Assessing a multi-method geophysical approach in the locating of unmarked graves under various seasonal conditions.

By

Andrew Frost
BAppGIS (Hons)

Thesis
Submitted to Flinders University
for the degree of

Doctor of Philosophy

College of Humanities, Arts and Social Science

February 2025

1 TABLE OF CONTENTS

2 ABSTRACT

This research used known burial sites to ascertain if there is an optimal seasonal time to conduct geophysical surveys to locate unmarked graves. This is important research as this was the first known study undertaken by the person who dug the graves in one study site, the certainty that there was no other anthropogenic interference between the burials. Also using known burials, of recent age, has firmly established the effectiveness of the chosen geophysical methods. This research is important to carry out in a South Australian context, as much of the research found in the literature is focused on climates that experience significantly more rainfall than South Australia.

My original contribution to knowledge is that in the soils typical of South Australia, it is the complexity of the soils physical and chemical characteristics that governs the effectiveness of geophysical methods in detecting human burials. Further to this I state that in the soils of South Australia, the relationship between soil moisture, radar velocity and resistivity are not linear relationships. As an addition to these points, I add to current knowledge in the discipline of Archaeology, that resistivity methods are slightly more effective in detecting burials in higher conductivity soils, as well as contributing my results of pXRF and Magnetic Susceptibility to the knowledge bank.

Burials are ubiquitous in the archaeological and forensic record, and the reliable detection of graves is an important challenge facing community groups, industry and law enforcement. Community groups and cemetery authorities look for reliable and cost-effective methods to help locate older burials and find space in ever filling burial grounds. Law enforcement authorities need rapid search methods and assurance that the conditions will not degrade the results. Locating burials sites is important as human remains occupy a unique position in an archaeological context, that being both a biological and cultural entity, able to connect contemporary society to a time and place from the past. Analysis of a burial using cross-disciplinary methodologies can allow revelation of many sophisticated sociocultural aspects of the past, these aspects can include social structure, population histories, diet and health, ritualized practices, as well as migrations and cosmologies

Geophysical methods are often used to locate unmarked graves due to their non-invasive nature and rapid site coverage, however, there are many factors that can influence, positively and negatively, the gathering, processing, and interpretation of geophysical data.

By using the same equipment over the life of this research, as well as a somewhat standard data process flow, the focus will be firmly on the subsurface matrix, how the soil and seasonal subsurface moisture levels affect the ability of these two geophysical methods in the pursuit of locating unmarked graves.

The two geophysical methods discussed within this study are active methods and so generate a signal (electrical and electromagnetic) that passes through the subsurface profile. Changes in these signals are then recorded. It can be seen then that the freedom and ease of these signals to pass through the subsurface profile is of paramount importance. The archaeological remains that are the targets of geophysics are typically in the subsurface profile, and because of this, the subsurface environment has a large influence on the effectiveness of these methods, due to changes in temperature, moisture levels, and soil type, to name a few.

The study sites are chosen as they offer the optimal above ground conditions, tended lawn as a ground cover, no grave furniture to impede the geophysical methods, and known burials. The lithologies presented at these sites are varied, so do offer contrast.

The subsurface matrix is a complex environment, this inhomogeneous nature of the subsurface matrix causes soil particles to be in contact with a variety of surfaces, these can be either permanently or variably charged. This then is a real soil system and is not simply composed of mixtures of pure minerals, but of materials covered with a variety of organic and inorganic films and coatings often bonded together into aggregates by various cementing agents. Subsurface soil moisture is the focus of much discussion in the literature. This subsurface soil moisture is largely dependent on naturally occurring precipitation, and so the relationship between the geophysical method and the soil structure will be examined to determine if there is an optimal time after these precipitation events that the geophysics can be conducted.

Using known graves will give instant feedback, with the potential for all burials to be identified with both geophysical methods. The results will be presented as a percentage of burials detected, the changes in radar velocity plus the changes in resistivity are compared to the seasonal precipitation recorded in previous days.

3 DECLARATION

I certify that this thesis: 1. does not incorporate without acknowledgment any material previously submitted for a degree or diploma in any university; 2.and the research within will not be submitted for any other future degree or diploma without the permission of Flinders University; and 3. that to the best of my knowledge and belief it does not contain any material previously published or written by another person except where due reference is made in the text.

Signed.....Andrew Frost.....

Date.....13/07/2024.....

4 ACKNOWLEDGEMENTS

An undertaking such as a thesis cannot be possible without support and belief from others.

I would like to take this opportunity to give heartfelt thanks to Pennie, an inspiration beyond belief, and Billie, who sat at my feet for the longest time.

My supervisor Associate Professor Ian Moffat, who did not seem to give up hope that I would, one day, actually finish.

Dr Amy Butler, who not only saved this thesis, but my life.

The writers of two of the best PhD theses I have ever read, Dr Xavier Mir Pellicer, National University of Ireland. Maynooth, and Dr Ian Brandes, University of New South Wales. Both had written a thesis of great complexity and simplicity.

This research would not have been possible without the consent of the study site cemeteries – Tatiara District Council and the Port Lincoln Sub-Branch of the Returned Services League.

Funding for this research was provided by the Australian Society of Exploration Geophysicists, and this research was also supported by an Australian Government Research Training Program (RTP) Scholarship.

5 LIST OF FIGURES

6 LIST OF TABLES

1 BACKGROUND

1.1 Introduction

Is there a seasonal time period wherein typical geophysical methods are most efficient in the detection of unmarked graves?

This is the question that underpins this research, and this chapter will provide a contextual background, and a review of the literature for this thesis. The role and scope of the practice of human burial is introduced, and why it is important to locate burials that are unmarked, or not otherwise recorded. The use of geophysics to detect these burials is widespread, and these methods are discussed, firstly in a general sense as applied to the discipline of Archaeology, and then in more detail as geophysical methods are used in the practice of locating unmarked burials. The reasoning behind the choice of study site is given, and the geology, geography, and seasonal conditions of the study sites are outlined. Soil is introduced, with discussion as to its make-up, both in general terms, and in further detail, along with the influence the physical and chemical properties exert on the efficiency of the geophysical methods. Parts of Australia are known to be climatically dry, so the role of subsurface moisture as a short temporal variable within the complex subsurface matrix is shown, and the relationship between this subsurface matrix, the moisture and the geophysical signals are explored further. Assumptions that have been found in the literature are given, in the context of soil and geophysical methods, and this thesis will examine these assumptions in an Australian context. It should be noted however, that while this thesis examines these detection methods in a seasonal context, there may not be an option of time and place for a search. This would be especially true in the Forensic context.

1.2 Burials

1.2.1 Overview

Why does locating unmarked graves matter? This chapter will explore the reasons why this research does matter, how the research fits into the broader archaeological and forensic framework, and why it is important for the geophysical discipline. Context around burials in modern times is given, both in a forensic sense and a cultural sense. Burials in the greater archaeological context are outlined, along with the crucial information that the dead can give us. This deeper understanding helps contemporary society understand the past. The human remains that may be in these graves, and how a burial may change the soil around it is also described, this gives context to the difficulty that is encountered in the location of unmarked graves.

1.2.2 Burials in a Contemporary Context

In Australia the burial of human remains within the post-European context usually takes place in registered cemeteries and is highly regulated. Modern funerary practices are well managed, with records accurately

kept, and burial sites marked (Ruffell et al. 2009:1). In South Australia, the Burial and Cremation Act, 2013 stipulates that Cemetery Authorities are required to maintain a plan of cemeteries that shows each site in which human remains are interred (*South Australia Burial and Cremation Act* 2013).

In accordance with these statutory regulations, contemporary records of burials are carefully maintained, more often digitally. In more historic times, however, these records can have become lost, or increasingly inaccurate. It cannot be assumed that in the past, those that maintained the records of burials were, in fact, literate. The physical location of the burial can become unmarked through many various ways, such as, desecration of burial sites; burials taking place in out of the way places (Conyers 2012:129); records being lost (Bevan 1991:1310; Conyers 2012:130; Purnell-Web 2012); gravesites not being marked (Purnell-Web 2012); clandestine burials (Larson et al. 2011:149); and as Indigenous burials (Conyers 2012:129; Garnaut et al. 2016; Gavin et al. 2015; Wallis et al. 2008). Once the location of a burial is lost, then the reliable detection of these burial sites becomes an important challenge to community and cultural groups, industry groups and law enforcement agencies. These groups require reliable detection to aid in acknowledging and honoring forgotten people, not only those from mainstream society, but also marginalized groups such as suicide victims or Indigenous burials that were never recorded.

Local authorities or church parishes require the extent of burials in an existing cemetery to aid future internments, or to guide future development. Law enforcement authorities require reliability in the search for clandestine burials. There is also a large social and ethical construct around burials, so utilizing non-destructive geophysical methods to locate burial sites offers a more ethical form of archaeology (Wadsworth et al. 2020:203).

As it has been estimated that approximately 117 billion people have been on earth over the entirety of human history, (Population Reference Bureau 2023), it can be imagined that there have been a large number of bodies disposed of in one way or another. From this it could be imagined that mortuary behavior has had a long history in hominins. Neanderthal skeletal remains have been recovered but given the passage of time that may have passed since death, it remains quite contentious whether the skeletal remains were from a burial or not. The burial ritual from those times may be quite different from what contemporary society consider to be normative behavior (Balter 2012; Burdukiewicz 2014; Kooijmans et al. 1989; Pomeroy et al. 2020:274). This modern behavioural development, was thought to have started in the Upper Paleolithic, yet Riel-Salvatore and Clark (2001:449) suggest that the deliberate burial of the dead and the use of grave goods started much earlier in the Middle Paleolithic. The pit at Sima de los Huesos in Spain also supports this (Carbonell and Mosquera 2006; Stiner 2017:256). The location of burial is shown to be an important behavioural development, with (Stiner 2017:252) providing summaries of burial places across the Middle and Upper Paleolithic periods. Cities all over the world are quickly running out of space to bury the dead, a thought that could well have been unthinkable in the early 19th century when the concept of

the garden cemetery first gained momentum. In the planning document “A Plan for Growing Sydney” (NSW Planning & Environment 2014), it is estimated that current space in the active cemeteries of Sydney will be in critical shortage by 2036. Accurately and reliably locating the remaining space within existing cemeteries becomes an important concern in the ability to maximise the available space (Hansen et al. 2014:14; Ruffell et al. 2009:1).

Xygalatas (2022) maintains that funerary rites have an important role for the living, allowing them to grieve, seek comfort, and face the reality of death, with Childe (1945:13) asserting that funerary practices are a manifestation of man’s spiritual culture. As cities worldwide struggle with finding enough space to bury the dead, the spiritual and cultural norms are also being challenged. In Hong Kong it is reported that the cost to house the dead outweigh the cost to house the living. Because of this, it is estimated that there are now some 200,000 cremated remains awaiting burial space. To help with this crisis the local government is promoting the scattering of ashes, but cultural beliefs do not support the scattering of any remains, preferring to have a single physical place to honor the ancestors (Keegan 2019). In Japan, authorities have been concerned about the lack of space available for burials since the 1970’s. To help foster innovative solutions the Buddhist community have promoted the practice termed ‘tree burials’, where the ashes can be interred, and a tree planted over the ashes. This has the benefit of supporting the cultural practices of visiting the burial site to honor the family members that have died (Mikles 2021). It was reported in 2017 that in England and Wales 23% of local authority burial grounds were either fully closed to new burials, or only open for burials in existing graves (Ministry of Justice 2007:8)

In Australia, cultural norms associated with burial are also changing. Natural burials are now offered. This type of burial replaces the wooden or metal coffin with easily composted materials, such as wicker or cardboard. The burials take place in a more natural bush environment with minimal or no grave markings (Falconer and Gould 2023). This type of burial would not only benefit the environment, but help create friendlier burial grounds, and aid the cooling of urban areas by providing greener areas. A further challenge to social norms is the concept of a composting burial, where the body is composted under accelerated conditions, resulting in 760 liters of soil in four weeks (Sheppard-Simms 2020). New, emerging technological driven methods of disposing of the dead are seen to continue on from a broader legacy of environmental activism. Conventional burial practices consume non-renewable resources, eg. wood, copper, steel for coffins, and reinforced concrete for grave sites. Below ground the embalmed body slowly decomposes releasing groundwater pollutants, above ground the well-manicured lawn cemetery consumes large quantities of water for maintenance (Westendorp and Gould 2021:5). See Figure 1.2.1 for a comparison between a traditional burial and a natural burial. Further challenging modern behaviors is the subtle return to more caring practices at the time of death, and it is here that the role of the death doula is placed. The death doula fulfils the role of companion, mentor and advocate, (Rawlings et al. 2020:13), a

move that some see as addressing the gender imbalances that are in place within the funeral industry (Westendorp and Gould 2021:3).

Because of this social importance, locating unmarked graves is essential in cultural resource management, importantly, the discovery of unmarked burial sites can lead to stabilization and protection of the burials from harm (Dionne et al. 2010:20). Historically, burial sites of indigenous peoples, unbaptized, diseased, suicide victims, or homosexual people were deliberately left unmarked, and located outside of consecrated grounds. In the recent SARS-Cov-2 (Covid 19) pandemic, thousands of bodies were buried hastily, often in mass graves (Raudon 2022; Reuters April 2021; Wallis et al. 2008).

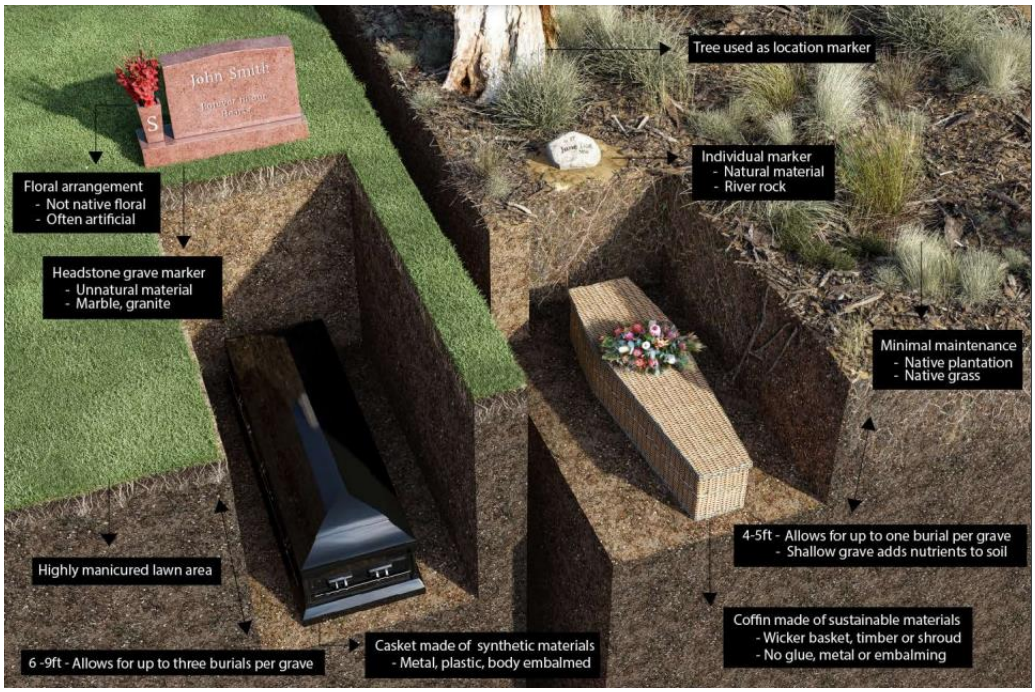

Figure 1.2.1: Diagrammatic representation of traditional versus natural burial practices. Image used with permission from Southern Metropolitan Cemeteries Trust. https://smct.org.au/murrun-naroon-natural-burials

There are different regulations in different countries that govern the exhumation of human remains and reuse of the burial site. For example, (Hansen et al. 2014:14) reports that in the USA human remains are left *in situ* in perpetuity, while the United Kingdom has a common 100 year rule. Several European countries, Netherlands, Switzerland, Sweden, Italy and Germany, have lease periods ranging from 10-30 years (Ferraz 2018). In South Australia a lease of a burial plot in one of the major metropolitan cemeteries can generally be for either 50 or 90 years, with large differences in the less populated regional cemeteries. As regulations governing exhumations within Australia are so tightly enforced, the opportunity to archaeologically examine human remains is rare, with more detail on this topic in Section 1.2.4 below.

1.2.3 Mass Graves

To this point the discussion has generally been about burials in more organized cemeteries. The subject of mass graves does require some mention. Mass graves are not a new phenomenon. Any time in history that a large number of people have died suddenly, their bodies may, invariably, have been interred in a mass grave. This type of burial is associated with war, criminal activity, slavery, natural disasters, or epidemic contagion, in other words, when exceptional circumstances supersede whatever normalized social rules are in place. This is either because of an urgent need to dispose of a large number of bodies, or because the dead are perceived as less than full citizens (Raudon 2022:85). Sadly, many examples of this type of burial exist. Soldiers killed in 19th century battles, Mexico-American War (1847-1850), Crimean war battlefields at Sebastopol, (1856), and Solferino, (1859), and the Franco- Prussian War, (1870-1871), were buried in communal graves (*War Graves on the 1914-1918 Western Front* n.d.). World War One saw unprecedented casualties, with the fallen often buried where they fell, with no record of where that may be (*War Graves on the 1914-1918 Western Front* n.d.). Other conflicts and disease occurrences over time have seen mass graves, Spanish Flu Pandemic 1918, Vietnam 1972, Sierra Leone 1991-2020, Rwanda 1994, Bosnia Herzegovina 1995, Cambodia 1995, East Timor 1999, Latin America 2002-2012, The Congo 2013, and currently Ukraine (Ashby 2011; Schreiber 2020; Xygalatas 2022).

Figure 1.2.2: Workers bury Covid victims in mass graves on Hart Island. (Coyne 2020) Image used with permission from NowThisImpact.

Since 2019 mass burials have been to the fore, as the SARS-Cov-2 pandemic spread across the world. Images from New York of the mass graves on Hart Island (Figure 1.2.2), and news reports of existing graves

in São Paulo, Brazil, being exhumed to make way for Covid burials, (Figure 1.2.3), highlights, firstly, how modern society is running out of space for burials in existing cemeteries and also shows contemporary methods of mass burials not associated with conflict or violence. Hart Island has been the burial place for the poor, unclaimed, or unidentified of New York, USA, since 1869. It is estimated that more than one million people have been buried there, (Mosher 2020), including victims of the Covid pandemic, and AIDS epidemic victims. The dead are interned three deep in large trenches, each trench holding 150 adults or 1000 babies (Raudon 2022:84). In Brazil, gravediggers and burials continued into the night, as authorities struggled to keep up with the rising death toll of the pandemic (Reuters April 2021). The inhumanity of mass graves is summed up by Raudon (2022:91) in that they (mass graves) "challenge the notion of individualized human remains, and mutes social connections". To be buried in an "indiscriminate mixed fashion is a lonely burial, separated from family, faith, or community".

It can be seen that mass graves arise from different causes, and the circumstances leading to the creation of the grave, and to a lesser extent the time since suspected burial, will dictate the investigation of the grave. If the suspected burial is within recent times, and is thought to be associated with criminal activity, armed conflict, or political unrest, then a forensic investigation may be called for. The United Nations considers mass graves created under these conditions to be matters of human rights, and to that end has created the Bournemouth Protocol that outlines the lawful and respectful protection of these sites, along with the ways in which they can be investigated in accordance with International law (Klinkner and Smith 2020). Haglund et al. (2001) have provided a commentary on the archaeology of mass graves. This commentary contains many case studies, some of which were located with the use of geophysical means.

This image has been removed for copyright reasons. The image can be viewed at https://www.theguardian.com/world/2021/apr/02/brazil-gravediggers-rush-to-exhume-bodies-to-make-space-for-covid-victims

Figure 1.2.3: Gravediggers exhuming bodies in Brazil. Photo (Reuters April 2021)

1.2.4 Burial in the archaeological context

Burials help us to understand how people once lived. The final disposition of the material body often reflects the social status of the dead, with rich variation in the mortuary practices shaped by social status and environment (Rains and Prangnell 2002:25; Raudon 2022:91). In an Archaeological context, the study of a cemetery, graveyard, burial site, or cremation site can yield much information from not only the subsurface, but also above ground as well (Muller 2021). Pardoe (1988:1) states that death is the last

disruptive rite of passage and that there is much to learn about a society by the examination of their response to death. Often, it is only the bones and grave goods that are left. These remains, plus the position of the body in the grave, and the location of the grave in the burial ground, are all that remain of a human life. Human remains occupy a unique position in an archaeological context, that being both a biological and cultural entity, able to connect contemporary society to a time and place from the past. Analysis of a burial using cross-disciplinary methodologies can allow revelation of many sophisticated sociocultural aspects of the past, these aspects can include social structure, population histories, diet and health, ritualized practices, as well as migrations and cosmologies (Stutz and Tarlow 2013:1). The material culture above ground can also tell a story, with the spatial arrangements of burials, in both more modern cemeteries and Indigenous burial grounds, often being due to social status, the grave decorations also a depiction of social status (Pate 2006:233).

The in-depth archaeological investigation of cemeteries in Australia is not extensive, with Anson and Henneberg (2004); Haslam et al. (2003); and Pitt et al. (2017) being exceptions that involved excavations. All of these studies of burials in post-colonial Australia have shown a variety of burial practices. They have also shown variable decomposition rates of the remains in the graves. The study of the Anglican Church of St Mary's in Adelaide, South Australia, exhumed burials from the period 1847 to 1925, (Anson and Henneberg 2004; Gurr et al. 2022). Pitt et al. (2017) was one of many Archaeologists that exhumed burials from the period 1792-1820 in the Old Sydney Burial Ground, while Haslam et al. (2003) exhumed burials from the period 1843-1875 at the North Brisbane Burial Grounds. As exhumations are rare in Australia, any that are undertaken become important, not only for the cultural artefacts they reveal, but to show rates of decomposition of human remains and burial accompaniments such as coffins etc. over a longer period of time. Some knowledge of what may be in the unmarked grave that has attracted the interest of a geophysical researcher is of value, but so little is known (Conyers 2016; Damiata et al. 2013; and Fiedler et al. 2009).

Neolithic burials had been excavated since the Renaissance, and in 1872, Émile Rivière described the first Paleolithic burial found in modern times. The body was decorated by perforated shells and covered with red ochre when found in the Balzi Rossi cave system in Italy. The notion that Paleolithic people had some kind of metaphysical beliefs challenged contemporary religious and intellectual beliefs of the time (Richard 2013:30–32). In the late Bronze Age many societal norms were challenged, and in these times Bruck, (1995:22), suggests that the dead took on strong symbolic concepts, adding further meaning to liminality, continuity and renewal. While not constrained entirely to the Bronze Age, it was in this period that many burial mounds were constructed, with these mounds becoming strong symbols in the landscape.

In the early Medieval Christian world, burials were conducted with an often, simple ceremony. Bodies were washed, wrapped in cloth, and then placed in either the ground, or a coffin. The corpse was laid out in an

extended position, with an east-west alignment that mimicked the alignment of the adjacent church. This simple pattern has been found in the hundreds of thousands of disinterred burials throughout medieval Europe (O'Sullivan 2013:261). Places of burial ranged from monasteries, major churches to minor parish cemeteries. Burials in monasteries were for the elite, with the position of burial dictated by rank or political position, while burials in churches were often according to affluence and influence (O'Sullivan 2013:271). Grave marking practices in the early Christian world derived from Roman customs. Grave markings were typically tombstones, with the name of the deceased marked on them. From the 10th century tombstones became more common, and by the 12th century grave markings started to take the shape of effigies of the deceased and symbolised their social rank (O'Sullivan 2013:265–266). This trend followed the trend of grave goods showing an increase of material culture (Childe 1945:15). While the elite and politically influential people were buried with elaborate markings in churches and monasteries, most people were buried in churchyards, and graves were often marked only by a mound of earth (O'Sullivan 2013:274).

In the Islamic world laws for burials were derived from the *ijtihad*, a set of laws based on deducted interpretation of the Koran. These laws from the Medieval period formed the basis of funeral manuals. Bodies were washed and wrapped in a shroud, or grave clothes. The bodies were placed in slots, either in the sides or the bottom of the grave shaft, with one body in each grave. Wooden planks are placed over the corpse, or mud bricks placed over the slot. Cemeteries were mostly used, these located outside of the town or village, with grave markings varying from a simple headstone with no markings, to elaborate cenotaphs. The latter were to mark the graves of more prominent or wealthier people (Petersen 2013:242–250).

In Australia, many Indigenous burials have been found, with many of the remains removed with no formal study involved, with (Pardoe 2013:741) stating that the majority of skeletal remains held by the South Australian Museum were exposed by development during the 19th century. However, Norman and Payne (2022:817) and Turnbull (2007:94) both describe the prevailing culture of the late 18th and early 19th century of procuring body parts and skeletal material of indigenous peoples from around the world. These skeletal remains were traded throughout a network of European collectors and Museums, often described as trophies of empire, and fetishized, commodified and consumed (Norman and Payne 2022; Pardoe 2013; Turnbull 2007).

Bowler (1998:128) described the discovery of the three burials at Lake Mungo as a new phase in Australia's human history. Bowler describes the labor-intensive ritual involved with the burial, called simply 'Mungo 3', as a phenomenon with 'extraordinary implications', as it represents the oldest example of burial adornment in the world, at the time of writing (Bowler 1998:151). Further south at Kow Swamp Thorne and Macumber (1972:316) recorded the burials found there. They note that the burials were full extension, crouching or tight flexion, with grave goods being stone artefacts, shells or marsupial teeth found also. Pate (2006:233–236) describes the burials at Roonka in some detail. Three types of burial pits were

described, shallow longitudinal pits with extended burials; deep circular shaft pits where the body was placed in a vertical position and allowed to slump down; and circular to oval pits where the body was placed on its side. The two former burial methods were from the early to late Holocene, with the latter dated to be from the late Holocene. Grave goods were found in most of the burials, and included stone and bone tools, bone and tooth headbands, necklaces, and pendants. As for the burials at Lake Mungo, the abundant use of ochres was noted. Pate (2006:233) also suggested that the use of material culture in the burial practices signaled the differences in social status. In the current post-processual archaeological context collaboration and negotiation became central pillars of the relationship between Anthropologists and Indigenous peoples. Repatriation of skeletal remains became more common, with community groups reporting that the reburials provide a direct link with their ancestral past (Pardoe 2013:738).

While the study of human skeletal remains can often be a controversial and emotive subject for many sections of the community, it is often these skeletal remains, and remnants of material culture as grave goods, that survive and can tell a story (Anson and Henneberg 2004:15; Owen and Pate 2014). The preservation of buried skeletal material is reliant on the soil surrounding the burial, wet clay was found to be an excellent preservative in a recent excavation in Piccadilly, United Kingdom, (Hilts 2023:57), and Bruck (1995:251) reports that excessively acidic or alkaline soils will not preserve bones, as human bone is a composite material, loosely described as a mineralized collagen, (Collins et al. 2002:384; Kibblewhite et al. 2015:250). The preservation of bones in an archaeological context is also closely correlated to the soil pH (Collins et al. 2002:386; Gordon and Buikstra 1981:566; Kibblewhite et al. 2015:250). The rate of decomposition of buried human skeletal material is also dependent on the amount, and pH, of available soil moisture, as well as the temperature of the surrounding soil.

Finding the buried remains of past peoples is a rare event, so any information that can be gleaned via scientific analysis becomes an important clue in human evolution. Examples of this include; Pomeroy et al. (2020:264) describe early Neanderthal burial practices from Shanidar Cave, Kurdistan; Stiner (2017:251) introduces the significance of burial location from Middle Paleolithic times; Swali et al. (2023) show the earliest evidence of Late Neolithic plague in Britain; Childe (1945) showed an extended shift towards cremation from the Paleolithic to the Late Neolithic periods; Owen and Pate (2014) show changes in landscape usage and modifications to socio-economic patterns after analysis of burial mounds; Anson and Henneberg (2004) nominate information about diet, social stratification, population origins, as well as changes in mortuary practices can all be extracted from the analysis of burial grounds and any skeletal remains exhumed; Radini et al. (2016) showed a relationship between the environmental particles on teeth and possible occupations. From skeletal remains DNA can be extracted, from grave goods dates of burial can be determined, and origins of any mineral objects, such as ochre, also determined, highlighting any possible trade routes.

1.2.5 What we might see – decomposition.

Locating unmarked human burial sites is important for a number of reasons, outlined in Section 1.2.2. An important question needs to be considered at this point, and that is, what human remains would be potentially within the subsurface matrix that a geophysical survey may locate?

If we consider a typical burial in the contemporary western world, ie a body in a simple wooden coffin (not lead or steel lined), placed in a grave with the soil replaced, or a body disposed of in a clandestine fashion. The human body will start the decomposition process approximately four minutes after death (Blom 2018:22). This decomposition will progress in two stages, pre and post skeletonization. The pre-skeletonization stage will follow a consistent series of four steps, consistent, but each step can be a little intertwined, and it must be noted that the body and coffin will each decompose in a different manner, almost separately. Vass (2001:191) suggests as a guide the formula 1285/ average temperature (C°) to determine the number of days to the skeletonization stage. These four pre-skeletonization stages are fresh, bloated, active decay and dry. The fresh stage is characterized by the onset of the stiffening of muscles (*rigor mortis*), the pooling of blood in the body (*livor mortis*), and the cooling of the body to ambient temperature (*algor mortis*). This stage can last from death to two days. The rupturing of cells and putrefaction signals the onset of the bloated stage. In this stage the formation of gases, such as ammonia, hydrogen sulphide, and VOC's take place, with this stage lasting from 2-10 days. These gases escape via ruptures in the skin in the active decay stage. These escaping gases will give the characteristic strong putrefaction odor, and this stage will last 11 – 42 days. The final stage takes place when the soft tissue and moist skin have finally decomposed, and will last 43 – 271 days (Blom 2018:8; Campobasso et al. 2001:20). The decomposition of the human body will be affected by many environmental, physical and chemical factors, both intrinsic and extrinsic. The environmental factors could include the soil temperature if buried, and ambient temperature if the body is on the surface; the ambient humidity and rainfall; and soil pH (Blom 2018:10–12; Van Belle et al. 2009:37; Vass 2001). Intrinsic factors that affect the decomposition are a complex mix and will be largely dependent on the individual physical and chemical body composition. Factors such as age at death, percentage of body fat, muscle and water, presence of disease, gut fauna, pH of physiological system are all very unique to each body. The soft tissue in the body will be attacked by bacteria, fungi, and protozoa, with this activity resulting in the production of inorganic gases, organic gases (termed volatile organic compounds (VOC)), and liquids (termed leachates). While human bone may last for thousands of years in some soils, the decomposition that occurs during the post-skeletonization stage is influenced by similar factors (Bevan 1991:1310; Collins et al. 2002; Kibblewhite et al. 2015:385). Bones that form the human skeleton are comprised largely of collagen fibers and hydroxyapatite ($CaCo_3$). Hydroxyapatite becomes soluble with increasing pH of any available soil moisture, and as this is dissolved, larger areas of collagen fiber are exposed to microbial activity (Collins et al. 2002:385; Kibblewhite et al.

2015:250). The activity of tree roots forcing open cracks can also accelerate the decomposition of bone, allowing increased microbial access to the collagen within the bone structure.

The rate of penetration through the grave soil of the VOC's and leachate will depend on the particle size and texture of the soil. The presence of any available soil moisture will also affect this dissolution, mobility, and sorption (Perrault et al. 2015:384). These compounds, both liquid and gas, that leech out of the body carry a charge, and it is this charge that will help bond the compound to any available charged soil particle. The subject of charged soil particles is dealt with in full in section 1.7, however, it must be stated here, that this bonding will weaken any possible bonding of soil particles and soil moisture. As the leachate compound-soil bonds weaken over time, gas is given off, and this is the residual odor of a burial site (Blom 2018:22; Brasseur et al. 2012:168; Perrault et al. 2015:2015). The primary function of many geophysical methods is the mapping of changes in subsurface resistivity, see Section 1.3, and these VOC's and liquid leachates will change the resistivity of the soil in the immediate vicinity of the burial (grave soil) (Pringle et al. 2010:127; Van Belle et al. 2009:38). How long the leachates and VOC's stay in the soil has been the topic of some study, with Van Belle et al. (2009:38) noting that nitrogen leached into grave soil during decomposition can still be traced up to 430 days after burial, Pringle et al. (2010:131) have recorded changes in soil conductivity after 2 years. No longitudinal study has been found where a human burial has been the subject of a geophysical survey to monitor the geophysical response, so it is largely unknown what part the decomposing flesh plays in the geophysical response. Several studies have been undertaken using pig carcasses (*Sus scrofa domesticus*), (Armstrong et al. 2016; Brasseur et al. 2012; Jervis et al. 2009; Perrault et al. 2015; Pringle et al. 2009; Schultz et al. 2016), pigs have been used as their chemical physiology closely represents that of a human. These studies have provided much data on VOC and leachate behavior, with rates of decomposition also monitored, but have not taken place over a large period of time, eg greater than 6 years.

The soil in which the burial takes place is physically altered, so it will show a different set of characteristics that will impact the results of a geophysical survey. In the act of burial, a grave shaft is dug, with the soil placed on the surface of the ground, near the grave. Human remains are placed into the grave, these remains may be in a wooden coffin, wrapped in cloth, or without any covering at all. The soil is then backfilled into the grave shaft. The backfilled soil has a greater percentage of space between the soil particles making up the soil profile, and whatever stratigraphic layers the grave shaft may have cut through are mixed. All these actions result in resistivity differences between the new grave shaft and the original soil profile. From the moment the grave shaft is filled in, the soil will slowly settle, and, over many years, the spaces between soil particles will reduce, reducing the differences in resistivity of the original soil, the grave fill, and the remains. Of course, while the turbated soil is slowly settling the coffin and remains are slowly decomposing. The environmental factors that affect the decomposition of the human body also affect the decomposition of the coffin, factors such as the soil pH, temperature, available soil moisture, soil

bacteria etc. Only two reports of exhumations from Australia that recorded the state of coffin decomposition were found. Rains and Prangnell (2002:27) reported on the 390 burials that were exhumed at the Lang Park, Brisbane site. This site was the first cemetery in use in the new settlement of Brisbane, and was in use for 34 years, starting in 1843. Grave sites discovered in the survey were reported as containing coffin outlines, coffin wood, with most of the excavated graves showing poor levels of preservation, and only three intact coffins found. In Sydney, Pitt et al. (2017) reported on the excavation of the Old Sydney Burial Ground, in use from 1792 - 1820. 68 graves were excavated, with only 57 showing evidence of a coffin. It is worth noting that both of these cemeteries were described as being 'wet', i.e. the soil having high levels of moisture, an ideal environment for the decomposition of organic material (Pitt et al. 2017:13; Rains and Prangnell 2002:21). Of particular note, in regard to locating burial sites by way of geophysical methods, when the body decomposes, but the coffin lid is intact, there is in effect, a void in the coffin. This will be highly visible within the geophysical survey.

Eventually the changes in resistivity will become quite subtle making the burial more difficult to detect with geophysical methods. The time taken to achieve this homeostasis within the soil profile is largely unknown (Dionne et al. 2010:27; Ruffell 2015:4). The results that are returned from a geophysical survey will depend firstly on how long the body has been buried. The method of burial will also affect the results, ie. the body in a coffin versus a shroud or laid in a supine position versus laying in a lateral position. The soil type, and any available soil moisture will also influence the geophysical results, this is discussed in depth in Section 1.4.3. Studies have reported excavating the grave after geophysical survey, and have linked the geophysical response to the direct detection of skeletal remains, (Damiata et al. 2013; Freeland et al. 2003; Ruffell 2015), and from these studies the chest cavity was the most recognizable feature. Other naturally occurring subsurface features that may be found in a burial ground, or the vicinity of a clandestine burial, could be tree roots, animal burrows, rocks or large stones. All of these objects could potentially show as results in a geophysical survey, and most can appear very much like a burial. However, (Ruffell 2015:4) reports that skeletal remains recovered from a beach sand environment comprising 50-70% shell, calcareous algae, and limestone fragments, showed no detectable changes in resistivity, and so recorded no result from geophysical survey. This aligns with Moffat et al. (2021:8) who states that under field conditions, a reliable detection of skeletal material is challenging.

To summarize; a geophysical survey of a potential human burial could show results from soil disturbance; the leachate within, and in the close vicinity of the grave soil; reflections from a casket, a tarpaulin or other wrappings; reflections from the skeletal remains; cuts through the naturally occurring stratigraphy; or any combination of these.

1.2.6 Burials Summary

Cemeteries and other places of human burial in the contemporary world can be places of quiet contemplation, a chance to connect with, or honor, those gone before, places of huge social and spiritual import. Contemporary places of human burial can also be places that signify immense violence or horror, as in mass graves found in places of conflict. Burial sites from pre-history contain much information of those that may be buried there, their communities, what they ate, who they traded with, where they had come from, and this information can help weave the tapestry of the deep past of contemporary man. A new problem with contemporary burial has been surfacing over the last few years, that is, cemeteries in large cities are quickly running out of space. The recent SARS-Cov-2 (Covid 19) pandemic has helped to highlight this, as cities in many countries that experienced a high death rate, quickly started to recycle burial sites in existing cemeteries. The search for those that may be missing, signs of criminal activity, or those that have died in conflict, the forensic application of geophysics is also of importance.

Geophysical methods have shown, and will be shown, to have some effectiveness in locating unmarked burial sites in all of the above scenarios, with the non-invasive and non-destructive nature of great significance. There has been a call for continued research into the applications of GPR, specifically targeting burials in different soils, different burial scenarios, and different micro-environments. Of particular note is their call for research into locating those remains that have been interred over a long period of time, as well as victims of war crimes that may be found in mass graves, (Schultz et al. 2006:615).

For all of these reasons, finding more effective ways of locating burial sites is of great interest to a number of disciplines, such as cemetery authorities, archaeology, forensic investigation, and war crime investigators. This research has been designed to address some of the many assumptions found in the literature, and the results will benefit all of those interested parties.

1.3 Geophysics

1.3.1 Overview

This section will outline in broad terms what geophysics is and general applications it can be used for. More detail will be given on how geophysics is used in Archaeology generally, and specifically, how locating unmarked graves benefits from geophysical methods. Two methods were chosen for this research, Ground Penetrating Radar (GPR), and Electrical Resistivity Tomography (ERT), these methods are outlined, and the reasoning behind their use is detailed. This section will build on the preceding sections by detailing how the complexity of the soil interacts with these geophysical methods, and the ways that the physical properties of an unmarked grave will interact with the geophysical pulse and currents.

1.3.2 Assumptions from the literature.

There are many assumptions around a geophysical survey that can be found in the literature. Those that are relevant to geophysical methods and have guided this research are listed below.

Doolittle and Collins (1995:102–106) *"Because it does not perform equally in all soils, GPR is an imperfect tool. Many soils, because of their high conductivity, are essentially radar opaque."*

"The realizable GPR investigation depths are less in areas where soluble salts are not leached from soil or where clays have cation-exchange capacities (high amounts of Ca, Mg, Na, and K)"

"Seasonal climatic variations do affect the differentiation of subsurface features. In most investigations, radar is not studied in a temporal mode".

(Hansen et al. 2014:15) "GPR may not be suitable…..where clay rich and saline soils are present in survey areas where radar waves become rapidly attenuated".

Gómez-Ortiz et al. (2010:112) *"Another limitation to the GPR technique corresponds to the signal attenuation produced when water saturated clayey material appears, making very difficult the interpretation of the radargrams".*

(Cassidy 2009:44) *"A material containing a high degree of free charges is effectively a conductor where the majority of the EM energy will be lost in the conduction process as heat. This is the reason why GPR is ineffective in higher-conductivity environments (e.g., saline conditions and high clay content)".*

Cassidy (2009:62) *"The effect of water is a constant theme within GPR, and as a basic rule of thumb: the relative permittivity of material increases with increasing water content (and therefore velocity decreases)".*

Van Dam et al. (2003:271) *"The minimum required textural variation necessary to produce GPR reflections of sedimentary structures is small. Even the smallest change in water content will cause a contrast in dielectric properties and, thus, reflection of EM energy".*

Daniels (2007:73) *"The velocity of propagation is primarily governed by the relative permittivity of a material, which depends primarily upon its water content".*

Dionne et al. (2010:28) *"GPR research similar to that of this study is necessary in other settings to determine optimal survey methodologies for unmarked burials in areas of contrasting environmental conditions and multiple time periods".*

Freeland et al. (2003:2) *"Simplified operation and interpretation for both novice and professional operators would greatly benefit law enforcement investigations, while also allowing the technology to be more effective and more widely utilized".*

Pringle et al. (2009:5) *"Resistivity can be a viable alternative to GPR surveys, particularly if the soil clay content is high or there are significant other non-target objects within the near surface".*

Dick et al. (2015:20) *"There are fewer studies using electrical resistivity to locate individual remains and indeed characterise mass burial sites".*

The assumptions above show that the nature of the subsurface matrix within a geophysical survey can become a large factor in the success of the survey, along with any possible subsurface moisture that may be within that matrix. Along with these environmental factors, is the call for simplified methodology, and using more than one method to located subsurface targets.

1.3.3 Introduction

A simple definition of the discipline of geophysics could be lateral and vertical mapping, by using non-invasive methods, the geology, geological structure, and anthropogenic artifacts beneath the Earth's surface (Environmental and Engineering Geophysical Society n.d.). A deeper definition of this discipline is the act of measuring, analyzing, and the interpretation of the subsurface of the Earth through the application of physical fields at the surface (Environmental and Engineering Geophysical Society n.d.; Reynolds 2011:3). The lateral and vertical mapping can be of a global resolution, as used by various geoscience disciplines, or of a finer resolution, as used by many disciplines in near surface prospection. No matter the size of the target of interest, it is the discontinuity of the physical or chemical properties of one subsurface region from its neighbors that geophysical methods will detect. These changes could be the density; magnetic susceptibility; elasticity; thermal conductivity; electric resistivity; dielectric permittivity; or radioactive levels (Sharma 1997:2). These changes in physical or chemical properties do, however, need to be of a magnitude of difference to register, regardless of what methodology of detection are used (Balkaya et al. 2021:2).

No matter what the target of a geophysical survey may be, nor if the survey is deep earth or near surface, the methods can fall into two categories, passive or active. The active methods, such as continuous wave electromagnetics, resistivity, or ground penetrating radar rely on a signal generated artificially and then sent into the subsurface matrix. The passive methods, such as magnetics, gravity, or radiometric, simply read the naturally occurring fields with no input. The application of either the active or passive methods has two common variables, one is the subsurface matrix that the active signal must penetrate, or the passive method must read, with the other being the interpretation of what is really just a vertical picture of what physics thinks the subsurface matrix looks like (Edwards 1977:1020).

1.3.4 Geophysics in Archaeology

As the applications of these physical fields at the surface are both non-invasive and non-destructive, the adaptation by the discipline of Archaeology has attracted much interest (Goodman and Piro 2013:3; Simyrdanis et al. 2016:2). Various geophysical methods are now routinely utilized across a spectrum of projects such as, subsurface foundations (Angelis et al. 2018; Balkaya et al. 2021; Correia 2019); burial sites (Aziz et al. 2016; Barone et al. 2016; Bladon et al. 2011; Booth and Pringle 2016; Conyers 2006; Moffat et al. 2021); stratigraphic mapping (Schöner et al. 2012; Simeoni et al. 2009; Van Dam et al. 2003), and many

more. Geophysics can be applied within the discipline of archaeology in three main ways. This can be prospection, extrapolation, or hypothesis testing.

When an archaeological investigation takes place, often, one of the first activities is a geophysical survey. This is due to the non-invasive nature, rapid deployment, and lower overall cost of a geophysical survey. In contrast, exploratory excavations by Archaeologists are subject to high financial and time costs (Balkaya et al. 2021:1; Cott 1997). This, then constitutes archaeological prospection. This survey is used in this manner to find areas of interest, with data being interpreted based on the experience of those involved. This interpretation is based on known patterns seen in the geophysical results, that may, in some way, correspond with patterns seen in results from the new site. These interpretations may, or may not, ignore the influence of subsurface geological features. After excavation, these features seen in geophysical results may, or may not, turn out to be archaeologically significant. A series of boulders laid within the subsurface profile as a result of natural causes can, at times, can be seen in geophysical results displaying similar patterns within the subsurface profile as anthropogenic material culture, such as building foundations (Moník et al. 2018; Simyrdanis et al. 2016). If excavation is carried out after this initial prospection, and anthropogenic material is found that is of interest, then geophysical methods can be used to further survey the area. This constitutes archaeological extrapolation. The initial results can then be marked over this new survey area to help locate further areas of interest. This extrapolation can extend existing knowledge over a wider area and helps build confidence in the geophysical results (Correia 2019:108). Archaeological results that are being returned in the field can give rise to further speculation or deeper questioning. This questioning can lead to a hypothesis. It is here that geophysics can be used to find further supporting, or unsupportive, information. The methods used in this case may often be different from those initially used, this gives a higher confidence level to the interpretation of results. This new information is consistent, or inconsistent, with the hypothesis, rather than to prove or disprove (Bevan 2000). This is because it is quite difficult with geophysical methods to say something does not exist, just because it is not detected.

These three applications of geophysics with the discipline of Archaeology are rarely clearly defined, and the range of potential subsurface material culture targets is large. One of these potential material culture targets that are ubiquitous within the archaeological record is the human burial. The non-destructive and non-invasive positions these geophysical methods as a culturally appropriate tool for cultural heritage management applications in cemeteries (Moffat et al. 2021:12; Wadsworth et al. 2020:203). The ability to image the soil's subsurface via geophysical methodology lends itself well to the detection of burials, both within archaeological prospection and forensic detection. Typical geophysics methodology for the detection of unmarked graves includes Ground Penetrating Radar (GPR) (Conyers 2011; Dionne et al. 2010; Martin 2015; Powell 2004; Sarris et al. 2018; Schultz and Martin 2011), Electrical Resistivity Tomography (ERT) (Martin 2015; Powell 2004; Sarris et al. 2018), Magnetic Susceptibility (Mag Sus) (Martin 2015; Powell

2004; Pringle et al. 2009; Sarris et al. 2018), and Earth Resistance (ER) (Martin 2015; Powell 2004; Schmidt 2008).

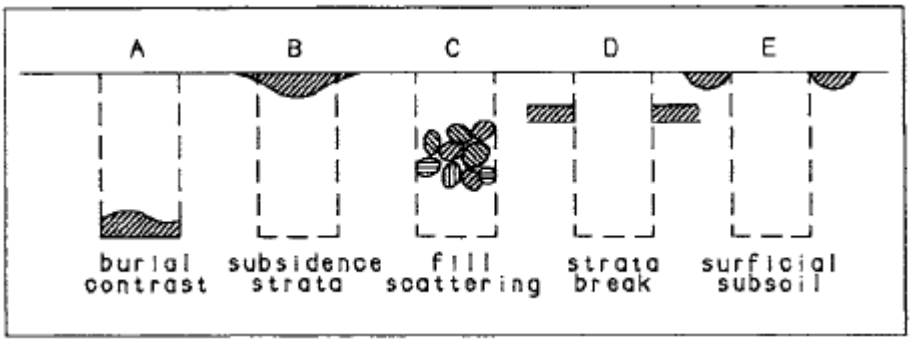

Figure 1.3.1: Diagrammatic representations of the physical changes to the subsurface matrix that is created during the act of human burial. (A) the contrast of the burial, contrasting soil and human remains. (B) soil from the surrounding area is eroded into the subsidence bowl. (C) intermingling the soil during the backfill process, introduces larger pore spaces and pathways for moisture. (D) the sides of the grave shaft are often straight. (E) often the overburden of the grave is spread out next to the grave. Image from Bevan (1991:1311) and used with permission.

The GPR pulse will reflect or refract when it encounters physical changes in the subsurface matrix. These physical changes could be the dielectric constant or the electrical resistivity, and these can change for a number of reasons. When a grave is dug for human burial, the removed soil is typically placed in an unstratified heap, next to the grave, in a truck for removal, or some other location specific collection method. There is a body placed in the grave, maybe in a coffin, swaddled in cloth, in a more natural wicker basket, or in a crime scene, just dumped in the grave. Then the grave shaft is refilled. These actions will disturb the natural stratigraphy of the subsurface matrix, the digging of the grave will slice through the natural stratigraphy, the intermingling of the soil will increase pore space and moisture content, and as the body decomposes leachates will permeate the soil adjacent the burial. These then, are the anthropogenic actions during a human burial that instigate changes in the subsurface matrix that a GPR may encounter, see Figure 1.3.1. (Bladon et al. 2011:249; Nobes 1999:10). Slightly contrary to these findings, Damiata et al. (2013:275), report that the dominant response is from the body, (cadaver or skeleton), and not the back fill or boundaries of the grave shaft. Their study undertaken in Florida, USA, found that the responses from cadavers and skeletal remains were hyperbolic reflections, and that these responses were near identical for a recent burial and skeletal remains after 19 months.

1.3.5 Forensic Geophysics

An important application of geophysical surveys is in the field of forensic investigation, with Buck (2003:5) suggesting that the potential is compelling. Locating a body within a forensic context has shown to bring

closure to family and assist with the psychological trauma associated with the sudden, perhaps violent, death. Legal precedent has shown that a body is an important piece of evidence, with the chances of successful prosecution increasing with this evidence (Berezowski et al. 2021:1). Geophysical methods offers the ability to cover a wide area quickly, as well as the non-invasive and non-destructive elements that are a key part of forensics, as any available evidence is safeguarded, preserving the sequence of search, recovery, identification and conviction (Pringle et al. 2009:2; Watters and Hunter 2004:23). Geophysical methods can be used within a forensic investigation in a number of ways, such as – identifying an undisturbed area that does not contain a grave, or defining anomalies that may be a grave, identifying actual locations of graves so these can be explored further with complimentary methods, and establishing the size of any possible grave (Watters and Hunter 2004:27). Graves may not be the only target. The ability of various geophysical methods to identify changes of physical and chemical properties within the subsurface can help identify any possible anthropogenic disturbances, even after a number of years. These targets could be a bunker, buried arms, leeching contaminants, tunnels etc. (Barone 2017:176).

Pringle et al. (2009:2) believes that geophysical methods are largely under-utilized, this is also emphasized by Berezowski et al. (2021) and Larson et al. (2011:151), who state that no one science contains all the skills necessary to conduct a systematic clandestine grave search. Ongoing research in the use of geophysics in forensic searches has proved to be a valuable resource, however, Schultz et al. (2016:73), calls for further controlled research, to add further understanding to the different variables that affect detections, and how GPR can be successfully applied.

1.3.6 Schmidt Precipitation Ratio

In 2017 a short research report was published by Schmidt et al. (2017), in which they outlined a theoretical precipitation ratio. This ratio was derived from the commonly held assumption that the detection of a ditch using the earth resistance method was more effective in a dry period that followed a high precipitation period. This assumption was based on the understanding that the bottom of a ditch could contain a high level of silt, and the backfill containing larger pore spaces. Both of these characteristics would trap moisture, and so, in a dryer period, the ditch would be left with a slightly higher level of moisture. It was theorised, and built on the results reported by Cott (1997), that this difference in soil moisture would return a lower resistivity value when surveyed with earth resistance methods. It is worth noting that the ditches in the report are Roman defensive ditches, located in Norwich, UK. The ratio was initially theorised to be the average rainfall in the last *d* days and the average rainfall over the month prior to the expected date of survey. This ratio was later refined, see equation 1.3.1, by predicting the number of days that would be *d.*

$$\boldsymbol{p(d) = \frac{average\ daily\ rainfall\ last\ d\ days}{average\ daily\ rainfall\ last\ 30\ days}}$$ **Equation 1.3.1**

This precipitation ratio was assessed in this research as a possible guide to when to carry out a geophysical survey in my study sites. The characteristics of a Roman ditch, soil dug, then backfilled increasing pore spaces, is not dissimilar to the characteristics of a grave.

1.4 Ground Penetrating Radar

The subsurface matrix is a complex environment, comprising a diverse mix of differing physical and chemical elements, some large, some small. All of these elements can influence the GPR pulse. In Section 1.4.4 it was discussed that of most interest was the presence/absence of moisture in the subsurface matrix, along with the grain size, and consequently, the size, shape, and connectivity of the pores. Bearing all this in mind, this chapter will build on that discussion and introduce the concepts of the Ground Penetrating Radar and how the soil and radar interact.

1.4.1 Theoretical Concepts

The Ground Penetrating Radar (GPR) is an electromagnetic (EM) reflection method, (Conyers 2004; Fotheringham 2013), and these electromagnetic, or radio, waves are used to probe lossy dielectric materials (Annan 2002:253, 2009:4). These lossy dielectric materials can be defined as a medium where some fraction of the electromagnetic wave power is lost as the wave propagates. This power loss is due to poor conduction (Cadence Design Systems 2022), and in Section 1.8.15 conduction from the perspective of the soil is discussed in more detail.

The application of these waves to sound the earth were developed using radio echo sounding of polar ice sheets (Reynolds 2011:535), with much subsequent developmental work being carried out in the glaciological field in the years 1950 – 1970. Further development took place as part of the Apollo Lunar Program, and after 1990 the applications of GPR had developed sufficiently for its use to be introduced in the fields of archaeology, environmental science, and geology. This is far from a complete history, that is not the aim of this research. A more complete history of the development of the GPR is provided by Annan, (2002). The development of Ground Penetrating Radar is now at a stage where it is routinely used in geological prospection (detection of cavities, subsistence mapping, glacial investigations, locating ice wedges, locating faults, and many other applications); environmental monitoring (contaminant plume mapping, landfill investigations, locating buried infrastructure, groundwater investigation etc.); glaciological prospection (ice thickness mapping, ice movement studies, snow stratigraphy mapping, detection of crevasses etc.); engineering analysis (road pavement analysis, railway ballast testing, void detection, locating reinforcing bars in concrete, location of utilities etc.); and archaeological survey (locating buried structures, detection of ancient roads, detection of voids, locating burial sites etc.); and forensic science (locating buried targets) (Reynolds 2011:536). Apart from the small personal cart described below, GPR is now used in aircraft, unmanned aerial vehicles (UAV), small watercraft, satellites, and mounted on vehicles.

A typical easily transported GPR system that may be used in the detection of unmarked graves would consist of a radar control system, receiving and transmitting antennae, and a power source (Conyers 2006; Koppenjan 2009:73; Reynolds 2011). The EM waves are pulsed at a high frequency (100-1000 MHz) in a cone shape, Figure 1.4.1, (Conyers 2004; Gómez-Ortiz et al. 2010). This finite frequency range is dictated by the physics of the EM wave itself. At low frequencies, the waves become diffusive and tend to be dispersed. At higher frequencies the depth of penetration becomes limited, due in part to the wave transitioning from conduction dominant to displacement dominant. This frequency range of 100 – 1000 MHz is termed the GPR plateau, Figure 1.4.1, (Annan 2002:254, 2009:10). Below this frequency the fields become diffusive, with pulses readily dispersing, and at higher frequencies there is an increase in signal absorption, to the point that penetration is limited. While at higher frequencies the penetration of the radar pulse is limited, with higher frequency comes a higher resolution. Conversely, radar pulses of lower frequency show less resolution.

The pulsed EM waves are reflected back from subsurface discontinuities and two parameters are read, the strength of reflection (amplitude) and the two-way travel time, in nanoseconds. These pulses are typically transmitted at extremely high rates, ranging from 25,000 to 50,000 pulses per second, and some control units are not capable of recording reflected waves of each distinct pulse. To overcome this issue the control system will use incremental sampling methods, these incremental samples will be used to produce a composite reflection trace (Conyers 2004; Daniels 2007). Waves that do not encounter a subsurface object that reflects them back, continue deeper into the ground until the energy finally dissipates (attenuation). Waves that encounter subsurface objects that are orientated in such a way as to reflect the wave pulses away from the receiver are not recorded, and these subsurface objects remain undiscovered (Annan 2009; Conyers 2004, 2016; Daniels 2007; Gómez-Ortiz et al. 2010; Jones 2008).

An important variable in the equipment used in GPR surveys is the frequency of the antenna used. With antennae of a wide range of frequencies available to the geophysics practitioner, the selection of antenna becomes a balance of depth vs resolution (Gómez-Ortiz et al. 2010:108). Rial et al. (2009:367) define resolution in a radar system as the ability to discriminate individual elements, in both horizontal and vertical planes, in the subsurface matrix. As the antenna used in this research is a pulsed radar that measures the two-way travel time, the vertical resolution will depend on the GPR system to differentiate reflections based on time. Bladon et al. (2011:249) states that this effect can be minimized by using an antenna of a different frequency. The horizontal resolution is based on two reflections, with origins located next to each other, at the same depth.

Schultz and Martin (2011:65) suggests that for the location of unmarked graves a mid-frequency antenna of 400-500 MHz will provide a favorable compromise between vertical resolution and depth of penetration. Doolittle and Collins (1995:102) comment further that a higher frequency antenna, (>500 MHz), will pick up

shallow features in low conductivity soils, and conversely a lower frequency antenna will improve the depth penetration in high conductivity soils. The conductivity of soils is expanded in Section 1.8.15. Adding considerable insight to the resolution/depth debate Damiata et al., (2013:274), argues that an antenna of suitable wavelength will provide the resolution capable of detecting human skeletal remains.

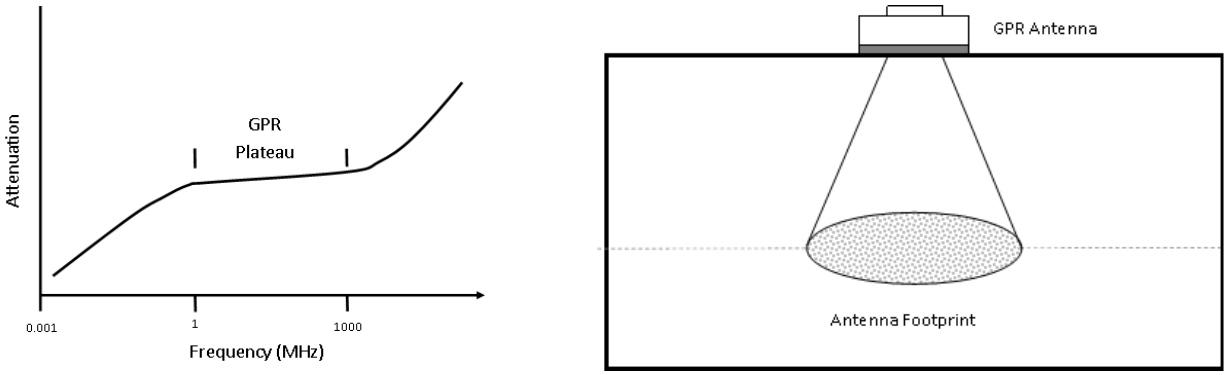

Figure 1.4.1: Left, the GPR plateau, where the radar pulse is most stable, and useable for GPR. Right, the diagrammatic representation of the radar pulse, originating from the antenna, and propagation out in a cone shape.

The receiving and transmitting antenna are usually both housed in a shielded enclosure. The shielding is an attempt by the manufacturers to keep the EM pulses from radiating out above the subsurface medium they are intended for. While the frequency range of the typical GPR is 100-1000 MHz centre frequency, most GPR systems use a dipole antenna, which transmits with a two-octave bandwidth. This means the actual frequency transmitted from the antenna can vary between one half and two times the centre frequency. This would mean that a 500 MHz centre frequency antenna would generate pulses with wavelengths ranging from 250 to 1000 MHz. Conceptually, this radar pulse would take the form of a bell shape, with equal distribution around the mean frequency, (Conyers 2004:39; Daniels et al. 2007:537). Figure 1.4.2 shows the theoretical bell-shaped curve of a 500 Mhz pulse, alongside the 500 MHz pulse recorded in a laboratory. The recorded pulse shows an asymmetrical 'spiky' distribution. This may be due to the irregularities in the construction of the antenna, or elsewhere in the electronics of other components in the system.

These waves move through the subsurface stratigraphy and are refracted, reflected, or diffused by physical or chemical changes in the subsurface matrix, Figure 1.4.3. These physical or chemical changes may take the form of variations in water content, changes in electrical or magnetic properties of the rock sediment or soil, bulk density changes at the stratigraphic interfaces, or the interface between archaeological features and the surrounding subsurface matrix (Bevan 1991:1311; Conyers 2004:25; Gómez-Ortiz et al. 2010:108).

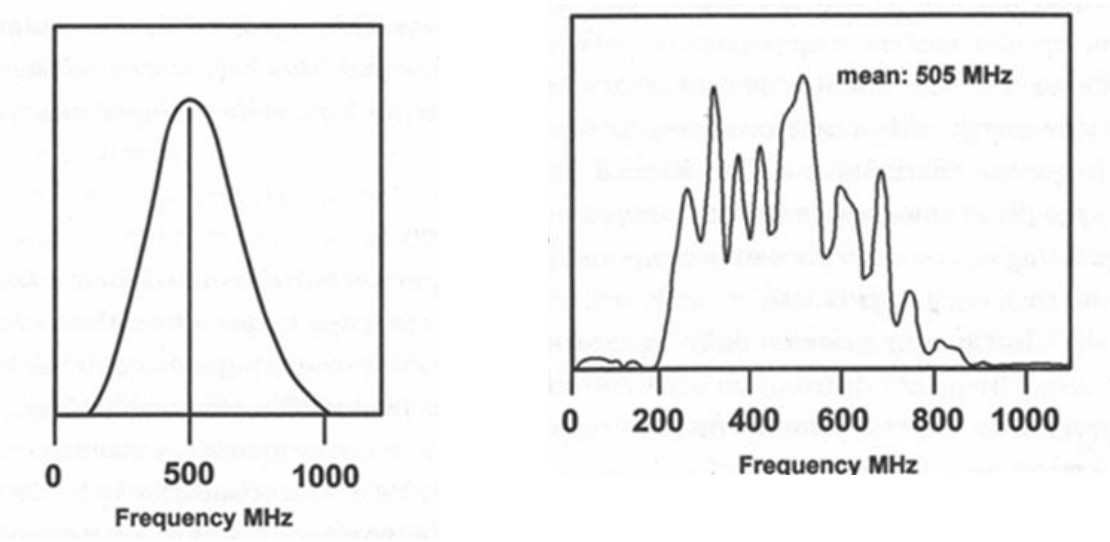

Figure 1.4.2: Diagrammatic conceptions of the GPR pulse. Top, with a centre frequency of 500 MHz, the conceptual GPR wave reaches from 250 – 1000 MHz. Below, the actual frequency recorded in a laboratory (Data: Conyers 2004:40).

This behavior of the EM pulse as it is transmitted through the subsurface is dependent on three characteristics of the subsurface, the relative permittivity, the electrical conductivity, and the magnetic permeability. By definition, the permittivity is the capacity of the soil to store electrical charge, and conductivity is the ability to transport an electrical charge. The magnetic permittivity is the magnetic equivalent of electrical permittivity, and is the capacity to store magnetic energy (Neal 2004:269). Scattering and geometric spreading of the energy of the EM pulse is further influenced by the presence of particles with similar dimensions to the wavelength. These particles will induce scattering, decreasing the transmission into the subsurface. As the pulse spreads into the subsurface in an expanding cone shape, this will decrease the energy with depth (Pellicer 2010:76).

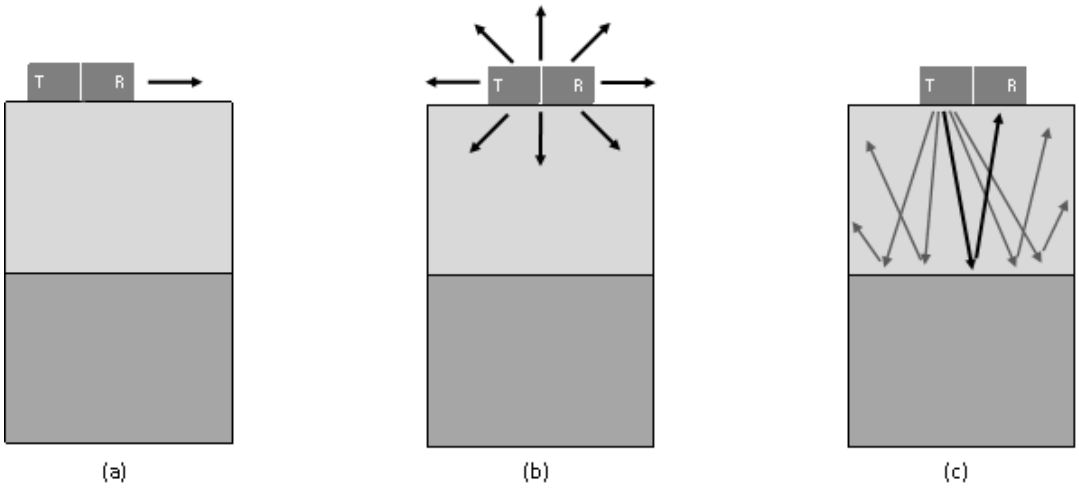

Figure 1.4.3: The GPR system in action. This consists of the transmitting antenna (T) and receiving antenna (R) that move together across the ground. The transmitting antenna acts as a point source (b) sending out the pulses in all directions. When the pulse encounters a change in resistivity in the subsurface matrix (c) these pulses will be reflected back to the receiving antenna. Not all transmitted pulses will be reflected back, some refract away from the antenna, and some will pass through any subsurface medium and attenuate.

Annan et al. (1991:2) and Neal (2004:272) both report that the amplitude sharpness of this reflection is dictated by the sharpness of which the permittivity changes, relative to the dominant wavelength. They suggest that wavelengths would be less than three of the size of the transition zone, (the distance over which there are changes in resistivity or permittivity), to return a sharp reflection. If the size of the transition zone is above this limit, the radar pulses are generally dispersed, or more general diffuse reflections are returned. However, Van Dam et al. (2003:258) states that very little is known about reflective effects of layering smaller than this transition zone.

The individual radar pulses are received by the receiving antenna, then recorded by the control box as a trace. These individual traces are the “A” scan, and are stacked next to each other producing a two-dimensional vertical profile, the “B” scan (Conyers 2004:12).

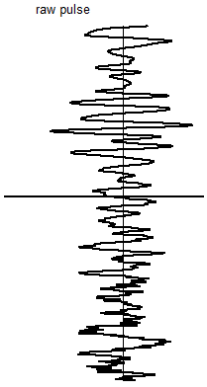

Figure 1.4.4: The 'A' scan.

Individual traces can be seen as the ‘A’ scan, or often referred to as the wiggle line (Figure 1.4.4). The scale of the reflection amplitude can be seen with the trace swinging from positive to negative.

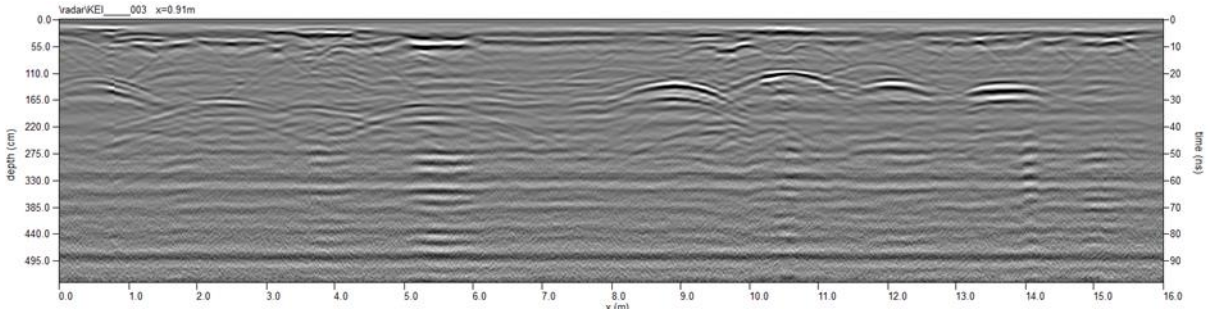

Figure 1.4.5: Typical GPR data displayed as a radargram, this is from the study site in Keith, South Australia.

Figure 1.4.5 shows a typical radargram, or ‘B’ scan. A radargram is made up of a series of scans, in this instance 1009 single scans. The radargram is also traditionally displayed in black and white, these colours depict the amplitude swing from positive to negative. On the left of the radargram is the indicative depth in cm, on the right is the indicative two-way travel time in ns. The scale on the bottom of the radargram is the distance travelled along the trace in m. This radargram is raw data, from this point the data undergoes a series of processing steps. Despite this showing raw data, several hyperbola’s can be seen, these are reflections, some stronger than others, from the burials. This supports Conyers who maintains that a subsurface target should be seen in raw data.

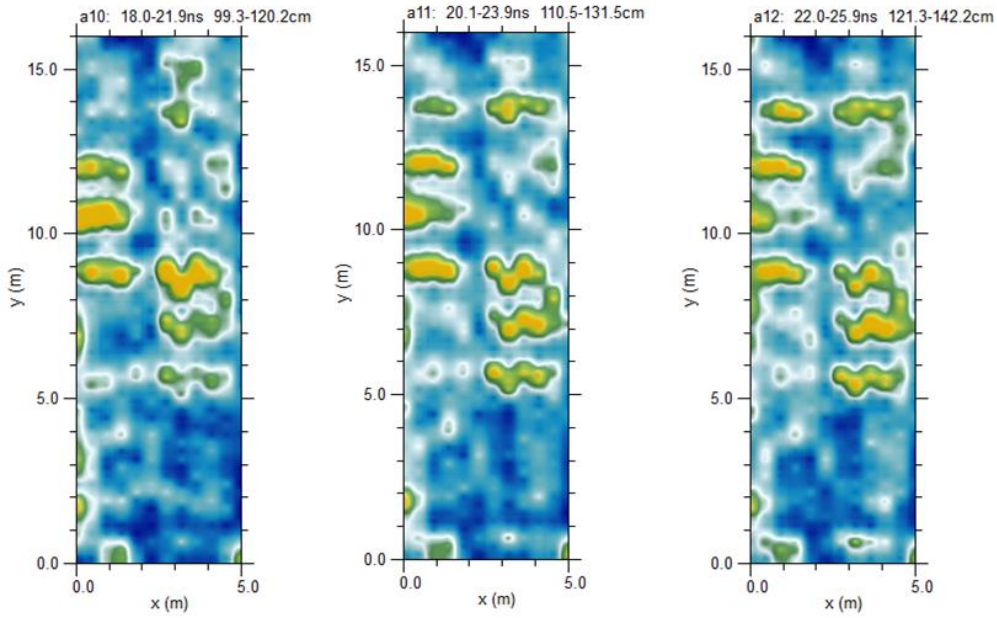

Figure 1.4.6: Time slices created from a series of radargrams to create the ‘C’ scans. These show the subsurface features (Burial sites in this case) at depths of 18 – 25.9 ns or 99.3 – 142.2 cm. These time slices are from the study rows in Keith Cemetery, Keith, South Australia.

After the radargrams are subject to processing, the cube of radargrams is sliced, the 'C' scans (Figure 1.4.6). The time slices show the amplitude swings, and these amplitude swings look more like the target subsurface features. These time slices can be gridded to form a 3D render of the subsurface. Figure 1.4.7 shows a series of time slices that start to form this 3D view.

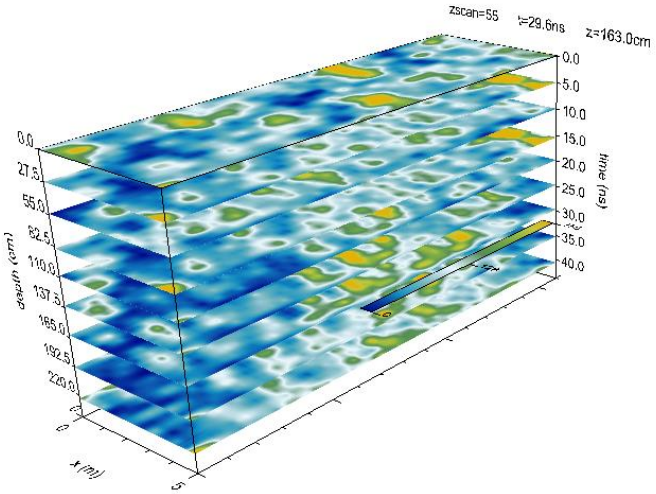

Figure 1.4.7: A series of time slices as depth increases. Scale on the left is the depth (cm), on the right is the two-way travel time (ns) and along the bottom is the travel distance. This is the start of the 3D view.

1.4.2 GPR Signal Processing

In this section a basic theoretical overview of processing a GPR signal will be given. Further specific information as to the processing steps used within this research is discussed in more detail in Methods, Chapter 2.

According to Daniels (2007:247) the primary goal of processing the GPR data is improving the signal to clutter ratio, (sometimes referred to as noise). Many of the most common processing techniques used to process GPR data have been developed for other applications, such as acoustic, ultrasonic and seismic geophysical applications. Many caution the over use of processing of the raw radargram, Luo et al. (2019:46) suggests a guided thought process is required, while Daniels (2007:247; Goodman (2009:236); Goodman and Piro (2013:62); Goodman (2012:166); Szymczyk and Szymczyk (2013:90) all warn that over-enthusiastic processing can add phantom features, while excluding features of interest. The subsurface matrix is a complex environment, any of the physical and chemical properties can reflect GPR data. Entities such as tree roots, changes in stratigraphy, rocks or stones, animal burrows, changes in soil moisture can all reflect GPR pulses under the right conditions. These reflections may not be sought by the geophysicist but are, in fact, still valid reflections. As GPR is time dependant, separating adjacent targets is straight forward if the targets are spaced further apart. If the targets are in close proximity, the processing becomes difficult to separate wavelet reflections (Daniels 2007:252).

Case studies found in the literature show these common processing steps, outlined below in Table 1.4.1;

Table 1.4.1: Common processing steps found in the literature.

Time zero correction	Balkaya et al. (2021:5) Hansen et al. (2014:16) Moffat et al. (2021:10) Aziz et al. (2016:401) Bladon et al. (2011:254) Schultz et al. (2016:62)
Gain	Balkaya et al. (2021:5) Marshallsay et al. (2021:96) Hansen et al. (2014:16) Aziz et al. (2016:401) Schultz et al. (2016:62)
Background Removal	Balkaya et al. (2021:5) Hansen et al. (2014:16) Aziz et al. (2016:401) Schultz et al. (2016:62) Bladon et al. (2011:254)
Bandpass Filter	Balkaya et al. (2021:5) Marshallsay et al. (2021:96) Moffat et al. (2021:10) Schultz et al. (2016:62)
Wobble	Balkaya et al. (2021:5) Marshallsay et al. (2021:96) Hansen et al. (2014:16) Moffat et al. (2021:10) Aziz et al. (2016:401) Schultz et al. (2016:62)
Butterworth Bandpass	Bladon et al. (2011:254) Hansen et al. (2014:16)
Migration	Hansen et al. (2014:16) Moffat et al. (2021:10) Aziz et al. (2016:401) Bladon et al. (2011:254)
Energy Decay	Moffat et al. (2021:10)
Average Trace Filter	Bladon et al. (2011:254) Marshallsay et al. (2021:96)

It can be seen from the above information that the primary function of the GPR survey is to gain deeper understanding of the subsurface matrix, and to spatially map these (Dionne et al. 2010:22). One important feature that is interpreted from the GPR data is the depth to these target features. Given the non-invasive nature of the GPR survey, being able to accurately map the depth and the orientation of subsurface features can sometimes suffice, preventing the destructive and expensive practice of excavation. The velocity of the wave can be accurately measured in a number of ways. The simplest of these is to identify reflections from known subsurface objects that are at known depths. These objects may have been buried for this purpose, or a part of the target has been exposed, such as a buried wall, or if coring takes place to identify changes in stratigraphy (Conyers 2004:102). These methods will undoubtably return the most

accurate indication of the depth of targets, but a Geophysics practitioner undertaking a GPR survey in a cemetery will not have the luxury of taking core samples down to the depth of a coffin.

The mapping of subsurface infrastructure is a good example of the value of knowing the velocity of the EM pulse, with the depth to pipes and cables being of paramount importance. Being able to cover large areas of ground and accurately map features at depth can also aid the archaeologist in understanding further subsurface features and stratigraphy at a landscape resolution. The subsurface matrix is not homogenous, neither vertically nor horizontally, but it will be constant during the GPR survey.

1.4.3 Soil and GPR

It is not known exactly what physical characteristic of the soil (e.g. grain size, orientation of grains, grain shape, pore space orientation), or what minimum variation of these characteristics control the actual EM pulse reflection (Van Dam et al. 2003:258). Adding to the complexity of the subsurface matrix that these physical characteristics show, is the electrochemical nature of the particle boundaries, plus the way that water is physically and chemically distributed within the matrix (Daniels 2007:95), and that any possible targets in the subsurface need to show a considerable permittivity contrast to the surrounding subsurface matrix to actually reflect the EM pulse. Ruffell, (2015:4), describes this problem in recounting a survey that was forensically searching for a body, buried in beach sand. The beach sand contained 50-70% shell, calcareous algae, and limestone fragments, and as these minerals showed little dielectric contrast to the skeletal remains, the skeletal remains were not detected by GPR survey.

1.4.4 Subsurface moisture

It has been shown that available water content, and subsequently the reflection of the EM pulse, from within an unsaturated subsurface matrix, is controlled by the size, distribution, and connectivity of the pore spaces, despite the difficulty in estimating these (Van Dam et al. 2003:270). Conyers (2004:101); Daniels (2007:73); van Dam et al. (2002:341) and others claim that the changes in soil moisture can dramatically change the GPR wave velocity, even during the survey. But these subsurface moisture changes can only be measured and understood if subsurface samples are taken during the survey, or there are appropriate measuring devices at the survey site. So, the complexity of the subsurface matrix and the subsurface moisture are rarely known at the time of a geophysical survey.

The moisture in the subsurface matrix will, at first, bond with the soil particles, forming a layer around charged particles. Colloidal forces will hold this bond. The available moisture that does not bond with particles becomes capillary water, this will be held by colloidal forces and the inherent surface tension, formed by the moisture, to the previously bonded water. This capillary water will act as a transition zone for further capillary action of the moisture. Moisture not attracted to soil solids is termed free water,

molecules of free water show an attractive force that is less than gravity, and so will move freely through the soil profile. All of this subsurface moisture moves through the soil profile via a complex maze of micropores. Further details of the physics of soil moisture, how it bonds with soil particles, and how it moves through these micropore passageways can be seen in Section 1.8.15. The EM pulse, emanating from the GPR, finds the low resistivity pathway through these micropores and travels through the subsurface matrix. Within the context of a human burial, the decomposing body will release many compounds, both liquid and gas. These leachates will bond to surrounding soil particles via charged molecules, with this act of bonding weakening the water/particle bond and increase the nutrient content of the grave soil, (Blom 2018:22; Brasseur et al. 2012:168; Perrault et al. 2015:377; Van Belle et al. 2009:38).

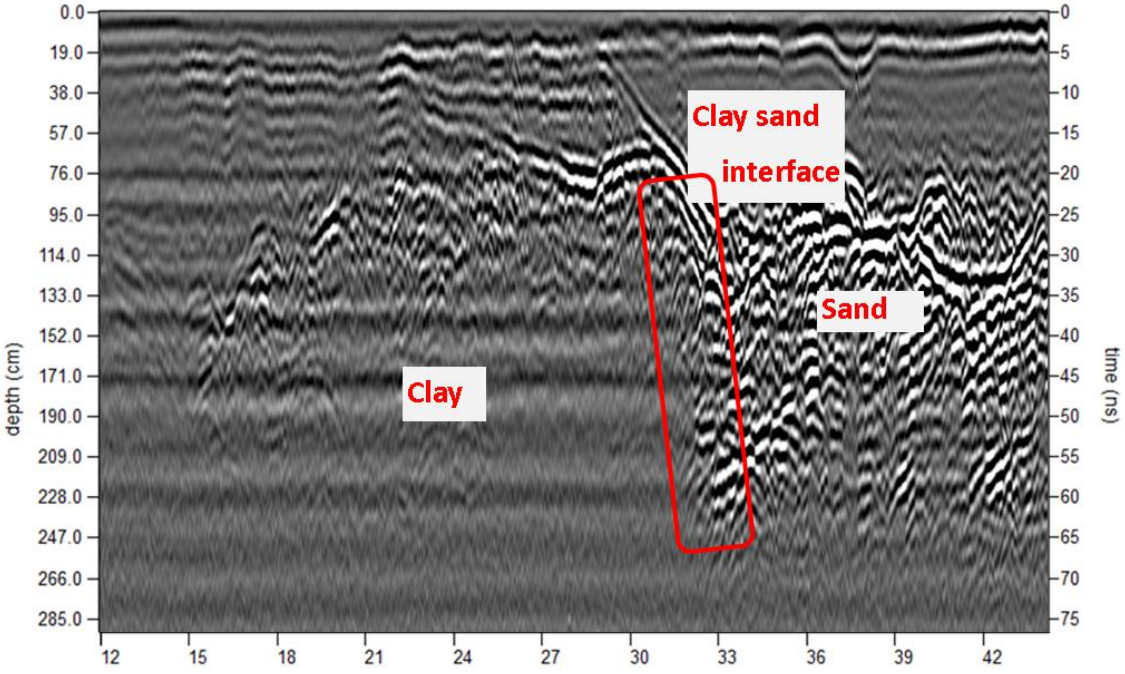

Figure 1.4.8: Radargram showing the effects that moisture plays in GPR. On the left is a clay deposit, to the right is a sand deposit. Soil moisture on the day this data was captured was high, and the clay/sand interface (highlighted) is quite prominant. This data was collected by the author on Norfolk Island, ground truthed by local workers.

An example of how soil moisture, and soil type, will affect the results of a GPR survey is seen in Figure 1.4.8. This radargram was recorded over a disused quarry. Some 70 years ago, this shallow quarry was backfilled with sand, and a golf course was created. There had been much rain at the time of this survey, and the ground held a high level of moisture. To the left is a clay deposit, and to the right is sand. The GRP pulse shows a high level of attenuation as it travels through the clay, and this is in contrast to the depth of penetration the radar achieves as it travels through the sand. The change in permittivity shows in the radargram as a sharp contrast in penetration depth. Further along the radargram, (Figure 1.4.9), a small, rising reflection is seen. This is the interface between the sand and gravel. These interfaces have recently been ground truthed.

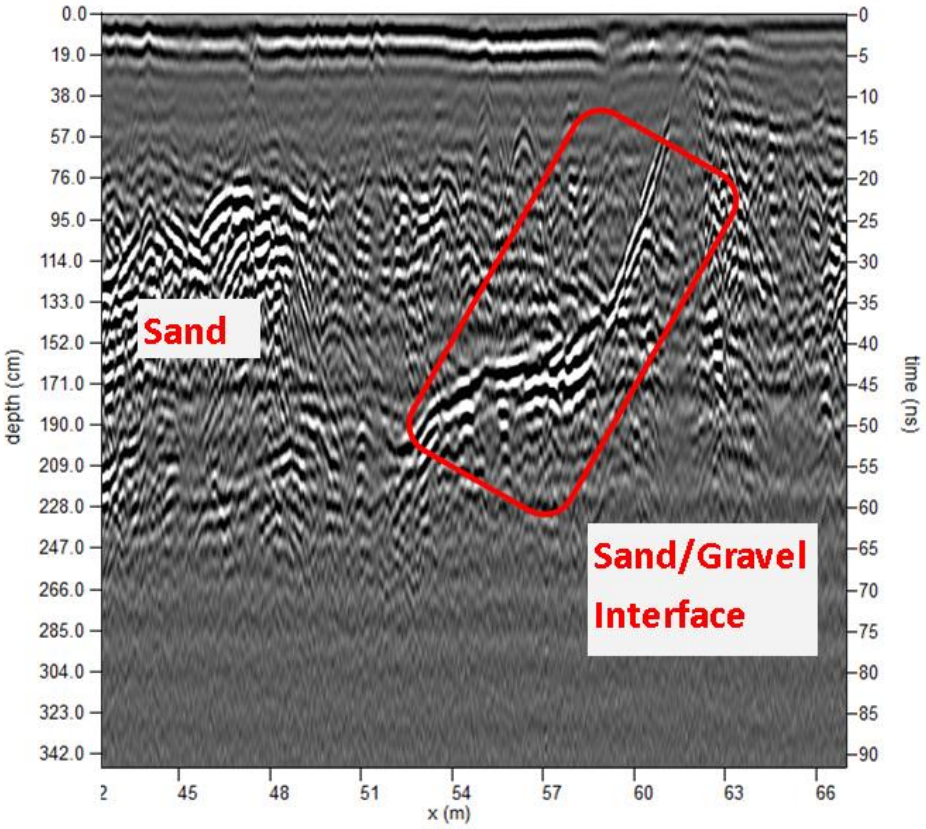

Figure 1.4.9: The same radargram a little further along. To the left is the sand deposit, with a sharp contrast highlighted that is a sand/gravel interface.

1.5 Earth Resistivity and Electrical Resistivity Tomography (ERT)

1.5.1 Theoretical Concepts

Injecting a DC current into the earth is another non-invasive, active, geophysical method, first developed in the early 20th century (Aizebeokhai 2010:3592). The method can be further defined into two categories, earth resistivity (ER) and electrical resistivity tomography (ERT). Methods using the earth resistivity techniques include the fixed probe method, and the operator moving a small set of probes manually after each reading is taken. As related technology has improved, portable computing, electronic controllers etc, the methods used in electrical resistivity has also improved (Aizebeokhai 2010:3592). The advent of multi-channel and multi-electrode systems has led to the rapid development of the ERT method. Electrical resistivity surveys have now become widely used in the fields of mineral prospecting, mining, engineering, hydrology, geotechnical, and archaeology (Aizebeokhai 2010:3592; Stummer et al. 2004:120). Being an active method, as is GPR, the interaction between characteristics of the subsurface matrix and the DC current will influence the passage of the DC current. Of these characteristics, it is again the presence/absence of subsurface moisture, and the passage of this moisture through the pore and

micropores in the subsurface that will influence the ability of the ERT to identify subsurface targets. This was shown by Cott (1997:6) who used earth resistivity in a longitudinal study over a Roman ditch. Earth resistivity can be measured using more than one method, all have in common electrodes being inserted into the ground, and a DC current activated. This section will introduce the concepts of ERT, subsurface electrical resistivity, and how these relate to the main research questions.

The purpose of an electrical resistivity survey is to determine the resistivity distribution of the subsurface matrix, by making measurements on the surface (Düztaş et al. 2017:7). This theory is based on the relationship between current, (*I* measured in amps), potential (*V* measured in Volts), and resistance (*R* measured in Ohms), as described by Ohm's Law, see Equation 1.5.1, (Martorana et al. 2023:2904; Pellicer 2010:51).

$$\boldsymbol{V = RI}$$ **Equation 1.5.1: Ohms law**

When conducting data collection, four electrodes are used, two current electrodes, (C_1 and C_2) and two electrodes to record the potential difference, (P_1 and P_2). These point electrodes are typically made of a conductive metal or alloy, in the case of this research they are magnesium electrodes. However, Angelis et al. (2018:210), describes the use of bentonite mud to attach electrodes to delicate surfaces. These electrodes are connected to a multi core cable, which is connected to a control box. The control box is connected to an external power source and is earthed, see Figure 1.5.1.

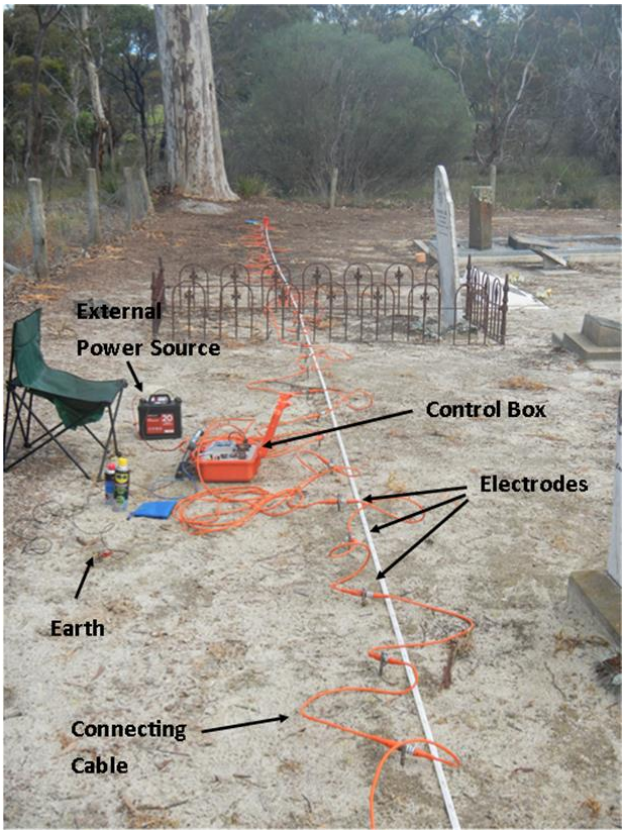

Figure 1.5.1: ERT components in operation.

The electrodes are equally spaced along a line, at a predefined spacing, with the resulting potential difference being measured between the pairs of current and potential electrodes (Aizebeokhai 2010:3594; Fotheringham 2013:11; Pellicer 2010:50; Samouëlian et al. 2005:3). The distance between electrodes is governed by factors such as desired resolution, the physical space at the survey site, the heterogeneity of the subsurface, and the depth of penetration required to map the target. Generally, the greater the distance between the electrodes, the greater the depth of penetration, with a corresponding loss of resolution (Aizebeokhai 2010:3595; Sarris et al. 2018:220).

If the subsurface matrix was a true homogenous environment, the electrical equipotential of the injected current will show a hemispherical pattern, see Figure 1.5.2, (Reynolds 2011:292; Samouëlian et al. 2005:3), and true resistivities would be returned. However, as mentioned many times in this thesis, the subsurface matrix is a complex environment. The DC current injected as part of an ERT survey will find its way between electrodes by following the path of least resistance. This then, is the apparent resistivity, and this represents a value that is an average resistivity over the total current path but are plotted at one depth point for each electrode pair. (Cardimona n.d.:1; Pellicer 2010:50; Witten 2006:306).

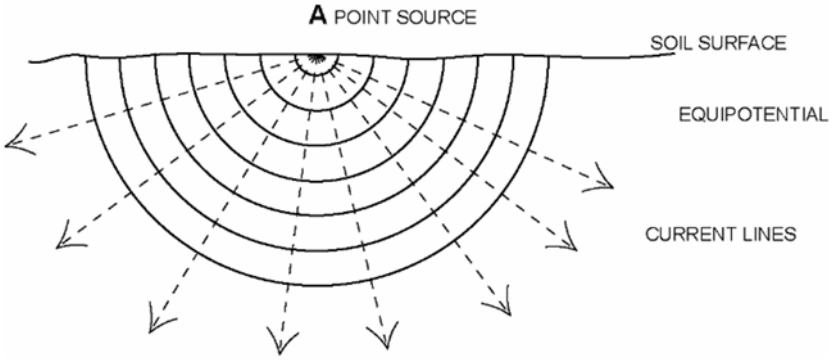

Figure 1.5.2: Theoretical current flow in a homogeneous half-space. Reproduced from Samouëlian et al. (2005:22) with permission from Elsevier.

The role and positioning of the injecting, (current), and measuring, (potential), electrodes is controlled by the use of various electrode configurations, or arrays. There are many array types traditionally used, these include the Wenner, Schlumberger, Dipole-Dipole, Pole-Dipole, Pole-Pole, and Gradient. Each array utilises different arrangements of electrodes, and provides different advantages and disadvantages (Aizebeokhai 2010:3595; Martorana et al. 2023:2905; Pellicer 2010:58; Sarris et al. 2018:220). It should also be noted that any apparent resistivity values recorded over the same structure can vary with differing array types (Aizebeokhai 2010:3595).

The often-used Wenner and Schlumberger arrays are sensitive to vertical resistivity variations, and less sensitive to horizontal variations. The Wenner array is preferred for surveys in noisy sites due to its high

signal strength, or good vertical resolution is required. The dipole-dipole array is the opposite, sensitive to horizontal variations and less sensitive to vertical variations in resistivity, see Figure 1.5.3. Thus, it is the preferred array for mapping vertical structures, such as cavities and dykes, or where good horizontal resolution is required (Aizebeokhai 2010:3596; Dahlin and Zhou 2004:397; Milsom and Erikson 2011:131; Pellicer 2010:58; Stummer et al. 2004:121). (Milsom and Erikson 2011:124) along with Sharma (1997:255) suggest that the Dipole-Dipole array most suited to Induced Polarisation, which is introduced below.

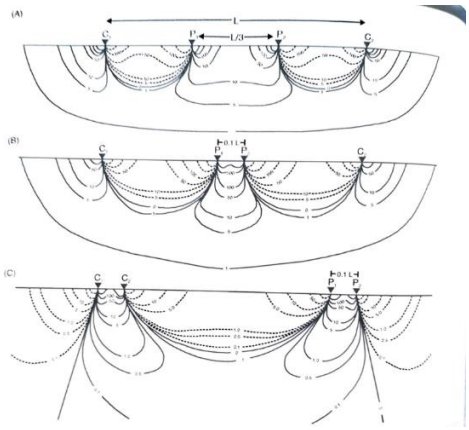

Figure 1.5.3: Indicative current paths for ERT arrays. (A) is a Wenner array, (B) is the Schlumberger array, and (C) is the Dipole-Dipole array. The contour lines are between the conducting electrodes (C_1 and C_2) and the potential electrodes (P_1 and P_2) and depict the current paths that are not refracted by bulk changes in resistivity. Image from Reynolds (2011:296) and used with permission from John Wiley & Sons.

Figure 1.5.4: Sensitivity distribution for Wenner (top), and Dipole-Dipole arrays (bottom). These distributions generated in res2mod modelling program.

Martorana et al. (2017a:35) note that the same arrays tend to be used, the decision based on ease of design and data acquiring software. Of interest is the common belief that the Wenner array is sensitive to vertical variations while the Dipole-Dipole array is more suited to horizontal variations. Is the subsurface disturbance in relation to a human burial a vertical or horizontal target? To understand this dichotomy further this research will use both the Wenner and the Dipole-Dipole arrays, and the results will be compared.

The sensitivity within the ERT context shows how different parts of the subsurface matrix contribute to the measured apparent resistivity. This contribution is weighted with the size of the sensitivity function, i.e., higher values of sensitivity show a higher influence on the measured value (Dahlin and Loke 2015:323; Pellicer 2010:58). Figure 1.5.4 shows the modelled sensitivity of the two arrays used in this research, the Wenner and Dipole – Dipole. Each model has four electrodes, and the areas of highest sensitivity (>128) can be seen to be on the surface, and adjacent to the electrode placements.

The Wenner array shows high sensitivity (>8) between the two potential electrodes, as well as outside of the conducting electrodes. Between the pairing of conducting and potential electrodes is an area of low negative sensitivity (<-2). The sensitivity model of the Dipole – Dipole array shows the highest sensitivity (>128) immediately adjacent the C_2 and P_1 electrodes, with the area between these two electrodes being an area of low negative sensitivity (<-2). These negative sensitivities can lead to counter intuitive effects, such as a highly resistive block in homogenous subsurface space with negative sensitivity would lead to a lower measured apparent resistivity (Dahlin and Loke 2015:323). When comparing the sensitivity models to the diagram of indicative current paths (Figure 1.5.2) it can be seen that the sensitivity contours do follow the indicative paths. The pattern of sensitivities are indicative of the strengths of each array, i.e., the 'flatter' shape of the low sensitivity (>2) of the Wenner is indicative of the sensitivity to vertical variations, as opposed to the more 'rounded' shape of Dipole – Dipole array, which has greater sensitivity to horizontal resistivity variations.

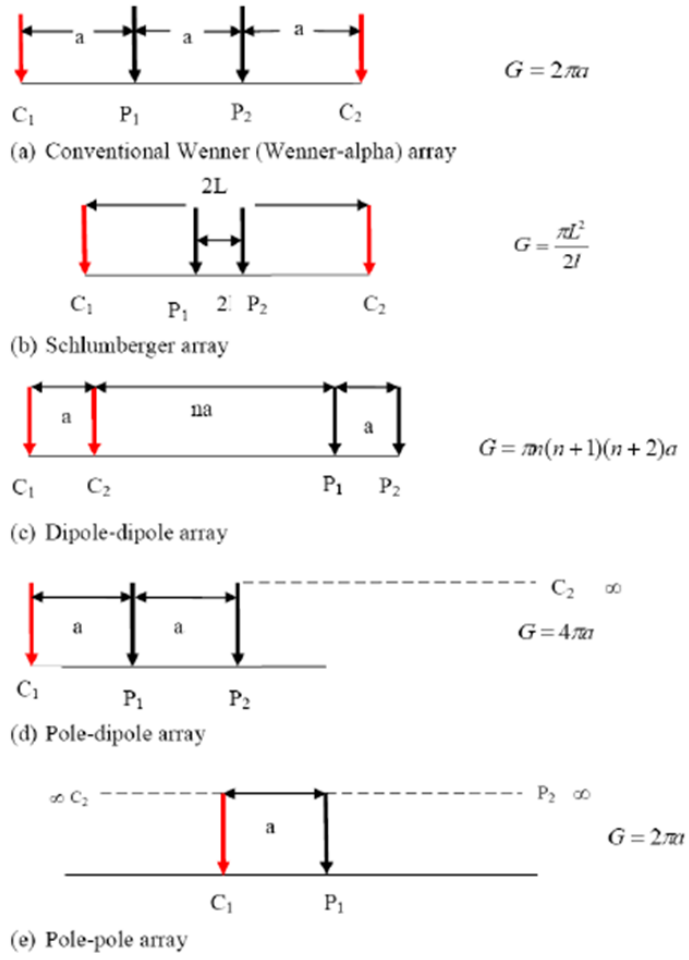

Figure 1.5.5: Typical ERT arrays. The distance, 'a', between electrodes is shown.

Figure 1.5.5 shows diagrammatically the common arrays in use. If we consider the Wenner array we can see the two current electrodes (C_1 and C_2), along with the two potential electrodes (P_1 and P_2). These four electrodes are equally spaced. For the first measurement, C_1 is electrode 1, P_1 is electrode 2, P_2 electrode 3, and C_2 is electrode 4. The first measurement point is the central point between electrode 2 and electrode 3. For the second measurement the configuration moves one electrode along the line, so C_1 becomes electrode 2, P_1 becomes electrode 3, P_2 becomes electrode 4, C_2 becomes electrode 5, and the measurement point is between electrodes 3 and 4. This is shown in Figure 1.5.6. This sequence is repeated until the final electrode grouping is used, in Figure 1.5.5 this would be electrodes 17 – 20, with the final data point being between electrodes 18 and 19. A schematic representation of this further sequence and location of data points can be seen in Figure 1.5.6.

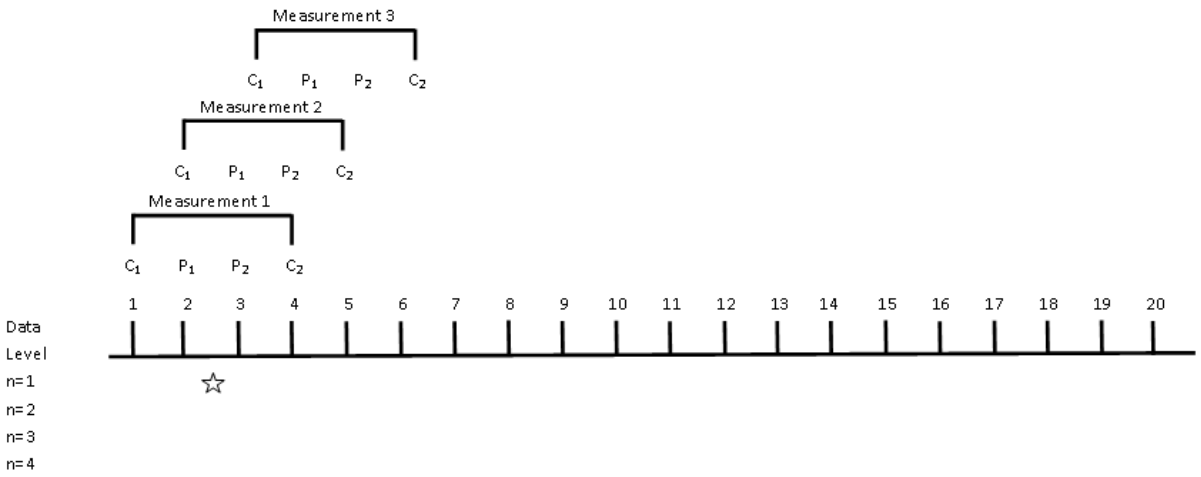

Figure 1.5.6: Schematic representation of the Wenner array. Measurement 1 uses electrodes 1-4, with the data point on level 1, between electrode 2 and 3. The electrodes then move one position along the line, with measurement 2 using electrodes 2-5, with the data point between electrodes 3 and 4.

The Dipole-Dipole array uses electrode pairing in a slightly different way. The two current electrodes (C_1 and C_2) stay adjacent, with the spacing between the current electrodes and potential electrodes (P_1 and P_2) increasing. For the first measurement C_1 is electrode 1, C_2 is electrode 2, P_1 is electrode 3 and P_2 is electrode 4. The first measurement point is the central point between electrode 2 and electrode 3. For the second measurement the configuration moves one electrode along the line, so C_1 becomes electrode 2, C_2 becomes electrode 3, P_1 becomes electrode 4 and P_2 becomes electrode 5, with the measurement point between electrodes 3 and 4. This pattern continues until the final electrode grouping is used, in Figure 1.5.7 this would be electrodes 17 – 20. For the next series, and level, of measurements the space between the C_1 and C_2 electrodes and P_1 and P_2 electrodes stays the same, but the space between C_2 and P_1 increases by one electrode. A schematic representation of these sequences and subsequent location of data points can be seen in Figure 1.5.7 This understanding of where the data point situated along the line of electrodes gives an opportunity to extract the resistivities in relation to the same burials as the hyperbolas found in the GPR results. This will give an opportunity to compare GPR velocity, resistivity and subsurface moisture levels.

Earth resistivity has been used to locate unmarked burials, and is regularly used in monitoring simulated burials, but the use of ERT is reported less in the literature. Doro et al. (2022:3) report that there is a scarcity of material in relation to mass graves. Dick et al. (2017) used GPR, magnetics, and earth resistivity to assess their effectiveness in locating known graves, concluding that the graves that were detected showed a low resistivity, and identified 39% - 58% of the graves, with soil types being the most influential variable.

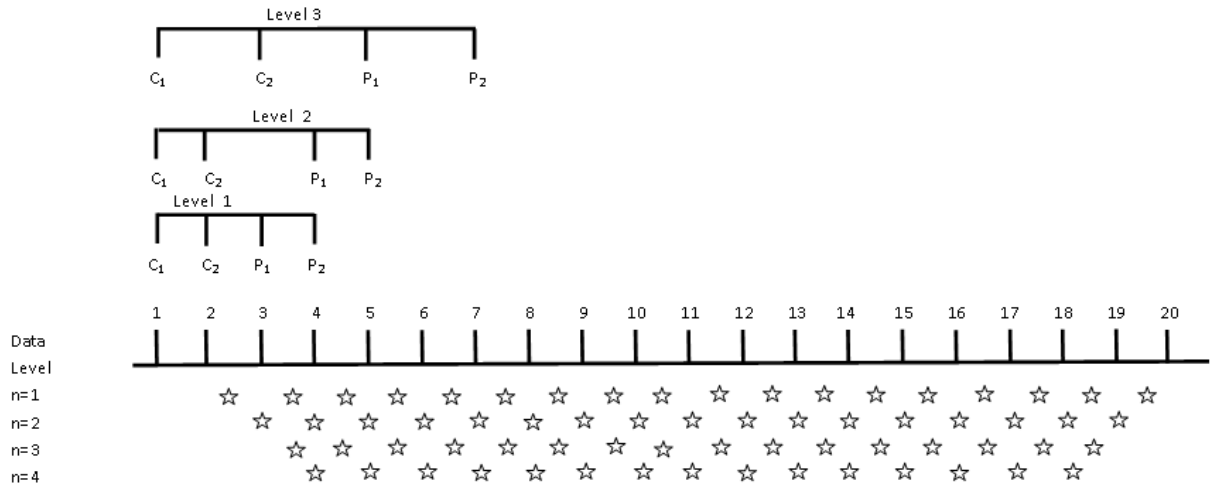

Figure 1.5.7: Schematic drawing of the Dipole-Dipole array. Measurement 1 used electrodes 1-4, with the data point at level 1, between electrode 2 and 3. The electrodes then move one position along the line, with measurement 2 using electrodes 2-5, with the data point between electrodes 3 and 4.

Hansen et al. (2014) used a similar premise in three cemeteries in Britian. The burials that are reported returned a high resistivity value. They did, however, caution that the effectiveness is in proportion to soil moisture, i.e., more effective in soils that contain higher moisture levels, and so very dependent on the soil type. Jervis et al. (2009) based the use of earth resistivity on the premise that the backfill in a burial will alter the resistivity due to increased pore space, and therefore increased moisture, this proved to be not the case. They used simulated burials of pigs to test this and concluded that the plume of decomposition fluids altered the conductivity of the soil surrounding the burial, and so was detectable using resistivity methods. Low resistivity values were recorded over burials of unwrapped pigs, with higher values over wrapped pigs. The wrapping was thought to contain the grave fluid and provide a high resistivity barrier. Pringle et al. (2009) used simulated burials of pigs to assess GPR and ERT over a twelve-month period. They concluded that the resistivity was lower in a grave that contained an unwrapped pig, and higher in a grave that contained a wrapped pig. Pringle et al. (2016) revisited the simulated burials of the previous study after a six-year period. They concluded that the unwrapped pig returned a low resistance value, due to the highly conductive decomposition fluid. The wrapped burial consistently returned a high resistance value. This study also reported that after a period of 5 years the grave fluid would have migrated away from the grave, making the burial harder to detect. Nero et al. (2016) used ERT to investigate a burial ground in Ghana. They report that possible graves that returned high resistivity values could have been burials that contained coffins, or a buried slab over the grave. Possible burials that returned a resistivity value close to the background value were thought to contain completely collapsed coffins. Possible burial sites that return high resistivity values were thought to contain higher moisture levels, either from grave fluid or subsurface

moisture. These burials were also surmised as being naked, i.e., not in a coffin. Doro et al. (2022) used ERT to delineate burial sites in simulated graves. This simulation included a mass grave containing human cadavers. They reported that high resistivities recorded were possibly due to a greater volume of air in the pores from the act of excavation and backfilling. The simulated burials that recorded a decrease in resistivity were thought to be from leachate. Buck (2003) tested GPR, magnetics, and resistivity in a forensics context in two cemeteries and a suspected murder site. Despite one site containing metal coffins, only one possible burial was detected. The researchers surmised that geophysics may be an effective forensic tool to narrow down potential search areas. Moffat (2023) used ERT to help in the forensic search to locate the burial site of children who went missing 52 years ago. He noted that the time taken to complete the survey would be an impediment in forensic searches, but the survey did reveal a large area of disturbed ground in the search area.

From the above review the characteristics of a human burial that may be detectable by earth resistivity or ERT methods are a lower resistivity due to decomposition fluids or a higher soil moisture level, a higher resistivity due to solid structures such as a vault or intact coffin, a wrapped body, or little or no grave fluids present.

1.5.2 Induced Polarisation (IP)

Induced polarisation is a technique that utilises the same equipment as ERT and measures the electrical chargeability of subsurface materials. Chargeability can be defined as the ability of a subsurface material to store and release charge when subject to an electric pulse (Wiberg and Jonsson 2017:16). Loke (2015:1) reports that ERT and IP are widely used together, as the ERT will provide general geological information about an area, and the IP will show the distribution of the mineral deposits. Dahlin et al. (2010:101) reports that the combination of IP and resistivity becomes a powerful tool in assessing landfills, as it is assumed that the leaching contaminates will change the resistivity.

In a typical ERT survey the current is applied across the four electrodes, and as it is abruptly stopped, the voltage across the electrodes does not drop to zero immediately, rather there is an immediate decrease which changes to a slow decay. This decay time can be in minutes or seconds. When the current is applied again over the next electrode pair, the potential increases suddenly, then gradually reaches the full value. This slow decay and increase within part of the signal is the Induced Polarisation (IP) (Düztaş et al. 2017:8; Reynolds 2011:376; Wiberg and Jonsson 2017:15). This is illustrated in Figure 1.5.8, in which the applied voltage (V) increases and decreases instantly as the current is switched on and off. The polarisation effect causes an overvoltage (Vp) that delays the response. The total measured voltage (Vo) is equal to the applied voltage and the overvoltage. The chargeability is measured by dividing the Vp with Vo (Wiberg and Jonsson 2017:17).

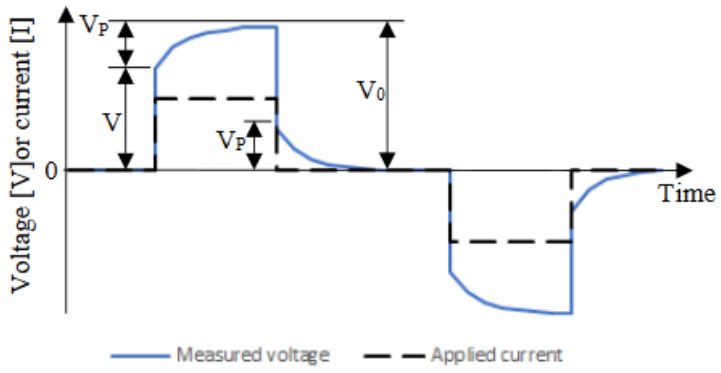

Figure 1.5.8: Diagrammatic representation of the subsurface injection of a pulse current. V indicates the applied voltage, Vo the total observed voltage, and Vp is the overvoltage created by polarisation effects in the subsurface matrix. Image from Wiberg and Jonsson (2017:17) and used with permission.

Apparent chargeability is measured in the beginning of an injected pulse, as the ground charges up during the delay time. This delay should be long enough to allow the ground to fully charge. The resistivity is measured during the remaining time of the pulse, termed the acquisition time. Traditionally during resistivity and IP measurements, the current is applied with an equal 50% on and 50% off timings. The resistivity is measured during the on-time and the IP is measured during the off-time.

It is physical and chemical characteristics of the subsurface that influences the Induced Polarisation. Within the IP survey geometry and environment of pore spaces is important in the IP response. Ionic concentration, grain size, the presence of clay, grain shape and pore throat diameter all affect the polarization of soil (Johansson et al. 2015:296; Milsom and Erikson 2011; Reynolds 2011:376; Slater 2007:178).

1.5.3 ERT, IP, and Soil

ERT utilises the flow of DC current through the subsurface profile, and the factors that influence this flow are the same as for the EM emanating from a GPR. Conductivity, resistivity, and permittivity, with all three variables being controlled by the physical and chemical characteristics within the subsurface matrix. These characteristics include the available soil moisture, the soil particle size and orientation, the connectivity of the micropores, and the electrolytic conduction of the subsurface moisture (Corwin and Lesch 2005:15; Pellicer 2010:51; Samouëlian et al. 2005:4; Stummer et al. 2004:120). As with the EM of a GPR passing through the subsurface, the DC current of the ERT survey will pass through the subsurface via three possible electrolytic pathways. These pathways being the liquid phase pathway formed with dissolved solids within the pore spaces, the solid/liquid pathway through exchangeable cations contained in clay minerals, and the solid pathway formed between soil grains that are in contact with one another (Corwin

and Lesch 2005:15; Samouëlian et al. 2005:4). The mineral grains within the subsurface are typically insulators, and conduction occurs via moisture laden pores or fissures. An exception to this is the minerals that comprise clay, which can be good conductors, due to the diffuse double layer formed on and between the particles (Fukue et al. 1999:43). Available moisture in the subsurface becomes an excellent conductor as it can contain ions from the subsurface (Neal 2004:269; Sharma 1997:208).

A high resistivity contrast between subsurface interfaces is required for targets to be detected by using the ERT method, and the greater the contrast, the easier the detection. The target also needs to be of a detectable size, shape and depth, and as the depth of the target increases its physical size and resistivity contrast need to increase to overcome the decrease in current density (Martorana et al. 2017b:2907; Witten 2006:314)

It is also the physical and chemical characteristics of the subsurface that influences the Induced Polarisation. Membrane polarisation occurs due to restrictions of ion movements in the pore fluid when electrical potential is applied. A grain surrounded by water will possess a negative surface charge which attracts positively charged ions in the pore fluid. When an external current is applied, ions will migrate towards the opposite charged pole. If no external current is applied ions will diffuse back into the pore fluid again. This migration explains why the measured potential does not drop to zero instantly when the current is switched off, or changes polarity (Wiberg and Jonsson 2017:16). In areas that contain clay in the subsurface matrix, the polarization effect is affected by ionic concentration, grain size, grain shape, and pore throat size (Johansson et al. 2015:296; Milsom and Erikson 2011; Reynolds 2011:376). Brandes (2005:2) reports that in areas of high clay percentage, (>15% content), the polarization effects decrease. This is due to the blocking of the pore pathways. In Section 1.8.10 the complexity of clay particles is discussed. The polarization within a subsurface containing clay particles is equally complex, as alluded to by Brandes. Chelidze and Gueguen (1999:12) suggest that the following are all possible in a subsurface matrix containing clay particles. In particles that display a thin surface, either a conductive film or a closed electrical double layer, polarization is strong at moderate partial saturations. If the subsurface contains conductive grains with a thin insulating envelope, a strong polarization is possible. This is due to thin dielectric shells having a large capacitance, this capacitance dies out at high frequency when the shells are shunted by displacement currents. If the particles contain open double layers at the solid-liquid interface, then at large saturations a free exchange of ions between the electrolyte and the EDL can produce out-of-phase currents. It is the behavior of soil particles that will be a key element in IP. In addition to these points, Slater (2007:178) postulates that from the IP response it should be possible to assess which of the above is more dominant in the subsurface, by the positive and negative IP response. If the IP survey returns a positive chargeability, then it is the pore volumes that are dominant, if the chargeability is negative, then the surface area is dominant.

1.5.4 Processing

The data collected is an apparent resistivity, a resistance value that is averaged along the line of equipotential injected current. The depth of this data point is dictated by the group of four electrodes used and is described in section 1.5.1. The data processing program will create model squares, see Figure 1.5.9, and uses the least squares inversion method to calculate a resistivity value that is as close as possible to the apparent resistivity. This closeness of fit is reported by a RMS value, and the results are displayed as a pseudosection (Martorana et al. 2017a:40; Samouëlian et al. 2005:63). This term pseudosection indicates that the data is not truly related to points within the vertical horizon, and added to the complexities of the subsurface, the pattern of apparent resistivities may not closely correspond to the subsurface targets (Edwards 1977:1020; Loke et al. 2013:149; Samouëlian et al. 2005:7).

The choice of arrays used to collect data can be dictated by the depth and shape of the subsurface target, i.e., Wenner for vertical variations, and Dipole-Dipole for horizontal variations. So too the processing can be varied depending on physical and chemical characteristics of the anticipated subsurface target. This refers to the shape, density, resistivity, etc. If the bulk resistivity interface between the target and surrounding subsurface matrix is strong, then Balkaya et al. (2021:104272), Cardarelli and De Donno (2019:44), and Dahlin et al. (2010:101) all suggest using an error-weighted chi-square fit, using a L1 norm to prevent a smooth transition in the model.

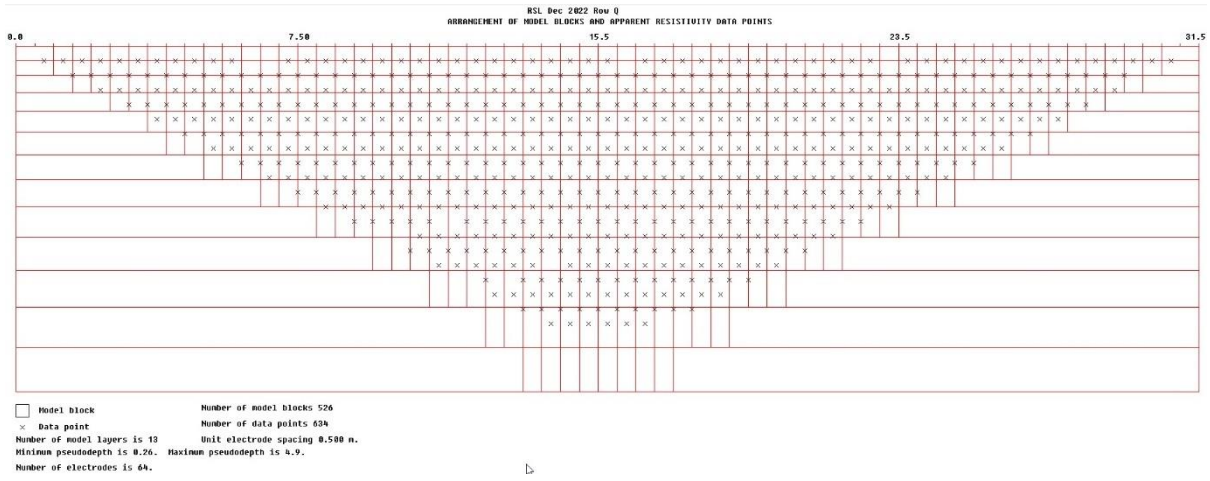

Figure 1.5.9: Inversion model blocks, as built by the Res2Dinv program.

Zhou et al. (2014:294) also describe the L1 and L2 norms by questioning the way the final tomogram needs to look, i.e., sharp versus smooth distributions. The L1 and L2 norms are inversion settings in Res2Dinv, the processing program used in this research. From Aarhus GeoSoftware (2022:75–76) the following are descriptions of these settings. The L1 constraint is considered the standard constraint and is recommended

for blocky inversions. The L1 inversion will attempt to minimise the square of differences between the measured and calculated apparent resistivities, while the L2 inversion setting will attempt to minimise the square of the changes in apparent resistivities. The L2 inversion setting will, in theory, produce a smoother transition between resistivity values, and is more suitable to a subsurface in which the resistivity values also change in a smooth manner. The issue of smoothness in the final tomogram is addressed by Loke et al. (2013:148), who states that the smoothing of resistivity data can sometimes block the true location of subsurface targets, and that using model cell sizes the electrode spacing provides an optimum compromise.

1.6 Simulation and modelling

1.6.1 Ground Penetrating Radar

The subsurface matrix is a complex environment, and in the context of GPR, many elements within this complex medium will influence the results of a GPR survey. A way to understand the interactions of the GPR pulse and the subsurface matrix is using a desktop simulator (Goodman and Piro 2013:11). Simulation programs can be GPRSIM© or gprMax (Goodman 1994; Zhang et al. 2023:115) with GPRSIM© termed a "Infinite slope method" and gprMax being a "finite-difference time-domain" method. Daniels (2007:37) also reports that other modelling methods use single frequency models, time domain models, ray tracing, discrete element methods, and method of moments. For this research GPRSIM© was used and is described here.

To successfully model the EM wave as it interacts with the subsurface matrix several items need to be defined. Obviously, the subsurface medium needs to be defined, in this case the shape, permittivity, conductivity, and magnetic permeability. These elements all relate to the ability of the subsurface to slow or allow passage of the electromagnetic pulse from the GPR. The antenna beam and pulse shape are required. The angles that the antenna radiates its pulses in is of great importance, as the refraction of the pulse is dependent on these initial angles. GPRSIM© assumes the use of a bow-tie antenna, which is common in archaeological applications. This type of antenna shows a pattern of main lobe, with side lobes approximately 60° from vertical, see Figure1.6.1.

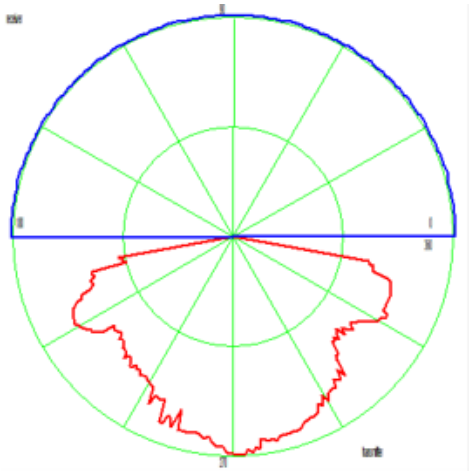

Figure 1.6.1:Diagrammatic representation of the antenna beam. The top semi-circle (in blue) is the receiving antenna, modelled for simplicity as 180°. The transmitting beam is below (in red), with the centre pulse and side-lobes shown. Image generated by GPRSIM.

The antenna pulse is modelled on a damped or Ricker wavelet. Current ground coupled antennas commonly used in archaeological surveys cannot achieve a sharp pulse of short duration (Conyers 2004:39), so a simple pulse is used. This is with the understanding that the true shape of any given antenna is not so simplified (Daniels 2007:197; Goodman and Piro 2013:26).

The reflection strength of GPR pulse from the subsurface model structures is related to the square root of the permittivity between materials. This gives an important clue as to the amount of energy reflected by electro-magnetic pulses off of subsurface interfaces, and if there is no significant change in permittivity, there is no reflection. As stated by Goodman and Piro (2013:16), the GPR is not a “gold” finder, rather a “contrast” finder.

Transmission and refraction both rely on the strength of contrast of subsurface materials. As transmission is the ability of the pulse to pass through subsurface materials, it is dependent on the conductivity, with no transmission through highly conductive materials. Refraction, on the other hand, is dependent on the permittivity, see Figure 1.6.2. Electro-magnetic pulses will change direction, refract, when passing through materials that cause changes in speed (Goodman and Piro 2013:16–18).

The electro-magnetic pulse travelling through the subsurface will either reflect, refract, or pass through materials, eventually attenuating. When modelling the EM pulse, the rate of attenuation is required, and this is largely dependent on the conductivity. The higher the conductivity, the faster the wave will dissipate, the energy lost as heat.

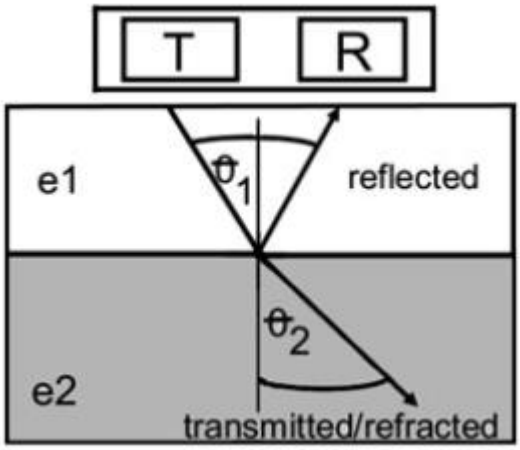

Figure 1.6.2: Diagrammatic representation of the reflection and transmission of a GPR wave. e1 and e2 are representations of materials where a contrast exists between them. Waves that are transmitted or refracted can be subject to attenuation (Data; Goodman and Piro 2013:17).

The final element that needs to be modelled is the raypaths. The GPR sends out pulses at regular intervals into the subsurface. Some of these pulses will reflect and return to the receiving antenna, with many more dissipating and never recorded. All of this is not known to the operator at the time of the GPR survey. Pulses can be refracted from the interface of two materials, then transmitted through another, then reflected by yet another material back to the antenna. All of this can be included into the model, with infinite number of possible pulse trajectories (Goodman and Piro 2013:29).

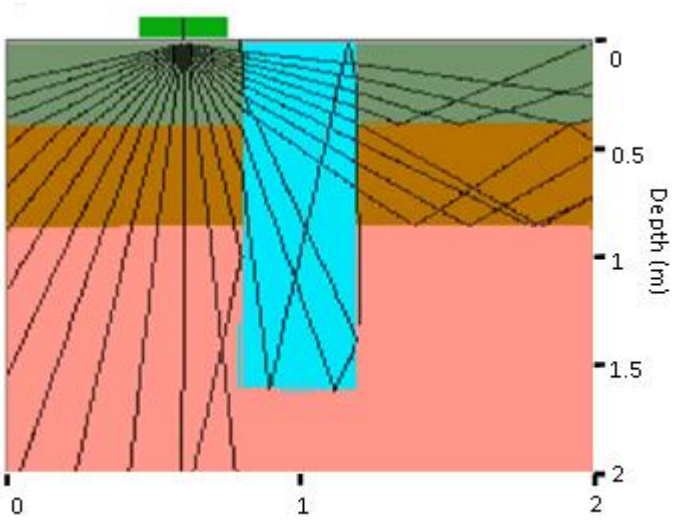

Figure 1.6.3: Simulation of a burial shaft. Three horizontal subsurface materials of differing permittivity can be seen, with the grave shaft (in teal) in the centre. The ray-paths are shown, and of note is the reflection of the pulses do not occur directly under the antenna. (Image generated by author in GPRSIM).

Examples of GPR modelling are scarce from the literature. Aziz et al. (2016:397) described using finite difference time domain modelling to simulate the responses over three different types of burials, in differing soil types and soil moisture contents. Giannopoulos (2005:760) give examples of GPR response over reinforcing bar in concrete, in both 2D and 3D. This was also with a finite difference time domain model. Zhang et al. (2023) also used the finite difference time domain method along with a random media to model the complex environment of road structures. Angelis et al. (2018:210) also used the finite difference time domain model to simulate wet areas and cracks in a wall of a Byzantine fortress. Millington et al. (2011) used the finite difference time domain model in conjunction with the Born approximation solution to model in 3D a forensic burial. Damiata et al. (2013:270) used the Infinite slope method of GPRSIM to simulate the different reflections of a burial pit versus skeletal remains. Pellicer (2010:136) used GPRSIM to model lithological, sedimentological and structural surfaces. Goodman (1994) and Goodman and Piro (2013) also present a number of examples of the infinite slope method used within GPRSIM.

1.6.2 Electrical Resistivity Tomography

The motivations to model the subsurface in an ERT context are the same as in a GPR context. The subsurface is a complex medium, and having an understanding of how the DC current will interact with this complexity will give insights into expected results. The simulation and modelling of the ERT process can be carried out in the Res2DMOD© program (Pellicer 2010:136), or by other mathematical means (Dahlin and Zhou 2004:52). In this research the models are created and run in Res2DMOD.

This program uses the finite-difference method to produce simplified models of a largely homogenous subsurface. This is achieved by dividing the synthetic surface into a number of blocks, with the potential resistance calculated at the nodes of this mesh (Loke 2016:3; Pellicer 2010:136). To successfully model the interactions between the DC current and the subsurface, characteristics of the subsurface needs to be included, along with parameters of the ERT array. The subsurface model contains the geometric shape of any theoretical stratigraphic layers, along with the resistivity of each of these layers. The type of array can be set, along with the number, and distance apart, of electrodes (Herring and Lewkowicz 2022:136).

Many examples of ERT modelling are found in the literature. Kilner et al. (2005:296) used synthetic modelling as a way of optimising survey configurations. The models used various stratigraphic layering of sand and clay, and by using differing thicknesses of these layers, the resolution required to check groundwater infiltration was established. Pellicer (2010:137) used Res2DMOD to model various stratigraphic layers. This layering ranged from simple low resistivity layer over a high resistivity layer, to a more complex model containing five types of sediments. Sedimentary layers were also modelled by Dahlin and Zhou (2004:52), who used synthetic models to assess the abilities of ten different array types to accurately detect the four different sedimentary scenario's. The method used for this analysis was not noted. Abdullah et al. (2018:3) created two different synthetic models to highlight the standard L and Corner array. The finite-element method within Matlab was used by Bièvre et al. (2018:103) to model the potential success of repairs to a dyke. The changes in subsurface moisture after rainfall events was simulated by Carey et al. (2017:40). They used a two-layer model, with resistivities dictated by field observations. The effects of negative IP values was examined by Dahlin and Loke (2015:324). They used Res2DMOD to construct a model with three horizontal layers, one of which is placed a block of much lower resistance. They found that negative chargeability can arise in shallow layers where the layers below have little or no chargeability. ERT data is typically, (but not always), gathered by laying out electrodes in a straight line. The effects of off-set electrodes was modelled by Robbins and Plattner (2018:67) who used the E4D software to test this effectiveness over a utility trench. Uhlemann et al. (2018:8) created a model to test 3D capabilities of Res3DMOD. The model comprised of a trapezoidal prism within a simple subsurface of a single resistivity. The modelling of graves was carried out by Doro et al. (2022:5), who used synthetic modelling of pigs and human burial. The model comprised of three layers, built to mimic the subsurface found around the burials, with additional resistivities of backfill and leachate both determined from the literature. The modelling of frozen/unfrozen interfaces in permafrost was shown by Herring and Lewkowicz (2022). The model used comprised of three layers, one mimicking a permafrost thaw layer, over two layers of frozen permafrost.

1.7 Geophysics Summary

Geophysical methods have become common across a wide range of disciplines such as engineering, archaeology, geology, forensic science, and asset detection. The non-invasive and non-destructive characteristics are vital to those that seek to 'see' the subsurface without disturbing it. One of the popular uses of geophysical methods is the location of unmarked graves, and that given the importance of this, there needs to be improvements in geophysical methodologies, as well as testing the limitations of different instruments in differing conditions (Dionne et al. 2010:20; Hansen et al. 2014:15). This research will add further original knowledge to the framework around these geophysical prospection surveys, be they within the forensic framework or the archaeological framework, and build on the work of Dionne et al. (2010:22; Hansen et al. (2014:15) and others who call for further research using more modern burials and differing geophysical methods.

Surveying the electrical resistivity of the earth has become common now in many different applications. Like other geophysical methods, such as GPR, it is non-invasive, which allows its use in forensic searches, as well as locating unmarked graves in cemeteries. From the literature, the success of this method does seem to be more dependent on the soil in the target area, but there is evidence that the burial and subsequent decomposition of a human body does alter the resistivity of the surrounding subsurface enough to be detectable. Using a method such as ERT in this research over known graves will give a good indication of the methods effectiveness.

Being able to model the interaction between the GPR pulse and DC current, and the complex subsurface matrix is of benefit. The use of forward modelling software for simulation allows the display of predicted results without any interference of the many possible subsurface elements. In both cases the simulation software gives the ability to compare results with changes in the crucial parameters of permittivity, conductivity, and resistivity of differing soils, along with being able to model the expected results of a human burial.

1.8 Soil

1.8.1 Overview

A ubiquitous part of the Archaeological record are human burials, and given that these are often underground, it should not be surprising that the soil is a focal point of this doctoral research. This section provides a literature review that will explore what soil is and reflect on the role of various factors in forming and influencing its properties. This will become a deep exploration of soil; however, this background is important as it sets the foundation for a central argument in this dissertation. Which is that soil is a complex, inhomogeneous medium whose properties play a significant role in highlighting the strengths and weaknesses of geophysical methods and technology. This exploration will examine how soil is categorised, how it has evolved and how this process shapes the interaction with geophysical methods. The types of soil are introduced, with the differences between them examined. The role that seasonally available moisture

plays in the ability of the subsurface to allow the passage of electromagnetic and DC currents is introduced, and the interactions between grains of soil and this available moisture are examined. This close examination of the subsurface medium is warranted as the literature contains several key assumptions which has directed this research.

1.8.2 Assumptions from the literature

There are many assumptions around a geophysical survey that can be found in the literature. Those that are relevant to soil and have guided this research are listed below.

> Salat and Junge (2010:2) "*…there is a suggestion of the existence of a threshold level for soil moisture with high clay content soils, above which an increase on soil moisture has a minimum impact on soil attenuation properties."*
>
> Jervis et al. (2009:272) "*…no previous study involving electrical resistivity or conductivity surveys over graves has been supported by direct measurement of porosity, moisture levels or fluid conductivity."*
>
> Tabbagh et al. (2000:395) "*Electrical permittivity …… depends on the liquid water content of the soil material….the application of GPR to soil sciences is an active domain of research."*
>
> Neal (2004:269–270) "*The most important conduction-based energy losses occur due to ionic charge transport in water and electro-chemical processes associated with cation exchange on clay minerals."*
>
> *"…the relationship between wave velocity and permittivity are violated with the introduction of high-conductivity substances, such as seawater and certain types of clay."*
>
> Fiedler et al. (2009:381) "*there have been very few studies that look at GPR and the soil properties of the area around the burial."*
>
> *"…clay and loam-enriched soil with a high water retention capacity, which are normally critical factors for a successful GPR survey…"*
>
> Conyers (2004:50–52) "*In a highly conductive medium, the electrical component of the propagating electromagnetic wave is rapidly conducted away, and when this happens, the wave as a whole dissipates."*
>
> *"Soil chemistry, especially the types and structures of different clay minerals also plays a role in radar energy transmission, but this mechanism is still poorly understood."*
>
> *"Other minerals in the ground, will create free ions, which allow for greater electrical conductivity. This includes carbonate minerals, or clay rich minerals."*
>
> Conyers (2004:101) "*Velocity is therefore influenced by water saturation differences as they are controlled by changes in the composition of sediment and soils."*

Arcone et al. (2008:2) "*Particle size of soil will affect permittivity…silt size and larger particles within a natural mineralogically complex soil and at a fixed volumetric water content should show little dispersion, attenuation rates of a few dB or less, and consistent value of permittivity."*

Ruffell (2005:2) "*Wet, clay-rich and wet, or salt impregnated ground still cause difficulty in obtaining images of the subsurface."*

Schultz et al. (2006:614) "*Mineral soils with high clay content can attenuate the EM wave propagation, thereby reducing the depth of penetration on the ground."*

The assumptions listed above tend to simplify the complex nature of the subsurface matrix. This complexity arises from the many diverse ways that soil is formed, giving rise to variations found from the micro to the landscape scale. This complexity and diversity are intriguing, and additionally, as the subsurface matrix is a constant variable across all study sites, it is a foundation for this research. The complexity and diversity are also reflected in the varied assumptions from the literature.

1.8.3 Soil

The word soil can refer to many different things, even when viewed through a geophysical lens. This is because the material that we term soil is a complex and varied medium containing a complex mix of salt and organic solutions, minerals, macroscopic and microscopic organisms, and organic matter (Dent et al. 2004:577). The complexity in the subsurface matrix is a product of the diverse environmental and soil-forming conditions that have occurred both in the past and present, (Hall et al. 2009). The word soil means different things to different people, with many views having anthropocentric tendencies rather than ecocentric ones. As discussed by Charman and Murphy (2000), a farmer sees the soil as a medium that facilitates the growth of a crop, while the builder or engineer often sees the soil as construction material or the basis of foundations. In both cases, an understanding of its current properties is needed to inform their next actions. However, deeper insights into the soil's history are generally not required in order to be able to achieve their desired outcome. In contrast, a geologist will explore the properties of the soil in a more natural and organic way. In a geophysical context, both the history and composition of the soil are important to understand, as it is these properties that will impact the geophysical survey.

In this thesis, soil refers to the weathered layers above the bedrock, and is described using the terms soil, or subsurface matrix.

1.8.4 Background of Australian Soil formation

The composition of the soil is very much the product of its history, and as in many facets of the soil, the relationship between bedrock lithology and soil type is complex. Whilst this section does explore these connections, more than a brief overview of this subject is beyond the boundaries of this research. Instead, the purpose of this section and overall research is to shape an understanding of the relationship between certain physical and chemical characteristics of the soil and the geophysical methods that have been used in this research.

Much of the geology of the Australian Continent is of Mesozoic age or younger, with areas of Australia's North-West dating from the Pre Cambrian (4.6 billion – 541 million years), to the younger Mesozoic (251-66 million years), in the east (Blewett 2012). This stable regolith (bedrock) geology has been the source of the soil across Australia, as, fundamentally, each small sample of soil has its origins in the weathering of bedrock. Bedrock can be defined as the material that has been altered from its original state and lying above unweathered bedrock, (Wald et al. 2013:614). This alteration of the unweathered bedrock is typically carried out by chemical or mechanical processes, such as oxidation of the iron bearing minerals, wedging due to ice crystal formation, or wedging due to plant root progression (St. Clair et al. 2015:534). Obviously, these processes require specific conditions to occur, for instance, the formation of ice requires suitable freeze-thaw conditions, or the action of plant roots require suitable conditions for plant growth. It must be pointed out here that this cycle of weathering of bedrock and the creation of soil is not unique to the Australian Continent, merely given in an Australian context.

The mineral makeup of bedrock will dictate the composition of the soil, i.e. the weathering of a granite will produce a soil with a high concentration of quartz, while the weathering of limestone will produce a soil with high levels of calcium carbonate. The minerality will also affect the pH values of the weathered material, with parent material such as granite generally producing more acidic sediments, while weathered material from limestone tending to be more alkaline. This weathering of bedrock is the starting point in soil formation, with the freshly eroded material becoming recently deposited river alluvium, hillslope colluvium that is unconsolidated, beach sand, or aeolian (windblown) deposits of dust or sand (Akinsunmade et al. 2019:1913; Blewett 2012:68; McKenzie et al. 2004; McNeill 1980:7; Queensland Government 2022). No matter what resolution this weathering process is viewed at, be it landscape or at a nano scale, the process is complex, takes time, and is spatially varied. Understanding the mechanisms that are involved with the formation of soils is important, this section will gradually dive deeper into this, with this knowledge influencing the discussions on soil that this research is based on.

1.8.5 The role of weathering in soil formation.

The breakdown, or weathering, of this regolith can be attributed to many individual processes. However, all processes can be classified into 1 of 3 general types – mechanical, chemical, or biological. These weathering processes act on the surface of primary materials in such a way as to grossly alter their physical and

chemical properties (McNeill 1980:6). These weathering processes are outlined in Table 1.8.1. and expanded below. Mechanical weathering involves the influence of a mechanical process in the disintegration of a rock without significant change in the mineralogical or chemical composition (Boggs 2016:3), with White (2006:83) nominating the mechanical weathering process as the starting point in all weathering. These mechanical or physical processes could include tree roots cracking the rock and allowing water to seep in. Under appropriate climatic conditions this water can freeze in low temperatures, expanding the crack. Rocks in water, such as a stream or ocean shoreline can be rubbed together by the movement of the water, and wind can blast small abrasive sand particles into rock. The stability of the Australian regolith has meant that many of the mechanical weathering processes seen in other continents is not as evident here, processes such as major tectonic movements, or large glacial activity. Understanding this process, and the parallels with the mechanical weathering of the bedrock gives greater insight into how the soil is formed. It must be noted that except in extremely hot, or extremely cold climates mechanical and chemical weathering act together, and it is difficult to separate their individual influences (Boggs 2016:3).

Chemical weathering is the changing of the rock structure due to chemical reaction. Rowell (1997:23) and White (2006:83) both describe how minerals are dissolved by water moving through the subsurface profile, with sodium chloride (NaCl) and gypsum being particularly susceptible to this weathering process. Water not only helps leech chemicals from the bedrock, but sustains plant life on the rocks, plants like the lichens produce chelates that chemically transform metallic elements from the decomposing rocks. Plant life also increases the amount of available CO_2 , increasing the solvent action of rainwater (White 2006:84).

Biological weathering can be defined as the disintegration of rocks as a result of the action of living organisms. The roots of plants can wedge rocks apart at a microscopic level, and as the root grows, so does the crack in the rock. Ants, termites, and larger burrowing vertebrates bring rocks to the surface, where the weathering process can happen rapidly (Akinsunmade et al. 2019:1913; Blewett 2012:68; Lech and Trewin 2013; McKenzie et al. 2004; McNeill 1980:7; Queensland Government 2022).

These weathering agents rarely act alone but can be seen as part of a more complex natural system, with spatial variations that may vary from microscopic to a more landscape scale and contribute to the subsurface matrix rarely being in a homogenous state (Hall 2015). These weathering events occur as small parts in a larger, more complex system, and so should be summarised together. As described above, with the weathering of the bedrock, these mechanical weathering processes rely on specific conditions to occur. The Australian Continent contains many diverse geological, climatic and environmental conditions. From the arid inland, where quartz laden sand is blown across rocky outcrops, and freezing nights and hot daytime temperatures, the humid and wet tropical north that facilitates lateritization, to the chemical

weathering that produces karst formations in limestone, the weathering of the Australian regolith can be diverse.

Table 1.8.1: Types of naturally occurring weathering processes.

Type of weathering	Process of weathering	Examples
Mechanical	Thermal expansion Abrasion and impact Pressure release Frost weathering Plant and animal activities	Water seeping into cracks and freezing. Rocks rubbing together in water. Wind blowing small particles over rock surface. Plant roots.
Chemical	Hydrolysis Carbonation Dissolution Oxidation	Acidic or alkaline water dissolving minerals in rock. Oxygen reacting with minerals in rock.
Biological	Plant roots Microbial activity Burrowing animals Human activities	Plant roots cracking rocks. Chemicals secreted by plants dissolving the rock. Animals scraping small holes into the rock. Human intervention

This diversity will facilitate the unique and complex weathering processes required. Once the bedrock has started to disintegrate, erosion can take place, moving the soil from its origin to form new sediments elsewhere. The weathering and erosion processes are constantly in action, with the severity waxing and waning over large temporal periods, and it is the minerals present within these parent materials that influence the weathering rate, as well as the composite components of soil (Charman and Murphy 2000:14; McKenzie et al. 2004:11). The weathering of bedrock and regolith is the origin of soil. The mineral material that this soil has come from, and the weathering processes it has been subject to will dictate the type and structure of this soil, and how this soil interacts with geophysical methods. From this understanding of the origin of soil how it is classified can be examined.

1.8.6 Classification of soils, an overview.

Just as there are many differing viewpoints in the understanding of soils, such as by farmers, engineers and geologists, there are differing ways of classifying the soil. Any number of samples of soil are inherently not the same, so their description should reflect these differences. Describing this pedology becomes important, for the details that aid the classification also impact the geophysical methods.

The composite components of soil can vary both horizontally and vertically, (McKenzie et al. 2004a:1), but it is the vertical plane or soil profile, that is of importance here, as it is initially important to geophysics. The vertical profile can be termed as a column of soil that extends downward from the surface, with the subsurface material being organized in layers, with the organization of these layers termed the soil horizon

(Charman and Murphy 2000:71). These layers are governed by the Law of Superposition – that is, in an undisturbed succession, one sequence of strata overlies another, then the upper sequence is the younger (Parker 2012:3). As this research progresses this will be shown to become important, as the sequence of strata did affect the geophysical methods in more than one study site. These layers, however, are subject to various soil-forming processes, or pedogenesis. Soil fauna, such as worms, termites etc. can mix layers, while the depletion and accumulation of clay, calcium carbonate or organic matter can create distinct layers, and clear horizons develop from the balance between these competing pedogenic activities. McKenzie et al. (2004:2) defines a horizon as a layer developed by soil-forming processes with morphological properties that differ from those layers above or below it.

Within Australia these horizons are classified according to the Australian Soil Classification System (Commonwealth Scientific and Industrial Research Organisation 2016). This classification system organizes the horizons into 'A', 'B', or 'C' horizons. The 'A' horizon is defined as the uppermost horizon, with the 'A1' horizon containing some humified organic matter, and often a darker colour. The 'A2' horizon is immediately below the 'A1' horizon and contains less organic matter or silicate clay than adjacent horizons. The 'B' horizon is classified as an "*illuvial, residual or other concentration of silicate clay, iron, aluminium, carbonate, gypsum, or manganese."* (Isbell 2021). Within this classification system there can be any number of horizons in the 'A' horizon, i.e. A1, A2, A3 etc., with the last horizon being a transition between the 'A' horizons and the 'B' horizons. Likewise, within the 'B' horizons, there can be any number, with the last 'B' horizon being the transition between the 'B' and 'C' horizons. The 'C' horizon is defined as partially weathered parent material (Charman and Murphy 2000:71).

The American system is similar in that there are several defined horizons. The uppermost is the 'O' horizon and is comprised of organic material or humus. The 'A' horizon contains mostly minerals derived from the parent material, mixed with organic material from the 'O' layer above. The 'E' layer is defined as the eluviated layer, this is derived from the leaching of clay, minerals and organic material from the 'A' layer. This leaching often leaves a concentration of sand and silt particles that are comprised mainly of quartz. The 'B' horizon is the subsoil and is rich in minerals that have leached down from the 'A' and 'E' layers above. The 'C' layer is defined as the parent material (Soil Science Society of America 2023). This scheme of classification of the soil horizons is similar to the Australian system, with the inclusion of the 'E' layer, see Figure 1.8.3.

The soil horizon classification system in use within the UK is, again, similar to the Australian system, with the following defined layers. The 'L' layer is organic litter above the soil profile. Below this is the 'O' layer, comprising the surface accumulation of organic matter overlying the mineral soil. The 'A' layer is the surface layer of mineral soil mixed with organic matter. The 'E' layer is the mineral layer underlying the 'O' or 'A' layer. This contains less organic material than the layers above. The 'B' layer is defined as subsoil

underlying the ‘O’, ‘A’, or ‘E’ layers that shows obvious alteration of the parent layers, with the ‘C’ layer below all of the above layers and shows very little evidence of alteration (weathering) but may contain and accumulation of soluble salts (GeoMon 2020).

The Australian soil horizon classification divides the vertical profile into horizons, generally with the youngest horizon at the surface, and the age increasing with depth. The structure of the soil changes through these horizons. Now that the vertical structure is described, the components of each horizon can be examined, and the interactions between these components expanded.

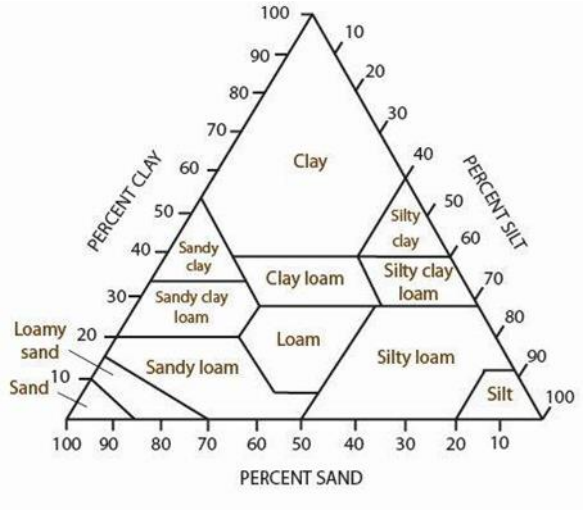

Figure 1.8.1: Soil texture classification according to proportion of sand, silt, or clay. Image reproduced with permission from Queensland Government (2021).

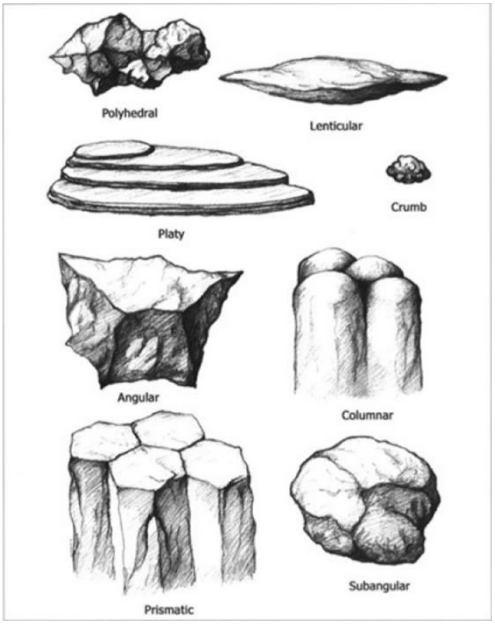

Figure 1.8.2: Common shape of peds. Image reproduced from McKenzie et al. (2004:8) with permission from CSIRO Publishing.

A

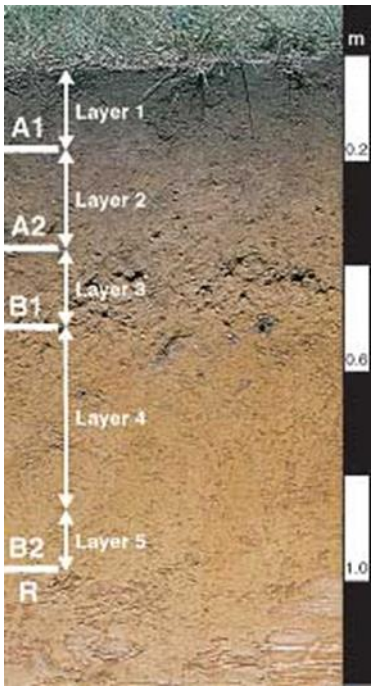

B

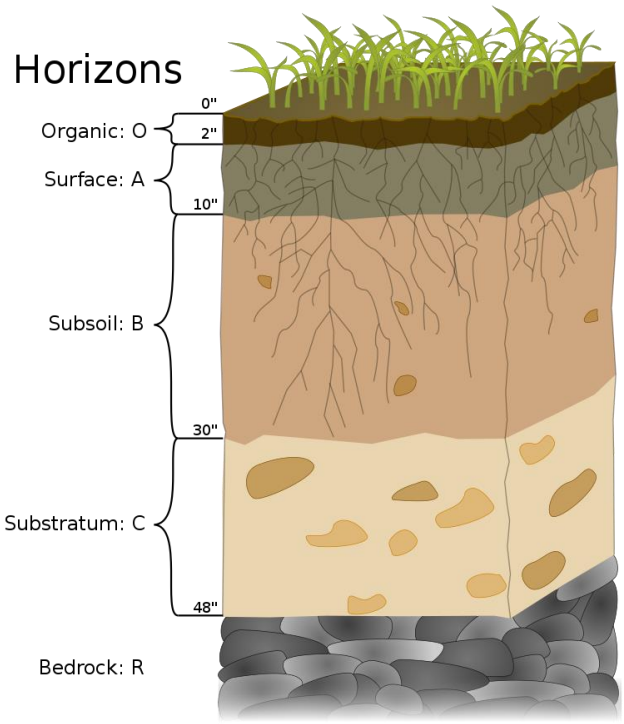

Figure 1.8.3: Pictorial example of soil horizons. Left (A) is the Australian system, and right (B) the American system. Image A reproduced from McKenzie et al. (2004a) with permission from CSIRO Publishing, and Image B reproduced with permission from Soil Science Society of America (2023).

1.8.7 Soil Texture, Soil Structure

The soil is classified in the first instance by the horizon it lies within, i.e. where the soil lies physically in a vertical profile. Further classification is used to describe the soil in closer detail, and it is here that the physical and chemical properties of the soil start to affect the geophysical methods.

Akinsunmade et al. (2019:1614) and White (2006:31) state that the texture of the soil changes slowly, over a large temporal period, and so is considered a permanent property. Physical attributes, such as texture, becomes the basis of the Australian soil classification system, which is based on field morphological data, that is, physical attributes that are easily identified in the field (Commonwealth Scientific and Industrial Research Organisation 2016). The physical properties used in soil classification are texture, structure and bulk density, colour, porosity, and consistency. These physical properties are all interrelated and exert influence on other qualities such as water saturation and compaction. It is these physical properties that also affect the passing of electromagnetic pulses through the subsurface profile, and so must be examined here.

Soil texture is closely related to particle size distribution, and is dependent on the proportion, by the percentage of the total, of sand, silt, and more importantly, clay within each sample. Table 1.8.2 provides a

summary of the broad field texture classes and percentages of clay in each texture classification. Soil texture and soil particle size are the foundation to understanding many soil behaviours, including the ability to retain water, the structure of the soil, the porosity of the soil, or the ease of a electro-magnetic pulse to pass, and it is the soil particle size that enables the grouping of soil samples into different soil types, see Figure 1.8.1, (Akinsunmade et al. 2019:1914; McKenzie et al. 2004a:6).

Table 1.8.2: Soil classifications based on clay content (McKenzie et al 2004:8).

Field Texture Group	Description	Approx. Clay Content
Sand	Nil to slight coherence	< 10%
Sandy Loam	Coherent but sandy to touch	10-20%
Loam	Coherent, spongy and smooth feel with no obvious sandiness	About 25%
Clay Loam	Coherent plastic bolus	30-35%
Light Clay	Plastic bolus. Smooth to touch	35-40%
Medium to Heavy Clay	Plastic bolus. Handles like plasticine.	> 40%

Soil structure, or more accurately the soil structural *form*, (Charman and Murphy 2000:174), is a quality that dictates how many physical, chemical and biological processes take place in anthropogenically altered and naturally occurring soils. These processes could be the transport of liquids through the subsurface profile, the penetration of roots, the decomposition of organic matter, or the proliferation of microbial life (Ghezzehei 2012:1). The inherent complexity that is the subsurface matrix displays a broad spectrum of spatial arrangement of primary soil particles. This broad spectrum ranges from the single grained structure, characterized by random arrangements of sand and silt particles that show little cohesion. Fresh deposits of loess or sand blown dunes are examples of the single grain structure. At the other extreme lie large cohesive massive structures of clay, electrostatically bonded. Between these two extremes soil particles form aggregated structures of infinite shape and size (Ghezzehei 2012:1). The structural form is also heavily influenced by soil particle size, with the structural form of soil being defined as the arrangement and organization of these particles and the resultant maze of pores between the particles. As these soil particles are heterogeneous in size and shape, soil structure is inherently complex and dynamic, with the bonding of these particles being equally diverse and complex. This complexity of pores becomes of great importance when we begin to describe, not only how water moves through the subsurface profile, but also the movement of electrical currents.

Despite this dynamic complexity, the soil particles within the structure are organized in a hierarchical fashion, where fine primary particles bond together to form the secondary particles, and these secondary particles then bond to form larger aggregates or peds (Charman and Murphy 2000:174; Ghezzehei 2012:1; McKenzie et al. 2004:7; White 2006:60). The peds, sometimes referred to as aggregates, are formed by the bonding of secondary particles that are subject to physical, chemical or biological influences. Examples of these influences include the chemical interaction of plant roots, (release of micronutrients and polymers),

anthropogenic compaction of the soil, swelling of the soil via osmotic effects of exchangeable irons, swelling of soil around the rhizosphere of plant roots, etc. (Charman and Murphy 2000:67; Ghezzehei 2012:5). These peds form distinctive shapes, see Figure 1.8.2, and, it can be seen, that as the shape of these peds are rarely uniform, (the inhomogeneous medium), there will be spaces between them. These spaces are the pore spaces, and while micropores can be caused from the irregularity of the peds, macropores can be caused by the activity of worms, plant roots, or soil shrinkage. The pore spaces give rise to the soil's porosity, or permeability, which is the measure of the ability of water to move through the soil profile (McKenzie et al. 2004a:7). This porosity can be generally classified by soil type, and McKenzie et al. (2004b:2) gives the following classification definitions, seen in Table 1.8.3.

Internal and external factors will influence the soil structure, these factors could be the available moisture, temperature fluctuations, subsurface biological activity, or anthropogenic interference, and given the dynamic and complex nature of soil structure, a universally accepted and quantifiable measure to describe soil structure has, to date, not been agreed to. To take a soil sample to inspect the structure requires digging or coring, further complicating the assessment and measure of soil structure (Charman and Murphy 2000:174; Ghezzehei 2012:1; McKenzie et al. 2004a:7).

Table 1.8.3: Water-soil characteristics of common soils (McKenzie et al. 2004b:3)

Soil Class	Dominant Characteristics	Soil Order
Deep sands	Rapid moisture infiltration Low moisture holding ability	Tenosols Podosols Rudosols Calcarosols
Coherent earth	Gradual or no horizon differentiation High surface infiltration Range from loamy sands to clay	Dermosols Kandosols Ferrosols Calcarosols Tenosols
Texture-contrast soils	Sharp increase in clay content between 'A' and 'B' horizon If the 'B' horizon is impermeable then there is a restricted capacity to absorb moisture	Kurosols Chromosols Sodosols
Cracking clays	Uniform, heavy textured profile Swelling and cracking common Very low permeability	Vertosol

Table 1.8.3 introduces a further soil classification term used within Australian soil classification systems, that is the soil order. These terms describe the highest order of classification, and a short description of each of these can be found in Figure 1.8.4.

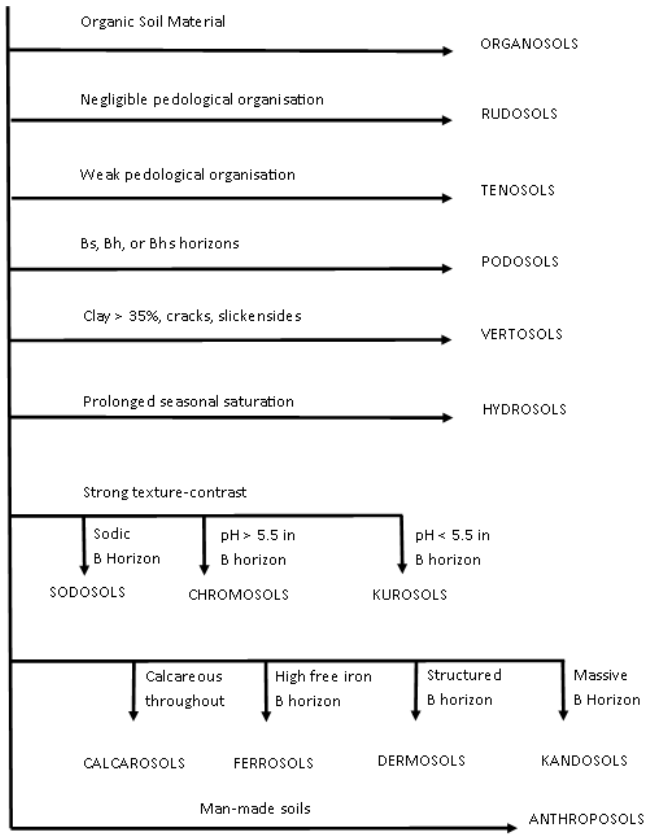

Figure 1.8.4: Schematic high level classification of soil orders found in the Australian Soil Classification system (Commonwealth Scientific and Industrial Research Organisation 2016).

The structure has been described as heterogeneous, dynamic and complex, and these qualities influence so many physical, chemical and biological processes. Interestingly these heterogeneous, dynamic and complex characteristics arise from the nature of weathering and mineralogy at the origins of the soil. This dynamic complexity ultimately will affect the geophysical methods so further investigations into the components of structure is needed.

1.8.8 Grain Size

The size and shape of these soil particles has great impact on the physical properties of the soil, i.e. the ability to hold water, the structural strength for building, or the ability of an electrical current to pass through (Rowell 1997:20). Grain size is also influenced by the minerality of the sample, and as we have seen above (Section 1.8.7), the grain size plays a part in determining, firstly the texture, and henceforth the bulk density, consistency, and porosity. Grain size is a fundamental attribute of soil, and thus an important descriptive property (Boggs 2016:1). Grain size is also the measure to determine what soil 'type' the sample is, and where it fits in the soil type triangle, see Figure 1.8.1. Within the Australian Soil Classification, the classification of soil type according to grain size is illustrated in Figure1.8.5, and White (2006:12) states that these grain size classifications are in agreement with the British Standards Institution, the United States

Department of Agriculture (USDA), and the International Union of Soil Sciences (IUSS). For this study the grains <2mm are of interest, the sands, silts and especially the clays.

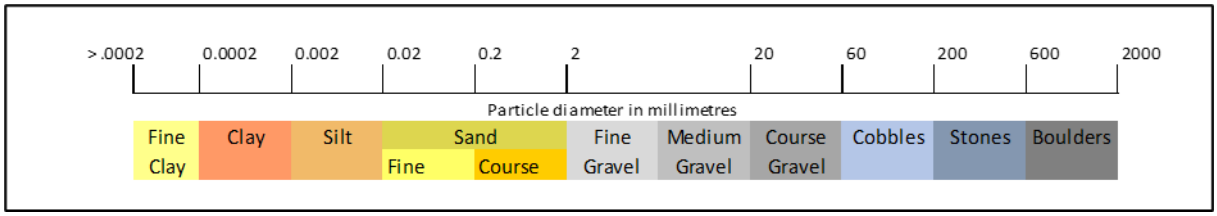

Figure 1.8.5: Australian Standard soil particle size classification. Image reproduced from McKenzie et al. (2004a:25) with permission from CSIRO Publishing.

Ghezzehei (2012:1) has described the arrangement of sand and silt particles as a single grain structure, arranged randomly with little cohesion. The grain size may vary, depending on how long they have been exposed to the weathering processes. These grains may be angular in shape, meaning that in the natural state, they may fit closely together (University of New South Wales 2007). Sand grains are often comprised of quartz, and being inert are considered noncohesive, meaning little chemical, electrical, or magnetic structure to help bond grains together.

Clay shows the smallest grain size and is of great importance within this research. The clay fraction of a soil sample is an important component of the subsurface matrix due to its electrostatic charge properties, and greatly increased surface area per unit mass (Goldberg et al. 2011:1; Qadir and Schubert 2002:279). The enhanced reactivity and large surface area of these particles is due to the rough surfaces of the individual particles, and a large number of surface controlled processes, i.e. precipitation, absorption reactions, nucleation and dissolution, involve colloidal particles (Goldberg et al. 2011:1). These colloids are characterized by an extremely complex and diverse polydispersivity, and are very dynamic, being subject to constant alteration that brings particles together (coagulation), or a disruption of aggregates (dispersion) (Goldberg et al. 2011:3). This ability to disperse becomes of critical importance when water is introduced into the soil profile.

From the mineral origins of soil, through the classification of the stratigraphic profile, determining the texture and type of a soil sample, the size of the grain has been a constant. It is this important physical characteristic that determines the interactions of many other physical influences, such as the passage of water and air through the soil profile. As the size is important, so then are the physical and chemical properties of the grain, and this is discussed below.

1.8.9 The Mineralogy of Soil

The mineralogy of the soil sample can also affect the bonding of the primary and secondary particles. Most sands in Australian soils are dominated by silicates or carbonates, with the silicate being derived from the mineral quartz, and limestone providing the carbonate. Silt shares a similar mineral profile but will contain smaller grain size and some component of clay, so primary and secondary minerals. Clay, being the most reactive inorganic component of soil, is composed mainly of secondary minerals, formed within the soil profile from primary minerals, and largely governs the behaviours and functions many soil properties (McKenzie et al. 2004a:11; Short 2006:7; Viscarra Rossel 2011:1). These clay components govern the behaviours via the control of movements of water (Viscarra Rossel 2011:9). Most of these secondary minerals found within clays show a crystalline surface structure, commonly arranged in two sheet structures, these being the octahedral or the tetrahedral sheet (Boggs 2016:107). Various combinations of these sheet structures give rise to many types of clay minerals, referred to broadly as layer silicate or phyllosilicates. The group that can be termed layer silicates comprise the clay types, Kaolin, Illite, Smectite and Vermiculite. The sheet structures within these layer silicates can be arranged in two different ways, these are termed 1:1 or 2:1 sheets. The 2:1 clays are defined as being structured with two tetrahedral sheets to one octahedral sheet (Canan 1999:5; Goldberg et al. 2011:152; Rowell 1997:25). The 2:1 structure differs from the 1:1 structure in that the bonding hydrogen atoms are no longer in place, and the sheets are held together by electrostatic forces. In certain clay types, such as smectite or vermiculite, this electrostatic bonding can be broken with the entry of water (Rowell 1997:25). The 1:1 clay structure refers to a type of layered clay mineral structure in which one tetrahedral sheet of silica (SiO_4) is sandwiched between two octahedral sheets of aluminum (AlO_6). This arrangement of silica and aluminum is called a 1:1 clay structure because there is a one-to-one ratio of silica to aluminum in each layer. The properties of 1:1 clay mineral is influenced by their crystal structure, as well as their chemical composition and the presence of impurities. They tend to be relatively unreactive and have low cation exchange capacities, making them useful for certain applications where stability is important, such as in ceramics production (Kumari and Mohan 2012:6).

A sample of sand contains particles that are relatively large, this allows a greater space between the grains, with these large particles forming random single grain structures as the grains possess little to form strong bonds. Clay particles, however, are much smaller, have been subject to many more eons of weathering, and as a consequence, carry an electrical charge, and it is this that first initiates the bonding. The small grain size and inhomogeneous shape of these grains restricts the spaces between, which in turn influences the passage of water and geophysical pulses through the subsurface matrix. How this bonding occurs, and the influences on water movement, is an important function of clay particles.

1.8.10 Cation Exchange in Clay

Sand, being a single grain structure made up of large grains, shows little bonding capability. Clay, conversely, consists of much smaller grains, and these grains carry a charge. This charge facilitates bonding,

and influences the passage of water, air, and geophysical electrical pulses. How does the charge on these small grains do this?

The clay particles are composed of stable secondary minerals, derived from primary minerals such as feldspar, mica, quartz etc. After eons of exposure to weathering the micro crystallite secondary particles positive charges are absorbed to the edges, these are cations. Cations are typically Calcium (Ca), Magnesium (Mg), Hydrogen (H), Potassium (K), or Sodium (Na) held loosely to the clay particle and can be exchanged for other cations, or more importantly in this research, go into solution with the introduction of water (McNeill 1980:5). Cation exchange, as well as conductivity pathways via moisture filled pores and passages, are possible due to the negative charge found on the face of these sheet structures, (Dept. Water, Land and Biodiversity Conservation 2002:32; McKenzie et al. 2004a:11), and while the face is negatively charged, the edges consist of broken tetrahedral and octahedral sheets, and the broken edges show a positive charge (Brandes 2005:7; Goldberg et al. 2011:20). While the clay particles are in aqueous suspension, the charge is neutralized by the hydrated ions of opposite charge. However, in sodic soils, the negatively charged surfaces of the clay particles are neutralized by the diffuse cloud of ions, in which the concentration of cations increase, and the concentration of anions decrease as the surface is approached. This balance is commonly called the 'Electrical Double Layer' (EDL) (Qadir and Schubert 2002:279). The EDL comprises of a cation rich zone, located next to the clay surface, this is relatively immobile and termed the 'Stern Layer'. Adjacent to this Stern Layer lies the Gouy diffuse mobile layer. This arrangement is diagrammatically shown in Figure 1.8.6, (Brandes 2005:4; Goldberg et al. 2011:16; White 2006:135). Cation exchange occurs between ions in the EDL and ions in solution, with the attraction and repulsion between clay particles being strongly influenced by the thickness of the EDL, although this is complicated by the non-homogenous shape and charge distribution of clay. These cations are electrostatically attracted to the negatively charged surface, and when the cation concentration is higher on the surface of particles, the cation will diffuse away into any available soil moisture, where there is a lower concentration (Brandes 2005:7; Qadir and Schubert 2002:279; White 2006:140). The pH value of the clay particle also influences the edge charge, with high pH, at times, even reversing the edge charge. Sumner (1993:688) expands this by stating that the inhomogeneous nature of the subsurface matrix causes soil particles to be in contact with a variety of surfaces, these can be either permanently or variably charged. The positively charged edge becomes less apparent under favorable chemistry and mineralogy conditions, resulting in a large EDL, which envelopes the edge region.

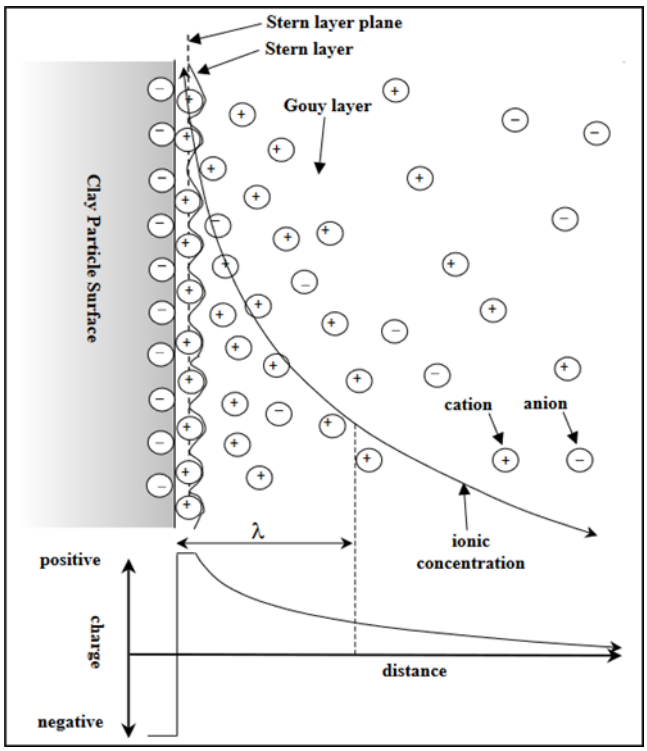

Figure 1.8.6: Diagrammatic representation of the Electrical Double Layer (EDL), surrounding the clay particles. Image reproduced from Brandes (2005:8)

Conversely, a small EDL will create higher edge-to-face charge differential, leading to positively charged clay particles becoming attached to negatively charged clay particle faces, (Brandes 2005:7; White 2006:140), with Sumner (1993:688) further clarifying that the opposite charge attraction requires dilute electrolyte conditions for the maximum attraction, and when the repulsive force in the double layer is less than the attractive force flocculation will occur. The presence of sodium, and the balance between sodium and calcium controls the attraction and repulsion forces, and this balance will determine sodic soil dispersing or flocculating (Brandes 2005:7; Sumner 1993:688; University of New South Wales 2007; White 2006:140). The opposite of flocculation is *dispersion*. Dispersion will occur when there is an abundance of sodium cations, these monovalent cations can only attach to one other particle and so individual platelets of clay are released from clay aggregates. When this occurs an inherently unstable structure is created, the microporosity is greatly reduced and the hydraulic conductivity is severely compromised, resulting in a subsurface matrix that is undesirable in the geophysical context (Nelson and Oades 1998:52; Qadir and Schubert 2002:280; University of New South Wales 2007).

Sumner (1993:717) nominates clay dispersion as a major mechanism that controls water movement in soil and Goldberg et al. (2011:168) states that the colloidal particles are stable as long as there is a balance between the attractive and repulsive forces acting on the particles. If repulsive forces predominate, then dispersion will occur. When attractive forces dominate, flocculation will occur. This statement very neatly encapsulates the most important characteristic of clay. How the attraction and repulsive forces are

generated, and how these forces are applied within the subsurface matrix is, naturally, as complex as the subsurface matrix is. One of the key influences, however, is moisture.

1.8.11 Water and Clay

The primary minerals have been weathered for eons and metamorphosed via weathering and erosion into secondary minerals. With a grain size < 2µm, correspondingly small spaces between them, (micropores), and a large surface area, these small grains of secondary mineral carry a charge. How water hydraulically moves through the soil horizon, and how this water interacts with the charged particles to affect changes in the attractive/repulsive forces is important.

Rainwater or irrigation water falls on the surface of the soil. A fraction runs off, with the remainder percolating down through the subsurface profile, under the force of gravity. As this water percolates downward, a small fraction is retained by the soil, with any remaining water eventually reaching the water table. This water in the soil Saarenketo (1998:74) divides into three categories: adsorption, or hygroscopic water; viscous or capillary water; and free water. Hygroscopic water is typically water molecules that are absorbed from the air. This molecular water will form as a layer around negatively charged mineral surfaces. Ions that do not hydrate occupy space and prevent hydrated ions from attracting water molecules with opposite charge. Moisture not bound in this way and does not respond to gravity is called capillary water. Capillary water is divided into two layers, inner and outer. The inner is in contact with the hygroscopic water, held by colloidal forces, and acts as a transition zone with the outer capillary water. The outer capillary water is controlled by colloidal force and surface tension. Water has the ability to form surface tension, so capillary menisci can form between particles and air in partially saturated soils. Free water is loosely attracted to soil solids, with an attractive force not as strong as gravity, so this free water will move through the soil profile (Saarenketo 1998:74).

When moisture is introduced to sodic soils the magnitude and direction of energy changes can set off slaking and swelling, spontaneous and mechanical dispersion and flocculation of dispersed clay particles (Qadir and Schubert 2002:279; Xiong et al. 2020:723). This process results in the reduction in size and total number of macropores at the surface, limiting rainfall infiltration. Generally, initial addition of moisture to sodic soils will lead to slaking and swelling, while continuous addition of moisture will increase the interparticle distance, with the clay particles moving into an independent state. This state is termed dispersion (Qadir and Schubert 2002:280; Rengasamy and Olsson 1991:941). This independent state will lead to degradation of the soil structure with the alteration of the geometry, or even creating blockages of the pores, negatively affecting the permeability of soil, further negatively influencing the infiltration rate and hydraulic conductivity (Qadir and Schubert 2002:283; Sumner 1993:696).

How the water moves through the complex maze of micropores requires deeper investigation in the context of this research. Under ordinary conditions water molecules are strongly attracted to soil particles, particularly clay particles. (Mitchell and Soga 2005:143–146). The clay particle is essentially hydrophilic, this encourages the water molecule to bond to the particle surface, or micropore space, via the hydrogen molecule, electrostatic forces, or the attractive forces between charged particles (Van der Waals force) (Li et al. 2016:136). As the clay particles bond together and form peds, neither the peds, nor the grains are uniform in size or shape, and so it follows that the spaces between, the pores, are not uniform either. Li et al. (2016:148) nominate three different types of pores that may be found in a sample of clay, these types are grouped according to size, (see Figure 1.8.7). Inter-particle spaces, or macropores are the largest and within these macropores water will form a bridge (a water bridge) between the particles. Intra-particle spaces, or micropores attract a film of water via capillary action, and Inter-layer spaces are more common in montmorillonite and attract water molecules to bond to the ends of sheets. Xiong et al. (2020:726) modelled this movement of water in micropores and found that water will be absorbed by the clay particle surface until saturation, and at that time the excess water will form a water bridge when two water films are close enough together to form an electrostatic bond. Both Li et al. (2016:148) and Xiong et al. (2020:731) state that the formations of these water bridges are heavily influenced by the pore width and the pore structure.

1.8.12 Sodic Soils

A small soil sample that has been weathered for many millions of years, would contain many grains < 2µm, the long period of exposure to weathering would have leeched and changed primary minerals to secondary minerals, and the grain would now carry a small electrical charge. This then is a sample that contains a large amount of clay particles, and if these clay particles contain a large percentage of unbound sodium, then they may be sodic clay particles. Rengasamy and Olsson (1991:936) note that some 28% of the Australian land area is affected by sodic soils.

Sodicity can negatively influence the structure of soil at the microstructure scale. Sodicity can also cause structural problems of inherent physical processes, problems such as slaking, swelling, or dispersion of the clay particles, with these issues often leading to interference of water and air movement, root penetration, plant available water holding capacity (Nelson and Oades 1998:52; Qadir and Schubert 2002:275), and of more concern to this research, the penetration and transmission of geophysical pulses.

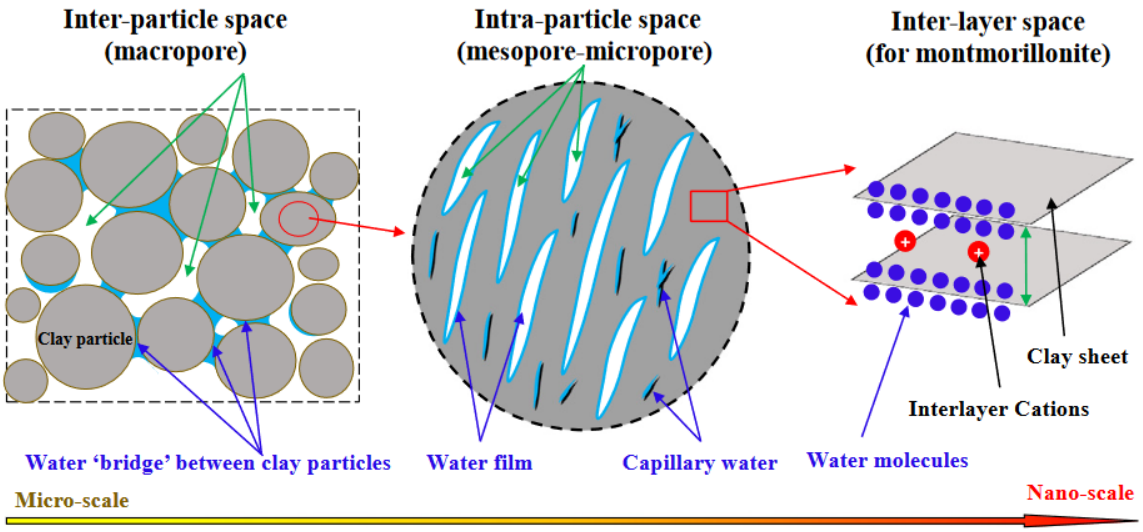

Figure 1.8.7: relationship between water and the three types of pores in clay. Image reproduced with permission from Li et al. (2016:148).

The level of sodicity in a soil is often described by the Exchangeable Sodium Percentage (ESP), or the Cation Exchange Capacity (CEC) (Mitchell and Soga 2005:167; Nelson and Oades 1998:52; Qadir and Schubert 2002:276). The CEC is a measure of the sum of exchangeable cations, these primarily being calcium (*Ca*), magnesium (*Mg*), potassium (*K*), hydrogen (H), and aluminium (*Al*). The University of New South Wales suggests that some correlation between weathering and CEC values exist. It is suggested that a high CEC value indicates a less weathered soil, as the primary minerals have not been leached out. From this they give a correlation between the CEC value and clay type, in Table 1.8.4. (University of New South Wales 2007).

Table 1.8.4: CEC values and clay possible clay types.

Clay	Gibbsite Goethite	Kaolinite	Illite Chlorite	Smectite	Vermiculite
Cmol+/kg	0-4	3-15	10-40	80-150	100-150

The ESP of a soil sample is determined by the sum of the possible exchange cations; calcium (*Ca*), magnesium (*Mg*), potassium (*K*) and aluminium (*Al*), see equation1.8.1. (Sumner 1993:685), however, argues that the typical characteristics displayed by sodic soils are at the upper limits of *Na* saturation, and that as *Na* saturation decreases, the need for total electrolyte concentration (TEC) increases to maintain the input of energy required.

$$ESP = 100(E_{Na}) / (E_{Ca} + E_{Mg} + E_{K} + E_{Na} + E_{Al})$$ **Equation 1.8.1: Exchangeable Sodium Percentage**

The numerical ESP value that defines sodicity in soil is variable. While Qadir and Schubert (2002:278) suggest that a value of 5 is suitable for Australian conditions, Rengasamy and Olsson (1991:935) suggest a value of 6, this being 6% of the total cation exchange capacity. Mitchell and Soga (2005:240) however, nominate a value of 2 as being the point of possible dispersion and a larger value range of 10-15 indicating probable dispersion. Both Qadir and Schubert (2002:278) and Rengasamy and Olsson (1991:935) justify their low values by claiming the complex and environmentally sensitive Australian soils generally contain a lower concentration of soluble minerals, especially Ca^{+}, necessary to maintain an electrolyte level during leeching, as well as Australian soils containing a high level of exchangeable Mg^{2+}. Despite the different opinions as to where sodicity sits in the ESP range, a high ESP usually indicates the presence of sodic soils, with other factors in the structure of the soil such as particle size distribution, electrical conductivity (EC), hydration, specific surface area, mineralogy, presence of cementing minerals such as oxyhydroxides of iron (Fe), silicone (Si), or aluminium (Al) (Nelson and Oades 1998:52).

Of greatest concern to geophysical surveys is the propensity of sodic soils to disperse. Dispersion is a process where individual platelets of clay are released from clay aggregates on the introduction of moisture (Mitchell and Soga 2005:239; Nelson and Oades 1998:52; Qadir and Schubert 2002:280). This release of clay particles reduces soil structural stability, and the now mobile particles can move within the subsurface matrix, resulting in pore blockage and reduced permeability (Fitzpatrick et al. 1994:1074; Nelson and Oades 1998:296; Sumner 1993:738). Of greatest note, is the dispersion of clay particles into solution. These freely moving particles have the ability to block pores, and blocked pores, with or without the presence of moisture, will attenuate electrical pulses and currents emanating from geophysical equipment.

The pH value of the water is critical to the dispersion tendency of sodic soils, with Rowell (1997:280) warning that the addition of rain water or low salinity irrigation water will exacerbate the dispersion of sodic particles. How water moves through soil that displays a tendency to disperse can become variable, as pore spaces may be blocked, Hall et al. (2009:88) states that the dispersive soils are only able to accept limited volumes of percolating water, due to the small size of pores, and the small percentage of pores that may be unblocked.

This becomes an important factor in geophysical surveys, as the introduction of moisture into the soil profile will physically and chemically change the characteristics of the subsurface matrix. Further, the subject of moisture is the soil is a thread that is common through the assumptions found in the literature and are guiding this research.

1.8.13 The Calcium Magnesium Ratio

The presence and concentration of these two cations within the subsurface can influence the chemical and mechanical properties of the soil. The concentrations of Calcium, (Ca), and Magnesium, (Mg), as

exchangeable cations is commonly termed the Ca:Mg ratio. The dominance of Calcium in the soil has been shown to promote aggregation and soil stability, whereas the dominance of Magnesium can facilitate dispersion. These effects are due to the difference in size at the molecular level, Mg has a smaller ionic radius, and therefore a larger hydration shell, (Dontsova and Norton 2002:184; Rengasamy et al. 1986:230; Zhang and Norton 2002:195). Studies have shown that the increased size of the hydration shell will cause an increase between particles, this is especially so in Mg saturated clay, (Dontsova and Norton 2002:184), and as the distance between particles increases, the force of attraction decreases. This results in a diminished Stern layer, directly affecting the stability of the colloidal system (Dontsova and Norton 2002:184; Rengasamy et al. 1986:229). Diminished attractive forces, and increased distance between particles results in a tendency for particles within a Mg dominant soil to disperse, Rengasamy et al. (1986:230) states that Mg dominant soils are more dispersive in low electrolyte conditions, whereas Zhang and Norton (2002:195) state that the effect of Mg was greater in non-calcareous soils. This tendency to disperse has a negative effect on the hydraulic conductivity of the soil, as the dispersed particles block the pore spaces. Pore spaces can be cleared with the introduction of moisture, with studies by Rengasamy et al. (1986:233) finding that in Mg dominant soils a greater amount of moisture is required to flocculate soils and help clear these pore spaces.

1.8.14 Permittivity

Two important factors of the subsurface matrix will affect the passage of a radar pulse and DC electric current. These factors are permittivity and conductivity. While a discussion of these two important properties of the subsurface should involve an element about electromagnetic and electrical currents, some will also involve the physical and chemical properties of the soil, and so this topic will be split over twosections. From the information preceding this section, it is clear that grain size and mineralogy, along with water content of the subsurface are foremost in discussions regarding geophysical methods. As Reynolds (2011:548) states, the subsurface matrix is a complex mixture of components, both geological and anthropogenic, and each of these components are likely to have a distinctive permittivity and conductivity. Despite these complex differences the topic of permittivity relies very much on water, and the interaction of water with grains within the subsurface matrix, and the electromagnetic (EM) and electrical currents used in geophysical surveys.

Witten (2006:235) defines permittivity, (also known as dielectric constant), as the measure of the energy taken for a radio wave to propagate through a material. This propagation takes the form of store and release of the EM energy, alternatively permittivity can be describes as the subsurface ability to restrict flow of free charge, or restrict the degree of polarization (Cassidy 2009:45; Knight 2001a:232). The term dielectric describes a class of subsurface materials that contain bonded electrical charges, (i.e. clay). These

charges allow the EM field to flow through the material, with loss of energy along the way. These losses are typically expressed as heat (Cassidy 2009:45). This ability to store and release EM energy varies dramatically, especially in the presence of bound or free water, and is a complex, frequency dependent quality with real and imaginary loss components. Canan (1999:28); Johnson and Poeter (2005:1); Knight (2001a:232); Neal (2004:268); and Salat and Junge (2010:1) all nominate permittivity as a key physical property of the subsurface matrix that determines radar pulse velocity, attenuation, and reflection coefficients, these three qualities all relate to the speed of the EM wave.

This relationship between the permittivity of a material and the EM wave is shown to be relative to a reference material, (usually a vacuum or air), with the wave speed being inversely proportional to the permittivity value, this is given by equation1.8.2, where the wave speed (*c*) is equal to the wave speed in air (c_{air}) divided by the square root of the material's permittivity ($\sqrt{e}$)

$$\boldsymbol{c = \frac{c_{air}}{\sqrt{e}}} \qquad \textbf{Equation 1.8.2}$$

This store and release concept is critical in understanding the complexities of permittivity. As described in section 1.8.10 clay particles show a negative charge of their faces, with a balancing positive charge on their edges. Canan (1999:2) suggests that the introduction of colloidal particles in the subsurface matrix will greatly alter the permittivity due to these electrical charges.

The EM wave moves via these negative and positive charges, with these charges becoming physically displaced in the process, this is termed polarization and has been introduced in section 1.5.2. This storage – release action by the electrons supplies energy to the propagated EM energy via displacement current, and by doing this gets slightly out of phase with the EM pulse, see Figure 1.8.8. This out of phase movement slows down the propagating EM wave, and this is the link between permittivity and velocity of the EM wave (Cassidy 2009:46–47). Water plays a critical role in the propagation of an EM wave or DC current. (Arcone et al. 2008:2) and Boggs (2016:54) states that the particle size will affect the permittivity as decreasing particle size increases specific surface area, which in turn, will convert free water to absorbed water. Within any sample of soil, water can be either free or bonded. Within soil a proportion of intergranular water will be bonded to the surface of the grains as a microscopic layer of absorbed water with restricted molecular rotation available. This well-known phenomenon is due to the inertia of bonded molecules and will produce a permittivity that is highly sensitive to low level water content variations. These variations have been observed in soils, clay and rocks (Cassidy 2009:51). These variations will depend on the degree of soil saturation, the percentage of clay and rock particles, the amount of compaction (high compaction will reduce pore space), the percentage of pore space, as well as the available ionic conductivity. In low

saturation levels, highly variable permittivity values can be seen from differing types of subsurface mixtures, and this is particularly true if phyllosilicate clay minerals are present (Cassidy 2009:51).

Annan (2002:263), however, suggests that while the electrical properties, in general, are understood, within more specific instances, the complexities and interactions are still subjects for research, and Table 1.8.5 shows a mix of common materials that may be found during an archaeological prospection survey, along with the typical permittivity and wave velocity values.

Table 1.8.5: Dielectric permittivity values for common materials (Reynolds 2011:551)

Material	Permittivity	Velocity (mm/ns)
Air	1	300
Water (fresh)	81-88	33
Water (sea)	81	33
Snow	1.4-3	164-252
Ice	2.5-8	78-157
Coastal sand (dry)	5-10	95-134
Sand (dry)	3-6	120-170
Sand (wet)	25-30	55-60
Silt (wet)	10	95
Clay (wet)	8-15	86-110
Clay (dry)	3	173
Agricultural land	15	77
“Average” soil	16	75

Canan (1999:2) and Knight (2001:240) both also point out that these figures are generally determined in laboratory conditions, and it must be remembered that these laboratory conditions are clean and homogenous materials are used in testing. Conditions such as this would rarely be encountered in the field, as the subsurface matrix is largely unknown at the time of the geophysical survey.

Permittivity is strongly dependent on water content (Salat and Junge 2010:1). This is the most important concept of permittivity that needs to be understood. The permittivity of soil samples is dependent on the complex mix of materials, each with its own permittivity, but it is the free or bonded water within these soil particles that affect the propagation of EM waves with greatest effect. Along with permittivity, the conductivity of the soil will affect any wave or pulse generated by geophysical methods, and it is this that is explored in the next section.

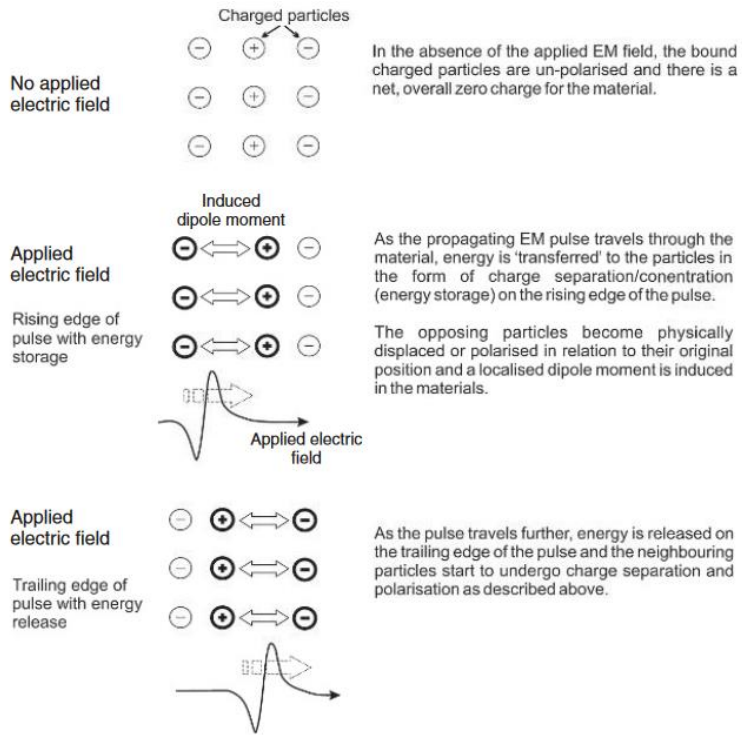

Figure 1.8.8: Conceptual representation of the process of storage/release, charge polarisation and the development of the dipole moment occurring when an electromagnetic wave is propagated through a material. Reproduced with permission from Cassidy (2009:47).

1.8.15 Conductivity

As discussed in section 1.8.14 above, permittivity will slow an EM wave down. In conjunction with permittivity, conductivity is an important factor of the subsurface matrix that will affect the pulses and waves generated by geophysical methods. As with permittivity, conductivity also straddles the discussion of the soil, along with the discussion on the actual geophysical methods.

The subsurface matrix is a complex medium, comprising many different natural geological and anthropogenic elements. Of these natural geological elements, soil and rock are very good insulators, showing a high resistivity. Neal (2004:269) describes conductivity as the measure of the ability to transport charge on application of a static electric field. The ability of the subsurface matrix to transport a charge will depend on several key factors. The porosity of the subsurface, which includes the size and shape of the pores, plus the number and size of interconnecting passages. The length of the interconnecting passages through the pore spaces is inversely proportional to the conductance of the path, with the cross-sectional area being proportional. The extent of water penetration into these pore spaces, with the concentration of electrolytes of the available water being important, as conductivity is an electrolytic process. The colloidal percentage of the surrounding subsurface will also be a factor (McNeill 1980:4). The colloidal content of the subsurface is of great importance, as Neal (2004:269) states that the ionic charge transport in water and the electro-chemical processes found in clay mineral cation exchange is where the most conduction-based

losses occur. In soils where available pore water is relatively pure, the contribution to conductivity is higher from the presence of the clay content, conversely in areas with saline pore water, it is the water that exerts the most influence, to the point of any possible conductivity being independent of clay content. Soils with a higher CEC will generally more conductive (McNeill 1980:4; Neal 2004:269).

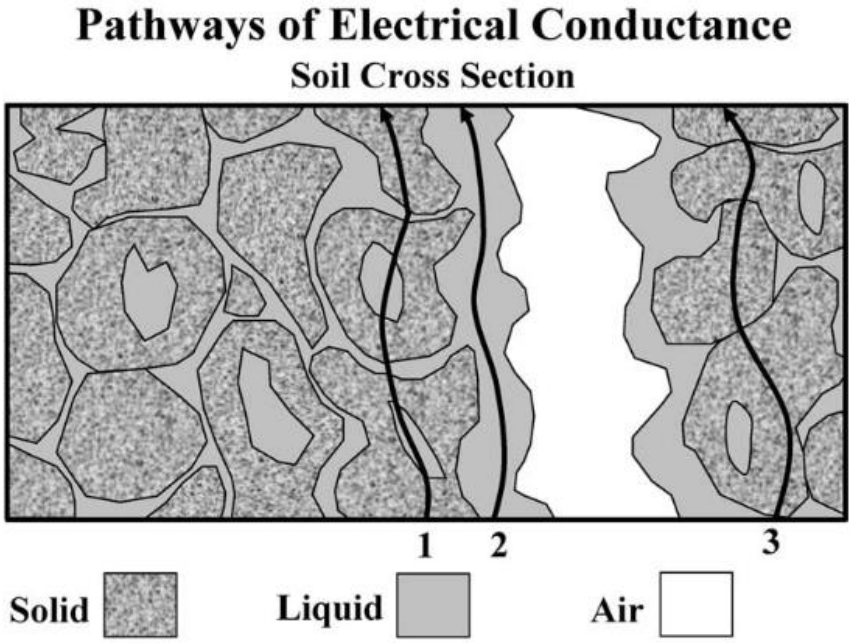

Figure 1.8.9: Diagrammatic representation of the three conductance pathways proposed by Corwin and Lesch (2005:15). Image used with permission.

Corwin and Lesch (2005:15) have proposed that there are three possible conductance pathways through the subsurface. These pathways are described as being via soil particles that are in direct and continuous contact with each other (3 in Figure 1.7.9); via dissolved solids that lay in soil water occupying large pores (1 in Figure 1.8.9); and finally, a solid liquid pathway via exchangeable cations associated with clay minerals. It can be seen from the description of these possible pathways that the conductance of soil is influenced by the amount of available ions that are from either clay minerals or water salinity, the amount of available water, and the bulk density of the soil (Corwin and Lesch 2005:15; Friedman 2005:48). Of these influences, the moisture profile is most complex. The moisture profile includes the porosity of the soil, the volume of water in these pore spaces, and the complexity of the interconnecting passage, which all vary with depth (Conyers 2004:50; McNeill 1980:19). Unfortunately measuring the conductivity is an equally complex process, with most being conducted in the laboratory, using relatively homogenous materials. This does not accurately reflect the spatial variability that is often experienced in the field (Friedman 2005:47). It is also very difficult to reconstruct soil moisture in laboratory samples.

Permittivity and conductance together are of great concern for geophysical surveys, first by permittivity's tendency to slow the EM waves down, with a lack of conductivity halting the pulse or current. By slowing the EM waves down, depth of penetration is compromised, attenuation also occurs at a shallower depth. A lack of conductivity will affect the EM waves in a similar fashion, shallow penetration and high rate of attenuation. Both of these natural phenomenon's are very sensitive to the quality and presence/absence of water content, along with the varied charges associated with clay particles in the subsurface matrix.

1.8.16 Soil Summary

This review has shown that soil is an extremely complex medium comprising an array of geological and anthropogenic materials. One of these complexities is the presence of clay particles, how they interact with each other, and how moisture changes these interactions. There are forces present in the subsurface matrix, firstly gravitational force to percolate water down through the soil profile, then electrostatic forces are needed to bond particles together, to bond water to clay particles, and to break those bonds. Gravity enabling the hydraulic movement of water is constant. The electrostatic forces that are within the soil particles are naturally held in equilibrium. This means that the force required for effective use of geophysics must be greater than the force holding water onto particle faces, or the force that had dispersed the clay particles, or the force that blocked micropores with this dispersed clay particles. This requirement becomes problematic, because if the EM wave, or DC current has been subject to attenuation, then the force required to proceed through the micropores is not enough. This has become an important point in this research.

1.9 Study Sites

1.9.1 Overview

This section will describe the three sites used in this study. These sites were strategically chosen, firstly on the age of the burials, then the type of cemetery, and if permission could be granted to conduct this research at each location. Descriptions of each cemetery are given, and an overview of soil classifications and underlying geology.

1.9.2 Study Sites

This project involved younger graves (dated from the mid-1980's) located in three existing cemeteries. These cemeteries are located in the South Australian rural towns of Bordertown, Keith and Pt Lincoln, (see Figure 1.9.1). All of these sites are garden cemeteries, i.e. are grassed with no grave furniture other than a headstone or plaque to mark the burial. Typically, burial sites of this age within registered cemeteries in Australia could be marked with ornate stone or metal outlines, stone headstones, metal or alloy flower holders, with the ground surface surrounding the burial being natural soil, small crushed stones, or even untended grass. The stone used for grave decoration could be granite or marble, with burial site surrounds

being concrete, granite, marble, or metal. Many of these grave decorations are raised above the surface of the surrounding ground, restricting the effective use of geophysical methods to probe the site of the burial. By using garden cemeteries that have an absence of intrusive grave furniture, along with an area of tended flat grass, these types of cemeteries provide the optimal ground surface conditions for the geophysical methods utilized in this study, see Figure 1.9.2.

Figure 1.9.1 Location of study sites within the State of South Australia.

These garden cemeteries are not frequently found in regional areas, as water for irrigation is not always readily available. There are garden cemeteries in the Adelaide metropolitan area that also provide these optimal conditions, Cheltenham; Enfield; West Terrace; and Centennial Park, but after negotiations to conduct this research at these cemeteries the relevant authorities were not able to grant permission. The lawn in the Bordertown and Keith cemeteries are occasionally irrigated via overhead sprinklers in the dryer months, two days per week for 45-60 minutes, at a rate of 12mm per hour. The lawn of Pt. Lincoln cemetery was not watered during this study. The lawn covering the Pt. Lincoln RSL Cemetery (Returned and Services League) is a mix of turf and weeds, patchy at times, and well mown to be quite short. The lawns at Bordertown and Keith are more carefully tended turf, and quite thick. The thickness is highlighted in Figure 1.9.3.

Figure 1.9.2: The Happy Valley cemetery complex, Pt Lincoln. Of note is the number of grave sites that are visible in the turf. To the left and top are non-garden cemeteries showing grave furniture. The contrast of the ground surface between these and the RSL lawn cemetery, centre, is marked. Having a clear surface allows easier access for geophysical methods in the locating of unmarked graves.

The age of the burials was an important consideration of which rows were used. This was dictated by the age of the burials in rows “P” and “Q” at the Pt. Lincoln RSL Cemetery, as these graves were amongst a larger number all hand dug by the author. Because of this, intimate knowledge of the burial sites, i.e. the size, shape and orientation are all known. Selecting burials of this age follows Fiedler et al. (2009:384), who suggested that undertaking geophysical research over much younger graves will give instant feedback. It is not known exactly what remains are in the burial shaft, but following Blom (2018:8 and Campobasso et al. (2001:20) from Section 1.2.5 (Burials) it can be assumed that after 271 days the final pre-skeletonization stage is completed, and that the older burials would still contain the remnants of the coffin, and extensive skeletal remains. The younger burials would be expected to contain an intact coffin, and extensive human remains. The burials in this research date from the period 1984 – 2019, are situated in well maintained, registered cemeteries, and so it is known that a burial took place, and the location of the burial is recorded. This follows Dionne et al. (2010:56; Hansen et al. (2014:28; and also Schultz et al. (2016:56) who all call for research involving more recent, known, human burials. Tables 1.9.1, 1.9.3, and 1.9.5 detail the ages of burials at each Cemetery.

Figure 1.9.3: Thickness of turf in Bordertown Cemetery, (left), and Keith Cemetery, (right).

1.9.3 Bordertown

The town of Bordertown is in the South-East of South Australia, with the cemetery on the eastern edge of the town, Figure 1.9.4. The recorded first burial took place in 1873. This is a large cemetery, covering some 25000 m², and contains over 1730 known interments. Rows “D” and “E” in the ‘Granite Lawn’ section are the target rows, with both rows containing 14 burial plots each. Of these 28 burial plots 12 have two burials, and one has three burials. Graves in these rows were backfilled with sand to approximately 10 cm above the coffin, then the soil from the grave was used to fill the remaining grave. This process is unique to Bordertown and gives gravediggers a warning when the grave is reopened for a second burial.

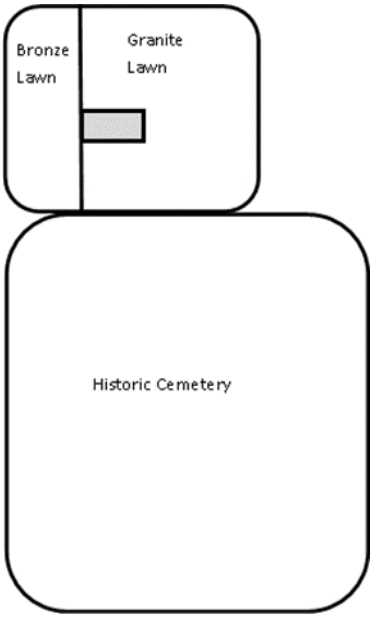

Figure 1.9.4: Above, location of Bordertown Cemetery in relation to the Bordertown township. Right, plan drawing of the Bordertown Cemetery. Rows D and E of the Granite Section are highlighted in grey.

Bordertown Cemetery is located within the Murray Basin with the underlying geology being Loxton Sand, (overlaying the Bookpurnong Formation), with an age given as Early Pliocene, Figure 1.9.5. The Loxton Sand is described as a regressive sequence of shallow water marine and marginal marine sediments, comprised of siliceous and clayey sand (Belperio 1995; Department of Energy and Mining 2022). The DEWNR soil classification data sheet for Bordertown is SE002 and SE003, (Hall et al. 2009). These two sample sites are 600 m and 700 m respectively from the cemetery. SE002 substrate is described as 'Tertiary sandy clays, ferruginised in places.' The descriptions of the horizons are red and dark brown heavy clay, gradual to red, brown and yellow heavy clay, and gradual yellowish-grey calcareous medium clay, (see Figure 1.9.6, with descriptions of soil classifications in Table 1.9.3).

Table 1.9.1: Bordertown Cemetery, age of burials for rows "D" and "E".

Bordertown														
Row "D"														
Grave No.	1	2	3	4	5	6	7	8	9	10	11	12	13	14
Burial 1	1995	1995	1995	1995	1995	1995	1995	1996	1996	1996	1996	1996	1996	1996
Burial 2	1996			1997	1999		1999		2015				2019	
Row "E"														
Burial 1	1997	1997	1997	1997	1997	1997	1997	1997	1997	1997	1997	1997	1996	1996
Burial 2			2019	1998			1998	1998			2005	2007	2018	
Burial 3							2017							

Classification site SE003 substrate is described as 'Pleistocene clays.' The description of the horizons is dark grey subangular blocky medium clay, gradual to grey medium-heavy clay, gradual to dark grey heavy clay, to brownish-grey heavy clay. Both of these classification sites are dominated by medium to heavy clays.

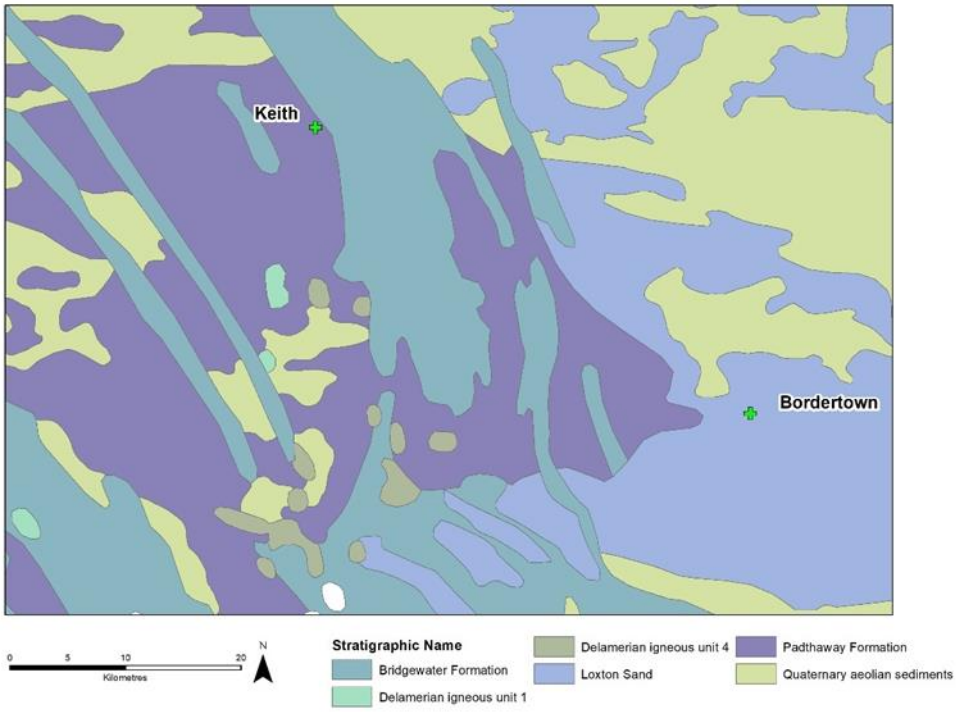

Figure 1.9.5: Geology of the Bordertown and Keith sites.

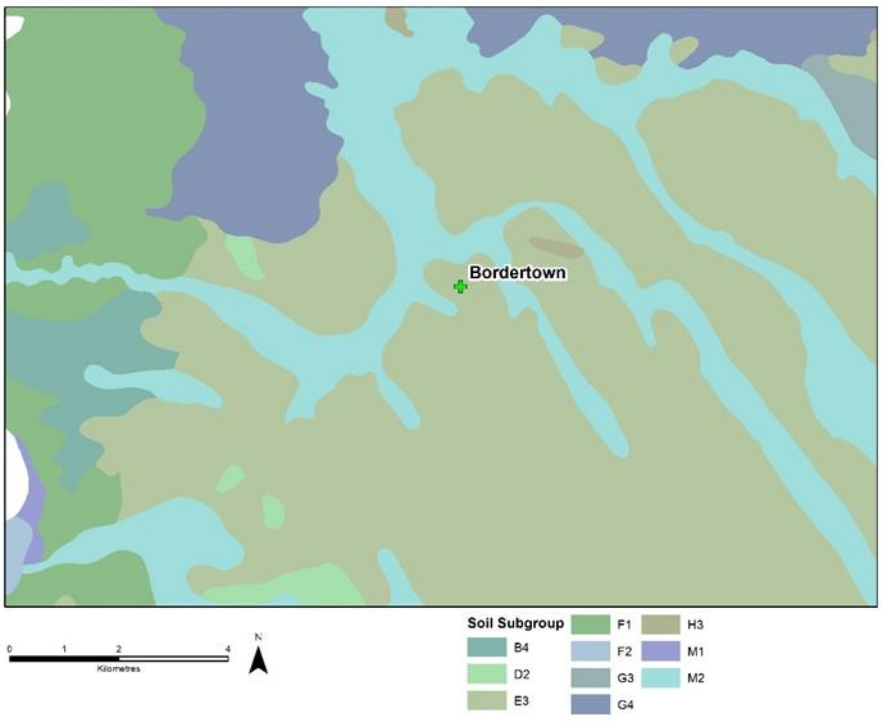

Figure 1.9.6: Soil subgroup, Bordertown

Table 1.9.2: Bordertown soil classification descriptions.

Soil Classification	Soil Group Description	Soil Type Description
B4	Shallow soils on calcrete or limestone	Shallow red loam on limestone
D2	Hard red-brown texture contrast soils with neutral to alkaline subsoil	Loam over red clay
E3	Cracking clay soils	Brown or grey cracking clay
F1	Deep loamy texture contrast soils with brown or dark subsoil	Loam over brown or dark clay
F2		Sandy loam over poorly structured brown or dark clay
G3	Sand over clay soils	Thick sand over clay
G4		Sand over poorly structured clay
H3	Deep sands	Bleached siliceous sand
M1	Deep uniform to gradational soils	Deep sandy loam
M2		Deep friable gradational clay loam

1.9.4 Keith

Keith is also in the South-East of South Australia, some 45 km to the north-west of Bordertown. The cemetery lies a short distance from the town, Figure 1.9.7, with the oldest recorded burial taking place in 1891, Table 1.9.3. This is a much smaller cemetery covering some 0.64 hectares and contains 620 recorded internments. Rows “H” and “I” are the target rows with both containing 10 burial plots each. Of these 20 burial plots, six have two burials. The graves here are dug with a mechanical digger, and the same soil is used to backfill.

Table 1.9.3: Keith Cemetery, age of burials of rows "H" and "I".

Keith										
Row “H”										
Grave no.	1	2	3	4	5	6	7	8	9	10
Burial 1	2000	1999	2018	1999	Empty	2000	1999	2000	1999	1998
Burial 2	2006					2011		2007		
Row “I”										
Burial 1	2001	2001	2001	2001	2001	2001	2001	2001	2000	1999
Burial 2	2001			2004	2011					

Keith Cemetery straddles the boundaries of the Coastal Quaternary and the Murray Basin provinces, with the rows involved in this research situated a mere 115 m from the boundary, Figure 1.8.6. The ages of both provinces are given as early to late Pleistocene (Department of Energy and Mining 2022). Within the boundary of the Coastal Quaternary province lies the Bridgewater Formation, which is described as ‘Calcreted aeolianite’, or coarse carbonate sands.

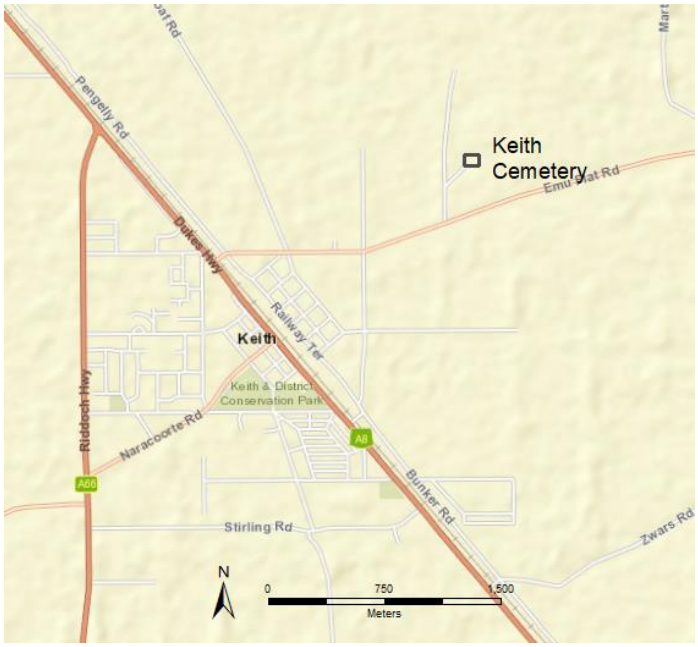

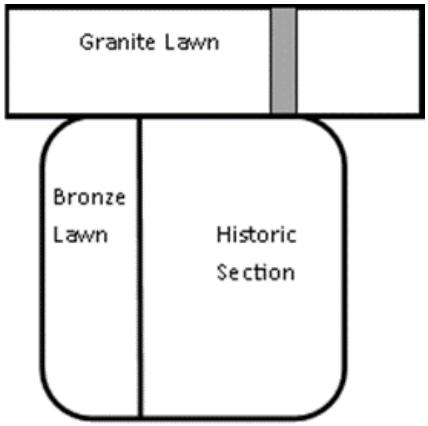

Figure 1.9.7: Above, location of the Keith Cemetery, in relation to the Keith township. Right, plan diagram of the Keith Cemetery. Study rows highlighted in grey.

Within the Murray Basin province lies the Padthaway Formation, with stratigraphy described as 'Silt, dolomite and sand of freshwater lagoons and swamps', with Belperio, (1995:223), describing this formation as lacustrine sediments that are deposited in interdune corridors, (Department of Energy and Mining 2022), see Figure 1.9.8, with a description in Table 1.9.4. The DEWNR soil classification site near Keith is SE043, this site is located some 3.5 km east of the cemetery. The substrate here is described as 'calcreted calcarenite', with the horizons described as grey loamy sand changing abruptly to light loamy sand, sharp to brown sandy clay.

The larger area of these two study sites, the South-East of South Australia, was once a shoreline, starting from the Middle to Late Miocene, and extending into the Quaternary. During this period the Australian Continent experienced sea levels ~100m above the present levels, as well mild tectonic activity (Belperio 1995:161). This ancient shoreline has left a series of coastal dune ranges, the Bridgewater Formation, with the interdune corridor plains being the Padthaway Formation. These dunes run in a general north-westerly orientation and can be seen in the geology and soil maps of the study sites, Figures 1.9.5 and 1.9.8. Pre-European, this area contained a large series of wetlands that covered approximately 46% of the landscape (South East Natural Resources Management 2022).

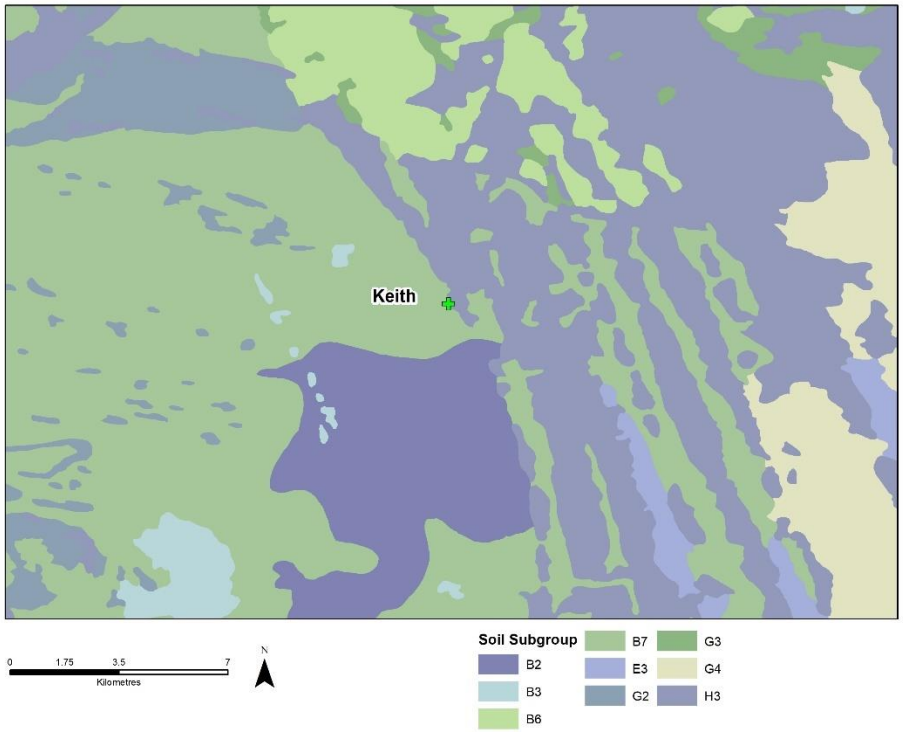

Figure 1.9.8: Soil subgroups, Keith

Table 1.9.4: Keith soil classification descriptions.

Soil Classification	Soil Group Description	Soil Type Description
B2	Shallow soils on calcrete or limestone	Shallow calcareous sandy loam on calcrete
B3		Shallow sandy loam on calcrete
B6		Shallow loam over red clay on calcrete
B7		Shallow sand over clay on calcrete
E3	Cracking clay soils	Brown or grey cracking clay
G2	Sand over clay soils	Bleached sand over sandy clay loam
G3		Thick sand over clay
G4		Sand over poorly structured clay
H3	Deep sands	Bleached siliceous sand

The climate of the South-East of South Australia is dominated by high winter rainfall, with corresponding high summer/low winter temperatures. The average rainfall for both Bordertown and Keith is 450 mm, with the majority of that rain falling after April, see figure 1.9.9.

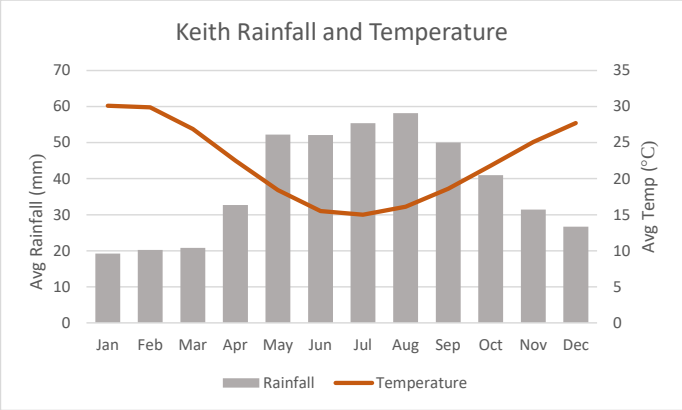

Figure 1.9.9: Mean annual average temperature and rainfall from the study stie at Keith, South Australia. (Data: Bureau of Meteorology 2024)

1.9.5 Pt Lincoln RSL

Port Lincoln is on the Eyre Peninsula, South Australia. The cemetery is a short distance north of the centre of the city, see Figure 1.9.10. This cemetery is part of a larger site comprising the Pioneer Cemetery and two parts of the Happy Valley Cemetery. The RSL Cemetery covers some 3350 m² and is the resting place of returned servicemen and women, and in later years partners were also buried here. Rows “Q” and “P” are the target rows, with both rows containing 18 burial plots each. Of these thirty-six burial plots, twelve have two burials, see Table1.9.5. All of these graves were dug by hand to a depth of 1.8 m, as in the time period of these initial burials the burial of spouses within this Cemetery was not allowed. If a double burial had been requested, the graves would have initially been dug to a deeper level. The graves were hand dug with the soil placed in a pile adjacent to the grave and refilled with the same soil after interment.

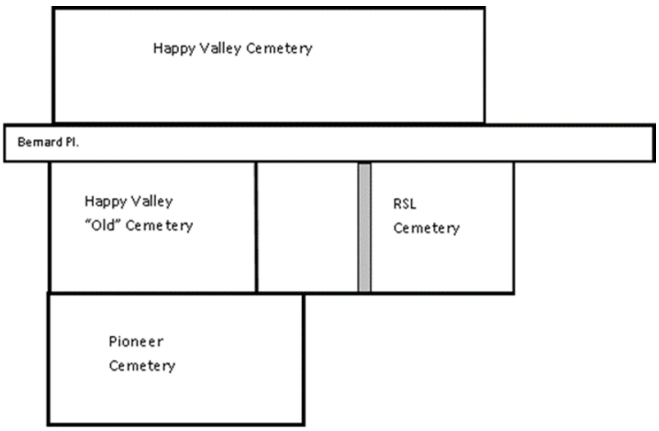

Figure 1.9.10: Above, location of the Happy Valley cemeteries in relation to the City of Pt. Lincoln, South Australia. Right, layout of the Happy Valley Cemetery complex, Pt Lincoln, South Australia. The cemeteries are split by a public road - Bernard Pl. The study rows are highlighted in grey.

The two rows in this research within the Pt Lincoln RSL Cemetery are situated some 50 m from the boundary of the Donington Suite and the Hutchinson Group. Both are part of the Gawler Craton, with the Hutchinson Group being part of the Cleve Subdomain. Ages for both are given as Palaeoproterozoic. The underlying geology of the Hutchinson Group is described as 'Quarzitic, pelitic and calcsilicate metasediment', while the geology of the Donington Suite is described as 'Megacrystic granite to grandiorite gneiss' (Department of Energy and Mining 2022) (see Figure1.9.15).

Table 1.9.5: Pt Lincoln RSL Cemetery, age of burials for rows "P" and "Q".

Pt Lincoln RSL														
Row "P"														
Grave no.	1	2	3	4	5	6	7	8	9	10	11	12	13	14
Burial 1	1984	1984	1984	1984	1984	1985	1985	1985	1985	1985	1985	1985	1984	1985
Burial 2	2001							1989		1990	2000	2000		2000
Grave No.											15	16	17	18
Burial 1											1985	1985	1985	1985
Burial 2											2004		2014	
Row "Q"														
Burial 1	1985	1985	1986	1986	1986	1986	1986	1986	1986	1986	1987	1987	1987	1987

Burial 2					1998		1996				2007			
Grave No.											15	16	17	18
Burial 1											1987	1987	1988	1988
Burial 2													1992	

This geology is evident on the ground, as in the adjacent Pioneer Cemetery there are granite outcrops some 150 m from the study rows. As this cemetery is within the boundaries of a major regional city, there is no agricultural soil classification site. From the DEWNR soil subgroup data the soil is given as being a mix of shallow soil on rock and loam over clay on rock, see Figure 1.9.16, with descriptions of soil classifications in Table 1.9.6. It is also worth noting that 80 m north of the study rows is a spring fed creek, this spring has long been diverted for commercial purposes. On the southern boundary of the RSL cemetery is an outflow of another storm-fed watercourse. Storm water will pool here after rain events, and presumably percolate down through the subsurface matrix over time. This pooling is only 20 m from the study rows.

As Pt Lincoln is located on the Lower Eyre Peninsula, the climate is more moderate, often described as 'Mediterranean', with a hot, dry summer, followed by a cool winter (Specht 1973). Pt Lincoln records a slightly higher annual rainfall than the South-East sites (420 mm), with a slightly lower average annual temperature (21.3°C), see Figure 1.9.11.

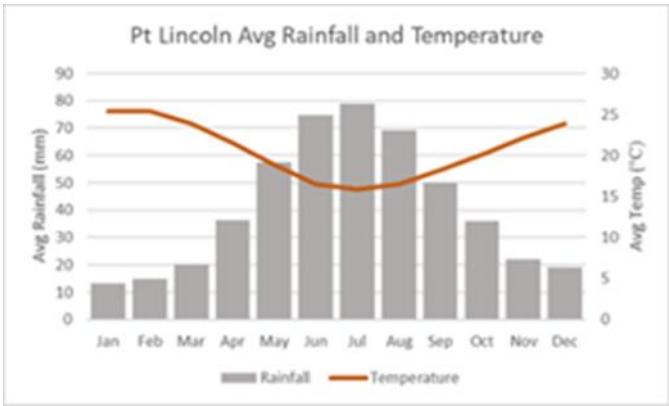

Figure 1.9.11: Average rainfall and temperature for Pt Lincoln. (Data: Bureau of Meteorology 2024)

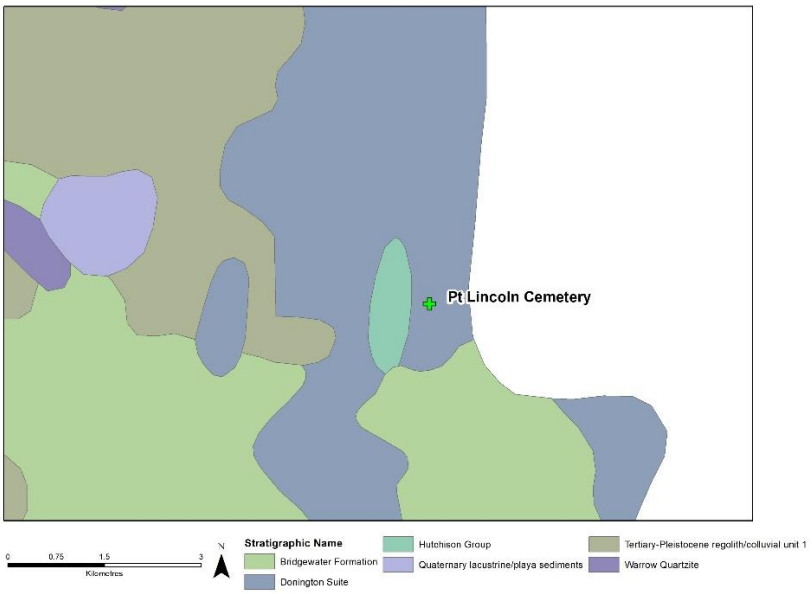

Figure 1.9.12: Geology, Pt Lincoln

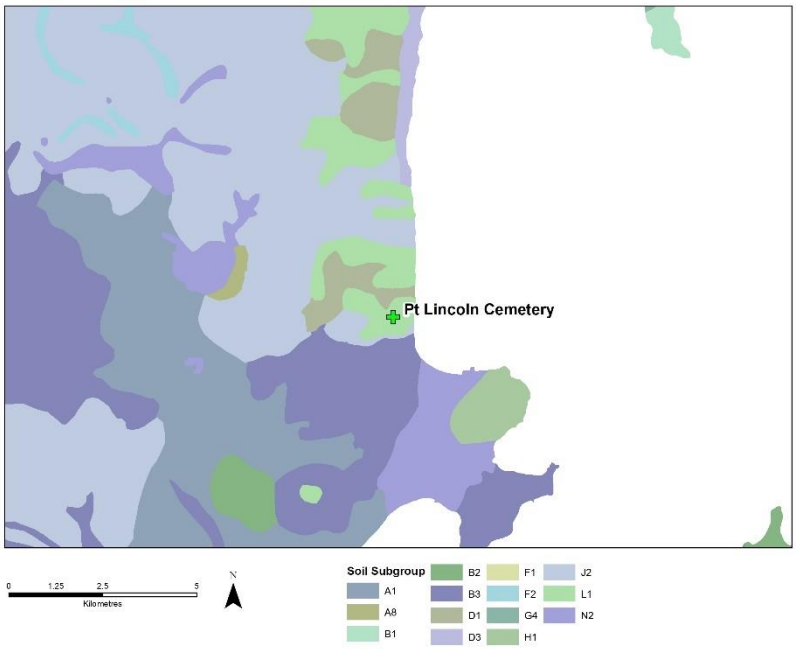

Figure 1.9.13: Soil subgroups, Pt Lincoln

Table 1.9.6: Pt. Lincoln soil classification descriptions.

Soil Classification	Soil Group Description	Soil Type Description
A1	Calcareous soils	Highly calcareous sandy loam
A8		Gypseous calcareous loam
B1	Shallow soils on calcrete or limestone	Shallow highly calcareous sandy loam on calcrete
B2		Shallow calcareous sandy loam on calcrete

B3		Shallow sandy loam on calcrete
D1	Hard red-brown texture contrast soils with neutral to alkaline subsoil	Loam over clay on rock
D3		Loam over poorly structured red clay
F1	Deep loamy texture contrast soils with brown or dark subsoil	Loam over brown or dark clay
F2		Sandy loam over poorly structured brown or dark clay
G4	Sand over clay soils	Sand over poorly structured clay
H1	Deep sands	Carbonate sand
J2	Ironstone soil	Ironstone soil
L1	Shallow soils on rock	Shallow soil on rock
N2	Wet soils	Saline soil

1.9.6 Study Sites Summary

The site of the RSL cemetery was a key feature of this study. The author hand dug the graves in the period 1984 – 1987. The rows at Bordertown and Keith were as close as possible aligned to these dates. All three sites are lawn cemeteries, this is a deliberate decision, as this type of cemetery provides the optimal above-ground conditions for the two geophysical methods used in this study. Using known burials as recent as this research has, should, in theory, provide a geophysical response from the burial site.

The Bordertown and Keith cemeteries are located in an area where the soil and geology display signs of being a depositional shoreline extending from the Middle to Late Miocene to the Quaternary Period. As both these sites are located within a larger agricultural region, the near-surface soil is well known. The area surrounding Bordertown is known to have an extensive clay presence, while the area surrounding Keith is known to be sandy. Being of depositional origin, it would be expected that the soil would show a large percentage of silica and sodium. The geology and soil in the area of the Pt. Lincoln RSL Cemetery is dominated by the presence of granite, gneiss, and limestone, and this does give a contrast to the two other sites.

1.10 Soil Testing

1.10.1 Outline

Soils are a complex medium, comprising a mix of minerals, salts and other organic solutions, organic matter, soil moisture, as well as various microscopic and macroscopic organisms. In a burial context, this complex mix will exert varying influences, in varying locations (Dent et al. 2004:577). Understanding this subsurface matrix will give deeper insights into the type of soil at each study site, and the effects that a particular soil type may have on the geophysical results. The soil tests used in this research were chosen as they helped tell the specific story of the study sites in a context that underlines the research. This Section will give an overview of these tests, and why they were chosen.

1.10.2 Grain Size

The size of grains in sedimentary soil is a fundamental attribute, and so becomes an important descriptive property. To make the concept of particle size a useful descriptive variable, there needs to be methods to quantify, classify, and summarize this, and this is where the measurement of the grain size fits. The size of the grains, and the mix of sizes, will determine the soil type, and provide a broad indication of the physical and chemical properties of the soils, as well as the weathering and erosion processes that the grains within the sample have been exposed to (Boggs 2016:45; Switzer 2013:11; Switzer and Pile 2015:331).

Several methods can be used to measure grain sizes. Large grains (>2 mm) can be measured by vernier, and samples that contain grains smaller than 2 mm are typically measured by sieving through a set of nested screens. Grains that are < 0.02 mm (fine silt and clay) can be measured in a number of different ways. The pipette analysis utilizes the sedimentation process; the photohydrometer also utilizes the settling process, but measures the changes of a beam of light; a sedigraph measures the grain size by determining the attenuation of an x-ray beam; the laser-diffraction analyzer assumes that particles of differing sizes will diffract a laser beam at different angles; and the electo-resistance analyzers measures particle size by the displacement of the particle in electrolyte (Boggs 2016:48; Switzer 2013:11).

The nested screens are sized according to the Udden-Wentworth scale, which is a geometric scale in which each value is one half as small as the preceding value. Due to the wide range of particle sizes contained in any soil sample, the logarithmic or geometric scales are more efficient in describing and quantitively displaying the size. If using a logarithmic scale to quantitively describe the particle sizes, negative values can be generated. To overcome this and allow particle size data to be expressed in units of equal value, the phi-Wentworth scale is used.(Switzer and Pile 2015:331). The relationship between the sieve mesh size and the phi-Wentworth scale is given in Table 1.10.1.

Table 1.10.1: Correlated relationship between phi sizes and Wentworth descriptions. (Switzer 2013:8).

Sieve Mesh Size (mm)	Size Terms
4	Fine Pebbles
2	Very Coarse Sand
1	Coarse Sand
0.5	Medium Sand
0.25	Medium Silt
0.125	Fine Silt

1.10.3 Magnetic Susceptibility

There is a magnetic field of some sort in everything around us, as the magnetic field is a product of electrons moving around the nucleus of an atom (Dearing 1988:4). The magnetic analysis of soil samples can provide information as to the origin of the minerals in the sample, the age the minerals were formed, the concentration of minerals and the grain size (Dalan and Banerjee 1998:8).

One method of magnetic analysis that is widely used is magnetic susceptibility, and this can be defined as a measure of the extent which a substance can be magnetized and is expressed as the ratio of the induced magnetization to the inducing field (Dalan and Banerjee 1998:6; Evans and Heller 2003:9). Once a soil particle is subject to an external magnetic field the alignment of the magnetic field of the particle will change, this is the isothermal remanence. Within each soil particle there are, at the atomic level, regions, or domains, of differing magnetic alignments. These domains are separated by narrow, (ca 0.1 μm), domain walls. These domain states vary in size and can be classified thus: ultrafine grains (≤0.03 μm), that are superparamagnetic (SP), stable single domain (SD) grains (0.03μm - 0.1μm), pseudo single domain (PSD) grains (0.1 - 20μm), and finally to multidomain (MD >20μm) (Dalan and Banerjee 1998:8; Evans and Heller 2003:14–15; Lowe et al. 2016:212). If there is remanence, then these domains have been subject to an external magnetic field, and the domains have aligned in the same orientation (Dalan and Banerjee 1998:8; Tarling 2007:16).

By applying various magnetic fields of varying frequencies to a sample, one can characterize the magnetic mineral composition, concentration, and grain size. The composition refers to the crystal structure and magnetic mineralogy, the concentration points to the mass fraction of the dominant magnetic carrier, and the magnetic grain size refers to the size dependent magnetic domain state of this magnetic carrier (Dalan and Banerjee 1998:8).

There are five main groups of behaviours that are displayed by minerals. Three of these groups are able to retain their magnetism and may be identified using remanence methods. These three return the strongest magnetic susceptibility values (Dearing 1988:4).

Ferromagnetism is commonly associated with iron and is not common in the natural environment. Ferromagnetic materials are highly magnetic. Ferrimagnetic materials contain common minerals such as magnetite, which is found in all igneous rock, some sedimentary rocks, and nearly all soils. These minerals contain magnetic moments that are aligned, but exist in two separate opposing, but unequal forces. This group of magnetic materials often dominate any susceptibility measurements. The canted antiferromagnetic group contains iron-based minerals such as hematite. This group contains two separate magnetic moments, but these moments are virtually equal, and so cancel each other out. Hematite is a very common mineral, occurring in most soils (Dearing 1988:4; Tarling 2007:15).

Weaker susceptibility values are returned from the paramagnetic group of minerals. These minerals typically contain small traces of iron and manganese, which, when subject to an external magnetic force, provide magnetic moments, with susceptibility values in the range of 10-3 – 10-5 SI units. Diamagnetic are the final group of minerals, this group typically contains calcium carbonate and quartz. When subject to an external magnetic force, minerals from this group show a weak, negative susceptibility value, typically < 10-5 SI units (Dearing 1988:4; Evans and Heller 2003:7; Tarling 2007:15).

In the Archaeological context magnetic susceptibility can be used to date material culture and sediments. Over many millions of years, the Earth's geomagnetic field has changed direction and intensity. The intensity and remanence orientation can be compared to known records to help understand depositional or creation date. Fired clay, pot remnants or bricks etc., can be measured for magnetic intensity (Tarling 2007:150). The Australian continent has a high iron content in soils, so the use of mineral magnetics has been somewhat constrained (Lowe et al. 2016:211). Nevertheless, magnetic techniques can be used to further the understanding in many Archaeological areas, with areas of interest pertinent to this research being (a) investigating the morphology of the sites, and the processes active in their formation; (b) further understanding the process of erosion and sedimentation of the site. Dalan and Banerjee (1998) cite several examples where magnetic susceptibility has been used to define morphology and anthropogenic earthworks of archaeological sites. These examples include burial mounds, rocks in fire pits, and hill forts.

In the area of erosion and sedimentation of archaeological sites the study of magnetics of a site can show how erosion may have changed the original shape of features such as earth mounds and assessing the magnetic susceptibility of samples taken from within the stratigraphy of a site will show the presence of magnetic minerals in sediments, these magnetic minerals may be due to cultural or natural processes (Dalan and Banerjee 1998; Lowe et al. 2016).

1.10.4 Soil Chemistry

X-Ray fluorescence (pXRF) analysis is a non-destructive technique that has been shown to be quick and cost efficient and can be used to quantify the inorganic component of a soil sample (Madden et al. 2022:2; Ravansari et al. 2020:1; Reddy et al. 2020:2; Shackley 2011:7; Trant et al. 2021:2; Williams et al. 2020:2). The unit used within this research was capable of detecting minute amounts of all elements between Fluorine, atomic number 9, and Uranium, atomic number 92.

An atom comprises an inner nucleus, (positively charged), and a collection of electrons, (negatively charged), that circle the nucleus. These electrons are arranged in shells, named K,L,and M, see Figure1.10.1. The X-ray Fluorescence will send a high energy photon pulse into the K shell, which will cause an electron to exit the atom in an excited state. To balance the electrons, and keep the atom in a stable condition, an electron from the L shell will replace the exited electron. To do this a small amount of excess energy is released. This released energy is quantised, and for each element that has an atomic number, this quantised value will always be the same for each individual element and will increase with an increase in the atomic number of the element (Bruker 2023; Ravansari et al. 2020:1; Shackley 2011:16).

Within the archaeological context pXRF analysis plays an important role in determining the overall characterisation of a soil sample.

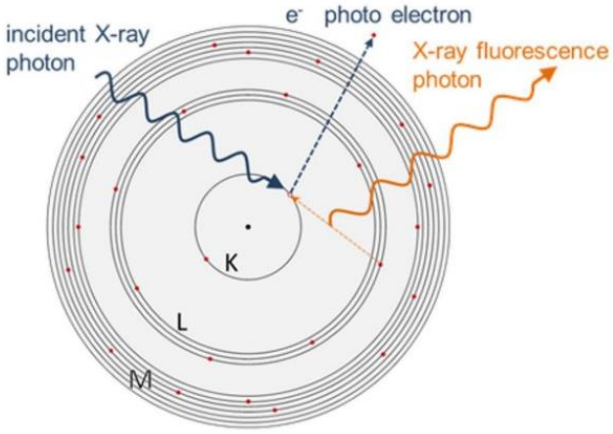

Figure 1.10.1: Diagrammatic representation of an atom, showing the K, L, and M shell. The X-ray fluorescence photon enters (top left), and top right, the excess energy is shed by the electron taking its place (X-ray fluorescence photon). Image reproduced with permission from Bruker (2023).

The chemical analysis returned from pXRF testing can give insights into the origins of the sample, past anthropogenic land uses, and environmental conditions that the sample may have been subject to. Chemical soil analysis has been successfully used as an interpretive tool to delineate, detect, and interpret discrete activity areas with archaeological sites (Gall 2012:96). Chemical analysis such as heavy metal contamination of graveyards (Madden et al. 2022:4), anthropogenic copper occurrences in Viking-age buildings (Trant et al. 2021:20), and phosphorus and calcium analysis within paleosol horizon (Romanis et al. 2021:5) have all been interpreted using pXRF analysis.

1.10.5 Exchangeable Sodium Percentage

In Section 1.8.12 (Sodic Soils), the function of sodicity was discussed. Determining the level of sodicity in a sample of soil is often carried out by testing the Exchangeable Sodium Percentage (ESP), (Mitchell and Soga 2005:167; Nelson and Oades 1998:52; Qadir and Schubert 2002:276). The ESP is determined by the percentage of exchangeable Sodium divided by the sum of the available exchangeable cations in the sample (Sumner 1993:685). The testing of ESP in this research was carried out by an external source. The test applied was an extraction method based on an Australian adaptation of the Rayment and Higginson test, (15D3), as described by (Rayment and Lyons 2011:356,386).

1.10.6 Soil Summary

From the preceding sections and chapters, it can be seen that the soil will exert a significant influence on the outcomes of this research. Using the soil classification data, and the descriptions of the underlaying geology of the study sites, gives an indication of the characteristics of the subsurface matrix that may be found, and what impacts this geology could place on the geophysical data captured. To underline this data,

soil testing will provide a deeper understanding of the physical and chemical characteristics of the subsurface matrix at each site, and it would be anticipated that a clearer picture of grain size, and the minerality of the samples will be of great value. This information can then be related back to the many assumptions found in the literature.

2 METHODS

2.1 Introduction

Two geophysical methods were used in this research, and following the research questions, were assessed for their suitability to locate unmarked graves. These methods, Ground Penetrating Radar (GPR) and Electrical Resistivity Tomography (ERT), were chosen as they both provide a non-invasive and non-destructive method of subsurface detection, as well as being well used techniques in the Archaeological context. The steps taken to gather data in this research are conventional, as are the data processing methods, and these are outlined in this chapter.

As the physical and chemical characteristics of the soil are so critical in these processes, and this research in general, the methods of soil analysis are given, along with the methods of assessing the subsurface moisture content, and general environmental precipitation as well.

2.2 Ground Penetrating Radar

At all three study sites, the GPR data was collected using the same methodology. A grid was laid out over the rows, with radar scan line spacing set to 50 cm, and configured in an orthogonal pattern to the orientation of the graves. Grid sizing for all sites can be seen in Table 2.2.1, with images of line spacing and orientations in Figure 2.7.1. This line spacing and orientation is consistent with Dionne et al. (2010:20); and Neal (2004:294) who recommends an orthogonal orientation to targets, Luo et al. (2019) who states that the scan spacing should be no greater than the anticipated targets, and Conyers (2011:28) who suggests an ideal scan space for the radar used here of less than one meter.

Table 2.2.1: GPR grid size and row numbers. Bordertown and Keith grids covered two rows due to the layout of the cemetery. Rows within the Pt Lincoln RSL Cemetery were configured differently, hence one GPR grid per row.

Study Site	Rows	Grid size (m)	Number of GPR lines	Figure number
Bordertown	“D” & “E”	5 x 21.5	11	3.7.1
Keith	“H” & “I”	5 x 16	11	3.4.1
Pt Lincoln RSL	“P”	3 x 25	6	3.11.1
	“Q”	3 x 25	6	3.11.1

A bi-directional, or ‘zig-zag’ pattern of moving along the GPR lines is used, this pattern involves data collection in one direction, then at the end of the line, collecting data in the opposite direction. This follows Goodman (1994) as the suggested data acquisition method.

Table 2.2.2: Radar setting used in this research.

Radar	Scan
400MHz	Samples 1024
T_Rate 100KHz	Format (bits) 16
Mode Distance	Range (nS) 100
GPS None	Diel 9.98
Rate 64	Scan/Unit 50.00

A Geophysical Survey Systems Inc (GSSI) SIR 3000 unit was paired with a 400MHz shielded bowtie antenna. Settings used can be seen in Table 2.2.2, and it should be noted that the Scan/Unit figure gives a scan spacing of 0.02 m. The GPR antenna was housed in a two-wheel push cart, (Figure 2.2.1), and the pulses were triggered by the distance wheel.

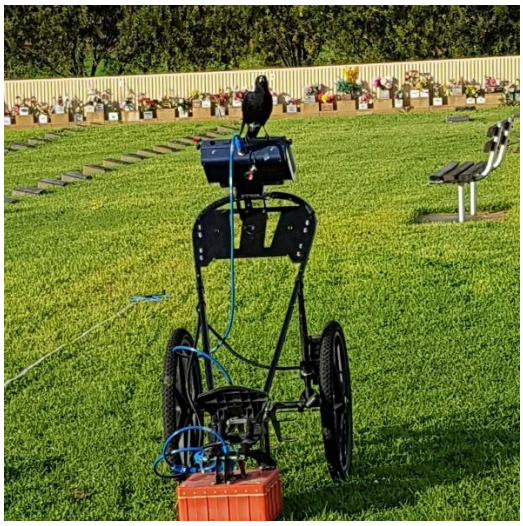

Figure 2.2.1 : The GSSI GPR radar used in this research.

2.2.1 Processing of GPR data

Processing of the raw radar data is undertaken to reduce the signal-to-noise ratio. This is to be undertaken with caution, so as to present an image that can be readily interpreted. Over-enthusiastic processing can add phantom features and exclude real features (Daniels 2007:247; Goodman 2009:236; Goodman and Piro 2013:62; Goodman 2012:166; Szymczyk and Szymczyk 2013:90). It is this reduction of clutter, or noise, that is the key objective in the processing steps outlined below.

Processing of the GPR data was carried out in GPR-Slice, (currently v7.0). A standard processing workflow was used, as given by (Goodman 2009:236), as well as (Balkaya et al. 2021:104272; Dionne et al. 2010:22; Goodman and Piro 2013:37; Gómez-Ortiz et al. 2010; Luo et al. 2019:40; Molina et al. 2016:108) and is outlined below. These processing steps are shown in Figure 2.2.1, with the progression of processing is

given from Figure 2.2.5 through to Figure 2.2.10 below. The aim of the GPR survey will dictate if all the steps are applied. For example, when used as an initial investigation technique, to find areas of interest, or Archaeological prospection, these processing steps can sometimes be reduced to the steps that are applied to the “B” scan. If the survey is aimed at an extrapolation or hypothesis testing exercise, then the full range of processing can be applied, and this can often result in the “C” scan, or 3D render. (See Section 1.4.1)

The goal of archaeological prospection is the detection of anomalous regions caused by physical and chemical changes in the subsurface matrix, (Trinks and Hinterleitner 2020), and to accurately achieve this the measurement of the depth of subsurface targets is important. This depth calculation is a function of the two-way travel time of the radar pulses, and to estimate this, the velocity of the wave propagation through the subsurface matrix is required, along with the time taken to travel from the transmitter antenna to the target and return to the receiving antenna (Ruffell 2005:2; Yelf and Yelf 2004). Determining the velocity of the wave propagation will be discussed later (see Section 2.2.2). As the GPR unit used in this study, (and many other units used generally), employ separate antennas for transmission and receiving there is a small time delay between the first signal transmitted, and this signal being subsequently received (Szymczyk and Szymczyk 2013:85; Zadhoush and Giannopoulos 2022:209). Other factors influencing this start time could be thermal drift, electronic instability, cable length, and variations of the antenna air gap (Zadhoush and Giannopoulos 2022:209), along with differences in operating temperatures (Neal 2004:274).

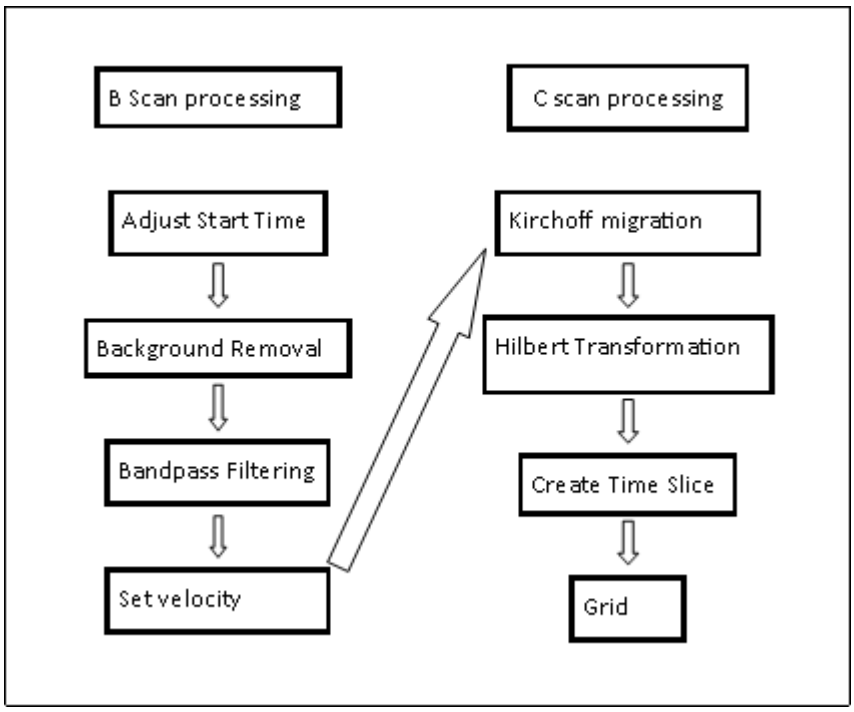

Figure 2.2.2: Schematic diagram of the radar processing workflow applied within GPR-Slice software and used in this study.

The method of adjusting this start time is to set a cut-off point at the start of the radar pulse, this can be at the first positive peak of the wavelet, the neutral position, or the negative peak (Conyers 2004:122; Goodman 2012:154; Yelf and Yelf 2004:159). Zadhoush and Giannopoulos (2022) undertook a study to determine to optimal position and concluded that trimming the pulse at the negative peak returned a depth calculation with greater consistency and accuracy. It is worth noting that the depth of their study was 30 cm, and the quoted depth accuracy for the negative peak method was 1.1 cm, with the positive peak method returning a depth accuracy of 2 cm. GPR Slice allows for three choices of start time adjustment, the threshold breach, the positive peak and the zero crossing. The positive peak was chosen in this study. Figure 2.2.2 shows this in detail, with Figure 2.2.6 showing the radargram trimmed to the new start time.

Background removal is the most commonly used processing filter and is used to remove banding noise across the radargram, Figure 2.2.7. Banding can be seen within a radargram as parallel horizontal lines, and these bands can be generated by changes in subsurface conductivity, nearby radio or electromagnetic devices, such as mobile phones, or variations in surface roughness (Conyers 2004:123). The GPRSlice© program used in this research achieves this by subtracting the average scan across a radargram from each individual trace within complete radargram (Goodman 2012:166; Hansen et al. 2014:16).

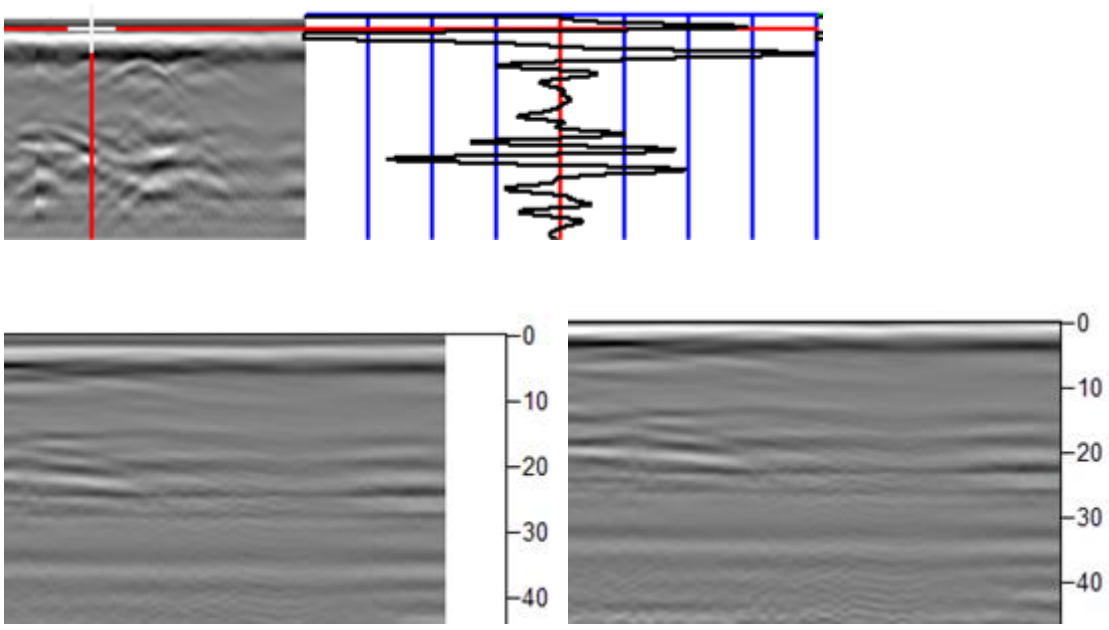

Figure 2.2.3: Left, raw radargram, right, radargram with the adjusted start time. Top, raw radargram with the corresponding wriggle line showing the positive peak that the start time was adjusted to.

Bandpass filtering is applied to reduce noise from unwanted high or low frequencies in the radar pulses (Conyers 2004:95; Goodman 2012:189; Hansen et al. 2014). Daniels (2007:255) suggest that additional noise can be introduced into the radargram by antenna ground interactions. To remove these frequencies, the radar pulses are converted using Fast Fourier Transforms (FFT) to the spectral domain. This allows the calculation of amplitudes and phases contained at each frequency of the radar pulse. Once the pulse is

displayed in the spectral domain the chosen frequencies can be removed or reduced. Following this, an inverse FFT is run to return the filtered radargrams to time domain signals (Goodman and Piro 2013:40; Szymczyk and Szymczyk 2013:87). Low-frequency noise can induce a significant DC drift, so the adjustment to the drift can be rectified as the bandpass frequencies are adjusted, (Goodman 2012:189). The bandpass filter dialog is shown in Figure 2.2.3, with the relevant radargram shown in figure 2.2.8.

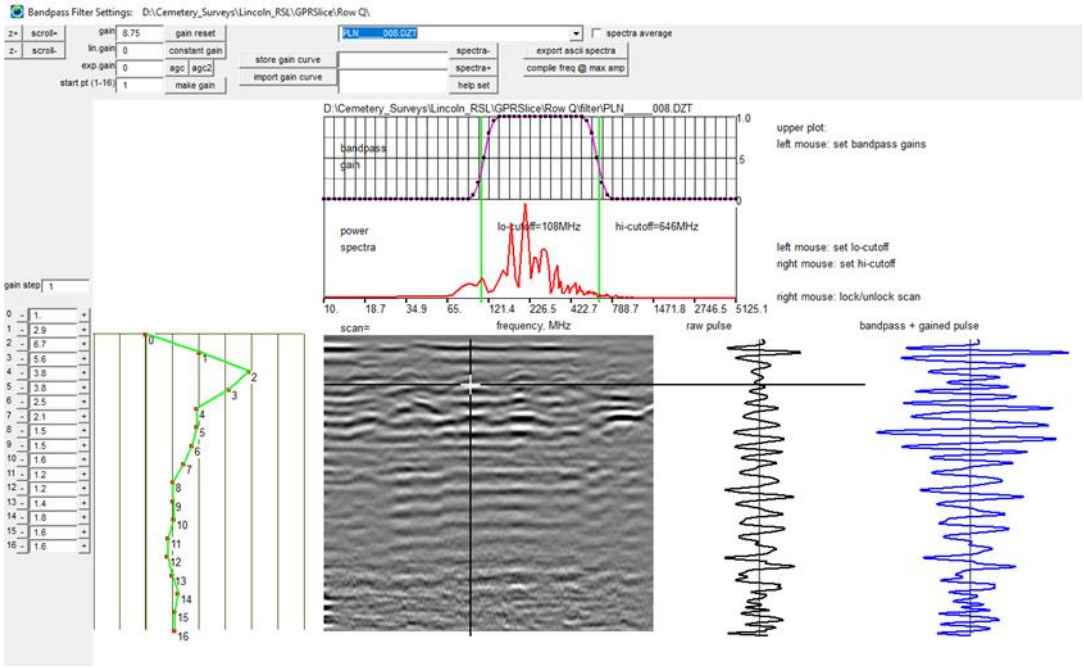

Figure 2.2.4: The bandpass filter dialog. The stepped gain is shown on the left, with the raw and filtered wiggle on the right. The radargram shows the first 400 traces of the target radargram. The spectral curve of the radar pulse is shown above, in red.

The velocity of the radar pulse as it travels through the subsurface matrix will vary due to many factors, outlined in Chapter 1.4. The velocity for each package of data, (i.e., each time the study site is visited and GPR data is recorded), is set via the hyperbola search function in GPR-Slice. This process is shown in Figure 2.2.4.

The result at this point in the processing workflow is a “B” scan, and at times this will suffice depending on the aims of the GPR survey. Processing workflow past this point will result in “C” scans, these are used for time slices or 3D rendering.

As shown in Chapter 1.4, the electro-magnetic pulse emanating from a GPR antenna spreads out in a cone pattern. Because of this feature, objects to the side, to the front, and to the rear of the antenna may reflect the electro-magnetic energy back to the receiving antenna and be recorded. Objects reflecting the radar pulses that are below the antenna return a two-way travel time that is smaller than reflecting objects that may be off to the side, and hence further away. The net effect of this is a hyperbolic pattern, (Conyers

2004:128; Goodman 2012:167; Hansen et al. 2014:16). The shape of these hyperbolas is dictated by the velocity of the radar pulses through the subsurface medium.

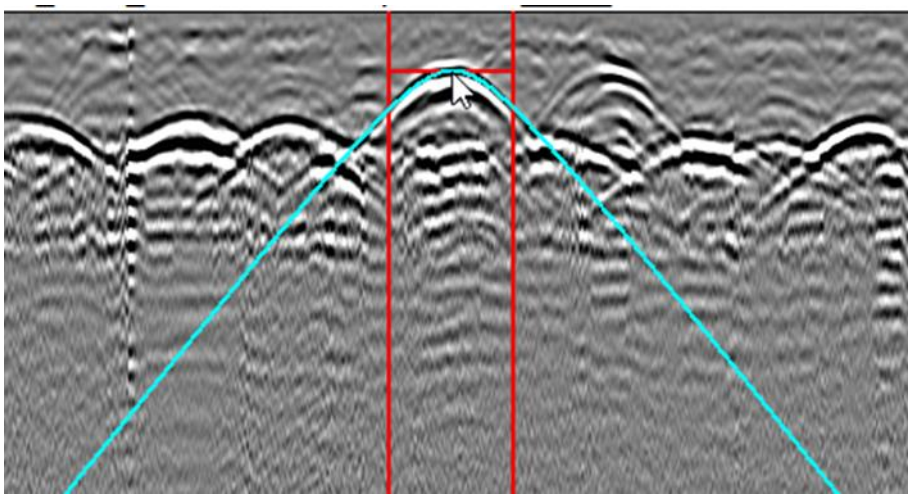

Figure 2.2.5: Example of fitting the synthetic curve to a hyperbola in the radargram (in cyan). This radargram is from the RSL Cemetery, data captured June 2021. Wave velocity in this instance is 0.150 m/ns.

The migration filter will remove hyperbolas from the radargram, Figure 2.2.9. The hyperbola that was generated in the velocity step is used. This hyperbola is fitted to a hyperbola found within the raw or partially processed radargram. This fitted hyperbola is then applied to the entire radargram, with all waves that fall along the hyperbola being added up with the resultant hyperbola placed at the vertex of the hyperbola. This then effectively collapses hyperbolic reflections found in the raw data to point reflections. Variable velocities and small errors can create pseudo reflections. Within the GPR-Slice program, the Kirchoff migration option was used. This method of migration is a velocity weighted summation process and includes corrections for wave obliquity and spherical spreading over the hyperbolic aperture (Goodman 2012:167; Neal 2004:306; Martorana et al. 2023:2897).

Hilbert transformations, Figure 2.2.10, convert radargram pulses to positive domain pulse envelopes. It achieves this via complex Fourier transformations (Goodman 2012:181). Conyers (2004:130) suggests that this transformation process can enhance reflections from subtle changes in subsurface resistivity.

All of these processing steps are pictured below. This series of radargrams is from the study site in Keith.

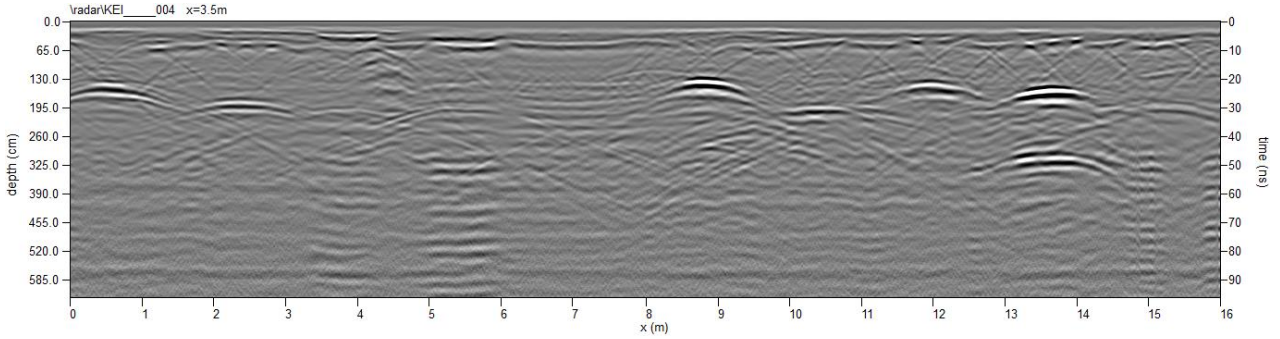

Figure 2.2.6: Raw data captured in July 2022. Some hyperbolae are visible along the radargram associated with the burial sites. Direction of data capture is left to right, with two-way travel time on the right, and unadjusted depth on the left.

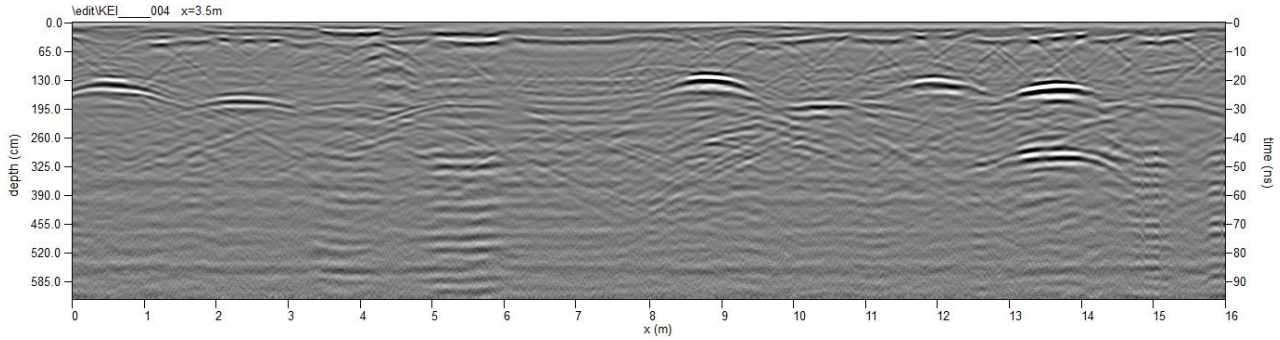

Figure 2.2.7: Start time adjusted, and this adjusts the depth (cm).

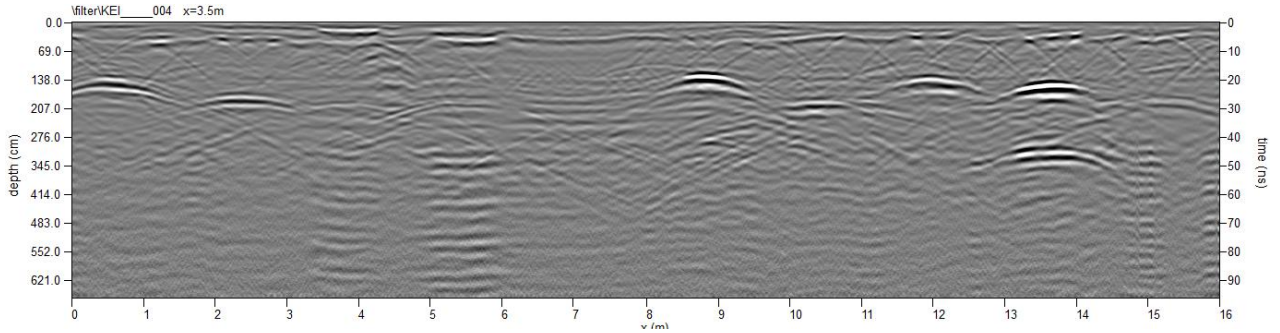

Figure 2.2.8: Background filter applied.

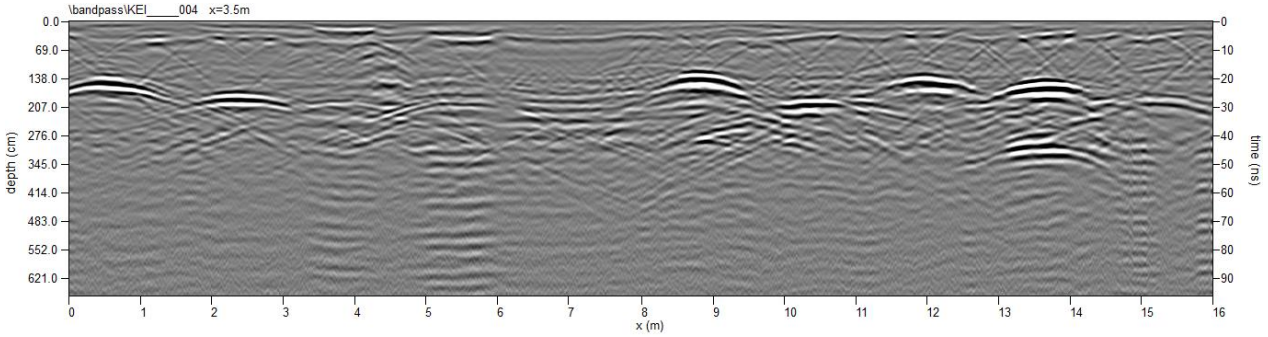

Figure 2.2.9:Bandpass filter applied. Low cut-off 103 MHz, high cut-off 662 MHz.

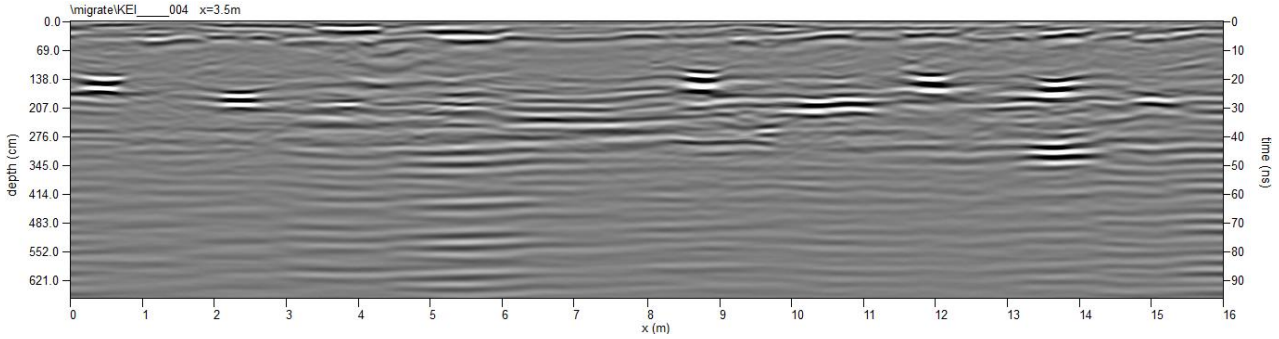

Figure 2.2.10: Migration applied. Hyperbolas have been collapsed to single reflections.

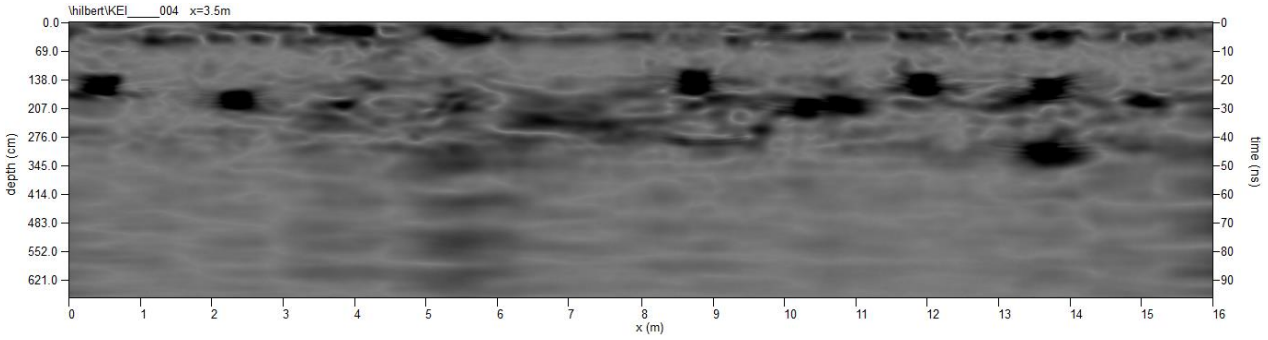

Figure 2.2.11: Hilbert transform applied. what could be a series of burials is now seen at around 30 ns, spaced evenly along the radargram. Grave 5 at 9.6 m contains no burial.

Once the processing of the raw radargram is completed, the processed radargrams can be further processed to yield time slices. Time slices represent the amplitudes of the recorded reflections mapped using multivariate interpolation and delivered as a raster interpretation of either depth or two-way travel time, across the entire GPR grid. Within GPR Slice this process is largely controlled by the program, but the allowable selectable options are given here. The thickness of the slices can be controlled by the number of slices, the percentage of overlap, or the time. The time of 3.7 ns was used with 45% overlap to create the slices. This time of 3.7 ns was suggested by Goodman, D. (pers conv 2024)

The action of desampling of the radargrams will take the spatial average of the pulses over a small distance along the radargram. These sampling distances are closely aligned to the profile spacing, in this study all profiles are spaced 50 cm apart. These spatial averages are then interpolated, either using an inverse distance weighted (IDW) average or by the Gaussian regression method of Kriging. This research used the IDW method with a weighting of 2 being applied. This method does not return a grid with a resolution as high as if Kriging is applied, but Goodman (2009:239) cautions the use of the Kriging interpolation method in archaeology. The process of creating the grid in a higher resolution may, inadvertently, not show larger reflection features. Following the creation of the grid using the IDW method a 3x3 low pass filter is applied. The final step in the grid process is a histogram autogain using 3 standard deviations.

2.2.2 Interpretation Methodology

At each study site there is one hyperbola that is constant, i.e. appears in radargrams in every visit. This provides the opportunity to measure the radar pulse velocity as it reflects from the same resistivity interface over an extended temporal period and compare this velocity to the available soil moisture at the time of data capture. This point will also be used to capture the resistivity and chargeability, as measured by the ERT, again over a temporal period. The distance along the radar and ERT lines is given for each site in Table 2.2.1.

Table 2.2.3: Hyperbola site used to capture velocity, resistivity and chargeability data.

Study Site	Row Number	Distance along Radar Trace (m)	ERT distance (m)
Bordertown	Row D	10.8	20.5
Keith	Row H	13.5	9
Pt Lincoln RSL	Row Q	14.5	15.5

The shape of the hyperbola is determined by the velocity of the pulse as it traverses the subsurface medium. Slower velocities will return narrow hyperbolas, while a faster velocity will return a broader hyperbola. The amplitude of the hyperbola will also be influenced by the changes in resistivity in the subsurface materials that the radar pulse encounters. The greater the change, the larger the amplitude of the wave that is reflected back (Conyers 2016:5).

Measuring the pulse velocity is part of the hyperbola search dialog in GPRSlice© and uses the hyperbola fit process. The left and right mouse keys are used to vary the synthetic hyperbola curve, allowing a good fit to the hyperbola displayed in the radargram, The result of this is shown in Figure 2.2.3, above.

2.3 Geophysical Forward Modelling Simulation

The electromagnetic pulse of a GPR, and the DC current of the ERT, are influenced by many physical and chemical characteristics as they pass through the subsurface. These influences include the frequency of the pulse, the various permittivity's the pulse and current encounter, the electrical conductivity, and the magnetic permeability. These characteristics of the subsurface matrix have all been outlined in previous sections. To give greater understanding of how these many subsurface characteristics influence the EM pulse and DC current, forward modelling is used. Forward modelling will give a more 'pure' result, as the characteristics that are built into the model will show in the results.

2.3.1 GPR Forward Modelling

The raw data from all of the study sites show multiple hyperbolas, so as a way of understanding this data obtained from the study sites and building on the discussion of decomposition (Section 1.2.5), a simulation algorithm has been utilized. This two-dimensional forward modelling was performed using GPRSIM© in an attempt to determine the source of the hyperbolas seen in the raw data. The synthetic profiles were generated for three scenarios, empty grave, grave with coffin and skeletal material, and grave with skeletal material. The latter was an attempt to simulate a burial site after the coffin had decomposed.

In the first series of models the permittivity of the background soil and fill were determined from the velocity of the radar waves seen in the radargrams from the Pt Lincoln RSL Cemetery site. The velocity of the undisturbed background soil was calculated from a hyperbola from a water pipe buried in the centre row, (ε_r = 12.7). The permittivity of the fill was calculated in two ways. Firstly, an average velocity was determined from a hyperbola located at the same place over all surveys (ε_r = 5.8 σ = 0.02). Then, following Damiata et al., (2013:275), another simulation was run with fill set at a higher permittivity and conductivity (ε_r = 8 σ = 0.01). The permittivity and conductivity for bone (ε_r = 13 σ= 0.149), was taken from Hammon et al., (2000:174). Following advice from D. Goodman, (pers comm 2023), a subsurface model for the burial contains three bands of soil, with increasing permittivity. Basic diagrammatic representations of each model are shown below and contains the permittivity and conductivity of the model elements. Greater detail of the settings used for these simulations are given in Table 2.3.1, with Figure 2.3.2 showing the three stratigraphic bands of soil, with corresponding permittivity's used for all subsurface materials.

Table 2.3.1: Settings used in GPRSim for the simulation.

Time window (ns)	60
Frequency (MHz)	400
Samples/Scan	1024
Overall Gain	10
Linear Gain	2
Exponential Gain	2

The theoretical wavepaths can be set, these are coded as to their path through the subsurface. These wavepath codes use R and T, R standing for reflection and T being transmission. Table 2.3.2 lists the wavepaths recorded in these simulations. R is a simple single reflection, RRR translates to three reflections, TR shows transmission through a permittivity change, followed by a reflection, etc. Graphical examples of these can be seen in Figure 2.3.1

Table 2.3.2: Wavepath codes used in these simulations.

R	RRRRR	TR
RR	TTRRTT	TTRRT
RRR	RT	RTRR

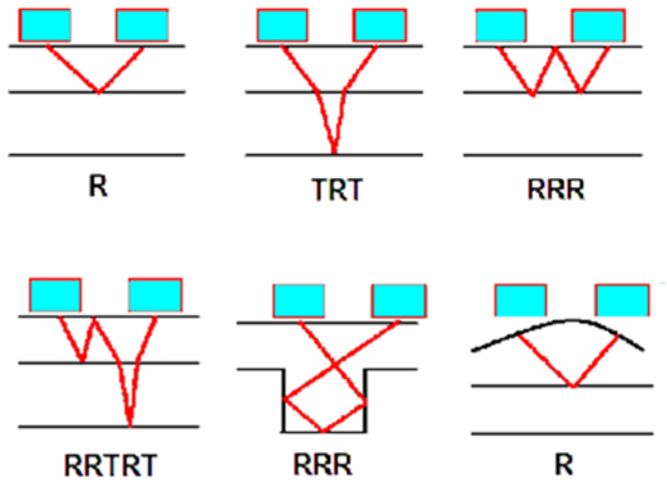

Figure 2.3.1: Graphical representation of various wavepaths used in simulation.

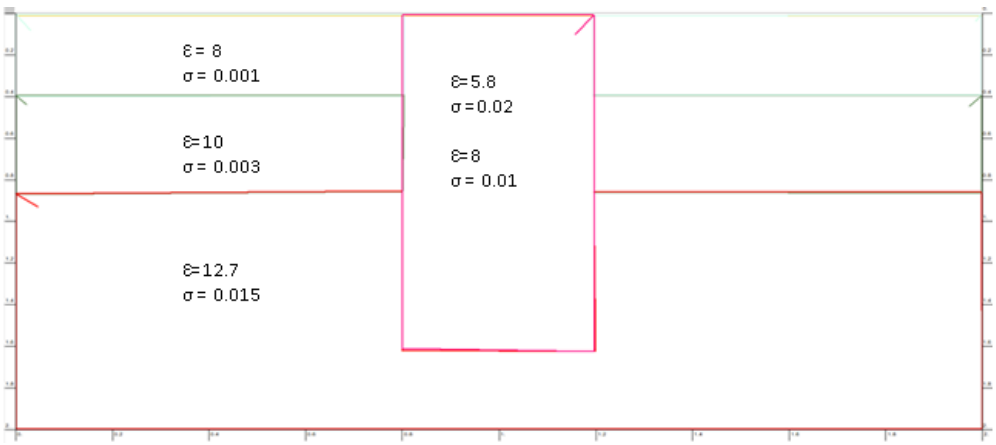

Figure 2.3.2: Simulation model for the cemetery burial. A model of a coffin, and skeletal meterial is added for further simulations. Permittivity and conductivity of each element is shown.

Pellicer (2010:172) has noted that permittivity interfaces with a low variation (0.0005) can be detected by raising the exponential gain to 10. The model for the empty grave, and the grave containing coffin and skeletal remains was re-run after the exponential gain was increased.

2.3.2 ERT Forward Modelling

The subsurface is a complex medium for measuring electrical resistivity, and the averaging of measured resistivity used in the Res2 results in difficulty in estimating true size and position of subsurface resistivity interfaces. As with GPR forward modelling, examining models of ERT behavior will give a clearer indication of the expected results over graves. The ERT models used the Res2DMOD program.

Two scenarios were modelled, an empty, backfilled grave, and a backfilled grave with skeletal remains. The elements of these two models followed the GPR models with three stratigraphic layers with decreasing resistivity. These resistivities are calculated from the conductivity used in each element of the GPR model. The arrays used in these models were the same as were used in data capture, the Wenner and Diploe-Dipole arrays. The electrode spacing was set at 0.5 m.

The resistivities used in the various models are given in Table 2.3.3

Table 2.3.3: Resistivity values used in the ERT Forward modelling

Element	Permittivity (F/m)	Conductivity (S/m)	Resistivity (Ωm)
Top stratigraphic layer	8	0.001	1000
Mid stratigraphic layer	10	0.003	333
Lower stratigraphic layer	12.7	0.015	67
Backfill soil	5.8	0.02	50
Backfill soil (high resistivity)	8	0.01	100
Skeletal material	13	0.149	6.7

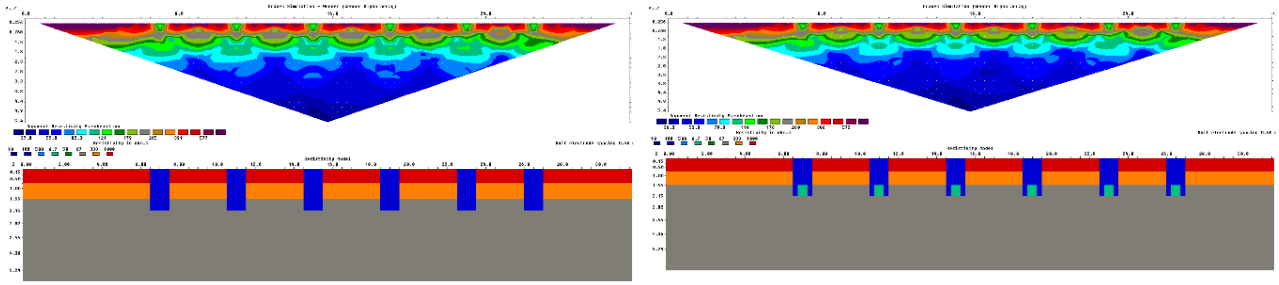

Figure 2.3.3: Resistivity model for Wenner array. Left, the backfilled grave, and right, the backfilled grave with skeletal remains.

2.3.3 Summary

The use of simulations that mimic a simplified version of one of the test sites has given a glimpse into how certain characteristics of the subsurface may influence the raw data. It must be stressed that the

subsurface is a complex medium, and the models used in these simulations do, by no means, fully replicate that complexity. However, having an understanding of how an EM pulse, as well as the DC current, will interact with the physical characteristics that may be seen in the subsurface around a burial site is valuable in the interpretation of the data in this research.

2.4 Electronic Resistivity Tomography (ERT)

The ERT data was recorded in slightly different ways across the three study sites. These differences were largely dictated by the usable space in each study site. In all sites, the ZZ Resistivity Universal 64 full channel resistivity meter was used to control the switching within protocols, with ZZ Resistivity Data Acquisition software used to set up arrays and record data capture. The site at Keith used an electrode spacing of 25 cm, with Bordertown and the Pt Lincoln RSL used a spacing of 50 cm. The protocols used in this study were the Wenner and Dipole-Dipole array. Survey parameters were set at 120V; 1 second on, 0.3 seconds off; IP and Res survey type; and K value set at 19, with all sites using 64 electrodes.

ERT data was processed using the Res2DINV© software. Prior to data import into Res2DINV© the raw data collected was converted using ZZGeo proprietary software into separate Wenner and Dipole-Dipole .inv files. These files are then imported into an excel spreadsheet with the recorded resistivity, chargeability, and electrode pairings, saved as a .txt files ready for importation into Res2DINV.

As described in Chapter 1.5.4 the processing of this data in Res2DINV software uses a least squares inversion mathematical approach. This approach, along with the wide application of Res2DINV within other geophysical resistivity methods, raises many options within the program. An overview of the options used in this study, along with justification of their use is as follows.

After import, raw data can be edited to remove outliers. The raw data is displayed as in Figure 2.4.1, the data points are in relatively straight lines. Outliers, or corrupt data points deviate from these straight lines, and can be deleted.

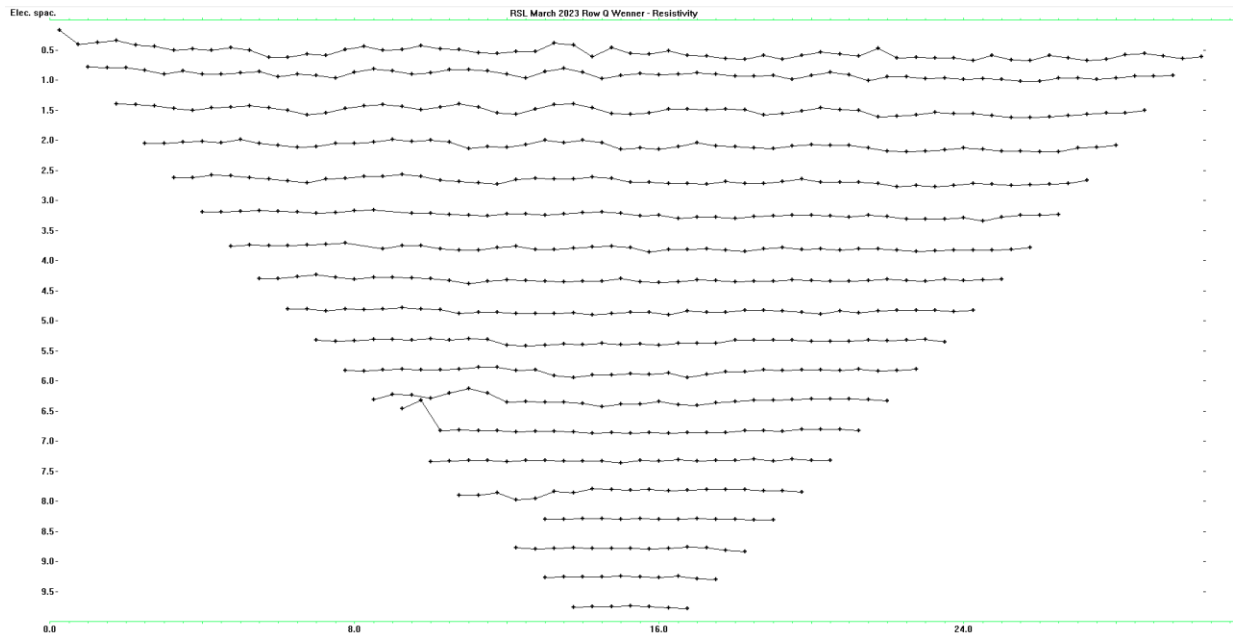

Figure 2.4.1: Raw data to be edited.

2.4.1 Processing of ERT data

There are many processing options within the Res2DInv software. Below are the options that have been changed to process the data gathered for this research, and the reasoning behind these decisions.

The type of inversion to be used can be selected. This option allows the selection of a smooth (L2 norm) or blocky (L1 norm) inversion method. The L1 method is used when the subsurface could be generally homogenous, but these homogenous layers are separated by sharp boundaries. This method is also recommended if the data contains outliers or random noise (Loke et al. 2003:182; Pellicer 2010:199). Under standard least-squares methods (L2) the square of the data misfit is used. This method then, is particularly sensitive to bad data points, ie those with larger misfits. By minimizing the sum of the absolute values of the data misfit, the L1 norm data misfit measure uses the standard least-squares formulation and iteratively reweights the least-squares method (Claerbout and Muir 1973; Loke et al. 2003:183). Comparison results can be seen in Figure 2.4.2. Following a series of tests over all study sites, the L1 inversion was chosen for Wenner data, and L2 for Dipole-Dipole.

There is an option to use a Standard Gauss-Newton or an incomplete Gauss-Newton least squares method. The incomplete is recommended where the number of data points is > 3000. The incomplete method uses an iterative linear conjugate-gradient approach to solve the least-squares equation, with a reported 1% accuracy. As the datasets in this study are well under the suggested 3000 data point limit, the standard method will suffice.

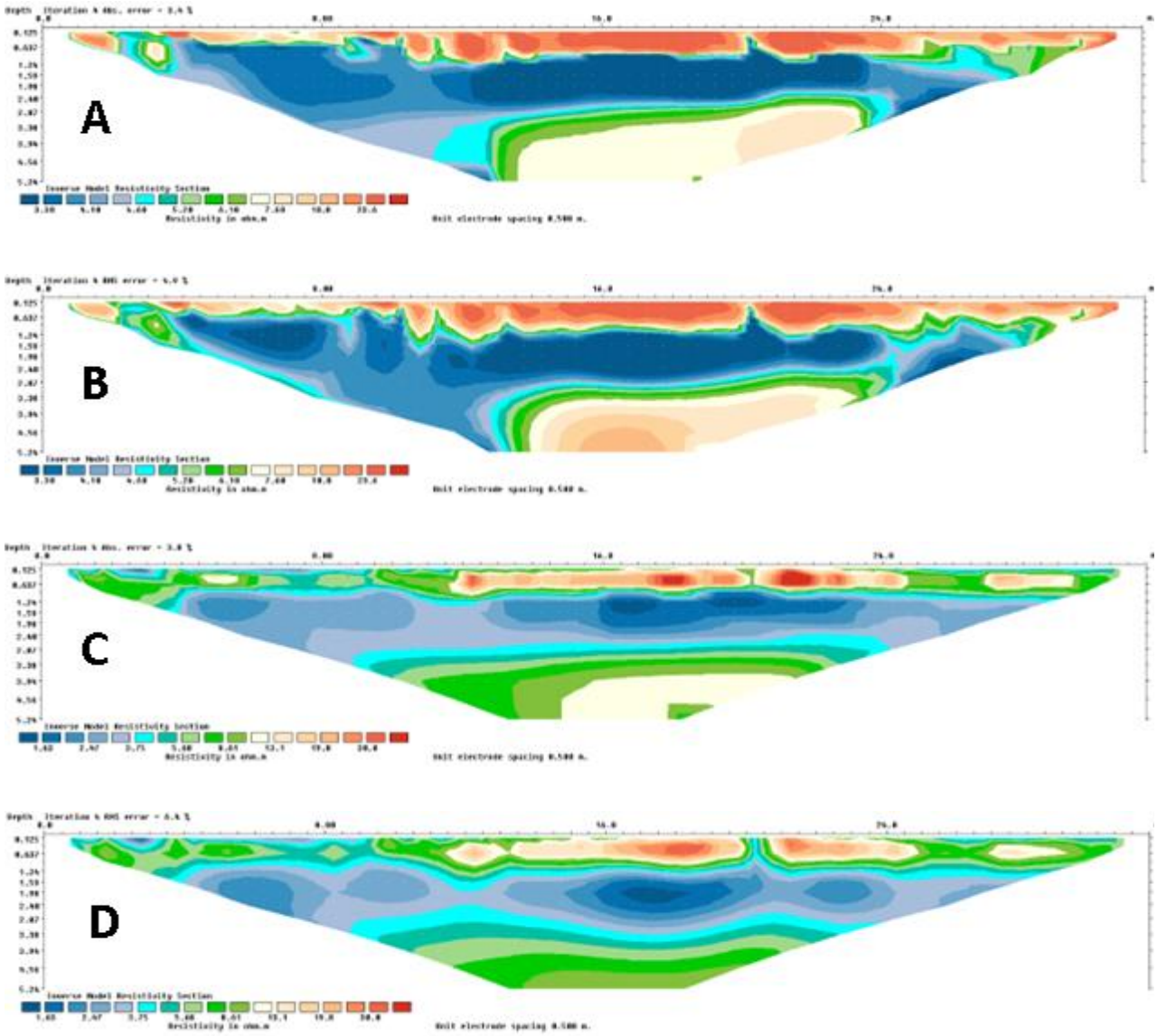

Figure 2.4.2: Comparison of the Li and L2 norm inversion methods. A – Dipole-Dipole inverted with the L1 norm, B – Dipole-Dipole inverted with the L2 norm. C- Wenner inverted with the L1 norm, and D – Wenner inverted with the L2 norm.

The data is recorded with the Induced Polarization (IP) measurement included. The addition of the IP data allows further options in processing. Following Kemna et al. (2000), a complex resistivity method is used for the inversion of apparent resistivity and IP data. Typically, the data misfit for the log of resistivity values shows a much larger range than the apparent IP values. Under normal processing conditions, this gives greater weight to reducing the data misfit of the apparent resistivity, as compared to the apparent IP. This can be controlled within the IP data weight option. The damping function affects the changes in IP values in each iteration as these are typically smaller than the change in apparent resistivity. By setting this option at a value of less than 1, (typically 0.1 – 0.25), a greater change in the values of IP is allowed.

The battery power source used in these ERT surveys does not always supply a suitable amount of current for a reliable IP survey, (typically < 1 amp), this can tend to introduce noise into the recorded IP values. This noise is seen as large values, and to counter this tendency a cutoff value is specified. In this case, the cutoff is set high, at 899 mV/V.

The upper and lower limits of the IP values can be specified. Aarhus GeoSoftware (2022:94) suggests that this range be kept under 1000 mV/V, although Brandes (2005) has shown that negative IP values are of worth, especially in the presence of flocculating clay in the subsurface matrix. As these studies have recorded a range of positive and negative values, this option of setting upper and lower limits has been disabled. As a follow on from this option, the IP model transformation can be specified. The square-root option will ensure that the IP values are always positive, and additionally, as over the course of this study, many negative values were recorded, this is not used. The second option is to use a range-bound model. This range bound will enforce the range set in the previous option, and as this has not been set, neither of these options are selected.

As noted above, this program uses the complex resistivity method, as outlined by Kemna et al. (2000), and as such, the optimal resistivity and IP, models are calculated simultaneously. Often the range of the resistivity data misfit is much larger than the range of the IP data misfit, and this will inadvertently show a more accurate resistivity model at the expense of the IP model in each iteration. Setting IP data weights, (see above), will help equal the iterations somewhat, but in this option, after the initial iteration, the IP data undergoes a separate inversion, so minimizing the data misfit of the IP data.

The smoothness constraints can be changed within the IP inversion. The robust inversion is discussed above, and as the subsurface matrix in this study has sharp interfaces of resistivity values, the L1 inversion method was selected. A different smoothness model can be selected for the IP inversion, ie use a more robust inversion for resistivity and a smooth constraint for the IP inversion, however, as outlined above, the subsurface matrix here calls for a robust inversion model for both the resistivity and IP inversions.

To further separate the resistivity and IP iterations an additional option of running separate inversions is offered. This option allows for separate inversion calculations for resistivity and IP, and the IP does have a small influence on the inversion of resistivity this option was chosen here.

After inversion is carried out data misfit points can be removed via the RSM error statistics dialog. These errors are shown in the form of a histogram that shows the distribution of the data points according to the percentage difference between the measured and calculated apparent resistivity values. What data points that are removed is user defined, although the RES2DINV help files suggest removing points that show a percentage difference >100% is recommended, see Figure 2.4.3

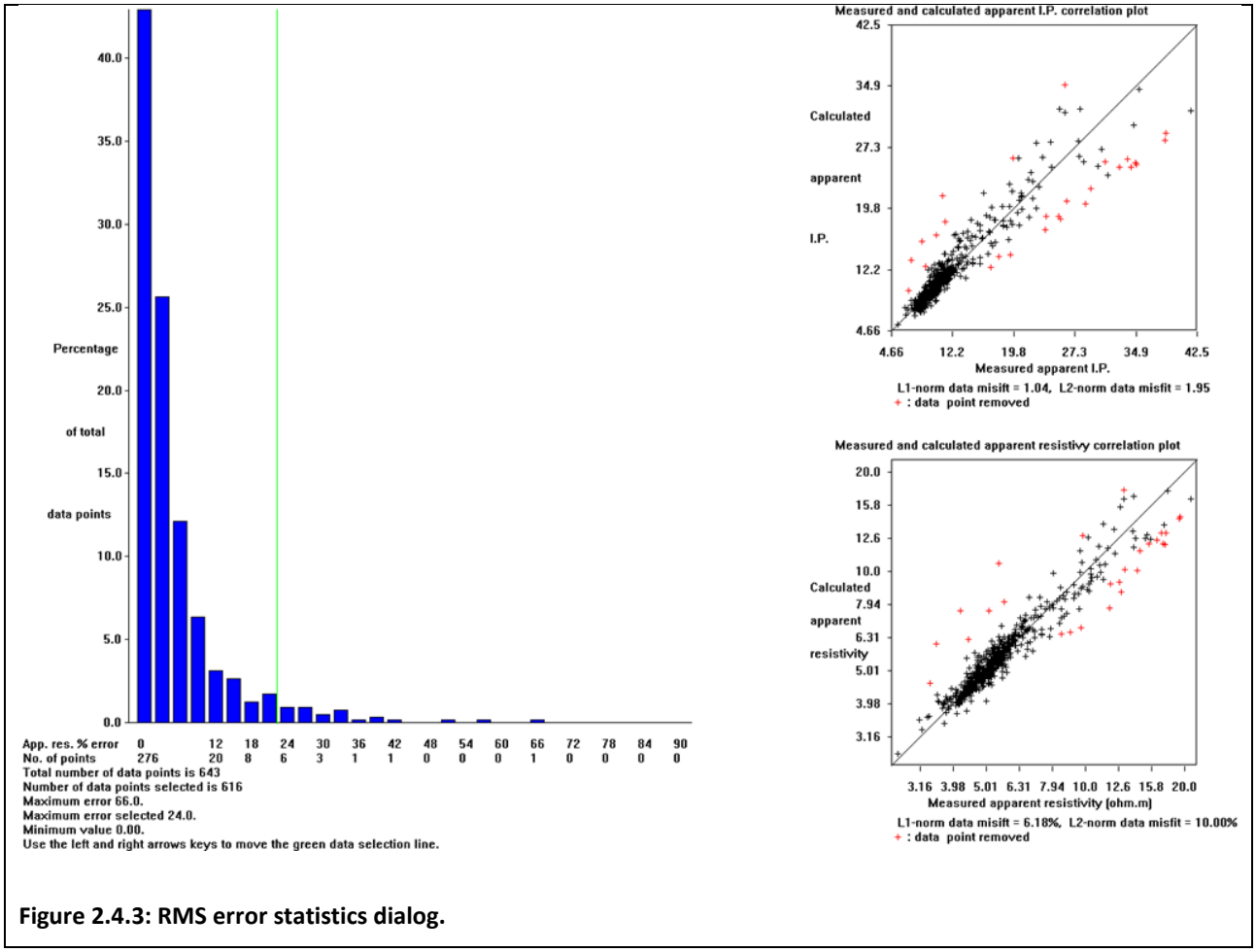

Figure 2.4.3: RMS error statistics dialog.

2.4.2 Interpretation Methodology

After inversion and RMS error removal, results are saved as xyz files. These files give the electrode configuration mid-point, the depth of measurement, the resistivity, conductivity and IP values. These resistivity values will be gathered from the burial that returns a reflection from each visit.

2.5 Soil Testing

Soil samples were gathered at depths of 30 cm, 60 cm, 100 cm, and 150 cm. One sample was taken at each depth from a grave in each study site cemetery, see Figures 2.5.1, 2.5.3, and 2.5.4. These samples were subject to Magnetic Susceptibility; X-Ray Fluorescence Spectroscopy (pXRF); grain size analysis; and Effective Cation Exchange Capability (ECE).

Each sample was tested for Magnetic Susceptibility using the Bartington MS3 coupled to the MS2B Dual Frequency Sensor, Figure 2.5.2. Samples were weighed and then tested twice. Drift correction was applied prior to testing, with a 5-second high frequency and a 5 second low frequency test applied to each sample. The high and low frequency tests were both repeated for each sample. Magnetic values were recorded in SI units.

The initial grain size analysis was carried out using the Endecotts sieve shaker, Figure 2.5.2. These sieves complied with ISO 3310. Sieve sizes were 4 mm, 2 mm, 1 mm, 0.5 mm, 0.25 mm 0.125 mm, and 0.063 mm.

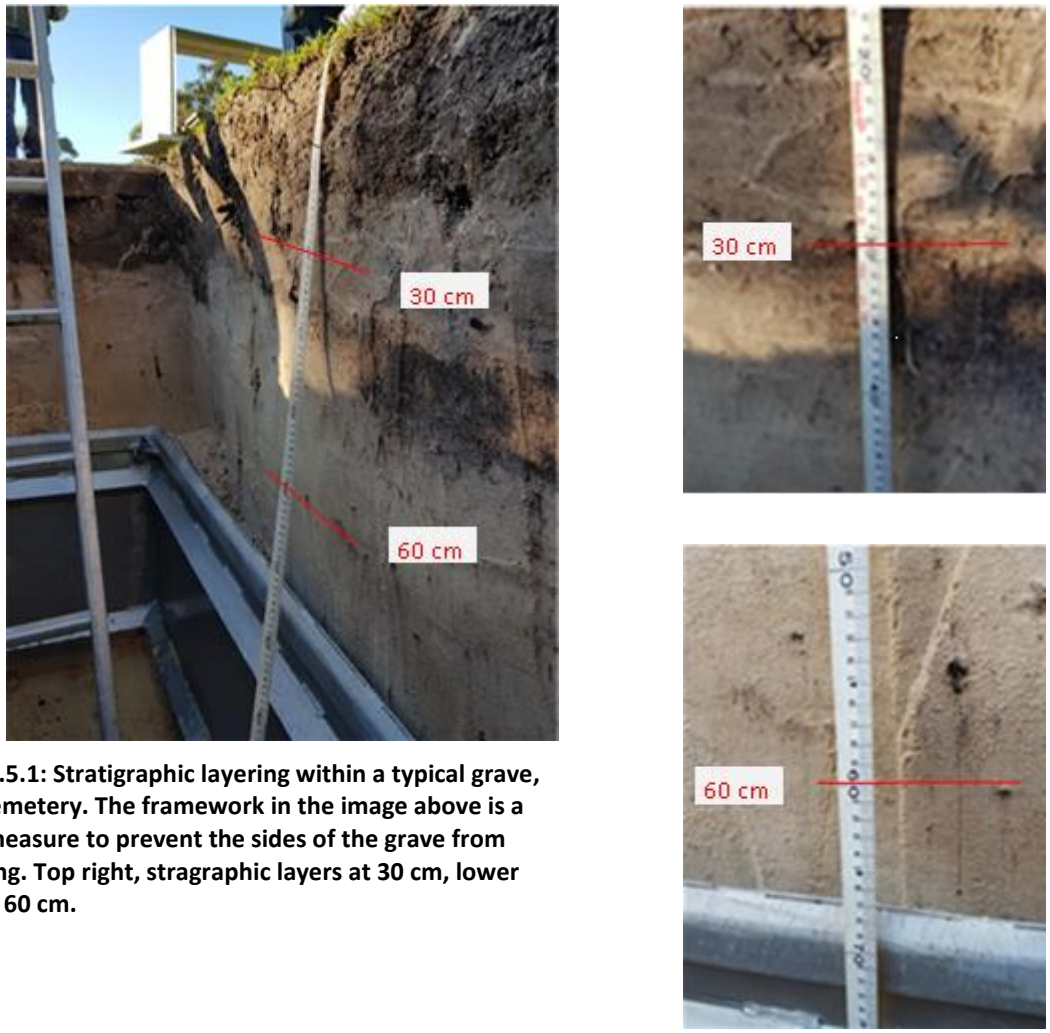

Figure 2.5.1: Stratigraphic layering within a typical grave, Keith Cemetery. The framework in the image above is a safety measure to prevent the sides of the grave from collapsing. Top right, stragraphic layers at 30 cm, lower right, at 60 cm.

These sieve sizes are in accordance with the Phi-Wentworth scale, which is a logarithmic scale, developed to add emphasis to the smaller grain sizes. Further grain size analysis was carried out on the RSL and Bordertown samples by using a Malvern Mastersizer 3000 laser diffraction unit. The decision to apply additional grain size analysis to these two sites is further discussed in Chapter 3.

The pXRF analysis was carried out using the Bruker Tracer 5i handheld unit, in Geoexploration 2020 mode. Sample cups of 32 mm were used with two shots of each sample being recorded.

Figure 2.5.2: The Endecotts four sieve shaker, and right, the Bartington MS3 and MS2B Magnetic Susceptibility sensor.

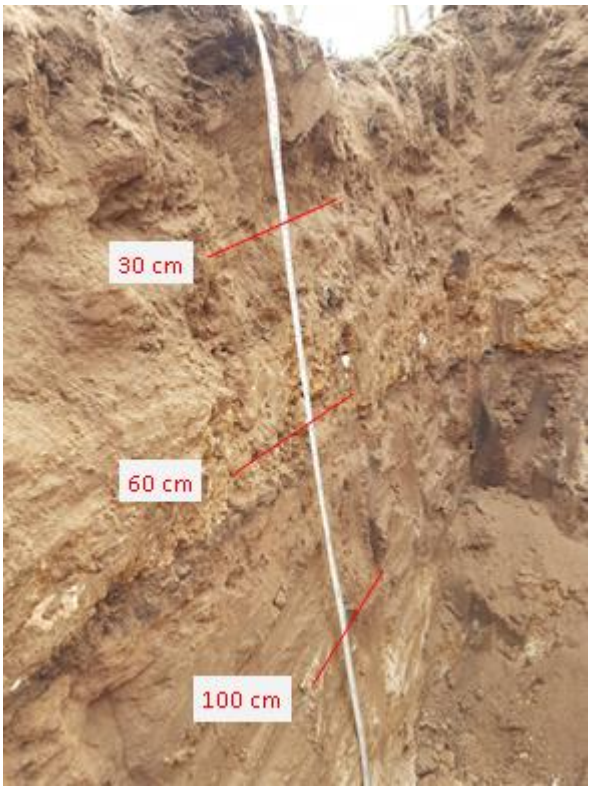

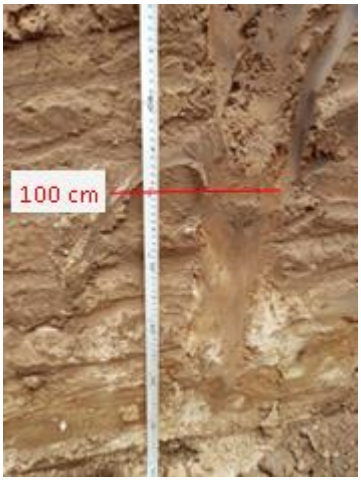

Figure 2.5.3: Stratigraphic layering within the grave, Bordertown Cemetery. Top right, stratigraphic layers at 30 cm and 60 cm, lower right, at 100 cm. Soil samples were taken at each site from these depths.

Effective Cation Exchange Capability (ECE) testing was carried out by the Southern Cross University Environmental Analysis Laboratory. The exchangeable cation test followed the methods of Rayment and Lyons (2011).

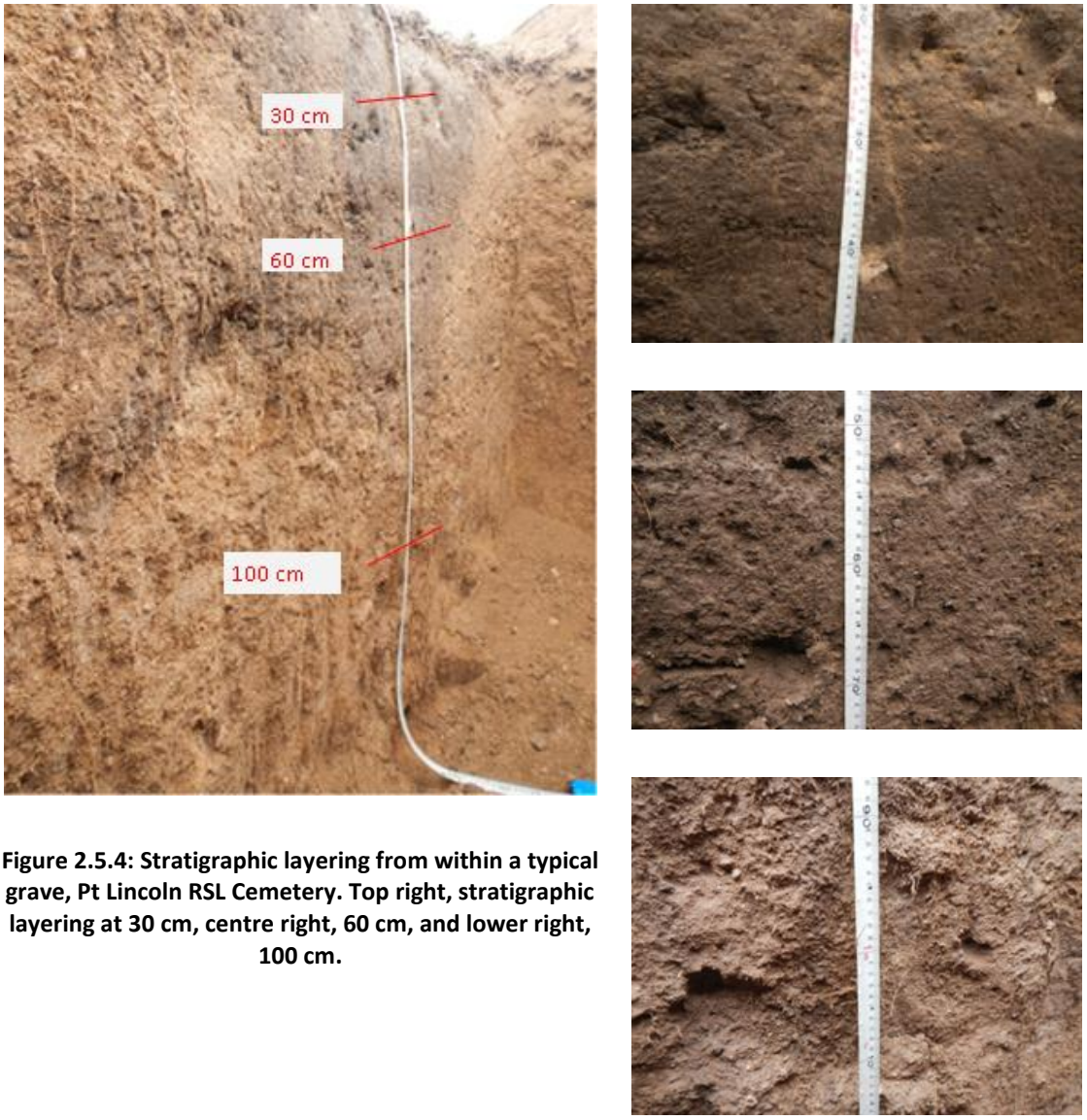

Figure 2.5.4: Stratigraphic layering from within a typical grave, Pt Lincoln RSL Cemetery. Top right, stratigraphic layering at 30 cm, centre right, 60 cm, and lower right, 100 cm.

2.6 Soil Moisture

Soil moisture was recorded using the Sentek Drill & Drop Bluetooth soil moisture probe. This unit records soil moisture levels at 10 cm intervals, from 15 cm to 85 cm. To install, a hole is bored into the ground, Figure 2.6.1, and the tapered probe is then pushed firmly into the hole. As the casing of the probe is tapered, an airproof fit between probe and soil is achieved, eliminating any possibility of water seeping

down between probe and soil. Data is uploaded to a cloud-based service, with moisture plots available online. Data has been downloaded and plotted for this record of study. Measuring the moisture levels in this way gives a very accurate picture of the amount of available subsurface moisture, irrespective of environmental factors, such as evaporation rates and surface runoff.

Figure 2.6.1: Installation of the moisture probe. Here the hole is drilled using supplied auger and electric drill.

In addition to this soil moisture data, the daily rainfall recorded at each site was obtained from the network of weather recording stations controlled by the Bureau of Meteorology (BOM). This data was downloaded from their web portal. Discrepancies in this data were very soon made apparent, and the correction of this data is ongoing, in conjunction with the BOM.

2.7 Study Sites

As outlined in Section 1.9 these study sites were chosen as they all were garden cemeteries and presented optimal above-ground conditions for the geophysical methods utilized in this study. This type of cemetery is not frequently found in the often-dry regional areas of South Australia, as water for irrigation is often scarce. A quick search via Google Earth at cemeteries located in major cities and towns throughout South Australia showed this scarcity quite clearly. The age of burial could not be controlled, for obvious reasons, and these ages are shown in Tables 1.9.1,1.9.3, and 1.9.5. The graves in Rows “P” and “Q” at the Pt Lincoln RSL cemetery were hand-dug in the period 1984 – 1988 by the author of this research. The rows that were

chosen to be used in this research at the Bordertown and Keith Cemeteries corresponded to that date range as closely as possible. The GPR lines and orientations of the rows used in this research are shown for each site in Figure 2.7.1.

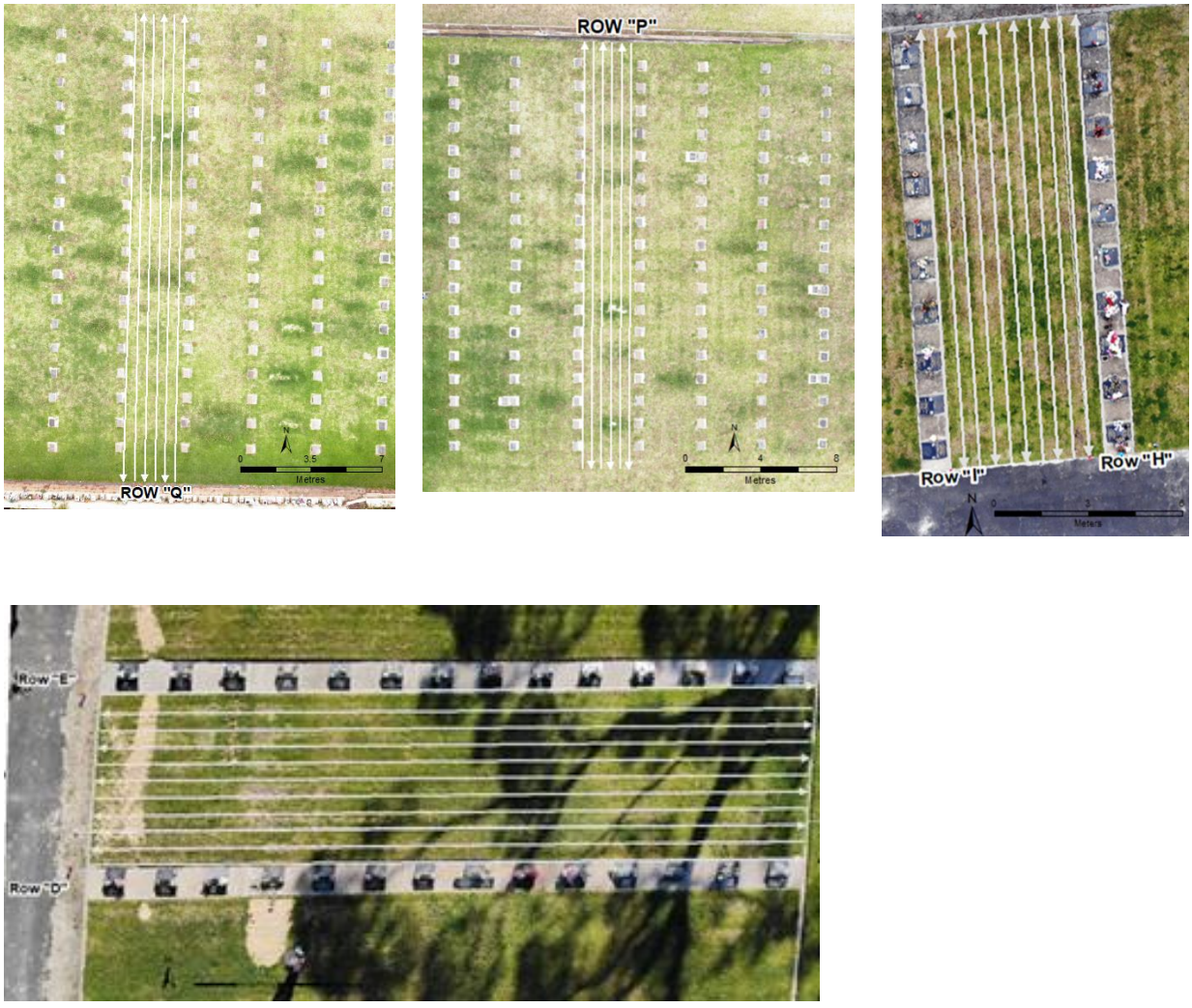

Figure 2.7.1: Study sites with direction of GPR lines shown. Bottom, Bordertown rows "D" & "E", top left, RSL row "Q", top centre RSL row "P", and top right, Keith Rows "I" & "H".

Each site was visited 4 times per year, as close as possible to every 3 months. To fit in with the Schmidt precipitation ratio model, it would have been preferable to have timed the visits to precipitation events, but it soon became apparent that this would have been impracticable, due to the precipitation frequency experienced over the length of the study, (see Appendix B for rainfall data for each site over the study period)

2.8 Summary

This chapter outlined the methods of data capture and the subsequent processing of this data. The data was captured in response to the research questions posed in Chapter 1, and followed the requirements of the data, as outlined in Chapter 2. The data in this research was captured using common methods, as could be followed by students, or those in the geophysics industry. The same methodology was followed with the processing of this data, even though more complex methods have sometimes been suggested. By keeping the capture and processing of the data to common methods and consistent through all study sites, the data stays as a constant in the research, along with the soil, and therefore it is the moisture in the soil that becomes the variable.

3 RESULTS

3.1 Introduction

This chapter presents the results from this research. These results are grouped by study site, and each site will contain the Ground Penetrating Radar (GPR) results, the Electrical Resistivity Tomography (ERT) results, the results of the soil testing, and soil moisture data. Also presented are the results from the GPR and ERT forward modelling.

The data from the GPR surveys is presented as radargrams. Each of these radargrams has a distance (m) scale on the bottom, on the left is a depth (cm) scale, and on the right is a travel time (ns) scale. The data is organised firstly by study site, then by date of data collection. Only 3 radargrams for each row will be shown in this section, these three lines pass over the widest part of the burial, and so will present the optimal possibility of containing reflections from the subsurface. Figure 3.4.1 demonstrates this. Along the top of each radargram is a series of dates. This is the position of the grave, and the burial date. A complete set of radargrams for each site is presented in Appendix A.

The ERT data is presented as an inversion plot. On the left of each inversion plot is the depth (m), along the top is a series of dates. This indicates the position of the grave and the date of burial. Both resistivity and Induced Polarisation data is presented, inverted using the Wenner and Dipole-Dipole protocols.

The inversions for the Wenner protocol and the Induced Polarisation, plus the inversion from the Dipole – Dipole protocol, and Induced Polarisation are shown, with the depth for all ERT models cut to a depth of 2 m.

A summary of the key results is presented in Table 3.15.1.

3.2 Ground Penetrating Radar Simulation

3.2.1 Introduction

The act of digging a grave, burying human remains, and refilling the grave will anthropogenically alter the physical characteristics of the soil. The theoretical concepts of these actions were introduced in section 1.3.4, with a description of the ways the physical characteristics, such as permittivity, conductivity, resistance, and arrangement of pore spaces could be detected. To further understand these assumptions, and examine how, in theory, the interactions of EM pulse and the subsurface matrix may appear in radargram form various simulations were performed.

A simulation of the GPR pulse was modeled under various scenarios, and following Bevan (1991:1311; Bladon et al. (2011:249) and Nobes (1999:10), these scenarios included a backfilled empty grave, a grave with a wooden coffin and skeletal material, and a grave with skeletal material and collapsed coffin. These simulations were to mimic a legal burial in a cemetery. Further to these simulations, the model was changed to show an empty burial pit, and a burial pit with skeletal remains. In these simulations the permittivity and conductivity of the soil was changed, following the literature, (Damiata et al. 2013:275; Hammon et al. 2000:174), these changes assumed a higher permittivity of the grave backfill. Simulations were also run with a higher exponential gain, this follows Pellicer (2010:172), who noted that subsurface permittivity interfaces of low variation (0.0016%) can be detected with a higher gain applied. This section will present these results.

3.2.2 GPR Simulation in a Cemetery Context

The model used to simulate a legal burial in a cemetery used three distinct soil horizons. These horizons were set with increasing permittivity ranging between Ɛ= 8 and Ɛ=12.7. This follows the permittivity calculated from a hyperbola from a buried pipe in the Pt. Lincoln RSL Cemetery. The grave shaft was set at a depth of 1.6 m and a width of 60 cm, with straight sides and perpendicular floor. This mimics a modern grave, but from the authors grave digging experience, older, early 19th century graves, were not always so neatly dug.

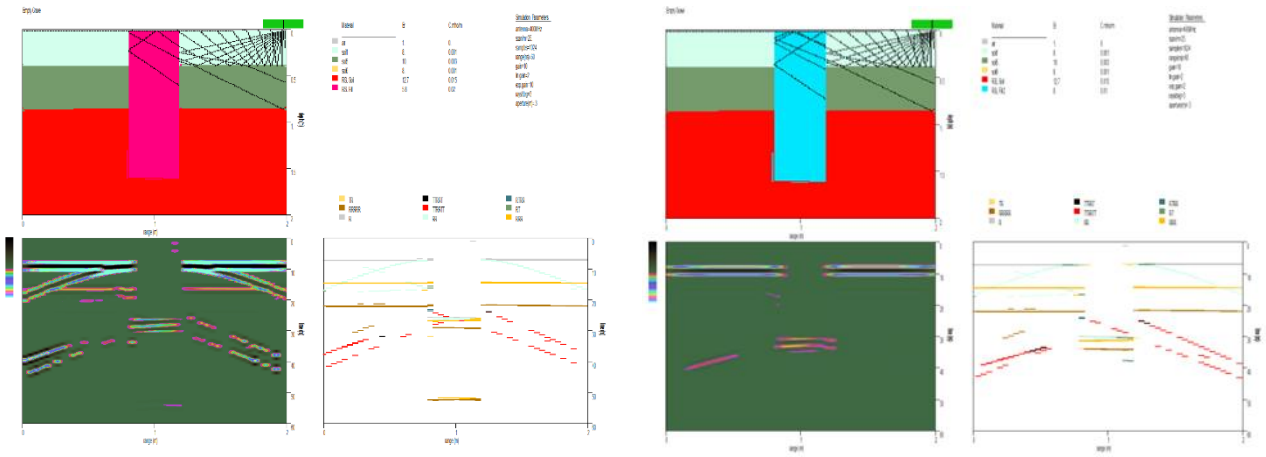

Figure 3.2.1: Left, empty grave. Backfilled soil permittivity = 5.8, exponential gain = 10. Right, empty grave. Backfilled soil permittivity = 8, exponential gain = 2.

Figure 3.2.1 shows the backfilled grave shaft with no burial. This simulation shows the reflections from just the shaft and the disturbed backfill. On the left there is a higher exponential gain applied. This shows the oblique reflections, a greater number of reflections of the second stratigraphic break, and a small increase in the reflections from the lid of the coffin.

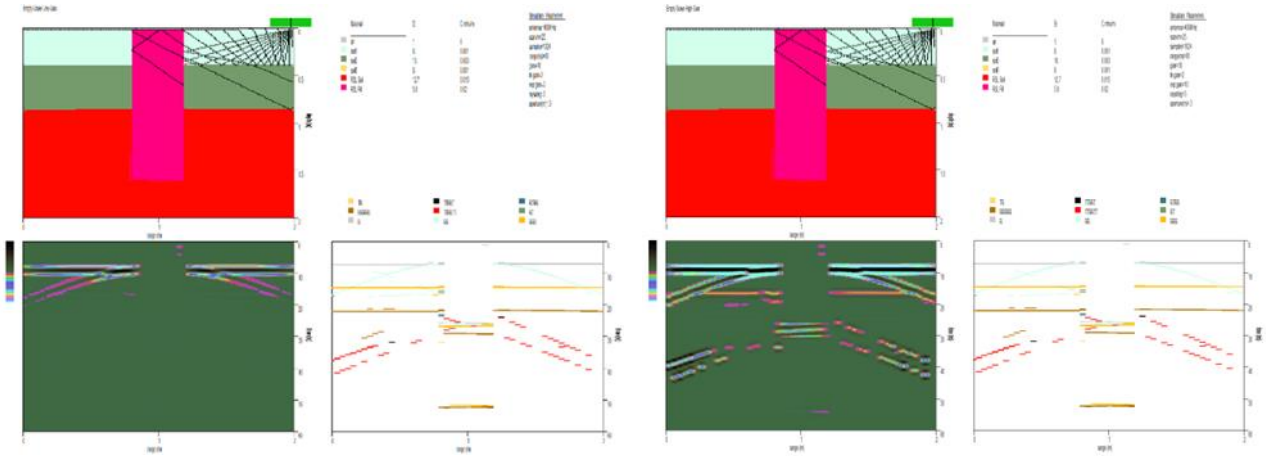

Figure 3.2.2: Left, Empty grave, backfilled soil permittivity = 5.8, exponential gain = 2. Right, empty grave, backfilled soil permittivity = 5.8, exponential gain = 10.

Figure 3.2.2 shows two simulations, with the backfilled soil having the same permittivity. The higher exponential gain used in the simulation of the right, again detects the permittivity interfaces of the stratigraphy, as well as the lid of the coffin. The oblique reflections can be seen, and from the legend these

are from two transmissions + two reflections + two transmissions (TTRRTT). This highlights the complexity of the path the EM pulses take through the subsurface.

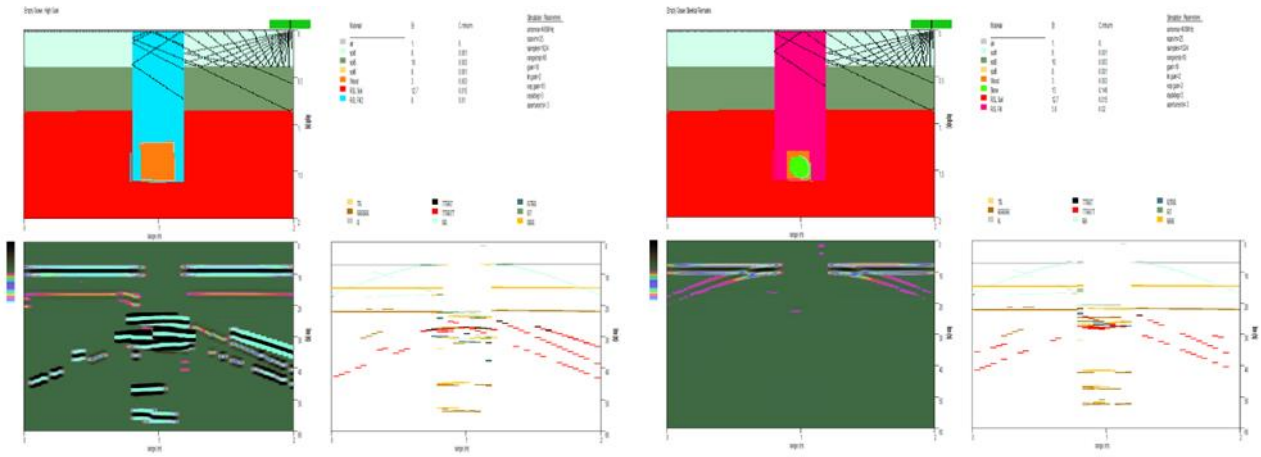

Figure 3.2.3: Left, backfilled grave with intact coffin. Backfilled soil permittivity = 8, exponential gain = 10. Right, backfilled grave containing coffin and skeletal remains. Backfilled soil permittivity = 5.8, exponential gain = 2.

A wooden coffin was added with a permittivity Ɛ=3. It was attempted to draw a coffin with thin wooden walls and an air-filled void inside, but the graphics limitations of the GPRSim program prevented this. Inside this wooden coffin was added a rounded shape representing skeletal material, Ɛ=13, Figure 3.2.3.

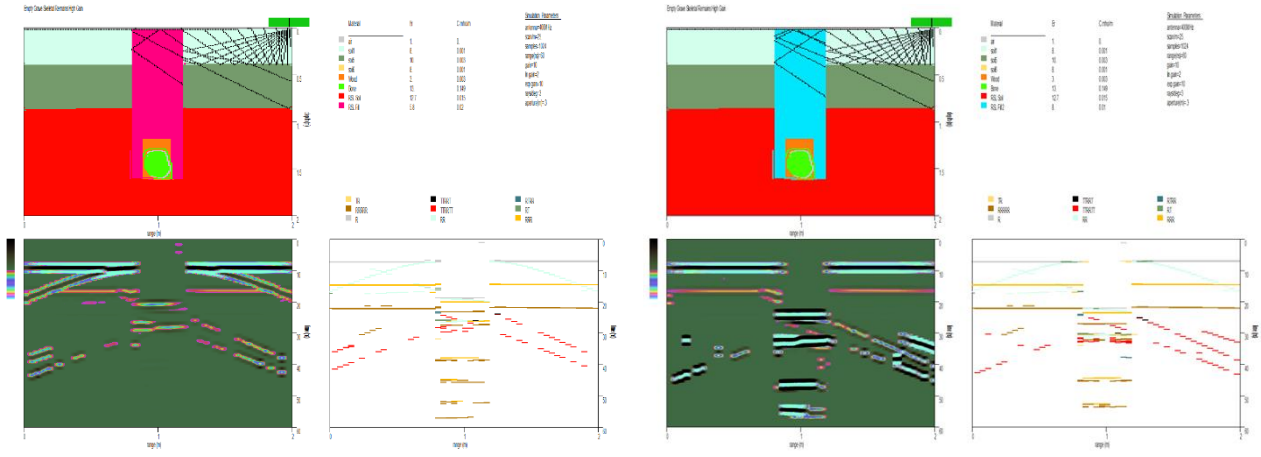

Figure 3.2.4: Left, backfilled grave, wooden coffin, and skeletal remains. Exponential gain = 10, and permittivity of backfilled soil = 5.8. Right, backfilled grave, wooden coffin, and skeletal remains. Exponential gain = 10, and permittivity of backfilled soil = 8.

Figure 3.2.4 illustrates the difference in backfill permittivity. The reflections seen below the grave shaft are categorized in the legend as RRR and RRRRR, meaning they are the result of many sequential reflections. These reflections could be assumed to be from the coffin or the bottom of the grave shaft. Figure 3.2.5 shows the same backfilled grave with skeletal remains, backfill permittivity is lowered to 5.8.

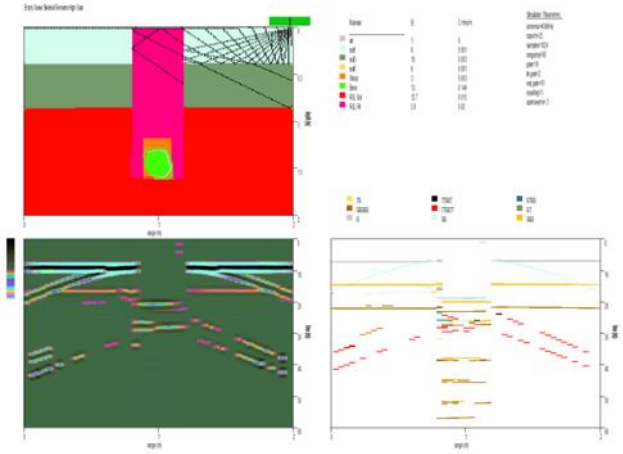

Figure 3.2.5: Backfilled grave with skeletal remains and intact coffin. Backfilled soil permittivity = 5.8, exponential gain = 10.

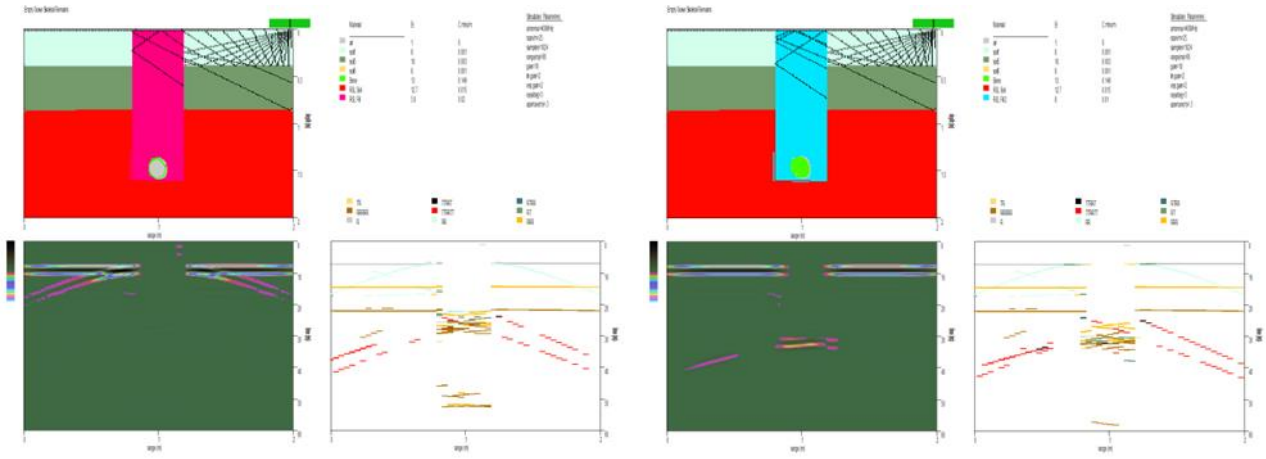

Figure 3.2.6: Left, backfilled grave with skeletal remains, no coffin. Backfilled soil permittivity = 5.8, exponential gain = 2. Right, backfilled grave with skeletal remains, no coffin. Backfilled soil permittivity = 8, exponential gain = 2.

Figure 3.2.6 shows a theoretical response from a GPR to a backfilled grave after the coffin has collapsed. This could be a common scenario in older burials, or burials in acid soils. There are a number of reflections

in the grave shaft that are from multiple reflections, (RRRRR, TTRRTT, and RRR), again highlighting the complexity of the radar path.

3.3 Electric Resistivity Tomography Simulation

The simulation models for ERT followed the same methods and aims of the GPR simulation. The models used were an empty, refilled grave, and a refilled grave with skeletal remains. The resistivities of each of the three stratigraphic layers were the same as in the GPR simulation. The electrode spacing was set to 50 cm, and both Wenner and Dipole-Dipole arrays were used.

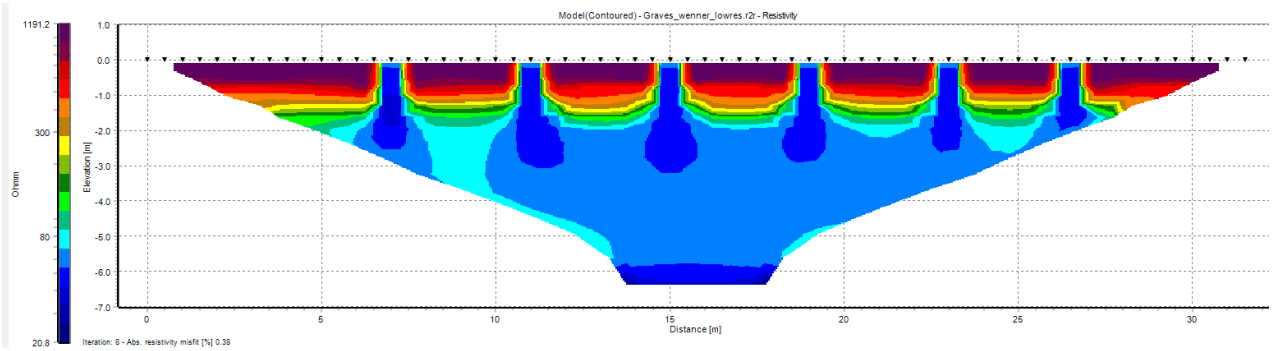

Figure 3.3.1: Result from simulation of the Wenner array, with low resistivity backfill.

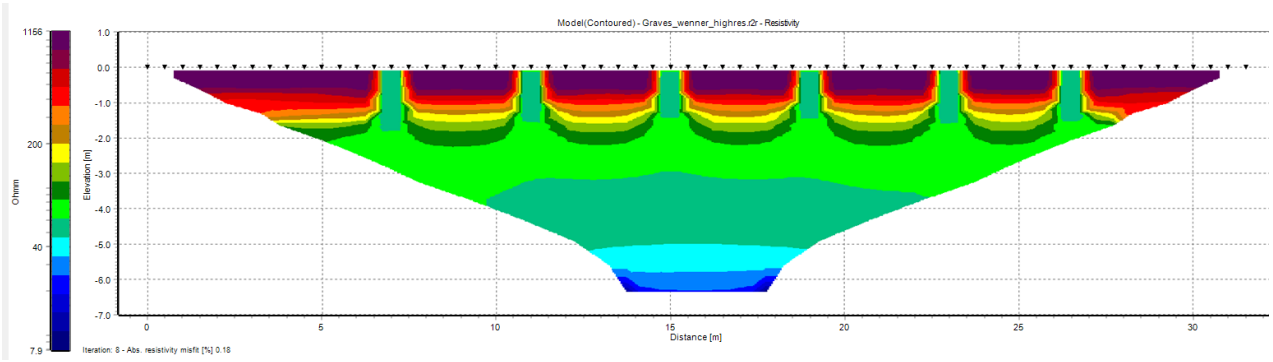

Figure 3.3.2: Result from simulation of the Wenner array, with high resistivity backfill.

The Res2MOD simulation of the Wenner array shows the six burial shafts with areas of higher resistivity in the spaces between them. These areas of higher resistivity are present in both the high, (Figure 3.3.2) and low resistivity fill models, (Figure 3.3.3). These extend to a depth of approximately 15 cm. Below these are layers extending the entire length of the ERT line of lower resistivity, in the high resistivity, (100 Ω-m), backfill model, to 40 cm, and the low resistivity model to the base depth of 60 cm. In the original model, Figure 3.3.1, the grave shafts extend to a depth of 200 cm, and this does not transfer to the simulated result.

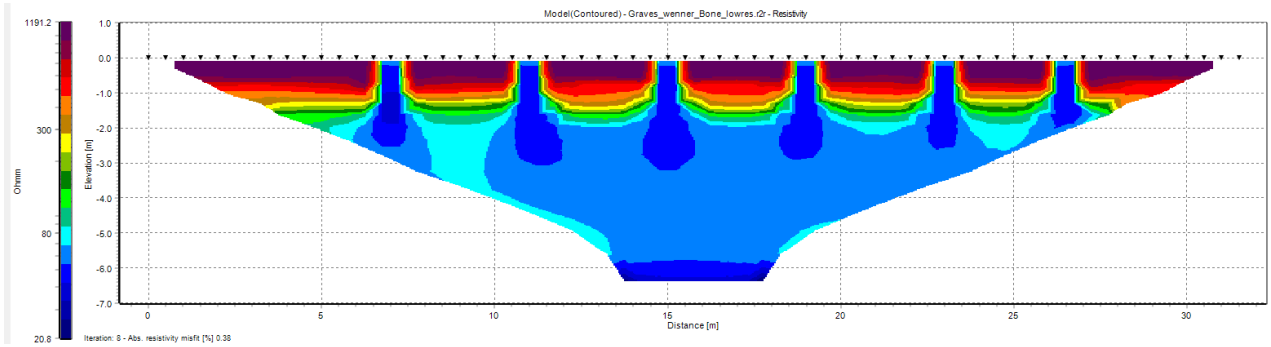

Figure 3.3.3: Result of simulation of Wenner array, backfilled grave with low resistivity backfill and skeletal remains.

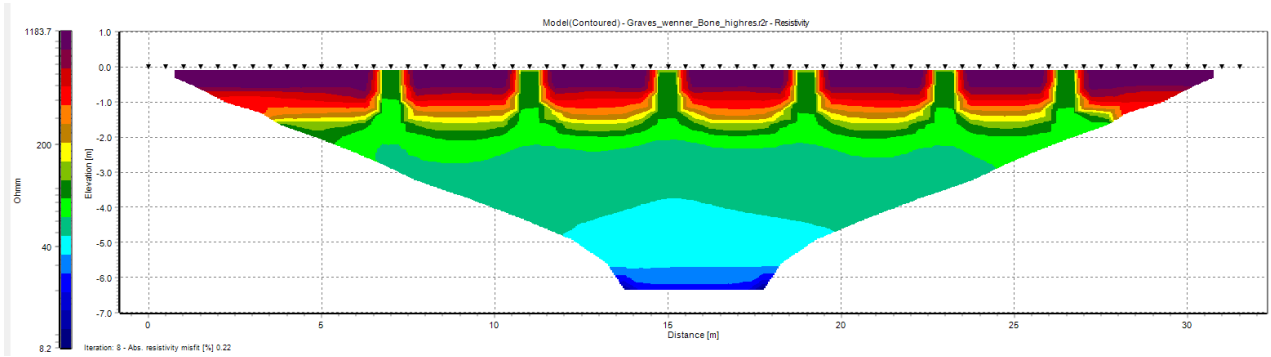

Figure 3.3.4: Result of simulation of Wenner array, backfilled grave with high resistivity backfill and skeletal remains.

The results of the Wenner array simulation containing skeletal remains show resistivity patterns of a similar nature to the non-skeletal remains model, Figure 3.3.4. The inclusion of skeletal remains in the bottom of the burial shaft has very little impact on the final model.

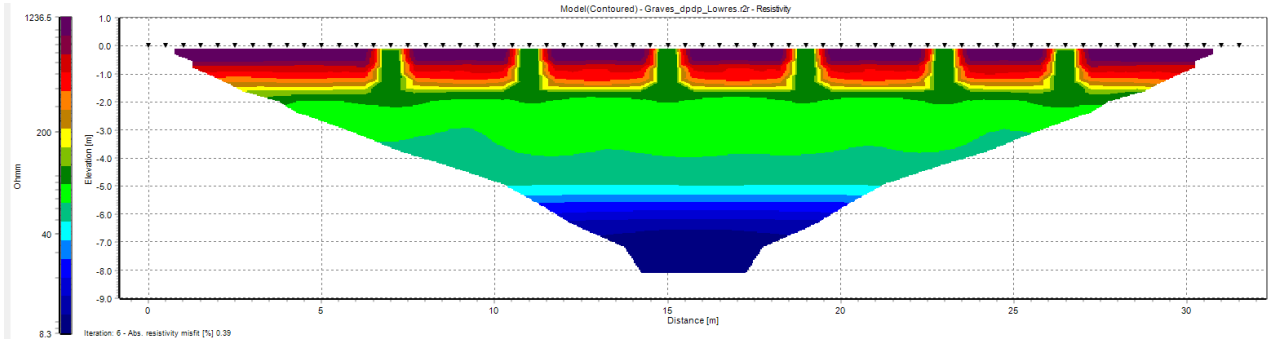

Figure 3.3.5: Result from simulation of Dipole-Dipole array, with low resistivity backfill.

The simulation from the Dipole-Dipole array shows the six burial shafts, between these are areas of higher resistivity. These areas of higher resistivity extend to a depth of approximately 20 cm, below this depth the resistivity to approximately 60 Ω-m, Figure 3.3.5. This area below the depth of 20 cm in the model using the higher resistivity backfill, (100 Ω-m) shows a homogenous soil profile, all at a resistivity of 60 Ω-m, Figure 3.3.6.

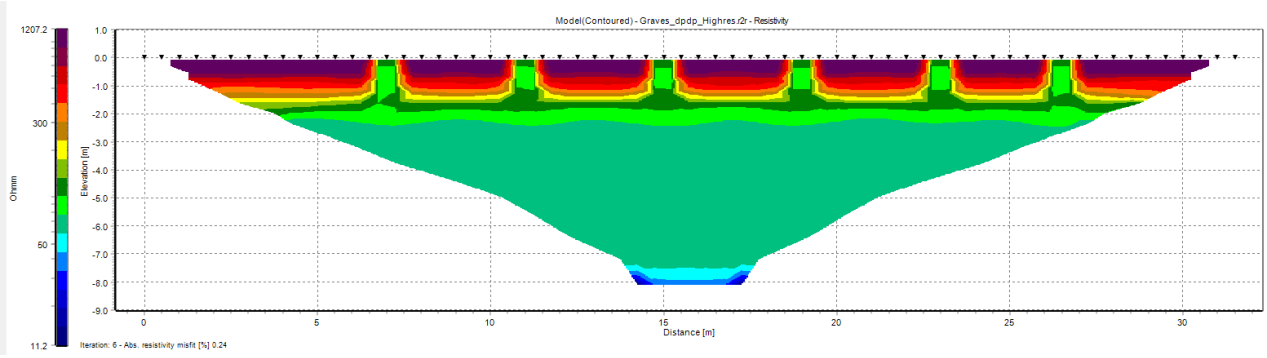

Figure 3.3.6: Result from simulation of Dipole-Dipole array, with high resistivity backfill.

The models that include skeletal remains do have some differences from the results with no skeletal remains. The model with higher resistivity backfill, (100 Ω-m), has returned the areas of higher resistivity between the burial shafts, but below these are areas approximately 2 m across of resistivity approximately 50 Ω-m, Figure 3.3.8. Surrounding this area is a homogenous area of approximately 60 Ω-m. The model with lower resistivity backfill, (50 Ω-m), shows these areas of approximately 50 Ω-m as extensions of the burial shaft, with small lower resistivity areas, (30-40 Ω-m) included in them, Figure 3.3.7.

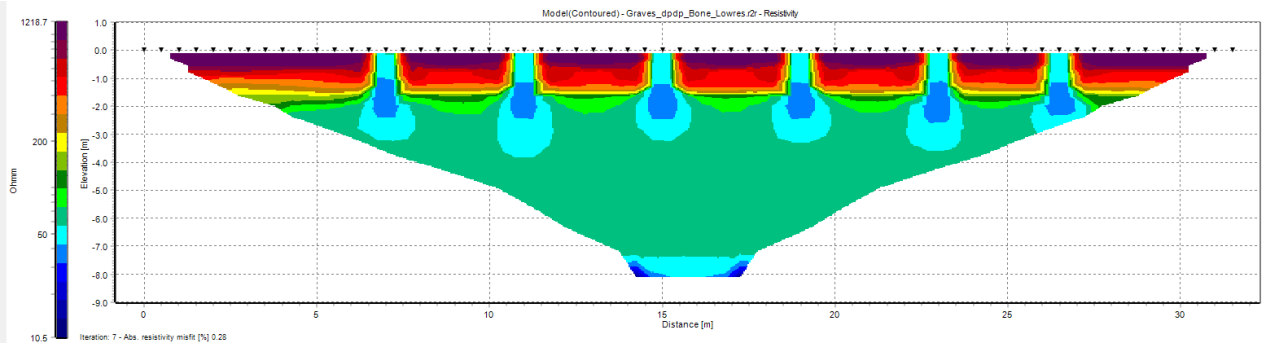

Figure 3.3.7: Result of simulation of Dipole-Dipole array, backfilled grave with low resistivity backfill and skeletal remains.

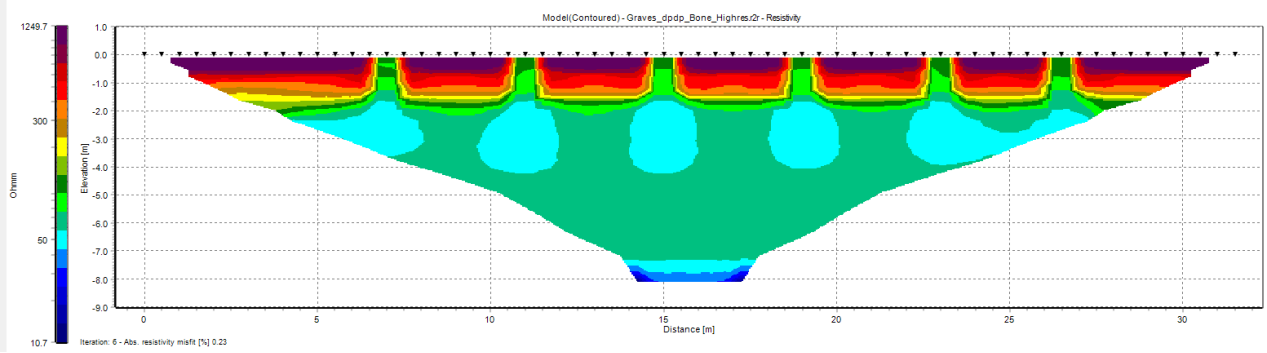

Figure 3.3.8: Result of simulation of Dipole-Dipole array, backfilled grave with high resistivity backfill and skeletal remains.

3.3.1 Summary

When utilizing geophysical methods to locate unmarked graves, there are a small number of theoretical resistivity interfaces that may reflect the GPR pulse. These being the disturbed backfill, the coffin, the edge of the grave shaft, skeletal remains, the moisture laden bottom of the grave shaft, or any combination of these. Constructing a simulation of these common interfaces gives a greater understanding of what the origins of reflections seen in a radargram may be. The simulations shown here are insightful, in that they show possible reflections with no interference from any other subsurface resistivity interface. The ERT models were set to show the changes in resistivity of the stratigraphic layers, as well as backfilled burial shafts. It should be noted that the ERT models included burial shafts to a depth of 200 cm. No results of these models included a change in resistivity below 30 cm that would indicate a burial shaft, despite the stratigraphic layers being set with resistivities of 1000 Ω-m, 333 Ω-m and 67 Ω-m. The differences in resistivity of these layers

3.4 Keith Cemetery

3.4.1 Introduction

Data for the Keith Cemetery was collected from rows H and I. This grid was 16x5 meters, and 11 lines of data were collected each visit, covering all of the grassed area, see Figure 3.4.1. Row H contained 9 burial sites, with row I containing 10 burial sites. GPR data was successfully collected on all visits, however, suitable ERT data was only collected on six occasions. The months within the period 2020-2023 that visits to this site are listed in Table 3.4.1

Table 3.4.1: Dates of visits to Keith Cemetery, and type of data collected.

GPR Data	ERT
Aug 2020	Aug 2020
Oct 2020	
Jan 2021	Jan 2021
Jan 2022	Jan 2022
May 2022	
July 2022	July 2022
Sept 2022	
Dec 2022	
March 2023	March 2023

From all the radargrams collected from Keith, one from Row H showed a reflection that was consistent from all visits. From these 11 radar lines, this one line will provide a soil velocity that will be compared to the resistance from the ERT data. The velocity and resistivity values are compared to soil moisture and/or seasonal rainfall. The results from the GPR show all nine of the burials being identified on 44% of the visits. Resistivity values range from 127.3 – 790.7 Ω-m for the Wenner array, 1233.8 – 144 Ω-m for the Dipole-

Dipole array. Chargeability values range from 739.8 – 27.6 nV/V for the Wenner array, and 747.9 – 41.5nV/V for the Dipole-Dipole array.

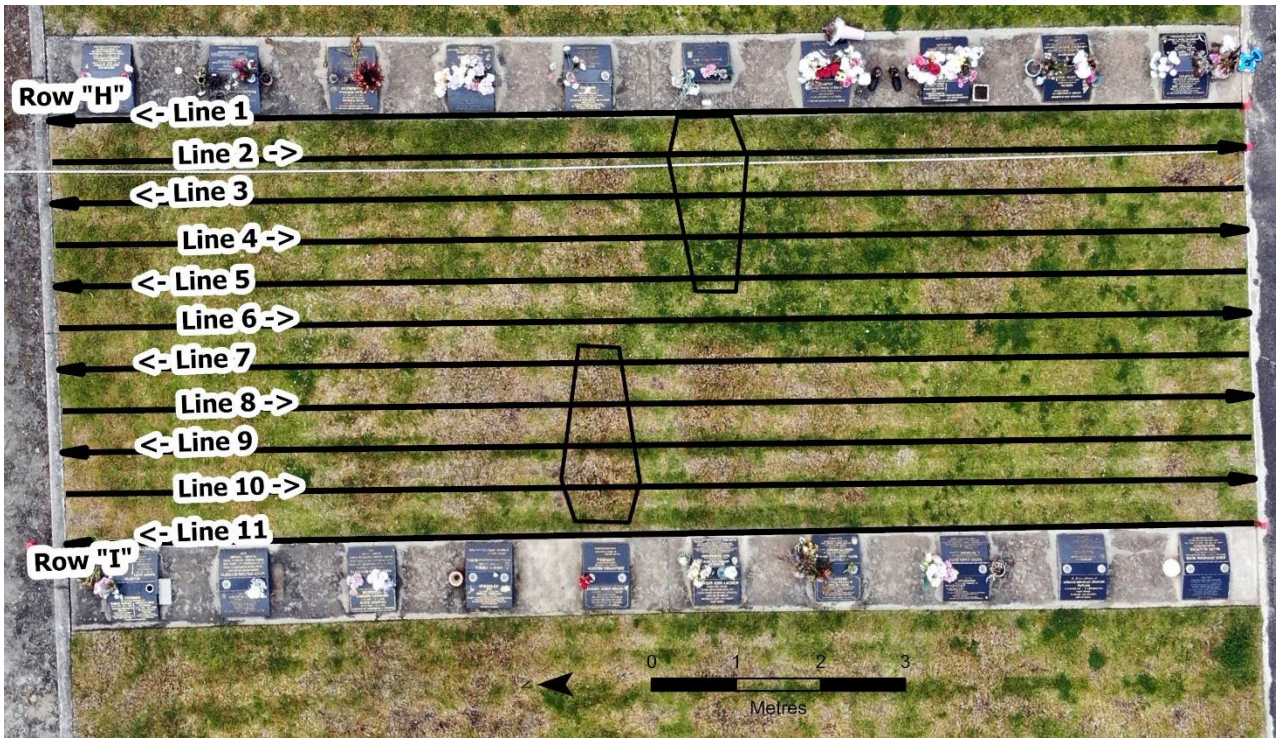

Figure 3.4.1: Rows H and I, Keith Cemetery. The GPR lines are shown, and as the data is collected in a "zigzag" method, every second line is in the opposite direction. The outlines of two graves are shown to illustrate that for Row H, lines 2,3 & 4 are over the widest point of the coffin, i.e. the shoulder and torso. The ERT line is between line 2 and line 3 in Row H.

3.5 Keith Cemetery Geophysics

3.5.1 August 2020

Data was collected in August 2020. There was 5 mm of rainfall in the week before this data was collected, and the ten-month rainfall plot is shown in Figure 3.5.1.

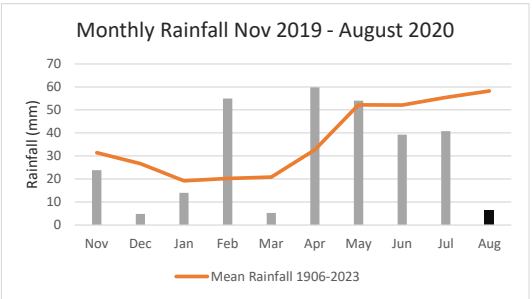

Figure 3.5.1: Rainfall in August 2020 for the ten months prior to data collecting. Months that the study site was visited over this period in black. (Rainfall and Temperature data from bom.gov.au)

The three radargrams from Row H, Figures 3.5.2,3.5.3, and 3.5.4, show a series of reflections (Figure 3.5.3, line 3 shows these clearly) ranging in depth of 110 – 165 cm. These reflections are quite planar in shape and show varying amplitude but similar polarity and are associated with the burials. Reflections from the burial shaft in the third grave, (date 2018), are highlighted in line 2, Figure 3.5.2. Highlighted as B in Figure 3.5.3, line 3, shows quite strong reflections from an empty plot that has not seen any anthropogenic interference. Highlighted in line 4, Figure 3.5.4, is a stratigraphic layer at approximately 30 cm depth. All burials can be identified in these radargrams. Attenuation of this data starts at ~300 cm.

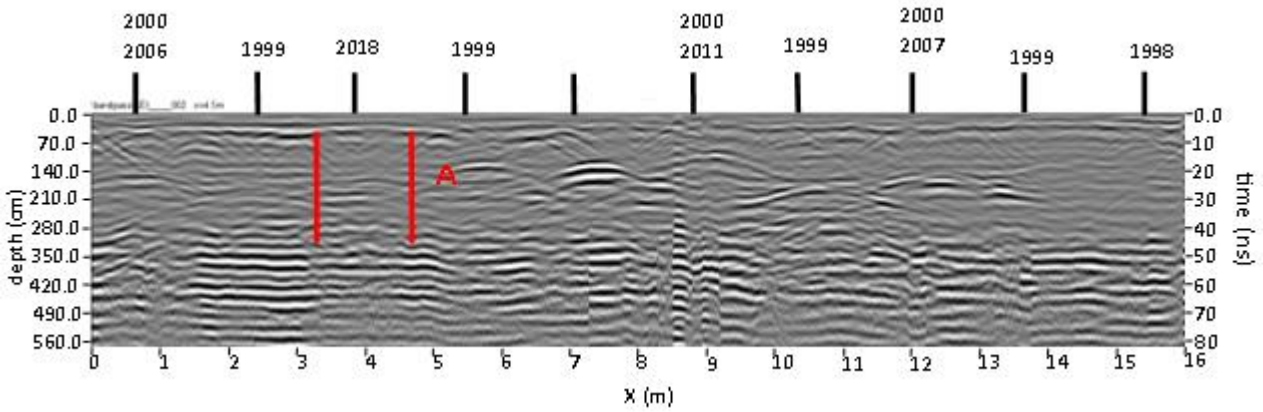

Figure 3.5.2: Keith Cemetery, August 2020, Row H, line 2. The reflections from the grave cut are highlighted in red.

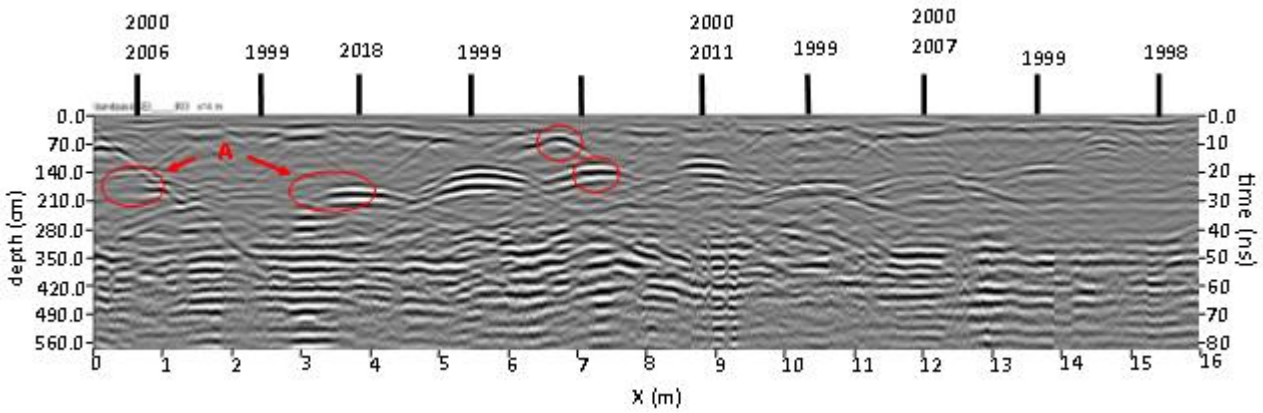

Figure 3.5.3: Keith Cemetery, August 2020, Row H, line 3. "A" shows the reversed polarity of the reflections, and "B" show reflections from a vacant plot.

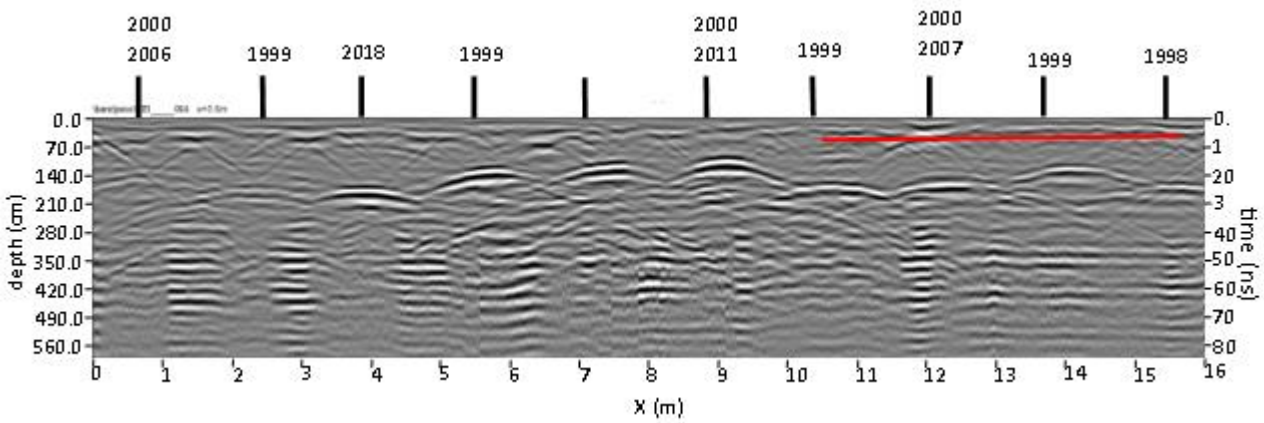

Figure 3.5.4: Keith Cemetery, August 2020, Row H, line 4. Highlighted in red is a horizontal reflection running along the entire radar line.

The resistivity and induced polarisation data was captured using the Wenner and Dipole – Dipole arrays, with electrode spacing of 25 cm. The resistivity data captured with the Wenner array, Figure 3.5.5, shows a large band of higher resistivity (>900 Ω-m) along the entire length of the ERT Line, this is between a depth of 20 cm and 1000 cm, and is above the burials. The maximum depth of penetration is ~1.2 m, shallower than expected.

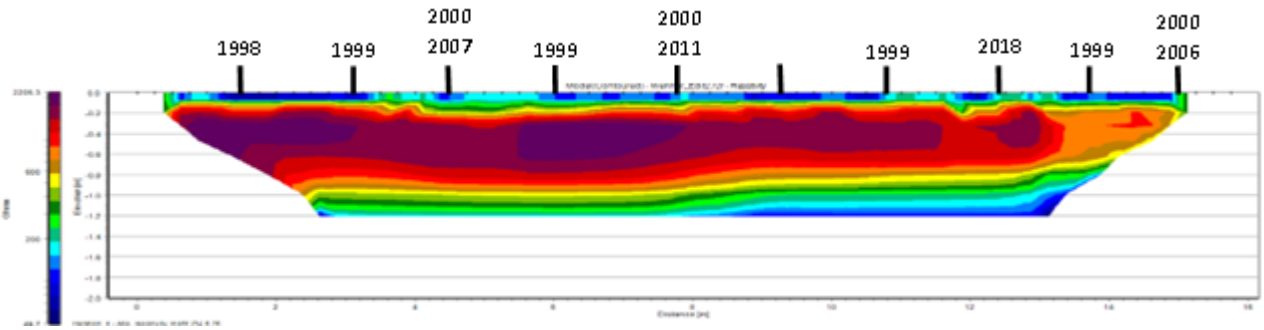

Figure 3.5.5: Resistivity data captured with the Wenner array, August 2020. Keith Cemetery, Row H.

The IP inversion from the Wenner data, Figure 3.5.6, also shows a thin layer to a depth of 20 cm. This thin layer shows chargeability values greater than 350 nV/V. These small areas of higher chargeability do not seem to be associated with burials. Below this to the maximum penetration depth is an area with chargeability less than 200 nV/V.

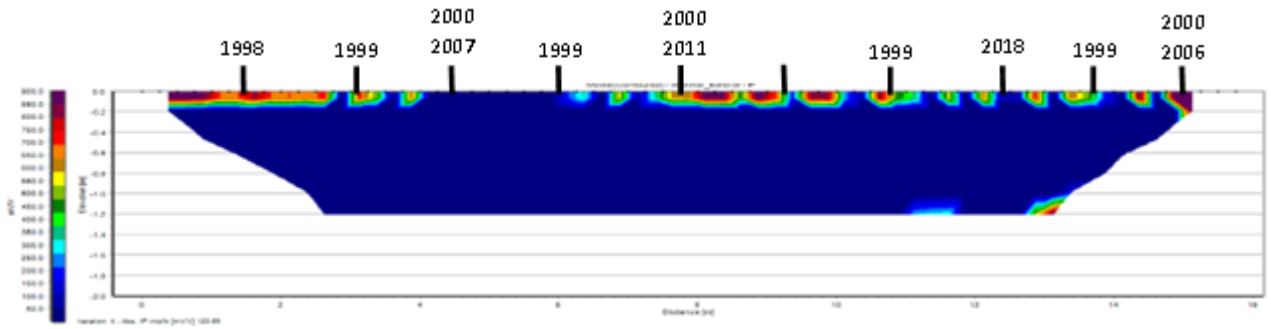

Figure 3.5.6: Induced Polarisation data captured with the Wenner array, August 2020. Keith Cemetery, Row H.

The resistivity data captured with the Dipole – Diploe array, Figure 3.5.7, shows higher resistivity above a depth of ~ 100 cm. Within this band are small areas of resistivities above 2000 Ω-m, these do seem to be associated with the burials, with 55% of the burials identifiable. The IP data, Figure 3.5.8, shows many small areas of chargeability greater than 350nV/V. These are scattered along the line and to a depth of 2000 cm. These areas do not seem to be associated with the burials.

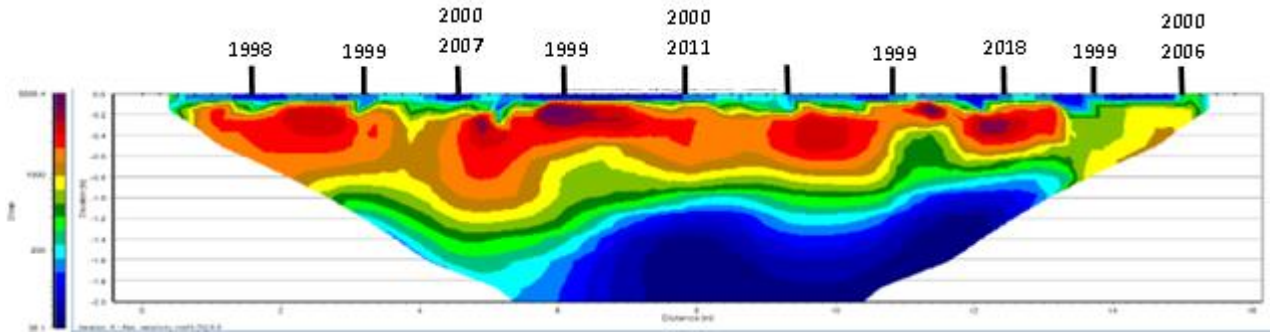

Figure 3.5.7: Resistivity data captured with the Dipole - Dipole array, August 2020. Keith Cemetery, Row H.

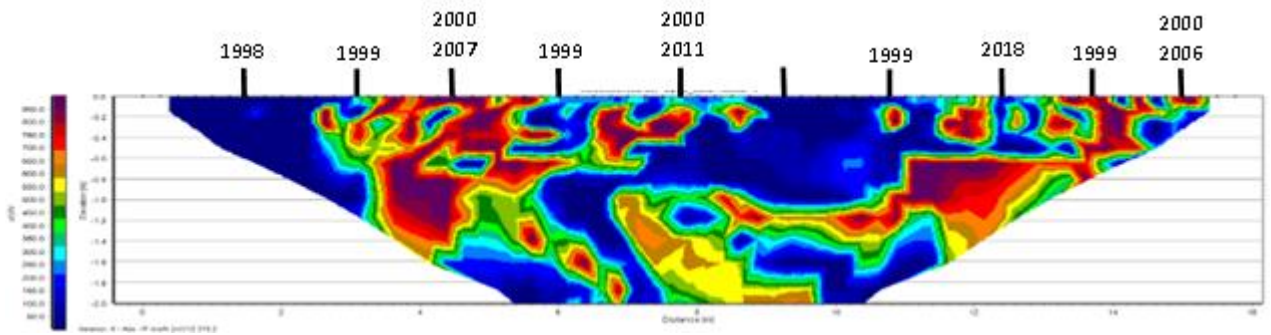

Figure 3.5.8: Induced Polarisation data captured with the Dipole - Dipole array, August 2020. Keith Cemetery, Row H.

3.5.2 October 2020

Data collected in October 2020. There was 4 mm of rainfall in the week before this data was collected, and the ten-month rainfall is shown in Figure 3.5.9. The results from the GPR show eight of nine of the burials being identified.

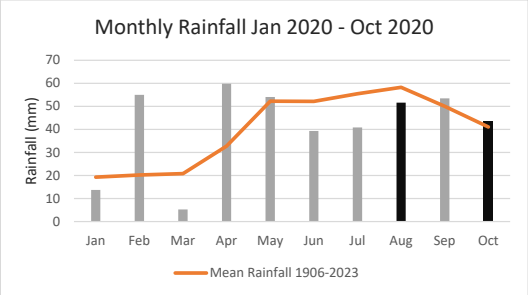

Figure 3.5.9 Rainfall in October 2020 for the ten months prior to data collecting. Months that the study site was visited over this period in black. (Rainfall and Temperature data from bom.gov.au)

The radargrams from Row H, Figures 3.5.11, 3.5.12, and 3.5.13, show a series of quite planar reflections, associated with the burials. There are some shallow stratigraphic breaks seen as the burial shaft cuts through the upper horizon. These are associated with the third from left burial (2018), the fourth from left burial (1999), and the eighth from left (2000/2007), and are outlined in red in Figure 3.5.11, line 2. Small shallow reflections are seen along the radar line, these are highlighted in Figure 3.5.12, line 3. There is a broken horizontal reflection seen at an approximate depth of 30 cm. This is highlighted in line 4, Figure 3.5.13. The reflections from the empty plot seen in August data, Figure 3.5.3, is not seen in these radargrams. Attenuation starts at a depth in this row of 250 cm. There was no suitable ERT data collected on this visit.

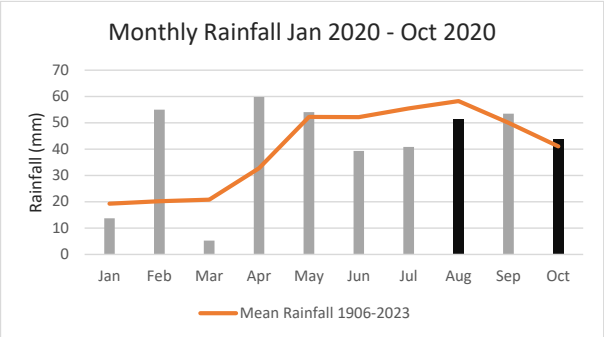

Figure 3.5.10: Rainfall in the ten months prior to the data collection visit, October 2020. Months that the study site was visited over this period in black.

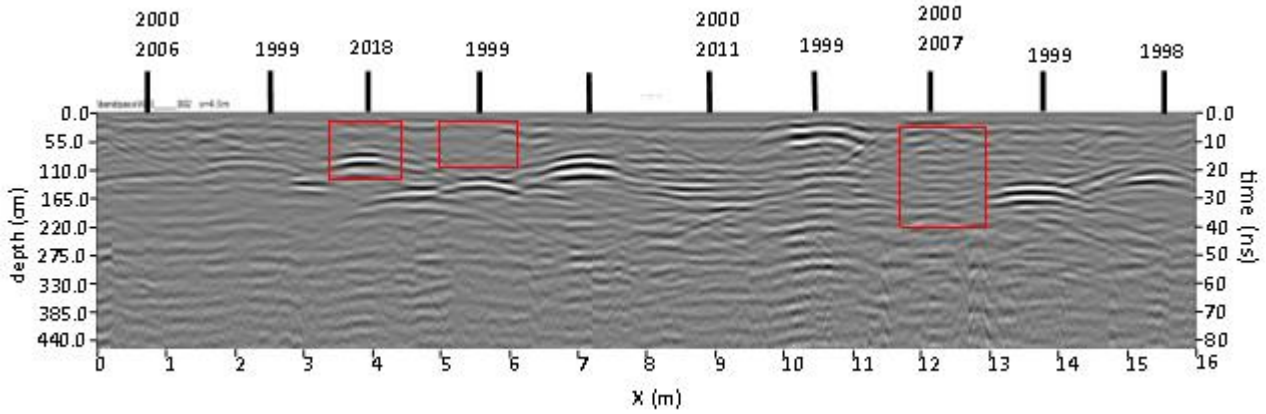

Figure 3.5.11: Keith Cemetery, October 2020, Row H, line 2. Stratigraphic breaks associated with grave cuts are outlined in red.

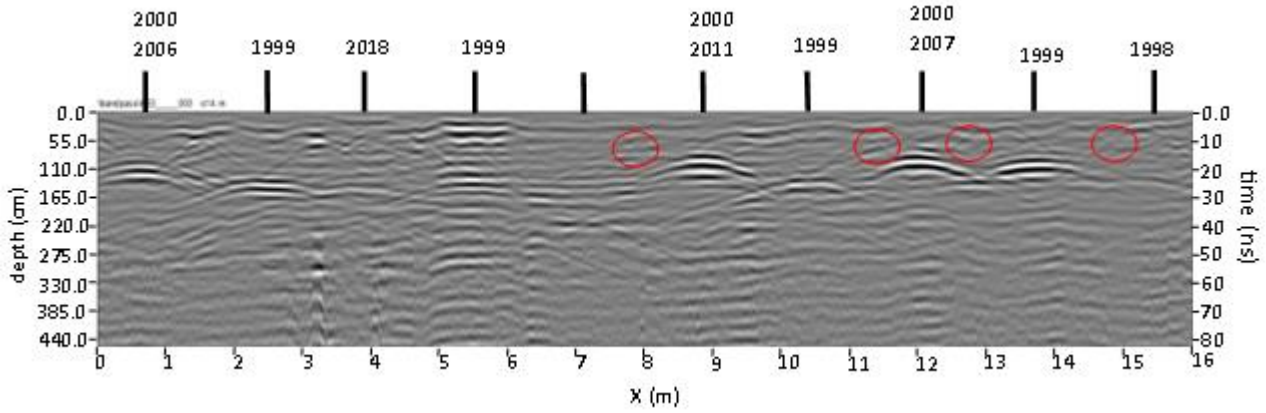

Figure 3.5.12: Keith Cemetery, October 2020, Row H, line 3. Small, shallow reflections are circled in red.

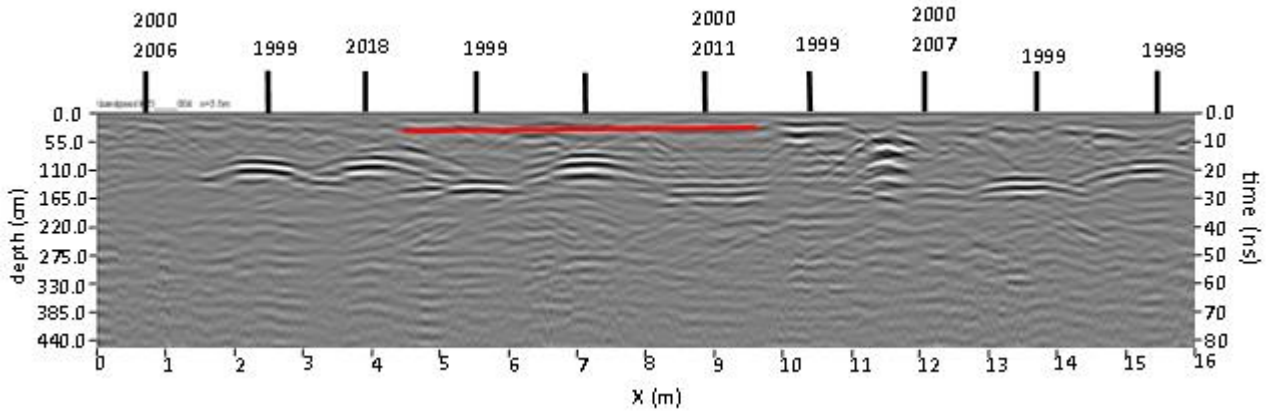

Figure 3.5.13: Keith Cemetery, October 2020, Row H, line 4. The broken horizontal reflection is underlined in red.

3.5.3 January 2021

Data collected in January 2021. There was 0.2 mm of rainfall in the week before this data was collected, and the rainfall in the ten months previous can be seen in Figure 3.5.14. Seven of nine burials can be identified.

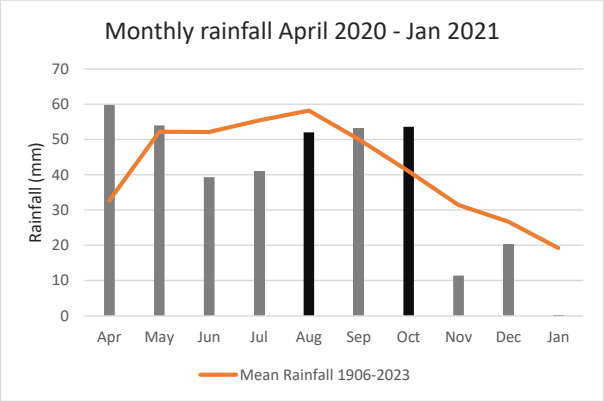

Figure 3.5.14: Rainfall in the 10 months prior to the data collection visit, January 2021. Months that this site was visited over this period are in black. (Rainfall and Temperature data from bom.gov.au)

The radargrams from Row H, Figures 3.5.15, 3.5.16, and 3.5.17, show the series of reflections seen in previous months that are associated with burials. These reflections show a planar shape, differing sizes, but all show the same polarity throughout. There are some reflections from infill related to the burial of 1999 located at 10.5 m, this is highlighted in Figure 3.5.15, line 2. Attenuation for this data starts at approximately 270 cm.

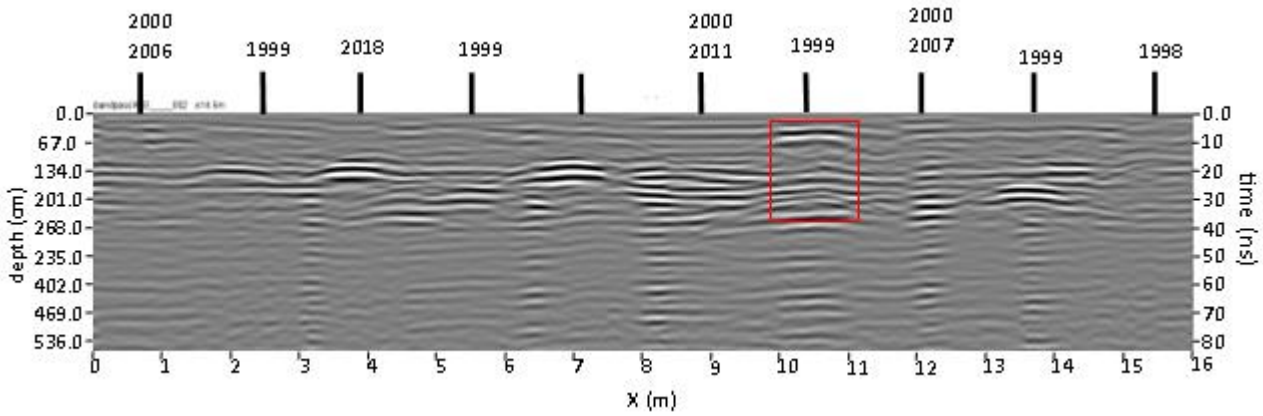

Figure 3.5.15: Keith Cemetery, January 2021, Row H, line 2. Infill associated with a burial is highlighted in red.

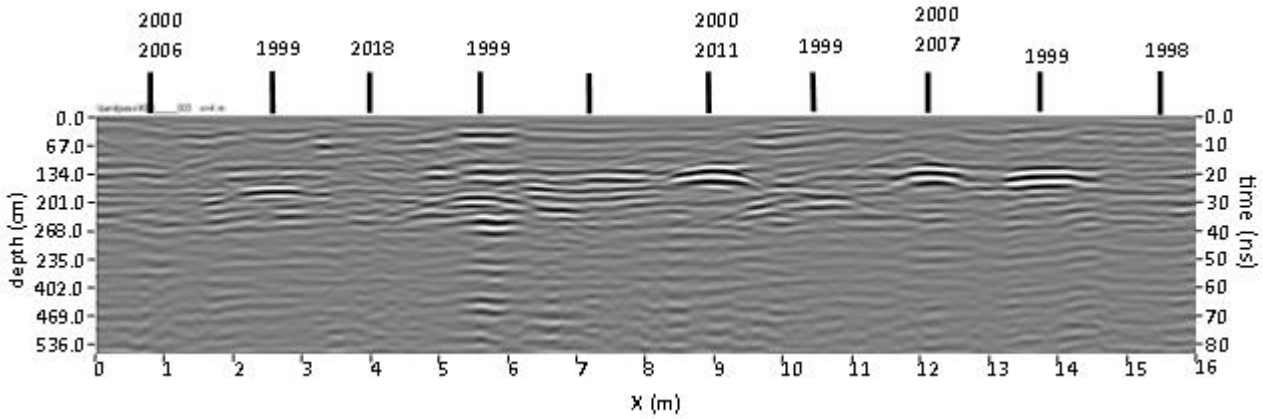

Figure 3.5.16: Keith Cemetery, January 2021, Row H, line 3.

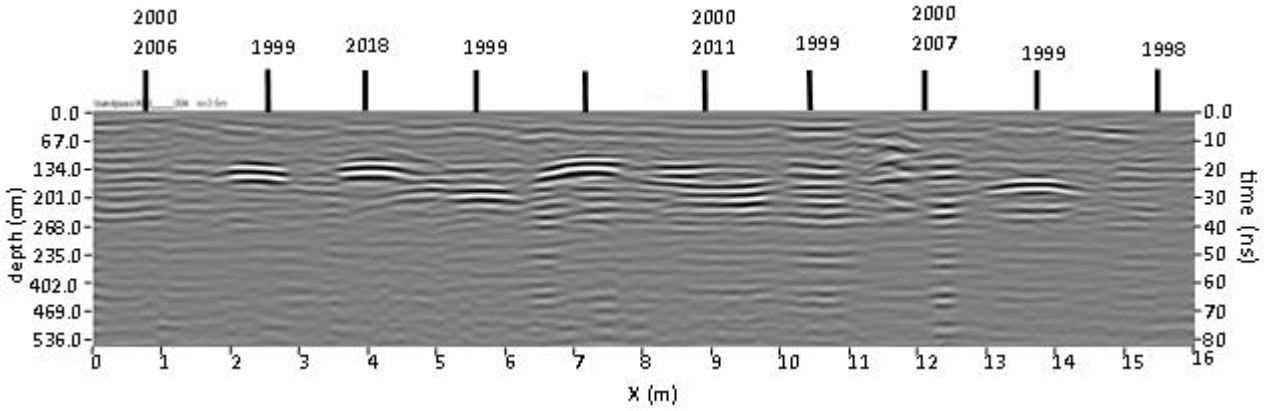

Figure 3.5.17: Keith Cemetery, January 2021, Row H, line 4.

The resistivity and induced polarisation data was captured using the Wenner and Dipole – Dipole arrays, with electrode spacing of 25 cm. The inversion plots from the Wenner resistivity, Figure 3.5.18 show layer with higher resistivity, (above 100 Ω-m), from a depth of 20 cm to 100 cm. Within this layer are smaller areas with resistivities above 600 Ω-m, these can be associated with the burials. The IP inversion plot shows an area that appears largely homogenous in nature, Figure 3.5.19. Two areas of higher chargeability, (above 300 nV/V), area associated with burials, with four very small areas on the surface also showing higher chargeability.

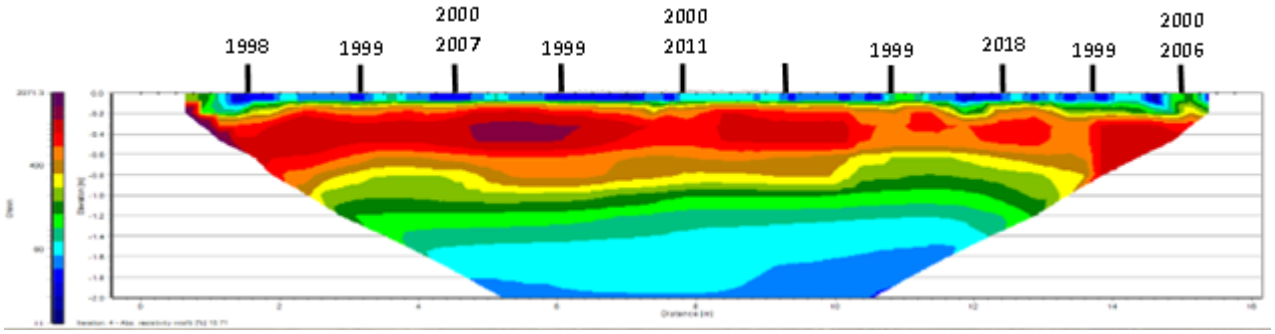

Figure 3.5.18: Resistivity data captured with the Wenner array, January 2021. Keith Cemetery, Row H.

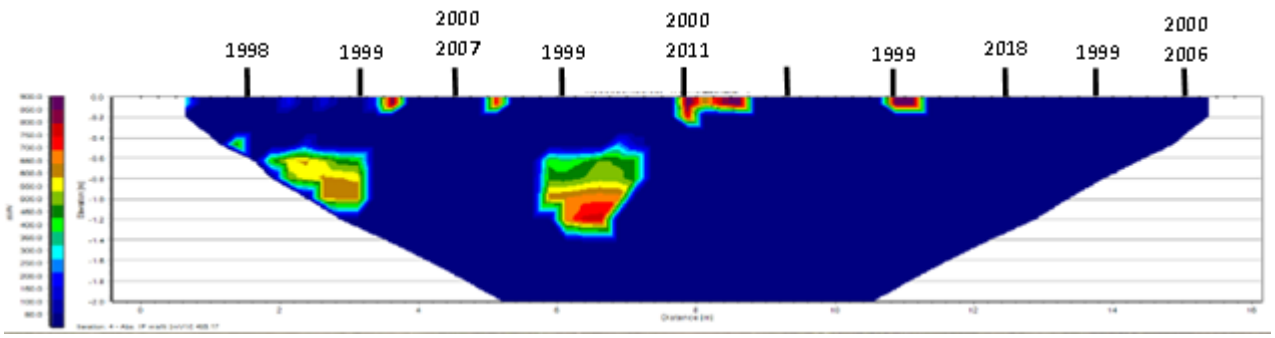

Figure 3.5.19: Induced polarisation data captured with the Wenner array, January 2021. Keith Cemetery, Row H.

The Dipole – Dipole array inversion, Figure 3.5.20, shows areas generally centred at a depth of 80 cm of resistivities above 300 Ω-m. These can be associated with the burials, with six of the nine burials identified. The IP plot from the Dipole-Dipole array, 3.5.21, also shows a largely homogenous area, with areas of chargeability above 700nV/V. These areas are not associated with the burials.

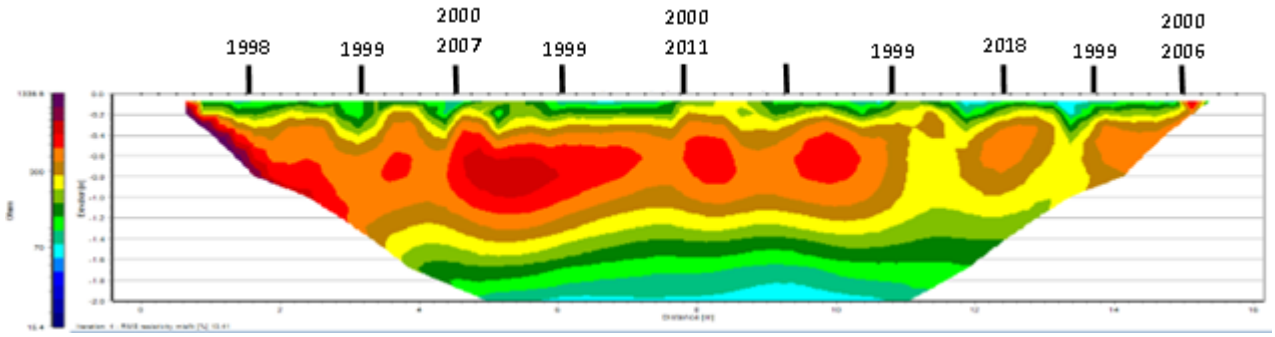

Figure 3.5.20: Resistivity data captured with the Dipole - Dipole array, January 2021. Keith Cemetery, Row H.

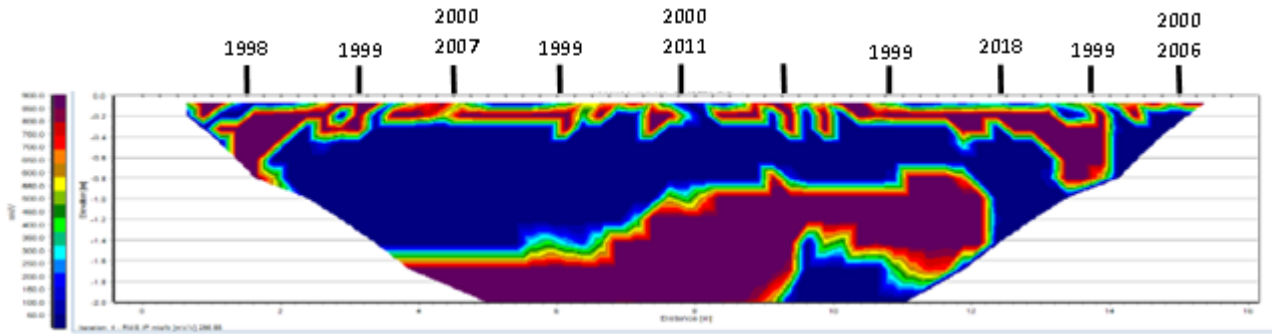

Figure 3.5.21: Induced polarisation data captured with the Dipole - Dipole array, January 2021. Keith Cemetery, Row H.

3.5.4 January 2022

Data collected in January 2022. There was 0 mm of rainfall in the week before this data was collected, the ten-month rainfall can be seen in Figure 3.5.22. Eight of the nine burials can be identified in these radargrams.

Of note in this series of radargrams, Figures 3.5.23, 3.5.24, and 3.5.25, is the line of high amplitude at approximately 30 cm. This corresponds with a change in subsurface horizon, this change is the delineation between the silicon rich sand below 30 cm, and the soil containing a higher percentage of organic material. The series of strong planar reflections is not as prevalent in this data, not all the reflections are visible, those that are vary in size and amplitude, but not polarity. Many shallow, small reflections are visible, these are highlighted in line 3, Figure 3.5.24. It is not known the origin of these small reflections. Attenuation starts at approximately 190 cm.

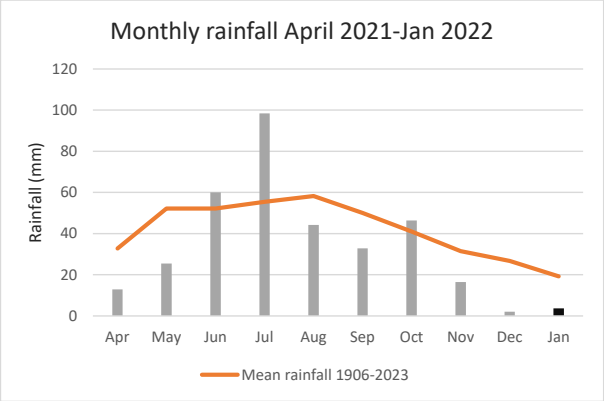

Figure 3.5.22: Rainfall at Keith, ten months prior to data collection. Months that this site was visited over this period in black. (Rainfall and Temperature data from bom.gov.au)

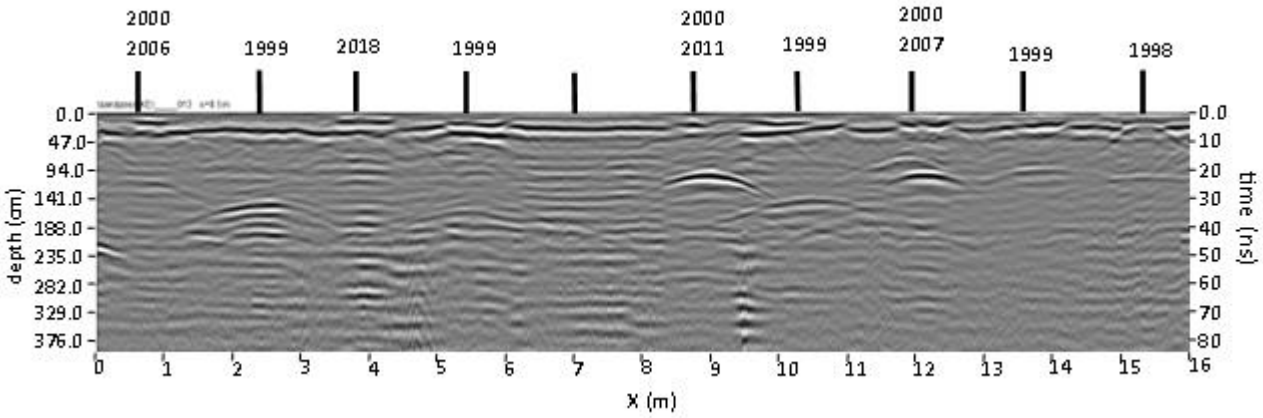

Figure 3.5.23: Keith Cemetery, January 2022, Row H, line 2. The stratigraphic layer at approximately 30 cm depth can be seen as a high amplitude reflection along the entire radar line.

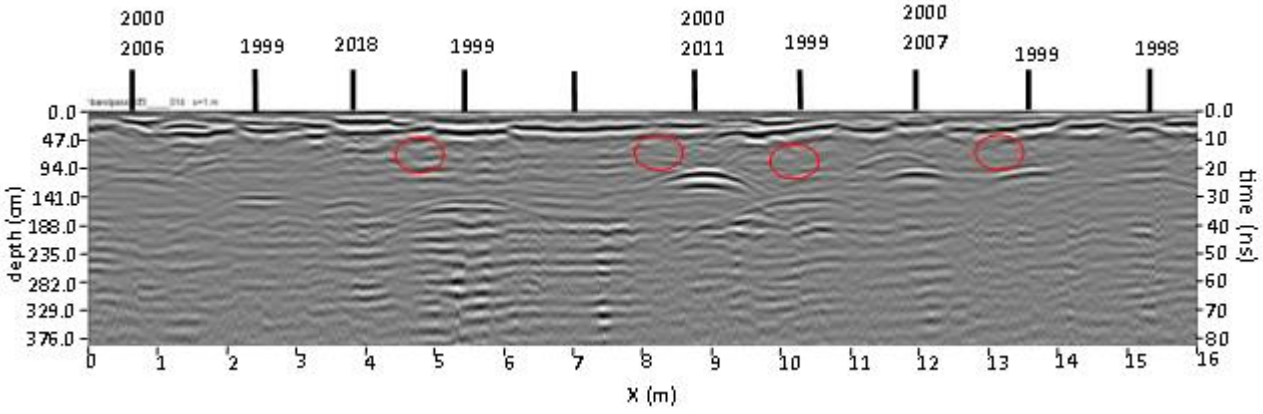

Figure 3.5.24: Keith Cemetery, January 2022, Row H, line 3. Small, shallow reflections are highlighted in red.

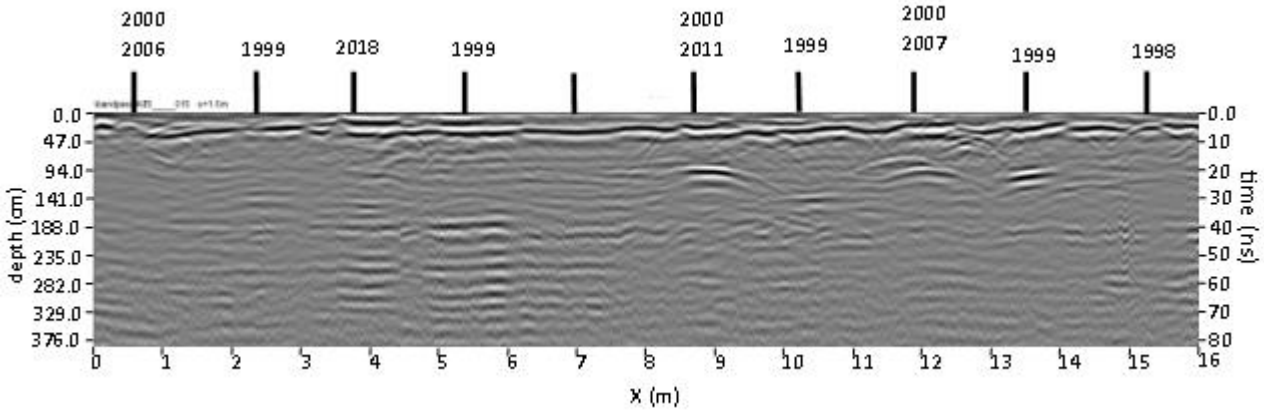

Figure 3.5.25: Keith Cemetery, January 2022, Row H, line 4.

The ERT results from this visit are the clearest captured so far. The Wenner resistivity data show a series of very shallow, (< 20 cm) low resistivity, (<150Ω-m), areas that are adjacent the position of the burials, Figure 3.5.26. This pattern does somewhat mimic the synthetic simulations. Below this the resistivity rises between 200 and 400 Ω-m, before dropping again at a depth below 140 cm. The IP data, Figure 3.5.27, captured with the Wenner array seems to be not of a quality to use. Unlike other months, the penetration of the ERT is ~140 cm, this could also indicate that the data is of poor quality.

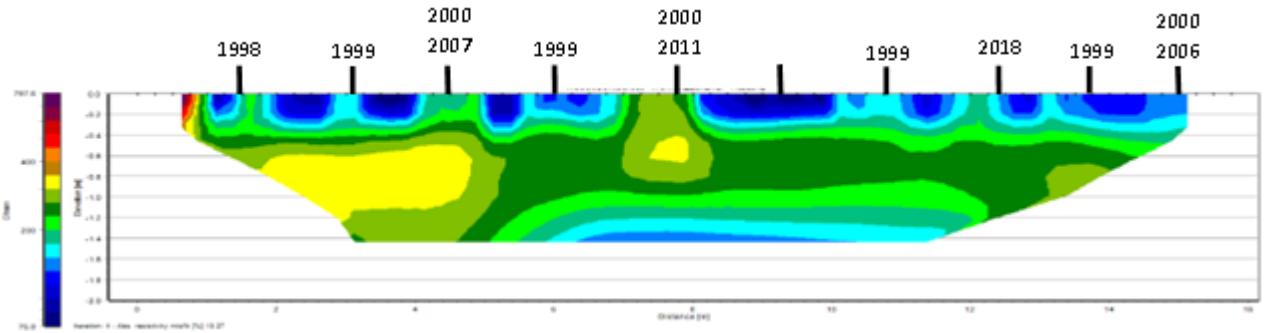

Figure 3.5.26: Resistivity data captured with the Wenner array, January 2022. Keith Cemetery, Row H.

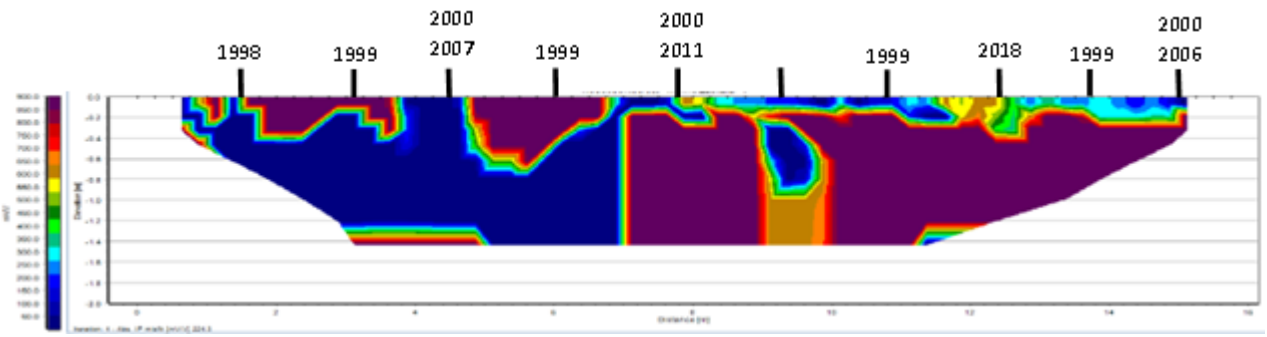

Figure 3.5.27: Induced polarisation data captured with the Wenner array, January 2022. Keith Cemetery, Row H.

The resistivity plot shows a wide band, (between depths of 20 cm and 100 cm), of higher resistivity, (> 300 Ω-m), along the length of the electrode line. Within this band are small discrete areas with resistivity over 350 Ω-m, Figure 3.5.28. These are associated with the burials. The IP plot, Figure 3.5.29, shows an area of high chargeability (>400nV/V) that extends along the entire plot, to a depth of 40 cm. In addition to this are two larger areas of similar chargeability at a deeper level.

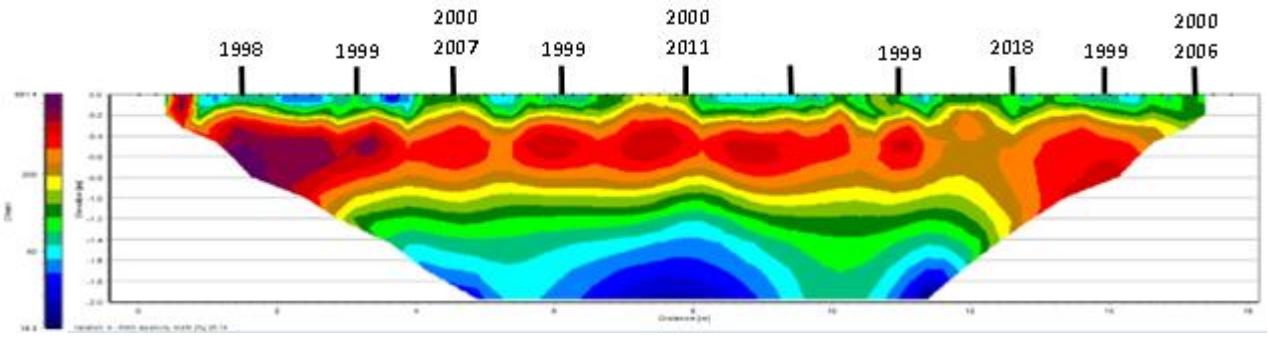

Figure 3.5.28: Resistivity data captured with the Dipole - Dipole array, January 2022. Keith Cemetery, Row H.

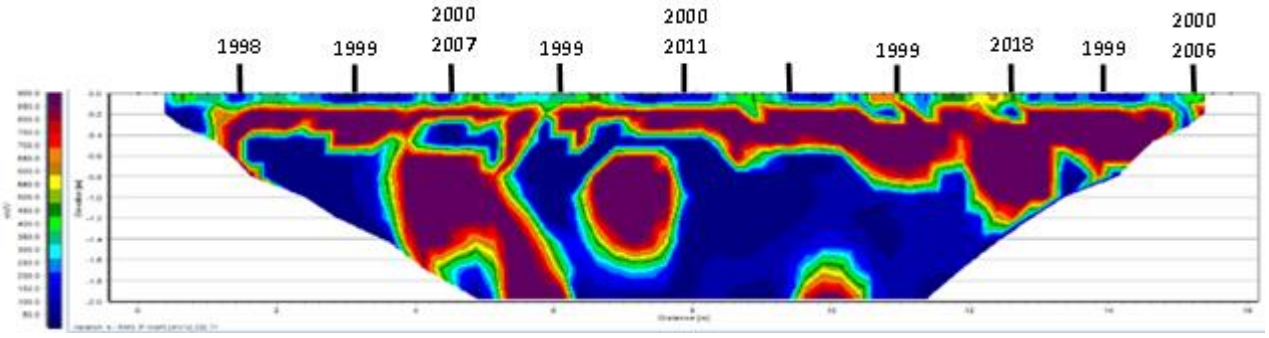

Figure 3.5.29: Induced polarisation data captured with the Dipole - Dipole array, January 2022. Keith Cemetery, Row H.

3.5.5 May 2022

Data collected in May 2022. There was 8.4 mm of rainfall in the week before this data was collected, and the rainfall in the previous ten months can be seen in Figure 3.5.30. Radargrams from Row H, Figures 3.5.31, 3.5.32, and 3.5.33 show a series of reflections, these are tending to be planar in shape, differing sizes, with a strong amplitude, and are associated with the burials.

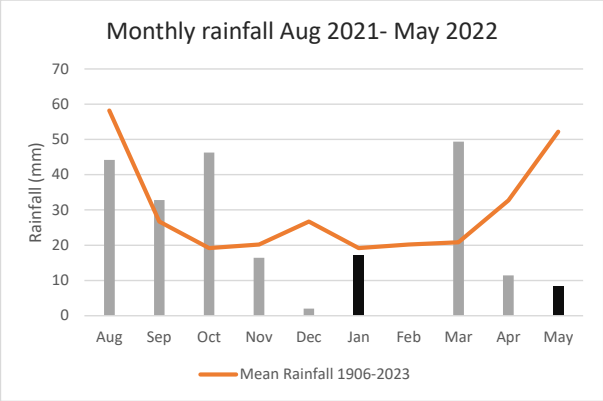

Figure 3.5.30: Rainfall in the ten months prior to the data collection visit, May 2022. Months that this site was visited over this period in black. (Rainfall and Temperature data from bom.gov.au)

The series of small, shallow reflections are highlighted in line 3, Figure 3.5.31. These reflections are mainly in the last five meters of the radar line. All nine burials can be identified in these radargrams. Attenuation of this data starts at approximately 220 cm.

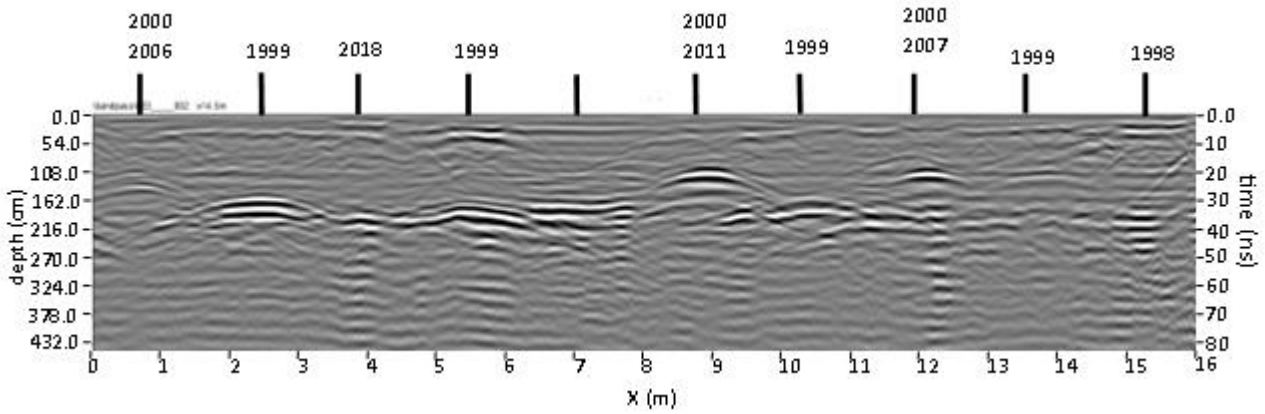

Figure 3.5.31: Keith Cemetery, May 2022, Row H, line 2.

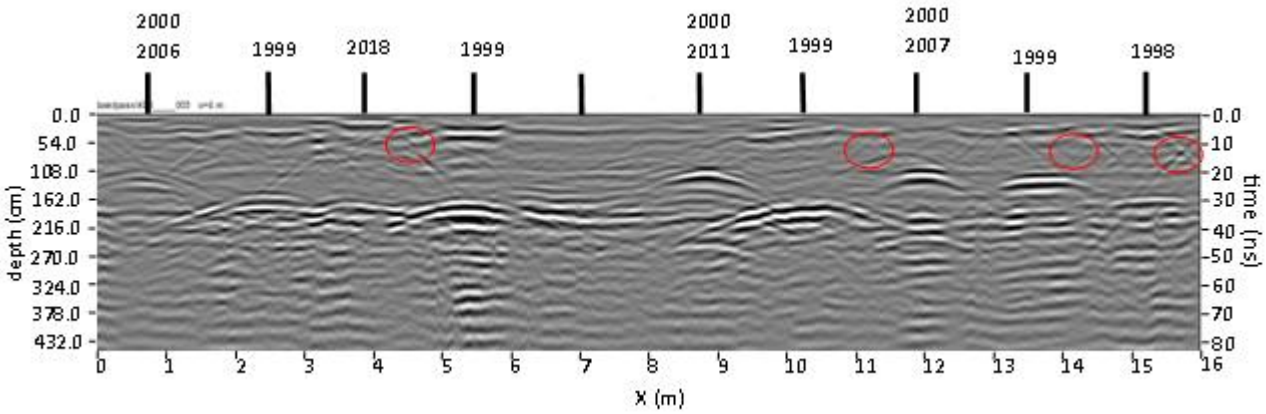

Figure 3.5.32: Keith Cemetery, May 2022, Row H, line 3. The small, shallow reflections are highlighted in red.

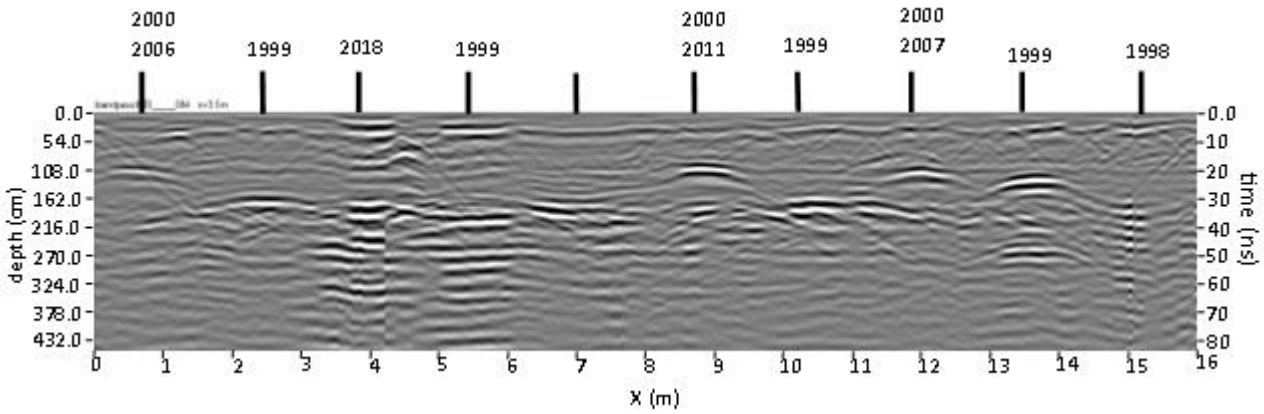

Figure 3.5.33: Keith Cemetery, May 2022, Row H, line 4.

There was no suitable ERT data from this visit due to technical issues with the equipment.

3.5.6 July 2022

Data collected in July 2022. There was 10.2 mm of rainfall in the week before this data was collected, the rainfall in the ten months prior to the visit can be seen in Figure 3.5.34.

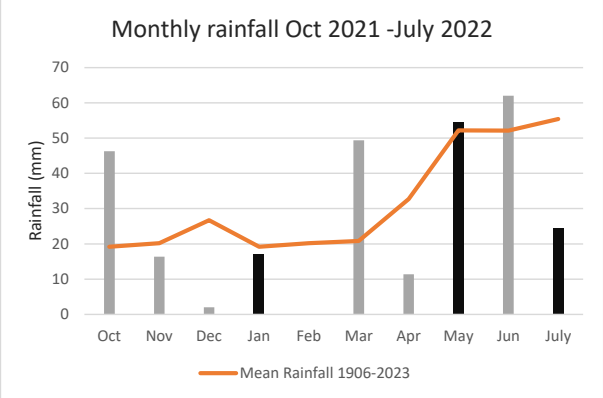

Figure 3.5.34: Rainfall in the ten months prior to the data collection visit, July 2022. Months that this site was visited over this period in black. (Rainfall and Temperature data from bom.gov.au)

The radargrams from data gathered in July 2022, Figures 3.5.35, 3.5.36, and 3.5.37, show very few of the strong planar reflections. The small, shallow reflections are more pronounced, these are highlighted in line 3, Figure 3.5.36. Eight of the nine burials can be identified in these radargrams. The attenuation is from a depth of 260 cm.

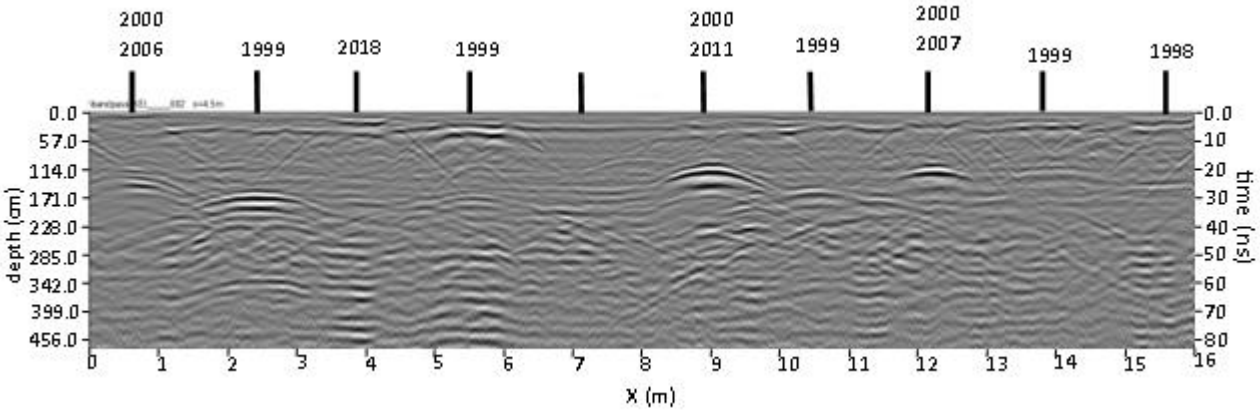

Figure 3.5.35: Keith Cemetery, July 2022, Row H, line 2.

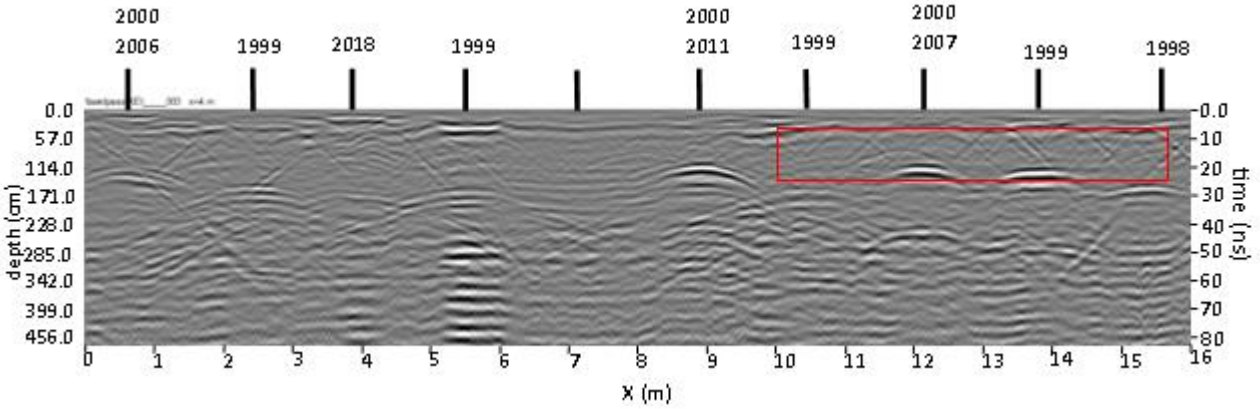

Figure 3.5.36: Keith Cemetery, July 2022, Row H, line 3. The small, shallow reflections are outlined in red.

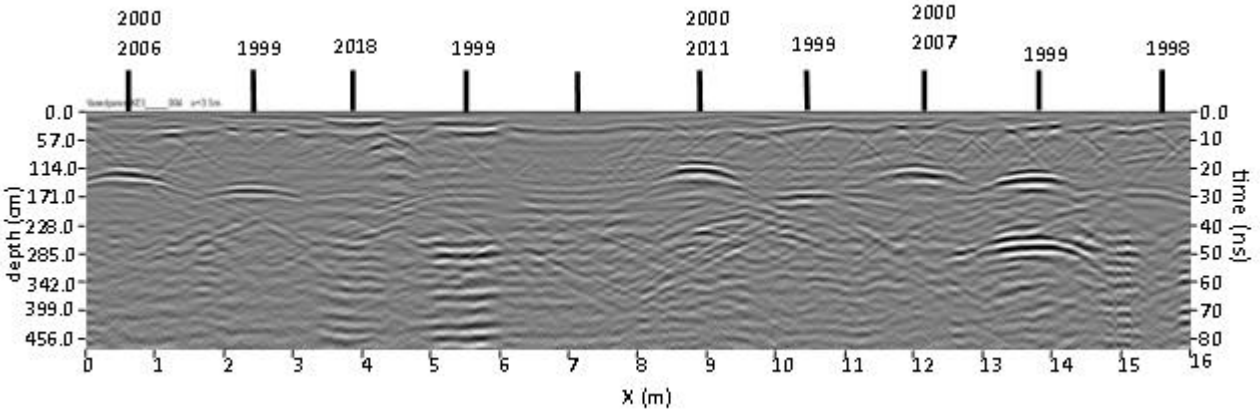

Figure 3.5.37: Keith Cemetery, July 2022, Row H, line 4.

The Wenner inversion plot shows resistivity increasing at a depth of 20 cm, to 500 Ω-m. Below this, to a depth of 100 cm the resistivity increases again, (above 700 Ω-m), with discrete areas of resistivity over 900 Ω-m. Within this layer > 700 Ω-m 6 burials can be identified, Figure 3.5.38. The IP from the Wenner array,

Figure 3.5.39, shows several small areas on the soil surface with chargeability > 250nV/V. In the remainder of the plot the chargeability drops to < 200nV/V.

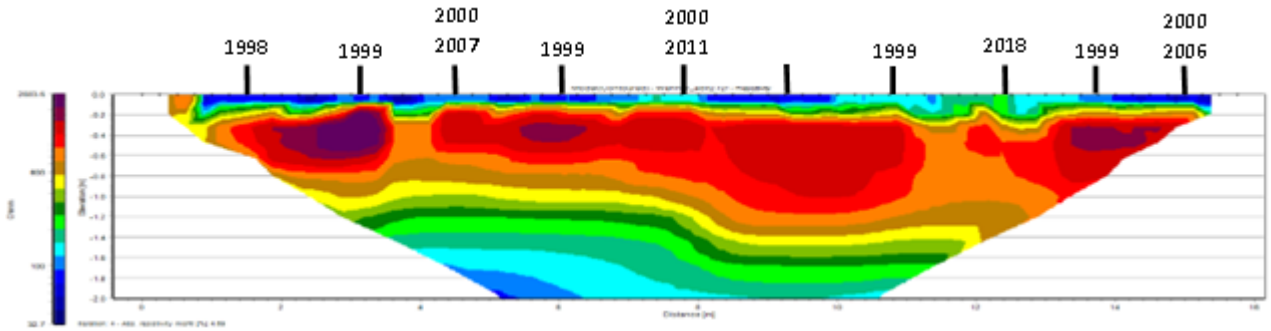

Figure 3.5.38: Resistivity data captured with the Wenner array, July 2022. Keith Cemetery, Row H.

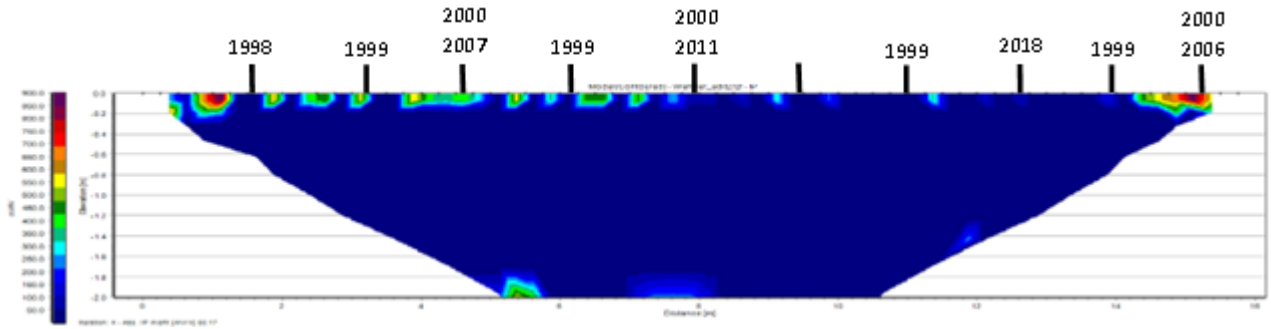

Figure 3.5.39: Induced polarisation data captured with the Wenner array, July 2022. Keith Cemetery, Row H.

The inversion plot from the Dipole- Dipole array shows a band of high resistivity (>519 Ω-m) extending along the length of the plot, and to a depth of 120 cm, Figure 3.5.40. Five areas within this band show a resistivity higher that 800 Ω-m, these are associated with the burials. The IP inversion shows a thin line of high chargeability (>550 nV/V) long the surface, Figure 3.5.41. Below this long the chargeability is largely low (<200 nV/V) for the entire plot, with the exception being an area at a depth of 160 cm, associated with the vacant plot.

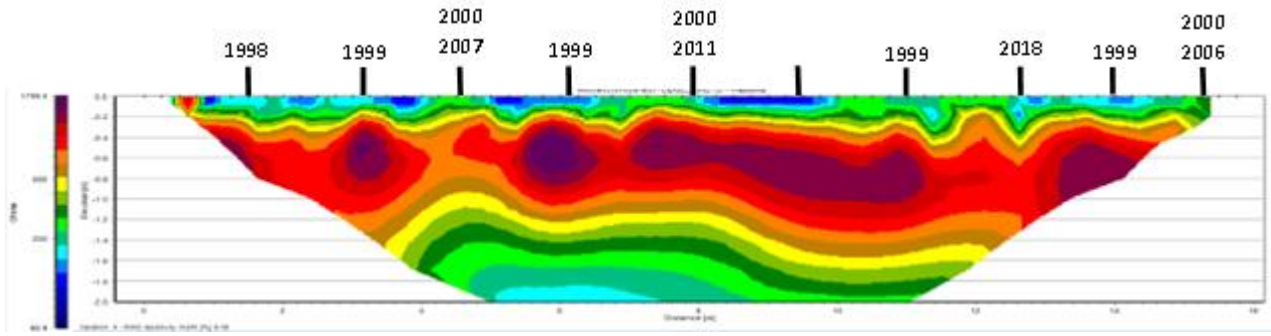

Figure 3.5.40: Resistivity data captured with the Dipole - Dipole array, July 2022. Keith Cemetery, Row H.

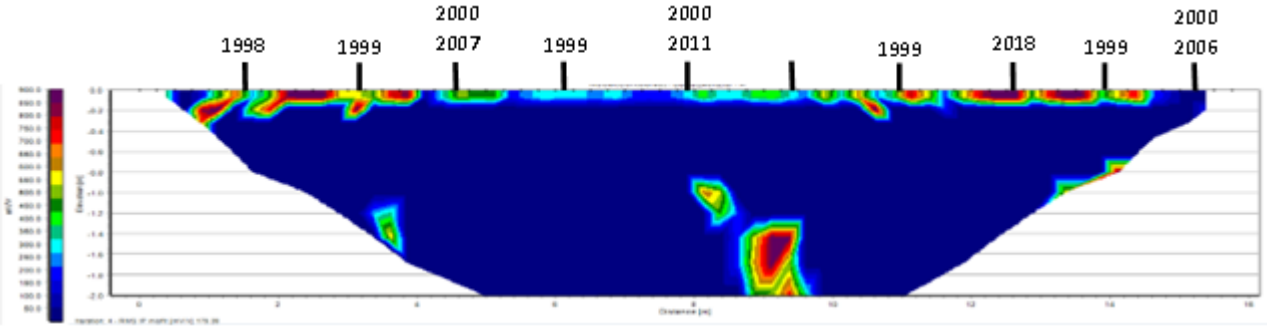

Figure 3.5.41: Induced polarisation data captured with the Dipole - Dipole array, July 2022. Keith Cemetery, Row H.

3.5.7 September 2022

Data collected in September 2022. There was 21 mm of rainfall in the week before this data was collected, the rainfall in the ten months prior to the visit can be seen in Figure 3.5.42. There was no ERT data collected on this visit due to equipment malfunction.

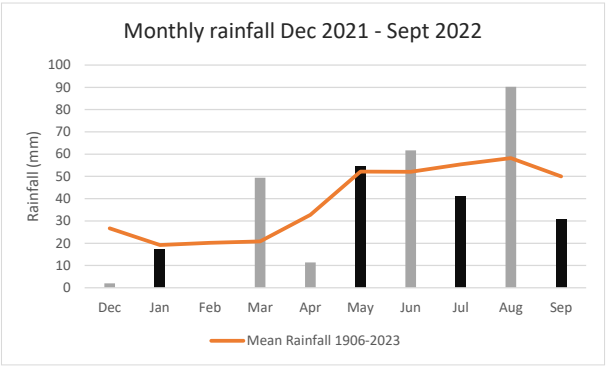

Figure 3.5.42: Rainfall in the 30 days prior to the data collection visit, September 2022. (Rainfall and Temperature data from bom.gov.au)

Radargrams from Row H, Figures 3.5.43, 3.5.44, and 3.5.45, show the series of flat reflections. These reflections do not all show high amplitude. The many small, shallow reflections are seen in line 3, Figure 3.5.44. There are some stratigraphic breaks that are associated with the burials, these are highlighted in line 4, Figure 3.5.45. Seven of the nine burials can be identified in these radargrams. Attenuation of this data starts at approximately 230 cm.

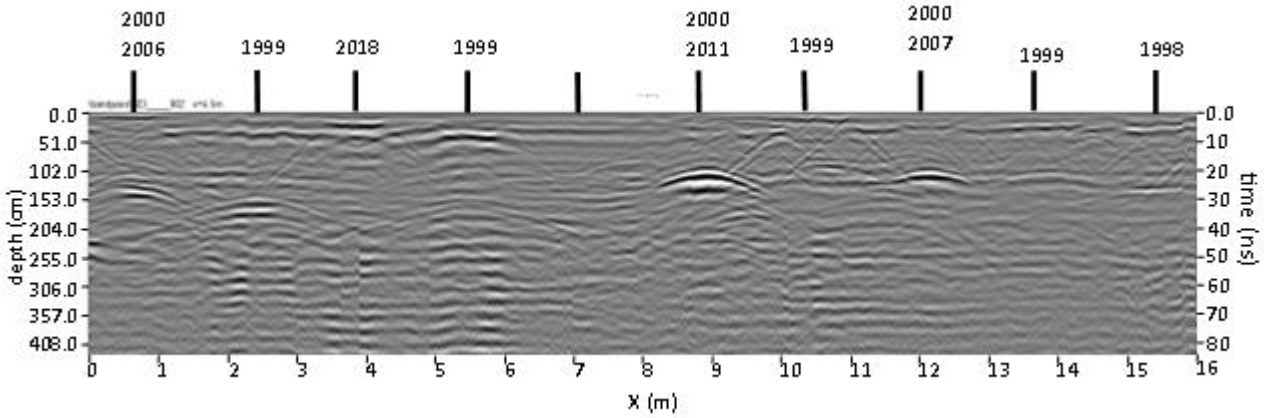

Figure 3.5.43: Keith Cemetery, September 2022, Row H, line 2.

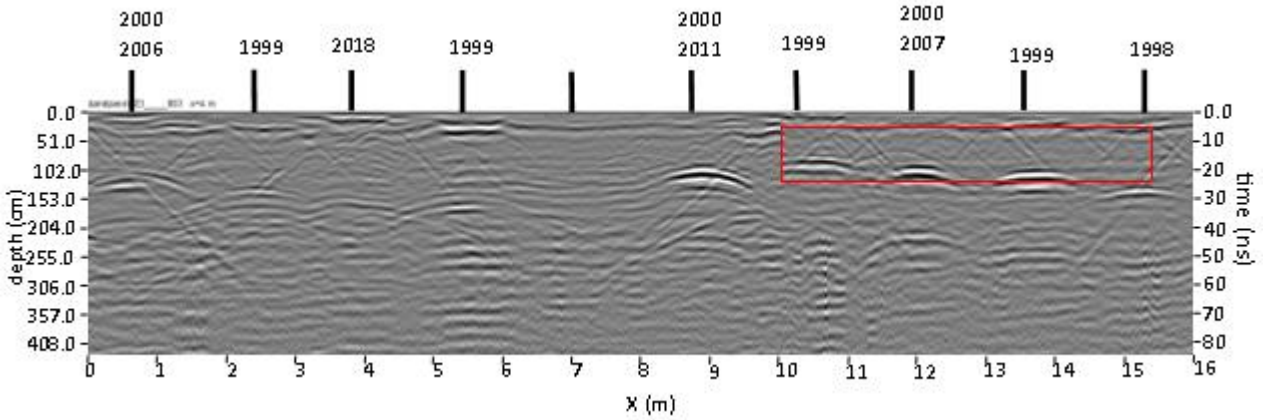

Figure 3.5.44: Keith Cemetery, September 2022, Row H, line 3. The small, shallow reflections are highlighted in red.

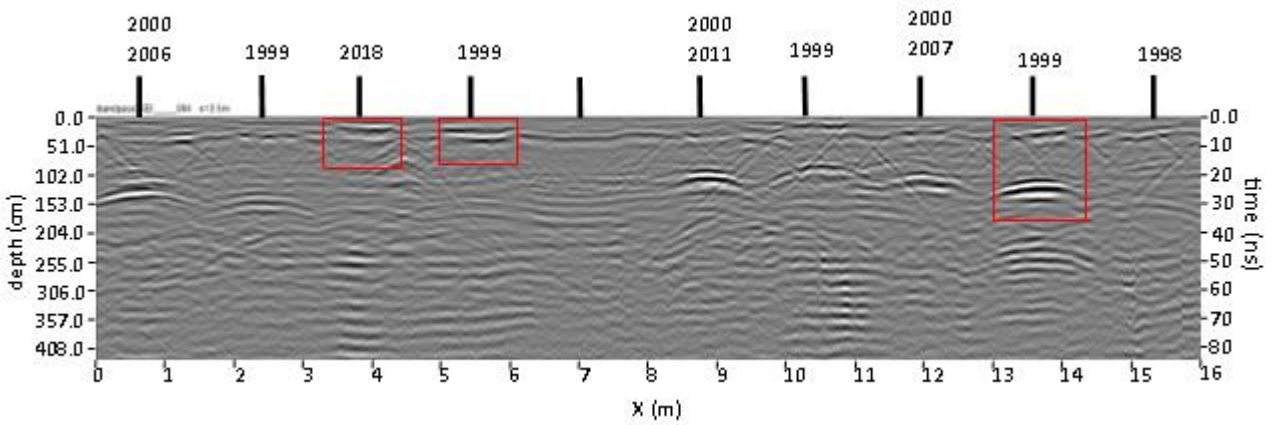

Figure 3.5.45: Keith Cemetery, September 2022, Row H, line 4. Stratigraphic breaks associated with the burials are highlighted in red.

3.5.8 December 2022

Data collected in December 2022. There was 0 mm of rainfall in the week before this data was collected, the rainfall in the ten months prior to the visit can be seen in Figure 3.5.46. There was no ERT data collected on this visit.

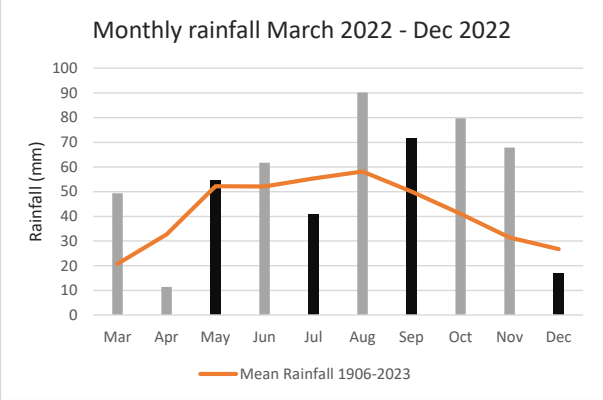

Figure 3.5.46: Rainfall in the 30 days prior to the data collection visit, December 2022. (Rainfall and Temperature data from bom.gov.au)

The radargrams from Row H, Figures 3.5.47, 3.5.48, and 3.5.49, show the series of planar reflections, these show a higher amplitude that in the previous months. The small, shallow reflections are again seen, these are highlighted in line 3, Figure 3.5.48. All nine of the burials can be identified in these radargrams. Attenuation in this group is approximately 230 cm.

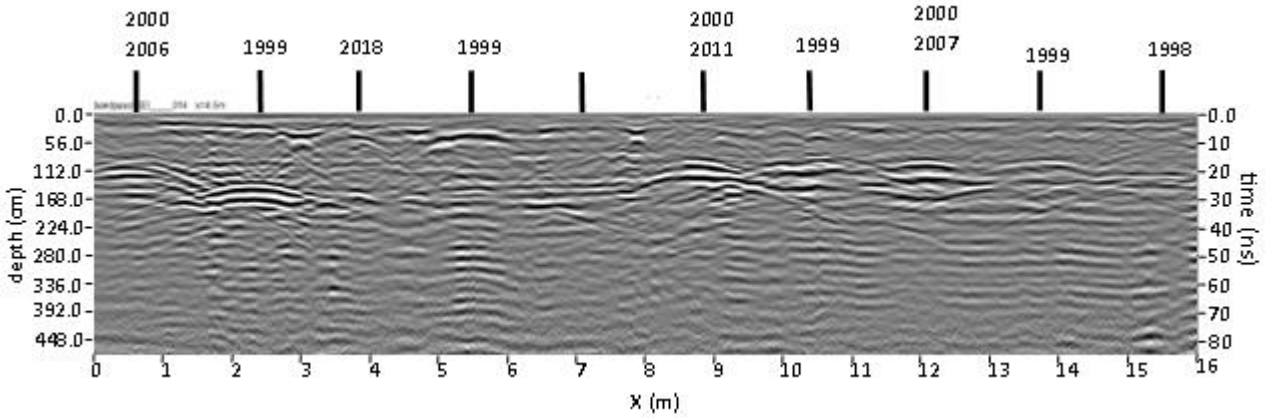

Figure 3.5.47: Keith Cemetery, December 2022, Row H, line 2.

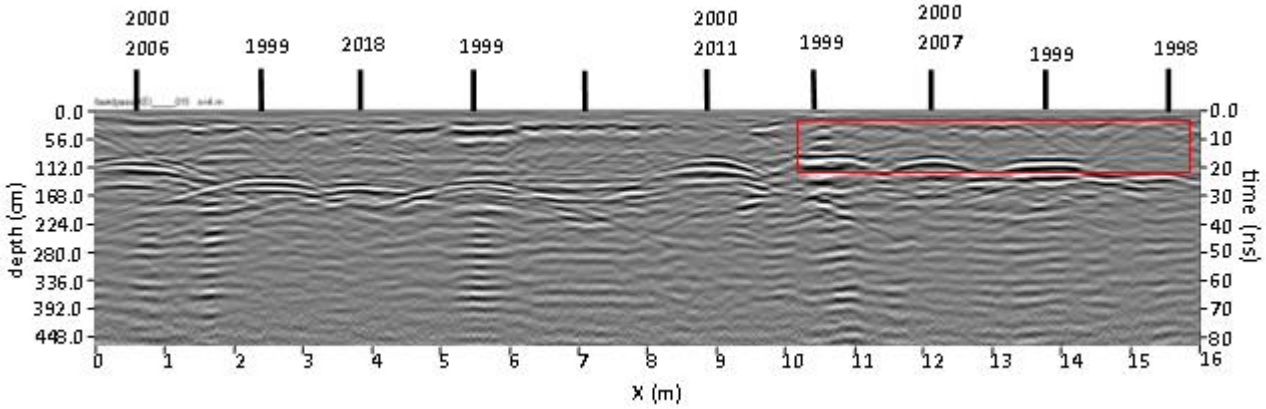

Figure 3.5.48: Keith Cemetery, December 2022, Row H, line 3. The small, shallow reflections are highlighted in red.

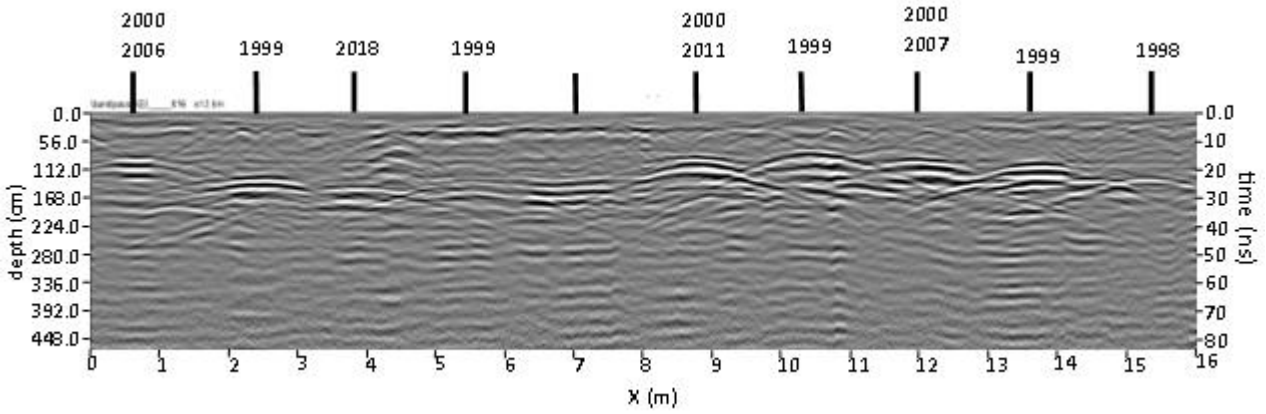

Figure 3.5.49: Keith Cemetery, December 2022, Row H, line 4.

3.5.9 March 2023

Data collected in March 2023. There was 7.9 mm of rainfall in the week before this data was collected, and the rainfall in the ten months prior to the visit can be seen in Figure 3.5.50.

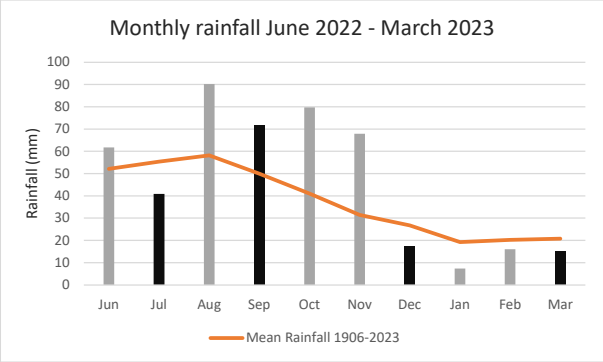

Figure 3.5.50: Rainfall in the 30 days prior to the data collection visit, March 2023. (Rainfall and Temperature data from bom.gov.au)

The radargrams from Row H, Figures 3.5.51, 3.5.52, and 3.5.53, show the series of reflections that are planar in shape. These reflections are not as high as in previous months, in line 2, Figure 3.5.51, several are not seen, and this is due to the slower radar velocity. The small shallow reflections are seen in line 4, Figure 3.5.53. In line 2, Figure 3.5.51, the stratigraphic layer at 30 cm is visible. Eight of nine burials can be identified in these radargrams. Attenuation starts at approximately 250 cm.

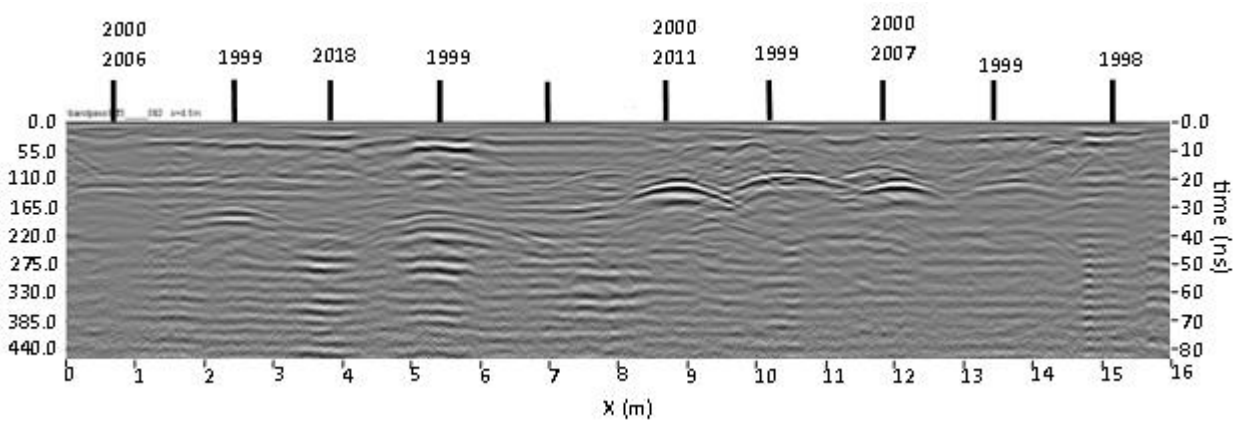

Figure 3.5.51: Keith Cemetery, March 2023, Row H, line 2.

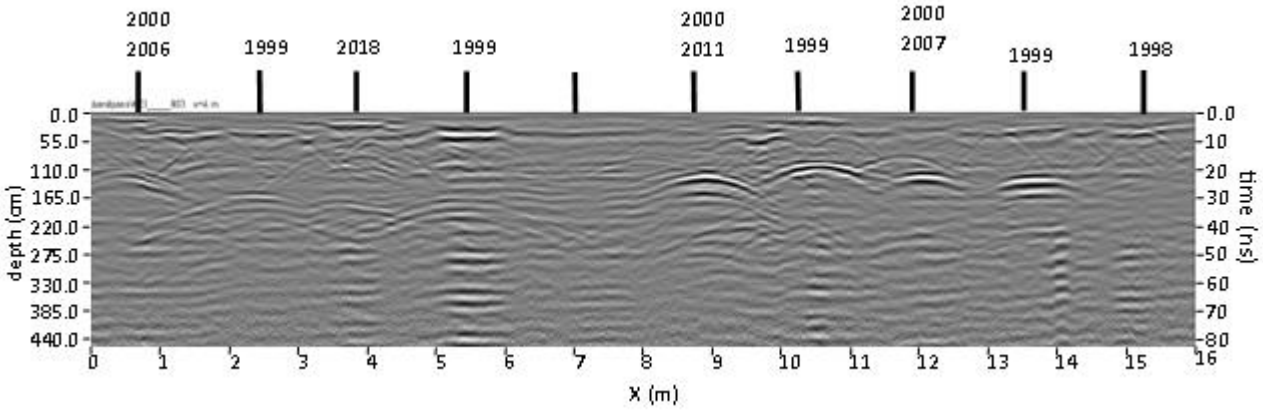

Figure 3.5.52: Keith Cemetery, March 2023, Row H, line 3.

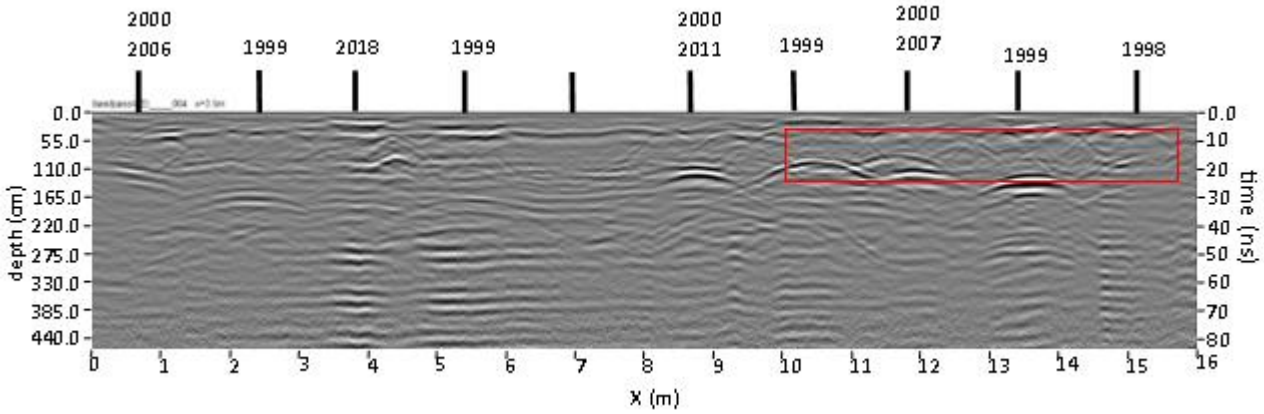

Figure 3.5.53: Keith Cemetery, March 2023, Row H, line 4. The small, shallow reflections are highlighted in red.

The inversion plot from the Wenner array, Figure 3.5.54, shows a shallow layer of low resistivity (<243Ω-m) along the length of the ERT line. Below this low resistivity layer, is a layer of higher resistivity (>351) that could be associated with the burials. The IP plot from the Wenner array, Figure 3.5.55, shows some areas of high chargeability (>528) at a shallow depth.

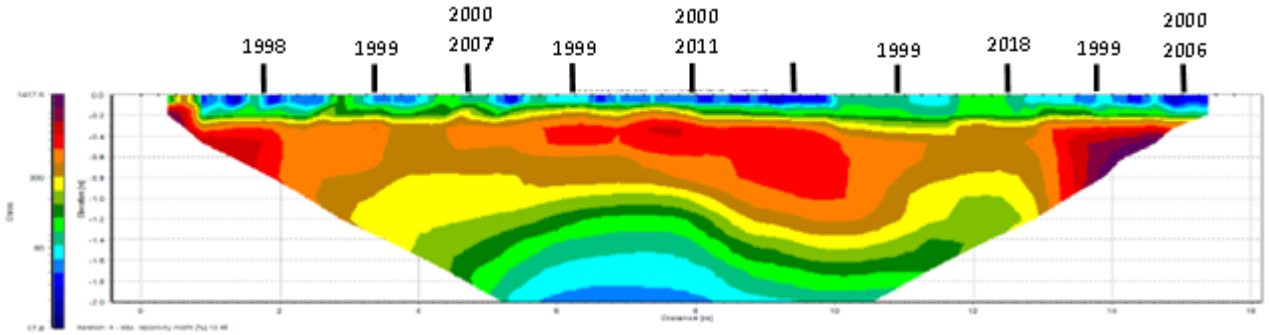

Figure 3.5.54: Resistivity data captured with the Wenner array, March 2023. Keith Cemetery, Row H.

The inversion plot from the Dipole-Dipole array, Figure 3.5.56, shows a shallow low resistivity layer (<222Ω-m) extending the length of the ERT line. Below this layer is a line of higher resistivity (>365Ω-m) that is associated with the burials. The IP plot, Figure 3.5.57, shows areas of high chargeability (>500) along the ground surface, then in areas to the depth of penetration.

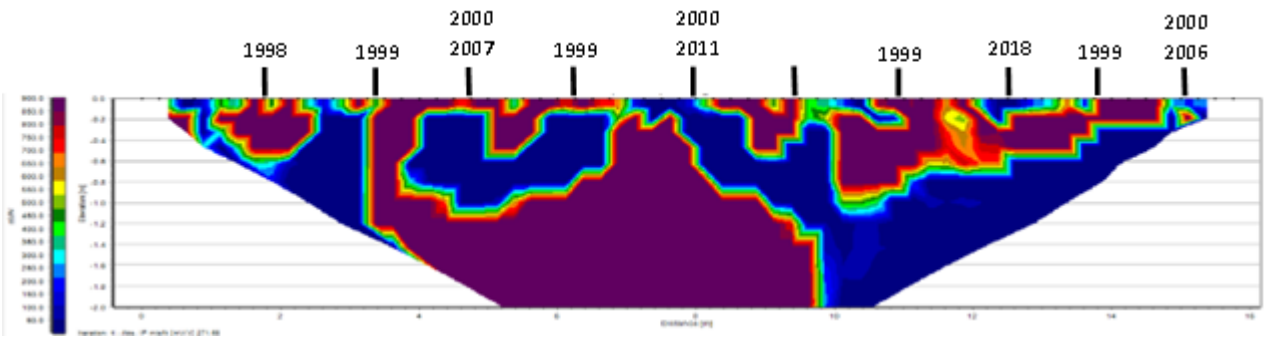

Figure 3.5.55: Induced polarisation data collected with the Wenner array, March 2023. Keith Cemetery, Row H.

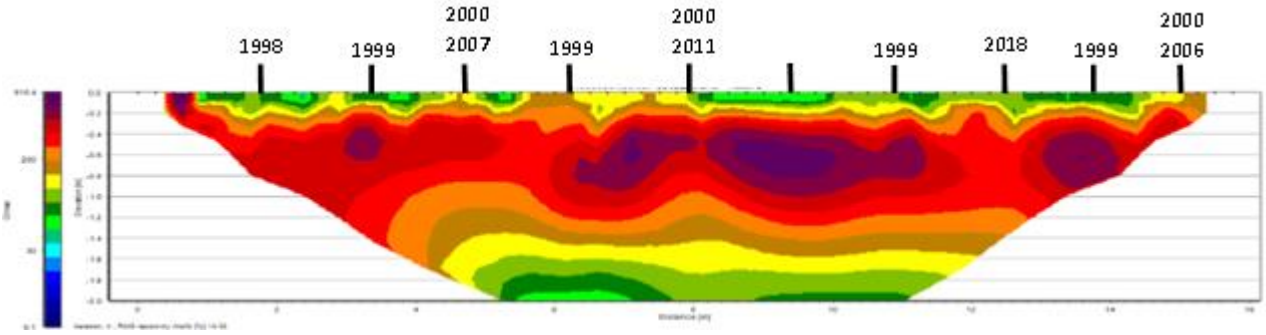

Figure 3.5.56: Resistivity data collected with the Dipole - Dipole array, March 2023. Keith Cemetery, Row H.

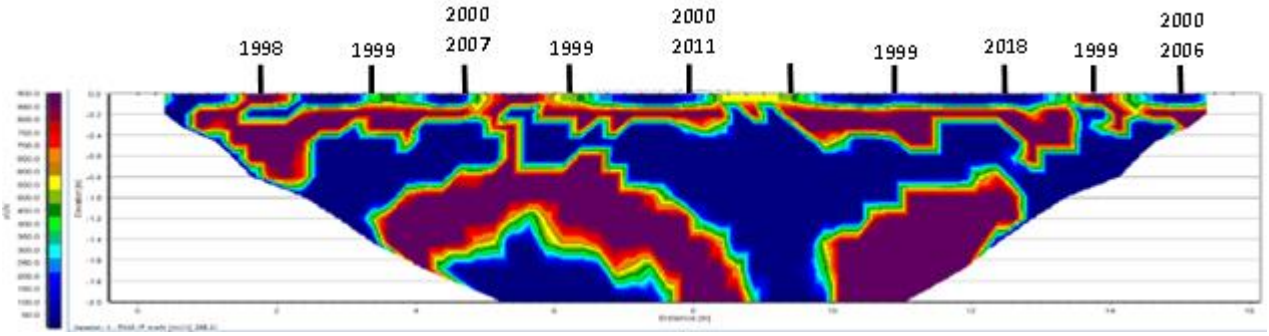

Figure 3.5.57: Induced polarisation data collected with the Dipole - Dipole array, March 2023. Keith Cemetery, Row H.

3.6 Keith Cemetery Soil

To understand the nature of the subsurface in the Keith Cemetery, detailed soil analysis was carried out. These are the results of those analyses.

3.6.1 Grain Size

Grain size analysis was carried out in the first instance using the nested sieve process.

Table 3.6.1: Nested sieve grain size results, Keith Cemetery.

Site	Sample Depth	Start weight	4mm	2mm	1mm	0.5mm	0.25mm	0.125mm	0.063mm	Base	Post weight	Loss
Keith	30cm	60.543	8.541	7.412	30.085	10.175	1.653	1.77	0.008		59.644	0.899
	60cm	60.682	0.617	0.274	34.369	18.341	4.414	0.281			58.296	2.386
	100cm	60.829	0.038	0.62	38.421	17.704	2.325	0.364	0.071		59.543	1.286
	150cm	60.167	0.197	0.253	42.847	13.628	1.49	0.856	0.062		59.333	0.834
Wentworth Scale			Granule	Very Course Sand	Coarse Sand	Medium Sand	Fine Sand	Very Fine Sand	Coarse Silt			

From Figure 3.6.1 and Table 3.6.1 the grain size analysis from the Keith Cemetery shows a large percentage of grains, at all depths, to be 0.5 mm or larger. The sample taken at 150 cm shows a larger percentage of grain sizes >1 mm, with very consistent sizing shown in the 60 and 100 cm samples. In all sample depths there is a very small percentage of grains <5 mm. On the Wentworth scale this places the grains in the coarse to coarse to medium sand category.

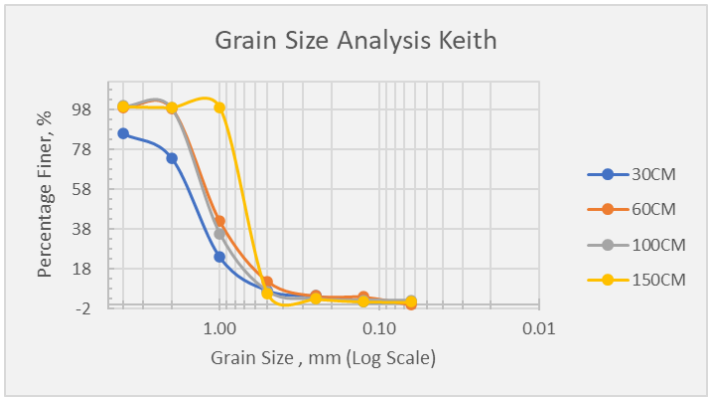

Figure 3.6.1: Nested sieve grain size plot, Keith Cemetery.

3.6.2 Magnetic Susceptibility

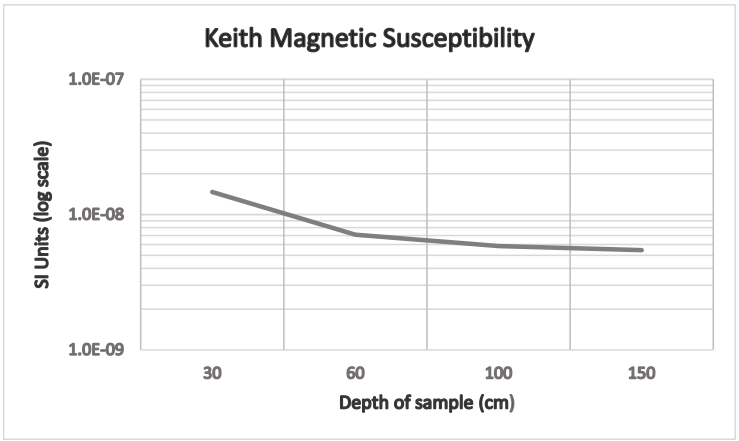

Figure 3.6.2: Low frequency magnetic susceptibility plot, Keith Cemetery.

The magnetic susceptibility results for Keith are shown in Figure 3.6.2. The subsurface found in the Keith Cemetery shows a very low susceptibility, indicating possible diamagnetic properties, although K_{lf}% is generally > 15. This is consistent with the sandy, depositional nature of the soil. Values also reduce with depth.

3.6.3 Soil Chemistry

X-ray fluorescence results from samples taken at the Keith Cemetery. The results in Table 3.6.2 show the ten most abundant chemical elements measured in the soil samples. These results are dominated by the presence of silicon (Si), which shows a consistent concentration throughout the sample depths. Also present at significantly lower concentrations are Calcium (Ca), Aluminium (Al), Potassium (K), Barium (Ba), and Sulphur (S). This is consistent with the depositional origins of the soil and could stem from the quartz in the sands.

Table 3.6.2: XRF chemical analysis, Keith Cemetery. The ten most abundant chemical elements are listed (ppm)

Element	30 cm	30 cm	60 cm	60 cm	100 cm	100 cm	150 cm	150 cm
Silica (Si)	142991	178758	177262	171842	195151	201644	197125	198472
Si Error	1558	1767	1748	1719	1846	1882	1858	1866
Calcium (Ca)	2668	3586	600	681	323	366	433	624
Ca Error	69	76	45	47	40	41	43	45
Aluminium (Al)	2385	2933	2537	2535	1940	1561	1537	1691
Al Error	636	695	656	652	655	653	648	652
Potassium (K)	1880	2616	2724	2437	2538	2521	2257	1978
K Error	75	82	81	79	79	79	77	73
Barium (Ba)	621	443	1298	0	456	979	1734	0
Ba Error	2660	2817	2547	2586	2572	2547	2636	2584
Sulfur (S)	602	649	488	490	485	514	518	548
S Error	79	82	74	74	75	76	77	77
Titanium (Ti)	476	754	0	585	390	565	0	424
Ti Error	6	6	6	6	6	6	6	6
Iron (Fe)	243	225	0	0	0	0	0	0
Fe Error	64	63	52	55	47	46	48	50
Zirconium (Zr)	166	115	90	139	76	178	138	88
Zr Error	8	7	7	8	7	8	7	7
Palladium (Pd)	166	206	176	170	174	155	190	195
Pd Error	29	29	27	28	26	26	27	27

3.6.4 Radar Velocity and ERT Resistivity

To analyse the effects of seasonal rainfall on velocity and resistivity, one hyperbola that is consistently detectable in all radargrams from all site visits is chosen. The velocity is recorded from all visits, as well as the relevant burial position. The resistivity from both array protocols is recorded from the same burial position and depth.

Table 3.6.3: Keith Cemetery resistivity and radar velocity results.

GPR Data	Velocity (m/ns)	ERT	Resistivity (Ω-m) Wenner array	Resistivity (Ω-m) Dipole – Dipole array
Aug 2020	0.11	Aug 2020	539.87	456.97
Oct 2020	0.118			
Jan 2021	0.134	Jan 2021	224.43	188.97
Jan 2022	0.1	Jan 2022	145.54	246.7
May 2022	0.108			
July 2022	0.114	July 2022	424.07	747.61
Sept 2022	0.098			
Dec 2022	0.116			
March 2023	0.09	March 2023	166.82	415.77

Table 3.6.3 gives the results of the velocity and resistivity according to the month of visit. May 2022 was the only month that recorded above average rainfall.

Table 3.6.4: Resistivity values for Wenner array.

Distance along ERT line (m)	Depth (cm)	Aug-20	Jan-21	Jan-22	Jul-22	Mar-23
8.5	78	680.14	283.91	178.46	492.3	211.17
8.5	104	565.54	239.65	156.6	468.67	174.3
8.62	91	652.88	275.4	183.99	434.82	189.68
8.62	117		247.03		445.32	165.01
8.75	78	686.52	268.51	150.35	434.11	191.41
8.75	104	573.2	234.17	154.32	448.21	174.32
8.88	91	594.59	238.34	148.1	405.33	182.53
8.88	117		228.92		403.34	149.82
9	78	625.89	258.85	153.63	420.99	187.75
9	104	529.17	224.48	137.17	414.77	164.74
9.25	78	560.56	211.72	154.46	444.39	191.08
9.25	104	540.8	218.89	144.59	421.31	172.52
9.38	91	495.67	197.84	160.88	464.58	191.47
9.38	117		193.35		386.4	158.95
9.5	78	508.83	165.43	182.92	507.95	214.13
9.5	104	490.64	209.02	135.01	404.56	174.95

Table 3.6.5: Resistivity values for Dipole - Dipole array.

Distance along ERT line (m)	Depth (cm)	Aug-20	Jan-21	Jan-22	Jul-22	Mar-23
8.5	87	569.12	202.97	129.96	728.98	424.75
8.5	105	501.78	181.17	212.32	626.22	448.66
8.62	73	587.5	207.42	129.96	804	
8.62	94	542.03	199.56	212.32	733.67	
8.75	70	621.65	205.78	322.68	933.91	310.54
8.75	105	434.25	164.3	212.42	667.74	411.91
8.88	73	682.08	271.85	186.71	833.29	
8.88	94		180.98	288	843.67	
9	70	698.5	267.94	379.75	1051.9	231.11
9	105	436.57	163.31	264.77	754.33	397.11
9.25	70	673.93	297.76	291.93	869.88	313.65
9.25	105	448.75	187.93	260.74	833.5	390.87
9.38	73	675.75	309.18	156.44	754.41	
9.38	94	527.38	229.73	252.09	693.85	
9.5	70	809.87	338.18	263.85	725.76	346.48
9.5	105	463.5	196.85	270.99	827.86	430.32

Tables 3.6.4 and 3.6.4 give the resistivity values of both array protocols. These distances and depths are of the model blocks from Res2DInv, and represent the width of the burial shaft, and the depth of the corresponding hyperbola.

3.7 Bordertown Cemetery

3.7.1 Introduction

Data for the Bordertown Cemetery was collected from rows D and E. This grid was 21.5x5 meters, and 11 lines of data were collected each visit, covering all of the grassed area, Figure 3.7.1. Row D contained 14 burial sites, with row E also containing 14 burial sites. GPR data was successfully collected on all visits, however, suitable ERT data was only collected on seven occasions. The ERT data was captured with the Wenner and Dipole – Dipole arrays, with an electrode spacing of 50 cm. Due to space restrictions, the electrodes extend past the end of the row, into a driveway. The edge of this driveway is at 9.8 m, or between the 20th and 21st electrode, see Figure 3.7.2. The months within the period 2020-2023 that visits to this site are listed in Table 3.7.1. From all the radargrams collected from Bordertown, one from Row D showed a reflection that was consistent from all visits. From these 11 radar lines, this one line will provide a soil velocity that will be compared to the resistance from the ERT data. The velocity and resistivity values are compared to soil moisture and/or seasonal rainfall.

The results from the GPR show no visits identified all fourteen of the burials, over all visits only 36% of the burials were identified. Resistivity values range from 1.63 – 36.9 Ω-m for the Wenner array, 3.3 – 131 Ω-m for the Dipole-Dipole array. Chargeability values range from 41.5 – 747.9 nV/V for the Wenner array, and 5.8 – 270 nV/V for the Dipole-Dipole array.

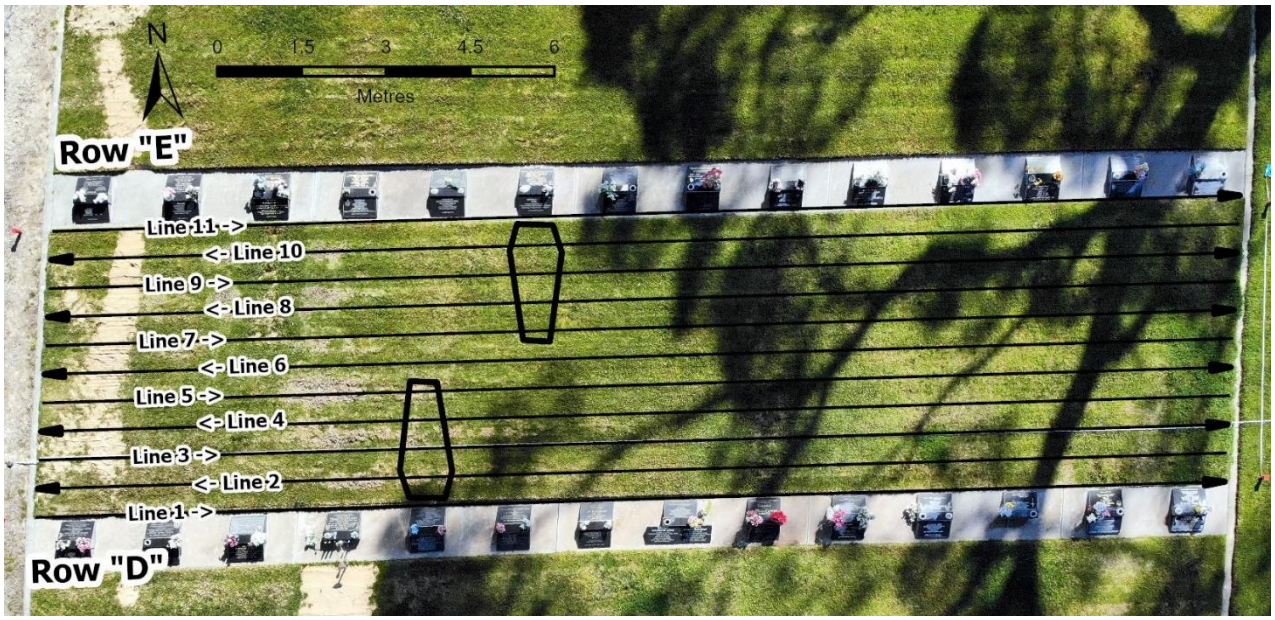

Figure 3.7.1: Rows D and E, Bordertown Cemetery. The GPR lines are shown, and as the data is collected in a "zigzag" method, every second line is in the opposite direction. The outlines of two graves are shown to illustrate that for Row D, lines 2 & 3 are over the widest point of the coffin, i.e. the shoulders and torso. The ERT line is between line 2 and 3 in Row D.

Table 3.7.1: Data collection months, Bordertown Cemetery.

GPR Data	ERT Data
Aug 2020	Aug 2020
Oct 2020	Oct 2020
Jan 2021	Jan 2021
Jan 2022	
May 2022	
July 2022	July 2022
Sept 2022	Sept 2022
Dec 2022	Dec 2022
March 2023	Mar 2023

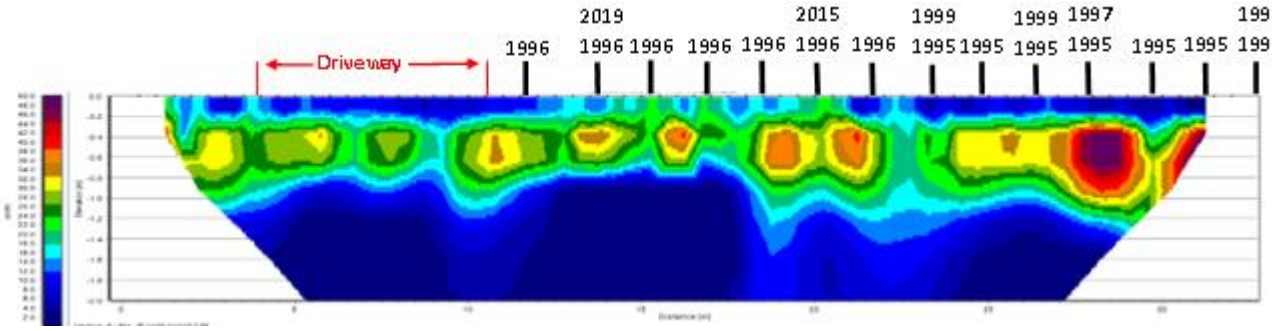

Figure 3.7.2: The layout of the ERT line along Row D, Bordertown Cemetery. To use the required total length of electrode spacing (31.5 m at 50 cm electrode spacing) the line extended past the end of Row D into a driveway. Beyond this driveway were two more graves that are not part of this research.

3.8 Installed Soil Moisture Meter

The moisture meter was installed in June 2021. This initial meter proved to be faulty and was replaced in March 2022.

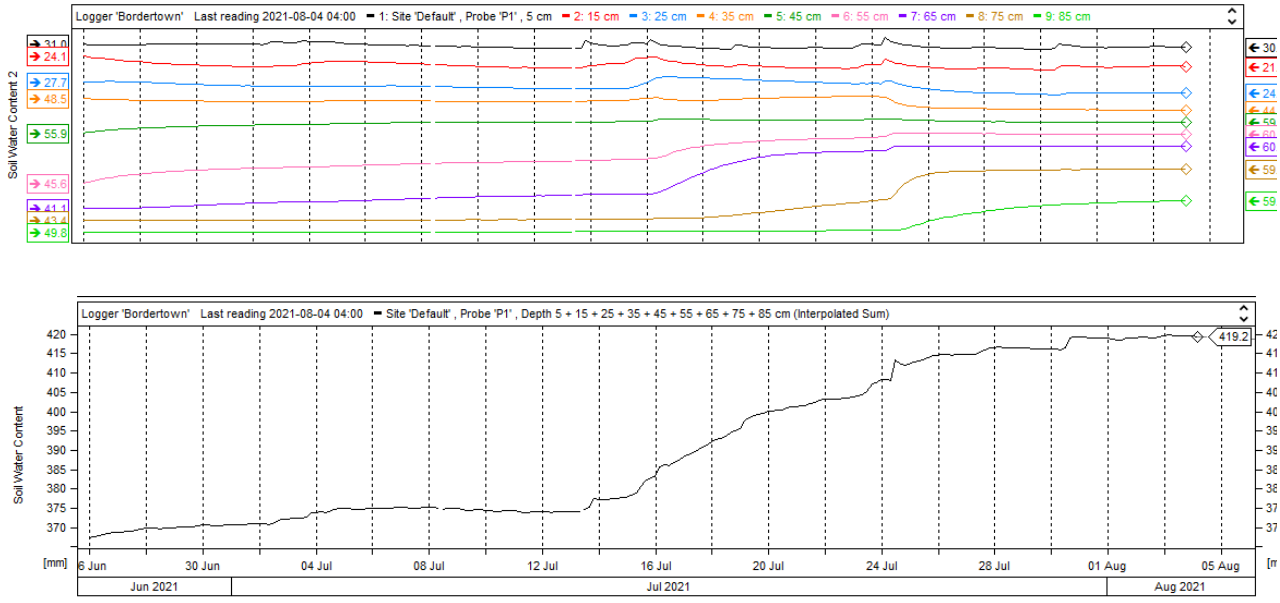

Figure 3.8.1: Moisture meter plot from initial installation. Top is the moisture levels (in mm) of each sensor. Bottom, overall soil moisture levels (in mm).

Figure 3.8.1 shows data from the initial installation. This is a period from 25 June 2021 until 4th August 2021. The uppermost plot shows the moisture level at each sensor depth, from 5 cm down to 85 cm in 10 cm increments. The lower plot shows the sum of all eight sensors as a total soil moisture content, in mm. This total soil moisture content shows a consistent moisture level until 13th July, when the total soil moisture content rises steadily over a period of seventeen days, then stays at a consistent level. The local official weather station recorded a rainfall event of 13.4 mm on July 5th, with no further rainfall events until after July 13th. The upper plot shows a small spike in moisture levels also recorded on the 13th July by the 5 cm sensor, this spike is replicated at 10 cm by a small rise in moisture, but not recorded by any deeper

sensors. On July 16th the sensors at a depth of 55 cm and below show a steady rise in moisture levels, the greatest rise is at 65 cm, this sensor recorded a rise from 41.1 mm to 60.1 mm over the period of recording.

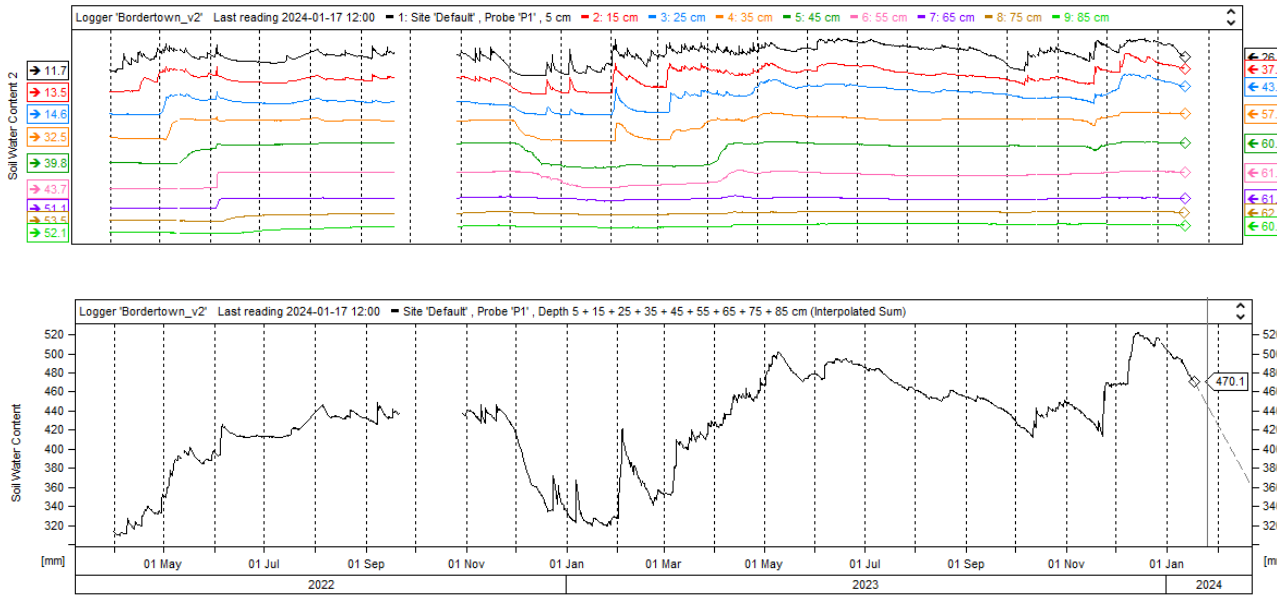

Figure 3.8.2: Moisture meter plot from the second installation.

Figure 3.8.2shows recorded moisture levels from the second installation, this sensor was installed on 30th March 2022. The period September 21 to October 28 shows an unexplained error in data capture, see "A" in Figure 3.8.3. In the period August 2021 to this installation on March 30th the total soil moisture dropped from 419 mm to 309 mm. The local official weather station recorded a total of 211 mm of rain during this period.

Total soil moisture spiked first on 29th April 2022, this is seen at sensor depth of 25 cm, then 5 days later at a depth of 35 cm, and a further 5 days and the soil moisture spikes again at a depth of 45 cm. The sensors below this depth do not record any changes in this period, see "B" in Figure 3.8.3. The local weather station recorded 7 mm on April 19th 2022, and a further 1.4 mm on April 20th 2022.

Another spike of 30 mm is recorded on 3rd June 2022, this is seen as spikes at all depths excluding the 85 cm sensor. The highest gain in soil moisture is recorded at depth of 55 cm, where the soil moisture increases by 16 mm in the 10 hours between the 5th and 6th June 2022, see "C" in Figure 3.8.3. The local weather station recorded a rainfall event of 32.4 mm on the 6th June 2022.

Between the 18th November and the 22nd December 2022 the total soil moisture dropped some 110 mm, and this drop is shown from the sensors at 45 cm and above, see "D" in Figure 3.8.3. The soil moisture recorded at 55 cm also recorded a small drop between the 15th December and the 22nd December 2022. Below 55 cm there was no change in soil moisture in this period. The local weather station recorded 32 mm of rain in this period.

On the 23rd December 2022 a sharp spike in soil moisture is recorded at the sensor depths of 5,15, and 25 cm. with the sensor at 15 cm showing the greatest increase of 15 mm over a two hour period, ("E" in Figure 3.8.3). The local weather station recorded a 6 mm rainfall event on 22nd December 2022.

Fourteen days (6th January 2023) later another soil moisture spike is recorded at the depths of 5 and 15 cm. At the depth of 5 cm the recorded soil moisture increased by 26.8 mm, ("F" in Figure 3.8.3). No rainfall had been recorded by the local weather station for the previous 15 days.

The 2nd of February 2023 saw another rainfall event, see "G" in Figure 3.8.3. This was recorded by the sensors to a depth of 35 cm and showed an increase of soil moisture of 27.9 mm, this increase was recorded over a period of 50 hours. The local weather station recorded 8.4 mm on the 2nd and 3rd of February.

Late on the 6th March 2023 another rainfall event was recorded by the sensors at 5 cm, 15 cm, and 25 cm. Over a period of 52 hours an increase of 11.5 at 5 cm, 25.6 mm at 15 cm and some 12 hours later 19.5 cm at a depth of 25 cm, see "H" in Figure 3.8.3. From this point the total soil moisture rose until a peak of 500 mm, recorded on May 10th, 2023, see "I" in Figure 3.8.3. This rise was replicated at the depths of 5 – 35 cm, but the sensors at 45 and 55 cm recorded one rise over a 17-day period, whereby the soil moisture recorded rose 23 mm. During this period (March 9th – May 10th) the local weather station recorded 84.9 mm of rain.

From this point in time, the moisture sensor has become a permanent installation to aid further research, but as the focus of this thesis ends in March 2023, no further discussion is required.

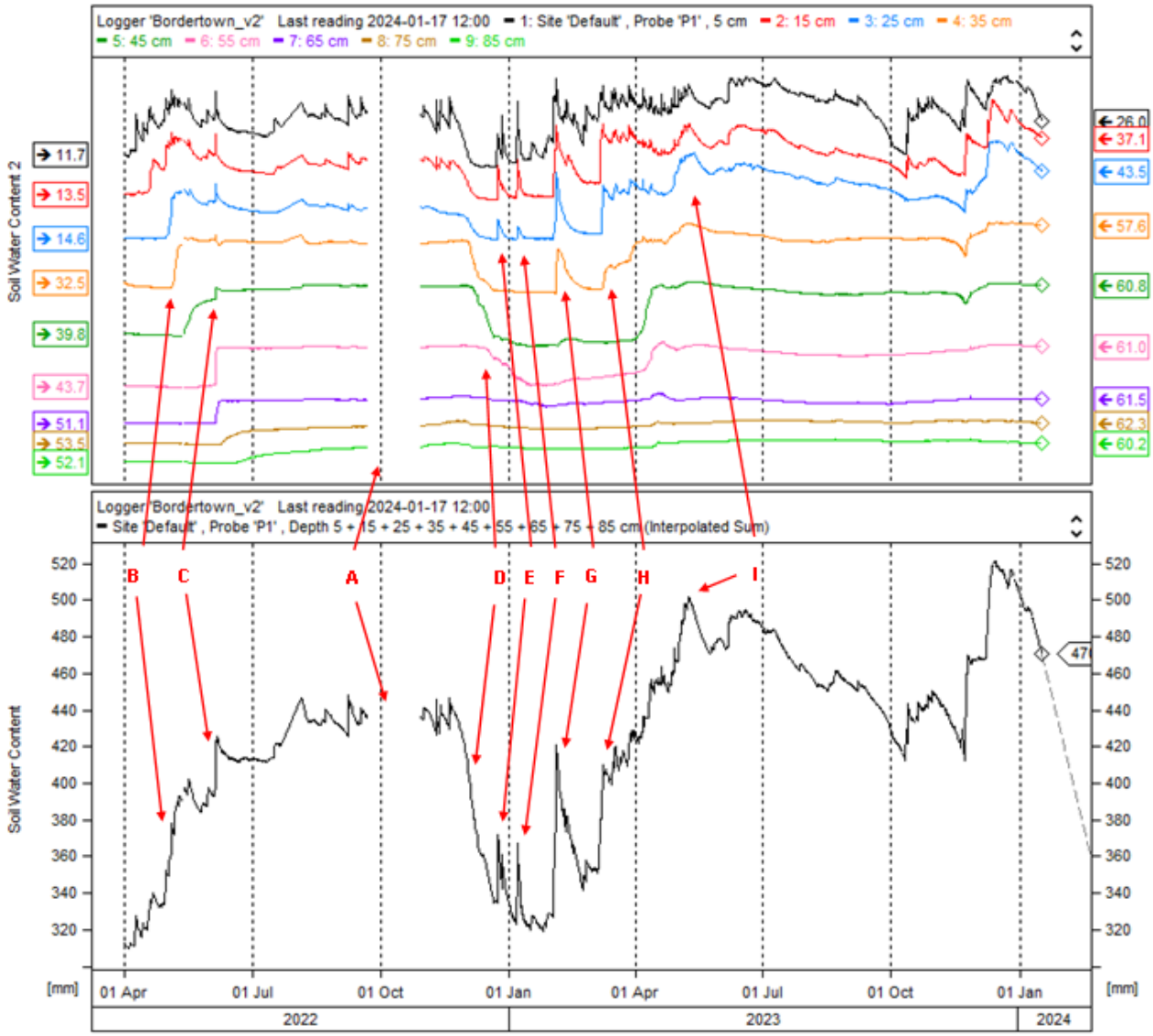

Figure 3.8.3: Bordertown moisture meter with key points highlighted.

3.9 Bordertown Cemetery Geophysics

3.9.1 August 2020

Data was collected in August 2020. There was 5 mm of rainfall in the week before this data was collected, and the ten-month rainfall plot is shown in Figure 3.9.1. Six of fourteen burials can be identified in the radargrams. The three radargrams from Row D shows a series of different reflections. Line 2 shows differing reflections at a depth between 50 – 100 cm. These are highlighted in Figure 3.9.2. Line 3 show reflections at the same depth range, these occur at the opposite end of the radargram. These are highlighted in Figure 3.9.3. Line 4 shows three stratigraphic breaks that may be associated with grave shafts, Figure 3.9.4. Attenuation of this data starts at ~110 cm.

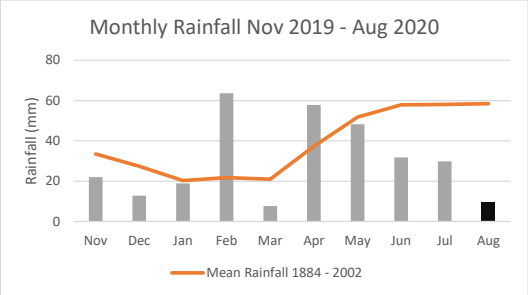

Figure 3.9.1: Rainfall in August 2020 for the ten months prior to data collecting. Months that the study site was visited over this period in black. (Rainfall and Temperature data from bom.gov.au)

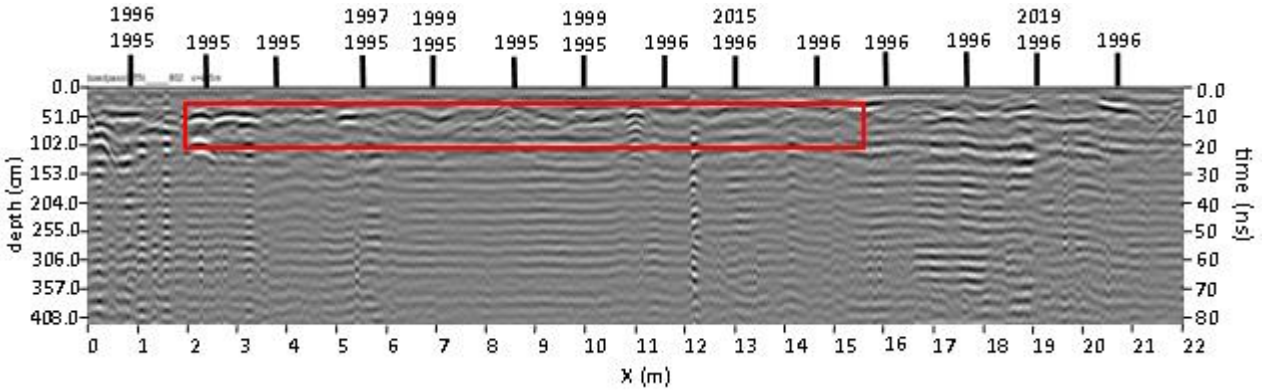

Figure 3.9.2: Bordertown Cemetery August 2020, Row D, line 2. The series of reflections are highlighted in red.

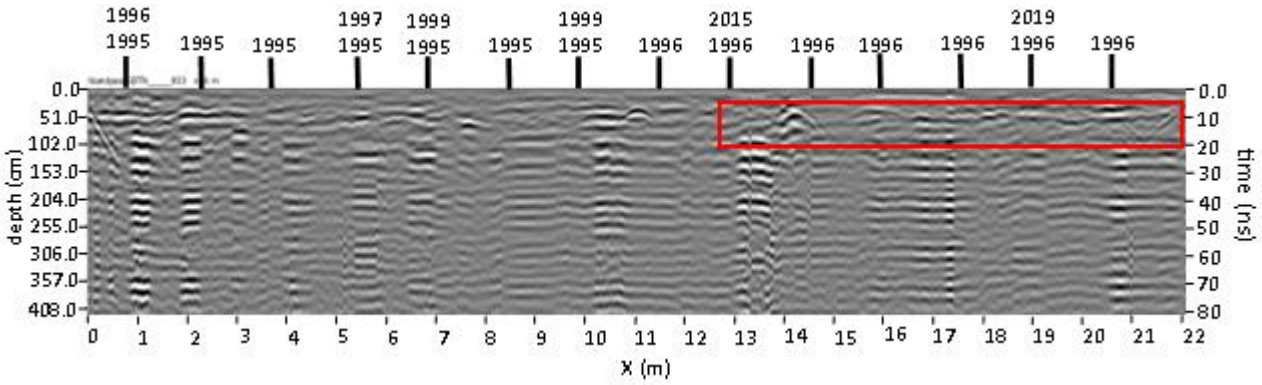

Figure 3.9.3: Bordertown Cemetery August 2020, Row D, line 3. The series of reflections are highlighted in red.

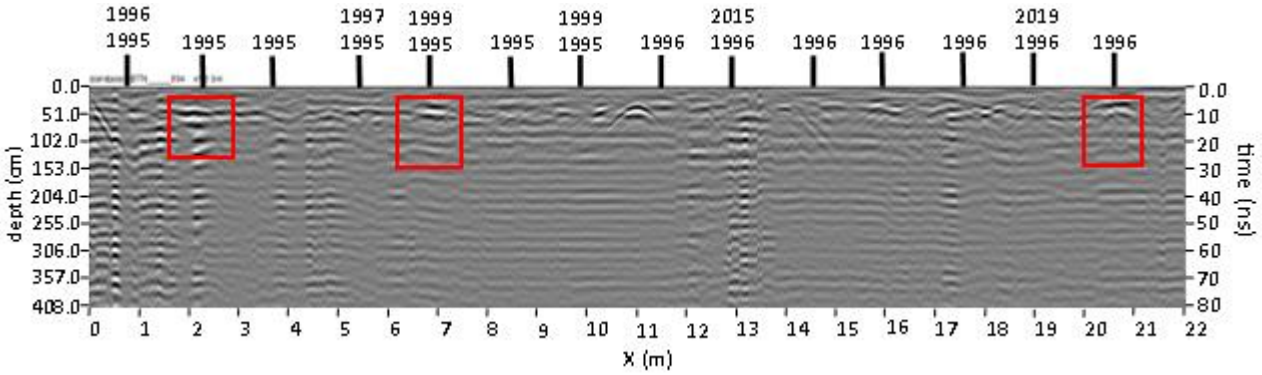

Figure 3.9.4: Bordertown Cemetery, August 2020, Row D, line 4. Stratigraphic breaks are highlighted in red.

The resistivity and induced polarisation data was captured using the Wenner and Dipole – Dipole arrays, with electrode spacing of 50 cm. The Wenner inversion, Figure 3.9.5, shows, at a depth of 80 – 100 cm, a drop in resistivity, (below 9 Ω-m). Areas of higher resistivity are seen above this depth these areas show resistivity values from 11 Ω-m to a high of 58.3 Ω-m. Nine of fourteen burials can be identified. Figure 3.9.6 shows the induced polarisation chargeability captured with the Wenner array. A layer of higher chargeability, (> 25 nV/V), extends down to a depth of 60 cm. Within this layer eight burials can be identified.

The IP inversion plot shows areas of higher chargeability, (> 26 nV/V), extending along the line. These areas could be associated with the burials, but the higher chargeability does extend into the driveway located at the start of the ERT line.

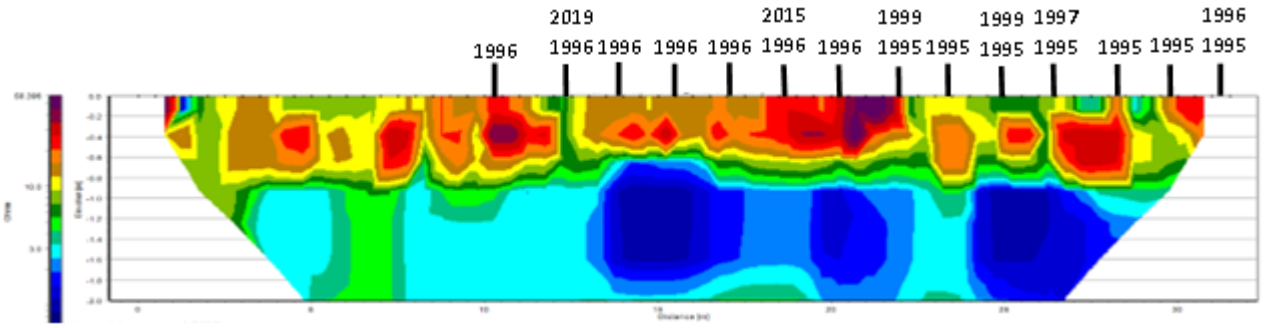

Figure 3.9.5: Resistivity data captured with the Wenner array, August 2020. Bordertown Cemetery, Row D.

The inversion of data captured by the Dipole – Dipole array, Figure 3.9.7, shows a layer along the entire line recording resistivity values > 15 Ω-m. This layer extends to a depth of between 60 and 80 cm and contains several discrete areas with resistivity > 50 Ω-m that are associated with burials.

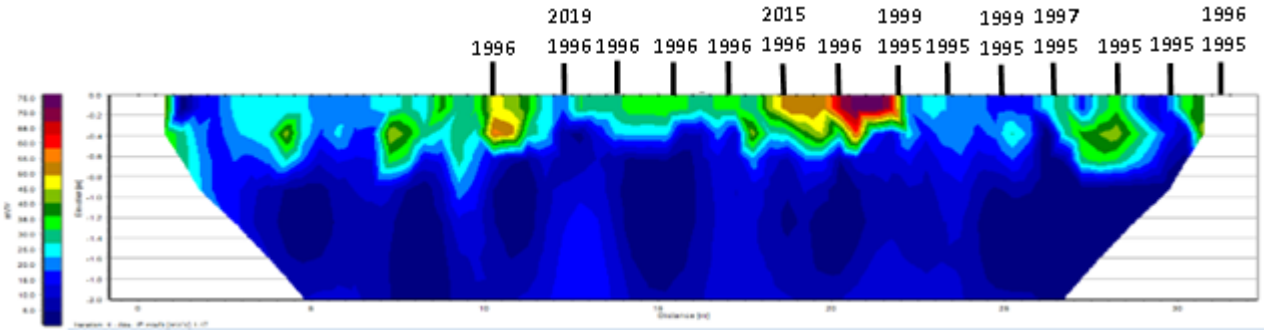

Figure 3.9.6: Induced Polarisation data captured with the Wenner array. August 2020. Bordertown Cemetery, Row D.

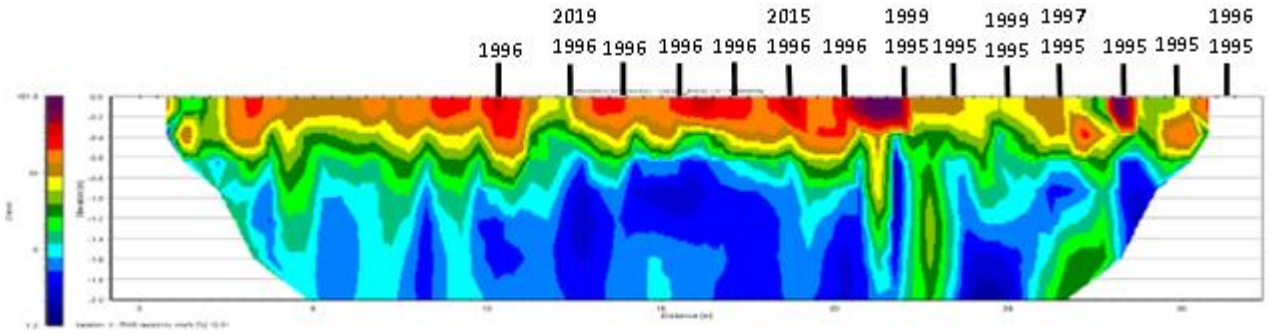

Figure 3.9.7: Resistivity data captured with the Dipole - Dipole array. August 2020. Bordertown Cemetery, Row D.

The IP data captured with the Dipole – Dipole array, Figure 3.9.8, shows a thin layer at depths between 20 and 40 cm, Figure 3.9.8. This layer records chargeability values > 80 nV/V, with two discrete areas > 120 nV/V that are associated with burials. This layer > 80 nV/V also extends into the driveway.

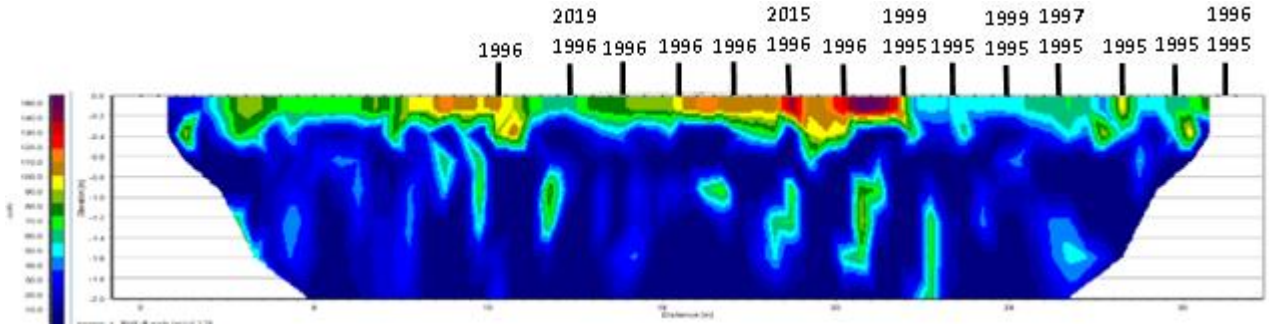

Figure 3.9.8: Induced polarisation data captured with the Dipole - Dipole array, August 2020. Bordertown Cemetery, Row D.

3.9.2 October 2020

Data was collected in October 2020. There was 3.3 mm of rainfall in the week before this data was collected, and the ten-month rainfall plot is shown in Figure 3.9.9. Six of fourteen burials are identified in these radargrams. Line 2 contains stratigraphic breaks visible at three locations, highlighted in red in Figure 3.9.10. Line 3 shows reflections at a shallow depth in the centre of the radargram, highlighted in red in Figure 3.9.11. Attenuation occurs at a shallower depth of approximately 70 cm.

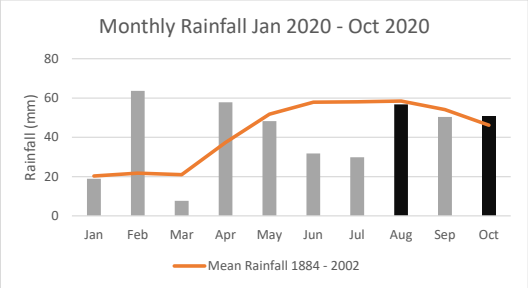

Figure 3.9.9: Monthly rainfall for the ten months prior to data collection. Months in which a visit occurred are in black. (Rainfall and Temperature data from bom.gov.au)

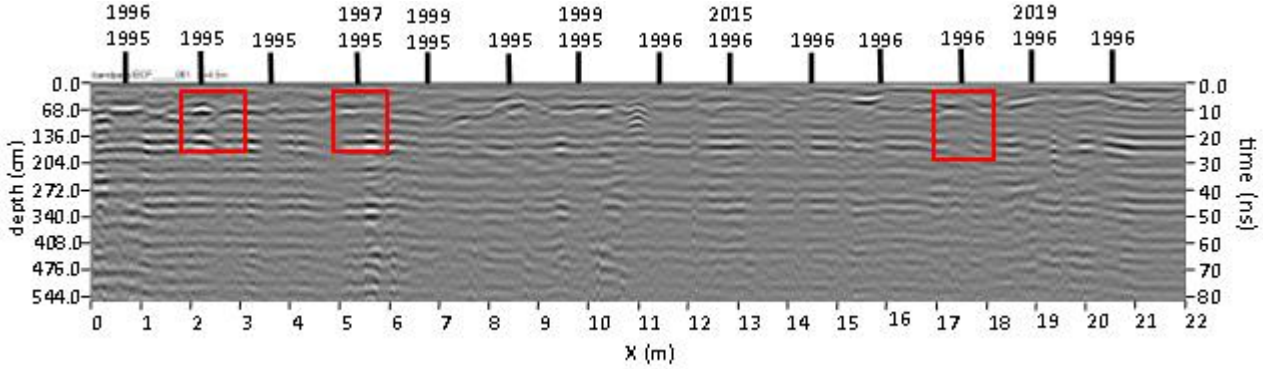

Figure 3.9.10: Bordertown Cemetery, October 2020, Row D, line 2.

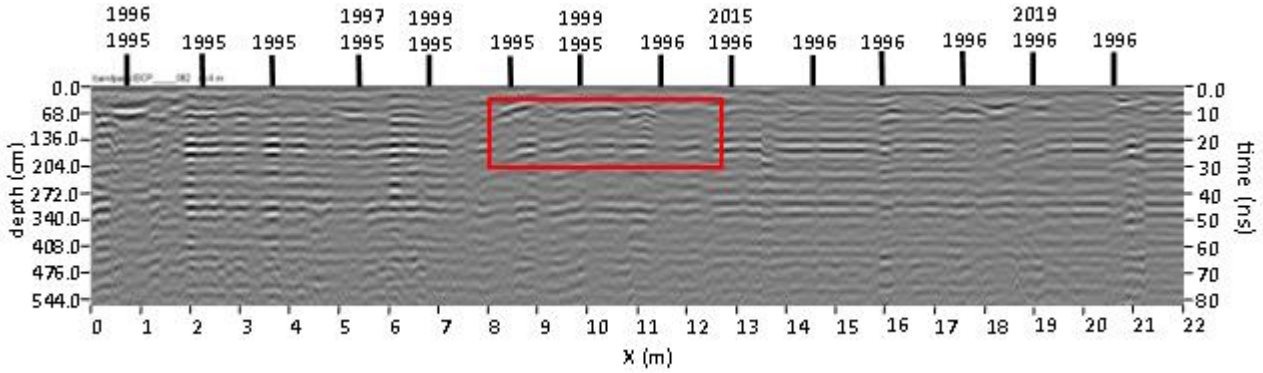

Figure 3.9.11: Bordertown Cemetery, October 2020, Row D, line 3

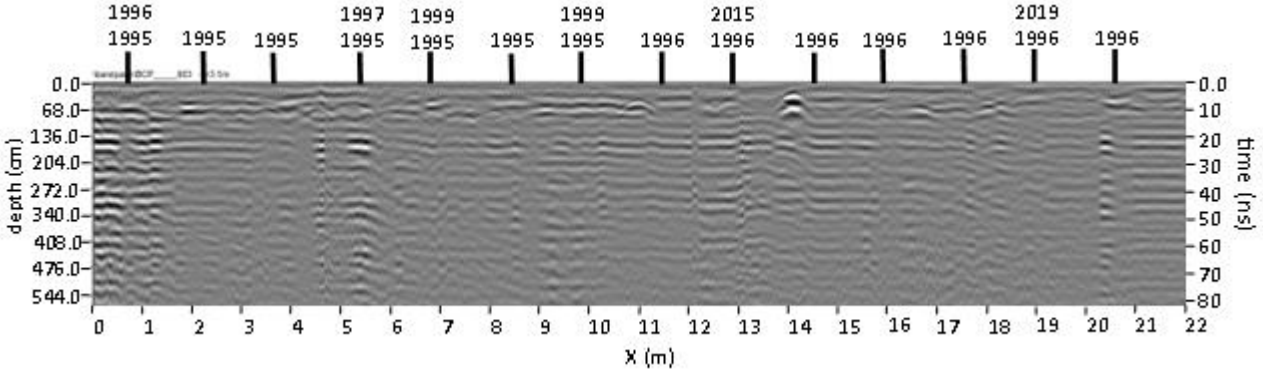

Figure 3.9.12: Bordertown Cemetery, October 2020, Row D, line 4.

The Wenner resistivity inversion, Figure 3.9.13, shows a layer at a depth between 20 cm and 120 cm of higher resistivity. The resistivity of this layer is greater than 7 Ω-m, to the maximum recorded of 36 Ω-m. Within this layer 8 burials can be identified. The IP inversion plot, Figure 3.9.14, shows many discrete areas with chargeability > 22 nV/V, these are associated with the burials, with eight burials being identified.

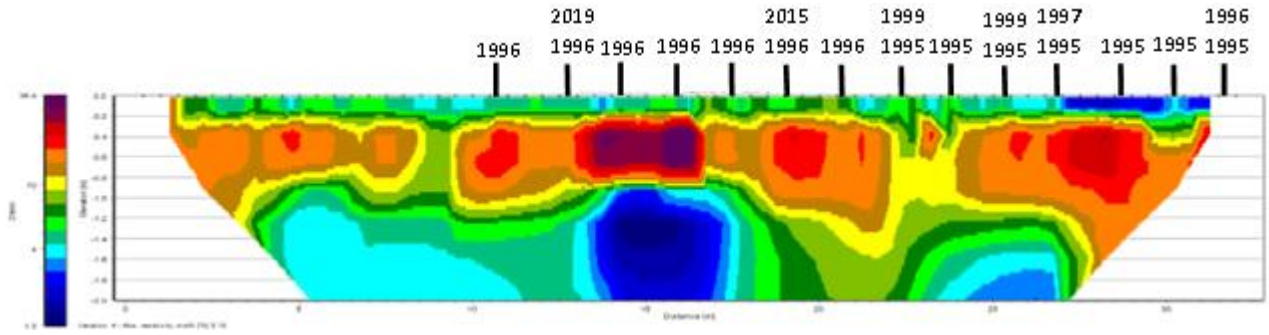

Figure 3.9.13: Resistivity data captured with the Wenner array, October 2020. Bordertown Cemetery, Row D.

The inversion of data captured with the Dipole – Dipole array shows a layer to a depth of approximately 60 cm, this layer records values above 10 Ω-m, with several discrete areas above 20 Ω-m that are associated with burials. There are also four areas extending to a depth 140 cm – 200 cm of higher resistivity, (> 15 Ω-m). These deeper areas are associated with burials.

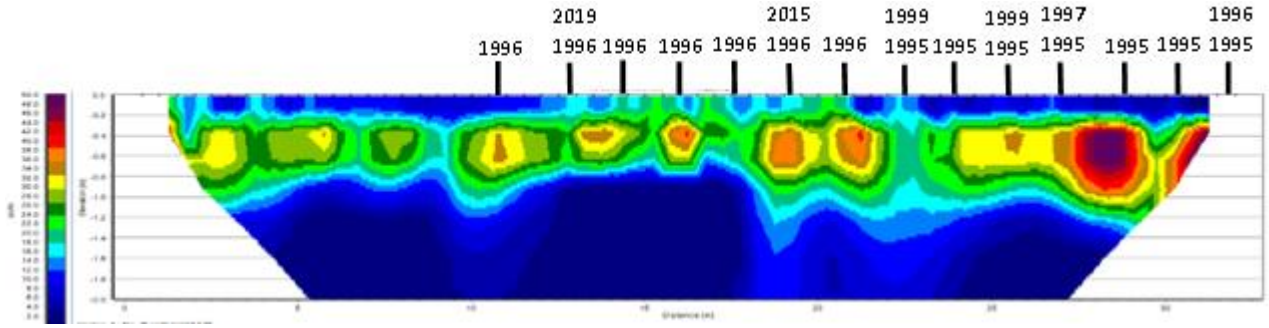

Figure 3.9.14: Induced polarisation data captured with the Wenner array, October 2020. Bordertown Cemetery, Row D.

Figure 3.9.15 shows the chargeability of data captured with the Dipole – Dipole array. This chargeability plot, Figure 3.9.16, shows a largely homogenous subsurface, with eight small areas to a depth of 40 cm, of higher chargeability, (> 50 nV/V).

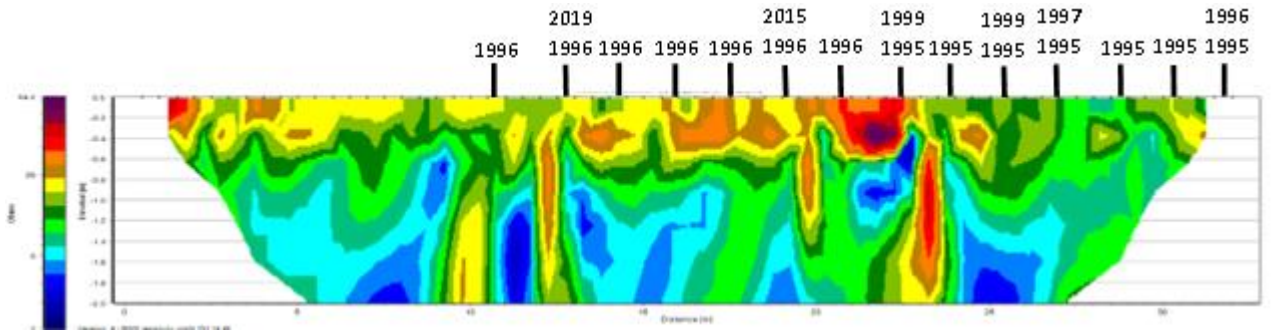

Figure 3.9.15: Resistivity data captured with the Dipole - Dipole array, October 2020. Bordertown Cemetery, Row D.

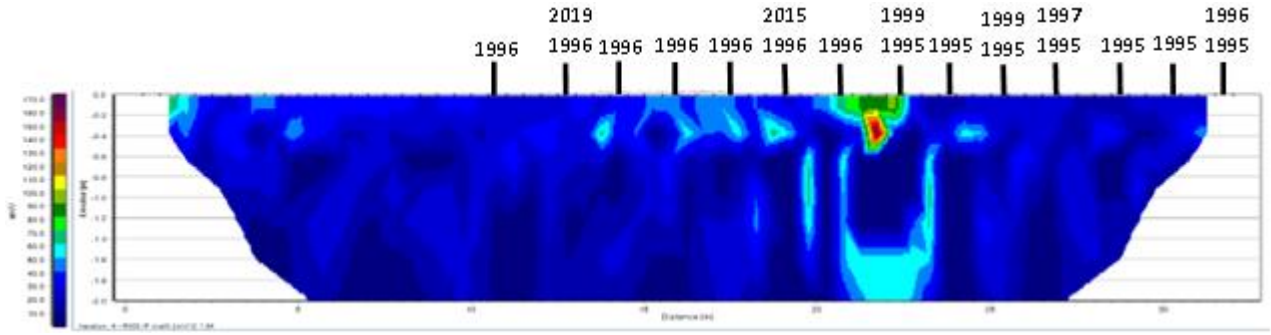

Figure 3.9.16: Induced polarisation data captured with the Dipole - Dipole array, October 2020. Bordertown Cemetery, Row D.

3.9.3 January 2021

Data was collected in January 2021. There was 0.6 mm of rainfall in the week before this data was collected, and the ten-month rainfall plot is shown in Figure 3.9.17.

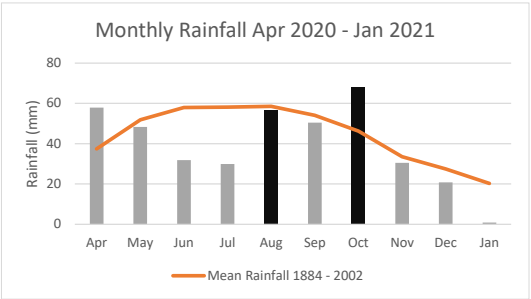

Figure 3.9.17: Monthly rainfall in the ten months prior to data collection. Months in which a site visit occurred in black. (Rainfall and Temperature data from bom.gov.au)

Three of fourteen burials are identifiable in these radargrams. The radargrams from this visit, Figures 3.9.18, 3.9.19, and 3.9.20, show very few reflections. Quite small stratigraphic breaks are seen in line 2, in

red in Figure 3.9.18. Line 4 shows one reflection in the centre of the radargram, this is highlighted in Figure 3.9.20. Attenuation does seem to start at the shallow depth of 50 cm.

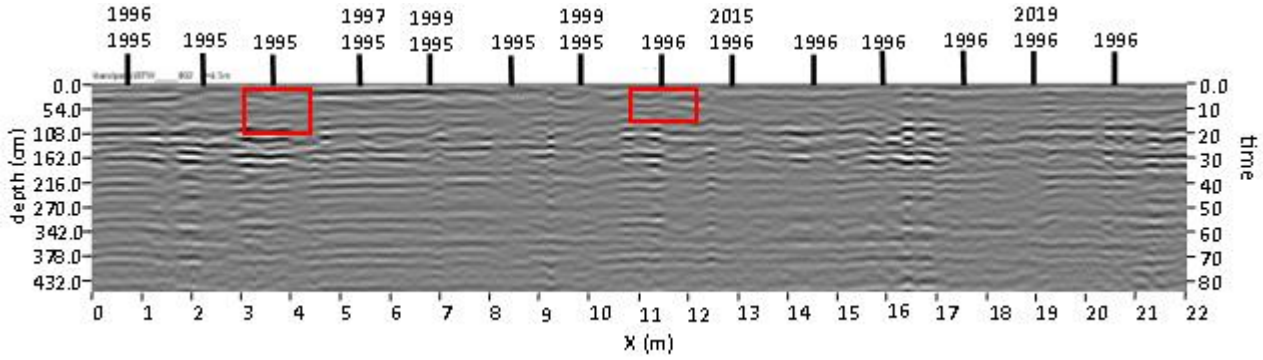

Figure 3.9.18: Bordertown Cemetery, January 2021, Row D, line 2.

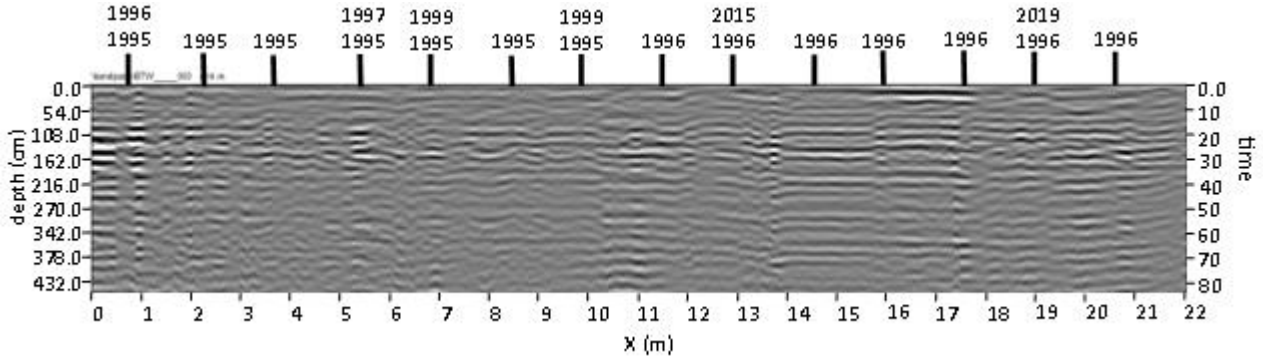

Figure 3.9.19: Bordertown Cemetery, January 2021, Row D, line 3.

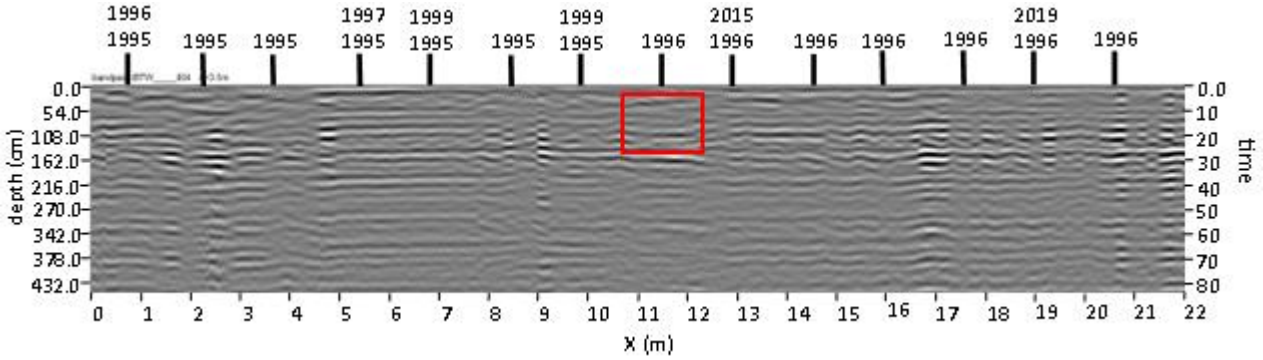

Figure 3.9.20: Bordertown Cemetery, January 2021, Row D, line 4. The small reflection is highlighted in red.

The resistivity data collected with the Wenner array, Figure 3.9.21, shows to a depth of approximately 100 cm, a layer of higher resistivity, (> 6 Ω-m). Within this layer are smaller areas of resistivity greater than 20 Ω-m, these areas are associated with burials. This layer also extends past the study site burials into the adjacent driveway.

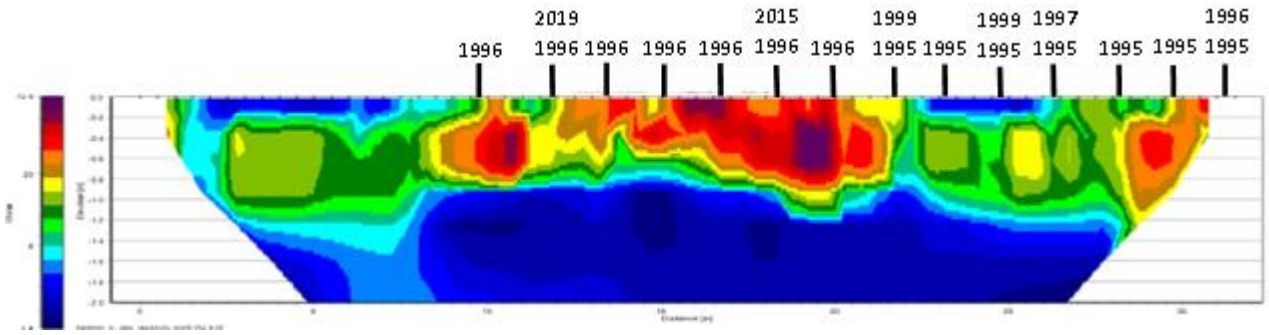

Figure 3.9.21: Resistivity data captured with the Wenner array, January 2021. Bordertown Cemetery, Row D.

The IP data captured with the Wenner array, Figure 3.9.22, mimics, to a certain extent the resistivity data. The layer to a depth of 60 cm extends through the area of the burials, this layer records a chargeability value > 25 nV/V. These higher chargeability values are associated with the burials.

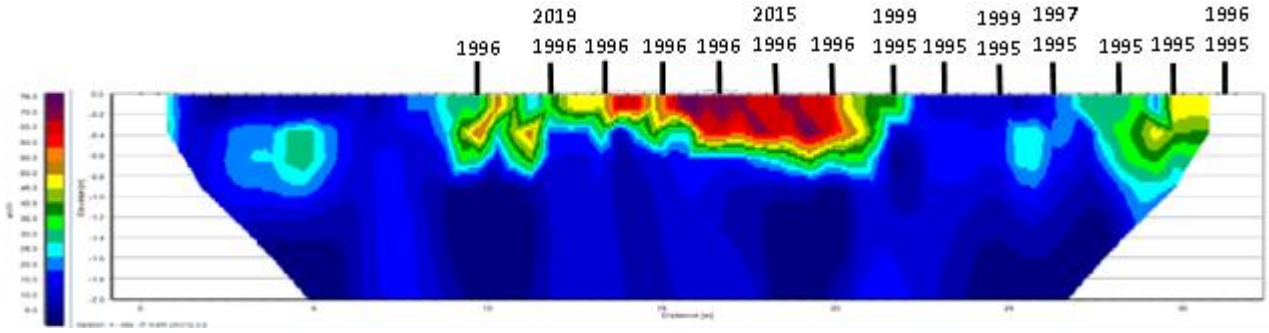

Figure 3.9.22: Induced polarisation data captured with the Wenner array, January 2021. Bordertown Cemetery, Row D.

Figure 3.9.23 shows the resistivity data captured with the Dipole – Dipole array. A layer extending to a depth of 100 cm records resistivity values greater than 7 Ω-m. Within this layer are smaller areas recording resistivity values of 60 Ω-m or more. These areas are associated with the burials, with ten burials being identified.

Figure 3.9.24 shows the IP data captured with the Dipole -Dipole array. This inversion shows small areas of chargeability above 80 nV/V, centred adjacent to the burials.

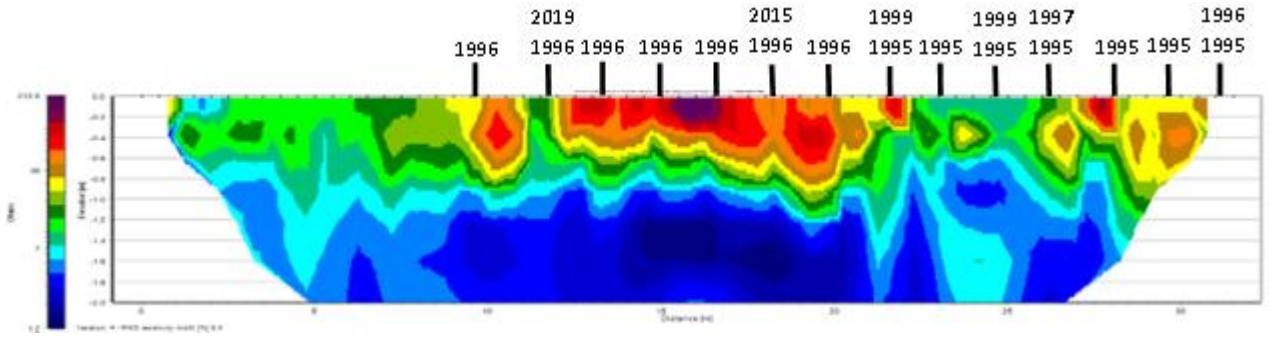

Figure 3.9.23: Resistivity data captured with the Dipole - Dipole array, January 2021. Bordertown Cemetery, Row D.

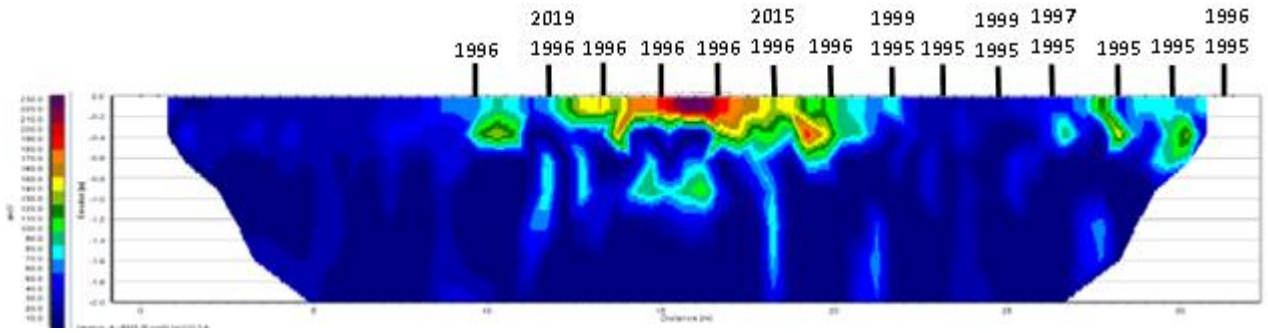

Figure 3.9.24: Induced polarisation data captured with the Dipole - Dipole array, January 2021. Bordertown Cemetery, Row D.

3.9.4 January 2022

Data was collected in January 2022. There was no recorded rainfall in the week before this data was collected, and the ten-month rainfall plot is shown in Figure 3.9.25. There was no ERT data captured on this visit. Four of the Fourteen burials are identifiable in these radargrams. The radargrams from January 2022 all show small reflections approximately above a depth of 60 cm. These reflections mainly show as stratigraphic breaks, these are highlighted in Figure 3.9.26 and Figure 3.9.27. Attenuation again starts at a shallow depth of approximately 50 cm.

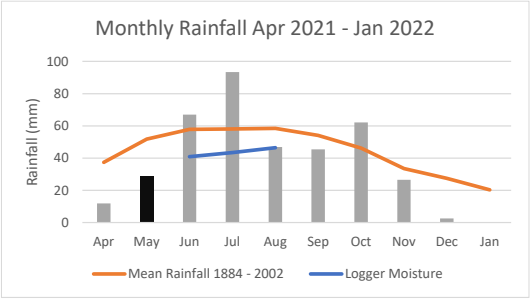

Figure 3.9.25: Monthly rainfall for the ten months prior to data collection. Months in which a site visit occurred are in black. (Rainfall and Temperature data from bom.gov.au)

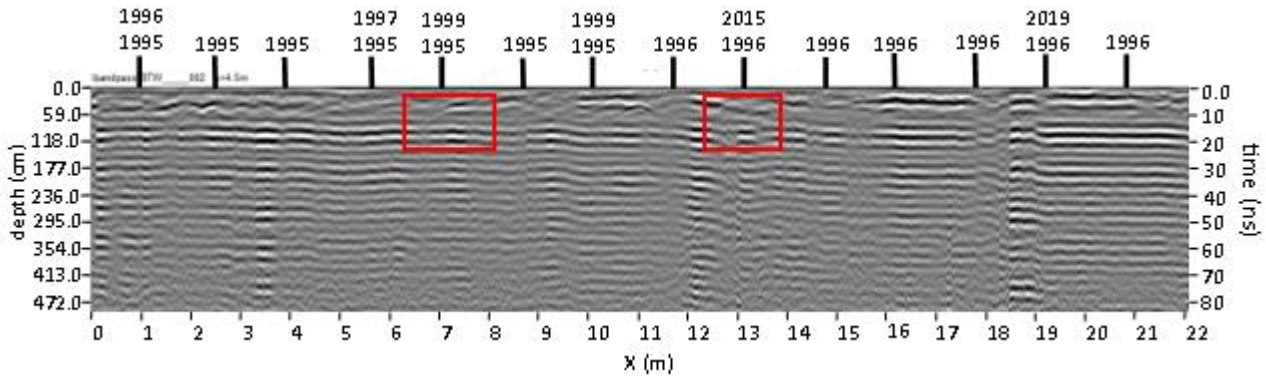

Figure 3.9.26: Bordertown Cemetery, January 2022, Row D, line 2. Stratigraphic breaks outlined in red.

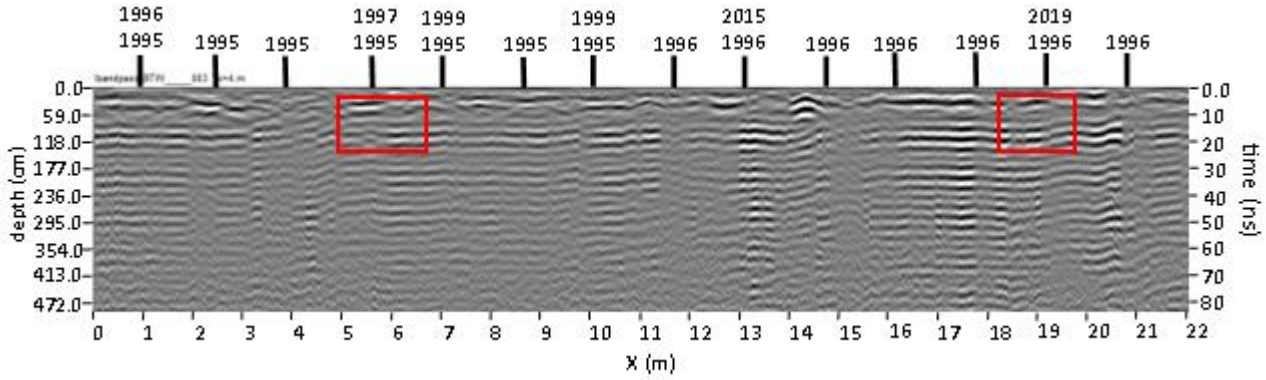

Figure 3.9.27: Bordertown Cemetery, January 2022, Row D, line 3.Stratigraphic breaks outlined in red.

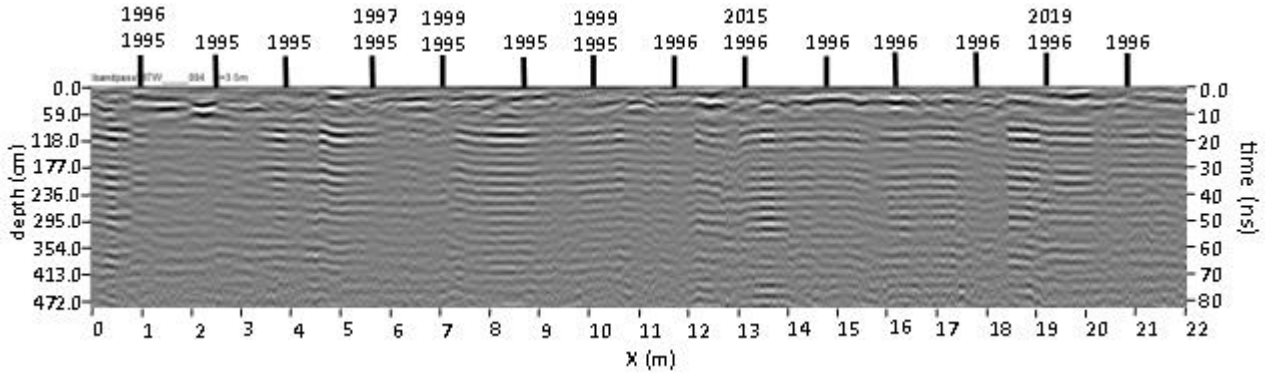

Figure 3.9.28: Bordertown Cemetery, January 2022, Row D, line 4.

3.9.5 May 2022

Data was collected in May 2022. There was 2.4 mm of rainfall in the week before this data was collected, with an additional 7.8 mm recorded on the day of collection. The ten-month rainfall plot is shown in Figure 3.9.29. There was no ERT data collected on this visit. Four of the fourteen burials are identifiable in these radargrams.

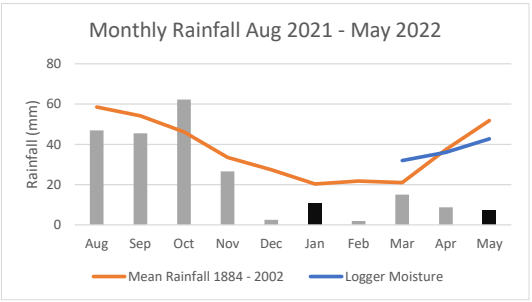

Figure 3.9.29: Monthly rainfall in the ten months prior data collection. Months in which a site visit occurred are in black. (Rainfall and Temperature data from bom.gov.au)

The radargrams from data gathered in May 2022, Figures 3.9.30, 3.9.31, and 3.9.32, all show a line of reflections at approximately 60 cm, below which attenuation starts. This line of reflections shows as a

stratigraphic layer, through which several breaks are present. These are highlighted in red in Figures 3.9.30, and 3.9.31.

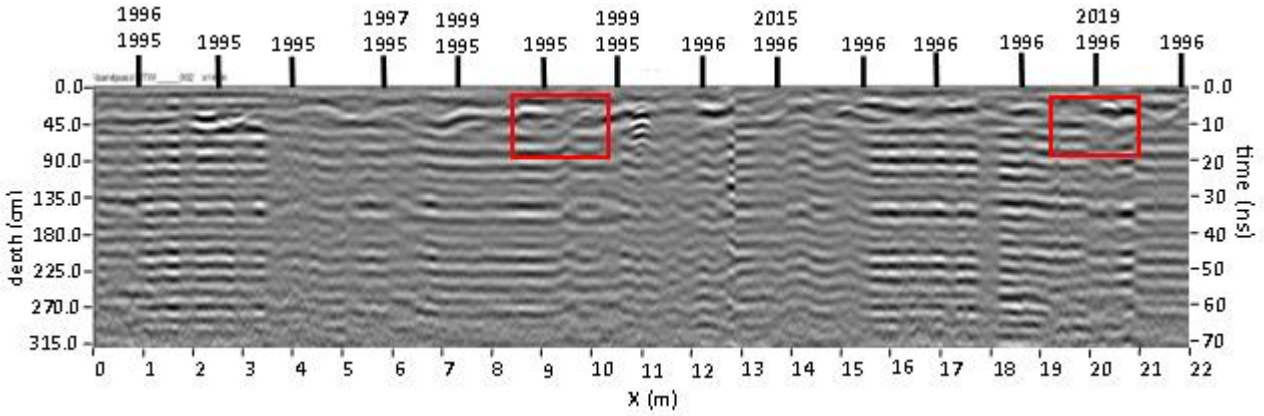

Figure 3.9.30: Bordertown Cemetery, May 2022, Row D, line 2. Stratigraphic breaks highlighted in red.

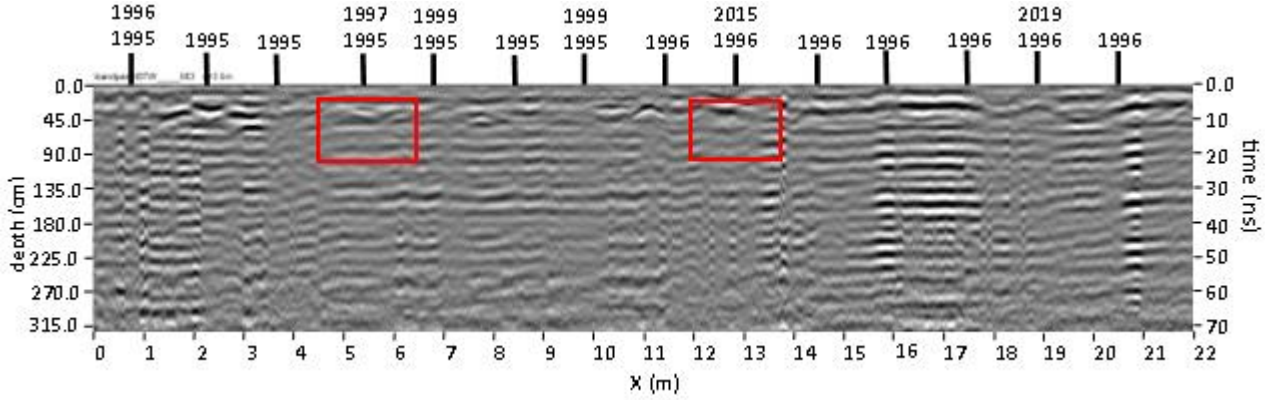

Figure 3.9.31: Bordertown Cemetery, May 2022, Row D, line 3. Stratigraphic breaks highlighted in red.

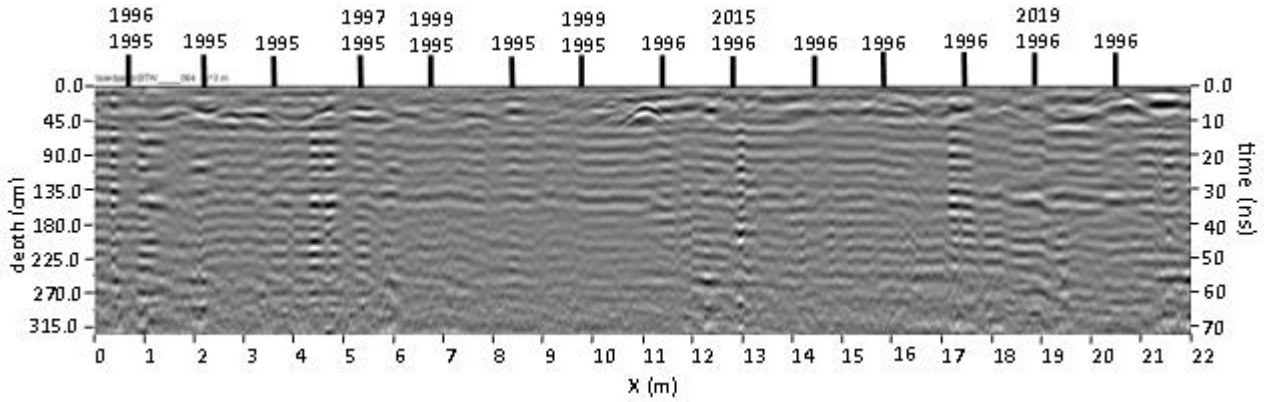

Figure 3.9.32: Bordertown Cemetery, May 2022, Rod D, line 4.

3.9.6 July 2022

Data was collected in July 2022. There was 8.8 mm of rainfall in the week before this data was collected, with an additional 2.4 mm recorded on the day of collection. The ten-month rainfall plot is shown in Figure 3.9.33. Six burials are identifiable in these radargrams.

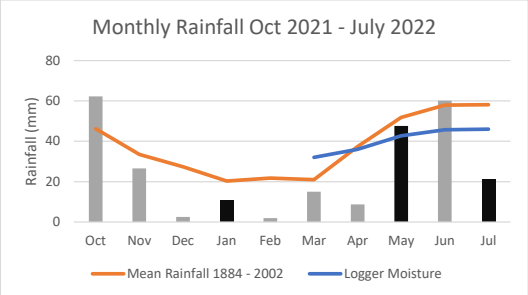

Figure 3.9.33: Monthly rainfall for the ten months prior to data collection. Months in which a site visit occurred are in black. (Rainfall and Temperature data from bom.gov.au)

The radargrams from this visit, Figures 3.9.94, 3.9.95, and 3.9.96, show a line of reflections through all radar lines. These appear as a stratigraphic layer, and are partly highlighted in line 3, Figure 3.9.95. Line 2 shows a reflection presenting a high amplitude, this is highlighted in Figure 3.9.94. Attenuation is deeper, starting at approximately 100 cm.

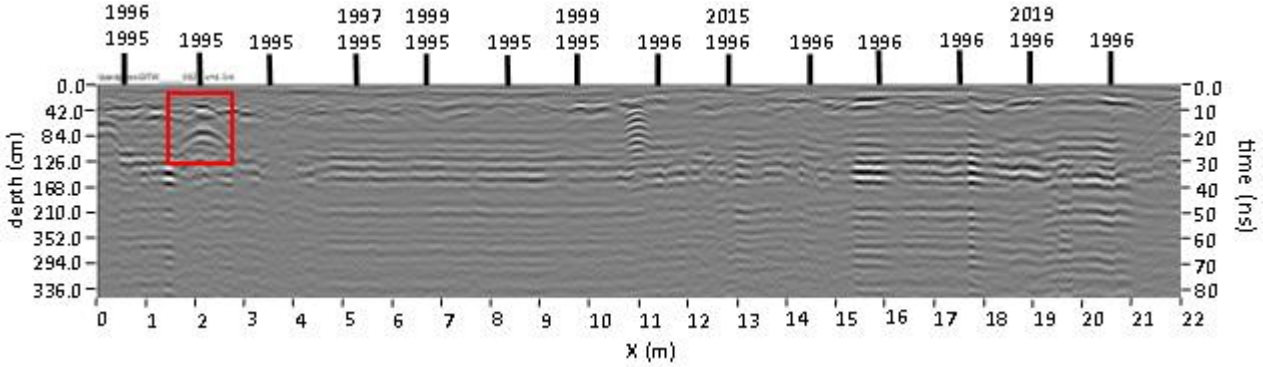

Figure 3.9.34: Bordertown Cemetery July 2022, Row D, line 2. The reflection showing the high amplitude is highlighted in red.

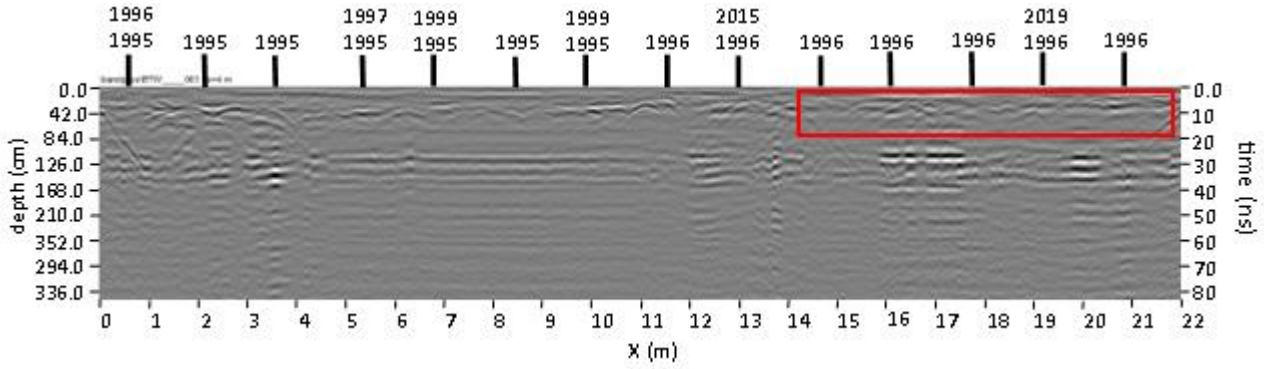

Figure 3.9.35: Bordertown Cemetery, July 2022, Row D, line 3. The line of reflections at 42 cm are highlighted in red.

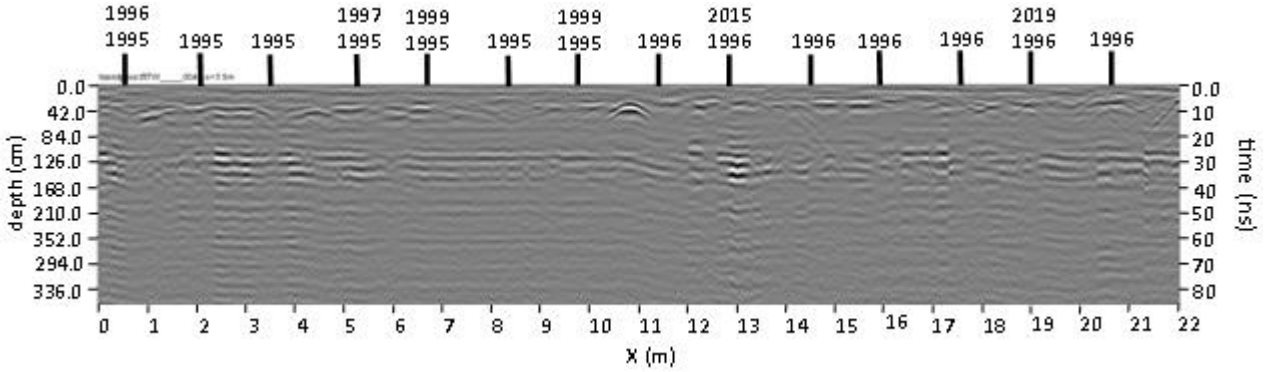

Figure 3.9.36: Bordertown Cemetery, July 2022, Row D, line 4.

The resistivity data, Figure 3.9.37, captured with the Wenner array shows a layer of higher resistivity, (> 5 Ω-m) above 80 cm. Within this layer are many discrete areas of higher resistivity, (> 10 Ω-m). These areas are associated with the burials.

The IP data, Figure 3.9.38, show a layer of chargeability above 25 nV/V, to a similar depth of 80 cm. Within this layer are discrete areas of higher chargeability, (> 25 nV/V), these discrete areas are associated with the burials.

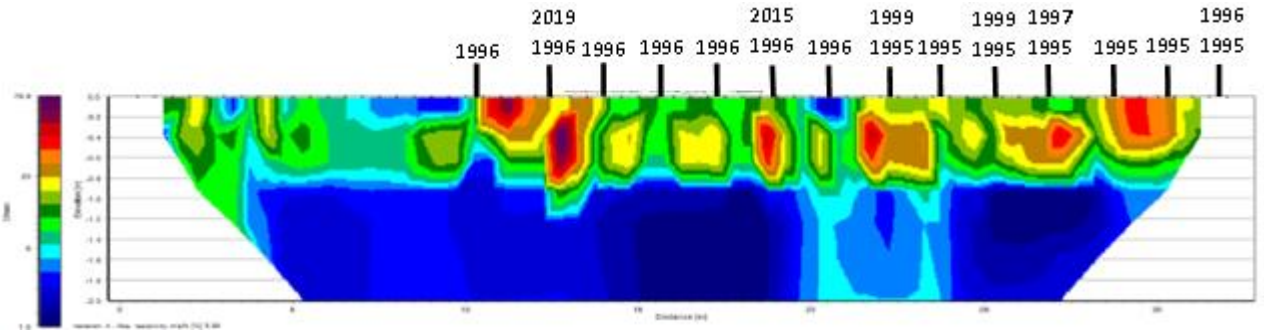

Figure 3.9.37: Resistivity data captured with the Wenner array, July 2022. Bordertown Cemetery, Row D.

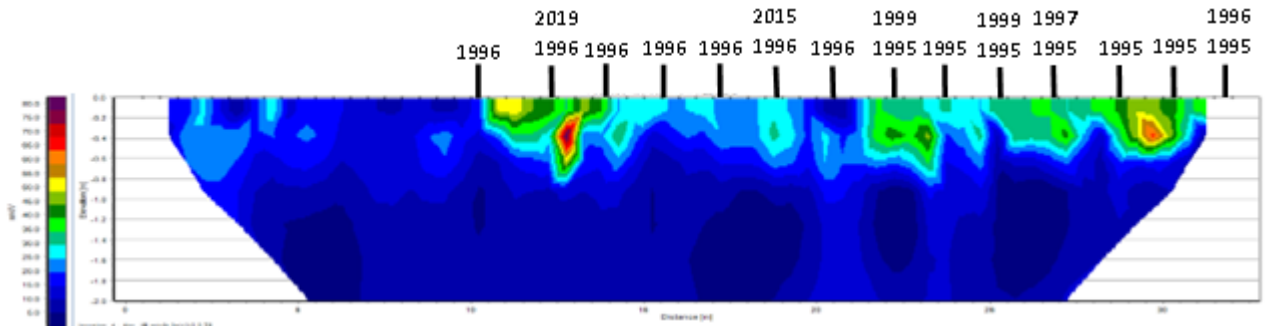

Figure 3.9.38: Induced polarisation data captured with the Wenner array, July 2022. Bordertown Cemetery, Row D.

The resistivity data captured with the Dipole – Dipole array, Figure 3.9.39, shows a high resistivity from the surface to a variable depth, approximately 80 -100 cm. The resistivity of this layer is above 10 Ω-m and includes smaller areas with resistivity above 30 Ω-m associated with the burials. Despite these areas being associated with the burials, individual burials are not easily identified.

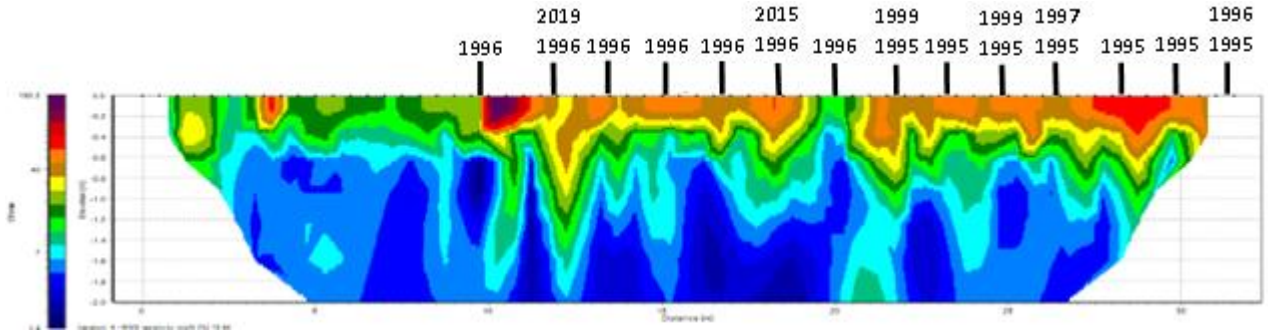

Figure 3.9.39: Resistivity data captured with the Dipole - Dipole array, July 2022. Bordertown Cemetery, Row D.

Figure 3.9.40 shows the IP data captured with the Dipole – Dipole array. A thin layer to a depth of 60 cm shows a mix of chargeability's above 70 nV/V. This layer is associated with the soil disturbance from burial, but no individual burials can be identified. Below this layer, in the homogenous sub surface are ten small, discrete areas with chargeability > 60 nV/V. Given the depth and position of these areas, they are possibly the coffins of the burials.

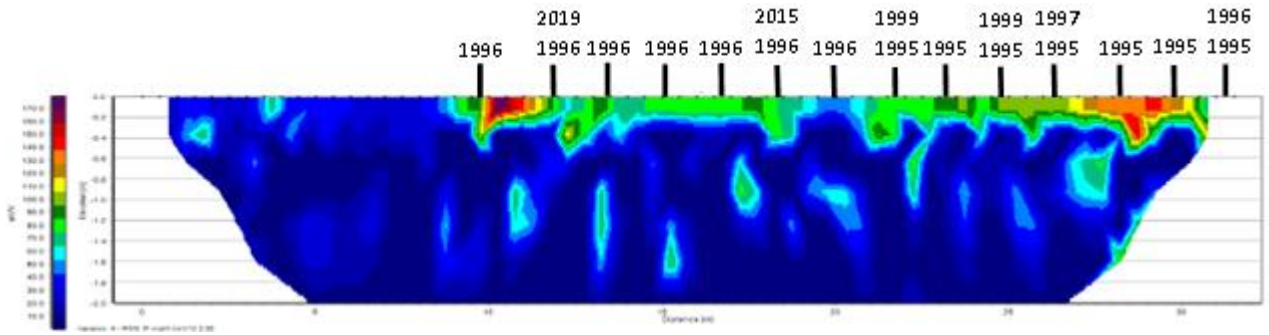

Figure 3.9.40: Induced polarisation data captured with the Dipole - Dipole array, July 2022. Bordertown Cemetery, Row D.

3.9.7 September 2022

Data was collected in September 2022. There was 14.8 mm of rainfall in the week before this data was collected, with an additional 0.4 mm recorded on the day of collection. The ten-month rainfall plot is shown in Figure 3.9.41. There was no ERT data collected on this visit.

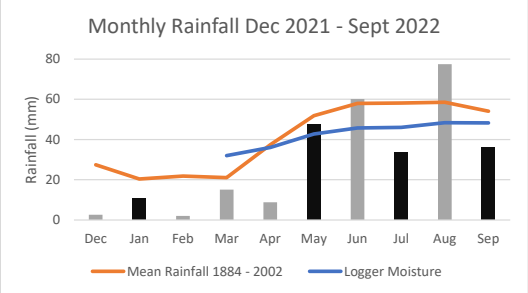

Figure 3.9.41: Monthly rainfall in the ten months prior to data collection. Months in which a site visit occurred are in black. (Rainfall and Temperature data from bom.gov.au)

Six of the fourteen burials can be identified in these radargrams. The radargrams from this visit show many strong reflections along the line, Figures 3.9.42, 3.9.43, and 3.9.44. These are partly highlighted in line 4, Figure 3.9.44. Line 3 contains stratigraphic breaks that are associated with grave cuts. These are highlighted in Figure 3.9.43. Attenuation starts at approximately 90 cm.

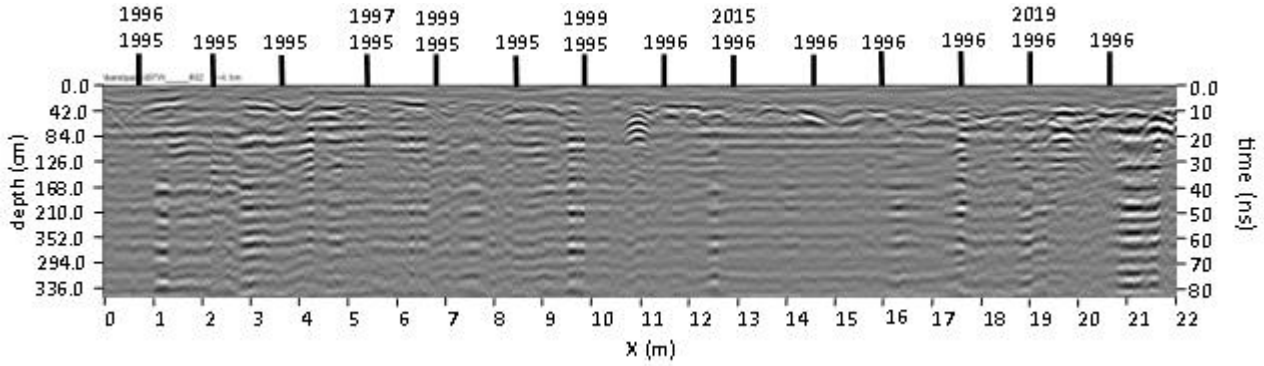

Figure 3.9.42: Bordertown Cemetery September 2022, Row D, line 2.

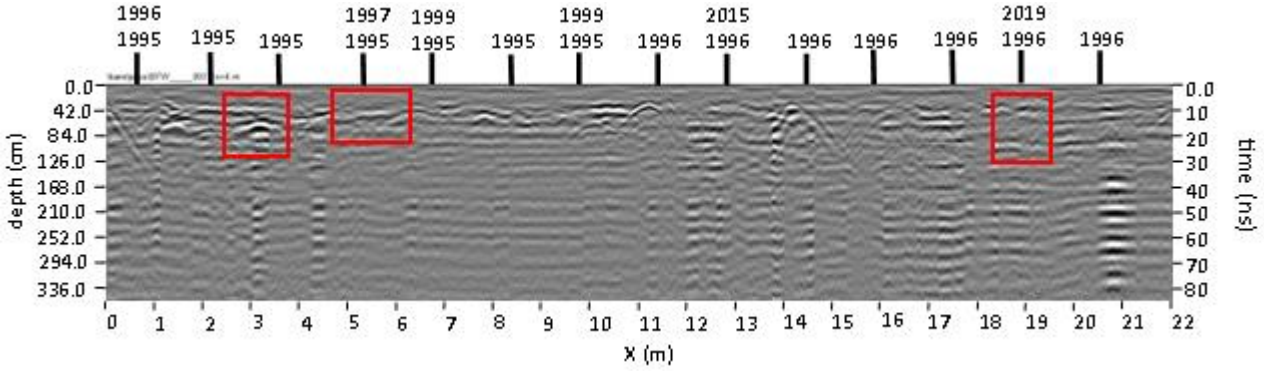

Figure 3.9.43: Bordertown Cemetery, September 2022, Row D, line 3. Stratigraphic breaks are highlighted in red.

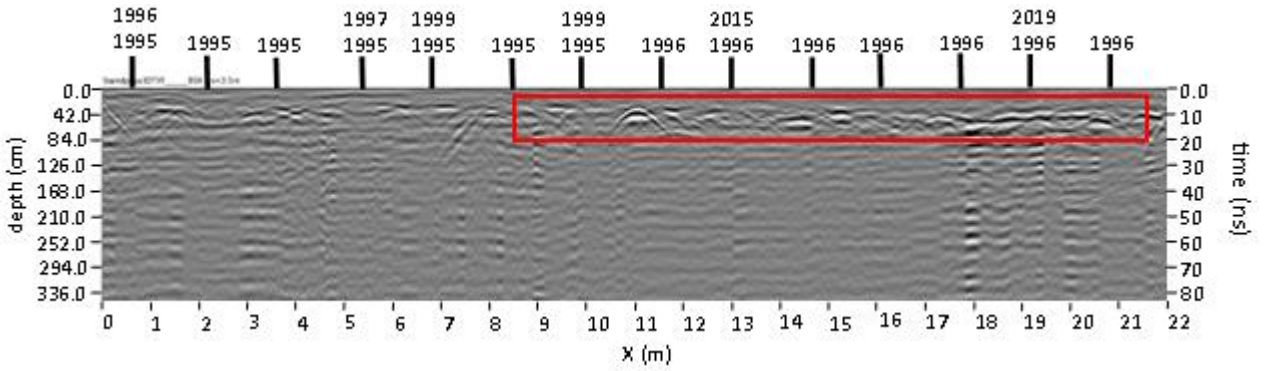

Figure 3.9.44: Bordertown Cemetery, September 2022, Row D, line 4. The reflections along the horizontal reflection is highlighted in red.

3.9.8 December 2022

Data was collected in December 2022. There was zero rainfall in the week before this data was collected.

The ten-month rainfall plot is shown in Figure 3.9.45.

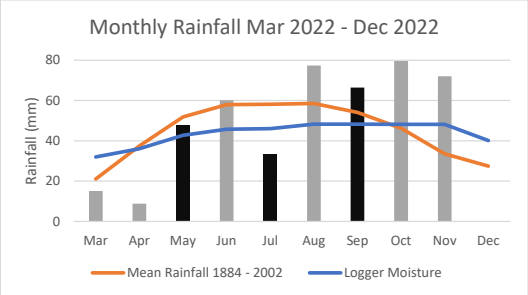

Figure 3.9.45: Monthly rainfall in the ten months prior data collection. Months in which a site visit occurred are in black. (Rainfall and Temperature data from bom.gov.au)

Eight of fourteen burials can be identified in these radargrams. The radargrams from December, Figures 3.9.46, 3.9.47, and 3.9.48, show the shallow line of reflections, in this data the line is a little deeper at 40 - 60 cm, outlined in Figure 3.9.48. There appears to be a stratigraphic layer at approximately 30 cm, this is underlined in Figure 3.9.47. Lines 3 and 4 show these reflections clearly. Attenuation starts at approximately 100 cm.

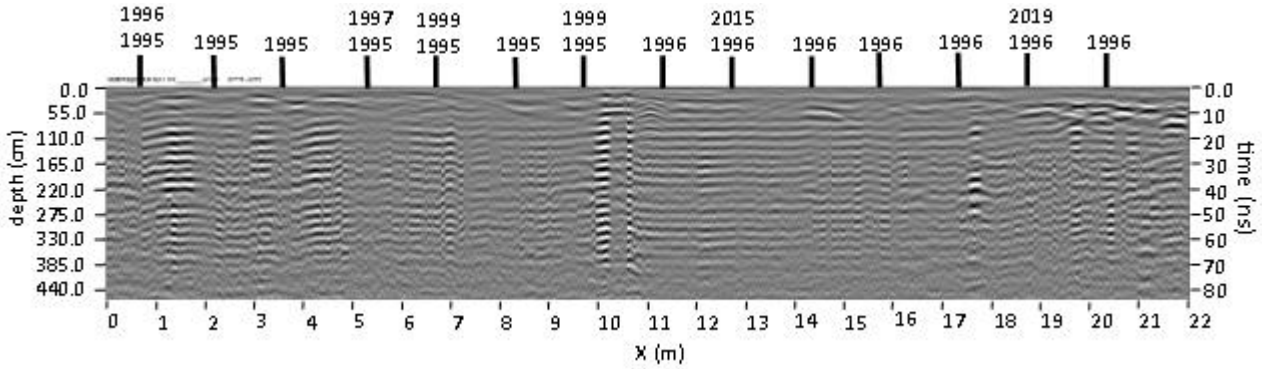

Figure 3.9.46: Bordertown Cemetery, December 2022, Row D, line 2.

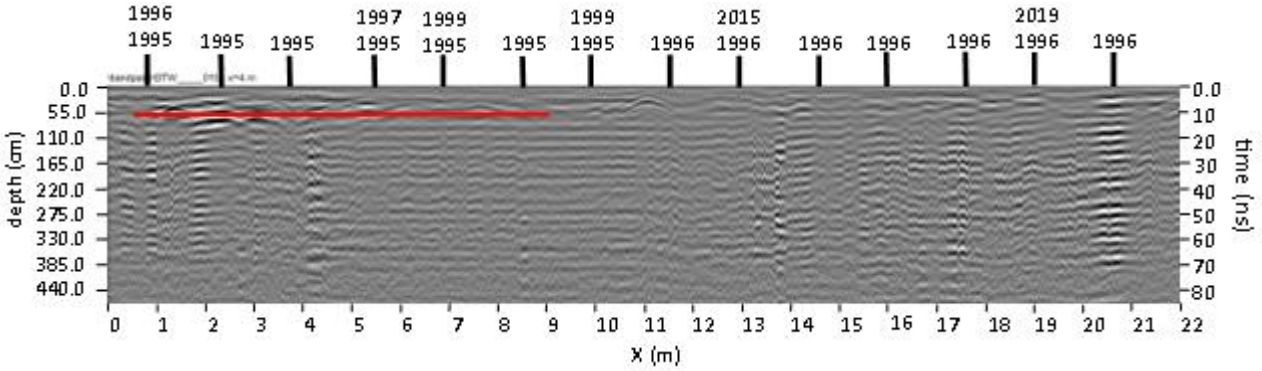

Figure 3.9.47: Bordertown Cemetery, December 2022, Row D, line 3. The stratigraphic layer is underlined in red.

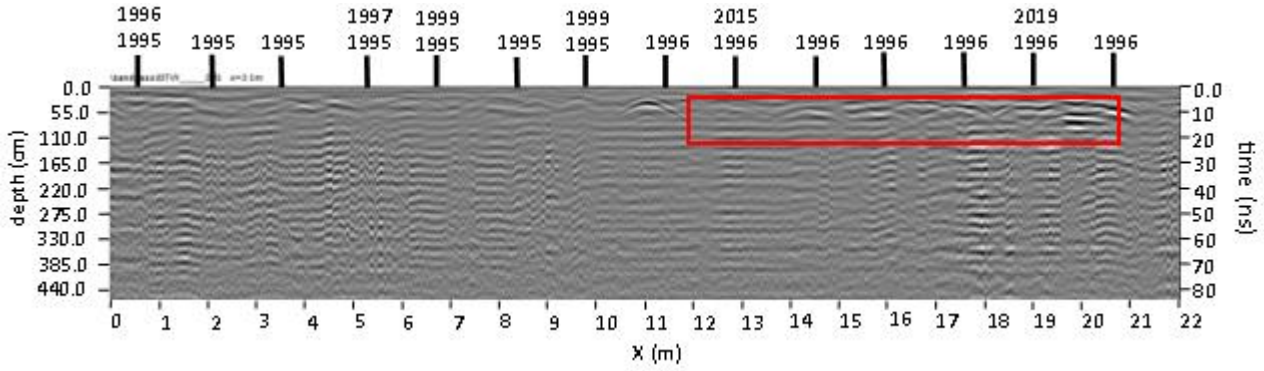

Figure 3.9.48: Bordertown Cemetery, December 2022, Row, line 4. The shallow line of reflections is outlined in red.

The resistivity data collected with the Wenner array, Figure 3.9.49, shows higher resistivity, (>15 Ω-m) above a depth of 60 cm. This layer extends past the burials into the driveway. Within this layer are smaller areas of resistivity above 22 Ω-m. It is difficult to clearly identify any possible burials in this layer.

The IP data, Figure 3.9.50, shows a very similar shaped band, with chargeability values above 35 nV/V. This band also extends past the area containing the graves. Below this high chargeability layer, are five small discrete areas with chargeability values between 20 – 40 nV/V. These smaller areas are possibly associated with the burials.

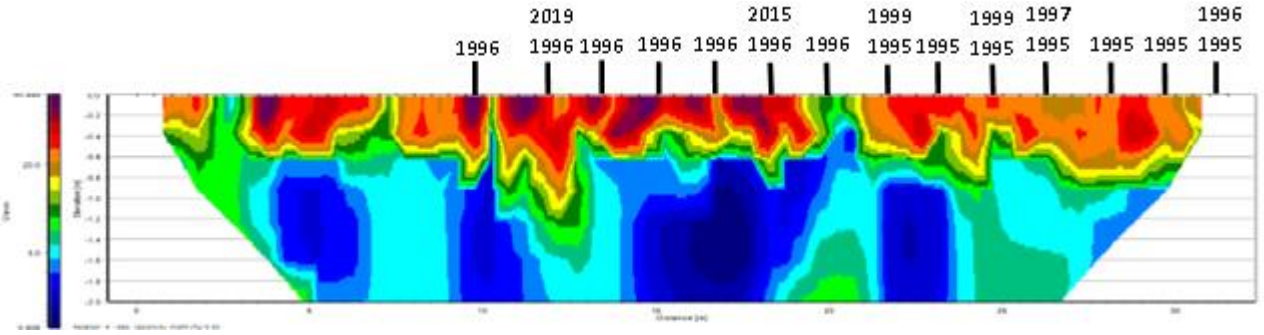

Figure 3.9.49: Resistivity data captured with the Wenner array, December 2022. Bordertown Cemetery, Row D.

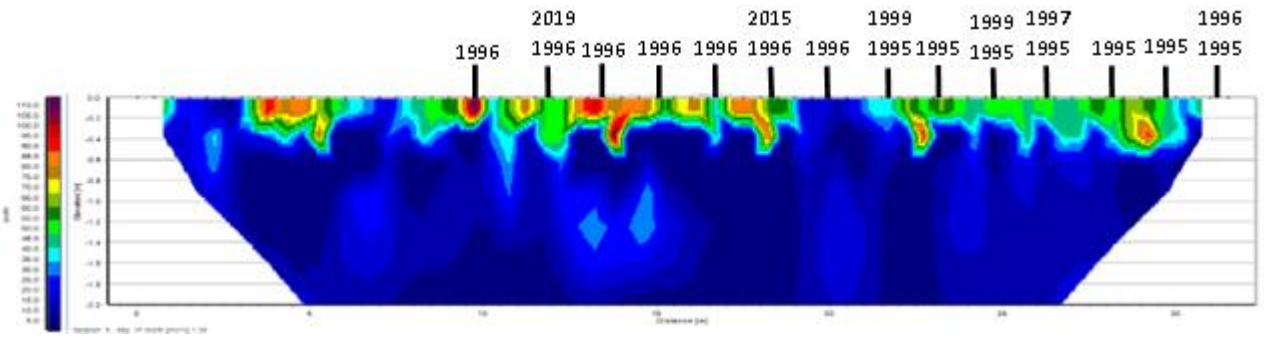

Figure 3.9.50: Induced polarisation data captured with the Wenner array, December 2022. Bordertown Cemetery, Row D.

The resistivity data captured with the Dipole – Dipole array, Figure 3.9.51, shows higher resistivity, (> 7 Ω-m), above a depth of 60 cm. Within this layer are several smaller, discrete areas with resistivity above 50 Ω-m, these smaller areas are associated with the burials. This layer also extends past the burials into the driveway. The IP data, Figure 3.9.52, shows a very shallow layer to 20 cm, with chargeability greater than 160 nV/V, within the area of the burials. Below this layer are several small discrete areas of chargeability between 120 and 160 nV/V, at depths of 80 – 180 cm. These discrete areas could possibly be associated with the burials.

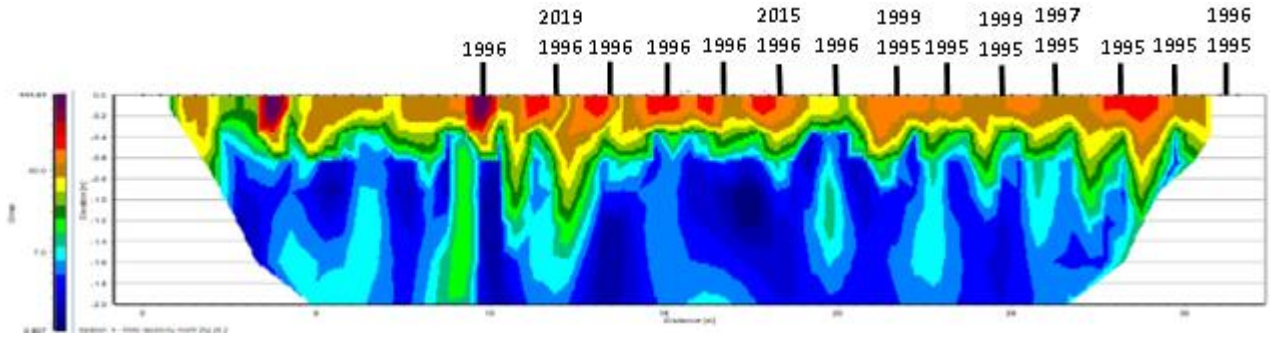

Figure 3.9.51: Resistivity data captured with the Dipole - Dipole array, December 2022. Bordertown Cemetery, Row D.

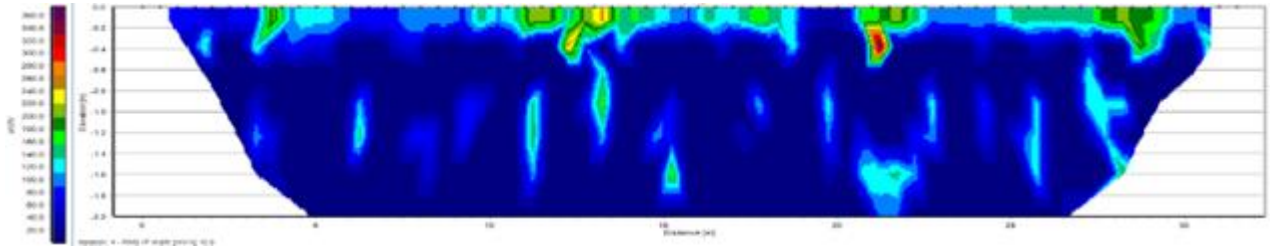

Figure 3.9.52: Induced polarisation data captured with the Dipole - Dipole array, December 2022. Bordertown Cemetery, Row D.

3.9.9 March 2023

Data was collected in March 2023. There was 6.1 mm of rainfall in the week before this data was collected. The ten-month rainfall plot is shown in Figure 3.9.53.

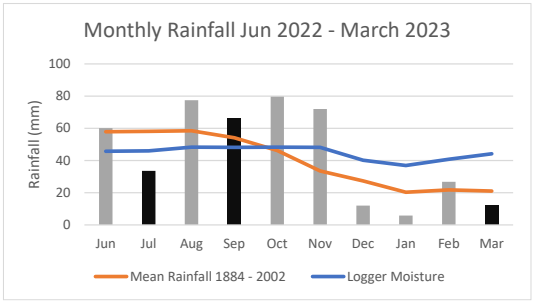

Figure 3.9.53: Monthly rainfall in the ten months prior to data collection. Months in which a site visit occurred are in black. (Rainfall and Temperature data from bom.gov.au)

Only three of fourteen burials are identifiable in these radargrams. The radargrams from March 2023, Figures 3.9.54, 3.9.55, and 3.9.56, show only a few reflections. Line 2, Figure 3.9.54, shows two stratigraphic breaks, these are situated at the 4 m mark and the 11 m mark. Line 3, Figure 3.9.55, shows a small line of shallow reflections, these are located from 9 m along the radargram. Attenuation in this data starts at approximately 100 cm.

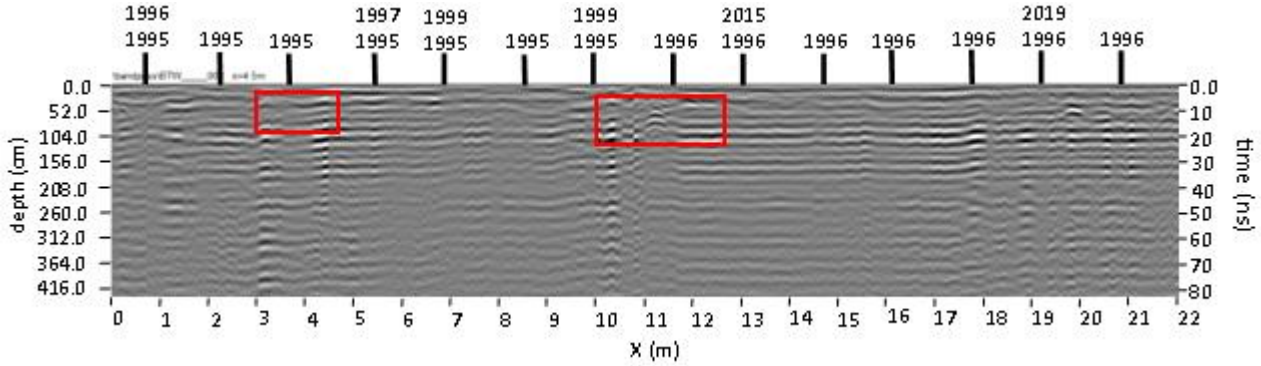

Figure 3.9.54: Bordertown Cemetery March 2023, Row D, line 2. Stratigraphic breaks are outlined in red.

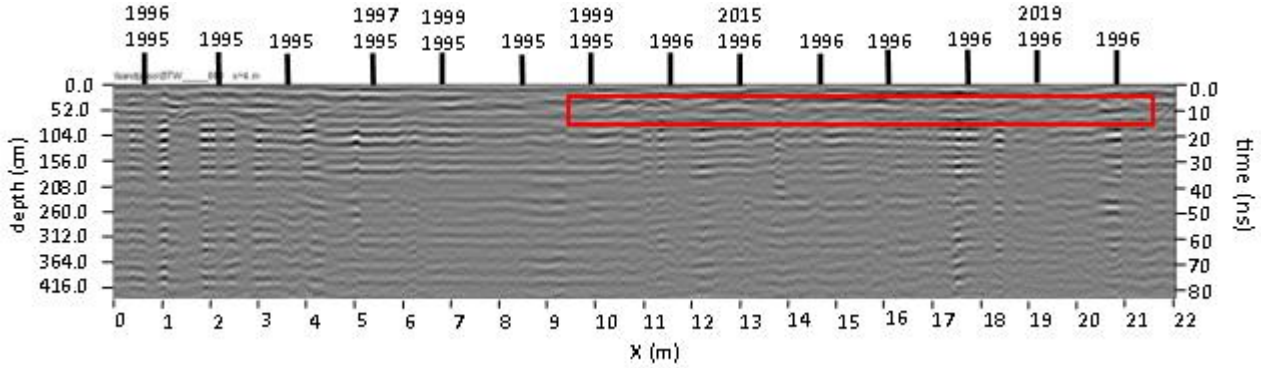

Figure 3.9.55: Bordertown Cemetery, March 2023, Row D, line 3. The line of shallow reflections is outlined in red.

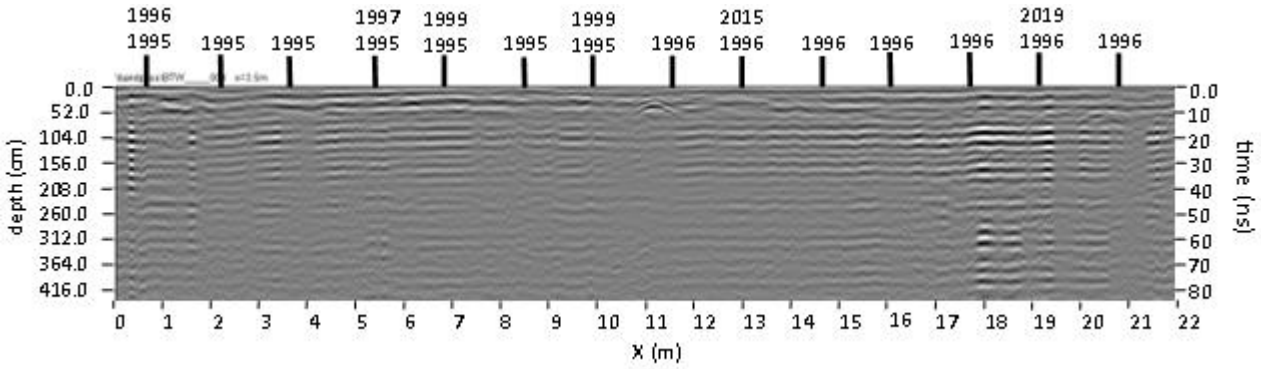

Figure 3.9.56: Bordertown Cemetery, March 2023, Row D, line 4.

The resistivity data that was collected with the Wenner array, Figure 3.9.57, shows resistivity values of 5 Ω-m or greater, extending down to a depth of approximately 80 cm. Within this layer of higher resistivity are areas containing resistivity values above 15 Ω-m, these areas are associated with the burials. The IP data, Figure 3.9.58, also shows a large area of chargeability above 20 nV/V within the area of all but one of the burials. There are no deeper areas of higher chargeability.

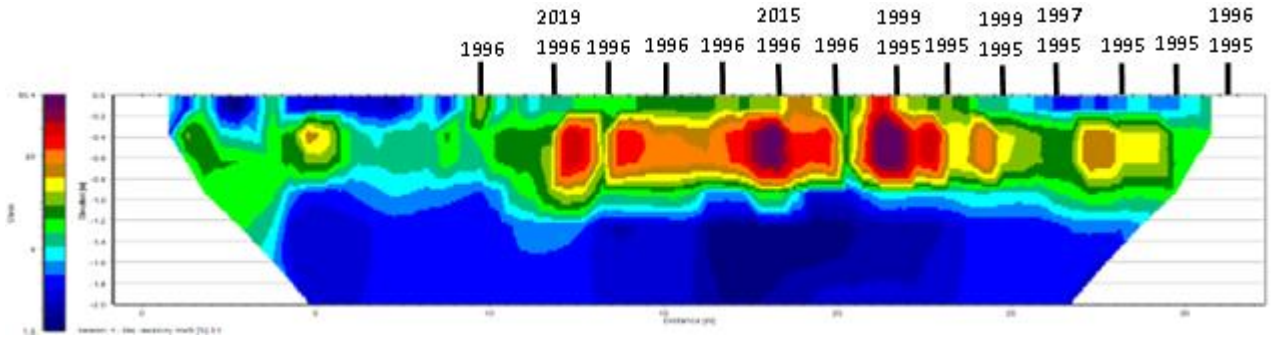

Figure 3.9.57: Resistivity data captured with the Wenner array, March 2023. Bordertown Cemetery, Row D.

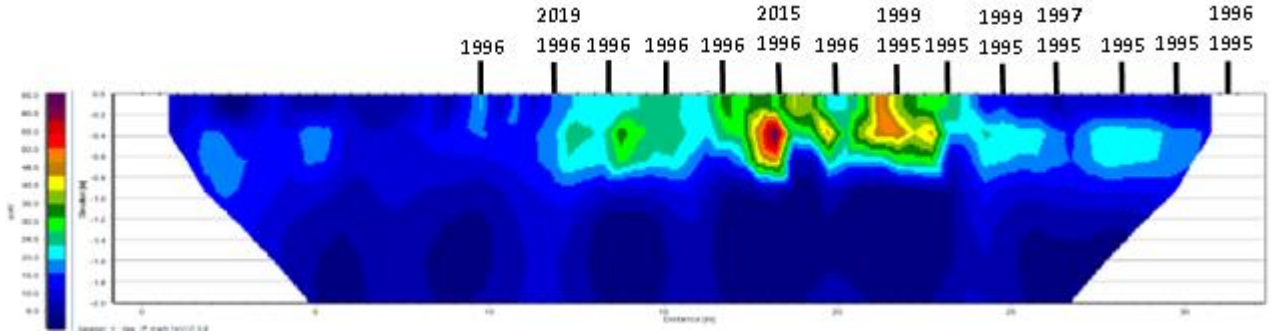

Figure 3.9.58: Induced polarisation data captured with the Dipole - Dipole array, March 2023. Bordertown Cemetery, Row D.

The resistivity data captured with the Dipole - Dipole array, Figure 3.9.59, shows higher resistivity values, (> 5 Ω-m), along the area of the burials, and extending onto the driveway. This band of higher resistivity extends to a depth of 100 cm. Within this band nine of the fourteen burials can be identified.

The IP data, Figure 3.9.50, shows this shallow band, with a chargeability of 35 nV/V or greater. This is largely contained within the area of the graves, and extends down to a depth of approximately 80 cm.

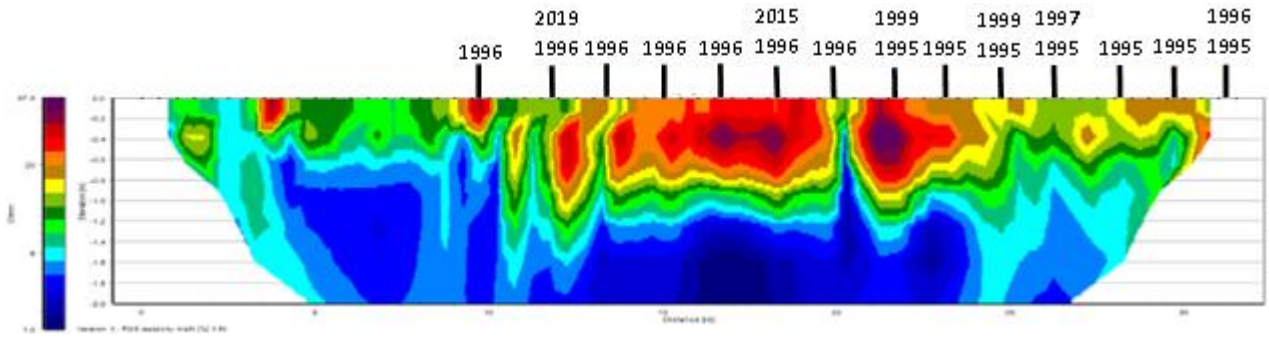

Figure 3.9.59: Resistivity data captured with the Dipole - Dipole array, March 2023. Bordertown Cemetery, Row D.

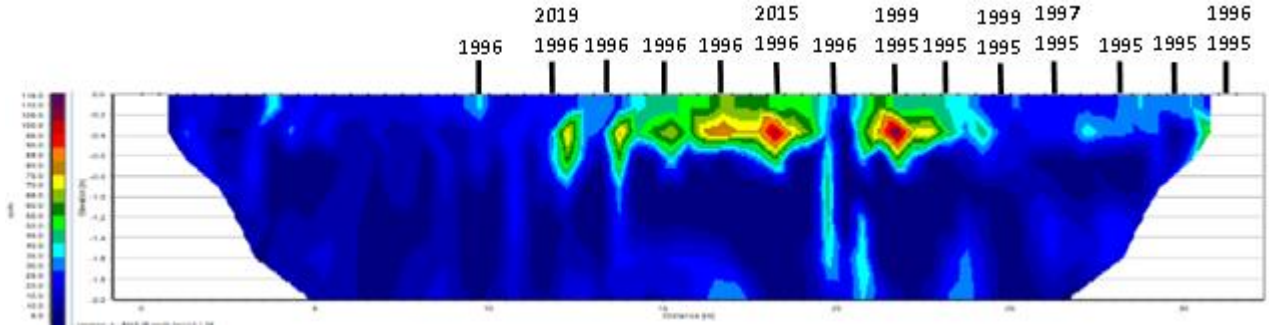

Figure 3.9.60: Induced polarisation data captured with the Dipole - Dipole array, March 2023. Bordertown Cemetery, Row D.

3.10 Bordertown Cemetery Soil

3.10.1 Grain Size

Grain size analysis was carried out in the first instance using the nested sieve process.

Table 3.10.1: Nested sieve grain size results, Bordertown Cemetery.

Site	Sample Depth	Start weight	4mm	2mm	1mm	0.5mm	0.25mm	0.125mm	0.063mm	Base	Post weight	Loss
Bordertown	30cm	60.234	1.921	2.15	3.437	2.93	9.197	29.234	9.325	1.74	59.934	0.3
	60cm	60.754	1.559	7.102	8.558	6.67	9.982	17.881	5.932	2.685	60.369	0.385
	100cm	60.662	11.554	3.919	5.91	5.209	9.123	16.53	4.215	2.436	58.896	1.766
	150cm	60.593	0.279	2.265	8.349	10.877	13.62	16.283	5.821	2.93	60.424	0.169
Wentworth Scale			Granule	Very Course Sand	Coarse Sand	Medium Sand	Fine Sand	Very Fine Sand	Coarse Silt			

From Table 3.10.1, and Figure 3.10.1, it can be seen that a large percentage of grains are < 0.5 mm and > 0.125 mm. The sample taken at 150 cm shows a larger percentage of grains 0.5-0.25 mm. On the Wentworth scale this soil can be classified as medium to very fine sand.

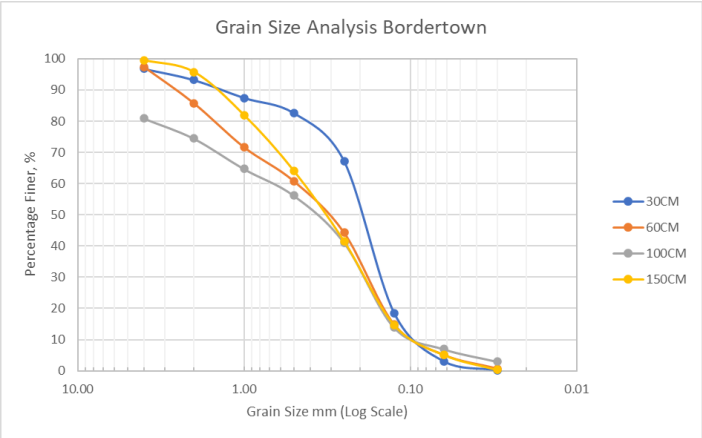

Figure 3.10.1: Nested sieve grain size plot, Bordertown Cemetery.

As the results of the sieve tests show a small percentage of the sample below 0.063mm, further testing was carried out using the laser diffraction process. The results with grain size < 1000 µm are presented below, in Table 3.10.2. These results show that at each subsequent sample depth the percentage of finer grains increases. Also of note is the higher percentage of grains 63 µm recorded with the laser diffusion process.

Table 3.10.2: Laser diffusion results. Values are a percentage of the total sample weight.

Site	Sample Depth	1000 µm	750 µm	500 µm	250 µm	125 µm	63 µm	31 µm	16 µm	8 µm	4 µm
Bordertown	30 cm	99.01	98.18	96.81	78.39	29.82	7.38	5.11	2.44	1.36	0.53
	60 cm	98.42	94.69	85.64	58.69	27.37	16.24	11.7	7.46	4.7	2.16
	100 cm	99.9	99.19	95.52	71.41	32.08	19.27	16.69	11.74	7.19	2.62
	150 cm	98.11	93.35	82.58	58.15	34.15	26.68	24.69	21.13	15.12	6.71
Wentworth Scale		Very Coarse Sand	Coarse Sand	Medium Sand	Fine Sand	Very Fine Sand	Coarse Silt	Medium Silt	Fine Silt	Very Fine Silt	Clay

The laser diffusion results show, at all depths, smaller grain size from the 159 cm sample, Figure 3.10.2. The percentage of grains <= 125 µm are considerably higher at this depth. The sample from 60 cm also show a higher percentage of grains < 125 µm.

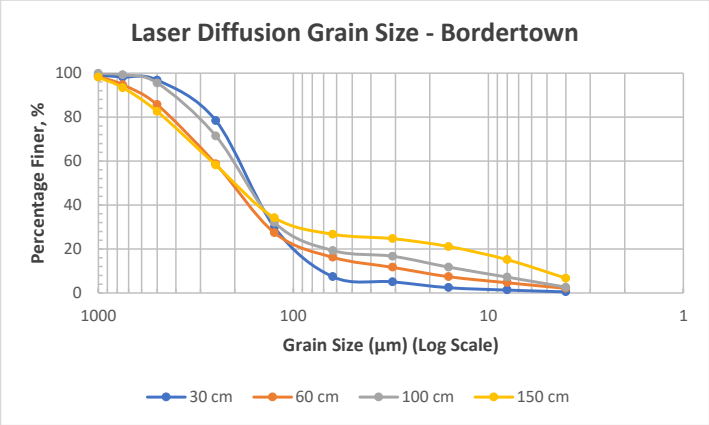

Figure 3.10.2: Grain size log plot from laser diffusion analysis.

3.10.2 Magnetic Susceptibility

The magnetic susceptibility results from the Bordertown samples are shown in Figure 3.10.3. Of note is the higher value for the 60 cm sample. Samples deeper than 60 cm show less magnetic potential. The frequency dependence is low for all samples, (<15% of the K_{lf})

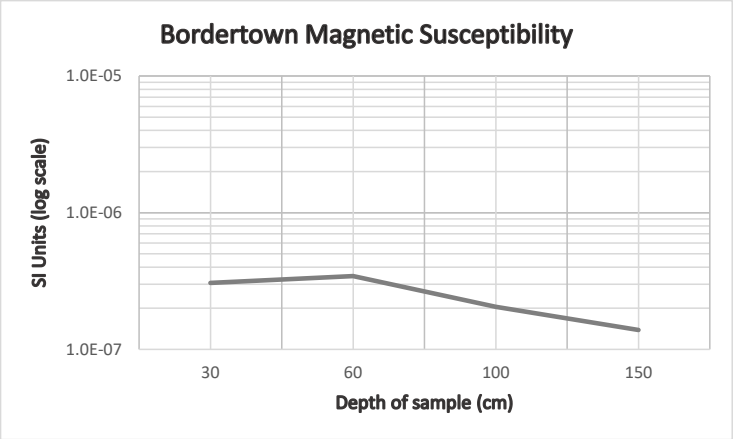

Figure 3.10.3: Bordertown magnetic susceptibility plot. These are low frequency values.

3.10.3 Soil Chemistry

X-ray fluorescence results from samples taken at the Bordertown Cemetery. These results in Table 3.10.3 show the ten most abundant chemical elements measured in the soil samples. These results are dominated by the presence of silica (Si), the concentration of which decreases, (273533 ppm – 142567ppm), throughout the sample depths. Also present at significantly lower concentrations are Aluminium (Al), Potassium (K), Calcium (Ca), and Iron (Fe), all of which increase in concentration significantly with depth.

Table 3.10.3: XRF chemical analysis, Bordertown Cemetery. The ten most abundant chemical elements are listed (ppm).

Element	30 cm	30 cm	60 cm	60 cm	100 cm	100cm	150 cm	150 cm
Silica (Si)	273533	273376	194293	196029	190470	188993	147164	142567
Si Error	2291	2290	1939	1948	1879	1866	1720	1694
Aluminium (Al)	20105	20540	36521	36609	47795	45305	36741	35699
Al Error	1223	1220	1561	1564	1708	1664	1616	1600
Potassium (K)	7156	7051	7344	7220	9719	8791	7268	7221
K Error	123	122	126	126	140	133	127	127
Calcium (Ca)	6902	7033	46341	46169	3602	3158	91359	93794
Ca Error	101	103	243	243	80	76	338	342
Iron (Fe)	5180	5278	19836	19894	29373	27743	26896	27061
Fe Error	108	108	200	201	230	225	243	244
Barium (Ba)	1778	522	1150	2476	129	1839	893	788
Ba Error	2408	2392	2535	2562	2569	2588	2631	2585
Titanium (Ti)	1039	1640	2203	1690	3015	2120	2438	2570
Ti Error	117	122	161	161	159	153	180	184
Phosphorus (P)	1008	1142	284	136	0	0	0	0
P Error	170	168	180	177	110	106	197	198
Sulfur (S)	821	887	924	960	568	613	1257	1141
S Error	97	97	98	100	84	84	104	103
Manganese (Mn)	296	200	190	273	67	255	137	126
Mn Error	28	28	29	29	29	30	30	31

3.10.4 Exchangeable Cation Levels

.

The laser diffusion grain size analysis of soil samples taken from the Bordertown Cemetery show a percentage of between 2 and 6% below 4µm. This indicates the presence of clay. This is consistent with the soil characterisation sheet, (Hall et al. 2009), which also states the soil type can be classified as sodic. These results warranted further testing to determine the levels of exchangeable cations and sodic capacity, see results Table 3.10.4 below.

Table 3.10.4: Percentage of exchangeable cation content, Bordertown Cemetery.

	30 cm	60 cm	100 cm	150 cm
Calcium (%)	82.2	71.3	36.5	44.3
Magnesium (%)	8.6	21.8	36.2	28.5
Potassium (%)	6.0	1.9	4.0	2.8
Sodium - ESP (%)	1.1	4.3	23.0	24.0
Aluminium (%)	0.4	0.1	0.1	0.0
Hydrogen (%)	1.8	0.6	0.3	0.3

The Effective Cation Exchange Capacity (ECE) value, (cmol+/kg) at each sample depth are 30cm - 10, 60cm - 26, 100cm – 24, and 150cm – 35. As nominated by Rengasamy and Olsson (1991:935) the cmol+/kg value of 6 is considered the starting value of sodic soil. The values returned from the Bordertown Cemetery are all > 20 cmol+/kg, and so can be considered heavily sodic, tending to extreme at greater depth.

3.10.5 Radar Velocity and ERT Resistivity

To analyse the effects of seasonal rainfall on velocity and resistivity, one hyperbola that is consistently detectable in all radargrams from all site visits is chosen. The velocity is recorded from all visits, as well as the relevant burial position. The resistivity from both array protocols is recorded from the same burial position and depth, see Table 3.10.5. May 2022 was the only month that recorded above average rainfall during the research period.

Table 3.10.5: Resistivity and Radar velocity by month of visit, Bordertown Cemetery.

GPR Data	Velocity (m/ns)	ERT Data	Resistivity (Ω-m) Wenner array	Resistivity (Ω-m) Dipole – Dipole array	Soil Moisture (mm)
Aug 2020	0.102	Aug 2020	8.02	7.87	
Oct 2020	0.136	Oct 2020	10.96	11.42	
Jan 2021	0.108	Jan 2021	16.18	15.88	
Jan 2022	0.118	Jan 2022	9.17		
May 2022	0.058				
July 2022	0.086	July 2022	6.74	10.74	60.2
Sept 2022	0.084	Sept 2022	6.76	7.07	60.77
Dec 2022	0.11	Dec 2022	4.48	4.98	60.64
March 2023	0.104	Mar 2023	11.55	9.36	48.13

Tables 3.10.6 and 3.10.7 give the resistivity values of both array protocols. These distances and depths are of the model blocks from Res2DInv, and represent the width of the burial shaft, and the depth of the corresponding hyperbola.

Table 3.10.6: Resistivity values - Wenner array.

Distance along ERT line (m)	Depth (cm)	Aug-20	Oct-20	Jan-21	Jan-22	Jul-22	Sep-22	Dec-22	Mar-23
20	52	8.646	12.063	25.12	16.706	8.37	5.467	4.3	10.237
20	104	4.198	9.439	7.666	7.104	4.267	4.813	1.746	6.337
20.25	78	4.641	10.882	14.026		4.399	4.105	2.589	8.179
20.25	130	3.732	7.649	5.424	5.977	3.982	4.419	2.586	5.981
20.5	104	4.36	9.073	8.671	7.81	3.746	4.501	2.461	7.54
20.5	156	3.876	6.994	4.985	4.284	5.11	3.861	3.261	5.11
20.75	78	6.445	9.98	9.395	11.24	5.224	7.134	4.111	10.382
20.75	130	3.814	7.567	6.728	5.307	4.729	4.459	2.805	5.556
21	52	12.381	10.948			8.994	10.371	6.942	17.424
21	104	4.65	8.196	7.69	7.347	4.719	4.939	3.707	6.431

Table 3.10.7: Resistivity values, Dipole - Dipole array.

Distance along ERT line (m)	Depth (cm)	Aug-20	Oct-20	Jan-21	Jul-22	Sep-22	Dec-22	Mar-23
20	70	11.695	11.475	19.32	15.494	11.176	6.905	10.754
20	105	3.82	8.492	4.939	8.464	7.037	3.526	5.627
20.25	62	12.016	11.642	19.142	13.568	9.24	5.546	11.789
20.25	104	4.623	8.93	7.335	8.146	24.544	3.557	5.874
20.5	70	6.11	10.683	16.243	10.686	5.559	3.959	9.653
20.5	105	3.482	8.741	3.968	6.877	3.893	3.619	5.034
20.75	62	6.55	11.805	16.3	8.667	6.073	4.826	8.436
20.75	104	3.97	9.199	4.295	5.684	15.87	3.062	5.337
21	70	3.023	11.475	8.406	5.307	3.311	3.692	6.194
21	105	4.418	9.853	5.103	6.296	19.279	3.972	5.02

3.11 Port Lincoln RSL Cemetery

3.11.1 Introduction

Data for the Pt. Lincoln RSL Cemetery was collected from rows P and Q. The grid for each row was 25x3 meters, and 11 lines of data were collected each visit, covering all of the grassed area, Figure 3.11.1. Row P contained 18 burial sites, with row Q containing 18 burial sites. The ERT data was captured with the Wenner and Dipole – Dipole arrays, with an electrode spacing of 50 cm. Due to space restrictions, the electrodes extend past the end of the row, into a driveway. The edge of this driveway is located between the sixteenth and seventeenth electrode, see Figure 3.11.12. The results from the GPR show no visits identified all eighteen of the burials, over all visits only 70% of the burials were identified. Resistivity values range from 65.2 – 601.7 Ω-m for the Wenner array, 54.1 – 2700.8 Ω-m for the Dipole-Dipole array.

Chargeability values range from 131 – 706.8 nV/V for the Wenner array, and 1 – 506.8 nV/V for the Dipole-Dipole array.

GPR data was successfully collected on all visits, however, suitable ERT data was only collected on seven occasions. The months within the period 2020-2023 that visits to this site occurred are listed in Table 3.11.1.

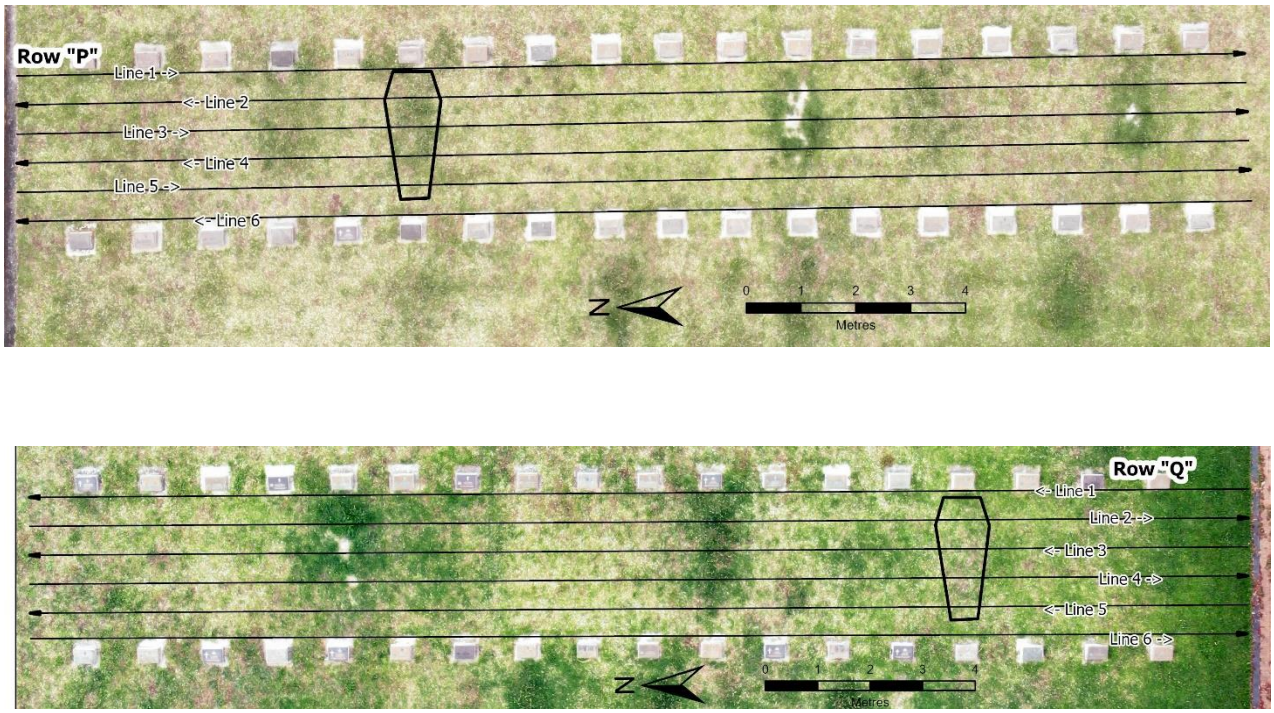

Figure 3.11.1: Rows P (top) and Q (bottom), Pt Lincoln RSL Cemetery. The GPR lines are shown, and as the data is collected in a "zigzag" method, every second line is in the opposite direction. For Row Q lines 2 & 3 are over the widest part of the coffin, i.e. the shoulders and torso. The ERT line is between lines 2 and 3 of Row Q.

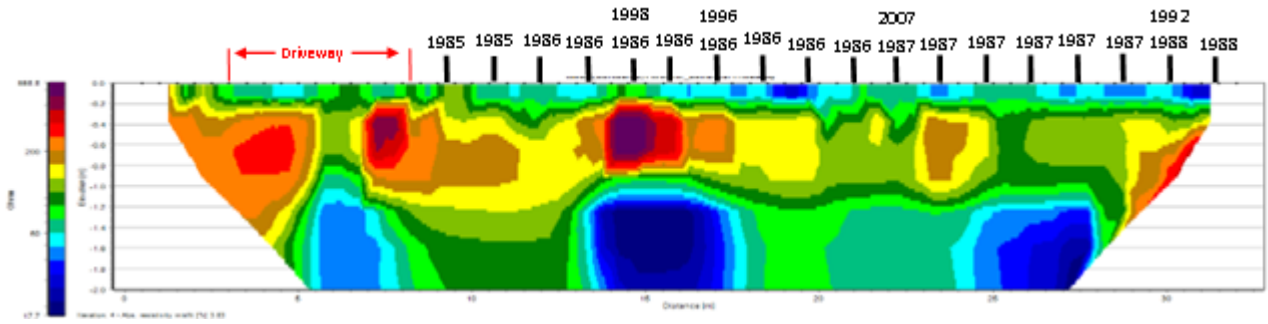

Figure 3.11.2: The layout of the ERT line along Row Q, Pt Lincoln RSL Cemetery. To use the required total length of electrode spacing (31.5 m at 50 cm electrode spacing) the line extended past the end of Row Q into a driveway. Beyond this driveway were two more graves that are part of Row P.

Table 3.11.1: Data collection months, Pt Lincoln RSL Cemetery.

GPR Data	Velocity (m/ns)	ERT Data

Sept 2020	0.068	Sept 2020
Dec 2020	0.128	Dec 2020
March 2021	0.154	
June 2021	0.144	June 2021
Jan 2022	0.13	Feb 2022
July 2022	0.134	July 2022
Sept 2022	0.128	
Dec 2022	0.126	Dec 2022
March 2023	0.154	March 2023

3.12 Installed Soil Moisture Meter

This soil moisture meter was installed on the 1st of June 2021 and has been recording the changes in soil moisture continuously. Overall seasonal high and low moisture levels can be seen in the total soil moisture plot, these seasonal changes amount to some 100 mm, see Figure 3.12.1.

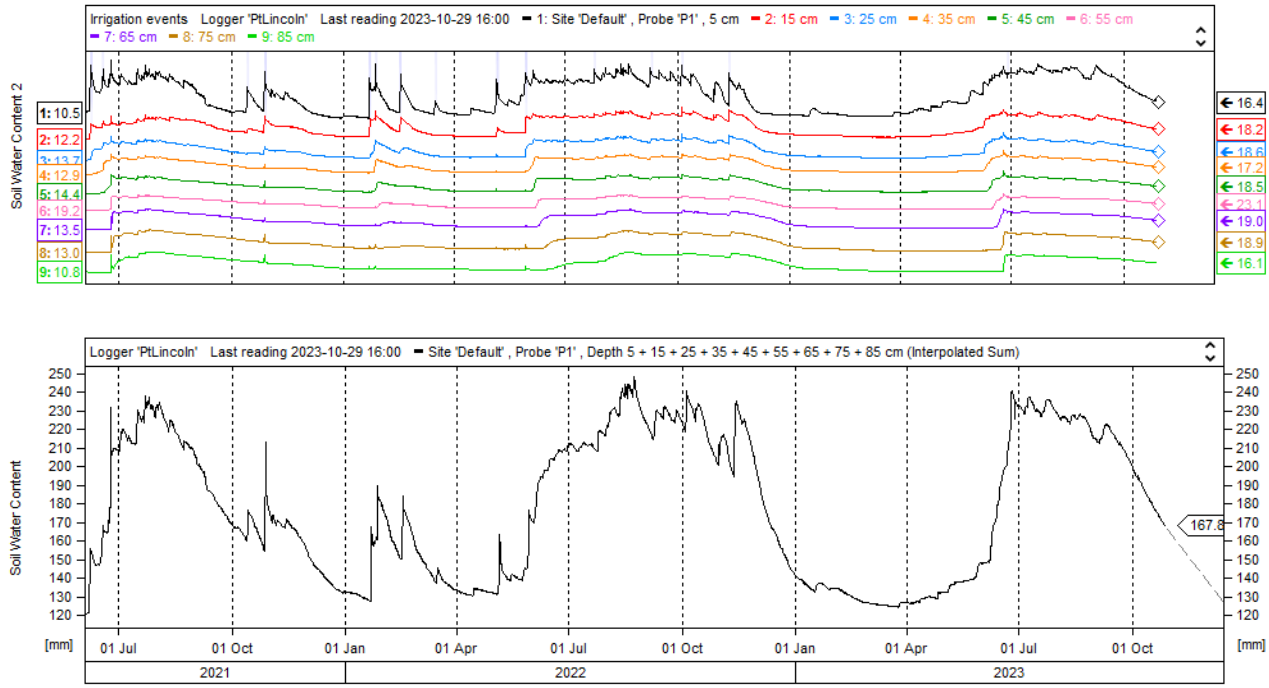

Figure 3.12.1: Moisture meter plot from the RSL Cemetery. Top is the moisture levels (in mm) of each sensor. Bottom, overall soil moisture levels (in mm).

June 23rd, 2021, saw a spike of some 13.8 mm. This soil moisture increase was over a period of 24 hours. This increase can be seen at all sensor levels. Two smaller increases in soil moisture preceded this, these were recorded on June 7th and June 17th, the total of these two rainfall events is 21.4 mm. The June 7th soil moisture increase can be seen at the 5 cm depth, the increase recorded on June 17th can be seen down to 45 cm only, (see "A" in Figure 3.12.2). In the period June 7 – June 24 the local official weather station recorded a total of 56.4 mm of rain.

Following the increase on June 23rd the total soil moisture rose to a seasonal peak of 237 mm on July 22nd. At this time the soil moisture levels at all sensor depths reached the seasonal maximum, with soil moisture at all depths declining slowly over the next few months, “B” in Figure 3.12.2. Over the period of this decline in soil moisture the local weather station recorded 102 mm of rain.

On the 14th October 2021 an increase of 14 mm is recorded by the 5 cm sensor, see “C” in Figure 3.12.2. No other depths recorded any increase, and the local weather station recorded 19.4 mm, plus a further 2.2mm on the 15th.

The next recorded rain event occurred on October 28th ,2021. The 5 cm sensor recorded an increase of 24 mm, with deeper sensors recording lower soil moisture increases, i.e. 10 mm at 15 cm, 4 mm at 25 cm, 2 mm at 35 cm, “D” in Figure 3.12.2. The local weather station recorded rainfall of 0.8 mm on the 27th and 11.4 mm on the 28th.

Over the next 86 days the total soil moisture fell from 189 mm to 126 mm, recorded on January 21, 2022, (see “E” in Figure 3.12.2). On this day a soil moisture increase was recorded by the 5 cm, 15 cm, 25 cm, 75 cm and 85 cm sensors. The largest increase of 23.5 mm was recorded at 5 cm, 11 mm at 15 cm, 2.1 mm at 25 cm, 0.5 mm at 75 cm and 1.4 mm at 85 cm. 47.4 mm of rain was recorded at the local weather station.

On January 26th, 2022 an increase of soil moisture was recorded by sensors at all depths, (“F” in Figure 3.12.2). The largest increase was of 16.1 mm, recorded at a depth of 5 cm. The local weather station recorded 47.2 mm on the 27th, but this could have been overnight. The sensor increases were recorded between 10pm and midnight.

Following this increase the total soil moisture fell from 189 mm to 149 mm over a period of 19 days, when another increase in soil moisture was recorded, down to a depth of 35 cm. See “G” in Figure 3.12.2.

On May 5th, 2022, another increase in soil moisture was recorded at 5 cm (20.3 mm), 15 cm (5.2 mm), 25 cm (2 mm), and 75 cm (1.4 mm). Eleven days later, May 26th, 2022, another small increase in total soil moisture of was recorded (138 mm to 144 mm), with a larger increase being recorded at all depths on May 30th, see “H” in Figure 3.12.2. The local weather station recorded 15 days containing a rain event, with a total of 48.2 mm of rain in the period May 5 – May 30.

The total soil moisture continued to rise from this date to a seasonal high of 248 mm, with all depths recording an increase. The sensors 65 cm and below recorded the greatest increase, between 9.3 mm and 9.5 mm, recorded on August 26th, 2022. “I” in Figure 3.12.2

From this seasonal high on August 26th, 2022, the total soil moisture fell to 194 mm over a period of 77 days. During this period of soil moisture decline, (“J” in Figure 3.12.2), there was seven recorded rain

events. One of these events was recorded at all depths, the others were not recorded below 45 cm. The local weather station recorded 111 mm of rain over this 77-day period.

On November 12th, 2022, the total soil moisture increased from 195 mm to 235 mm. This increase was recorded at a depth of 5 cm (20 mm), 15 cm (7 mm), 25 cm (4.9 mm), and at a depth of 35 cm (3.4 mm). Sensors below 35 cm did not record any increase in soil moisture, “K” in Figure 3.12.2. The local weather station recorded 14.2 mm of rain on November 12, followed by 42 mm on November 13th.

Following this November rain event, the soil moisture decreased to a seasonal low of 123 mm, recorded on March 26, 2023.

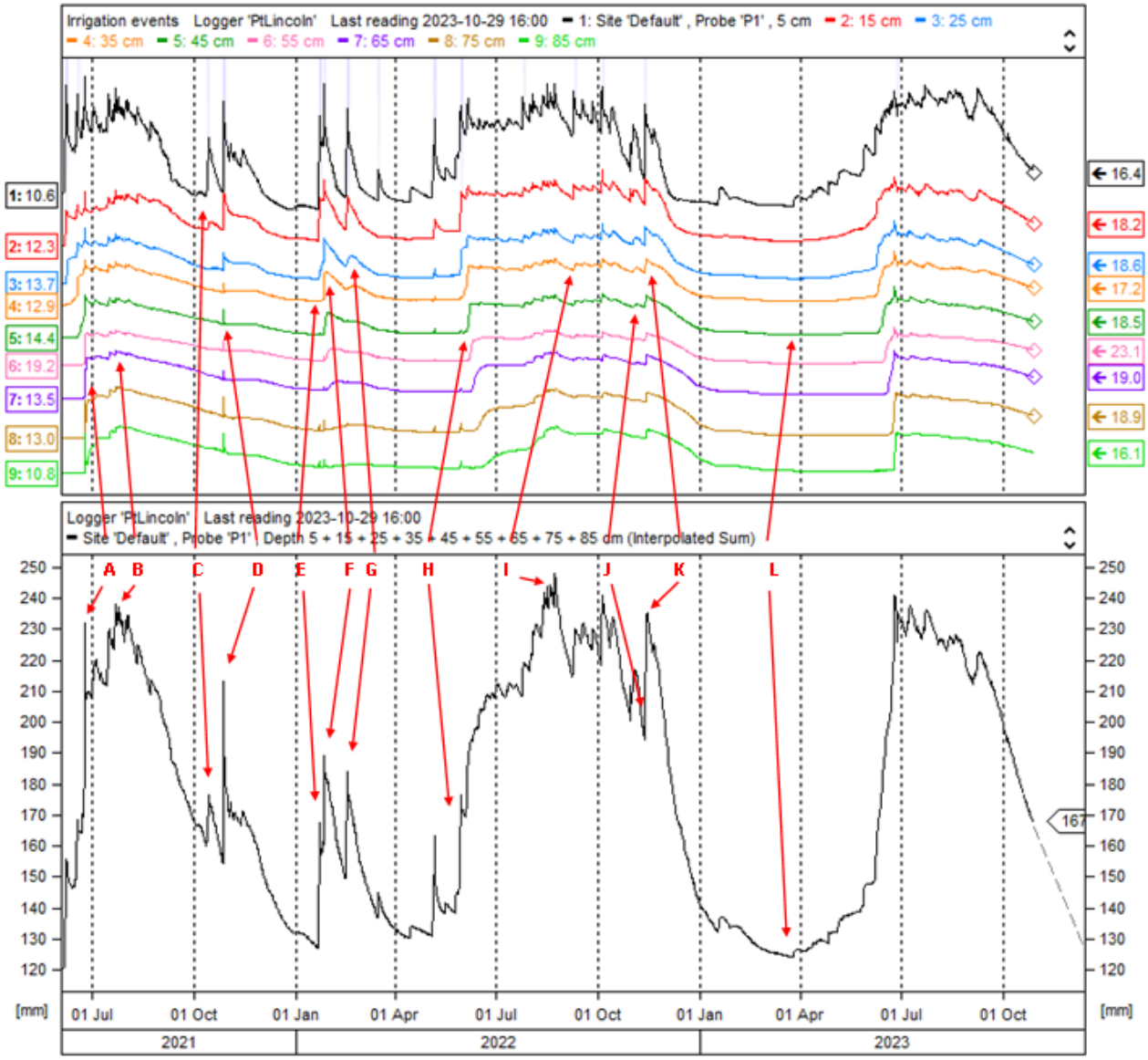

Figure 3.12.2: Pt Lincoln RSL moisture meter with key points highlighted.

3.13 Pt Lincoln RSL Geophysics

3.13.1 September 2020

Data was collected in September 2020. There was 14.8 mm of rainfall in the week before this data was collected. The ten-month rainfall plot is shown in Figure 3.13.1.

Fourteen of the eighteen burials in Row Q can be identified in these radargrams. The radargrams from September 2020, Figures 3.13.2, 3.13.3, and 3.13.4, show many reflections along the radar line. Depth of penetration is more than 4.5 m, with attenuation starting at approximately 2.5 m. Reflections that are smaller in amplitude and size can be seen at a shallower depth, (circled in red, Figure 3.13.3). A horizontal reflection can be seen in line 4, (“B” in Figure 3.13.4), from 16 m along the radar line.

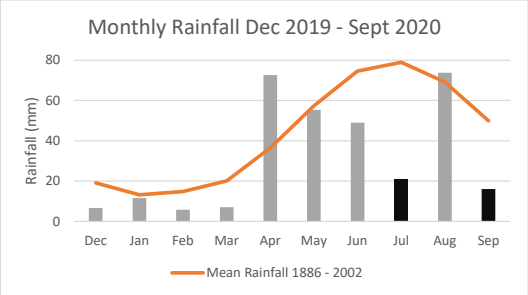

Figure 3.13.1: Monthly rainfall in the ten months prior to data collection. Months in which a site visit occurred are in black. (Rainfall and Temperature data from bom.gov.au)

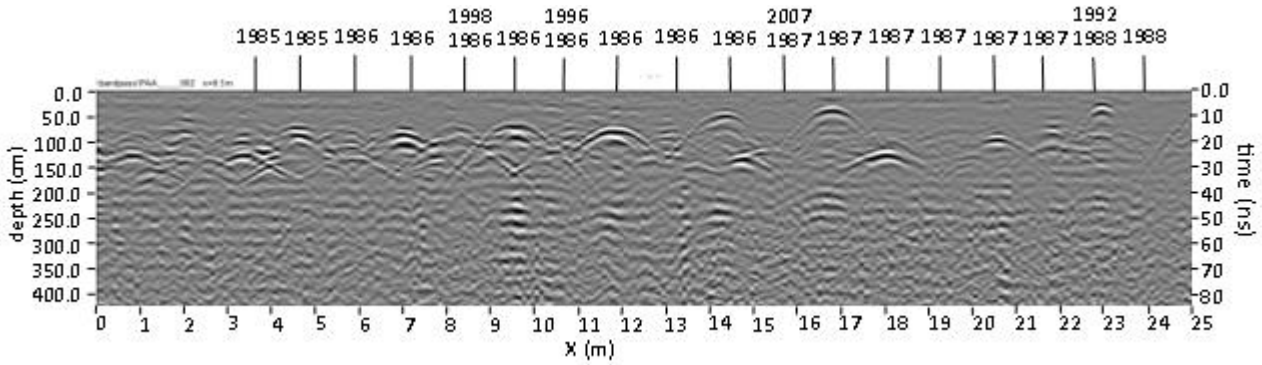

Figure 3.13.2: Pt Lincoln RSL Cemetery September 2020, Row Q, line 2.

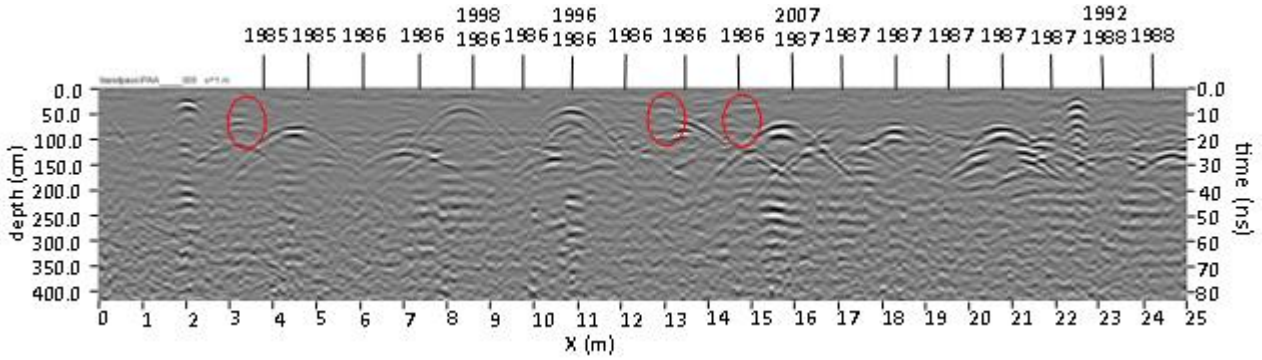

Figure 3.13.3: Pt Lincoln RSL Cemetery, September 2020, Row Q, line 3.

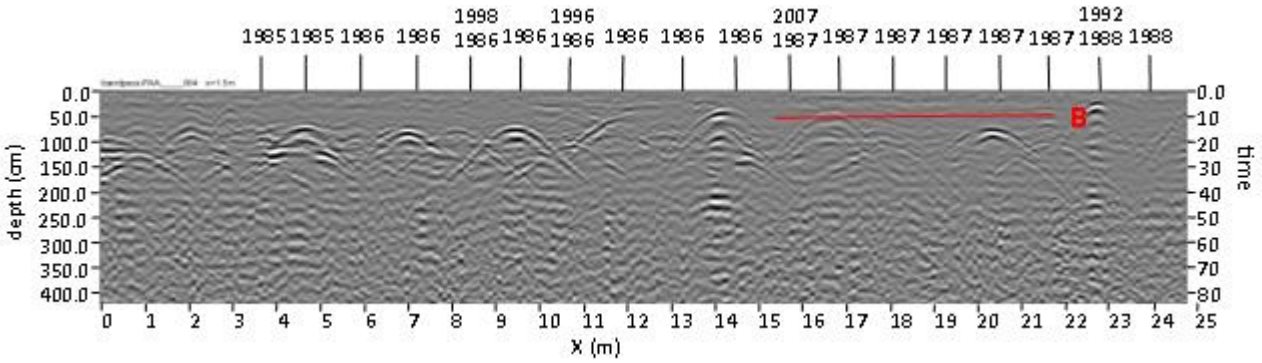

Figure 3.13.4: Pt Lincoln RSL Cemetery, September 2020, Row Q, line 4.

The resistivity data captured with the Wenner array, Figure 3.13.5, shows a large band, to a depth of 120 cm with resistivity values greater than 90 Ω-m. Within this band are discrete areas with resistivity values > 170 Ω-m. Four burials can be identified in this layer.

The IP data, Figure 3.13.6, shows a band of higher chargeability at depths 20 cm to 80 cm. The chargeability of this band ranges from 300 nV/V to 900 nV/V. Although this band extends the entire length of the ERT line, through the area of burials into the driveway, it can be assumed that higher chargeability is due to the location of the burials.

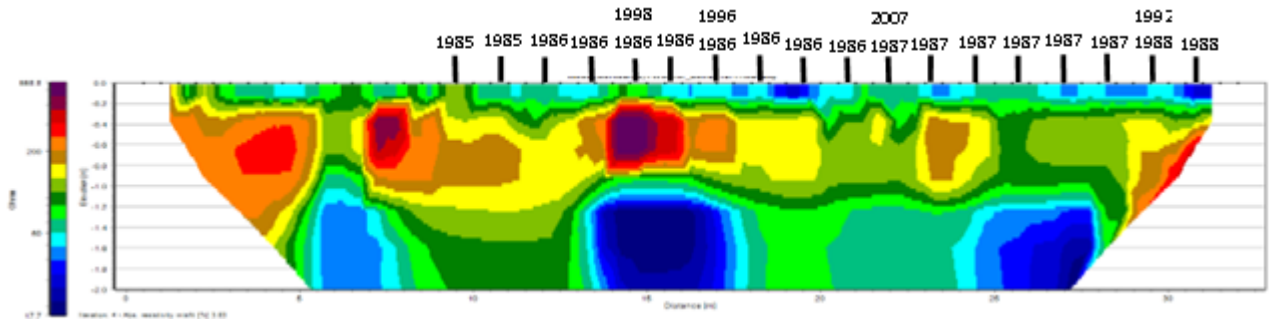

Figure 3.13.5: Resistivity data captured with the Wenner array, September 2020. Pt Lincoln RSL Cemetery, Row Q.

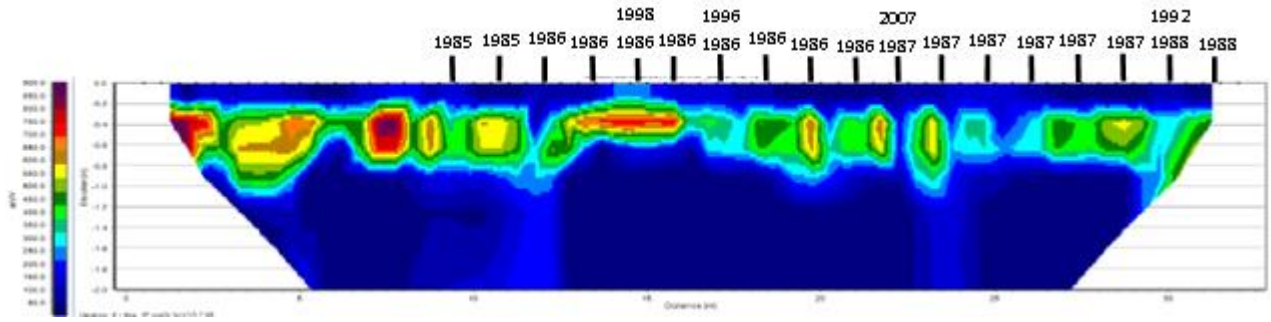

Figure 3.13.6: Induced polarisation data captured with the Wenner array, September 2020. Pt Lincoln RSL Cemetery, Row Q.

The resistivity data captured by the Dipole – Dipole array, Figure 3.13.7, shows a less homogenous subsurface than the Wenner inversion. A number of small, discrete areas of resistivity in the range of 150-200 Ω-m are within a depth range of 40 - 100 cm. These discrete areas are not confined to the area containing the burials, but thirteen of the eighteen burials can be identified.

The IP data captured with the Dipole – Dipole array, Figure 3.13.8, shows a similar pattern. Chargeability values in the depth range of 40 - 80 cm are higher than 400 nV/V. Several small areas recording a chargeability above 550 nV/V are within the area of the burials.

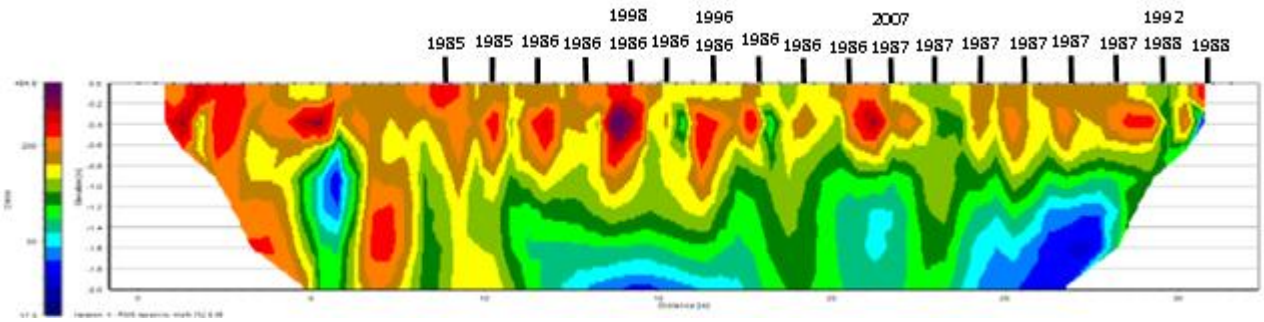

Figure 3.13.7: Resistivity data captured with the Dipole - Dipole array, September 2020. Pt Lincoln RSL Cemetery, Row Q.

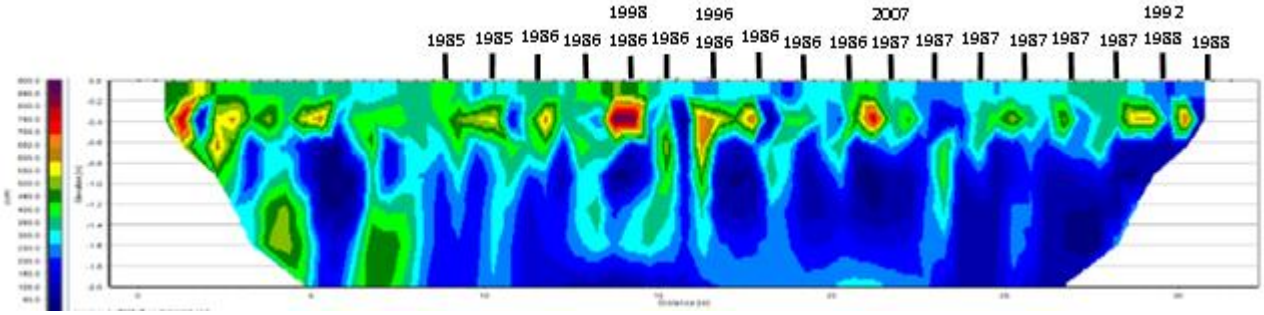

Figure 3.13.8: Induced polarisation data captured with the Dipole - Dipole array, September 2020. Pt Lincoln RSL Cemetery, Row Q.

3.13.2 December 2020

Data was collected in December 2020. There was 3 mm of rainfall in the week before this data was collected. The ten-month rainfall plot is shown in Figure 3.13.9.

Eleven of the eighteen burials in row Q can be identified in these radargrams. The radargrams from December 2020 all show strong reflections along the length of the radar line, Figures 3.13.10, 3.13.11, and 3.13.12. Lines 2 and 3 show these reflections clearly, while in line 4 the reflections are not evident, this line being over a narrower section of the grave. Smaller reflections, circled in red, Figure 3.13.11, can be seen in line 3. The horizontal reflection seen in the September radargrams is not seen here. Depth of penetration is greater than 6.9 m, with attenuation starting at approximately 2.5 m.

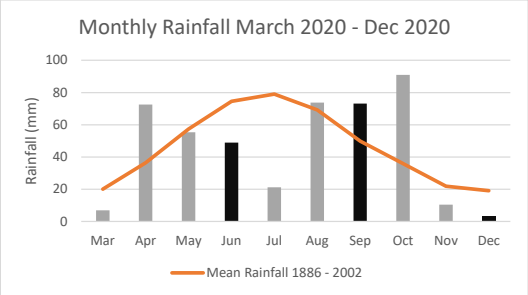

Figure 3.13.9: Monthly rainfall in the ten months prior to data capture. Months in which a site visit occurred are in black. (Rainfall and Temperature data from bom.gov.au)

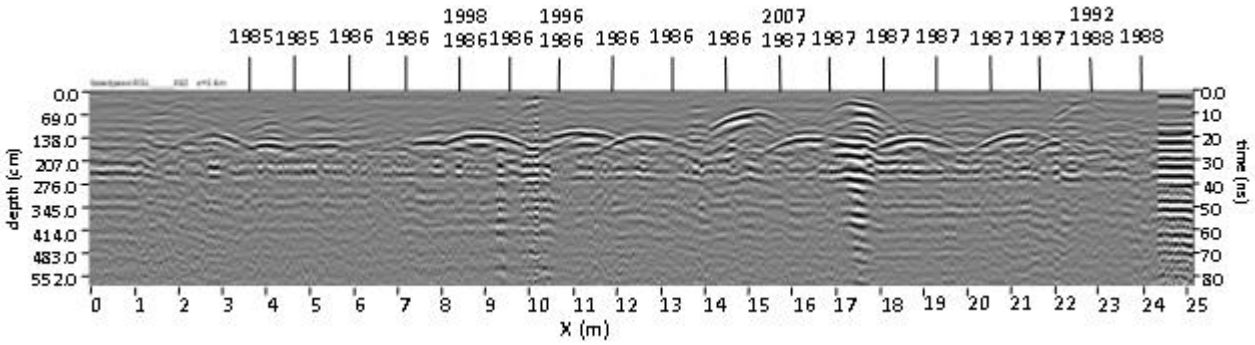

Figure 3.13.10: Pt Lincoln RSL Cemetery, December 2020, Row Q, line 2.

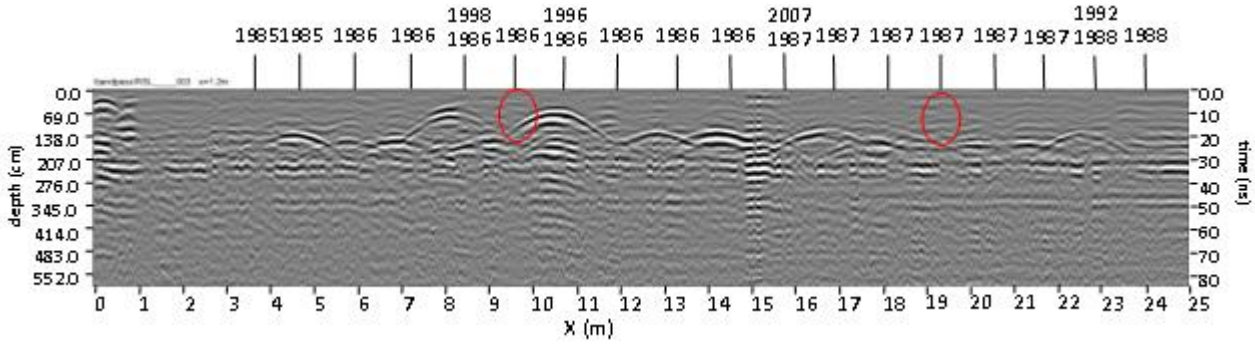

Figure 3.13.11: Pt Lincoln RSL Cemetery, December 2020, Row Q, line 3.

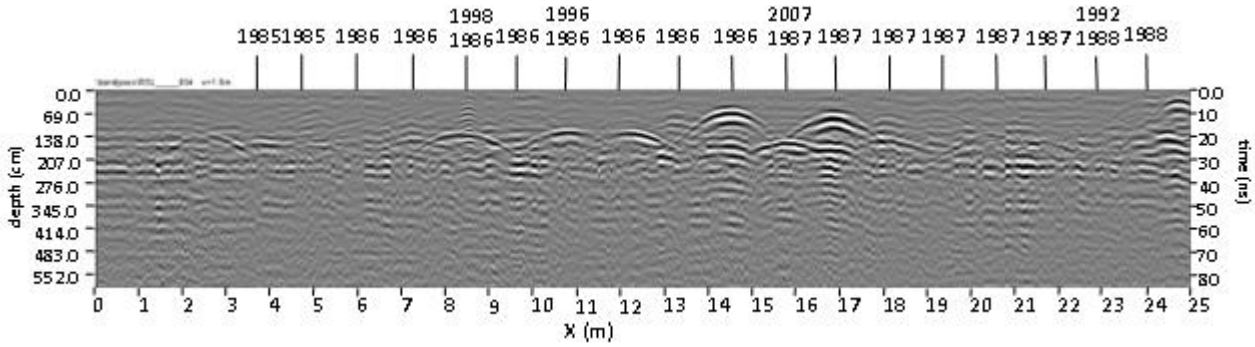

Figure 3.13.12: Pt Lincoln RSL Cemetery, December 2020, Row Q, line 4.

The resistivity data captured with the Wenner array, Figure 3.13.13, shows a wide band of higher resistivity above 150 Ω-m. This band lies between the depths of 20 and 100 cm. Within this band are smaller, discrete areas of resistivity above 300 Ω-m. These smaller areas can be associated with the burials.

The higher chargeability shown in the IP data plot, Figure 3.13.14, lies to a depth between 60 and 80 cm, and shows values greater than 550 nV/V. This band extends past the burials into the driveway.

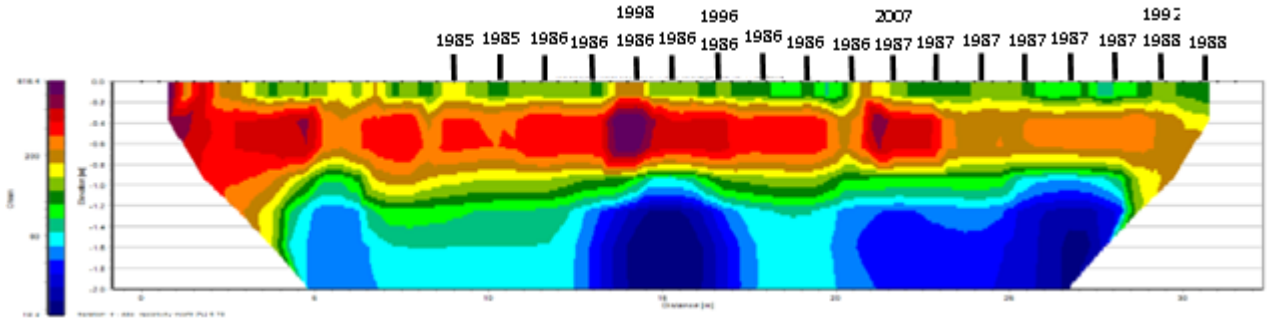

Figure 3.13.13: Resistivity data captured with the Wenner Array, December 2020. Pt Lincoln RSL Cemetery, Row Q.

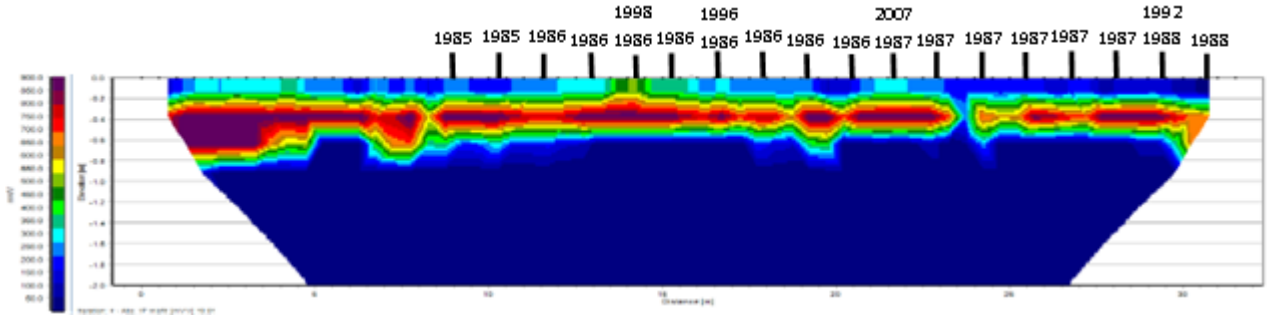

Figure 3.13.14: Induced polarisation data captured with the Wenner array, December 2020. Pt Lincoln RSL Cemetery, Row Q.

The resistivity data collected using the Dipole – Dipole array, Figure 3.13.15, shows a band of resistivity greater than 150 Ω-m, between the depths of 20 and 100 cm. Within this band are smaller, discrete areas of resistivity greater than 300 Ω-m, these can be associated with the burials. There is a similar band of higher chargeability in the IP data plot, Figure 3.13.16. The chargeability of this band is greater than 550 nV/V, and within this band burials can be identified.

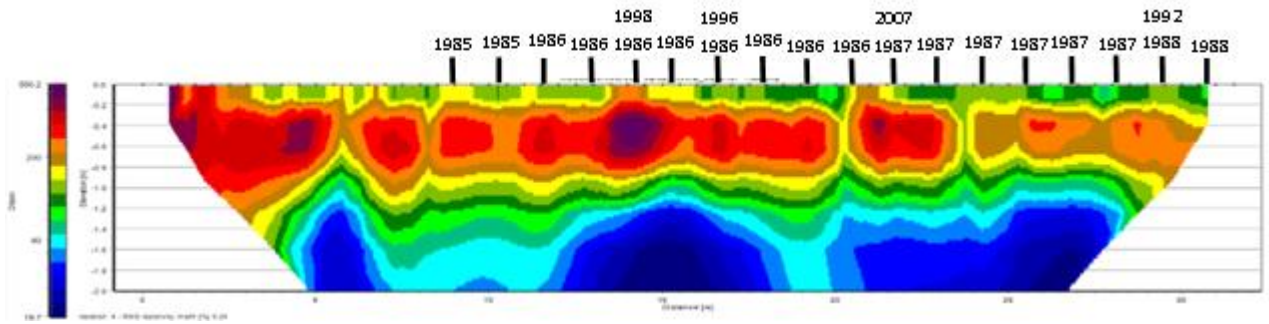

Figure 3.13.15: Resistivity data captured withe the Dipole - Dipole array, December 2020. Pt Lincoln RSL Cemetery, Row Q.

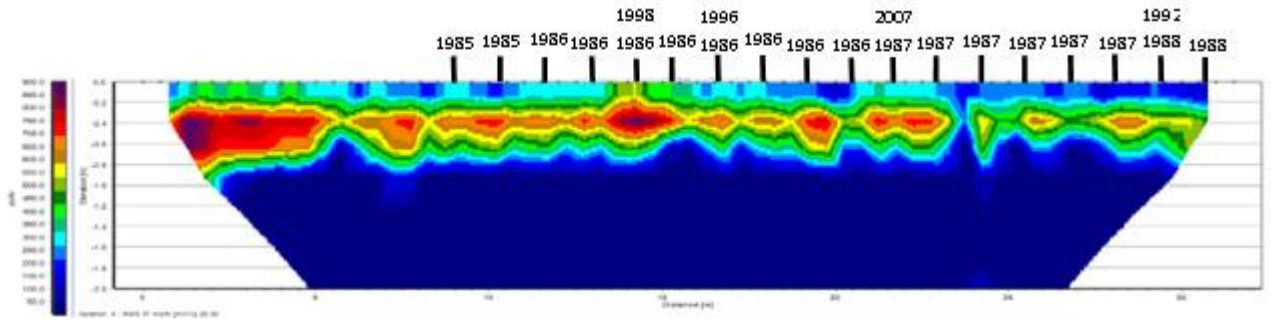

Figure 3.13.16: Induced polarisation data captured with the Dipole - Dipole array, December 2020. Pt Lincoln RSL Cemetery, Row Q.

3.13.3 March 2021

Data was collected in March 2021. There was 0.4 mm of rainfall in the week before this data was collected. The ten-month rainfall plot is shown in Figure 3.13.17. There was no ERT data collected on this visit.

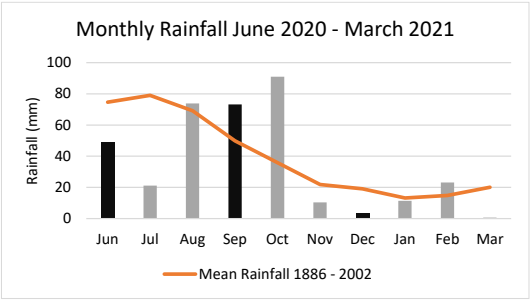

Figure 3.13.17: Monthly rainfall in the ten months prior to data capture. Months in which a site visit occurred are in black. (Rainfall and Temperature data from bom.gov.au)

The radargrams from data gathered in March 2021 show a line of strong reflections along the entire length of the radar line. Line 3, being over the widest part of the grave shows the reflections clearly. Lines 2 and 3 show a shallow horizontal reflection, ("A" in Figure 3.13.18), and line 4 shows the smaller, shallow reflections circled in red, Figure 3.13.20. Fourteen of the eighteen burials in row Q can be identified in these radargrams.

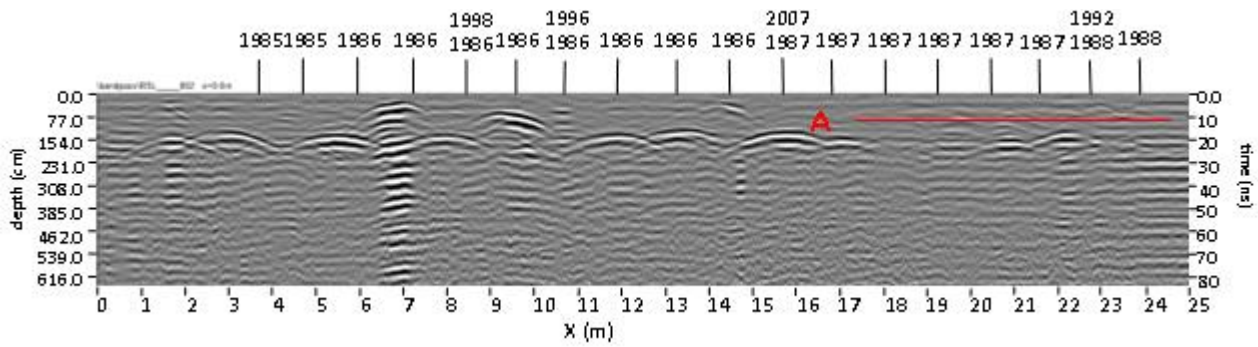

Figure 3.13.18: Pt Lincoln RSL Cemetery March 2021, Row Q, line 2.

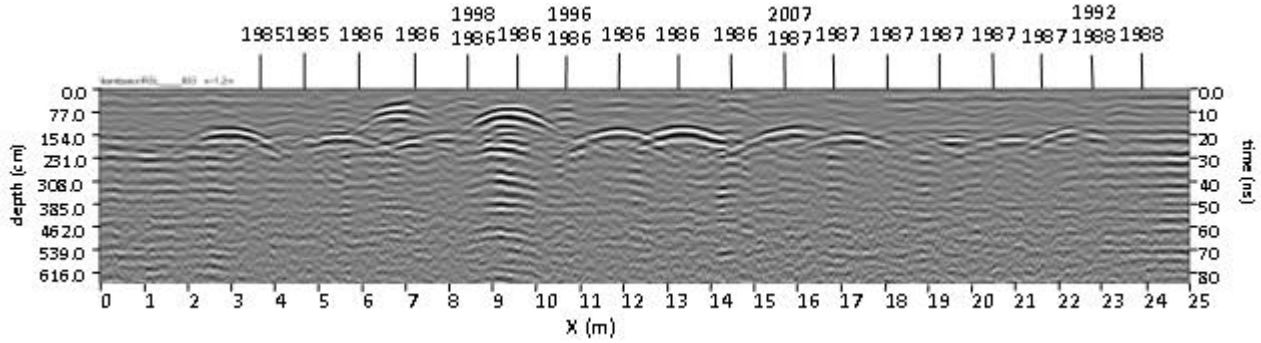

Figure 3.13.19: Pt Lincoln RSL Cemetery, March 2021, Row Q, line 3.

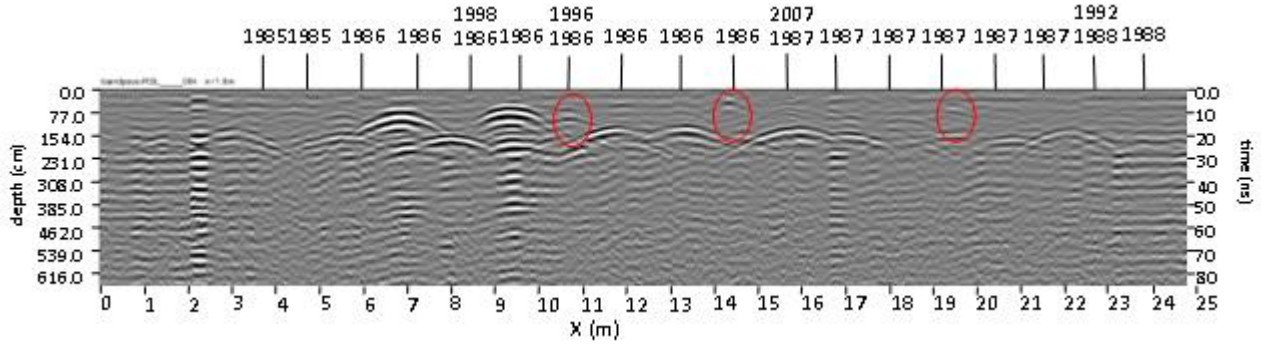

Figure 3.13.20: Pt Lincoln RSL Cemetery, March 2021, Row Q, line 4.

3.13.4 June 2021

Data was collected in March 2021. There was 17.8 mm of rainfall in the week before this data was collected. The ten-month rainfall plot is shown in Figure 3.13.21. There was no ERT data collected on this visit.

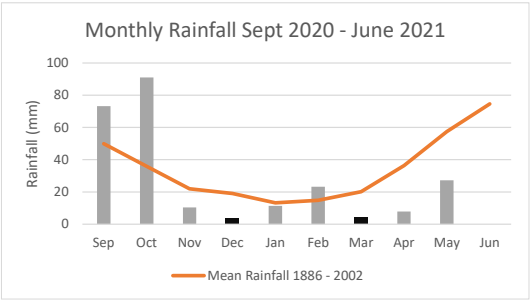

Figure 3.13.21: Monthly rainfall in the ten months prior to data collection. Months in which a site visit occurred are in black. (Rainfall and Temperature data from bom.gov.au)

The radargrams from June 2021 show reflections the entire length of the radar line, Figures 3.13.22, 3.13.23, and 3.13.24. There are shallower reflections above these, circled in red, along with the horizontal reflection, “A” in Figure 3.13.24. Depth of penetration is 6.5 m with attenuation starting at approximately 2 m. Fourteen of the eighteen burials in row Q can be identified in these radargrams.

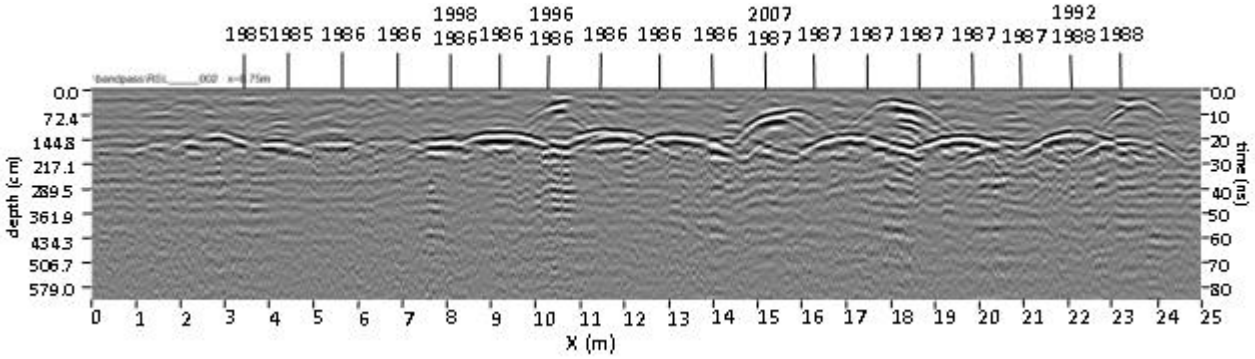

Figure 3.13.22: Pt Lincoln RSL Cemetery June 2021, Row Q, line 1.

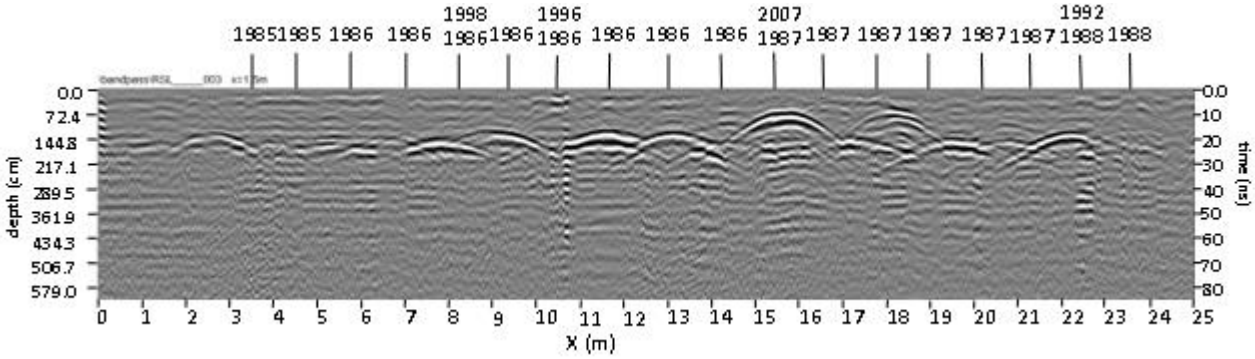

Figure 3.13.23: Pt Lincoln RSL Cemetery, June 2021, Row Q, line 2.

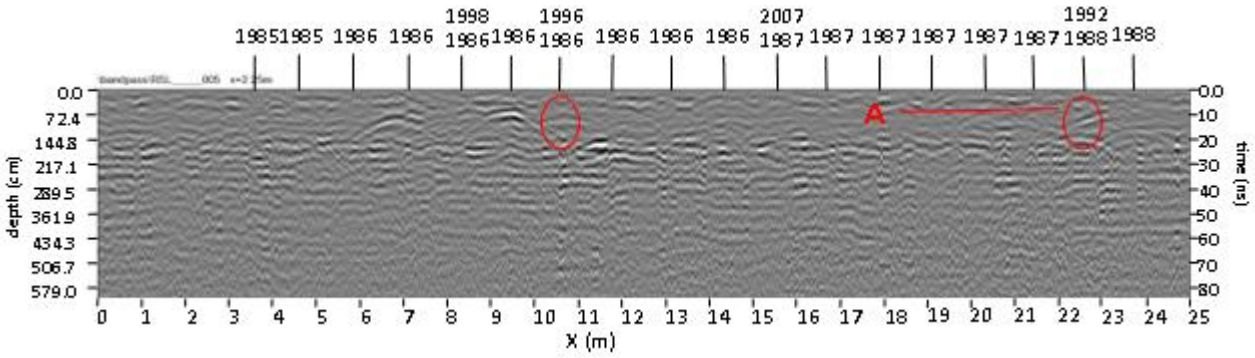

Figure 3.13.24: Pt Lincoln RSL Cemetery, June 2021, Row Q, line 3.

3.13.5 February 2022

Data was collected in February 2022. There was 50.6 mm of rainfall in the week before this data was collected. The ten-month rainfall plot is shown in Figure 3.13.25.

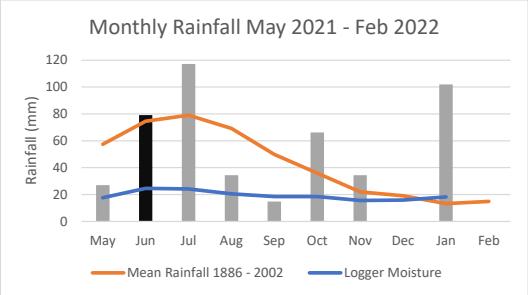

Figure 3.13.25: Monthly rainfall in the ten months prior to data capture. Months in which a site visit occurred are in black. (Rainfall and Temperature data from bom.gov.au)

The radargrams from February 2022 show many reflections along the line of graves, Figures 3.13.26, 3.13.27, and 3.13.28. However, these have not been recorded along the entire line, as in previous data. There are still smaller and shallower reflections, circled in red, Figure 3.13.26. The horizontal reflection seen in previous radargrams is highlighted in Figure 3.13.27. Depth of penetration is 4.8 m, with attenuation starting at approximately 2 m. Thirteen of the eighteen burials in row Q can be identified in these radargrams.

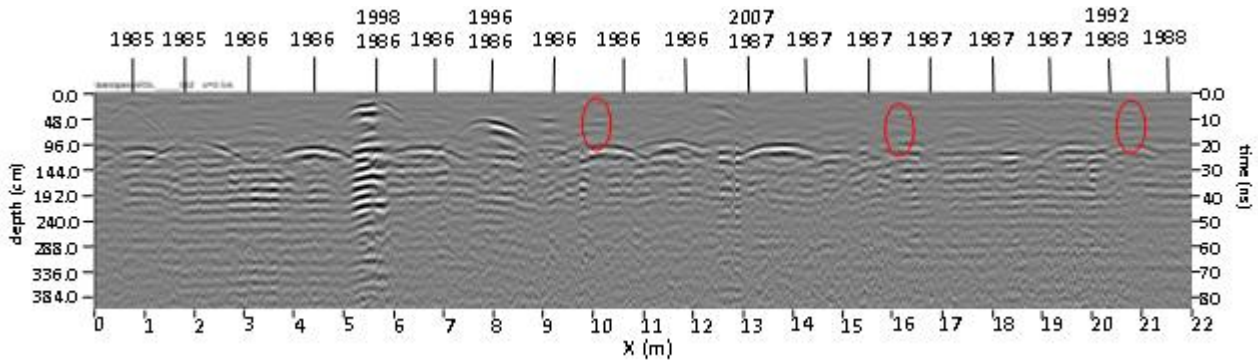

Figure 3.13.26: Pt Lincoln RSL Cemetery February 2022, Row Q, line 2.

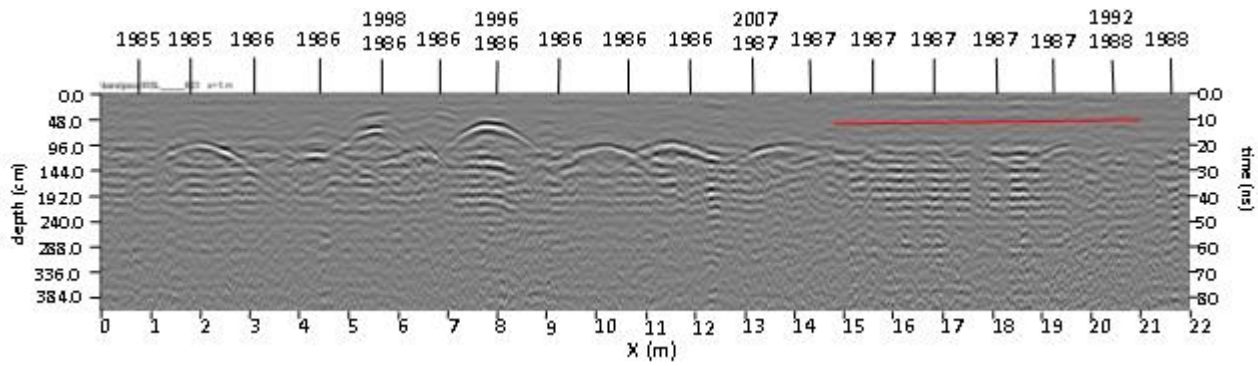

Figure 3.13.27: Pt Lincoln RSL Cemetery, February 2022, Row Q, line 3.

The resistivity data captured by Wenner array, Figure 3.13.29, shows several discrete areas at a depth range of 40 – 140 cm. Resistivities for these areas range from 300 - 400 Ω-m. These are along the entire line and can be associated with the burials. The IP data, Figure 3.13.30, shows a similar pattern with several discrete areas along the ERT line. These areas show a chargeability greater than 550 nV/V, and are located at the same depth as the Wenner resistivities.

The resistivity data captured with the Dipole – Dipole array, Figure 3.13.31, also presents several areas with resistivity greater than 300 Ω-m. These areas extend along the entire ERT line and are associated with the burials. The IP Data captured by Dipole – Dipole array, Figure 3.13.32, mimics the resistivity data to an extent. The chargeability values within the discrete areas is greater than 400 nV/V, and are generally constrained above a depth of 120 cm.

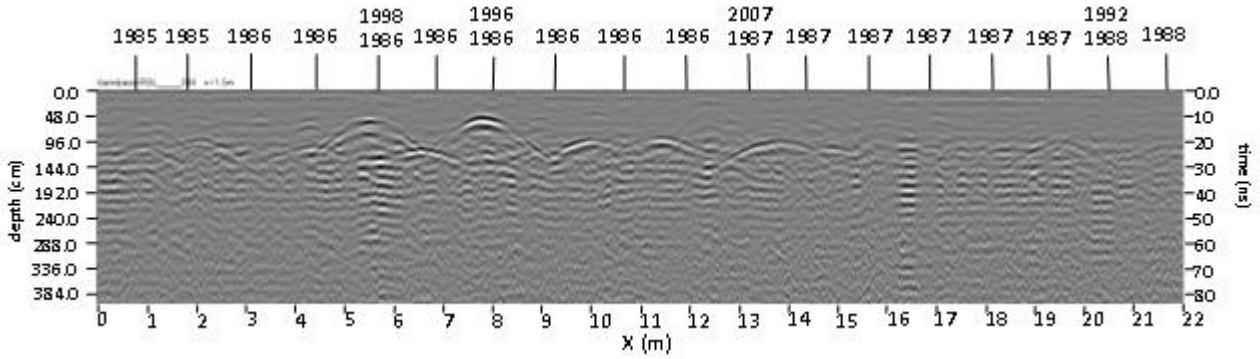

Figure 3.13.28: Pt Lincoln RSL Cemetery, February 2022, Row Q, line 4.

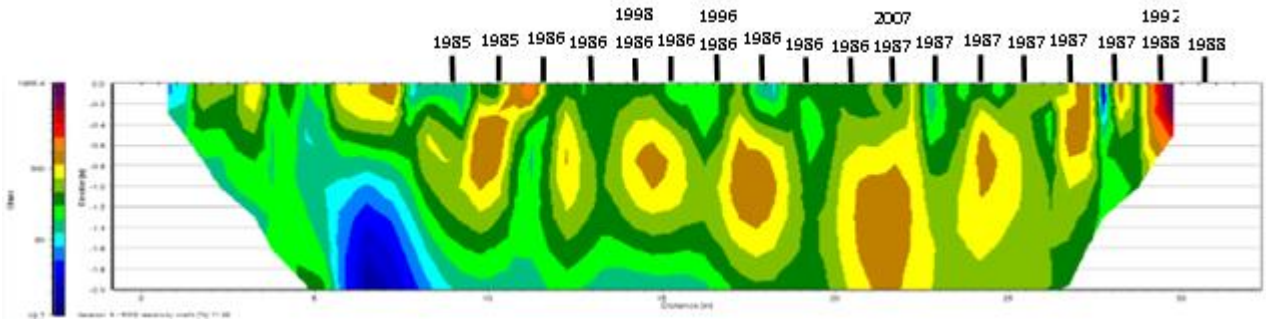

Figure 3.13.29: Resistivity data captured with the Wenner array, February 2022. Pt Lincoln RSL Cemetery, Row Q.

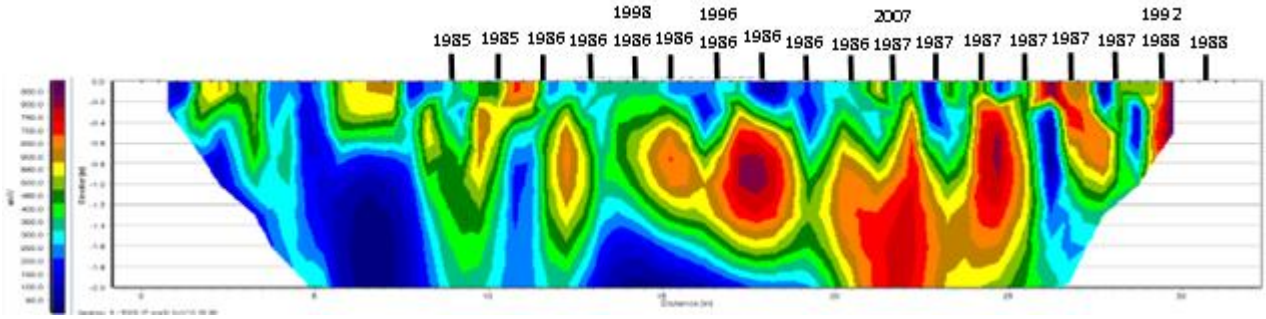

Figure 3.13.30: Induced polarisation data captured with the Wenner array, February 2022. Pt Lincoln RSL Cemetery, Row Q.

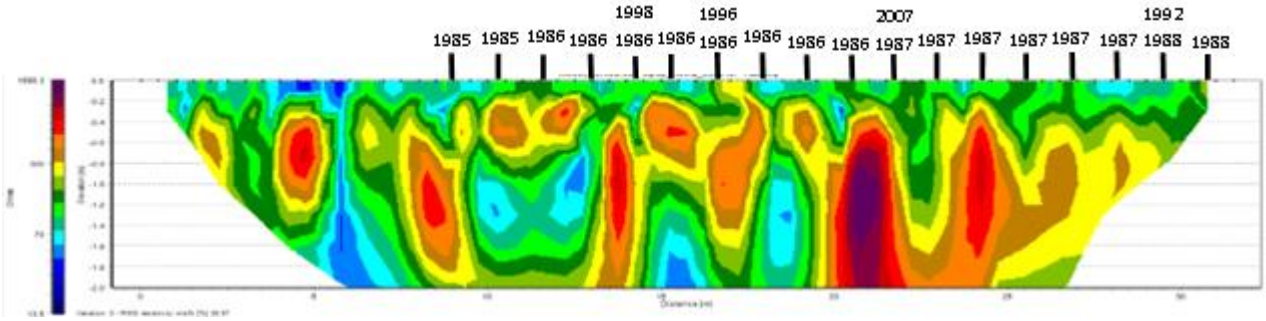

Figure 3.13.31: Resistivity data captured with the Dipole - Dipole array, February 2022. Pt Lincoln RSL Cemetery, Row Q.

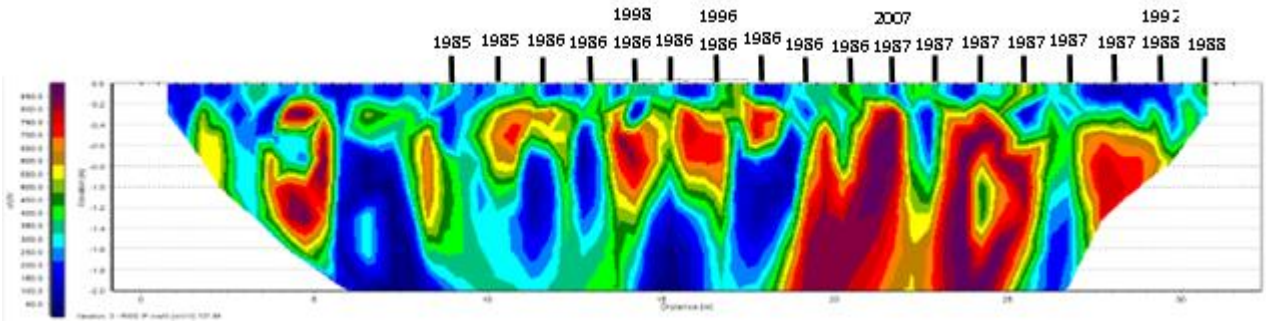

Figure 3.13.32: Induced polarisation data captured with the Dipole - Dipole array, February 2022. Pt Lincoln RSL Cemetery, Row Q.

3.13.6 July 2022

Data was collected in July 2022. There was 4.2 mm of rainfall in the week before this data was collected.

The ten-month rainfall plot is shown in Figure 3.13.33.

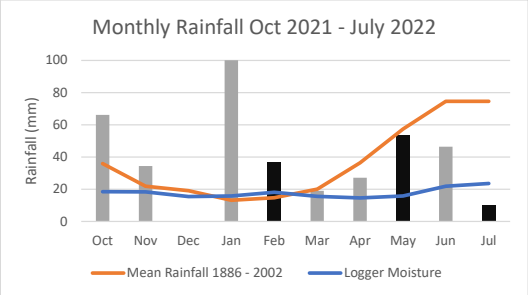

Figure 3.13.33: Monthly rainfall in the ten months prior to data collection. Months in which a site visit occurred are in black. (Rainfall and Temperature data from bom.gov.au)

The radargrams from the July 2022 data capture show a line of reflections along the entire radar line, Figures 3.13.34, 3.13.35, and 3.13.36. These reflections are large, both in amplitude and geographic size, and are especially clear in the first 18 m of the line. There are numerous smaller reflections at a shallow depth, circled in red in Figure 3.13.36, while in Figure 3.13.34, the shallow horizontal reflection is highlighted. Eleven of the eighteen burials can be identified in these radargrams, mainly from the large hyperbola.

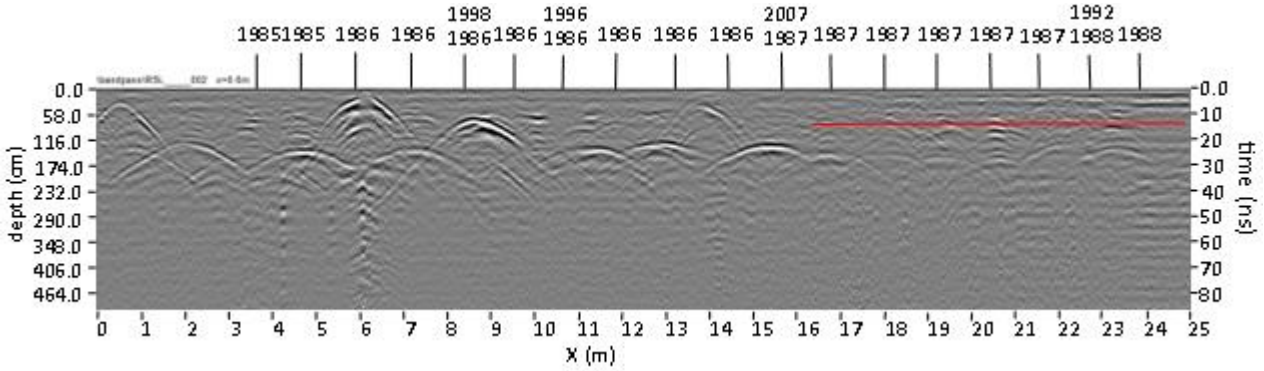

Figure 3.13.34: Pt Lincoln RSL Cemetery, July 2022, Row Q, line 2.

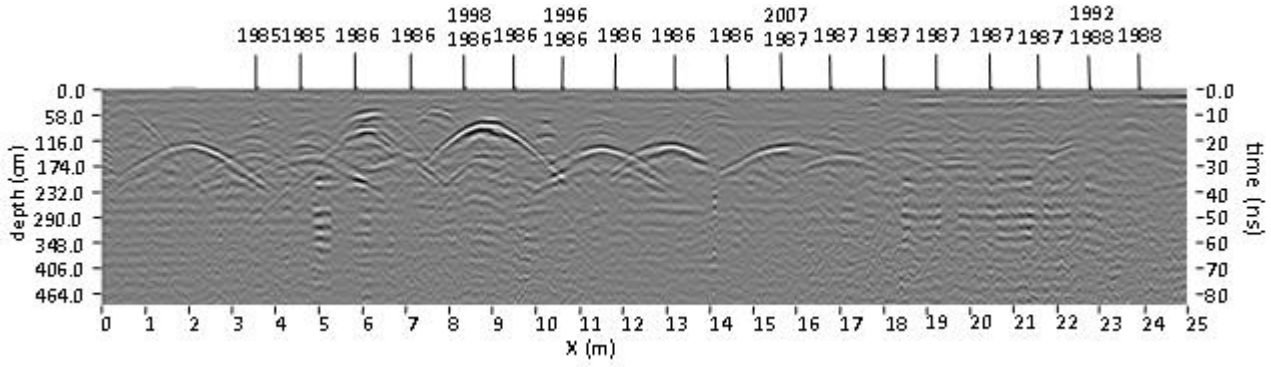

Figure 3.13.35: Pt Lincoln RSL Cemetery, July 2022, Row Q, line 3.

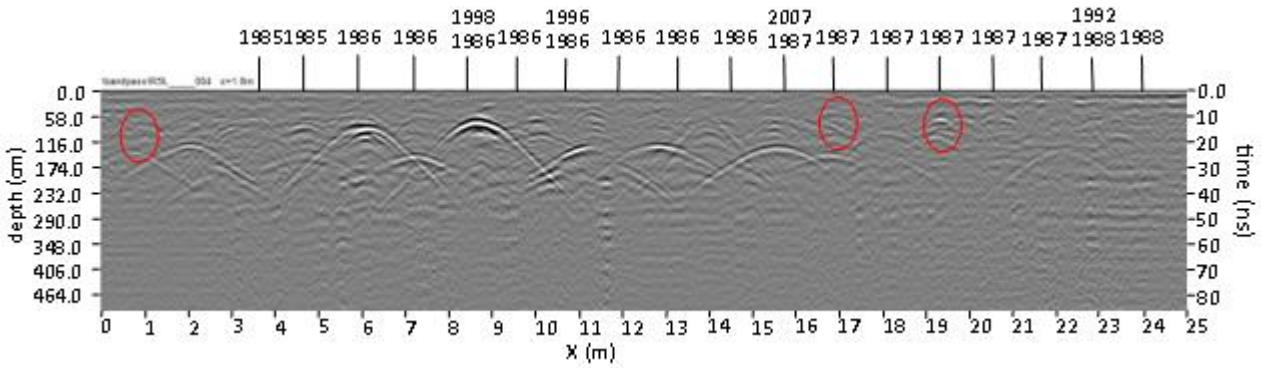

Figure 3.13.36: Pt Lincoln RSL Cemetery, July 2022, Row Q, line 4.

The resistivity data captured with the Wenner array, Figure 3.13.37, shows a layer to 1.2 m of resistivity values above 160 Ω-m. Within this layer no discrete areas are presented, only two of the burials could be identified.

The IP data, Figure 3.13.38, shows a similar shallow layer, with high chargeability values greater than 550 nV/V. This layer is to a similar depth of 100 cm, and below this the chargeability seems largely homogenous with a value below 130 nV/V. From this data no burials could be identified.

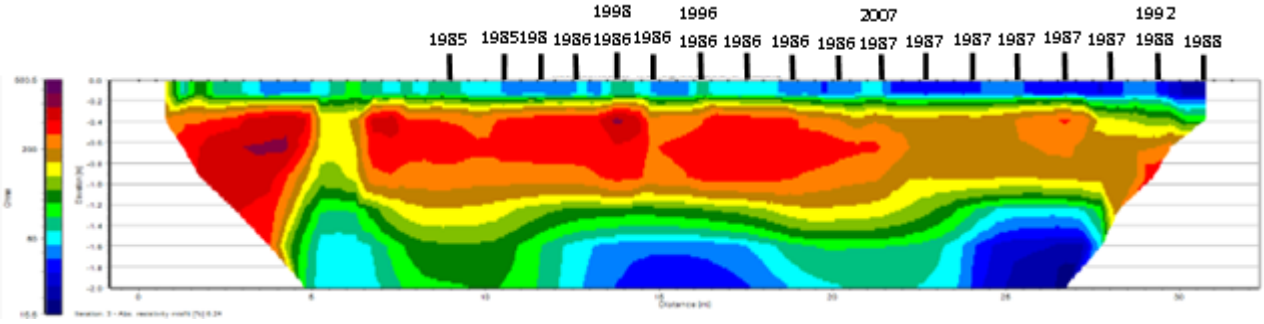

Figure 3.13.37: Resistivity data captured with the Wenner array, July 2022. Pt Lincoln RSL Cemetery, Row Q

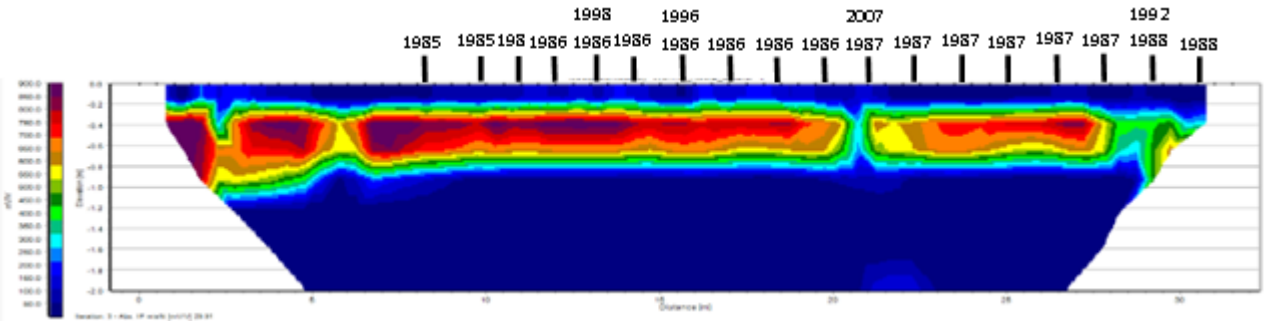

Figure 3.13.38: Induced polarisation data captured with the Wenner array, July 2022. Pt Lincoln RSL Cemetery, Row Q.

The resistivity data captured by the Dipole – Dipole array, Figure 3.13.39, shows several discrete areas with recorded resistivities above 200 Ω-m. These areas can be associated with the burials.

The IP data, Figure 3.13.40, shows a very similar pattern, with higher chargeability values recorded between the depths of 40 -160 cm. The chargeability of these areas is greater than 400 nV/V.

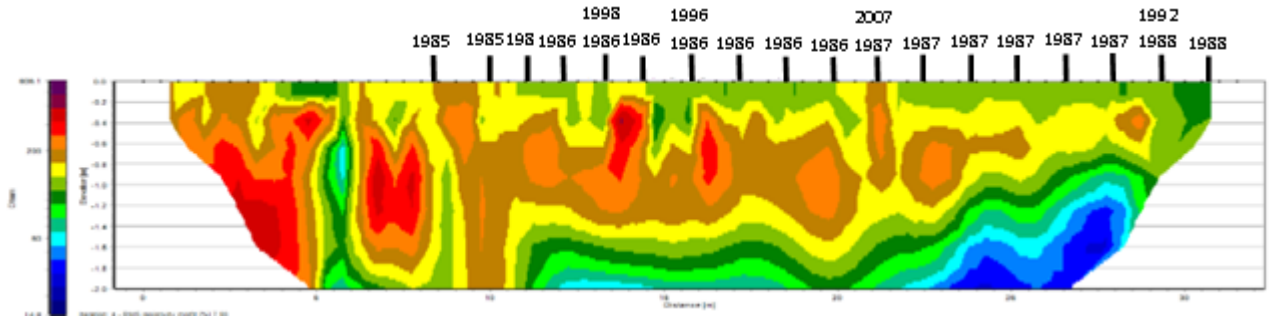

Figure 3.13.39: Resistivity data captured with the Dipole - Dipole array, July 2022. Pt Lincoln RSL Cemetery, Row Q.

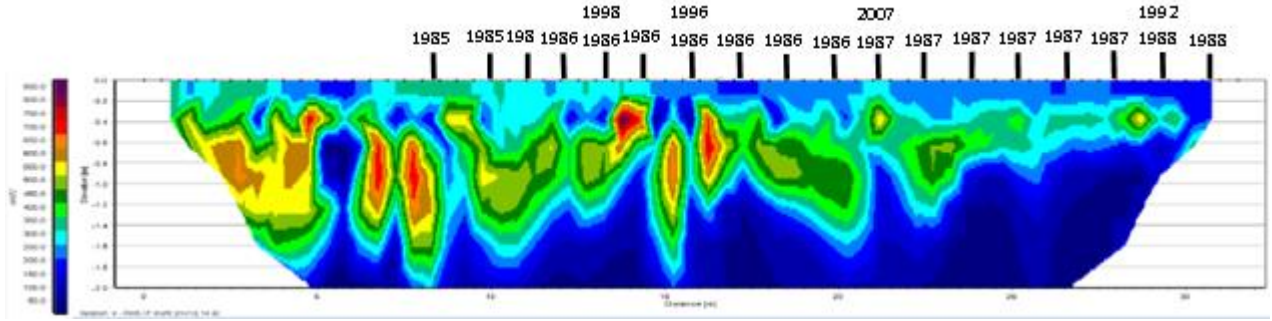

Figure 3.13.40: Induced polarisation data captured with the Dipole - Dipole array, July 2022. Pt Lincoln RSL Cemetery, Row Q.

3.13.7 September 2022

Data was collected in September 2022. There was 4 mm of rainfall in the week before this data was collected. The ten-month rainfall plot is shown in Figure 3.13.41. There was no suitable ERT data collected on this visit. Fourteen of the eighteen burials in row Q can be identified in these radargrams.

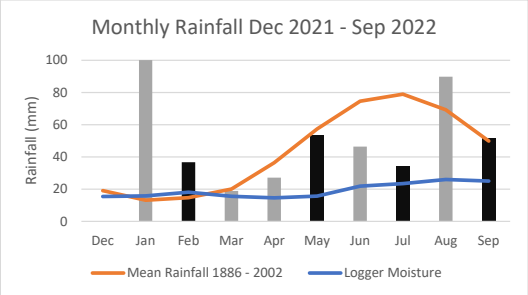

Figure 3.13.41: Monthly rainfall in the ten months prior to data collection. Months in which a site visit occurred are in black. (Rainfall and Temperature data from bom.gov.au)

The radargrams from data captured in September 2022 show the line of strong reflections, Figures 3.13.42, 3.13.43, and 3.13.44. These reflections are large in amplitude and geographic size but do not extend past 17 m with the same strength. These large hyperbola allow identification of the burial sites. Smaller reflections at a shallower depth can be see, these are circled in red in Figure 3.13.43.

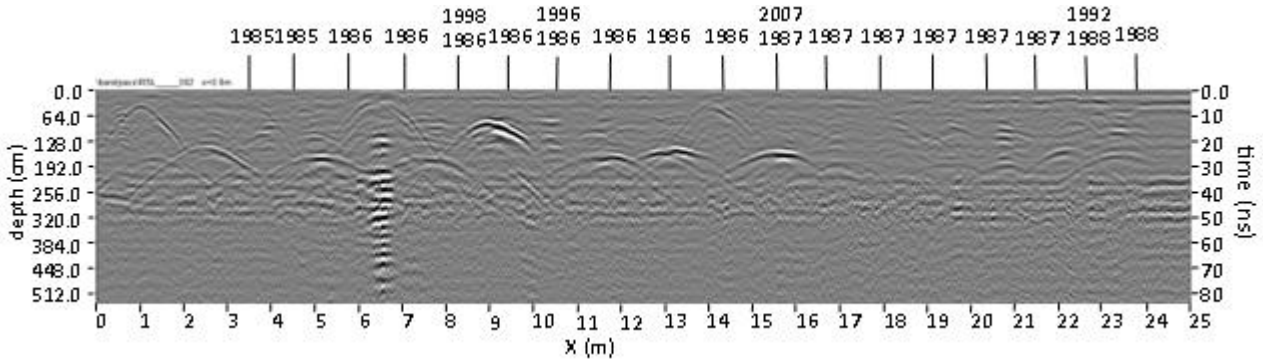

Figure 3.13.42: Pt Lincoln RSL Cemetery September 2022, Row Q, line 2

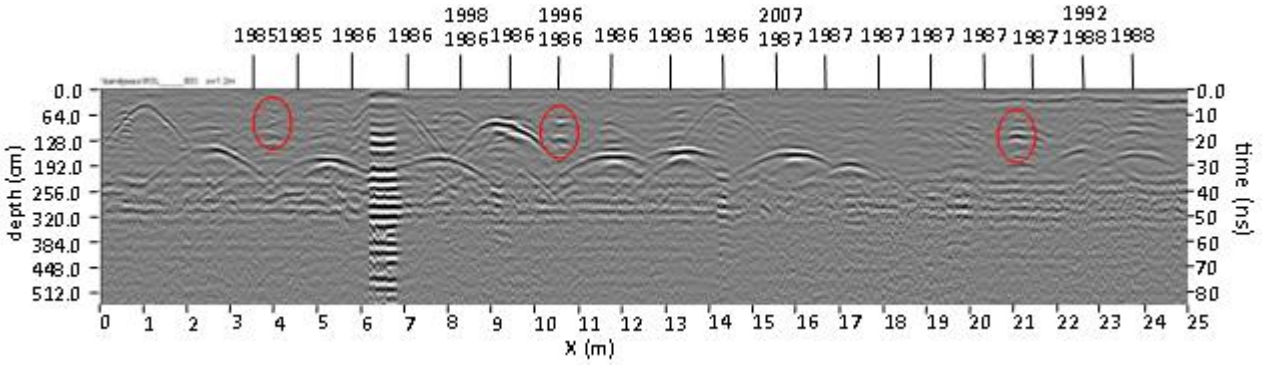

Figure 3.13.43: Pt Lincoln RSL Cemetery, September 2022, Row Q, line 3.

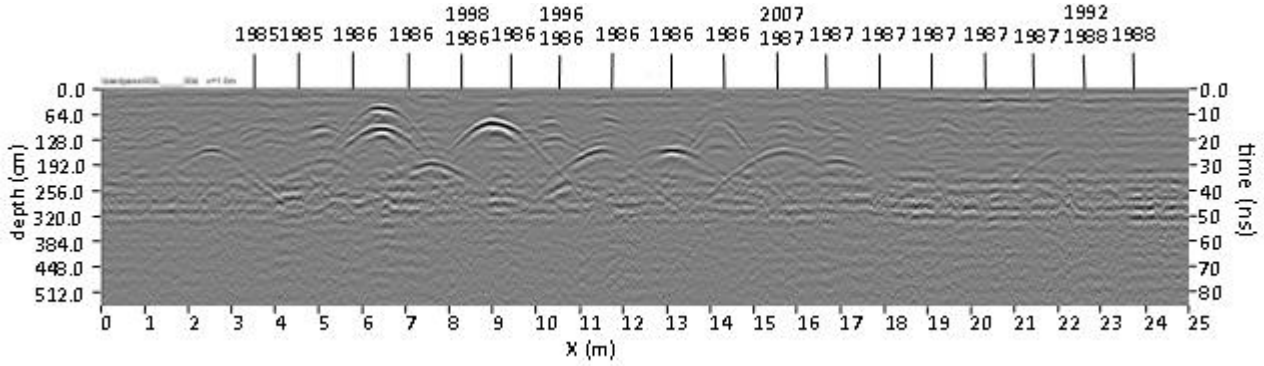

Figure 3.13.44: Pt Lincoln RSL Cemetery, September 2022, Row Q, line 4.

3.13.8 December 2022

Data was collected in July 2022. There was 5.4 mm of rainfall in the week before this data was collected. The ten-month rainfall plot is shown in Figure 3.13.45

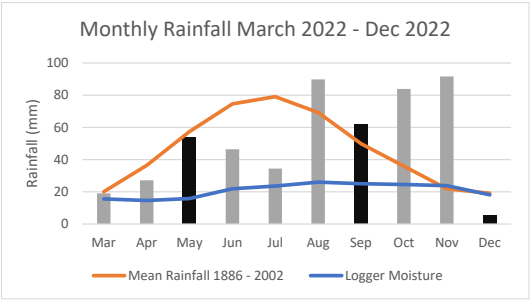

Figure 3.13.45: Monthly rainfall in the ten months prior to data collection. Months in which a site visit occurred are in black. (Rainfall and Temperature data from bom.gov.au)

The radargrams in Figures 3.13.46, 3.13.47, and 3.13.48 show the line of strong reflections as in previous months. Here they extend past 17 m to the entire radar line. Smaller, shallow reflections are seen, and are highlighted in red in Figure 3.13.47. The stratigraphic layer is also clearly seen, (in red, Figure 3.13.48), and this extends for most of the radar line. Twelve of the eighteen burials in row Q can be identified in these radargrams.

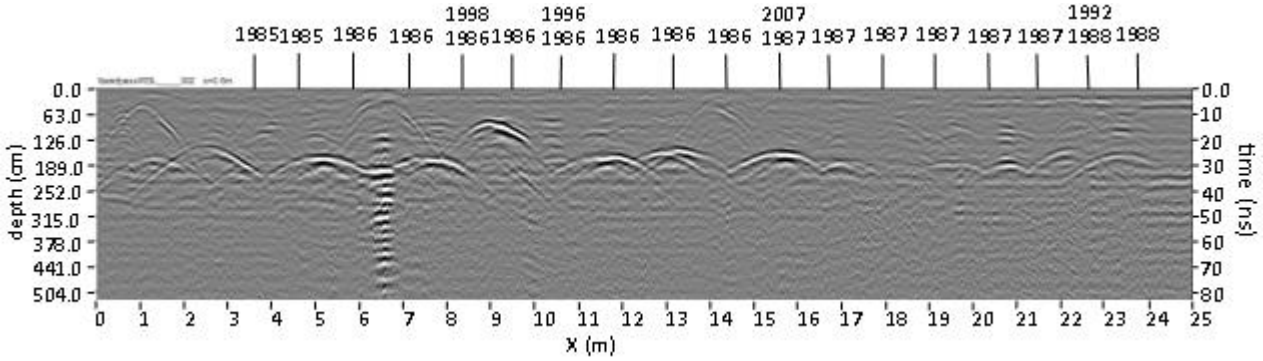

Figure 3.13.46: Pt Lincoln RSL Cemetery December 2022, Row Q, line 2.

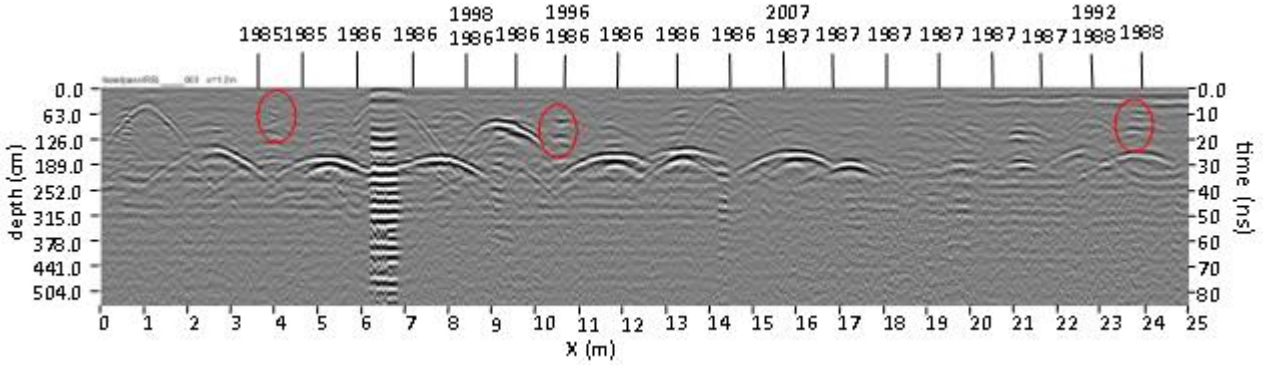

Figure 3.13.47: Pt Lincoln RSL Cemetery, December 2022, Row Q, line 3.

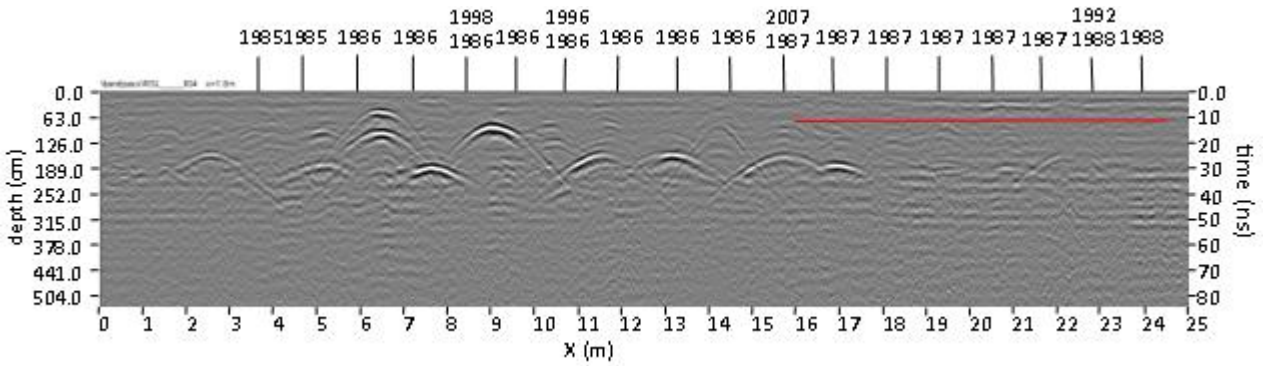

Figure 3.13.48: Pt Lincoln RSL Cemetery, December 2022, Row Q, line 4.

The resistivity data captured by Wenner array, Figure 3.13.49, shows a uniform band with higher resistivities above 150 Ω-m along the entire ERT line. Within this band are several smaller, discrete areas with resistivity values above 300 Ω-m. These smaller areas can be associated with the burials.

The IP data, Figure 3.13.50, shows a similar pattern, with chargeability values above 500 nV/V within the band that lies between the depths of 20 – 80 cm. Within this band are smaller areas of chargeability above 700 nV/V, these are associated with the burials.

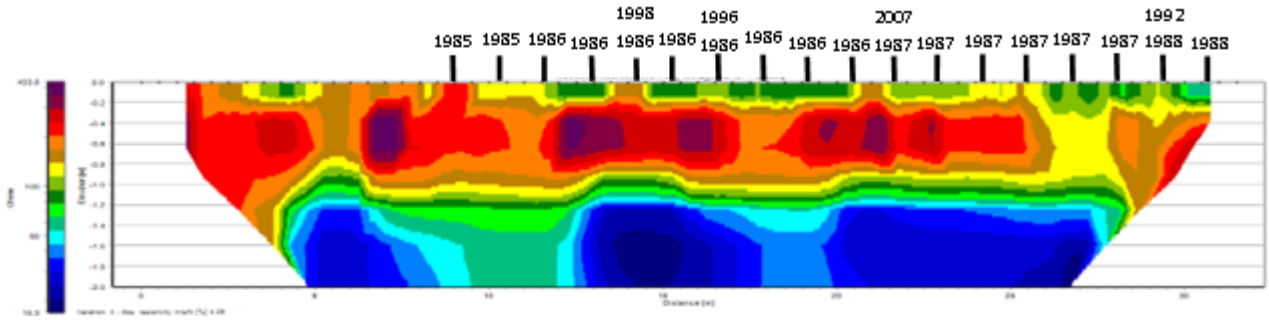

Figure 3.13.49: Resistivity data captured with the Wenner array, December 2022. Pt Lincoln RSL Cemetery, Row Q

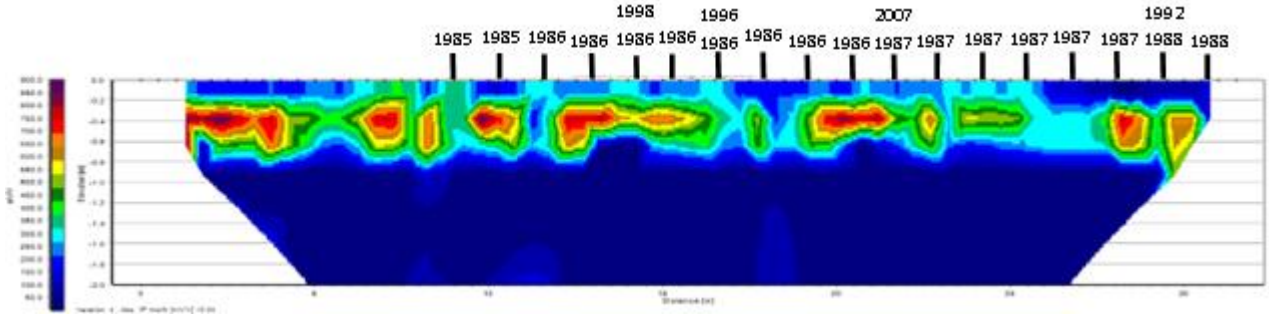

Figure 3.13.50: Induced polarisation data captured with the Wenner array, December 2022. Pt Lincoln RSL Cemetery, Row Q

The resistivity data captured with the Dipole – Dipole array, Figure 3.13.51, shows resistivity values above 250 Ω-m from the surface to approximately 80 cm. These higher values extend along the entire ERT line, any identification of burial sites could only be at a shallow depth.

The IP data, Figure 3.13.52, shows chargeability values above 550 nV/V, again, at a shallow depth less than 60 cm. Below this depth the chargeability is less than 400nV/V.

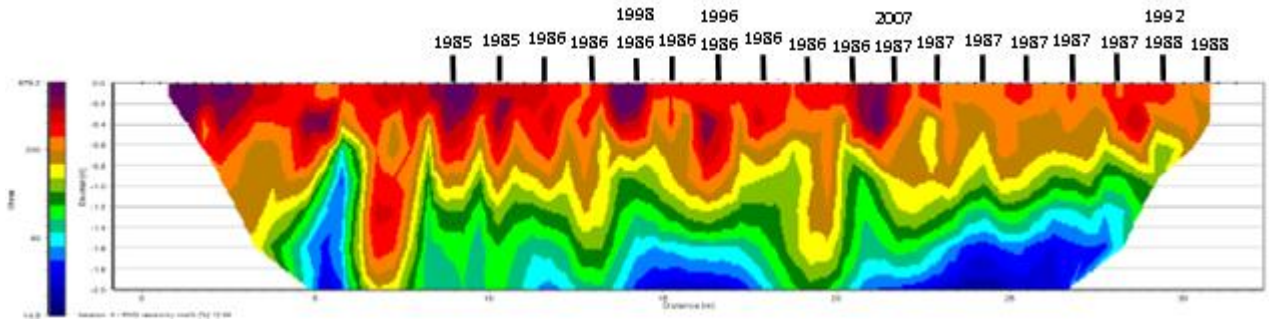

Figure 3.13.51: Resistivity data captured with the Dipole - Dipole array, July 2022. Pt Lincoln RSL Cemetery, Row Q

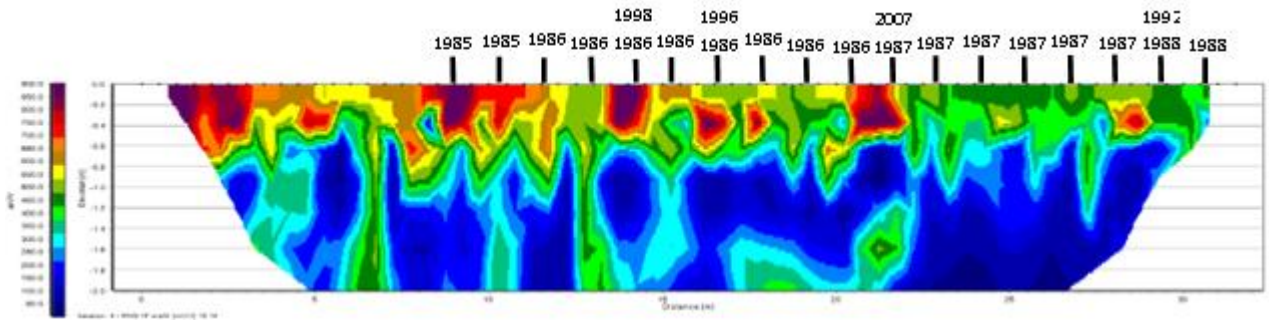

Figure 3.13.52: Induced polarisation data captured with the Dipole - Dipole array, July 2022. Pt Lincoln RSL Cemetery, Row Q

3.13.9 March 2023

Data was collected in March 2023. There was 6.1 mm of rainfall in the week before this data was collected. The ten-month rainfall plot is shown in Figure 3.13.53. Twelve of the eighteen burials in row Q are identified in these radargrams.

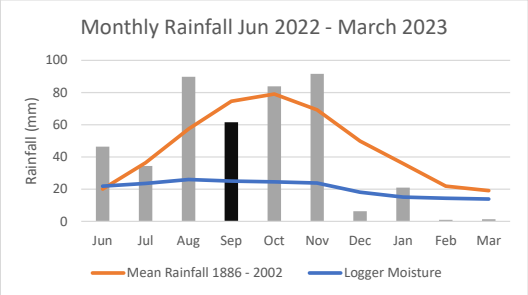

Figure 3.13.53: Monthly rainfall in the ten months prior to data collection. Months in which a site visit occurred are in black. (Rainfall and Temperature data from bom.gov.au)

The radargrams from data captured in March 2023, Figures 3.13.54, 3.13.55, and 3.13.56, show the strong reflections along the entire length of the line. As with previous months, smaller reflections are seen at a shallower depth, these are circled in red in Figure 3.13.55. The shallow stratigraphic layer is highlighted in red in Figure 3.13.56.

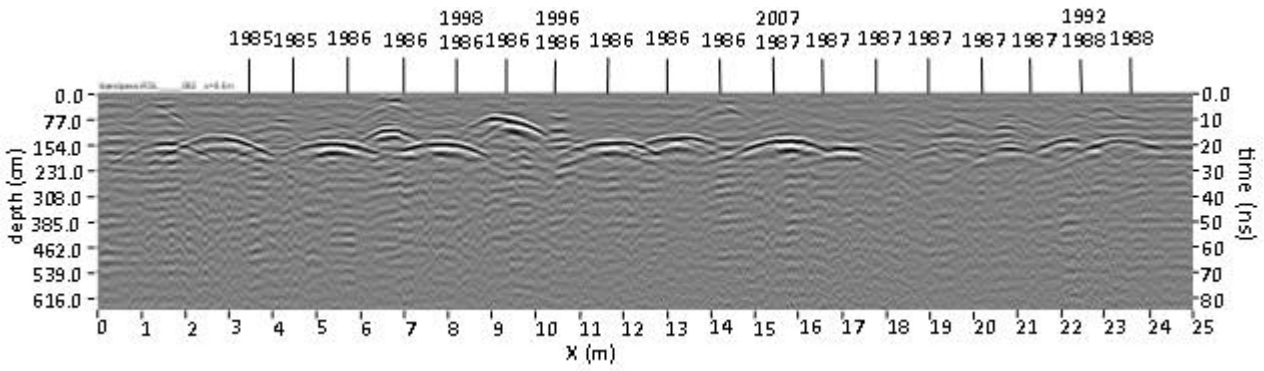

Figure 3.13.54: Pt Lincoln RSL Cemetery March 2023, Row Q, line 2.

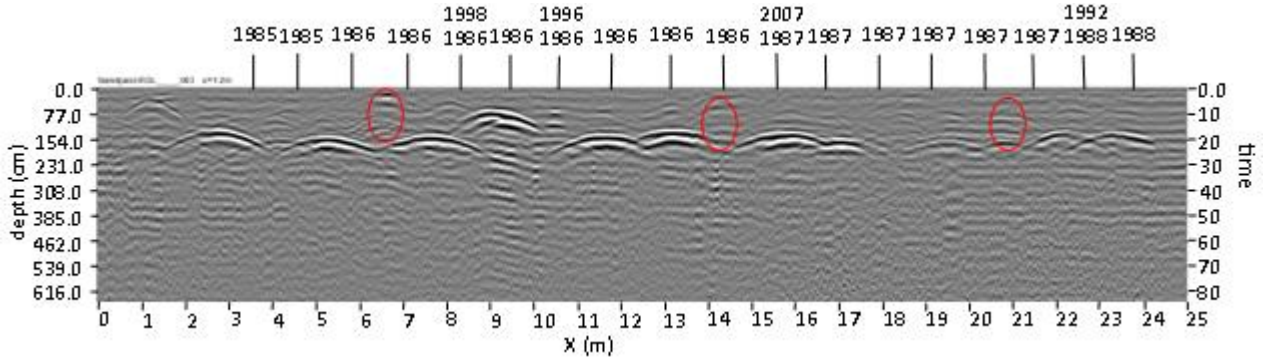

Figure 3.13.55: Pt Lincoln RSL Cemetery March 2023, Row Q, line 3.

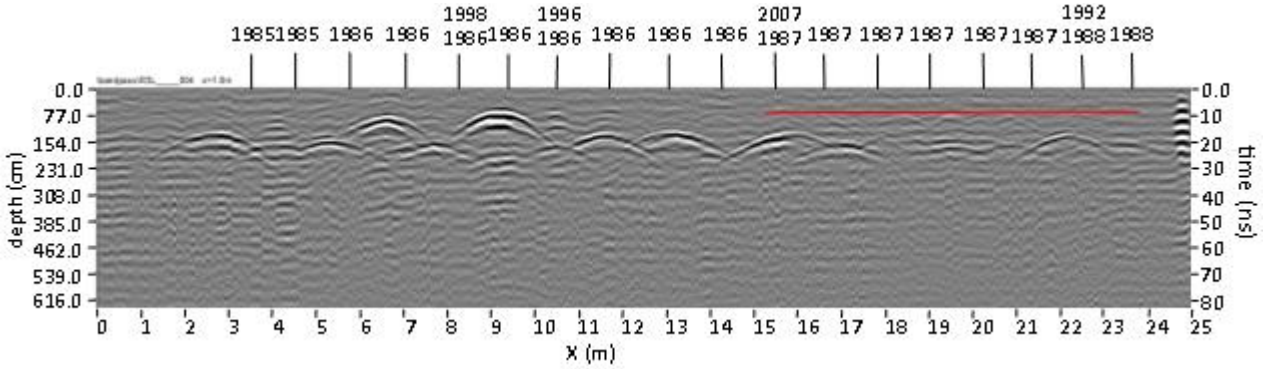

Figure 3.13.56: Pt Lincoln RSL Cemetery March 2023, Row Q, line 4.

The resistivity data captured with the Wenner array, Figure 3.13.57, shows a band of higher resistivities to a depth of 100 cm. The resistivity values in this band are greater than 200 Ω-m, with smaller areas greater than 400 Ω-m associated with the burials.

The IP data in Figure 3.13.58 shows a layer with chargeability values greater than 350 nV/V, above a depth of 80 cm. This layer extends the entire length of the ERT line in a quite uniform shape. From this layer no burials can be identified.

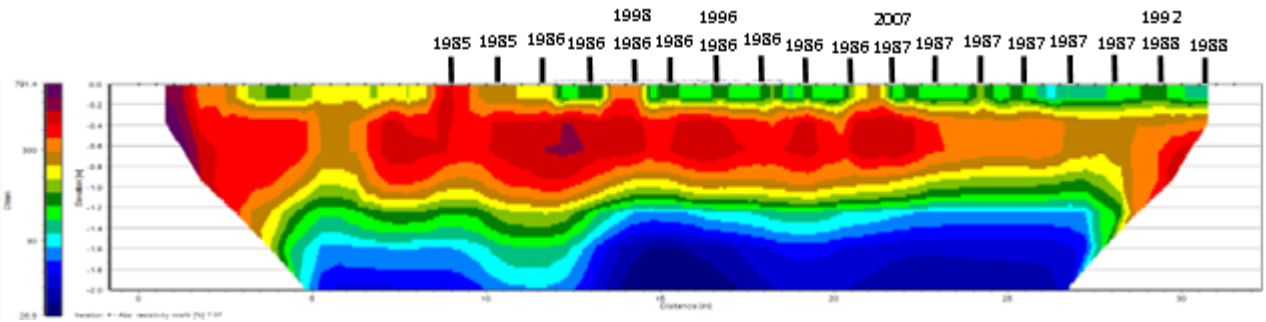

Figure 3.13.57: Resistivity data captured with the Wenner array, March 2023. Pt Lincoln RSL Cemetery, Row Q

The resistivity data captured with the Dipole – Dipole array, Figure 3.13.59, does not present as a consistent band or layer. The resistivity values above 300 Ω-m occur from the surface to depths of 40 – 140 cm. Within this layer, several areas of higher resistivity do occur, these record values above 500 Ω-m, and are generally bound by the area of the burials. The IP data, Figure 3.13.60, shows a similar inconsistency. Despite this inconsistency, some areas with higher chargeability values recorded above 700 nV/V do lie within the bounds of the burials.

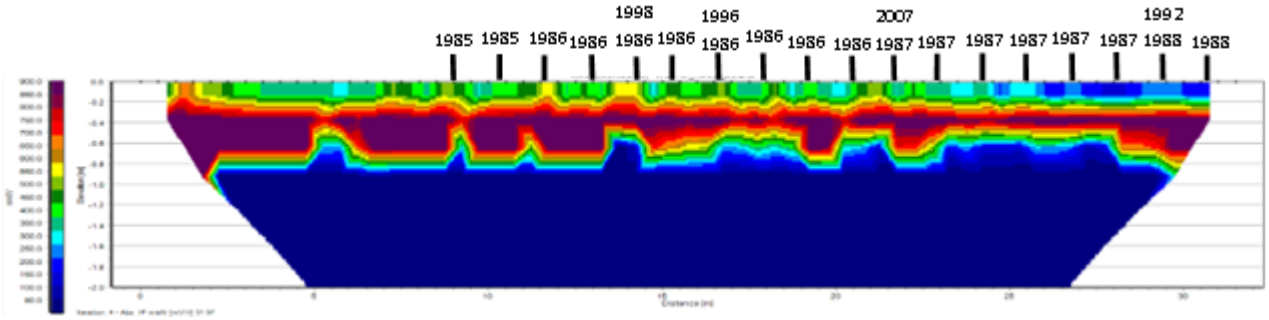

Figure 3.13.58: Induced polarisation data captured with the Wenner array, March 2023. Pt Lincoln RSL Cemetery, Row Q.

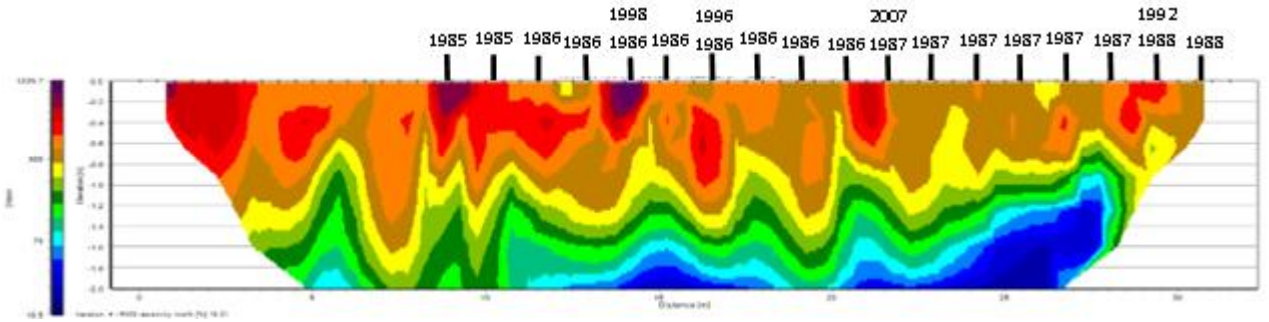

Figure 3.13.59: Resistivity data captured with the Dipole - Dipole array, March 2023. Pt Lincoln RSL Cemetery, Row Q.

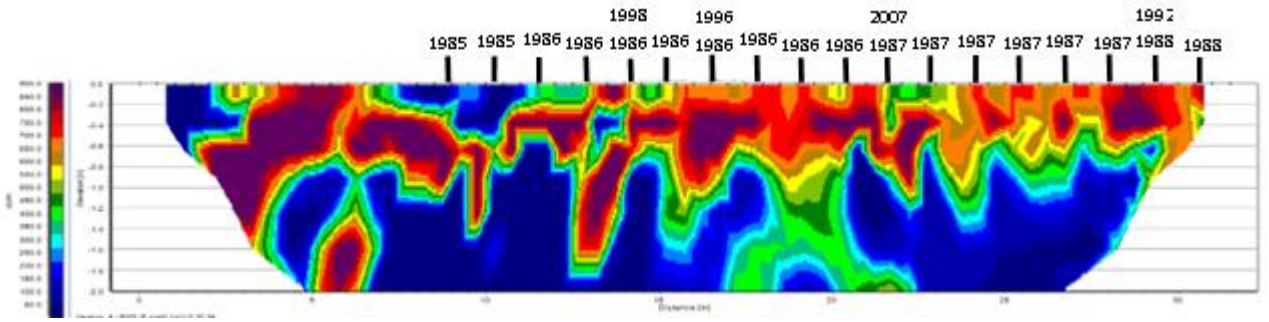

Figure 3.13.60: Induced polarisation data captured with the Dipole - Dipole array, March 2023. Pt Lincoln RSL Cemetery, Row Q.

3.14 Pt Lincoln RSL Soil

3.14.1 Grain Size

The grain size analysis was undertaken in the first instance using the nested sieve method.

Table 3.14.1: Grain size from nested sieve analysis, Pt Lincoln RSL.

Site	Sample Depth	Start weight	4mm	2mm	1mm	0.5mm	0.25mm	0.125mm	0.063mm	Base	Post weight	Loss
RSL	30cm	60.277	4.235	7.204	10.092	13.351	21.197	3.809	0.117	0.024	60.029	0.248
	60cm	60.42	1.724	6.773	7.872	14.99	23.64	4.03	0.351	0.05	59.43	0.99
	100cm	60.744	4.055	2.792	3.759	10.35	32.635	5.808	0.174	0.043	59.616	1.128
	150cm	60.352	2.891	2.946	3.976	12.728	24.327	10.095	1.927	0.683	59.573	0.779
Wentworth Scale			Granule	Very Course Sand	Coarse Sand	Medium Sand	Fine Sand	Very Fine Sand	Coarse Silt			

From Table 3.14.1 and Figure 3.14.1 it can be seen that a large percentage of grains are < 0.5 mm and > 0.125 mm. The sample taken at 150 cm shows a larger percentage of grains 0.5-0.25 mm. On the Wentworth scale this soil can be classified as medium to fine sand.

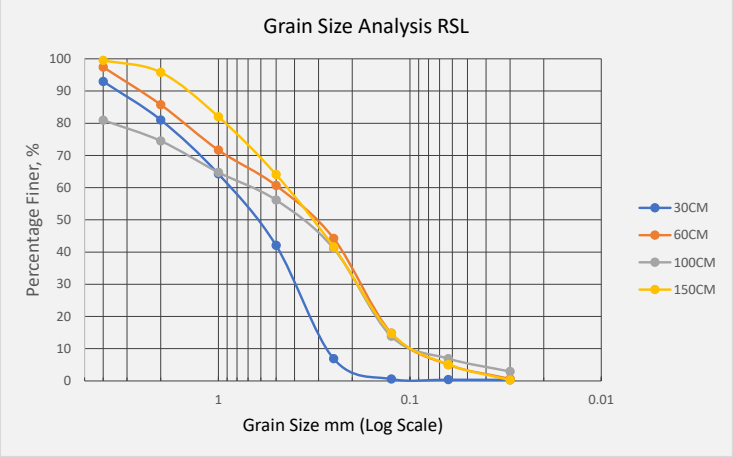

Figure 3.14.1: Nested sieve grain size plot, Pt Lincoln RSL Cemetery.

As the results of the sieve tests show a small percentage of the sample below 0.063mm, further testing was carried out using the laser diffraction process. The results are presented below in Table 3.14.2 and Figure 3.14.2for grain size <= 1000 µm. The laser diffraction results show the deeper 150 cm sample contains a greater concentration of finer grains. The sample taken at 60 cm contains a lower concentration of grains <= 63 µm.

Table 3.14.2: Grain size laser diffraction results, Pt Lincoln RSL Cemetery.

Site	Sample Depth	1000 µm	750 µm	500 µm	250 µm	125 µm	63 µm	31 µm	16 µm	8 µm	4 µm
RSL	30 cm	99.7	96.59	84.55	51.18	29.81	22.25	15.82	10.66	6.38	3.36
	60 cm	98.47	91.42	70.82	28.43	11.48	9.14	6.94	5.15	3.43	1.92
	100 cm	99.69	96.32	84	53.58	35.6	25.93	16.37	10.15	5.91	2.87
	150 cm	99.26	96.14	85.77	57.62	38.14	28.17	18.97	12.64	7.79	4.23
Wentworth Scale		Very Coarse Sand	Coarse Sand	Medium Sand	Fine Sand	Very Fine Sand	Coarse Silt	Medium Silt	Fine Silt	Very Fine Silt	Clay

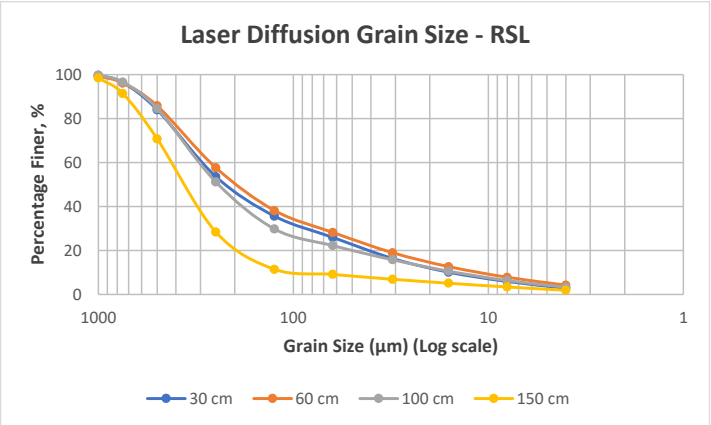

Figure 3.14.2: Grain size log plot from laser diffusion analysis.

3.14.2 Magnetic Susceptibility

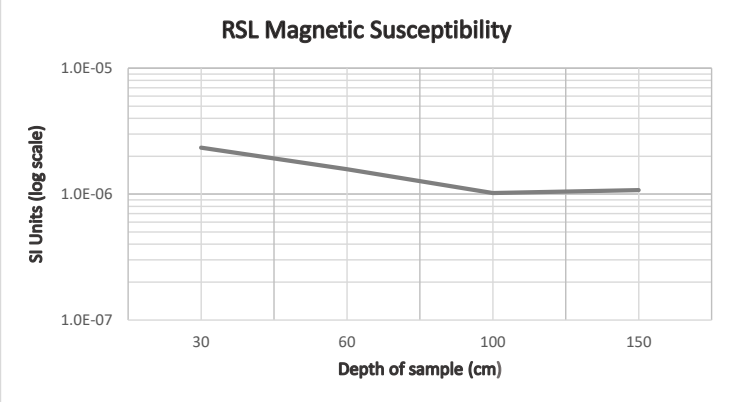

Figure 3.14.3: Pt Lincoln RSL magnetic susceptibility plot. These are low frequency values.

The magnetic susceptibility results, see Figure 3.14.3, from the Pt Lincoln RSL Cemetery show higher values at the 30 cm depth, these values drop at the 100 cm depth. The frequency dependence value is > 15% for all samples. All magnetic susceptibility values are high, indicating possible magnetic material in the grains.

3.14.3 Soil Chemistry

X-ray fluorescence results from samples taken at the Pt Lincoln RSL Cemetery, Table 3.14.3. These results show the ten most abundant chemical elements measured in the soil samples. These results are dominated by the presence of Calcium (Ca) the volume of which increases with depth. Also present at slightly lower concentrations are Silicon (Si), Aluminium (Al), Iron (Fe), and Potassium (K).

Table 3.14.3: XRF chemical analysis, Pt. Lincoln RSL Cemetery. The ten most abundant chemical elements are listed (ppm).

Element	30 cm	30 cm	60 cm	100 cm	100 cm	150 cm	150 cm
Calcium (Ca)	179856	180087	208512	248234	249873	280972	288373
Ca Err	464	464	497	542	543	578	586
Silica (Si)	40547	42365	26420	24283	21296	33046	32122
Si Err	1023	1038	904	918	889	1041	1037
Aluminium (Al)	19074	19308	15283	15887	15436	20155	20101
Al Err	1301	1298	1194	1252	1239	1411	1410
Iron (Fe)	16497	16567	12319	9781	9824	10105	9919
Fe Err	212	212	191	178	179	184	184
Potassium (K)	6737	6854	4817	3789	3627	4034	4526
K Err	125	124	108	100	99	105	110
Magnesium (Mg)	2172	2174	2358	4217	4029	5320	5511
Mg Err	2681	2683	2699	2823	2812	2914	2931
Sulphur (S)	1602	1710	1627	1696	1631	1942	1862
S Err	114	114	114	116	117	126	125
Titanium (Ti)	1520	1535	904	1010	1147	1422	1882
Ti Err	178	170	167	173	160	189	204
Strontium (Sr)	1490	1450	1358	1671	1653	2255	2247
Sr Err	22	22	22	24	24	28	28
Barium (Ba)	1223	648	1668	1286	360	763	388
Ba Err		2531	2577	2639	2664	2665	2624

3.14.4 Exchangeable Cation Levels

As the grain size analysis showed the presence of clay at all depths, further testing was carried out to determine the levels of exchangeable cations and hence sodic capacity. The results are presented in Table 3.14.4.

Table 3.14.4: Percentage of exchangeable cation content, Pt Lincoln RSL Cemetery

Calcium (%)	86.5	88.2	90.6	89.7
Magnesium (%)	7.2	7.1	6.2	5.6
Potassium (%)	4.9	2.4	0.6	0.3
Sodium - ESP (%)	1.1	1.0	2.2	3.2
Aluminium (%)	0.1	0.1	0.1	0.1
Hydrogen (%)	0.3	1.2	0.4	1.2

The Effective Cation Exchange Capacity (ECE) value, (cmol+/kg) at each sample depth are 30cm - 24, 60cm - 23, 100cm – 21, and 150cm – 21. As nominated by Rengasamy and Olsson (1991:935) the cmol+/kg value of 6 is considered the starting value of sodic soil. The values returned from the Pt Lincoln RSL Cemetery are all > 20 cmol+/kg, and so can be considered heavily sodic.

3.14.5 Radar Velocity and ERT Resistivity

To analyse the effects of seasonal rainfall on velocity and resistivity one hyperbola that is consistently detectable in all radargrams from all site visits is chosen. The velocity is recorded from all visits, as well as the relevant burial position. The resistivity from both array protocols is recorded from the same burial position and depth, see Table 3.14.5.

Table 3.14.5: Resistivity and Radar velocity by month of visit, RSL Cemetery.

GPR Data	Velocity (m/ns)	ERT Data	Resistivity (Ω-m) Wenner array	Resistivity (Ω-m) Dipole – Dipole array	Soil Moisture (mm)
Sept 2020	0.122	Sept 2020	94.7	103.6	
Dec 2020	0.152	Dec 2020	104.6	101.8	
March 2021	0.168				
June 2021	0.150				11.3
Jan 2022	0.112	Feb 2022	177.6	149	12.2
July 2022	0.122	July 2022	127.3	136.7	16.37
Sept 2022	0.102				22.65
Dec 2022	0.106	Dec 2022	95.5	94	18.09
March 2023	0.184	March 2023	152.3	138.5	11.22

Table 3.14.6: Resistivity values - Wenner array

Distance along ERT line (m)	Depth (cm)	Sep-20	Dec-20	Feb-22	Jul-22	Dec-22	Mar-23
15	52	139.37	203.89	202.45	155.56	140.29	238.76
15	104	107.87	124.75	180.51	139.73	99.42	194.81
15.25	78	112.94	144.09	193.23	139.96	108.3	191.51
15.25	130	91.735	100.21		123.02	88.074	151.42
15.5	52	125.34	248.66	187.37	129.68		281.1
15.5	104	94.589	101.43	185.17	127.88	90.192	141.16
15.75	78	96.716	141.78	160.97	123.9	114.45	181.98
15.75	130	92.956	87.534		124.61	78.498	123.78
16	52	132.82	231.72	163.66			307.07
16	104	86.411	109.51	167.12	121.52	121.52	150.64

Tables 3.14.6 and 3.14.7 give the resistivity values of both array protocols. These distances and depths are of the model blocks from Res2DInv, and represent the width of the burial shaft, and the depth of the corresponding hyperbola.

Table 3.14.7: Resistivity values - Dipole - Dipole array.

Distance along ERT line (m)	Depth (cm)	Sep-20	Dec-20	Feb-22	Jul-22	Dec-22	Mar-23
15	83	134.53	144.51	302.48	171.55	133.46	10.256
15	105	92.683	86.866	156.28	120.99	73.174	15.079
15.25	62	150.88	190.39	179.82	179.1	195.67	344.51
15.25	104	112.13	115.98	64.977	142.69	106.15	161.89
15.5	83	132.25	156.68		159.42	153.14	286.78
15.5	105	110.84	101.67	170.78	145.5	88.371	155.86
15.75	62	150.69	192.18	222.96	157.95	190.54	349.82
15.75	104	101.01	102.72	214.15	135.14	100.69	180.84
16	83	114.41	123.09	260.22	140.96	123.35	225.72
16	105	101.64	101.99	138.85	139.35	101.74	179.16

3.15 Summary

Table 3.15.1: Summary Results of Geophysical methods and soil analysis presented in this thesis.

Site	Method	% graves detected	Lithology	Soil Type	Mean Grain Size	Magnetic Susceptability (SI)	Mean Resistance (Ω-m)	Mean Velocity (m/ns)
Keith	GPR	91	Calcreted aeolianite	Coarse Sand	1 mm	8.275E-09		0.109
	Wenner	53					308.2	
	DPDP	68					418.5	
RSL	GPR	70	Quarzitic, pelitic and calcsilicate metasediment	Fine to Very Fine Sand	0.25-0.125 mm	1.50186E-06		
	Wenner	19					120.1	0.135
	DPDP	26					146.5	
Bordertown	GPR	36	Siliclastic clayey sand	Very fine sand to coarse silt	0.125-0.063 mm	2.48504E-07		0.1
	Wenner	54					6.2	
	DPDP	55					8.8	

Two geophysical methods were used in three different study sites. These study sites were all situated in garden cemeteries, with existing graves dating from the years 1984 to 2019. The GPR data were processed to produce radargrams for analysis. From these radargrams, three were chosen for analysis, these were the radargrams that ran over the widest part of the grave, see Figures 3.4.1, 3.7.1 and 3.11.1. From these three radargrams, one hyperbola was chosen that was consistently seen at the same grave site location over the study period. The velocity of this reflection was calculated. At every visit to a study site GPR data was recorded, and the full set of radargrams is available in Appendix A. The radargrams from each site varied in the number and shape of reflections, as well as the depth of attenuation.

ERT data were collected using the Wenner and Dipole – Dipole arrays, with resistivity and Induced Polarisation data collected. These data were inverted to produce 2D depth sections for analysis. From this inverted data the resistivity from a depth and location as close as possible to the recorded hyperbola within the GPR data were recorded. ERT data was not recorded at every visit to the study sites. Of the three sites, the ERT data collected from the Bordertown Cemetery overall showed lower resistivity and chargeability levels for both the Wenner and Dipole – Dipole arrays. The resistivity and chargeability levels for Keith and Pt Lincoln were similar. The high and low values for all sites are in Table 3.15.2. The low resistivity values recorded at Bordertown point to a soil that is highly conductive, a soil that contains a high percentage of dissolved ions.

Table 3.15.2: High and low resistivity and chargeability values, all sites. Resistivity values in Ω-m, chargeability values in nV/V.

Site	Protocol	Value	Low Value	High Value
RSL	Wenner	Resistivity	65.2	601.7
		Chargeability	131	706.8
	DPDP	Resistivity	54.1	2700.8
		Chargeability	1	506.8
Keith	Wenner	Resistivity	127.3	790.7
		Chargeability	27.6	739.8
	Dpdp	Resistivity	144	1233.8
		Chargeability	41.5	747.9
Bordertown	Wenner	Resistivity	1.63	36.9
		Chargeability	7.2	65.7
	Dpdp	Resistivity	3.3	131
		Chargeability	5.8	270

Soil samples were collected from each site, these samples were collected at depths of 30, 60, 100 and 120 cm. These samples were subject to analysis to determine the grain size, the chemical composition, and the magnetic susceptibility. The grain size analysis initially involved a standard nested sieve. As the samples from both Bordertown and Pt Lincoln resulted in a small sample from each site less than 63µm, i.e. below the lower limit of the sieves, further size analysis was carried out using a laser diffraction method, see Figure 3.15.1. These samples were also further tested to determine the exchangeable cation levels, as the diffraction analysis showed the possible presence of clay. X-Ray fluorescence was used to analyse the chemical composition of each sample, with results of the ten most abundant elements from each site in Tables 3.6.2, 3.10.3, and 3.14.3. The magnetic susceptibility analysis, see Figure 3.15.2, showed the magnetic capability of each sample, and this was linked to the chemical composition, grain size, and depositional method. The results confirm that the sites have very different soil compositions, ranging from depositional sand in Keith, to heavily sodic at Bordertown.

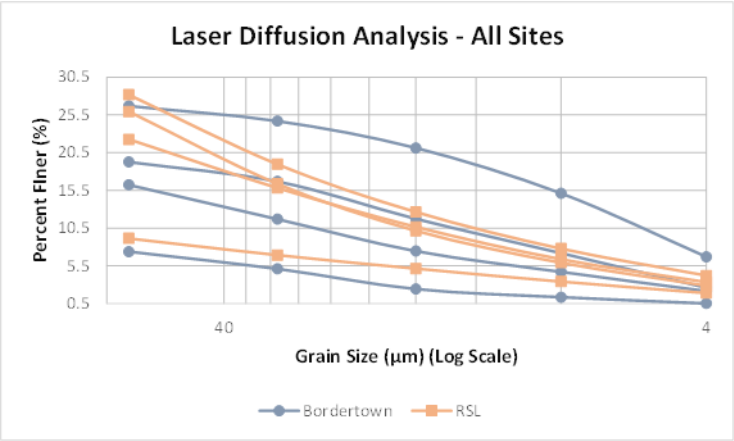

Figure 3.15.1: Results for grain size analysis for all sites by laser diffusion.

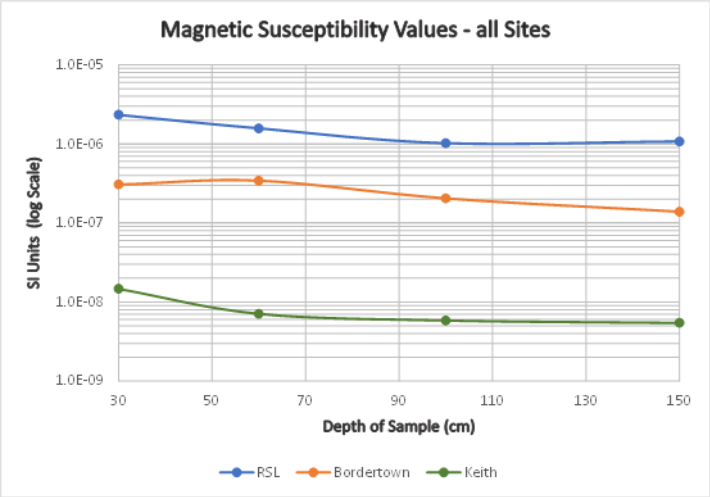

Figure 3.15.2: Magnetic Susceptibility Values - all sites.

Seasonal rainfall data was collected in two scales. On the landscape scale, rainfall data used was recorded by the national weather authority, the Bureau of Meteorology. This authority operates weather stations covering all of Australia, and daily rainfall is recorded, available online. The complete dataset from three study sites is available in Appendix B. On a more local scale, subsurface moisture probes were installed at the sites of Bordertown and Pt Lincoln RSL. These two probes constantly recorded the moisture levels on eight depths, from 5 cm to 85 cm. This data was uploaded periodically via Bluetooth connection. The results from these probes show firstly that there is a disconnect between the official recorded rainfall and the actual rainfall. The probes also show that the time between rainfall and the moisture reaching depths below 50 cm is inconsistent, ranging from hours to weeks.

All three sites recorded months of above average rainfall over the 34 months of this research, Keith 13, Bordertown 9, and Pt Lincoln 14.

4 DISCUSSION

4.1 Introduction

This research seeks to answer the primary question “Is there a seasonal time period wherein typical geophysical methods are most efficient in the detection of unmarked graves”. Further to this primary question is the evaluation of the Schmidt Precipitation Ratio within the South Australian climatic conditions. The approach to evaluating this question is to use two geophysical methods that are commonly used in the detection of unmarked graves, and study sites located in contemporary cemeteries. These study sites were situated on differing geologies, calcreated aeolianite at Keith, quartzitic, pelitic and calsilicate metasediment at Bordertown, and fluviolacustrine and coastal aeolian sediment at Pt Lincoln. The annual rainfall ranges from 420 mm at Pt Lincoln to 450 mm at Bordertown and Keith. Common data collection methods are used, as well as simple, common data processing methods, both easily replicated.

This research has been carried out in South Australia, and as such, some of the results are specific, not only to the local soil and climatic conditions, but may be relevant to other locations across the world.

4.2 Schmidt Precipitation Ratio

The ability to predict the optimal time to undertake a geophysical survey to locate unmarked graves would constitute a significant breakthrough in geophysical prospection. This ratio, (Schmidt et al. 2017), was conceived and developed in the wetter climate of the UK and is based on the soil moisture of a ditch showing a contrast in conductivity at a point where the soil has reached full saturation, see Section 1.3.6. Despite reporting a high success rate of this predictor, (Schmidt et al. 2017), sadly, application of a similar seasonal formula in the much dryer climate of South Australia is not as successful. For example, the visit to Keith in January 2021 was preceded by 0.2 mm of rain, (77% of burials detected), January 2022, no rain in the week preceding the visit, (100% of burials detected), July 2022 visit to Pt Lincoln was preceded by 4.2 mm of rain, (61% of burials detected), with the September and December 2022 visits preceded by 4 mm and 5.4 mm respectively, (77% & 66% of burials detected). Simply put, there has not been enough consistent rainfall for the application of a predictive formula based on 30 days rainfall, in the climatic conditions of South Australia.

Schmidt et al. (2017) also assumes that evapotranspiration and the downward movement of moisture are equal. As seen in the soil moisture meter data, (Figures 3.8.1 and 3.12.1), what precipitation that does fall, does not always peculate down through the stratigraphic layers to a depth that could possibly influence the geophysical results, in the case of Bordertown, past 55 cm.

4.3 Assumptions from the Literature - Geophysics

Geophysics is the act of measuring and interpreting the subsurface of the Earth, using one or more of a multiple of methods. This research has concentrated on two of these methods, Ground Penetrating Radar, and Electrical Resistivity Tomography, both active methods, and common in the application of locating unmarked graves. These assumptions were first introduced in Section 1.3.2, and are concerned with the performance of the GPR, the relationship between geophysical methods and the soil, geophysical methods and seasonal changes, and a comparison between GPR and ERT. These assumptions have guided this research, and each are addressed context of the lithology and climate of South Australia.

> Doolittle and Collins (1995:102–106) *"Because it does not perform equally in all soils, GPR is an imperfect tool. Many soils, because of their high conductivity, are essentially radar opaque."*
>
> *"The realizable GPR investigation depths are less in areas where soluble salts are not leached from soil or where clays have cation-exchange capacities (high amounts of Ca, Mg, Na, and K)"*
>
> *"Seasonal climatic variations do affect the differentiation of subsurface features. In most investigations, radar is not studied in a temporal mode".*

The first assumption is true in South Australian soils. The overall resistivity ranges recorded at all sites showed the soil from the Bordertown study site to have a mean resistance of 6.2 Ω-m from the Wenner array, and 8.8 Ω-m from the Dipole-Dipole array. These values are 50 times less than the mean value recorded at Keith. As conductivity and resistivity share an inverse relationship, the conductivity at Bordertown is high, and the radar opaque nature of the soil was reflected in the radar data, which returned an average attenuation depth of 80 cm across all visits, (Keith attenuation average depth is 244 cm, and Pt Lincoln average attenuation depth is 262 cm). These radargrams showed a low signal to noise ratio, and low clarity, with a mean total percentage of graves detected at 36%. The question, then, is, at what conductivity or resistivity does this opacity stop? The soil from the RSL cemetery in Pt Lincoln returned a mean resistivity 20 times greater than Bordertown Cemetery, (120 Ω-m and 146 Ω-m), with 70% of the burials detected, so between the mean resistance of 6 Ω-m at Bordertown and the 120 Ω-m of Pt Lincoln this opaque phenomenon stops. This is not reported in any other literature.

This second assumption is true for the soil in Bordertown Cemetery, where the Cation Exchange Capacity (CEC) returned a high of 35 cmol+/kg, and an average over all sample depths of 24 cmol+/kg. From Section 1.8.12 it is suggested that a high CEC value in soils indicate a less weathered soil, with little leaching of primary minerals, (University of New South Wales 2007), this supports the assumption. However, the soil from the Pt Lincoln RSL Cemetery returned an average of 22 cmol+/kg over all sample depths and showed a suitable penetration depth. This then

becomes the one of the most significant findings of this research. Both soils show high CEC values, but the average attenuation depth of Bordertown is 80 cm with the average in the RSL Cemetery being 260 cm. The resistivity values from the RSL Cemetery are 20 times greater. The differences, from the results of this research, are the dispersive characteristic of the soil from Bordertown, especially at the sample depth of 60 cm, and the Calcium/Magnesium ratio. This finding should become the basis of further research.

In this research Ground Penetrating Radar was used over known burials across a large temporal period, and there were variations in the numbers of burials detected in all sites, (Figures 4.7.1,4.7.2 and 4.7.3). While this research did record variations across visits at all sites, these variations were not correlated to either seasonal change or seasonal rainfall. For example, January 2021 and January 2022, (mid-summer in South Australia) the burials detected were 77 % with 0.2 mm of rain the previous week and 88% with 0 mm of rain in the previous week respectively. July 2022, mid-winter in South Australia, the percentage detected was 88% with 10.2 mm of rain in the previous week. Bordertown January 2021 21% of burials were detected with 0.6 mm of rain in the week previous, January 2022 saw 28% of burials detected with 0 mm of rain in the week previous. Mid-winter, July 2022, saw 42% of burials detected with 8.8% of rain in the week previous. The summer visits to Pt Lincoln saw 61% of burials detected in December 2020, with 3 mm of rainfall in the week previous, December 2022 saw 66% of burials detected with 5.4 mm of rain in the week previous. Mid-winter visit in June 2021 saw 77% of burials detected with 17.8 mm of rain the week previous.

(Hansen et al. 2014:15) *"GPR may not be suitable…..where clay rich and saline soils are present in survey areas where radar waves become rapidly attenuated".*

Gómez-Ortiz et al. (2010:112) *"Another limitation to the GPR technique corresponds to the signal attenuation produced when water saturated clayey material appears, making very difficult the interpretation of the radargrams".*

(Cassidy 2009:44) *"A material containing a high degree of free charges is effectively a conductor where the majority of the EM energy will be lost in the conduction process as heat. This is the reason why GPR is ineffective in higher-conductivity environments (e.g., saline conditions and high clay content)".*

These three assumptions, from Hansen et al. (2014); Gómez-Ortiz et al. (2010); Cassidy (2009) have been shown to be true, at only one site. The attenuation seen in radargrams from the Bordertown Cemetery is high, and from Table 3.15.1 the mean resistance is 6.2 Ω-m and 8.8 Ω-m for Wenner and Dipole-Dipole arrays respectively. The percentage of grains below 4μm at 100 cm is 2.6%, (Table 3.10.2), however, the percentage of grains below 4μm at 100 cm is 2.8% for the RSL cemetery, with radargrams showing less attenuation, see Table 3.14.2. While the influence of clay

particles in the soil is strong from the literature of Brandes (2005), Qadir and Schubert (2002), and White (2006), results from this research suggest, firstly, that there are other characteristics of the subsurface that also affect the attenuation, and secondly, the term 'high clay content" is misleading. As stated above, and in Tables 3.10.2 and 3.14.2 the percentage of grains below 4μm at 100 cm in Bordertown and Pt Lincoln is 2.6% and 2.8% respectively. From this result the soil in Pt Lincoln has a slightly higher clay content but shows a greater depth of attenuation (262 cm Pt Lincoln, 81 cm Bordertown), and higher percentage of burials detected, (70% Pt Lincoln and 36% Bordertown). Further studies are required to confirm and validate these findings.

Cassidy (2009:62) *"The effect of water is a constant theme within GPR, and as a basic rule of thumb: the relative permittivity of material increases with increasing water content (and therefore velocity decreases)"*.

Daniels (2007:73) *"The velocity of propagation is primarily governed by the relative permittivity of a material, which depends primarily upon its water content".*

Yes, the permittivity and velocity have an inverse relationship. At each study site the velocity increased as the permittivity decreased, see Section 2.2.2 for velocity measuring methods, however, this relationship is not consistent with changes in soil moisture, nor with seasonal rainfall at all sites. Results of radar velocity from this research can be seen in Tables 3.6.4, 3.10.5, and 3.14.5. Only at Keith, where the deep, bleached sand soil shows a larger mean grain size, (1 mm), and very low magnetic susceptibility, ($8.2x10^{-9}$), did the increase in permittivity occur in the month that recorded above average rainfall. The soils at Bordertown and Pt Lincoln with smaller mean grain size, (0.25-0.125 mm and 0.125-0.063mm), higher magnetic susceptibility, ($2.4x10^{-7}$ and $1.5x10^{-6}$), and the presence of sodic dispersive clay, did not record seasonal rainfall consistently percolating down through the stratigraphic profile. As the stratigraphic layers below a depth of 55 cm did not consistently record a change in moisture, the permittivity did not change, (see Figure 3.8.1).

Van Dam et al. (2003:271) *"The minimum required textural variation necessary to produce GPR reflections of sedimentary structures is small. Even the smallest change in water content will cause a contrast in dielectric properties and, thus, reflection of EM energy".*

This assumption is partially true in the soils of South Australia. The change in soil moisture will affect the dielectric properties, this can be seen in the changes to radar velocity and permittivity of the soil after rainfall events, see Tables 3.6.4, 3.10.5, and 3.14.5. But these soil moisture changes do not consistently change the reflections from subsurface structures of contrasting resistivities, i.e. the changes in resistivity associated with the burials. A possible explanation for this might be that in the subsurface of Bordertown, the moisture content may be experiencing a rise or fall, but not at

levels that would alter the reflections, or at a depth that stratigraphic layers show changes in resistivity.

Dionne et al. (2010:28) *"GPR research similar to that of this study is necessary in other settings to determine optimal survey methodologies for unmarked burials in areas of contrasting environmental conditions and multiple time periods".*

This research has answered this request from Dionne et al. (2010). The three study sites are contrasting in subsurface matrix and the South Australian climate is in contrast to Florida, where Dionne undertook their research. Orlando, Florida has an average annual rainfall of 1350 mm (53 inches) compared to the average annual rainfall of 420 mm - 450 mm for the study sites in this research. While Dionne visited the Florida site once, the study sites in this research were visited multiple times, see Tables 3.4.1, 3.7.1, and 3.11.1, this temporal period allows seasonal variations to become apparent.

Freeland et al. (2003:2) *"Simplified operation and interpretation for both novice and professional operators would greatly benefit law enforcement investigations, while also allowing the technology to be more effective and more widely utilized".*

This research showed methods that were simple and easily replicated. While this could be seen as a comment on methodology, this research and its findings can add to the confidence to operators and those undertaking time sensitive forensic investigations that seasonal rainfall may not influence the survey.

Pringle et al. (2009:5) *"Resistivity can be a viable alternative to GPR surveys, particularly if the soil clay content is high or there are significant other non-target objects within the near surface".*

This research does support this assumption. The ERT results from the soil with the highest clay content, Bordertown, showed a 54 % and 55% detection rate for the Wenner and Dipole-Dipole arrays respectively. While resistivity may be more effective in soils with higher conductivity, these soils in the Southern Australian context may lack moisture content or friability, and so the soil becomes too hard to insert electrodes from survey methods other than ERT, where electrodes are hammered in. In these soils, this precludes the use of equipment such as the Geoscan RM15 resistance meter system.

Dick et al. (2015:20) *"There are fewer studies using electrical resistivity to locate individual remains and indeed characterise mass burial sites".*

This study did include electrical resistivity in contrast to the GPR. The results showed that the resistivity method was marginally more effective in the clay subsurface found in the Bordertown

Cemetery, (36% for GPR, 54% and 55% for Wenner and Dipole-Dipole respectively). However, the work effort to undertake an ERT survey vs a GPR survey was greater than the efficiency gains. For example, the GPR survey of rows D and E in the Bordertown Cemetery measured 107 m², and comprised 11 GPR lines 50 cm apart, took less than an hour. In comparison, the ERT survey of one line in one row took over two hours to set up and acquire data. This highlights the big disadvantage of ERT in locating unmarked graves, and that is the time taken to survey one line, and unless multiple lines are surveyed, subsurface features can easily be missed. There are alternative Earth Resistivity (ER) methods, some of which are quicker than ERT, such as the Geoscan RM15, and these methods would be applicable in a garden cemetery, such as the cemeteries in this research. But these cemeteries do not contain unmarked graves due to their young age. Older cemeteries in dryer Australian climatic conditions lack the soil moisture for these alternatives to be effective.

4.4 Assumptions from the Literature - Soil

The subsurface is a complex, inhomogeneous medium, whose properties are significant in highlighting the strengths and weaknesses of any geophysical method or technology. These assumptions were first introduced in Section 1.8.2, and are concerned with soil moisture, the physical and chemical characteristics of the soil in a grave shaft, and in the vicinity of graves, and the complex chemistry of soil. These assumptions have guided this research. Each of these assumptions are addressed from findings in this research, and in the context of the lithology and climate of South Australia.

Salat and Junge (2010:2) *…there is a suggestion of the existence of a threshold level for soil moisture with high clay content soils, above which an increase on soil moisture has a minimum impact on soil attenuation properties.*

There is little support for this assumption from this research, but it must be noted that the soils in this research did not reach saturation point. Results from Bordertown show changes in attenuation, permittivity, and velocity, (which is inversely proportional to permittivity), but these changes are not correlated to the rainfall in the previous five or fifteen days. These results were the same for all sites and soil types in this study.

Jervis et al. (2009:272) *…no previous study involving electrical resistivity or conductivity surveys over graves has been supported by direct measurement of porosity, moisture levels or fluid conductivity.*

This research did incorporate subsurface moisture sensors, with the data recorded providing crucial and important information on the hydraulic conductivity of the soils. Sections 3.8 and 3.12 give the results of these sensors. The key outcomes of both sites were how little of seasonal rainfall

percolated down through the subsurface to levels below 55 cm, and the time after rainfall that soil moisture below this depth increased.

Tabbagh et al. (2000:395) *Electrical permittivity …… depends on the liquid water content of the soil material….the application of GPR to soil sciences is an active domain of research.*

An interesting finding of this research is that the permittivity of soil found in South Australia is not directly related to the available soil moisture, as in some soils, the available seasonal rainfall does not permeate to any great depth through the subsurface profile. This is noted in the soil classification data sheet, (Hall et al. 2009), where it is noted that the soil contains 'slowly permeable subsoil'. Tabbagh is suggesting that permittivity is an area that needs more research in the application of soil sciences.

Neal (2004:269–270) *The most important conduction-based energy losses occur due to ionic charge transport in water and electro-chemical processes associated with cation exchange on clay minerals*.

…the relationship between wave velocity and permittivity are violated with the introduction of high-conductivity substances, such as seawater and certain types of clay.

There is support for the first assumption in this research. The attenuation is certainly higher in the soils of Bordertown, but not from the chemically and physically similar soils of the RSL Cemetery. From the soil moisture sensor data, there is certainly moisture being retained at depths to 85 cm at both sites. A possible explanation for this may be the dispersive nature of the Bordertown soil, and the possibility of the available soil moisture blocking the capillary pore spaces. Further to blocked pore spaces, the energy losses may be explained by the ionic charge energy that the soil moisture needs to unblock the capillary pore spaces dissipates as the moisture percolates down through the subsurface profile.

Neal states that the relationship between permittivity and velocity, and conductivity and attenuation, break down with the introduction of higher conductivity materials, such as clay. This research does not support this in total but does note that the range of mean resistance values recorded in the soils of Bordertown and the RSL Cemetery that contain clay, is greater than the range recorded at Keith, see Table 3.1.15. To be fully supported from the results in this research, the resistivity values, (and by proxy the permittivity), of the subsurface at the RSL Cemetery would need to be lower to reflect presence of a comparable concentration of conductive elements to the subsurface of Bordertown, (Tables 3.10.5 and 3.14.5).

Fiedler et al. (2009:381) *there have been very few studies that look at GPR and the soil properties of the area around the burial.*

…clay and loam-enriched soil with a high water retention capacity, which are normally critical factors for a successful GPR survey…

This research did look at the soil in which the burials took place, but Fiedler was referring more to the study of leachate and how that can influence the detection of burials. The soil from the RSL Cemetery was a mix of clay and loam, and from the soil moisture sensors, the soil moisture is retained and does not completely drain away. GPR results from the RSL Cemetery were good, with 70% of burials detected, however, it does seem possible that these results are due to the chemical characteristics as much as the physical characteristics.

Conyers (2004:50–52) *In a highly conductive medium, the electrical component of the propagating electromagnetic wave is rapidly conducted away, and when this happens, the wave as a whole dissipates.*

Soil chemistry, especially the types and structures of different clay minerals also plays a role in radar energy transmission, but this mechanism is still poorly understood.

Other minerals in the ground, will create free ions, which allow for greater electrical conductivity. This includes carbonate minerals, or clay rich minerals.

The results from this research support these assumptions, with the following notes. The term "highly conductive" is subjective. The soil from the Bordertown Cemetery saw a high amount of attenuation, with low signal to noise ratio, and few reflections from below a depth of 60 cm, and a lower mean resistivity value, (Table 3.1.15). However, can this soil be defined as highly conductive? The chemical properties do play a significant role in the transmission of EM waves. The comparison of the similar soils of the RSL and Bordertown cemeteries show this, (see Sections 3.10 and 3.14). This research nominates that the differences in Calcium, Magnesium, and Sodium are the primary factors in the effectiveness of the geophysical methods, in the lithology of the study sites of South Australia.

Conyers (2004:101) *Velocity is therefore influenced by water saturation differences as they are controlled by changes in the composition of sediment and soils.*

This study has been unable to demonstrate that the saturation of the soils will influence radar velocity to any significant degree. This can be possibly explained by the lack of seasonal rainfall experienced in South Australia over the extensive study period. It has been shown by the soil moisture sensor data that a significant rainfall event could possibly unblock pore spaces and so therefore affect radar velocity, but very few of these events were experienced.

Arcone et al. (2008:2) *Particle size of soil will affect permittivity…silt size and larger particles within a natural mineralogically complex soil and at a fixed volumetric water content should show little dispersion, attenuation rates of a few dB or less, and consistent value of permittivity*.

There was no support for this assumption from this research. The larger soil grain particle size from the Keith Cemetery, (1 mm mean), showed changes to the permittivity after the same amount of seasonal rainfall fifteen days previous to data collection on three occasions, and seven occasions with the same amount of rainfall the previous five days.

Ruffell (2005:2) *Wet, clay-rich and wet, or salt impregnated ground still cause difficulty in obtaining images of the subsurface.*

In this assumption Ruffel is stating that despite the technological advances in GPR, there are still environmental conditions that will preclude the capturing of good data. While not specifically encountering wet conditions, this research supports this assumption. Of the three study sites used in this research, the subsurface chemical and physical characteristics of Bordertown returned a lower percentage of graves detected (36%) by GPR, see Table 3.1.15. The subsurface is a complex medium, and subsurface conditions cannot be known, or indeed controlled, by the geophysics practitioner.

Schultz et al. (2006:614) *Mineral soils with high clay content can attenuate the EM wave propagation, thereby reducing the depth of penetration on the ground.*

There is support from this research for this assumption, but with one caution. The presence of clay alone will not necessarily facilitate attenuation, rather, it is the chemical and physical characteristics of the soil particles, and how these particles allow moisture to move among them that is a prime instigator of attenuation in the soils of South Australia.

4.5 Study Sites Discussion

The three study sites were chosen for quite particular reasons. The graves in rows P and Q within the RSL Cemetery, Pt Lincoln, were all hand dug by the author. This, then, becomes a unique factor in this research, as it is not known if any other research has been conducted by the person who dug the graves. As these graves were all hand dug, the size, orientation, and depth are known, and cannot be disputed. The graves in these rows dated from the period 1984 - 1985, so, if possible, other cemeteries to be included in the study should ideally be of a similar age. The Keith and Bordertown Cemeteries were chosen as they are both garden cemeteries, and within the same local government region. The burials in Bordertown were from

1995, and Keith 1998. All three sites shared similar annual rainfall, Pt Lincoln 490 mm, Bordertown 487 mm, and Keith 460 mm.

4.5.1 Keith Cemetery

The GPR data collected at Keith was of a consistent quality, showing a high signal to noise ratio, and clarity of reflections. Over the nine visits the number of burials that could be identified was consistently high, (91%), with attenuation also starting at a consistent depth of 240 cm through all visits. There were three visits that saw any significant rainfall prior to data collection, May 2022 - 8.5 mm, September 2022 – 21 mm, and March 2023 – 7.9 mm, with the latter two months recording above average rainfall. Only the visit in May 2022 saw the percentage of burials detected rise above the average, with 100% detection. Detection of burials was achieved by the interpretation of hyperbolas, and to a lesser extent, the interpretation of grave cuts through the stratigraphy. Prior studies, primarily from Van Dam et al. (2003:258), have stated that in uniform stratigraphic profiles, the source of reflections has remained unsolved. The current study found that in the soil of the Keith Cemetery, the majority of reflections associated with burials are hyperbolas associated with the intact coffin.

The ERT data collected with the Wenner array identified, on average 53% of the total burials. The visit in January 2022 returned 100% of the burials. In the week before this visit no rainfall was recorded. The inversion plot, Figure 3.5.25, shows small areas of approximately 50 cm wide, and to a depth of 40 cm. The arrangement of these areas closely mimics the pattern returned from the forward modelling, (Figures 3.3.1 and 3.3.2). This was the only visit that this pattern was observed. From this it could be assumed that the values used in the simulation closely reflected the geology and grave fill at the time. It is of interest that on other visits that experienced no rainfall, (December 2022 – no rain), or very little, (January 2021 – 0.2 mm), these patterns of resistivity in the ERT results are not replicated. There is very little that could identify any grave fluid plume, from the literature of Pringle et al. (2010) and Van Belle et al. (2009) this is not a surprising result. The base of the grave shaft is ~1.8 m, and not only is there nothing to indicate grave fluids, but there is also little that indicates the expected changes in resistivity a coffin or grave shaft would give.

The official soil classification data, (Department of Energy and Mining 2022), has the Keith Cemetery classified as “B7”, described as ‘Sand over brown clay on calcrete’. However, from the soil analysis, and visual inspection, the soil at the Keith study sight should be classified as “H3”, with a description of ‘Deep bleached sand’. See Figure 2.5.1 for images of the subsurface profile of a grave in the Keith Cemetery. However, the soil samples taken at the Keith Cemetery support the soil classification of depositional sand. The study rows are some 20 m from the boundary given in the soil spatial data, this then becomes an unreliable source of soil type information, and any site near a boundary should be questioned. This follows Conyers (2012:108) who notes the difficulty in obtaining accurate soil information before a geophysical

survey. The analysis of the soil samples shows large grain sizes, (mean = 1 mm), high silica content, and low magnetic susceptibility, ($8.2x10^{-9}$), all consistent with this classification of deep, bleached sand. The soil profile shows little horizon development, illustrated by the high percentage of grains between 0.5 -1 mm, (average 25. 6 %), at all sample depths.

There were significant variations in the results of the soil analysis below 30 cm. The sample taken at 30 cm showed finer grain size, higher magnetic susceptibility, and a higher concentration of calcium (Ca). This would be consistent with either the application of top dressing to create the well-maintained lawn, or a result of the weathering process in action. Between 30 cm and 150 cm the soil analysis shows the depositional sand is quite homogenous.

4.5.2 Bordertown Cemetery

The GPR data collected at Bordertown is of a consistent quality, although this quality could be said to be poor, showing a low signal to noise ratio, and low clarity, with a low average of 36% burials detected.

The majority of the GPR data from this site show reflections in a band between 30 and 70 cm, although attenuation is generally deeper than this. There were three visits that saw any significant rainfall prior to data collections, July 2022 – 8.8 mm, September 2022 – 14.8 mm, and March 2023 – 6.1 mm, with the latter two months recording above average rainfall. The detection of burials was achieved mainly by grave cuts through the upper stratigraphy, as stated, there is very little information in the radargram below 70 cm. The ERT data of both the Wenner and Dipole-Dipole array's show a change in resistivity at a depth of 80 cm. Below this depth, lower resistivities are recorded, above higher resistivities, with the lower resistivities showing little variation. Both arrays returned low percentage of burial detected, 54% and 55 %. The IP data from both protocols showed little changes in chargeability below the depth of 40 cm, with the exception of October 2020, where 71% of the burials can be detected. There is some indication of what could be interpretated as grave fluids in some of the Dipole-Dipole results, specifically the October 2020 results, and to a lesser extent, the December 2022 results. It could be conceivable that the IP results from October 2020, noted above, are from leachate plumes, not direct indications of a burial. Prior studies by Dick et al. (2017:17) and Pringle et al. (2010:127) have indicated that the plume of leachate from a decomposing body would increase conductivity, (decrease resistivity), and the October 2020 results do support this. The previous studies also suggest that leachate may be harder to detect in clay soils, as the physical characteristics of the soil would trap the leachate fluids in the grave shaft. If these small areas of lower resistivity are signs of leachate plume, then they are detectable beyond the time frame suggested by Pringle et al. (2010) and Van Belle et al. (2009).

There is nothing in the literature that discusses leachate and Induced Polarisation. Perhaps the most unexpected finding is that these lower resistivity areas that could be associated with leachate plumes

extend down past 2 m, this is unexpected as the moisture meter shows little soil moisture changes below 65 cm.

The soil analysis shows a stratigraphic layer at 60 cm that is heavily sodic, returning a cmol+/kg value of 26. The soil is classified as sandy clay loam with sodic tendencies, with the grain size and Exchangeable Cation level analysis supporting this classification. Of note is the high concentration of Calcium (Ca) in the soil chemistry. The concentration rise at 60 cm, (46255 ppm), drop at 100 cm, (3380 ppm) then rise again at 150 cm, (92576 ppm). The concentration of Iron (Fe) also rises significantly at 60 cm, (from 5229 at 30 cm to 19865 ppm). This increase in iron is reflected in the magnetic susceptibility, which recorded a small rise at 60 cm, (30 cm low frequency 3.07 $x10^{-7}$, high frequency 2.75 $x10^{-7}$, 60 cm low frequency 3.44 $x10^{-7}$, high frequency 3.27 $x10^{-7}$). These findings are consistent with the soil classification data sheet, (Hall et al. 2009), which describes an abrupt change from sandy loam to red brown heavy clay. Fitzpatrick et al (1994) and Hall et al. (2009) also describe a reduction in hydraulic conduction in the soil profile. This is reflected in both the radar results, high attenuation at an average depth of 81 cm and, the ERT results. The results from the moisture sensor also show a reduction of hydraulic conductivity below 55 cm.

The subsurface moisture meter installed initially failed after two months, and this was not detected for some ten months later. This left a large amount of important data not recorded. What the subsurface moisture meter does show, however, is that the naturally falling rain does not percolate down through the soil. Despite climatic conditions, the moisture levels below 65 cm stays at a steady level throughout the data recording period.

4.5.3 Pt Lincoln RSL Cemetery

The GPR data collected from the RSL Cemetery in Pt Lincoln was of a high consistent quality, with a high signal to noise ratio, and high level of clarity. The percentage of burials detected was also consistent across all visits, with an average of 70%. There were three visits in which significant rainfall was recorded prior, September 2020 with 77% of burials detected, June 2021 with 77% of burials detected, and February 2022 with 72% of burials detected, with all three months recording above average rainfall. It is worth noting that in the months of September 2020, March 2021, and September 2022 77% of burials were also detected, with all three months receiving less than monthly average rainfall.

The ERT data returned a very low percentage of burials detected, 19% from the Wenner array and 26% from the Dipole-Dipole array. On visits that coincided with above average rainfall, such as February 2022, whereby 101.6 mm of rain fell in the 30 days before the visit, the percentage of burials detected rose to 50% from the Wenner array and 44.4% from the Dipole-Dipole array. September 2020 saw 64 mm of rain in the 30 days before the visit, and the percentage from the Wenner array stayed low at 22.2%, and the Dipole-Dipole array rose to 72.2%. These results are not consistent, which is a surprising result given that

the literature states that resistivity decreases with an increase in moisture, Berezowski et al. (2021:12; Bièvre et al. (2018:100; Cott (1997:36), and others. The results from the IP data were also not consistent, but on two occasions the IP from the Wenner returned a higher percentage of burials detected.

The soil samples returned the highest magnetic susceptibility due to the high level of Iron (Fe) found consistently in all sample depths, pXRF results, see Table 3.14.3. Iron content was not part of the analysis of exchangeable cations where Calcium (Ca) is recorded as being more abundant. The CEC values for the 30 cm and 60 cm samples return 24 and 23 cmol+/kg respectively, and while the levels of exchangeable cations are high the ESP is 1.1%, which is below the sodic threshold (Rengasamy and Olsson 1991; Qadir and Schubert 2002). This is a surprising result as these CEC values are similar to those from Bordertown, but these two soils are physically very different.

The subsurface moisture meter recorded soil moisture over a 16-month period and showed the high and low of seasonal rainfall that would be expected in this area. The soil moisture below the 65 cm sensor showed subtle seasonal variations, with heavy downpours and seasonal changes being evident above this depth.

The soil analysis of samples taken at the Bordertown and RSL Cemeteries returned very similar results. Grain size was similar, with mean grain size being 0.125-0.063 mm for Bordertown and 0.25-0.125 mm for the RSL, with an average of 3% sample weight below 4µm from Bordertown and 3.1% from the RSL. The average CEC over all samples was 24 cmol+/kg for Bordertown and 22 cmol+/kg for the RSL. While the levels of exchangeable cations were similar the ESP differs. Average ESP at Bordertown was 24%, while Pt Lincoln returned an average of 1.9%. The mean magnetic susceptibility was a little further away with $1.5x10^{-6}$ for the RSL and $2.4x10^{-7}$ for Bordertown. The average annual rainfall was also comparable. The difference from the analysis was the higher concentration of Calcium (Ca) in the samples from the RSL, and this is a surprising result of this research. This higher concentration of Ca is discussed in more detail in the soil section below.

4.6 Ground Penetrating Radar

The use of a Ground Penetrating Radar within the discipline of Archaeology, for many different purposes, is wide spread (Angelis et al. 2018; Berezowski et al. 2021; Garnaut et al. 2016; Lowe 2012; Sarris et al. 2018) and others. One of these purposes is the location of unmarked graves, locating these has many social, scientific, and legal benefits. There are many assumptions in the literature, Cassidy (2009); Conyers (2004); Daniels (2007); Fiedler et al. (2009); Neal (2004); Salat and Junge (2010), and others, that include soil moisture, and how a lack or abundance of soil moisture can affect the outcome of a GPR survey. Having the assurance that soil moisture levels do, or do not, affect GPR in the climatic conditions of South Australia,

gives confidence in being able to undertake a GPR survey of a possible burial site at an optimal time, when soil moisture conditions are conducive.

There are alternative processing steps aligned to both of these common geophysical methods. Methods such as the Multi-Trace coherence analysis, as reported by Trinks and Hinterleitner (2020), or noise reduction in GPR (Zhang et al. 2022), or the introduction of machine learning from Green (2020), and while these are all valid steps, in this study it was decided that the methods of data capture and processing needed to be kept at a more simple or common usage level. The reasons behind this decision are quite clear. Firstly, by keeping the methods constant, any student, or industry worker, could pick up the conclusions of this research and be confident in following the methods; secondly, by approaching the methods in this manner, the methods of data capture and processing remain a constant, not a variable; and thirdly, by selecting any processing steps of a more 'advanced' nature for one study site over another should, ideally, consist of a robust statistical decision-making process. To employ a step such as this would detract from the robust simplicity of the first two points.

The methods of collecting the radar data in the three study sites was consistent. Grid patterns were followed, with lines of data collected at each visit, all sites using a 50 cm spacing. The data collection method and data processing steps both stayed consistent, the physical and chemical characteristics of the soil stayed the same, the only variable was the available soil moisture from seasonal rainfall.

One of the many interesting findings of this research were the reflections seen in the radargrams from the Keith Cemetery. On three occasions, in the months August and October 2020, and January 2021 there was a strong reflection, (approximately 95 cm wide) from an empty plot centred at a depth of ~100 cm. See Figures 3.5.3, 3.5.12, 3.5.17. As well as this reflection, a series of small reflections are seen from all but one visit. These small reflections are at a depth range of ~ 50 – 100 cm and extend the length of the radargram. See Figures 3.5.13, 3.5.25, 3.5.33, 3.5.37, 3.5.45, 3.5.49, and 3.5.54. These reflections are interesting, the empty plot has had no anthropogenic disturbance, neither has the ground between the burials. The soil analysis from an adjacent plot shows an almost homogenous subsurface of deep, bleached sand, with no small objects, tree roots, or animal burrows. It is mentioned several times in the literature that familiarity with the interpretation of radargrams in regard to burials is required, (Damiata et al. 2013; Watters and Hunter 2004). Further to this, when studying GPR responses to aeolian deposits Van Dam et al. (2003:258) reported that it is not known in great detail if it is grain size, grain density, or porosity that is creating the reflection. They go on to remark that little is known about reflections from layers smaller than a quarter wavelength, the assumed vertical resolution. If there was no prior knowledge of the subsurface in this row at the Keith Cemetery, the reflection from the vacant plot could easily be interpreted as a burial. Likewise, the line of small reflections could be interpreted as anthropogenic in origin, or could be what Conyers (2012:137) terms 'out of phase' reflections from subsurface features some distance from the antenna.

Intimate knowledge of the subsurface is not always available to the geophysics practitioner, official soil data is not always accurate, and complexities exist in the subsurface from landscape to molecular scale. When interpreting GPR data a buried rock can look like a grave marker, or tree roots can show reflections consistent with burials.

4.6.1 Radar velocity

The radar velocity from data captured at the Keith Cemetery does change over the study period, from a low of 0.092 m/ns to a high of 0.134 m/ns, but there is no correlation to the rainfall, one day, five days, or fifteen days prior the data capture. For example, in the one month that recorded above average rainfall, May 2022, the slowest velocity, (0.092 m/ns) was recorded. As this soil is medium to coarse sand, with underlying lithology described as silt, dolomite and sand, any available soil moisture from rainfall would percolate through quickly. This relationship between soil moisture and velocity is a general trend, and not strictly linear.

The velocity from Bordertown shows no relationship to the available soil moisture. The fastest velocity recorded (0.136 m/ns) was in a month where 49.1 mm of rain fell in the previous fifteen days, but the second fastest, (0.118 m/ns), was recorded in a month with no rainfall in the previous fifteen days. The one month that recorded above average rainfall recorded a velocity that was 10% less than the mean.

Velocity recorded at the RSL Cemetery in Pt Lincoln also shows little relationship to the available soil moisture. The one month that recorded above average rainfall, (July 2022), recorded a velocity 4% greater than the mean. The month that recorded the fastest velocity, (0.154 m/ns, March 2023), recorded no rain in the five days previous, and only 1.4 mm in the fifteen days previous to data being recorded. The visit that recorded 100.2 mm of rain in the fifteen days previous, (February 2022), recorded a velocity of 0.13 m/ns.

From these results it is hard to support the assumption that velocity and soil moisture share an inverse relationship, (Cassidy 2009:62), in the soils and seasonal conditions of South Australia. This position is clearly shown in the following Figure 4.6.1. Perhaps though, results of this research does show a contrast with comments made by Conyers (2012:107) in regard to the effect of magnetic conductivity in soil. Conyers postulated that a high magnetic permeability could possibly diffuse the magnetic component of the radar pulse, and hence help create attenuation, as magnetic permeability is equal to magnetic susceptibility +1. The soil of the RSL Cemetery did record the highest magnetic susceptibility, as well as the highest mean radar velocity, so these results do not support Conyers. A possible explanation for this might be that, while the magnetic susceptibility was the highest recorded for this research, it may not be high enough to affect the magnetic component of the radar pulse.

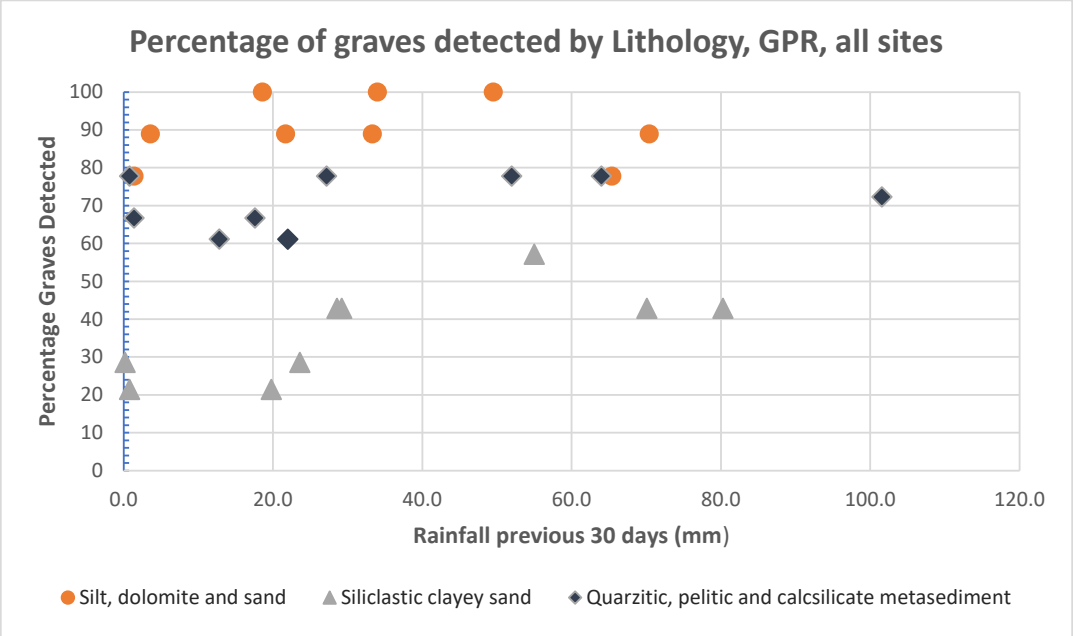

Figure 4.6.1: Percentage of burials detected by GPR, all sites. The percentage of detection is grouped by the unique Lithology of each site.

4.7 Electrical Resistivity Tomography

Electrical resistivity surveys have become widely used since the advent of multi-channel and multi-electrode systems. These surveys are routinely used in mineral prospecting, mining, engineering, hydrology, and archaeology (Aizebeokhai 2010; Stummer et al. 2004). The ERT, and earth resistivity methods in general measure the interaction between an injected DC current and the various characteristics in the subsurface matrix. Of these many characteristics, it is the presence/absence of subsurface moisture, along with the passage of this moisture through the pores and micropores that influence the ability of the ERT to identify subsurface targets.

There were questions about the suitability of each of the arrays used in this research (Aizebeokhai 2010:3595; Martorana et al. 2023:2905; Pellicer 2010:58; Sarris et al. 2018:220). The Wenner array is reported in the literature to be more sensitive to vertical variations, (Aizebeokhai 2010:3596; Dahlin and Zhou 2004:397; Milsom and Erikson 2011:131; Pellicer 2010:58; Stummer et al. 2004:121), while the literature reports the Dipole-Dipole array showed greater suitability to horizontal variations, see Figure 1.5.3, and is preferred for sites with vertical structures (Milsom and Erikson 2011:131; Stummer et al. 2004:121). Martorana et al. (2017:2907) and Witten (2006:314) both indicate that a subsurface target of ERT is required to be, not only large enough contrast in resistivity, but also, of a detectable size, shape and depth. They go on to indicate that the size and resistivity contrast must increase as the depth increases to counter the decrease in current density. A series of burials could, conceivably, fit both descriptions, the

horizontal plane is evenly broken and in the vertical plane conceptionally there are bulk resistivity changes from a burial shaft.

To assist in conceptualizing how the output of inversion would appear in an ERT plot, modelling was carried out for both array's, with the model containing a series of burial shafts, and differing resistivities, see Section 1.6.2. Only on two occasions were the ERT results of a similar pattern to the forward modelling.

One interesting finding of this research applies to the comments of Annan et al. (1991:2) and Neal (2004:272), who have stated that the amplitude sharpness of the GPR reflection is in response to the sharpness in change of permittivity, or resistivity. Amplitude sharpness is defined by Neal (2004:272) as a function of the width of the transition zone, relative to the dominant wavelength. If a wavelength is less than three times the size of a transition zone, then a sharp amplitude reflection occurs. If a wavelength is greater than three times the size of the transition zone, then typically, dispersion and more diffuse reflections occur. The reflections associated with the burials in Keith and the RSL Cemeteries have a large amplitude, and following Annan and Neal, therefore there should be a detectable change in resistivity. These changes were not detected by the ERT, despite Keith using an electrode spacing of 25 cm, and the RSL 50 cm. It is not known if these changes in resistivity were not detected because of the choice of array, the on/off settings in Induced Polarisation data capture, or the moisture levels in the soil were not optimal for an ERT array to detect them.

Over all sites and all visits, neither of the arrays showed to be more effective in all environments in identifying burial sites. In the Calcreated aeolianite, (medium to coarse sand), at the Keith Cemetery the Wenner detected 53%, (mean resistance 308.8 Ω-m), the Dipole-Dipole 68%, (mean resistance 418.5 Ω-m). This was the highest detection rate in this research. In the Fluviolacustrine and coastal aeolian sediment, (coarse silt to very fine sand), of the Bordertown cemetery, the Wenner detected 54%, (mean resistance 6.2 Ω-m), with the Dipole-Dipole detecting 55%, (mean resistance 8.8 Ω-m). The quartzitic, pelitic and calsilicate metasediment, (fine to medium sand), of the RSL Cemetery the Wenner detected 19% of burials, (mean resistance 120.1 Ω-m), while the Dipole-Dipole detected 26%, (mean resistance 146.5 Ω-m). The fact that at each site the mean resistance of the arrays varied is supported by Aizebeokhai (2010:3595).

From the literature of Johansson et al. (2015:296); Reynolds (2011:373); and Wiberg and Jonsson (2017:18) the IP process is sensitive to grain size, shape and surface chemistry, and so therefore there is a relationship between grain size and relaxation time. In light of these theories, IP should be more effective with a subsurface with larger grain sizes, e.g. the deep, bleached sand of Keith Cemetery would be ideal. Further to this Brandes (2005:2) does state that in soils with a clay content greater than 15% the polarisation effect will decrease. Dahlin et al. (2010); Johansson et al. (2015); and Wiberg and Jonsson (2017) all suggest that IP is a useful tool in the assessment of landfills for contaminant leaching, due to chemical contaminant having an insular effect on the grain surfaces. Given this position, one could assume that the measurement

of the chargeability of the subsurface should show any changes that grave fluids are present and detectable. Neither of these statements proved to be true in this research.

4.7.1 Resistivity

The mean resistivity results from this research further support results given by Doro et al. (2022:2), who state that resistivity methods work well in conductive soils, but not their statement that soil moisture and precipitation aid the detection of buried remains. Research from Hansen et al. (2014); Jervis et al. (2009) and Nero et al. (2016) have all stated that as soil moisture increases, resistivity decreases. From the resistivities measured over the grave in all three sites, this is not the case. Only one month that a survey took place recorded above average rainfall, July 2022 in the RSL Cemetery. The mean resistivity recorded over the grave in this month, (8.9 Ω-m), was average over all visits, for both arrays. In the month that received 100 mm of rain, (February 2022), a mean resistivity of 190 Ω-m was recorded, the same resistivity was recorded in March 2023, with 1.4 mm of rain in the 30 days previous. Similar results are found from other sites.

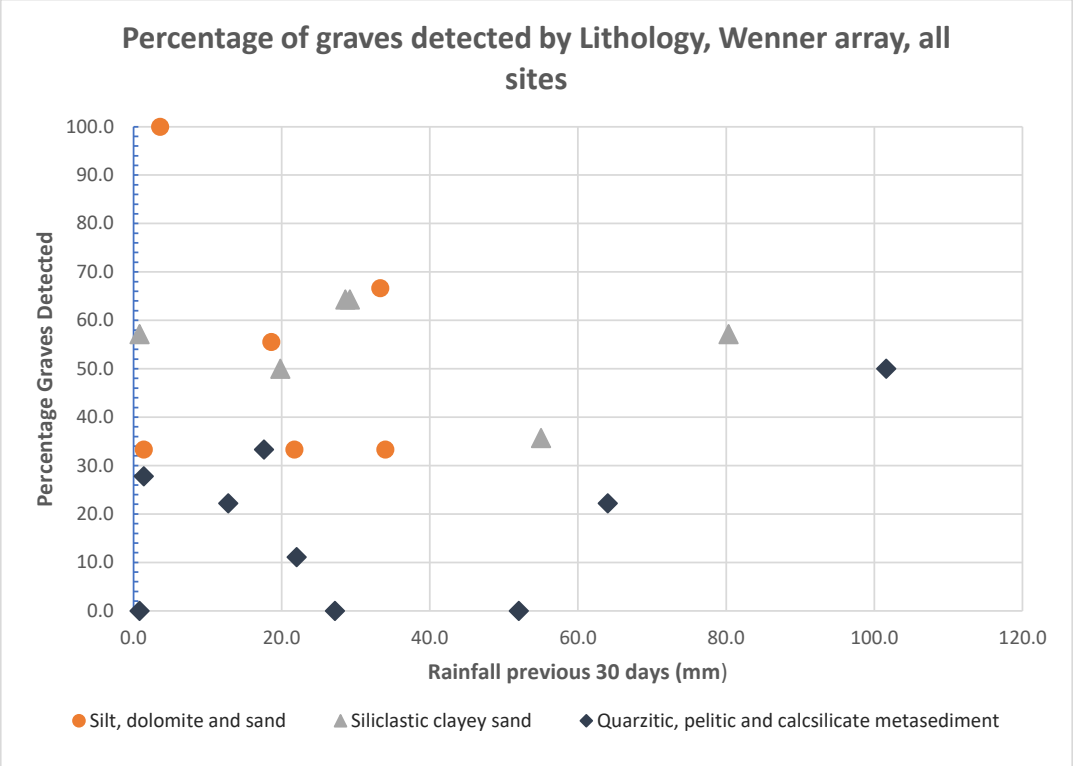

Figure 4.7.1:Percentage of burials detected by Wenner array, all sites. The percentage of detection is grouped by the unique Lithology of each site.

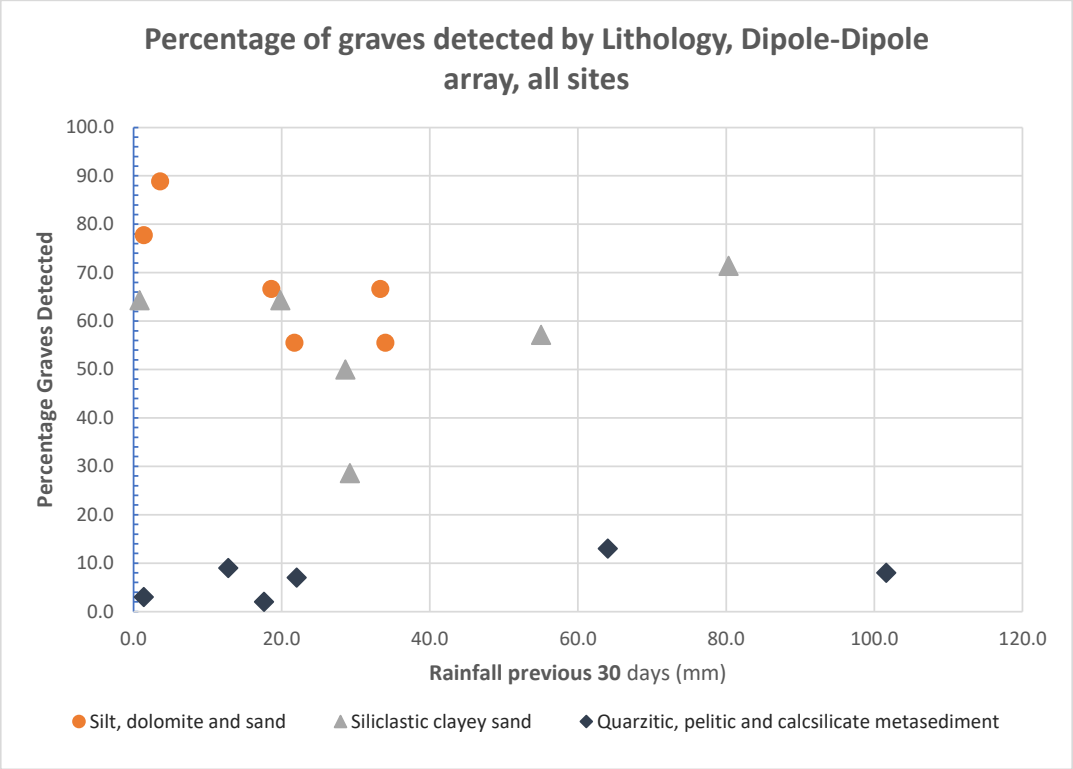

Figure 4.7.2: Percentage of burials detected by Dipole-Dipole array, all sites. The percentage of detection is grouped by the unique Lithology of each site.

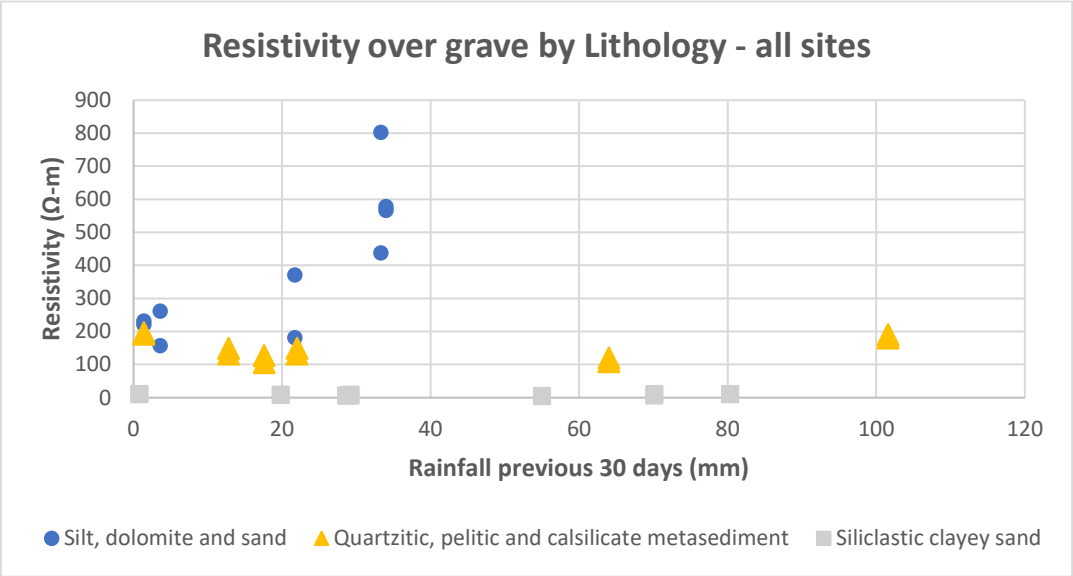

Figure 4.7.3: Mean resistivities recorded over the target grave, Wenner and Dipole-Dipole array, all sites.

4.8 Soil

The anthropological remains that are the targets of geophysics are typically in the complex, inhomogeneous subsurface profile, the properties of this medium have a large influence on the

effectiveness of these methods, due to changes in temperature, moisture levels, and soil type, to name a few. Of these naturally occurring variables in the subsurface, soil moisture is the one that has the greatest variability over a short temporal period, with the subsurface soil moisture being dependent on naturally occurring precipitation. Given this dependance, the relationship between the geophysical method and the soil structure has been examined to determine if there is an optimal seasonal time after precipitation, and so ensuring maximum effectiveness of the geophysical methods.

There are some interesting findings within the soil analysis. The individual magnetic susceptibility analysis returned expected results from each cemetery. The high magnetic susceptibility from the Pt Lincoln samples is consistent with the high concentrations of iron, (average 12144 ppm across all depths). This is not surprising, given the numerous granite outcrops in close proximity to the rows involved with this research. The results from the Bordertown Cemetery samples, however, are greater than those from the RSL Cemetery, (average 20157 ppm across all depths). The depositional deep bleached sand from the Keith Cemetery returned the lowest magnetic susceptibility. This is consistent with Dearing (1988:6); Quijano et al. (2014:1811); Shirzaditabar and Heck (2021:233), who state that silica and calcium carbonate rich soils can be classified as diamagnetic, a classification which shows little or negative magnetic susceptibility. What is unexpected is the percentage frequency dependance (PFD). Dearing (1988:17) and (Kodama et al. 2014:780) nominate the PFD as being an indicator of the presence of ultrafine, (< 0.03µm), superparamagnetic ferrimagnetic minerals, (SP), in the soil. The presence of these SP sized particles has been suggested to be an indicator of the pedogenesis process. Samples that contain these ultrafine minerals will show lower values measured in the high frequency range, while samples that do not contain these minerals should show identical high and low frequency values.

The PFD for the RSL Cemetery is very consistently between 6 and 11%, with an average over all depths being 9.49%, with the PFD for Bordertown showing a range of 3-11%, with an average of 9.62%. Despite the difference in overall low frequency values in Figure 3.15.1, and mean susceptibility in Appendix E, these values are very similar and point to soils with generally a similar degree of development. From Table 3.10.3, the low PFD value of 3.6% from the 60 cm sample could be an error, if taken as an error, then the PFD percentages through the subsurface profile show a consistent degree of pedogenesis. The PFD values through the subsurface profile for the RSL Cemetery, Appendix E show that samples from a depth of 150 cm have a lower percentage, and so this can be inferred as being a less developed soil. Samples from Keith Cemetery returned PFD values between -58 and 29%. This is a large variation and includes negative values. Soil such as sampled from Keith that are high in silica, and have large grain size, would be expected to return a low PFD, but the variation of the PFD values could suggest either sampling or measurement error, or as Kodama et al. (2014:780) suggests, the susceptibility is so low it is close to instrument noise. These PFD values point to the soil found in the Keith Cemetery are quite undeveloped, while the soils from the Bordertown and Pt Lincoln Cemeteries show the result of a high degree of pedogenesis.

The phrases ‘high clay content’, or ‘clay content’, or ‘highly conductive soils’ are common phrases found in the literature, Bevan (1991); Conyers (2012); Hansen et al. (2014); Jones (2008); Molina et al. (2016); Pringle et al. (2009); Ruffell (2005); Watters and Hunter (2004), and many others, often with no quantitative definition. This research has found that the amount of clay particles in the soil is not as important as the chemical and physical characteristics. For example, the particle size at a depth of 100 cm from the Bordertown samples is 2.6%, and at the same depth the sample from Pt Lincoln is 2.8%, see Tables 3.10.2 and 3.14.2. The percentage of burials detected at Bordertown is 36% and Pt Lincoln 70%, so the clay particle content alone was not a factor in the results.

The sodic nature of the Bordertown soil was noted by Hall et al. (2009), and further evidence was found in the Exchangeable Sodium Percentage (ESP) analysis, where the average for Bordertown was 13.1 with a maximum of 24 cmol+/kg. While the sodic index was high the Cation Exchange Capacity (CEC) of both sites was also high. The average CEC at Bordertown through all sample depths is 24 cmol+/kg. Compared to this, the CEC from Pt Lincoln is 22 cmol+/kg, with friable soil though all sample depths. This high sodicity was thought to be the underlying influence of the ‘clodding’ found in the soils of Bordertown, for the grain size analysis does not show a high percentage of clay present. Prior studies by Nelson and Oades (1998:52) note that sodicity will affect the soil at a molecular level, and that any dispersion within the subsurface profile can create an inherently unstable structure, often resulting in hardsetting, low friability, and high strength (Nelson and Oades 1998:52; Qadir and Schubert 2002:280). This high strength is due to the strength of the bonds between exchangeable electrons within the Electrical Double Layer, (EDL). These bonds are broken with the introduction of moisture, but only if the force of the water molecules is greater than the force of the van der Waals attraction between clay molecules (Sumner 1993:697). Unfortunately the potential energy, or force, that the water molecules exert to break these bonds is not regenerated, and previous studies from Rengasamy and Olsson (1991:940) have shown that the interactive force of the water molecules is weakened through this interaction. As mentioned in the literature review, Goldberg et al. (2011:168) nominates the balance between the forces of attraction and repulsion are the most important characteristics of clay, and the results of this research show that for an active geophysical method to be effective in clay soil, the force of the pulse needs to be greater than these naturally occurring forces.

Further differences found within the CEC analysis is the higher percentage of base saturation calcium found in the RSL soil, 89% vs 59% along with the Calcium/Magnesium ratio, average 14 cmol+/kg for the RSL compared to 3.8 cmol+/kg for Bordertown. In previous studies Barzegar et al. (1994:191) has reported that under an electron microscope, soils with a high Ca content show increased spaces between the micro particles that surround sand particles, and this can result in lower tensile strength. This position is supported by Dontsova and Norton (2002:184), who suggest that the larger hydration shell of the Magnesium (Mg) molecule will result in an increased distance between particles.

4.8.1 Soil Moisture

Perhaps the most unexpected finding of this research is the manner in which soil moisture, in the form of seasonal rainfall, percolates down through the soil in the Bordertown and Pt Lincoln RSL Cemetery's. The installed subsurface moisture sensors show very clearly that a considerable amount of rainfall is required before soil moisture levels below 45 cm in Pt Lincoln RSL, and 55 cm at Bordertown change to any significant extent. From the soil analysis, and initial understanding that Bordertown contained sodic soil, this could be expected at this location, but for the Pt Lincoln RSL Cemetery, this result was entirely unexpected. Increases in soil moisture below a depth of 45 cm in the RSL Cemetery occur after considerable sustained rainfall has fallen. This retention of available soil moisture at Bordertown corresponds with finding from Doolittle et al. (2007:417) who have stated that, in dry conditions, moisture that is retained in capillary space, (pore spaces), is sufficient to influence the electrical conductivity of the subsurface. Furthermore, Doolittle et al. (2007:417), postulates that in semi-arid conditions exchangeable cations accumulate in the upper part of the subsurface profile, producing high attenuation. While Bordertown is not classified as semi-arid, many months prior to visits saw no, or very little rain.

In prior studies from Barzegar et al. (1994:186), Nelson and Oades (1998:52), and Sumner (1993:698) it is noted that the hydraulic conductivity, or the ability of water to percolate down through the subsurface profile, is sensitive to the Exchangeable Sodium percentage, (ESP). Their research shows that in Australian soils with an ESP as low as 5, the hydraulic conductivity is severely restricted. Doolittle et al. (2007:417) further states that sodic soils, (defined in this case by sodium absorption ratio >=13) are highly conductive and so unsuitable for GPR.

Previous studies by (Rengasamy et al. 1986:230), and (Zhang and Norton 2002:203) have reported that in addition to the effect ESP has on hydraulic conductivity, the Ca:Mg ratio is also a factor in hydraulic conductivity. This is due to the larger size of the Mg hydration shell, and the tendency of Mg dominate soils with a ESP > 5 to become dispersive (Rengasamy et al. 1986:230; Sumner 1993:717). Comparison of the findings of this study with Rengasamy et al. (1986:233) confirms that the pore spaces in the subsurface at the Bordertown Cemetery do appear to be blocked, and it is only after considerable rainfall that there is partial unblocking and moisture percolation to deeper levels. The difference in Ca:Mg ratio found in the RSL Cemetery dictates that this is not applicable, and a greater level of moisture is percolating down through the soil profile.

4.9 Implications of this research.

GPR remains the most reliable geophysical method to locate unmarked graves in the soils of South Australia. ERT has been stated to be effective in locating sloping bulk resistivity interfaces, (Milsom and Erikson 2011; Reynolds 2011:294) but seems to be unreliable in locating subsurface features that are the size and subsurface orientation of a burial. Seasonal rainfall does not play a major role in changing the effectiveness of these geophysical methods. The most influence goes to the chemical and physical characteristics of the soil, and the soils' ability to transport and store the little moisture that is available. The ability to transport and store moisture allows a more effective transportation of the EM pulse and DC current. The results of this research show that whatever moisture the soil receives via rainfall, not all of it will continue to percolate down through the subsurface profile, this can be seen in the results of the soil moisture sensors, (see Figures 3.8.2 and 3.12.1). In the case of the dispersive soil found in Bordertown Cemetery, very little of the rainfall that fell, percolated below a depth of 60 cm. The dispersive nature of the soil effectively blocked the soil pore spaces. Prior studies have noted this phenomenon (Brandes 2005; Qadir and Schubert 2002; Shainberg and Letey 1984; Sumner 1993).

In a forensic context, the grave fluids, or leachate plume, are not always detectable using resistivity methods. From the literature, Van Belle et al. (2009:38) reported detecting traces of nitrogen from decomposition after 430 days, and Pringle et al. (2010:131) reports that changes in soil conductivity are detectable after 730 days (2 years). Given the burials in this study took place between 3 and 37 years ago, these previous studies would suggest that they would be old enough for the leachate plume to have dispersed, or at least dispersed to an extent that is not detectable by resistivity methods. This question does lead to further research.

4.10 The Value of this Research

This research has significant scientific value. As the author dug the graves in the RSL cemetery, there can be no doubt as to the shape, depth, the orientation of the graves, nor the material of the coffin. There is no doubt either that there are no anthropological artefacts in the soil in between the graves. The cemeteries in Keith and Bordertown are under the administration of the same local authority, they also confirm the depth, orientation, and absence of anthropological artefacts in the soil.

From such a robust methodology, this study delivers equally robust empirical evidence that both supports and challenges aspects of the many assumptions widely accepted within the geophysical discipline, see Sections 1.3.2 and 1.8.2. It has been important to undertake this research in the context of the South Australian climatic conditions, as much of the research is focused on climates that experience significantly more rainfall than South Australia. This research has followed Dionne et al. (2010); Hansen et al. (2014); and Schultz et al. (2016), who have all called for further research into the geophysical responses over

known human burials, and of Schmidt et al. (2017), who called for the testing of the precipitation ratio in differing climates.

This then gives increased confidence in those that undertake geophysical surveys for unmarked graves, law enforcement agencies in their search for clandestine burials, and to a lesser extent, other subsurface archaeological targets. The average number of burials detected per lithology also can give the geophysics surveyor a target range of possible subsurface targets that may be detected in similar subsurface conditions.

5 CONCLUSION

This research set out to establish whether there was an optimal seasonal period in which to undertake a geophysical survey to locate unmarked graves. This research has shown, that in the soils and climatic conditions found in South Australia, there is no optimal seasonal period that would significantly increase the possibility of detecting burials.

Other original contributions to knowledge are:

- In the soils of South Australia, the soil's physical and chemical characteristics are the primary drivers that govern the effectiveness of the geophysical methods in detecting human burials.
- In the soils of South Australia, the relationship between the available moisture is in the subsurface and the radar velocity is not a direct relationship.
- In the soils of South Australia, the relationship between whatever available moisture is in the subsurface and the resistivity is not a direct relationship.
- In the soils of South Australia, the hydraulic conductivity is such that any seasonal rainfall does not always percolate down through the subsurface profiles. In the subsurface profile of Bordertown this depth was 55 cm, while in the subsurface of Pt Lincoln a precipitation event greater than 60 mm was required to percolate down beyond 85 cm.

Other findings that further current knowledge in the Archaeology discipline are:

- While resistivity methods are slightly more effective in detecting burials in higher conductivity soils, the GPR remains the most important tool in locating unmarked graves over a range of soil types.

- The results of the portable X-Ray Fluorescence (pXRF) analysis add further to the current knowledge base, in that there is now a direct comparison between geophysical effectiveness and the soils mineral composition.
- The results of the magnetic susceptibility analysis add further to the current knowledge base, in that there is now a direct comparison between geophysical effectiveness and the magnetic susceptibility of a soil.
- The term “high clay content” is ubiquitous in geophysics literature. This research showed that even in low clay content soils, the effectiveness of the GPR is compromised. For example, the clay content at Bordertown is 2% clay particles at 100 cm, and as reported by Bevan (1991); Conyers (2011, 2006); Dionne et al. (2010) and Doolittle et al. (2007), the radar data showed sever attenuation, a low signal to noise ratio, lower penetration and an ‘opaqueness’ to the radar pulse.
- Following Hansen et al (2014), who call for studies in sites with contrasting soil types, and Schultz (2016), who calls for studies of burials over longer temporal periods, this research has delivered a body of work that can further knowledge of the relationship between geophysical targets and the surrounding soils.

From the several significant findings of this survey, it can be stated that this research has made an important contribution to the use of geophysical methods in the detection of human burials, and to Archaeological prospection in general.

The reasons behind this research, and why it was important are discussed in Section 1.2. The current literature was interrogated to understand burials in a contemporary context, the symbolism and ritual associated with burials, and how this symbolism and ritual have helped shape grieving in the modern world. Reports from around the world were presented to help describe how the shortage of space to intern the deceased is impacting those cities, and how the detection of unmarked graves becomes important in that context. Future trends such as natural burials, and composting the dead were also discussed. A consequence of conflict and epidemic disease through the ages, mass graves are often deliberately hidden. The importance and sensitivity associated with efforts to locate these graves is discussed. Burials in the deep past were examined, and the role that symbolism played in the evolution of hominin’s is described. The literature describing the role of burials in Archaeological science is presented, this literature tells of early symbolism and how scientific analysis can help give important information on the lives of those interned. Decomposition of a human body was discussed, as it is important to try to understand what remains could possibly be in a grave site after a period. The literature described recent studies that document decomposition rates, and the role of geophysics in helping document this process.

Section 1.3 introduced the concepts of geophysics, with the two methods of Ground Penetrating Radar (GPR) and Electrical Resistivity Tomography (ERT) being the focus of this research. Assumptions from the

literature that focused on these two geophysical methods were presented. The role of geophysical methods within Archaeological science were discussed, and definitions of archaeological prospection, archaeological extrapolation, and archaeological hypothesising were expanded on. From the literature the five most common subsurface conditions within the context of a burial that impact geophysical methods are presented, (Bevan 1991:1311). The role and importance of using geophysical methods in forensic science are also discussed, (Buck 2003; Pringle et al. 2009; Watters and Hunter 2004, and others). This chapter also bbriefly introduced the Schmidt Precipitation Ratio. This was presented in a short report by Schmidt et al. (2017) and is an attempt to mathematically predict the optimal time for geophysical survey using the precipitation over a thirty-day period.

Section 1.4 gives a theoretical overview of Ground Penetrating Radar (GPR), from the literature a short historical view, (Annan 2002; Reynolds 2011), and the uses for this technology. The reasoning for the antenna used in this research is given from the literature, (Bladon et al. 2011: Gómez-Ortiz et al. 2010; Schultz and Martin 2011). The theoretical characteristics of the radar wave are discussed, (Conyers 2004: Daniels et al. 2007), with further detail from the literature of Bevan (1991); Conyers (2004); and Gómez-Ortiz et al. (2010). GPR signal processing is introduced, with common processing steps given from the literature, (Balkaya et al. 2021; Marshallsay et al. 2021; Moffat et al. 2021; Schultz et al. 2016, and many more). Cautions were given from the literature of Daniels (2007); Goodman (2009, 2012); Luo et al. (2019); Szymczyk and Szymczyk (2013), and others, that over processing can introduce phantom features. Caution was also raised over the complexity of the subsurface matrix, and that this complexity can show in data as reflections. The relationship between soil, soil moisture and the GPR was introduced. Van Dam et al. (2003) postulated in the literature that which of the many physical characteristics of the subsurface matrix controlled the GPR pulse reflection, with Daniels (2007) adding that the chemical characteristics were of a similar nature. The available moisture within the subsurface matrix is an important element, with literature from Conyers (2004); Daniels (2007); Van Dam et al. (2002) and others claiming that soil moisture can change GPR pulse velocity, even during an active survey. How moisture moved through the soil at a capillary level was described, and how grave fluids also bond to soil particles, affecting the grain/water balance and bonding. It was also suggested by Conyers (2004) that appropriate soil moisture measuring devices would help understand soil moisture changes. This research did use soil moisture sensors, installed at Bordertown and Pt Lincoln.

Electrical Resistivity Tomography (ERT) and earth resistance (ER) in general were introduced in Section 1.5. A short history from the literature of Aizebeokhai (2010) and Stummer et al. (2004) was outlined. The literature of Martorana et al. (2023) and Pellicer (2010) described Ohms law, which is the basis of measuring resistivity. The different patterns of electrodes used with ERT are introduced, with literature from Aizebeokhai (2010); Martorana et al. (2023); Pellicer (2010); and Sarris et al. (2018) describing the various array types and the advantages of each. From this literature the array types used in this research

were chosen, with a question raised as to which would be more effective in detecting a line, (horizontal resistivity changes), of burials, (vertical resistivity changes). A caution from the literature of Aizebeokhai (2010) that resistivity measured by different array types can differ proved correct from the results of this research. The effect of grave fluids was discussed from the literature of Jervis et al. (2009) and Pringle et al. (2009) who have researched over many years by burying pigs. The subject of Induced Polarisation, (IP), is introduced as an adjunct to the ERT process. The differences between IP and ERT, and how IP fits into the ERT process is explained from the literature of Düztas et al. (2017); Reynolds (2011); and Wiberg and Jonsson (2017). The literature of Milsom and Erikson (2011) as well as Reynolds (2011) gives context to the interaction between the IP process and the subsurface matrix. The interaction between the soil and the DC current of the ERT and IP process is examined through the literature of Corwin and Lesch (2005); Pellicer (2010); Samouëlian et al. (2005); Stummer et al. (2004) and others. The interaction between a grain of soil and moisture is described, with a description of how the DC current passes through the micropores within the subsurface matrix. The membrane polarisation that a grain of soil undergoes when subjected to an external charge is explained by the literature of Milson and Erikson (2011) and Reynolds (2011). The complex role that clay particles in soil play in the IP process is given by Brandes (2005), with Chelidze and Gueguen (1999) nominating the behavior of soil particles as the key element in Induced Polarisation.

The processing of ERT data is outlined by the literature of Martorana et al. (2017) and Samouëlian et al. (2005). The least squares inversion method is used, and model squares are created that represent the centre point between the two electrodes that have measured the apparent resistivity. The smoothness of the final tomogram is controlled by the L1 and L2 norms settings in the initial processing. The discussion as to these norms stemmed from the literature of Aarhus GeoSoftware (2022) and Zhou et al. (2014).

Section 1.6 introduced the forward modelling of GPR and ERT. Different programs are available for this, each using a different process. These processes are introduced by the literature of Daniels (2007); Goodman and Piro (2013); and Zhang et al. (2023). The creation of the GPR model is guided by the literature of Goodman and Piro (2013), with different models used to simulate burials with the backfilled soil of differing resistivities. The ERT model was constructed following the literature of Loke (2016) and Pellicer (2010), with the program using a finite-difference method. Many instances of ERT modelling is found in the literature, with reports from Abdullah et al. (2018); Dahlin and Zhou (2004); Kilner et al. (2005); Pellicer (2010); and others, with Doro et al. (2022) modelling the burial of pigs to simulate a human burial.

Section 1.8 introduces the complex medium known as soil. The EM pulse and DC currents pass through this medium, and so the subsurface matrix becomes the primary influence in geophysics. A number of assumptions are introduced from the literature of Arcone et al. (2008); Conyers (2004); Fiedler et al. (2009); Jervis et al. (2009); Neal (2004); Ruffell (2005); Salat and Junge (2010); Schultz et al. (2006); Tabbagh et al

(2000) that shape this research. A brief background of the Australian geology, how it is formed, and weathering processes is given in the literature of Akinsunmade et al. (2019); Blewett (2012); McKenzie et al. (2004) and McNeill (1980). The role of weathering and how this complex process breaks down the regolith is introduced. From the literature of Hall (2015) comes the insight that weathering is part of a complex natural system, with spatial variations in size from macroscopic to landscape scale, and these systems contribute to the subsurface rarely being a homogenous unit. An overview of the soil classification system is taken largely from the literature of Charman and Murphy (2000) and McKenzie et al. (2004), and it is here that the theory of soil profiles is given, with a description of the Australian system and how this relates to international systems from the literature of Charman and Murphy (2000), GeoMon (2020), Isbell (2011), and the Soil Science Society of America (2023). The complexity of soil texture and structure is introduced, along with the physical properties that are applicable to classifying soil. These physical properties are texture, structure, colour, porosity and consistency, with the percentage of clay particles in any given sample the defining factor. These descriptions are from the literature of Akinsunmade et al. (2019) and McKenzie et al (2004), with a Table from McKenzie et al. (2004) illustrating the classifications with corresponding clay content. The soil structure describes the arrangement of the primary soil particles. This spatial arrangement of primary soil particles ranges from the single grained structure characterized by sand or silt, to the large electrostatically bonded massive structures of clay. Between these extremes soil particles form aggregated structures of infinite shape and size (Ghezzehei 2012). This complex and dynamic structural form that soil adopts is heavily influenced by particle size, and along with the structural form, the particle size and arrangement of particles are termed peds, these peds form distinctive shapes, rarely uniform, and between these peds are the pore spaces. These pore spaces become one of the passageways of soil moisture, and ultimately the geophysical pulse or current (Charman and Murphy 2000; Ghezzehei 2012; McKenzie et al. 2004; and White 2006). To understand this soil structure at the time of a geophysical survey would require digging or coring, and as both activities disrupt the structure of the soil, are not feasible to the geophysics operator.

One of the most important physical characteristics of soil is the particle size. The grain particle size dictates the texture, density, consistency, porosity, the ability to hold water, and the ability for an electrical current to pass through (Boggs 2016; Rowell 1997). The size, and percentage of total sample weight thereof dictates the soil type. It is here that the Australian Soil Classification is introduced, and from the literature of White (2006), this local classification is aligned to other international standards. The arrangement of sand and silt as a single grain structure is described by Ghezzehei (2012). Goldberg (2011) along with Qadir and Schubert (2002) introduces the complexity of a grain of clay. The clay particle is electrostatically charged, this charge will govern the extremely complex and diverse polydispersivity and make the clay particle quite dynamic. The mineralogy of the soil is discussed from literature by McKenzie et al. (2004); Short (2006; and Viscarra Rossel (2011). The majority of the sands in Australia are comprised of silicates or

carbonates, with the silicate being derived from the primary mineral's quartz, and limestone being the provider of carbonates. Silt is a mixture of sand and clay, so shares primary and secondary minerals, with clay being composed mainly of secondary minerals. Canan (1999); Goldberg et al. (2011); and Rowell (1997) describe the typical physics of these secondary minerals, these being the octahedral or tetrahedral sheet arrangement. These sheets can form various combinations within clay minerals, typically termed layer silicates or phyllosilicates, and typically arranged in either 1:1 or 2:1 sheets. The 1:1 sheets comprise a sheet of silica between two sheets of aluminium and are quite inert. The 2:1 sheets are held together by electrostatic forces. These electrostatic forces are supplied by cations. Cations are the positive charges found on the edges of stable secondary minerals that typically make up clay particles (McNeill 1980). The characteristics of these cations, the way that the charge is held, and the important role of the electrical double layer, (EDL), are supplied by the literature of Brandes (2005); Goldberg et al. (2011); and white (2006). Cation exchange occurs between ions in this EDL, the strength of the attraction or repulsion is described by the literature of Brandes (2005); Qadir and Schubert (2002); and White (2006). The overall concentrations of these exchangeable cations will determine if the soil is considered sodic, with the balance of sodium, calcium, and to a lesser degree magnesium controls the attraction/repulsion force. From Nelson and Oades (1998); Qadir and Schubert (2002); and University of New South Wales (2007) comes a description of how dispersion occurs, the consequences of which is microporosity being compromised. The presence of moisture in the subsurface matrix is introduced, with the ways that this moisture moves through the subsurface profile is described by the literature of Saarenketo (1998). How this movement is disrupted is termed dispersion, a function of repulsion between clay particles (Qadir and Schubert (2002); Rengasamy and Olsson (1991). The concentrations of unbound sodium in clay particles gives rise to what is termed sodic soil. This is determined by the Cation Exchange Capacity (CEC), a measure of the sum of exchangeable cations. As well as the CEC, the Exchangeble Sodium Percentage (ESP), a ratio of sodium to other cations is quoted by Mitchell and Soga (20005); Nelson and Oades (1998); Qadir and Schubert (2002). A further qualitative measure of soil texture is introduced as the Calcium/Magnesium ratio by the literature of Dontsova and Norton (2002); Rengasamy et al. (1986); and Zhang and Norton (2002). The importance of this ratio is explained as a dominance of calcium will affect the soil stability and promote particle aggregation. The literature of Cassidy (2009); Reynolds (2011); Witten (2006) and others introduces the subject of permittivity in soil. This is important in a geophysical context, as permittivity will slow the geophysical pulse or current. A counter force to permittivity is conductivity, and this description comes from the literature of Corwin and Lesch (2005); McNeill (1980); Neal (2004) and others. Both permittivity and conductivity are dependent on many of the complex physical and chemical characteristics of the soil particles. Finally the magnetic properties of the soil are introduced from the literature of Conyers (2012); Neal (2004) and Olhoeft (1998). Several groups of magnetics are discussed, along with the physical changes that occur at the nucleus of the molecule to facilitate a magnetic moment.

Section 1.9 introduces the three study sites and the rationale for their selection. The underlying geology is described, as well as the surface geology. Section 1.9 describes the soil analysis methods that will be used to determine the physical and chemical characteristics of the soil samples taken from the study sites.

Chapter 2 introduces the methodology used in this research. The geophysical methods used are the Ground Penetrating Radar (GPR) and Electrical Resistivity Tomography (ERT). Data acquisition of radar data follows the literature of Conyers (2011); Dionne et al. (2010); Goodman (1994), and others. Processing this data follows the literature of Conyers (2004); Daniels (2007); Goodman (2012); Hansen et al. (2014) and many others. The processing steps were kept to common practice as per the research outline. The ERT data was captured and processed following literature by Claerbout and Muir (1973); Loke et al. (2003); Pellicer (2010) and others. Results are presented in Chapter 3. The results from the soil testing show three contrasting soils, from coarse to medium sand through to medium to fine silt with clay content. Results from the GPR showed a difference in the ability of the radar to detect a burial, according to soil type, corresponding results from the ERT showed a similar pattern.

The Discussion in Chapter 4 reflects on the purpose of this research and gives a short description of the lithology of the study sites. The Schmidt Precipitation Ratio, Schmidt et al. (2017), is described, and the results in the South Australian context are given. The many assumptions from the literature, Sections 1.3.2 and 1.8.2, are answered, either in support or against, with reasoning stemming from the research. The results of each study site are discussed, with the Bordertown and RSL Cemetery sharing very similar subsurface characteristics. The results of the GPR and ERT are discussed, and results related back to the literature. The complex medium that is soil is discussed, with results of the soil analysis also described. Implications and value of the research are given.

5.1 Limitations of this Study

This research used two geophysical methods and measured their effectiveness in detecting human burials over known graves. The methods used were typical and followed literature from Conyers (2011); Dionne et al. (2010); Luo et al. (2019); and Neal (2004). Despite the success of these methods, there are some areas that limited the scope of this research, primarily equipment failure, equipment loan procedures, and the need to use garden type cemeteries to provide the optimal above ground conditions.

The subsurface moisture sensors provided a unique insight into the hydraulic conductivity of the differing subsurface at each study site, and how seasonal rainfall moved through this subsurface. However, this study was also limited by these sensors, firstly, the sensor initially installed in Bordertown Cemetery failed. Ten months passed before this was discovered, resulting in the loss of data. One of these sensors installed in Keith Cemetery would have broadened the scope of the study and provided a contrast of the characteristics of hydraulic conductivity in sand. Using wireless sensors instead of Bluetooth sensors would

have allowed remote downloading. This last option was dismissed by the local government authority as a potential breach of safety for visitors to the cemetery. Installing the sensors at the start of the study, rather than at the start of the second year would have given another 12 months of data.

The ERT equipment did not prove to be reliable. There were six site visits that did not result in the capture of ERT data. There were issues with the control box, these would not manifest until in the field and set up. Prior checking of the equipment was not possible. This study did not evaluate the effectiveness of ERT with differing electrode spacings at each site. Bordertown and the RSL Cemeteries could have been successfully evaluated with a smaller spacing, and the comparison would have provided useful contrast to the same array over the same graves with a different resolution.

Visiting the sites immediately after a significant rainfall event could have provided important information on how seasonal rainfall affects the radar velocity and ERT resistivity. Planning for each visit needed to occur on occasions many weeks in advance.

Study site selection was based on the criteria outlined in section 1.8.2. Garden cemeteries are rare in South Australia, but others do exist. While the sites used in this research returned interesting and important results, expanding the number of sites would have increased the lithologies and seasonal rainfall available, giving a larger data pool to determine the effectiveness of the geophysical methods.

5.2 Recommendations for further studies

This research addressed several assumptions found in the literature, these are listed in Section 4.3 and 4.4, as well as the primary research question, 'Is there an optimal seasonal period to undertake geophysical surveys?' The results from this research have addressed these assumptions, with several intriguing questions arising from the results. These questions can lay a foundation for further research in geophysical methods, and how these interact with the complex subsurface matrix.

There was little indication of any leachate in the results. From the literature, (Blom 2018; Dick et al. 2017, and Pringle et al. 2010), signs of leachate have not been detected in resistivity results past a temporal period of two years. From this lack of results a closer study of VOC leachate and its effect on the bonding of clay particles could be considered, this would follow Perrault et al. (2015), who have questioned the influence of particle size and texture plays in VOC sorption. Further to this point, ERT surveys could be undertaken over burials of a more recent age, in an attempt to ascertain at what age this leachate dissipates to an extent that it cannot be detected by these geophysical methods.

There is little in the literature on the subject of Induced Polarisation and locating burials. Given that IP is used to monitor leaching of buried waste, (Dahlin et al. 2010; Johansson et al. 2015; Wiberg and Jonsson 2017), it can be assumed that the leaching of grave fluids would provide a suitable study for the application of Induced Polarisation. Induced Polarisation showed much promise from the literature, (Dahlin et al. 2010), due to the chemical changes the grains supposedly undergo when surrounded by grave fluids, but the application of IP in this research was not effective. From this position further experimental investigations are called for to validate results from the literature with the soils of South Australia.

Features in the subsurface matrix are rarely of two dimensions only, (Loke and Barker 1996; Loke et al. 2013). Using ERT in a square array showed some promise in the literature, (Abdullah et al. 2018; Aizebeokhai 2010; Argote-Espino et al. 2013), if the issues of resolution can be addressed. Capturing suitable data in a small area rather than in a straight line could potentially also address the issue of time and effort required to initiate an ERT survey. Fully developing these surveys in a 3D space needs more development and research.

Negative chargeability and negative resistivity were an interesting issue in this research, and extensively discussed by Brandes (2005). At this time, Res2DInv converts negative to positive values, but Brandes (2005) has shown the negative values are a strong indicator of clay particles in the subsurface. Further investigation of negative chargeability and resistivity, and how this can be incorporated into the processing programs would be of interest.

The highly conductive soil found in the Bordertown Cemetery proved also to be dispersive, with a high electrostatic force holding particles together. This research showed that the chemical and physical characteristics of soil such as this leads to high attenuation in the radar data, and correspondingly little effective penetration from the DC current used in the ERT. This research was conducted with a 400 MHz radar antenna, with the ERT using 120 v in each DC pulse. Further experimental investigations might explore employing pulses of higher voltage in antennas, as well as a higher voltage in the ERT, with the increase in power theoretically being enough to break the electrostatic forces and provide passage for the radar pulse and ERT current.

From the results there was very little indication of grave shaft or backfill, contrary to findings of Bevan (1991). Therefore, the act of digging a grave and backfilling did not change the resistivity enough to be detectable to the GPR or ERT. Future studies could investigate if a radar antenna of a different frequency could detect these common features, as well as investigating the effectiveness of GPR and ERT over graves that use various soils in backfill. These studies could give valuable information as to the percentage of change in resistivity that can be detected. There was also some discussion of resolution from Gómez-Ortiz et al. (2010); Rial et al. (2009); and Schultz and Martin (2011). This could become an important issue for

future research, studies could be undertaken over buried objects of differing sizes with differing frequency antennas to determine what size object can reliably be detected by each frequency.

The role of Magnetic permittivity and its effect on the radar pulse is under researched, (Conyers 2012). The magnetic qualities of the soil in the Pt Lincoln RSL Cemetery proved to be of significance. Further research could also be conducted to determine the effects of magnetic permittivity and how it could affect the two geophysical methods from this research.

This research was over a finite period. A longer term study over the same graves could be beneficial, as the period in which this study was conducted recorded seasonally below average rainfall. A longer term study would include any changes that may be climate change driven.

More broadly, the sites of Keith and Bordertown were 47 km apart, with a difference in elevation of 60 m. Two sites so close, yet the soil and underlying lithology presenting as opposites. As the origins of this part of South Australia is largely accepted as being from a shoreline deposition, an interesting question has arisen as to why are the soils so different?

6 REFERENCES

Aarhus GeoSoftware 2022, 'Res2dinvx64 Rapid 2-D Resistivity and Ip Inversion Using the Least Squares Method'.

Abdullah FM, Loke MH, Nawawi M and Abdullah K 2018, 'Optimized perimeter arrays for 3D resistivity survey in urban areas: a comparison with standard L and Corner arrays', *EAGE-HAGI 1st Asia Pacific Meeting on Near Surface Geoscience and Engineering*, Yogyakarta, Indonesia, doi:10.3997/2214-4609.201800426.

Aizebeokhai AP 2010, '2D and 3D geoelectrical resistivity imaging: Theory and field design', *Scientific Research and Essays*, 5(23):3592–3605.

Akinsunmade A, Tomecka-Suchoń S and Pysz P 2019, 'Correlation Between Agrotechnical Properties of Selected Soil Types and Corresponding Gpr Response', *Acta Geophysica*, 67(6):1913–1919, doi:10.1007/s11600-019-00349-4.

Angelis D, Tsourlos P, Tsokas G, Vargemezis G, Zacharopoulou G and Power C 2018, 'Combined application of GPR and ERT for the assessment of a wall structure at the Heptapyrgion fortress (Thessaloniki, Greece)', *Journal of Applied Geophysics*, 152:208–220, doi:10.1016/j.jappgeo.2018.04.003.

Annan AP 2002, 'GPR—History, Trends, and Future Developments', *Subsurface Sensing Technologies and Applications*, 3:253–270.

Annan AP 2009, 'Electromagnetic Principles of Ground Penetrating Radar', in *Ground Penetrating Radar Theory and Applications*, Elsevier, doi:10.1016/B978-0-444-53348-7.00001-6.

Annan AP, Cosway SW and Redman JD 1991, 'Water table detection with ground-penetrating radar', in *SEG Technical Program Expanded Abstracts 1991*, *SEG Technical Program Expanded Abstracts 1991*, Society of Exploration Geophysicists, doi:10.1190/1.1888793.

Anson T and Henneberg H 2004, 'A solution for the permanent storage of historical skeletal remains for research purposes: A South Australian precedent that keeps scientists and the Church community happy', *Australian Archaeology*, 58(1):15–18, doi:10.1080/03122417.2004.11681776.

Arcone S, Grant S, Boitnott G and Bostick B 2008, 'Complex permittivity and clay mineralogy of grain-size fractions in a wet silt soil', *GEOPHYSICS*, 73(3):J1–J13, doi:10.1190/1.2890776.

Armstrong P, Nizio KD, Perrault KA and Forbes SL 2016, 'Establishing the volatile profile of pig carcasses as analogues for human decomposition during the early postmortem period', *Heliyon*, 2(2):e00070, doi:10.1016/j.heliyon.2016.e00070.

Ashby E 2011, 'Archaeological Approaches to Forensic Casework in New Zealand: Review and Future Directions', 63.

Aziz AS, Stewart RR, Green SL and Flores JB 2016, 'Locating and characterizing burials using 3D ground-penetrating radar (GPR) and terrestrial laser scanning (TLS) at the historic Mueschke Cemetery, Houston, Texas', *Journal of Archaeological Science: Reports*, 8:392–405, doi:10.1016/j.jasrep.2016.06.035.

Balkaya Ç, Ekinci YL, Çakmak O, Blömer M, Arnkens J and Kaya MA 2021, 'A challenging archaeo-geophysical exploration through GPR and ERT surveys on the Keber Tepe, City Hill of Doliche, Commagene (Gaziantep, SE Turkey)', *Journal of Applied Geophysics*, 186:104272, doi:10.1016/j.jappgeo.2021.104272.

Balter M 2012, 'Did Neandertals Truly Bury Their Dead?', *Science*, 337(6101):1443–1444, doi:10.1126/science.337.6101.1443.

Barone PM 2017, 'Forensic Geophysics', in R Di Maggio and PM Barone (eds) *Geoscientists at Crime Scenes*.

Barone PM, Swanger KJ, Stanley-Price N and Thursfield A 2016, 'Finding graves in a cemetery: Preliminary forensic GPR investigations in the Non-Catholic Cemetery in Rome (Italy)', *Measurement*, 80:53–57, doi:10.1016/j.measurement.2015.11.023.

Barzegar AR, Murray RS, Churchman GJ and Rengasamy P 1994, 'The strength of remolded soils as affected by exchangeable cations and dispersible clay', *Soil Research*, 32(2):185–199, doi:10.1071/sr9940185.

Belperio A 1995, 'Quaternary', in JF Drexel, WV Preiss, and AJ Parker (eds) *The Geology of South Australia. Vol. 2: The Phanerozoic*, Bulletin / Geological Survey of South Australia, Mines and Energy, South Australia, Geological Survey of South Australia, Adelaide.

Berezowski V, Mallett X, Ellis J and Moffat I 2021, 'Using Ground Penetrating Radar and Resistivity Methods to Locate Unmarked Graves: A Review', *Remote Sensing*, 13(15):2880, doi:10.3390/rs13152880.

Bevan BW 1991, 'The search for graves', *GEOPHYSICS*, 56(9):1310–1319, doi:10.1190/1.1443152.

Bièvre G, Oxarango L, Günther T, Goutaland D and Massardi M 2018, 'Improvement of 2D ERT measurements conducted along a small earth-filled dyke using 3D topographic data and 3D computation of geometric factors', *Journal of Applied Geophysics*, 153:100–112, doi:10.1016/j.jappgeo.2018.04.012.

Bladon P, Moffat I, Guilfoyle D, Beale A and Milani J 2011, 'Mapping anthropogenic fill with GPR for unmarked grave detection: a case study from a possible location of Mokare's grave, Albany, Western Australia', *Exploration Geophysics*, 42(4):249–257, doi:10.1071/EG11018.

Blewett R 2012, *Shaping a Nation: A Geology of Australia.*

Blom G 2018, 'Chemical Detection of Non Volatile and Semi-Volatile Decomposition Markers from Clandestine Gravesites.', Staffordshire University.

Boggs S 2016, *Principles of Sedimentology and Stratigraphy*, 5th edn, Pearson, USA.

Booth AD and Pringle JK 2016, 'Semblance analysis to assess GPR data from a five-year forensic study of simulated clandestine graves', *Journal of Applied Geophysics*, 125:37–44, doi:10.1016/j.jappgeo.2015.11.016.

Brandes IM 2005, 'The Negative Chargeability of Clays' PhD Thesis, UNSW Sydney, Sydney, Australia., doi:10.26190/UNSWORKS/21965.

Brasseur C, Dekeirsschieter J, Schotsmans EMJ, de Koning S, Wilson AS, Haubruge E and Focant J-F 2012, 'Comprehensive two-dimensional gas chromatography–time-of-flight mass spectrometry for the forensic study of cadaveric volatile organic compounds released in soil by buried decaying pig carcasses', *Journal of Chromatography A*, 1255:163–170, doi:10.1016/j.chroma.2012.03.048.

Bowler JM 1998, 'Willandra Lakes revisited: environmental framework for human occupation', *Archaeology in Oceania*, 33(3):120–155, doi:10.1002/j.1834-4453.1998.tb00414.x.

Brasseur C, Dekeirsschieter J, Schotsmans EMJ, de Koning S, Wilson AS, Haubruge E and Focant J-F 2012, 'Comprehensive two-dimensional gas chromatography–time-of-flight mass spectrometry for the forensic study of cadaveric volatile organic compounds released in soil by buried decaying pig carcasses', *Journal of Chromatography A*, 1255:163–170, doi:10.1016/j.chroma.2012.03.048.

Bruck J 1995, 'A place for the dead: the role of human remains in Late Bronze Age Britain'.

Bruker 2023, *The Principles of XRF Spectrometry*, https://www.bruker.com/en/products-and-solutions/elemental-analyzers/xrf-spectrometers/how-does-xrf-work.html, accessed 28 August 2023.

Buck S 2003, 'Searching for Graves Using Geophysics.', *Journal of Forensic Sciences*, 48(1):5–11.

Burdukiewicz JM 2014, 'The origin of symbolic behaviour of Middle Palaeolithic humans: Recent controversies', *Quaternary International*, 326–327:398–405, doi:10.1016/j.quaint.2013.08.042.

Cadence Design Systems 2022, 'Wave Propagation in Lossy Dielectrics', *Resource Systems Analysis*, https://resources.system-analysis.cadence.com/blog/msa2021-wave-propagation-in-lossy-dielectrics, accessed 23 November 2022.

Campobasso CP, Di Vella G and Introna F 2001, 'Factors affecting decomposition and Diptera colonization', *Forensic Science International*, 120(1):18–27, doi:10.1016/S0379-0738(01)00411-X.

Canan B 1999, 'Dielectric Properties of Mixtures of Clay-Water-Organic Compounds', 371.

Carbonell E and Mosquera M 2006, 'The emergence of a symbolic behaviour: the sepulchral pit of Sima de los Huesos, Sierra de Atapuerca, Burgos, Spain', *Comptes Rendus Palevol*, 5(1):155–160, doi:10.1016/j.crpv.2005.11.010.

Cardarelli E and De Donno G 2019, 'Advances in electric resistivity tomography: Theory and case studies', in *Innovation in Near-Surface Geophysics*, Elsevier, doi:10.1016/B978-0-12-812429-1.00002-7.

Cardimona S n.d., 'ELECTRICAL RESISTIVITY TECHNIQUES FOR SUBSURFACE INVESTIGATION'.

Carey AM, Paige GB, Carr BJ and Dogan M 2017, 'Forward modeling to investigate inversion artifacts resulting from time-lapse electrical resistivity tomography during rainfall simulations', *Journal of Applied Geophysics*, 145:39–49, doi:10.1016/j.jappgeo.2017.08.002.

Cassidy NJ 2009, 'Electrical and Magnetic Properties of Rocks, Soils and Fluids', in H Jol (ed) *Ground Penetrating Radar Theory and Applications*, Elsevier, doi:10.1016/B978-0-444-53348-7.00002-8.

Charman PE and Murphy BW 2000, *Soils: Their Properties & Management*, 2nd edn, Oxford Press.

Chelidze TL and Gueguen Y 1999, 'Electrical spectroscopy of porous rocks: a review—I.Theoretical models', *Geophysical Journal International*, 137(1):1–15, doi:10.1046/j.1365-246x.1999.00799.x.

Childe VG 1945, '4. Directional Changes in Funerary Practices During 50,000 Years', *Man*, 45:13–19, doi:10.2307/2793007.

Claerbout JF and Muir F 1973, 'Robust Modelling with Erratic Data', *GEOPHYSICS*, 38(5):826–844, doi:10.1190/1.1440378.

Collins MJ, Nielsen–Marsh CM, Hiller J, Smith CI, Roberts JP, Prigodich RV, Wess TJ, Csapò J, Millard AR and Turner–Walker G 2002, 'The survival of organic matter in bone: a review', *Archaeometry*, 44(3):383–394, doi:10.1111/1475-4754.t01-1-00071.

Commonwealth Scientific and Industrial Research Organisation 2016, *The Australian Soil Classification*, https://www.clw.csiro.au/aclep/asc_re_on_line_V2/append2.htm, accessed 30 March 2022.

Conyers LB 2011, 'Discovery, mapping and interpretation of buried cultural resources non-invasively with ground-penetrating radar', *Journal of Geophysics and Engineering*, 8(3):S13–S22, doi:10.1088/1742-2132/8/3/S02.

Conyers L 2004, *Ground-Penetrating Radar for Archaeology*, AltaMira Press, California.

Conyers L 2006, 'Ground Penetrating Radar Techniques To Discover and Map Historic Graves', *Hostorical Archaeology*, 40(3):64–73.

Conyers LB 2011, 'Discovery, mapping and interpretation of buried cultural resources non-invasively with ground-penetrating radar', *Journal of Geophysics and Engineering*, 8(3):S13–S22, doi:10.1088/1742-2132/8/3/S02.

Conyers L 2012, *Interpreting Ground-penetrating Radar for Archaeology*.

Conyers L 2016, *Ground-Penetrating Radar for Geoarchaelogy*, Wiley & Sons, Oxford.

Correia A 2019, 'Archaeological Geophysics in Portugal: Some Survey Examples', in G El-Qady and M Metwaly (eds) *Archaeogeophysics*, Natural Science in Archaeology, Springer International Publishing, Cham, doi:10.1007/978-3-319-78861-6_5.

Corwin DL and Lesch SM 2005, 'Apparent Soil Electrical Conductivity Measurements in Agriculture', *Computers and Electronics in Agriculture*, 46(1):11–43, doi:10.1016/j.compag.2004.10.005.

Cott P 1997, 'The Effect of Weather on Resistivity Measurements over a known Archaeological Feature' PhD Thesis, University of Bradford.

Coyne M 2020, 'New York Inters Bodies In Mass Burials On Island Amid Coronavirus Crisis', Forbes, accessed 25 May 2023, https://www.forbes.com/sites/marleycoyne/2020/04/10/new-york-inters-bodies-in-mass-burials-on-island-amid-coronavirus-crisis/?sh=10ad5dbe47c8, accessed 25 May 2023.

Dahlin T and Loke MH 2015, 'Negative apparent chargeability in time-domain induced polarisation data', *Journal of Applied Geophysics*, 123:322–332, doi:10.1016/j.jappgeo.2015.08.012.

Dahlin T, Rosqvist H and Leroux V 2010, 'Resistivity-IP mapping for landfill applications', *First Break*, 28(8), doi:10.3997/1365-2397.28.8.40742.

Dahlin T and Zhou B 2004, 'A numerical comparison of 2D resistivity imaging with 10 electrode arrays', *Geophysical Prospecting*, 52(5):379–398, doi:10.1111/j.1365-2478.2004.00423.x.

Dalan RA and Banerjee SK 1998, 'Solving archaeological problems using techniques of soil magnetism', *Geoarchaeology*, 13(1):3–36, doi:10.1002/(SICI)1520-6548(199801)13:1<3::AID-GEA2>3.0.CO;2-9.

van Dam RL, van den Berg EH, van Heteren S, Kasse C, Kenter JAM and Groen K 2002, 'Influence of Organic Matter in Soils on Radar-Wave Reflection: Sedimentological Implications', *Journal of Sedimentary Research*, 72(3):341–352, doi:10.1306/092401720341.

Damiata BN, Steinberg JM, Bolender DJ and Zoëga G 2013, 'Imaging skeletal remains with ground-penetrating radar: comparative results over two graves from Viking Age and Medieval churchyards on the Stóra-Seyla farm, northern Iceland', *Journal of Archaeological Science*, 40(1):268–278, doi:10.1016/j.jas.2012.06.031.

Daniels DJ 2007, *Ground Penetrating Radar*, 2nd ed, K Chang (ed), Institution of Engineering and Technology, London.

Dearing J 1988, 'Environmental Magnetic Susceptibility', https://bartingtondownloads.com/wp-content/uploads/OM0409.pdf, accessed 10 September 2023.

Dent BB, Forbes SL and Stuart BH 2004, 'Review of human decomposition processes in soil', *Environmental Geology*, 45(4):576–585, doi:10.1007/s00254-003-0913-z.

Department of Energy and Mining 2022, *South Australian Resources Information Gateway (SARIG)*, *SARIG Map*, https://map.sarig.sa.gov.au/.

Dept. Water, Land and Biodiversity Conservation 2002, 'Assessing Agricultural Lands', https://data.environment.sa.gov.au/Content/Publications/Assessing-Agricultural-Lands.pdf.

Dick HC, Pringle JK, Sloane B, Carver J, Wisniewski KD, Haffenden A, Porter S, Roberts D and Cassidy NJ 2015, 'Detection and characterisation of Black Death burials by multi-proxy geophysical methods', *Journal of Archaeological Science*, 59:132–141, doi:10.1016/j.jas.2015.04.010.

Dick HC, Pringle JK, Wisniewski KD, Goodwin J, van der Putten R, Evans GT, Francis J, Cassella JP and Hansen JD 2017, 'Determining geophysical responses from graves', *Geophysics*, 82(6):1–52.

Dionne CA, Wardlaw DK and Schultz JJ 2010, 'Delineation and Resolution of Cemetery Graves Using a Conductivity Meter and Ground-Penetrating Radar', *Technical Briefs in Historical Archaeology*, 5:20–30.

Dontsova KM and Norton LD 2002, 'CLAY DISPERSION, INFILTRATION, AND EROSION AS INFLUENCED BY EXCHANGEABLE Ca AND Mg':, *Soil Science*, 167(3):184–193, doi:10.1097/00010694-200203000-00003.

Doolittle JA and Collins ME 1995, 'Use of Soil Information to Determine Application of Ground Penetrating Radar.', *Journal of Applied Geophysics*, 33:101–108.

Doolittle JA, Minzenmayer FE, Waltman SW, Benham EC, Tuttle JW and Peaslee SD 2007, 'Ground-penetrating radar soil suitability map of the conterminous United States', *Geoderma*, 141(3):416–421, doi:10.1016/j.geoderma.2007.05.015.

Doro KO, Kolapkar AM, Bank C-G, Wescott DJ and Mickleburgh HL 2022, 'Geophysical imaging of buried human remains in simulated mass and single graves: Experiment design and results from pre-burial to six months after burial', *Forensic Science International (Online)*, 335, doi:10.1016/j.forsciint.2022.111289.

Düztaş E, Kurtuluş B, Erdem G, Sağır C, Gürcan T, Avşar Ö, Regnier J-L, Coz ML and Razack M 2017, 'Electrical Resistivity Tomography (ERT) and Induced Polarization (IP) Applied to Karst Alluvium: Case Study from Azmak Spring, Mugla, Turkey'.

Edwards LS 1977, 'A MODIFIED PSEUDOSECTION FOR RESISTIVITY AND IP', *GEOPHYSICS*, 42(5):1020–1036, doi:10.1190/1.1440762.

Environmental and Engineering Geophysical Society n.d., *What is Geophysics?*

Evans M and Heller F 2003, *Environmental Magnetism*, Academic Press, London.

Falconer K and Gould H 2023, *Our cemeteries face a housing crisis too. 4 changes can make burial sustainable.*, *The Conversation*, https://theconversation.com/our-cemeteries-face-a-housing-crisis-too-4-changes-can-make-burial-sustainable-205987, accessed 6 September 2023.

Ferraz R 2018, *Cemetery Overcrowding is Leading Europe to Recycle Burial Plots*, *TalkDeath*, https://www.talkdeath.com/cemetery-overcrowding-leading-europe-recycle-burial-plots/, accessed 2 June 2023.

Fiedler S, Illich B, Berger J and Graw M 2009, 'The effectiveness of ground-penetrating radar surveys in the location of unmarked burial sites in modern cemeteries', *Journal of Applied Geophysics*, 68(3):380–385, doi:10.1016/j.jappgeo.2009.03.003.

Fitzpatrick R, Boucher S, Naidu R and Fritsch E 1994, 'Environmental Consequences of Soil Sodicity', *Australian Journal of Soil Research*, 32:1069–1093.

Fotheringham T 2013, 'Comparison of Geophysical Techniques to Determine Depth to Bedrock in Complex Weathered Environments of the Mount Crawford Region, South Australia.', University of Adelaide, Adelaide.

Freeland RS, Yoder RE, Miller ML and Koppenjan S 2003, 'Forensic application of sweep-frequency and impulse GPR', in S Koppenjan and H Lee (eds), *Ninth International Conference on Ground Penetrating Radar (GPR2002)*, Santa Barbara, CA, doi:10.1117/12.462241.

Friedman SP 2005, 'Soil properties influencing apparent electrical conductivity: a review', *Computers and Electronics in Agriculture*, 46(1–3):45–70, doi:10.1016/j.compag.2004.11.001.

Fukue M, Minato T, Horibe H and Taya N 1999, 'The micro-structures of clay given by resistivity measurements', *Engineering Geology*, 54(1):43–53, doi:10.1016/S0013-7952(99)00060-5.

Gall MJ 2012, 'It's Elemental! A Case Study in the Use of Multi-element Geochemical Analysis as an Aid in Locating Cultural Features at the Foundation Site', *Northeast Historical Archaeology*, 41(1):96–125, doi:10.22191/neha/vol41/iss1/6.

Garnaut J, Jordan C, Vella A, Bailey M and Moffat I 2016, 'Ground penetrating radar investigations at the Lake Condah Mission Cemetery: locating unmarked graves in areas with extensive subsurface disturbance', *Artefact: the Journal of the Archaeological and Anthropological Society of Victoria*, 39:8–14, doi:10.3316/ielapa.242588357627092.

Gavin LJ, Hoskin T, Witten B, Shragge J, Petersen A and Deeks J 2015, 'Geophysical remote sensing of a historical aboriginal gravesite in Quairading, Western Australia', *ASEG Extended Abstracts*, 2015(1):1–4, doi:10.1071/ASEG2015ab030.

GeoMon 2020, *Soil Classification*, https://www.geomon.co.uk/geology-of-anglesey/soils-of-wales/soil-classification/.

Ghezzehei T 2012, 'Soil Structure', in PM Huang, Y Li, and ME Sumner (eds) *Handbook of Soil Sciences: Properties and Processes, Second Edition.*, CRC Press, Boca Raton, Fla.

Giannopoulos A 2005, 'Modelling ground penetrating radar by GprMax', *Construction and Building Materials*, 19(10):755–762, doi:10.1016/j.conbuildmat.2005.06.007.

Goldberg S, Lebron I, Seaman J and Suarez D 2011, 'Soil Colloidial Behavior', in PM Huang, Y Li, and M Summer (eds) *Handbook of Soil Sciences: Properties and Processes*, Taylor & Frances.

Gómez-Ortiz D, Martín-Crespo T, Martín-Velázquez S, Martínez-Pagán P, Higueras H and Manzano M 2010, 'Application of Ground Penetrating Radar (gpr) to Delineate Clay Layers in Wetlands. a Case Study in the Soto Grande and Soto Chico Watercourses, Doñana (sw Spain)', *Journal of Applied Geophysics*, 72(2):107–113, doi:10.1016/j.jappgeo.2010.07.007.

Goodman D 1994, 'Ground-Penetrating Radar Simulation in Engineering and Archaeology', *GEOPHYSICS*, 59(2):224–232, doi:10.1190/1.1443584.

Goodman D 2009, *Seeing the Unseen: Geophysics and Landscape Archaeology*, S Campana and S Piro (eds), CRC Press, Boca Raton.

Goodman D 2012, 'GPR-Slice User's Manual', 388.

Goodman D and Piro S 2013, *GPR Remote Sensing in Archaeology*, Springer Berlin Heidelberg, Berlin, Heidelberg, doi:10.1007/978-3-642-31857-3.

Gordon CC and Buikstra JE 1981, 'Soil pH, Bone Preservation, and Sampling Bias at Mortuary Sites', *American Antiquity*, 46(3):566–571, doi:10.2307/280601.

Gurr A, Kumaratilake J, Brook AH, Ioannou S, Pate FD and Henneberg M 2022, 'Health effects of European colonization: An investigation of skeletal remains from 19th to early 20th century migrant settlers in South Australia', *PLoS ONE*, 17(4):e0265878, doi:10.1371/journal.pone.0265878.

Haglund WD, Connor M and Scott DD 2001, 'The archaeology of contemporary mass graves', *Historical Archaeology*, 35(1):57–69, doi:10.1007/BF03374527.

Hall J 2015, 'Terroir and subregionality', *Australian and New Zealand Grapegrower and Winemaker*, (618):57–61.

Hall J, Maschmedt D and Billing N 2009, *The soils of Southern Australia. The South Australian Land and Soil Book Series.*, Govt of South Australia, Adelaide.

Hammon WS, McMechan GA and Zeng X 2000, 'Forensic GPR: finite-difference simulations of responses from buried human remains', *Journal of Applied Geophysics*, 45(3):171–186, doi:10.1016/S0926-9851(00)00027-6.

Hansen JD, Pringle JK and Goodwin J 2014, 'GPR and bulk ground resistivity surveys in graveyards: Locating unmarked burials in contrasting soil types', *Forensic Science International*, 237:e14–e29, doi:10.1016/j.forsciint.2014.01.009.

Haslam M, Prangnell J, Kirkwood L, McKeough A, Murphy A and Loy TH 2003, 'A Lang Park mystery: Analysis of remains from a 19th century burial in Brisbane, Queensland', *Australian Archaeology*, 56(1):1–7, doi:10.1080/03122417.2003.11681743.

Herring T and Lewkowicz AG 2022, 'A systematic evaluation of electrical resistivity tomography for permafrost interface detection using forward modeling', *Permafrost and Periglacial Processes*, 33(2):134–146, doi:10.1002/ppp.2141.

Hilts C 2023, *Current Archaeology*, https://reader.exacteditions.com/issues/110281/page/57, accessed 31 May 2023.

How Many People Have Ever Lived on Earth? 2023, *Population Reference Bureau*, https://www.prb.org/articles/how-many-people-have-ever-lived-on-earth/, accessed 28 May 2023.

Isbell R 2021, *Glossary*, *The Australian Soil Classification*, https://www.soilscienceaustralia.org.au/asc/soilglos.htm, accessed 6 February 2023.

Jervis JR, Pringle JK and Tuckwell GW 2009, 'Time-lapse resistivity surveys over simulated clandestine graves', *Forensic Science International*, 192(1–3):7–13, doi:10.1016/j.forsciint.2009.07.001.

Johansson S, Fiandaca G and Dahlin T 2015, 'Influence of non-aqueous phase liquid configuration on induced polarization parameters: Conceptual models applied to a time-domain field case study', *Journal of Applied Geophysics*, 123:295–309, doi:10.1016/j.jappgeo.2015.08.010.

Johnson RH and Poeter EP 2005, 'Iterative use of the Bruggeman-Hanai-Sen mixing model to determine water saturations in sand', *GEOPHYSICS*, 70(5):K33–K38, doi:10.1190/1.2049348.

Jones G 2008, 'Geophysical Mapping of Historic Cemeteries', *Technical Briefs in Historical Archaeology*, 3:25–38.

Keegan M 2019, 'Hong Kong Real Estate Now More Expensive for the Dead Than The Living', The Guardian, https://www.theguardian.com/cities/2019/apr/23/dead-pricey-hong-kong-burial-plots-now-more-expensive-than-living-space.

Kemna A, Binley A, Ramirez A and Daily W 2000, 'Complex resistivity tomography for environmental applications', *Chemical Engineering Journal*, 77(1–2):11–18, doi:10.1016/S1385-8947(99)00135-7.

Kibblewhite M, Tóth G and Hermann T 2015, 'Predicting the preservation of cultural artefacts and buried materials in soil', *Science of The Total Environment*, 529:249–263, doi:10.1016/j.scitotenv.2015.04.036.

Kilner M, West LJ and Murray T 2005, 'Characterisation of glacial sediments using geophysical methods for groundwater source protection', *Journal of Applied Geophysics*, 57(4):293–305, doi:10.1016/j.jappgeo.2005.02.002.

Klinkner M and Smith E 2020, *The Bournemouth Protocol on Mass Grave Protection and Investigation*, United Nations Human Rights Special Procedures, https://www.icmp.int/wp-content/uploads/2022/02/mass_graves_project_english-4.pdf, accessed 26 June 2023.

Knight R 2001a, 'Ground Penetrating Radar for Environmental Applications', *Annual Review of Earth and Planetary Sciences*, 29(1):229–255, doi:10.1146/annurev.earth.29.1.229.

Knight R 2001b, 'Ground Penetrating Radar for Environmental Applications', *Annual Review of Earth and Planetary Sciences*, 29(1):229–255, doi:10.1146/annurev.earth.29.1.229.

Kodama K, An Z, Chang H and Qiang X 2014, 'Quantification of magnetic nanoparticles with broad-band-frequency magnetic susceptibility measurements: a case study of an upper loess/palaeosol succession at Luochuan, Chinese Loess Plateau', *Geophysical Journal International*, 199(2):767–783, doi:10.1093/gji/ggu299.

Kooijmans LPL, Smirnov Y, Solecki RS, Villa P, Weber T and Gargett RH 1989, 'On the Evidence for Neandertal Burial', *Current Anthropology*, 30(3):322–330.

Koppenjan S 2009, 'Ground Penetrating Radar Systems and Design', in H Jol (ed) *Ground Penetrating Radar Theory and Applications*, Elsevier.

Kumari N and Mohan C 2012, 'Basics of Clay Minerals and Their Characteristic Properties.', in G Nascimento (ed) *Clay and Clay Minerals*, IntechOpen.

Larson DO, Vass AA and Wise M 2011, 'Advanced Scientific Methods and Procedures in the Forensic Investigation of Clandestine Graves', *Journal of Contemporary Criminal Justice*, 27(2):149–182, doi:10.1177/1043986211405885.

Lech ME and Trewin CL 2013, *Weathering, Erosion, Landforms and Regolith: Teacher Notes and Student Activities*, 2nd edition, Geoscience Australia, Canberra.

Li J, Li X, Wang X, Li Y, Wu K, Shi J, Yang L, Feng D, Zhang T and Yu P 2016, 'Water distribution characteristic and effect on methane adsorption capacity in shale clay', *International Journal of Coal Geology*, 159:135–154, doi:10.1016/j.coal.2016.03.012.

Loke MH, Acworth I and Dahlin T 2003, 'A Comparison of Smooth and Blocky Inversion Methods in 2d Electrical Imaging Surveys', *Exploration Geophysics*, 34(3):182–187, doi:10.1071/EG03182.

Loke MH 2015, 'Determination of model reliability in 3-D resistivity and I.P. inversion', *ASEG Extended Abstracts*, 2015(1):1–4, doi:10.1071/ASEG2015ab046.

Loke MH 2016, 'Res2DMOD. Rapid 2D resistivity and I.P. forward modeling using the finite-difference and finite-element methods.'

Loke MH, Chambers JE, Rucker DF, Kuras O and Wilkinson PB 2013, 'Recent developments in the direct-current geoelectrical imaging method', *Journal of Applied Geophysics*, 95:135–156, doi:10.1016/j.jappgeo.2013.02.017.

Lowe K 2012, 'Review Of Geophysical Applications in Australian archaeology', *Australian Archaeology*, 74(1):71–84, doi:10.1080/03122417.2012.11681936.

Lowe KM, Shulmeister J, Feinberg JM, Manne T, Wallis LA and Welsh K 2016, 'Using Soil Magnetic Properties to Determine the Onset of Pleistocene Human Settlement at Gledswood Shelter 1, Northern Australia: SOIL MAGNETIC PROPERTIES AND HUMAN SETTLEMENT IN AUSTRALIA', *Geoarchaeology*, 31(3):211–228, doi:10.1002/gea.21544.

Luo TXH, Lai WWL, Chang RKW and Goodman D 2019, 'GPR Imaging Criteria', *Journal of Applied Geophysics*, 165:37–48, doi:10.1016/j.jappgeo.2019.04.008

Madden C, Pringle JK, Jeffery AJ, Wisniewski KD, Heaton V, Oliver IW, Glanville H, Stimpson IG, Dick HC, Eeley M and Goodwin J 2022, 'Portable X-ray fluorescence (pXRF) analysis of heavy metal contamination in church graveyards with contrasting soil types', *Environmental Science and Pollution Research*, 29(36):55278–55292, doi:10.1007/s11356-022-19676-z.

Marshallsay J, Moffat I and Beale A 2021, *Geophysical investigations of the Tabernacle (Yilki) Cemetery, Encounter Bay, South Australia*, Open Science Framework, doi:10.31219/osf.io/7cnrh.

Martin P 2015, 'An Evaluation of Geophysical Methods for Detection of Toddler Graves.', University of Mississippi, Oxford.

Martorana R, Capizzi P, D'Alessandro A and Luzio D 2017a, 'Comparison of different sets of array configurations for multichannel 2D ERT acquisition', *Journal of Applied Geophysics*, 137:34–48, doi:10.1016/j.jappgeo.2016.12.012.

—— 2017b, 'Comparison of different sets of array configurations for multichannel 2D ERT acquisition', *Journal of Applied Geophysics*, 137:34–48, doi:10.1016/j.jappgeo.2016.12.012.

Martorana R, Capizzi P, Pisciotta A, Scudero S and Bottari C 2023, 'An Overview of Geophysical Techniques and Their Potential Suitability for Archaeological Studies', *Heritage*, 6(3):2886–2927, doi:10.3390/heritage6030154.

McKenzie N, Jacquier D, Isbell R and Brown K 2004a, 'Properties of Soil', in *Australian Soils and Landscapes: An Illustrated Compendium*, CSIRO.

—— 2004b, 'Soil Function within ecosystems', in *Australian Soils and Landscapes: An Illustrated Compendium*, CSIRO.

McNeill J 1980, 'Electrical conductivity of soils and rocks, Technical Note TN-5.', *Geonics Limited*5–22.

Mikles N 2021, *Lack of burial space is changing age-old funeral practices, and in Japan 'tree burials' are gaining in popularity*, *The Conversation*, http://theconversation.com/lack-of-burial-space-is-changing-age-old-funeral-practices-and-in-japan-tree-burials-are-gaining-in-popularity-161323, accessed 2 June 2023.

Millington TM, Cassidy NJ, Nuzzo L, Crocco L, Soldovieri F and Pringle JK 2011, 'Interpreting complex, three-dimensional, near-surface GPR surveys: an integrated modelling and inversion approach', *Near Surface Geophysics*, 9(3):297–304, doi:10.3997/1873-0604.2010010.

Milsom J and Erikson A 2011, *Field Geophysics*, 4th edn, Wiley-Blackwell.

Mitchell JK and Soga K 2005, *Fundamentals of Soil Behaviour*, 3rd edn.

Moffat I 2023, *How we're developing underground mapping technologies - lessons from the Beaumont case.*, *The Conversation*, https://theconversation.com/how-were-developing-underground-mapping-technologies-lessons-from-the-beaumont-case-90687.

Moffat I, Garnaut J, Jordan C, Vella A, Bailey M and Corporation GMTO 2021, *Ground penetrating radar investigations at the Lake Condah Mission Cemetery: Locating unmarked graves in areas with extensive subsurface disturbance*, Open Science Framework, doi:10.31219/osf.io/xm245.

Molina CM, Pringle JK, Saumett M and Evans GT 2016, 'Geophysical monitoring of simulated graves with resistivity, magnetic susceptibility, conductivity and GPR in Colombia, South America', *Forensic Science International*, 261:106–115, doi:10.1016/j.forsciint.2016.02.009.

Moník M, Lenďáková Z, Ibáñez JJ, Muñiz J, Borell F, Iriarte E, Teira L and Kuda F 2018, 'Revealing early villages – Pseudo-3D ERT geophysical survey at the pre-pottery Neolithic site of Kharaysin, Jordan', *Archaeological Prospection*, 25(4):339–346, doi:10.1002/arp.1713.

Mosher D 2020, *Over 1 million unclaimed bodies are buried on a little-known island in New York City — a mass graveyard where some coronavirus victims will go to rest*, *Business Insider*, https://www.businessinsider.com/story-of-potters-field-on-hart-island-2016-6, accessed 25 May 2023.

Muller S 2021, '"Oh, Early Vanished from a Parents Eye": "Childness" and child memorialisation in the South Australian cemetery, 1836-2018 CE.', Flinders University, Adelaide.

Neal A 2004, 'Ground-Penetrating Radar and Its Use in Sedimentology: Principles, Problems and Progress', *Earth-Science Reviews*, 66(3–4):261–330, doi:10.1016/j.earscirev.2

Nelson P and Oades J 1998, 'Organic Matter, Sodicity and Soil Structure', in ME Sumner and R Naida (eds) *Sodic soils: distribution, properties, management, and environmental consequences*, Topics in sustainable agronomy, Oxford University Press, New York.

Nero C, Aning AA, Danuor SK and Noye RM 2016, 'Delineation of graves using electrical resistivity tomography', *Journal of Applied Geophysics*, 126:138–147, doi:10.1016/j.jappgeo.2016.01.012.

Nobes DC 1999, 'Geophysical surveys of burial sites: A case study of the Oaro urupa', *GEOPHYSICS*, 64(2):357–367, doi:10.1190/1.1444540.

Norman H and Payne AM 2022, 'Nowhere Else but Home: A National Resting Place for Indigenous Australian Ancestral Remains', *Curator: The Museum Journal*, 65(4):817–834, doi:10.1111/cura.12526.

NSW Planning & Environment 2014, 'A Plan For Growing Sydney', 146.

Olhoeft GR n.d., 'Electrical, Magnetic, and Geometric Properties that Determine Ground Penetrating Radar Performance'.

O'Sullivan D 2013, 'Burial of the Christian Dead in the Later Middle Ages', in S Tarlow and L Stutz (eds) *The Oxford Handbook of the Archaeology of Death & Burial*, Oxford University Press.

Owen T and Pate D 2014, 'A Kaurna burial, Salisbury, South Australia: Further evidence for complex late Holocene Aboriginal social systems in the Adelaide region', *Australian Archaeology*, 79(1):45–53, doi:10.1080/03122417.2014.11682018.

Parker AJ 2012, *The Geology of South Australia*, JF Drexel, WV Preiss, and AJ Parker (eds), Mines and Energy, South Australia, Geological Survey of South Australia, Adelaide.

Pardoe C 1988, 'The cemetery as symbol. The distribution of prehistoric Aboriginal burial grounds in southeastern Australia', *Archaeology in Oceania*, 23(1):1–16, doi:10.1002/j.1834-4453.1988.tb00178.x.

—— 2013, ‘Repatriation, Reburial, and Biological Research in Australia’, in *The Oxford Handbook of The Archaeology of Death & Burial*, Oxford University Press.

Pate D 2006, ‘Hunter-gatherer social complexity at Roonka Flat, South Australia’, 226–241, doi:10.13140/2.1.2496.8648.

Pellicer X 2010, ‘Geophysical Characterisation and Evolutionary Model.’, National University of Ireland, Maynooth.

Perrault KA, Stefanuto P-H, Stuart BH, Rai T, Focant J-F and Forbes SL 2015, ‘Detection of decomposition volatile organic compounds in soil following removal of remains from a surface deposition site’, *Forensic Science, Medicine, and Pathology*, 11(3):376–387, doi:10.1007/s12024-015-9693-5.

Petersen A 2013, ‘The Archaeology of Death and Burial in the Islamic World’, in S Tarlow and L Stutz (eds) *The Oxford Handbook of the Archaeology of Death and Burial*, Oxford University Press.

Pitt N, Casey M, Lowe A and Stocks R 2017, ‘The Old Sydney Burial Ground’, 3–23.

Pomeroy E, Hunt CO, Reynolds T, Abdulmutalb D, Asouti E, Bennett P, Bosch M, Burke A, Farr L, Foley R, French C, Frumkin A, Goldberg P, Hill E, Kabukcu C, Lahr MM, Lane R, Marean C, Maureille B, Mutri G, Miller CE, Mustafa KA, Nymark A, Pettitt P, Sala N, Sandgathe D, Stringer C, Tilby E and Barker G 2020, ‘Issues of theory and method in the analysis of Paleolithic mortuary behaviour: A view from Shanidar Cave’, *Evolutionary Anthropology: Issues, News, and Reviews*, 29(5):263–279, doi:10.1002/evan.21854.

Powell K 2004, ‘Detecting buried human remains using near-surface geophysical instruments’, *Exploration Geophysics*, 35(1):88–92, doi:10.1071/EG04088.

Pringle JK, Cassella JP and Jervis JR 2010, ‘Preliminary soilwater conductivity analysis to date clandestine burials of homicide victims’, *Forensic Science International*, 198(1–3):126–133, doi:10.1016/j.forsciint.2010.02.005.

Pringle JK, Jervis JR, Roberts D, Dick HC, Wisniewski KD, Cassidy NJ and Cassella JP 2016, ‘Long-term Geophysical Monitoring of Simulated Clandestine Graves using Electrical and Ground Penetrating Radar Methods: 4-6 Years After Burial’, *Journal of Forensic Sciences*, 61(2):309–321, doi:10.1111/1556-4029.13009.

Pringle JK, Jervis JR and Tuckwell GT 2009, ‘Comparison of Time-lapse GPR and Resistivity over Simulated Clandestine Graves’, in *Near Surface 2009 - 15th EAGE European Meeting of Environmental and Engineering Geophysics*, *Near Surface 2009 - 15th EAGE European Meeting of Environmental and Engineering*

Geophysics, European Association of Geoscientists & Engineers, Dublin, Ireland, doi:10.3997/2214-4609.20146988.

Qadir M and Schubert S 2002, 'Degradation processes and nutrient constraints in sodic soils', *Land Degradation & Development*, 13(4):275–294, doi:10.1002/ldr.504.

Queensland Government 2022, *How Soils Form*, https://www.qld.gov.au/environment/land/management/soil/soil-explained/forms#:~:text=They%20are%20produced%20from%20rocks,help%20break%20down%20parent%20material, accessed 2 December 2022.

Quijano L, Chaparro MAE, Marié DC, Gaspar L and Navas A 2014, 'Relevant magnetic and soil parameters as potential indicators of soil conservation status of Mediterranean agroecosystems', *Geophysical Journal International*, 198(3):1805–1817, doi:10.1093/gji/ggu239.

Radini A, Buckley S, Rosas A, Estalrrich A, Rasilla M de la and Hardy K 2016, 'Neanderthals, trees and dental calculus: new evidence from El Sidrón', *Antiquity*, 90(350):290–301, doi:10.15184/aqy.2016.21.

Rains K and Prangnell J 2002, 'Background to the University of Queensland Archaeological Services Unit's Lang Park Salvage Excavations: History, Significance Assessment and Methods', *Queensland Archaeological Research*, 13:21–30, doi:10.25120/qar.13.2002.65.

Raudon S 2022, 'Huddled masses: The shock of Hart Island, New York', *Human Remains and Violence: An Interdisciplinary Journal*, 8(1):84–101, doi:10.7227/HRV.8.1.6.

Ravansari R, Wilson SC and Tighe M 2020, 'Portable X-ray fluorescence for environmental assessment of soils: Not just a point and shoot method', *Environment International*, 134:105250, doi:10.1016/j.envint.2019.105250.

Rawlings D, Litster C, Miller-Lewis L, Tieman J and Swetenham K 2020, 'The voices of death doulas about their role in end-of-life care', *Health & Social Care in the Community*, 28(1):12–21, doi:10.1111/hsc.12833.

Rayment G and Lyons D 2011, 'Ion-exchange properties', in *Soil Chemical Methods - Australasia*, CSIRO.

Reddy PS, Mohanty B and Rao BH 2020, 'Influence of Clay Content and Montmorillonite Content on Swelling Behaviour of Expansive Soils', *International Journal of Geosynthetics and Ground Engineering*, 6(1):1, doi:10.1007/s40891-020-0186-6.

Rengasamy P, Greene R and Ford G 1986, 'Influence of magnesium on aggregate stability in sodic red-brown earths', *Soil Research*, 24(2):229, doi:10.1071/SR9860229.

Rengasamy P and Olsson K 1991, 'Sodicity and Soil Structure', *Australian Journal of Soil Research*, 29(6):935–952.

Reuters April 2021, 'Brazil's Gravediggers rush to exhume bodies to make space for Covid victims', The Guardian, accessed 25 May 2023, https://www.theguardian.com/world/2021/apr/02/brazil-gravediggers-rush-to-exhume-bodies-to-make-space-for-covid-victims, accessed 25 May 2023.

Reynolds J 2011, *An Introduction to Applied and Environmental Geophysics*, 2nd edn, Wiley-Blackwell, London.

Rial FI, Pereira M, Lorenzo H, Arias P and Novo A 2009, 'Resolution of GPR bowtie antennas: An experimental approach', *Journal of Applied Geophysics*, 67(4):367–373, doi:10.1016/j.jappgeo.2008.05.003.

Richard N 2013, 'Did Prehistoric Man Bury His Dead?', in *The Oxfrd Handbook of the Archaeology of Death & Burial*, Oxford University Press.

Riel-Salvatore J and Clark GA 2001, 'Grave Markers: Middle and Early Upper Paleolithic Burials and the Use of Chronotypology in Contemporary Paleolithic Research', *Current Anthropology*, 42(4):449–479, doi:10.1086/321801.

Robbins AR and Plattner A 2018, 'Offset-electrode profile acquisition strategy for electrical resistivity tomography', *Journal of Applied Geophysics*, 151:66–72, doi:10.1016/j.jappgeo.2018.01.027.

Romanis T, Sedov S, Lev S, Lebedeva M, Kondratev K, Yudina A, Abrosimov K, Golyeva A and Volkov D 2021, 'Landscape change and occupation history in the Central Russian Upland from Upper Palaeolithic to medieval: Paleopedological record from Zaraysk Kremlin', *CATENA*, 196:104873, doi:10.1016/j.catena.2020.104873.

Rowell D 1997, *Soil Science Methods and Applications*.

Ruffell A 2005, 'Searching for the IRA "Disappeared": Ground-penetrating Radar Investigation of a Churchyard Burial Site, Northern Ireland', *Journal of Forensic Sciences*, 50(6):1–6, doi:10.1520/JFS2004156.

Ruffell A 2015, 'A RAG System for the Management Forensic and Archaeological Searches of Burial Grounds', *International Journal of Archaeology*, 3(1):1, doi:10.11648/j.ija.s.2015030101.11.

Ruffell A, Donnelly C, Carver N, Murphy E, Murray E and McCambridge J 2009, 'Suspect burial excavation procedure: A cautionary tale', *Forensic Science International*, 183(1–3):e11–e16, doi:10.1016/j.forsciint.2008.10.013.

Saarenketo T 1998, 'Electrical properties of water in clay and silty soils', *Journal of Applied Geophysics*, 40(1–3):73–88, doi:10.1016/S0926-9851(98)00017-2.

Salat C and Junge A 2010, 'Dielectric permittivity of fine-grained fractions of soil samples from eastern Spain at 200 MHz', *GEOPHYSICS*, 75(1):J1–J9, doi:10.1190/1.3294859.

Samouëlian A, Cousin I, Tabbagh A, A. B and Richard G 2005, 'Electrical resistivity survey in soil science: A review', *Soil and Tillage Research*, 83:173–193, doi:10.1016/j.still.2004.10.004.

Sarris A, Kalayci T, Moffat I and Manataki M 2018, 'An Introduction to Geophysical and Geochemical Methods in Digital Geoarchaeology', in C Siart, M Forbriger, and O Bubenzer (eds) *Digital Geoarchaeology*, Natural Science in Archaeology, Springer International Publishing, Cham, doi:10.1007/978-3-319-25316-9_14.

Schmidt A 2008, 'Electrical and magnetic methods in archaeological prospection', in S Piro and S Campana (eds) *Seeing the Unseen. Geophysics and Landscape Archaeology*, Taylor & Francis, doi:10.1201/9780203889558.pt2.

Schmidt A, Fry R, Parkin A, Bonsall J and Gaffney C 2017, 'When the Time Is Right: The Impact of Weather Variations on The Contrast in Earth Resistance Data', *12th International Conference of Archaeological Prospection*, Archaeopress Archaeology, University of Bradford.

Schöner W, Boeckli L, Hausmann H, Otto J-C, Reisenhofer S, Riedl C and Seren S 2012, 'Spatial Patterns of Permafrost at Hoher Sonnblick (Austrian Alps) - Extensive Field-measurements and Modelling Approaches', *Austrian Journal of Earth Sciences*, 105(2):154–168.

Schreiber M 2020, 'Rwanda's Genocide Ended 26 Years Ago. Survivors Are Still Finding Mass Graves', NPR, accessed 25 May 2023, https://www.npr.org/2020/07/16/891815028/rwandas-genocide-ended-26-years-ago-survivors-are-still-finding-mass-graves, accessed 25 May 2023.

Schultz JJ, Collins ME and Falsetti AB 2006, 'Sequential Monitoring of Burials Containing Large Pig Cadavers Using Ground-Penetrating Radar', *Journal of Forensic Sciences*, 51(3):607–616, doi:10.1111/j.1556-4029.2006.00129.x.

Schultz JJ and Martin MM 2011, 'Controlled GPR grave research: Comparison of reflection profiles between 500 and 250MHz antennae', *Forensic Science International*, 209(1–3):64–69, doi:10.1016/j.forsciint.2010.12.012.

Schultz JJ, Walter BS and Healy C 2016, 'Long-term sequential monitoring of controlled graves representing common burial scenarios with ground penetrating radar: Years 2 and 3', *Journal of Applied Geophysics*, 132:60–74, doi:10.1016/j.jappgeo.2016.06.015.

Shackley MS 2011, 'An Introduction to X-Ray Fluorescence (XRF) Analysis in Archaeology', in MS Shackley (ed) *X-Ray Fluorescence Spectrometry (XRF) in Geoarchaeology*, Springer New York, New York, NY, doi:10.1007/978-1-4419-6886-9.

Shainberg I and Letey j 1984, 'Response of Soils to Sodic ad Saline Conditions', *Journal of Agricultural Science*, 52(2), https://hilgardia.ucanr.edu/fileaccess.cfm?article=152852&p=VAFSNP, accessed 28 March 2024.

Sharma P 1997, *Environmental and Engineering Geophysics*, Cambridge University Press.

Sheppard-Simms E 2020, *Ashes to ashes, dust to..compost? An eco-friendly burial in just 4 weeks.*, *The Conversation*, https://theconversation.com/ashes-to-ashes-dust-to-compost-an-eco-friendly-burial-in-just-4-weeks-127794, accessed 6 September 2023.

Shirzaditabar F and Heck RJ 2021, 'Characterization of soil magnetic susceptibility: a review of fundamental concepts, instrumentation, and applications', *Canadian Journal of Soil Science*, 102(2):231–251, doi:10.1139/CJSS-2021-0040.

Short AD 2006, 'Australian Beach Systems—Nature and Distribution', *Journal of Coastal Research*, 221:11–27, doi:10.2112/05A-0002.1.

Simeoni MA, Galloway PD, O'Neil AJ and Gilkes RJ 2009, 'A procedure for mapping the depth to the texture contrast horizon of duplex soils in south-western Australia using ground penetrating radar, GPS and kriging', *Soil Research*, 47(6):613, doi:10.1071/SR08241.

Simyrdanis K, Papadopoulos N and Cantoro G 2016, 'Shallow Off-Shore Archaeological Prospection with 3-D Electrical Resistivity Tomography: The Case of Olous (Modern Elounda), Greece', *Remote Sensing*, 8(11):897, doi:10.3390/rs8110897.

Slater L 2007, 'Near Surface Electrical Characterization of Hydraulic Conductivity: From Petrophysical Properties to Aquifer Geometries—A Review', *Surveys in Geophysics*, 28(2):169–197, doi:10.1007/s10712-007-9022-y

Soil Science Society of America 2023, *Soil Horizons*, https://www.soils4teachers.org/soil-horizons/.

South Australia Burial and Cremation Act 2013, https://www.legislation.sa.gov.au/lz?path=%2FC%2FA%2FBURIAL%20AND%20CREMATION%20ACT%202013.

South East Natural Resources Management 2022, 'Landscapes of the South-East'.

Specht RL 1973, 'Structure and Functional Response of Ecosystems in the Mediterranean Climate of Australia', in F di Castri and HA Mooney (eds) *Mediterranean Type Ecosystems: Origin and Structure*, Ecological Studies, Springer, Berlin, Heidelberg, doi:10.1007/978-3-642-65520-3_8.

St. Clair J, Moon S, Holbrook WS, Perron JT, Riebe CS, Martel SJ, Carr B, Harman C, Singha K and deB. Richter D 2015, 'Geophysical imaging reveals topographic stress control of bedrock weathering', *Science*, 350(6260):534–538.

Stiner MC 2017, 'Love and Death in the Stone Age: What Constitutes First Evidence of Mortuary Treatment of the Human Body?', *Biological Theory*, 12(4):248–261, doi:10.1007/s13752-017-0275-5.

Stummer P, Maurer H and Green AG 2004, 'Experimental design: Electrical resistivity data sets that provide optimum subsurface information', *GEOPHYSICS*, 69(1):120–139, doi:10.1190/1.1649381.

Stutz L and Tarlow S 2013, 'Beautiful Things and Bones of Desire; Emerging Issues in the Archaeology of Death and Burial', in *The Oxford Handbook of The Archaeology of Death and Burial*.

Sumner M 1993, 'Sodic soils - New perspectives', *Australian Journal of Soil Research*, 31(6):683–750, doi:10.1071/SR9930683.

Swali P, Schulting R, Gilardet A, Kelly M, Anastasiadou K, Gloke I, McCabe J, Williams M, Audsley T, Loe L, Fernandez-Crespo T, Javier O, Walker D, Clare T, Cook G, Hodkinson I, Simpson M, Read S, Davy T, Silva M, Hajdinjak M, Bergstrom A, Booth T and Skoglund P 2023, 'Yersinia Pestis Genomes Reveal Plague in Britain 4000 Years Ago.', *Nature Communications*, 14(2930):1–9, doi:https://doi.org/10.1038/s41467-023-38393-w.

Switzer A and Pile J 2015, 'Grain Size Analysis', in I Shennan, A Long, and BP Horton (eds) *Handbook of sea-level research*, Wiley works, AGU, Wiley, Hoboken, NJ.

Szymczyk M and Szymczyk P 2013, 'Preprocessing of GPR data', *Image Processing and Communication*, 18(2–3):83–90, doi:10.2478/v10248-012-0082-3.

Tabbagh A, Dabas M, Hesse A and Panissod C 2000, 'Soil resistivity: a non-invasive tool to map soil structure horizonation', *Geoderma*, 97(3–4):393–404, doi:10.1016/S0016-7061(00)00047-1.

Trant PLK, Kristiansen SM, Christiansen AV, Wouters B and Sindbæk SM 2021, 'Sampling density and spatial analysis: a methodological pXRF study of the geochemistry of a Viking-Age house in Ribe, Denmark', *Archaeological and Anthropological Sciences*, 13(1):21, doi:10.1007/s12520-020-01243-7.

Tarling D 2007, *Palaeomagnestism Principles and Applications in Geology, Geophysics and Archaeology*, Chapman and Hall, London.

Thorne A and Macumber P 1972, 'Discoveries of Late Pleistocene Man at Kow swamp, Australia', *Nature*, 238:316–319.

Trinks I and Hinterleitner A 2020, 'Beyond Amplitudes: Multi-Trace Coherence Analysis for Ground-Penetrating Radar Data Imaging', *Remote Sensing*, 12(10):1583, doi:10.3390/rs12101583.

Turnbull P 2007, 'Scientific Theft of Remains in Colonial Australia', *Australian Indigenous Law Review*, 11(1):92–102.

Uhlemann S, Wilkinson PB, Maurer H, Wagner F, Johnson T and Chambers J 2018, 'Optimized survey design for Electrical Resistivity Tomography: combined optimization of measurement configuration and electrode placement.', *Geophysical Journal International*, 214(1):108–121, doi:https://doi.org/10.1093/gji/ggy128.

University of New South Wales 2007, *TerraGIS*, http://www.terragis.bees.unsw.edu.au/index.html, accessed 27 April 2023.

Van Belle LE, Carter DO and Forbes SL 2009, 'Measurement of ninhydrin reactive nitrogen influx into gravesoil during aboveground and belowground carcass (Sus domesticus) decomposition', *Forensic Science International*, 193(1–3):37–41, doi:10.1016/j.forsciint.2009.08.016.

Van Dam RL, Van Den Berg EH, Schaap MG, Broekema LH and Schlager W 2003, 'Radar reflections from sedimentary structures in the vadose zone', *Geological Society, London, Special Publications*, 211(1):257–273, doi:10.1144/GSL.SP.2001.211.01.21.

Vass AA 2001, 'Beyond the grave – understanding human decomposition', *Microbiology Today*, 28:190–193.

Viscarra Rossel RA 2011, 'Fine-resolution multiscale mapping of clay minerals in Australian soils measured with near infrared spectra', *Journal of Geophysical Research*, 116(F4):F04023, doi:10.1029/2011JF001977.

Wadsworth WTD, Bank C-G, Patton K and Doroszenko D 2020, 'Forgotten Souls of the Dawn Settlement: A Multicomponent Geophysical Survey of Unmarked Graves at the British American Institute Cemetery', *Historical Archaeology*, 54(3):624–646, doi:10.1007/s41636-020-00251-7.

Wald JA, Graham RC and Schoeneberger PJ 2013, 'Distribution and properties of soft weathered bedrock at ≤ 1 m depth in the contiguous United States', *Earth Surface Processes and Landforms*, 38(6):614–626, doi:10.1002/esp.3343.

Wallis L, Moffat I, Trevorrow G and Massey T 2008, 'Locating Places for Repatriated Burial: A Case Study from Ngarrindjeri Ruwe, South Australia', *Antiquity*, 82:750–760.

War Graves on the 1914-1918 Western Front n.d., http://www.greatwar.co.uk/war-graves/ww1-war-graves.htm, accessed 25 May 2023.

Watters M and Hunter JR 2004, 'Geophysics and burials: field experience and software development', *Geological Society, London, Special Publications*, 232(1):21–31, doi:10.1144/GSL.SP.2004.232.01.04.

Westendorp M and Gould H 2021, 'Re-Feminizing Death: Gender, Spirituality and Death Care in the Anthropocene', *Religions*, 12(8):667, doi:10.3390/rel12080667.

White R 2006, *Pricipals and Practice of Soil Science. the Soil as a Natural Resouce.*, fourth, Blackwell Science.

Wiberg A and Jonsson H 2017, 'Application of ERT and IP for localisation of chlorinated hydrocarbons at a former dry-cleaning facility' MSc, Lund University.

Williams R, Taylor G and Orr C 2020, 'pXRF method development for elemental analysis of archaeological soil', *Archaeometry*, 62(6):1145–1163, doi:10.1111/arcm.12583.

Witten A 2006, *Handbook of Geophysics and Archaeology*, Equinox Publishing, London.

Xiong H, Devegowda D and Huang L 2020, 'Water Bridges in Clay Nanopores: Mechanisms of Formation and Impact on Hydrocarbon Transport', *Langmuir*, 36(3):723–733, doi:10.1021/acs.langmuir.9b03244.

Xygalatas D 2022, *How burying the dead keeps the living human*, *The Conversation*, http://theconversation.com/how-burying-the-dead-keeps-the-living-human-181590, accessed 26 May 2023.

Yelf R and Yelf D 2004, 'Where Is True Time Zero?', in *Proceedings of the Tenth International Conference on Grounds Penetrating Radar*, *GPR 2002*, IEEE.

Zadhoush H and Giannopoulos A 2022, 'Optimizing GPR time-zero adjustment and two-way travel time wavelet measurements using a realistic three-dimensional numerical model', *Near Surface Geophysics*, 20(2):208–226, doi:10.1002/nsg.12193.

Zhang L, Tang J, Li Y, Liu Z, Chen W and Li G 2022, 'GPR denoising via shearlet transformation and a data-driven tight frame', *Near Surface Geophysics*, 20(4):398–418, doi:10.1002/nsg.12212.

Zhang XC and Norton LD 2002, 'Effect of exchangeable Mg on saturated hydraulic conductivity, disaggregation and clay dispersion of disturbed soils', *Journal of Hydrology*, 260(1):194–205, doi:10.1016/S0022-1694(01)00612-6.

Zhou J, Revil A, Karaoulis M, Hale D, Doetsch J and Cuttler S 2014, 'Image-guided inversion of electrical resistivity data', *Geophysical Journal International*, 197(1):292–309, doi:10.1093/gji/ggu001.

7 APPENDICES

7.1 Appendix A Ground Penetrating Radar results

7.1.1 Keith Cemetery Radargrams

Keith Cemetery rows H and I. Data captured August 2020

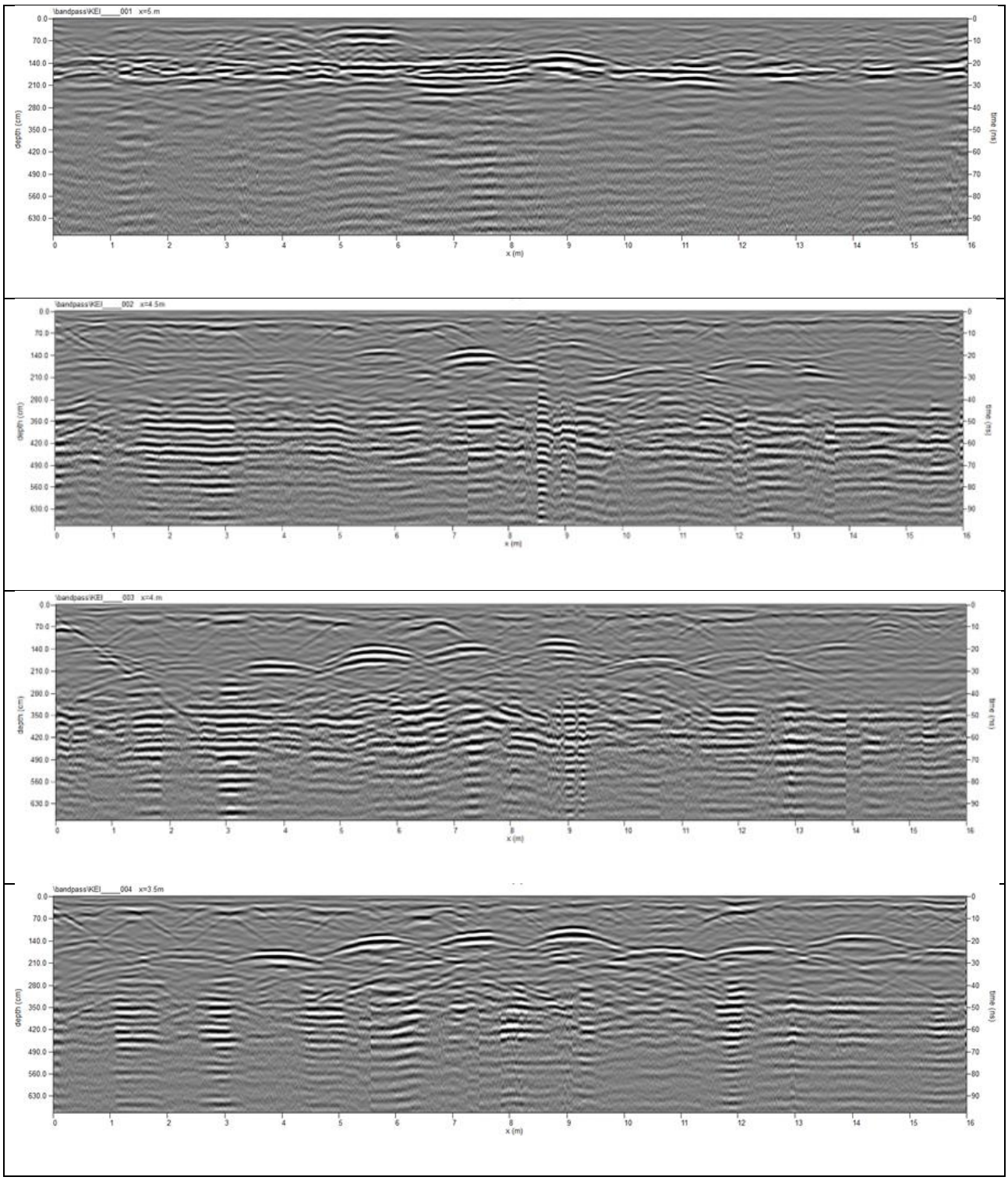

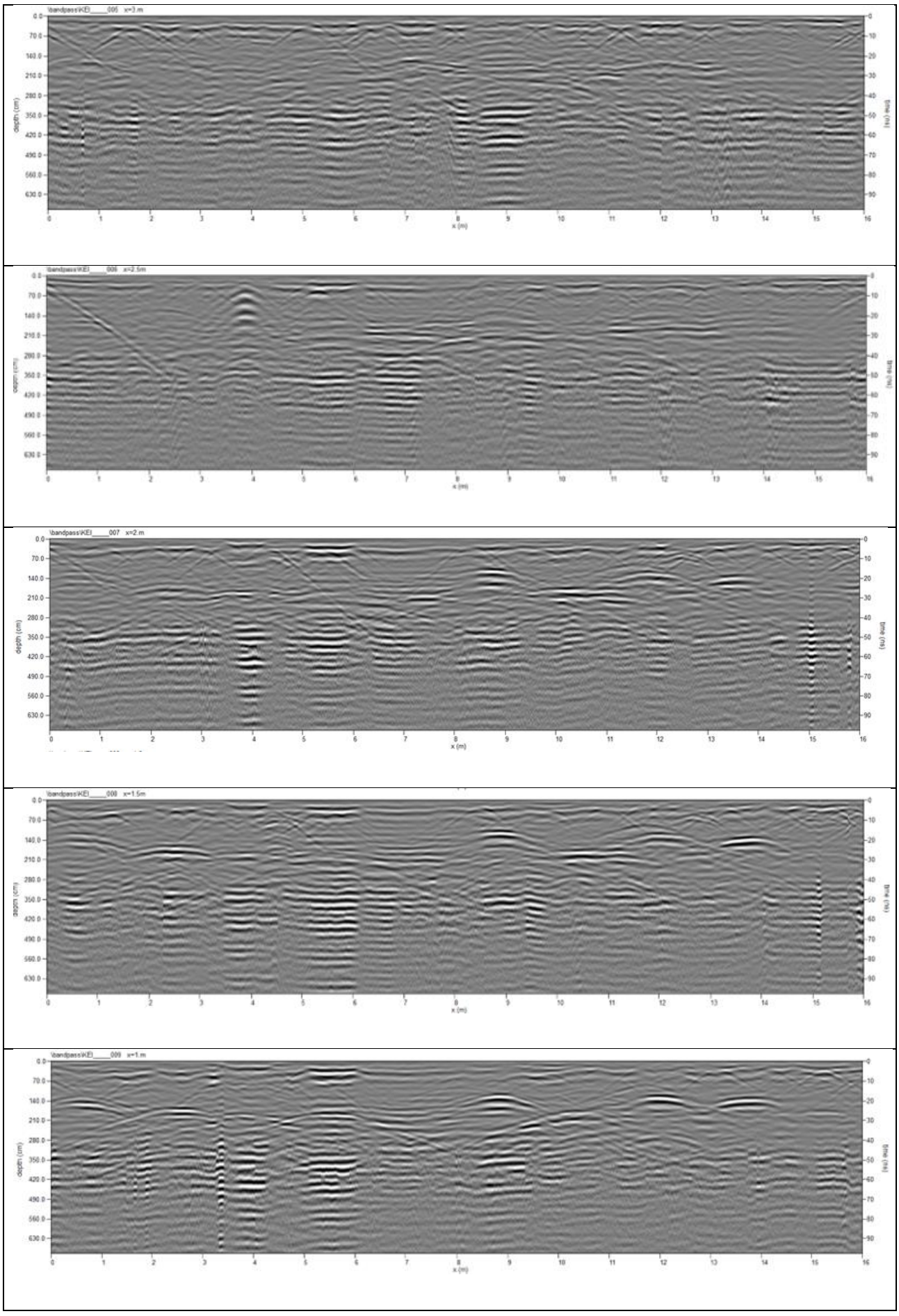
\bandpass\KEI____005 x=3 m
\bandpass\KEI____006 x=2.5m
\bandpass\KEI____007 x=2 m
\bandpass\KEI____008 x=1.5m
\bandpass\KEI____009 x=1 m
depth (cm)
time (ns)
x (m)

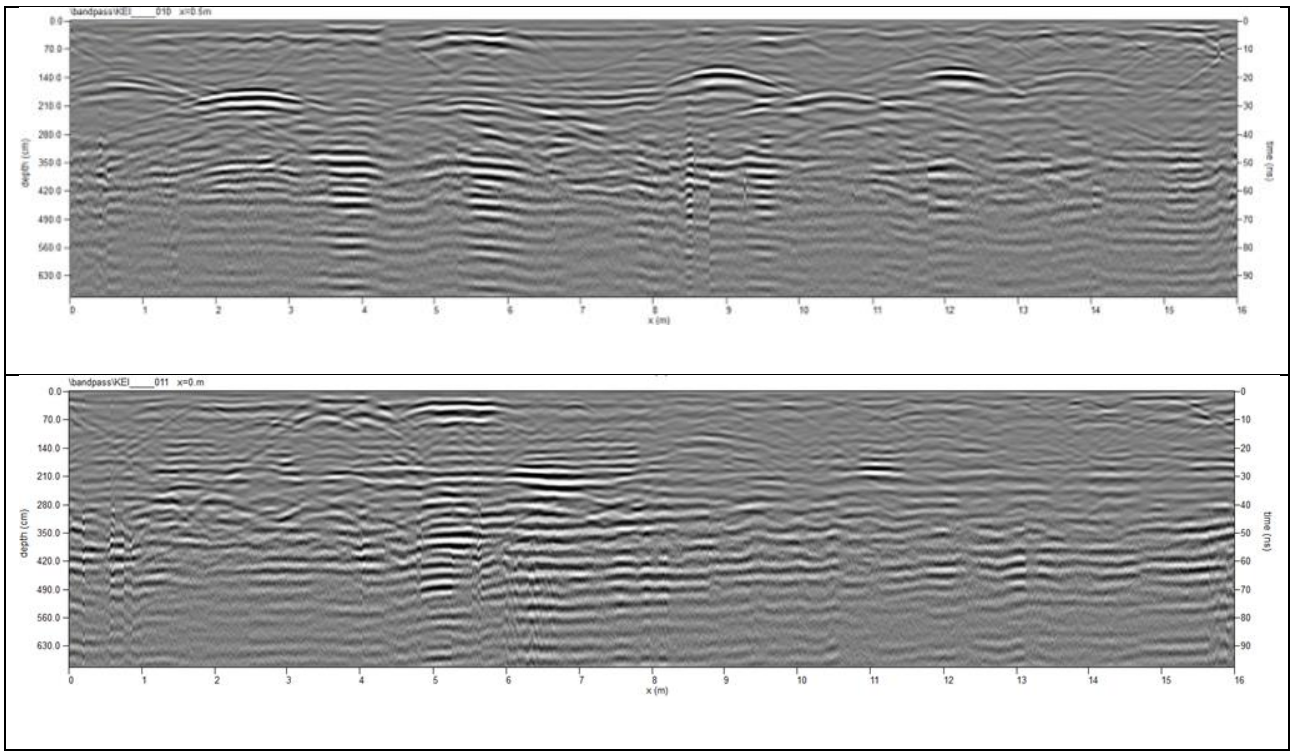

Keith Cemetery Rows H and I. Data collected October 2020

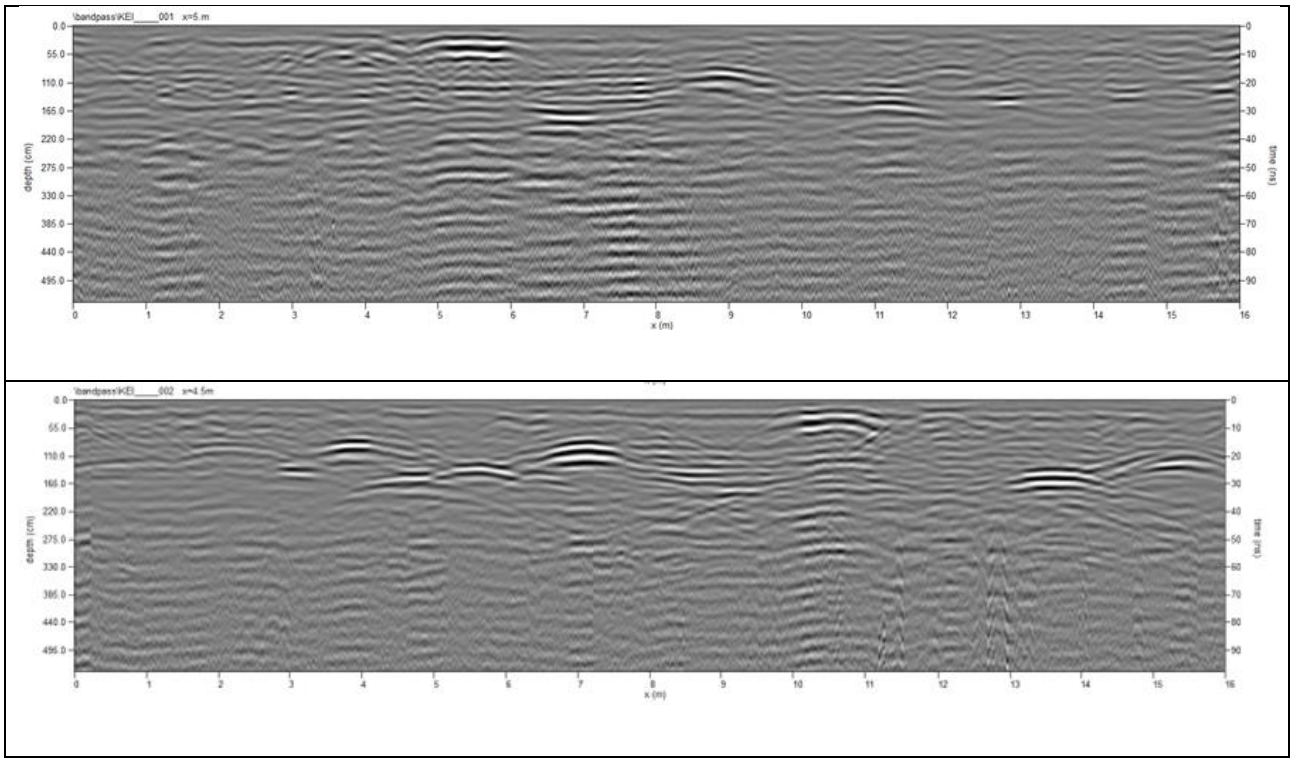

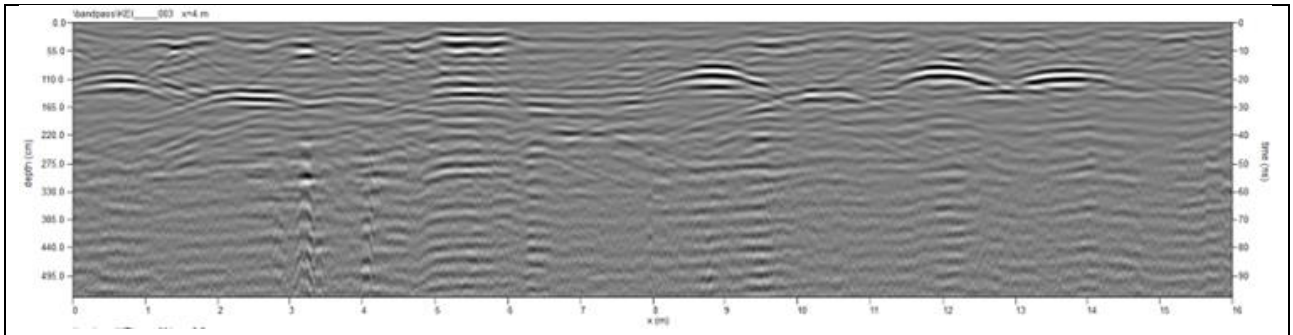
\bandpass\KEI____003 x=4 m
depth (cm)
time (ns)
x (m)

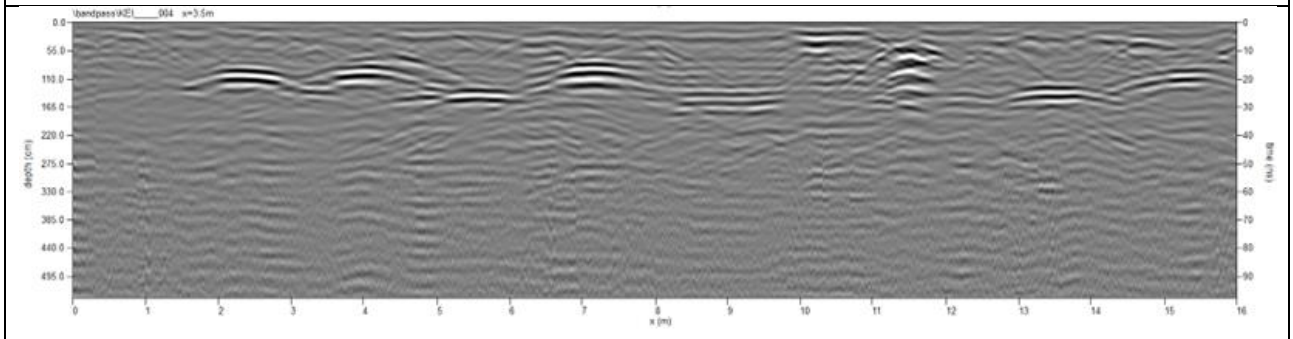
\bandpass\KEI____004 x=3.5m
depth (cm)
time (ns)
x (m)

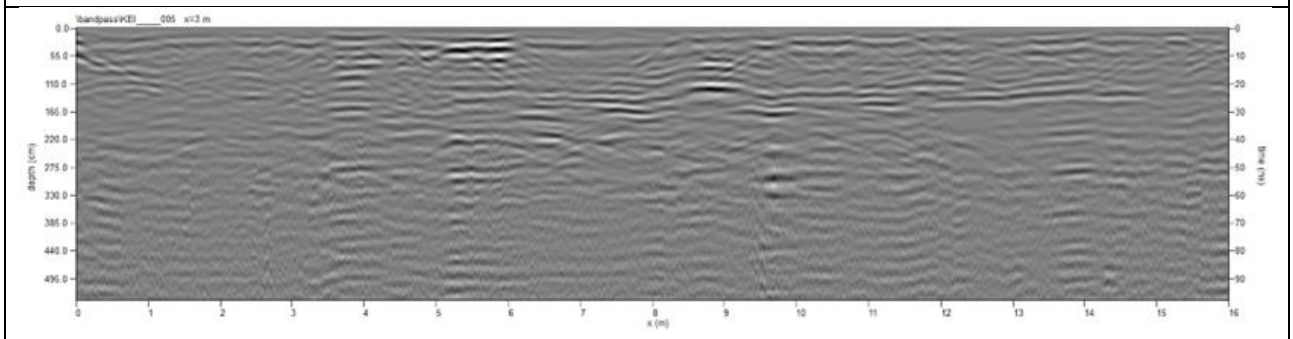
\bandpass\KEI____005 x=3 m
depth (cm)
time (ns)
x (m)

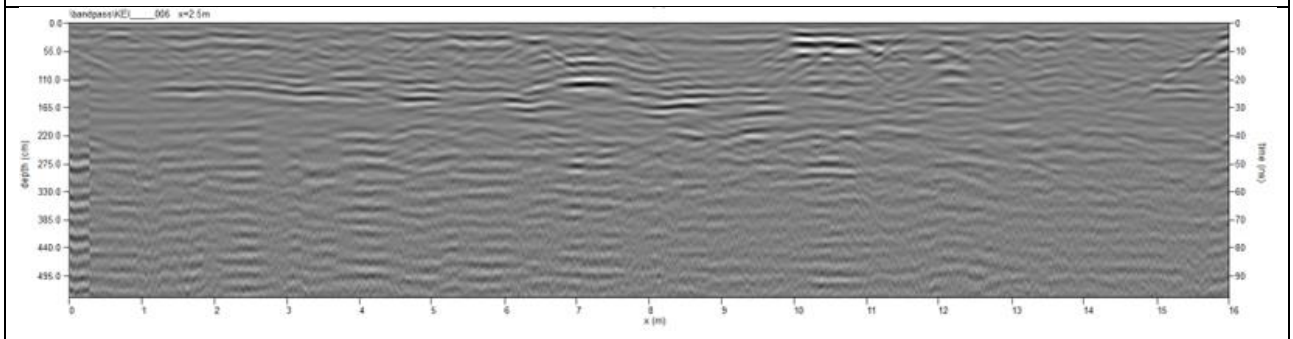
\bandpass\KEI____006 x=2.5m
depth (cm)
time (ns)
x (m)

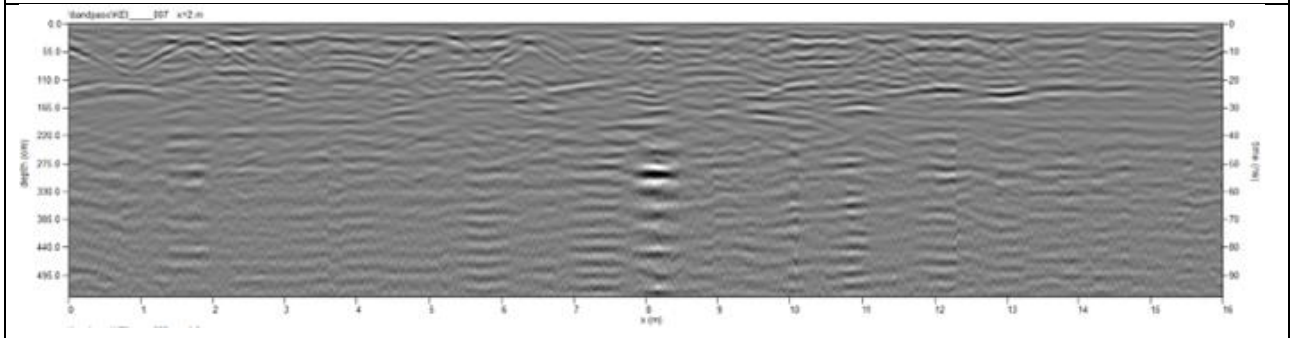
\bandpass\KEI____007 x=2 m
depth (cm)
time (ns)
x (m)

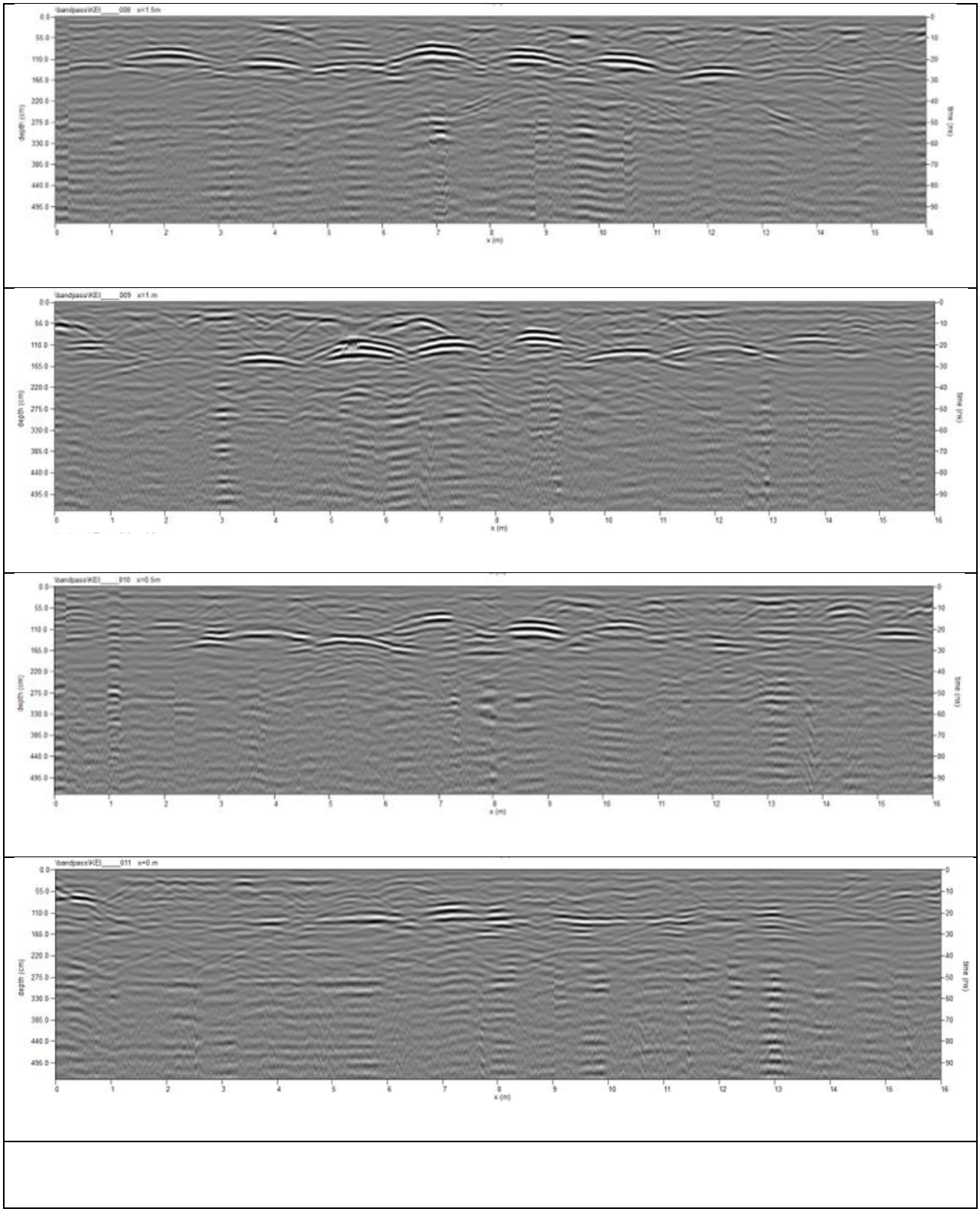

Keith Cemetery rows H and I. Data collected January 2021

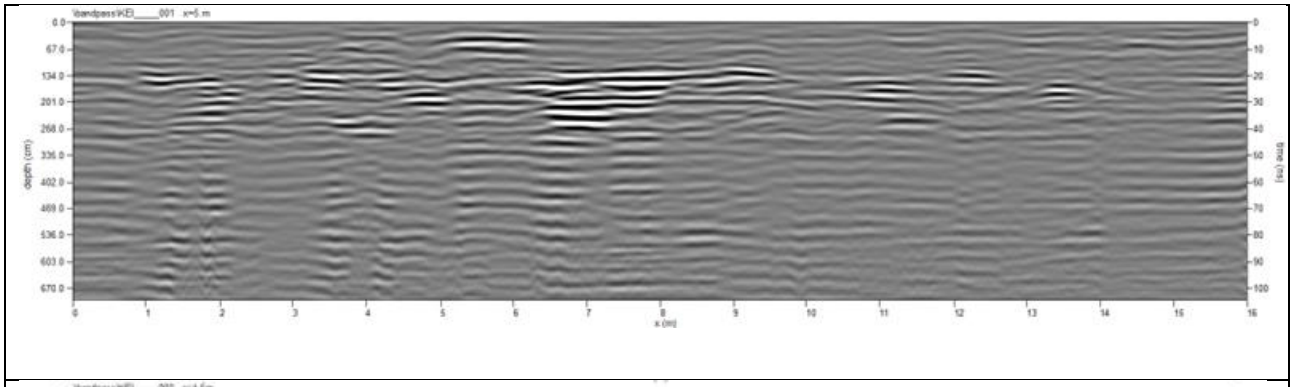
\bandpass\KEI_____001 x=5 m
depth (cm)
time (ns)
x (m)

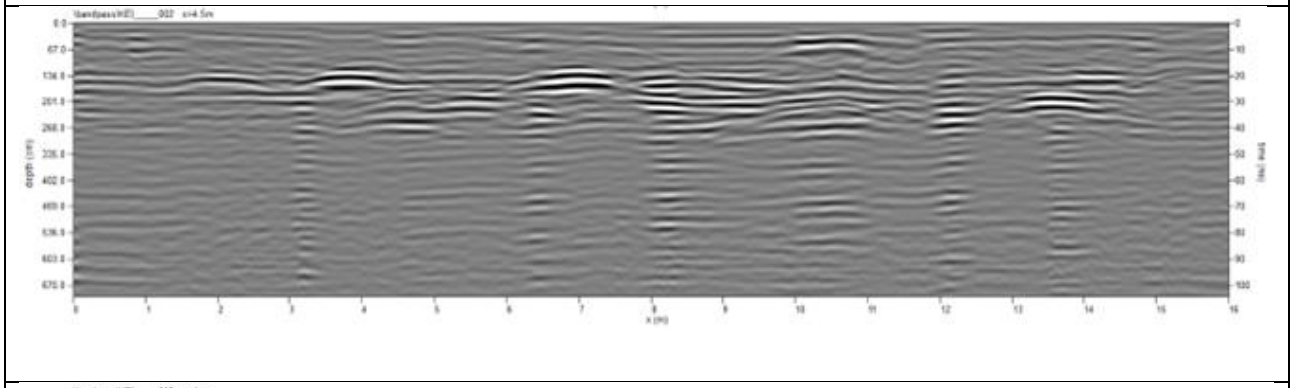
\bandpass\KEI_____002 x=4.5m
depth (cm)
time (ns)
x (m)

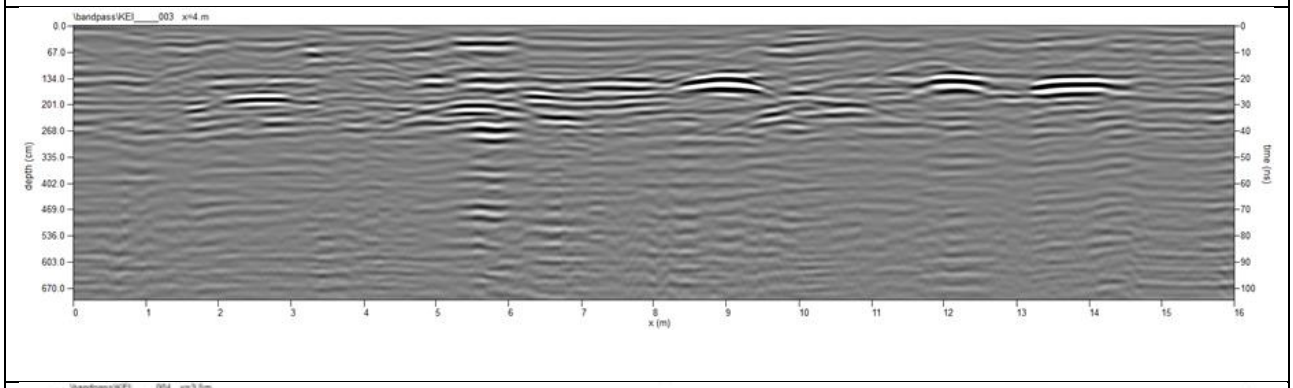
\bandpass\KEI_____003 x=4 m
depth (cm)
time (ns)
x (m)

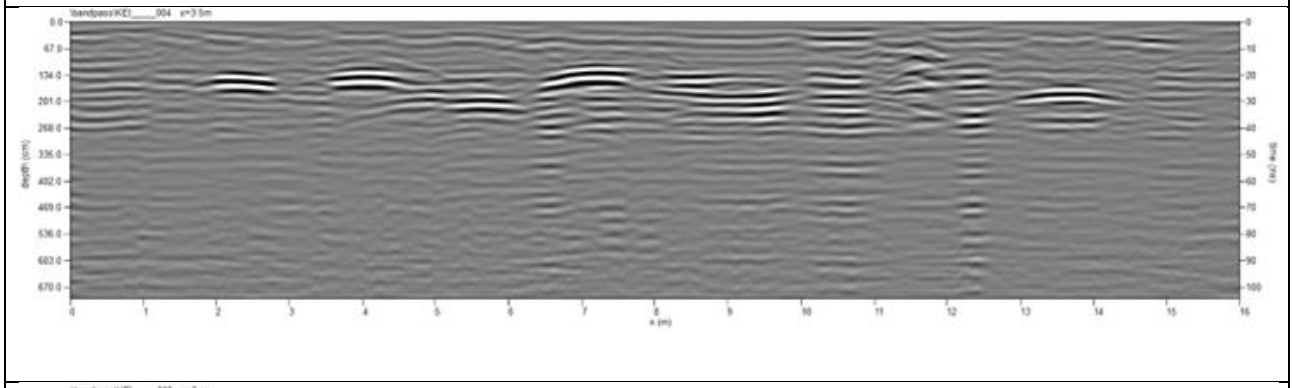
\bandpass\KEI_____004 x=3.5m
depth (cm)
time (ns)
x (m)

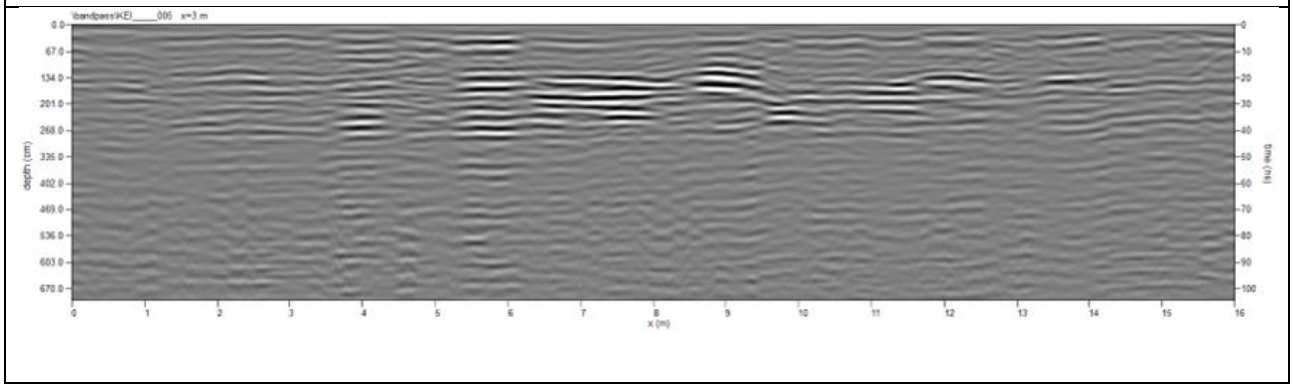
\bandpass\KEI_____005 x=3 m
depth (cm)
time (ns)
x (m)

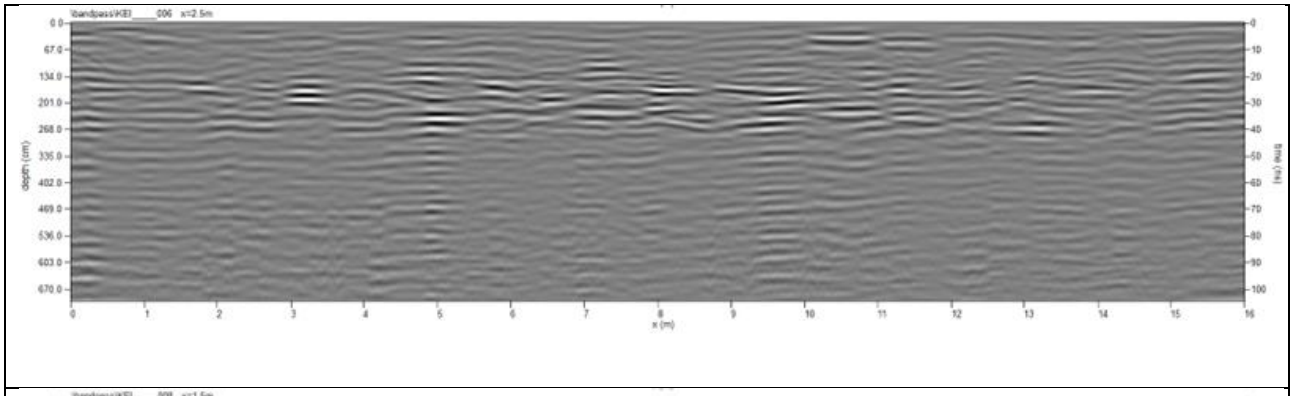
\bandpass\KEI____006 x=2.5m
depth (cm)
time (ns)
x (m)

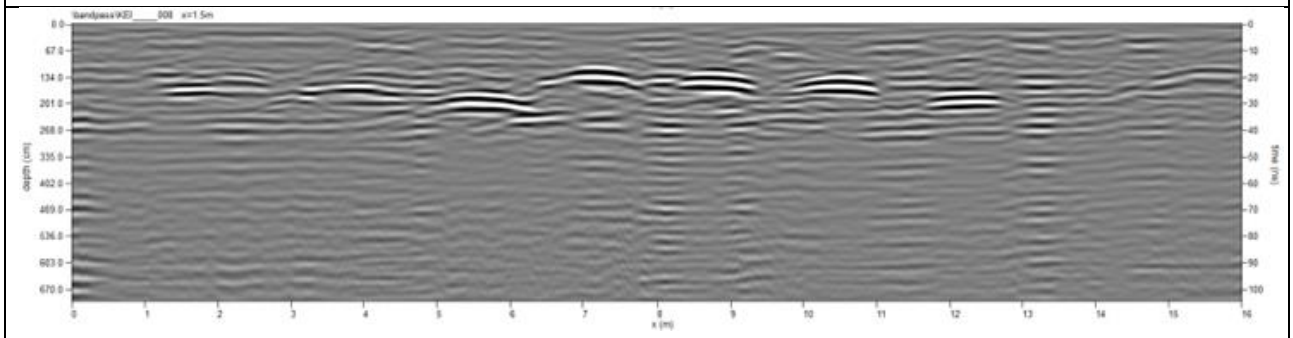
\bandpass\KEI____008 x=1.5m
depth (cm)
time (ns)
x (m)

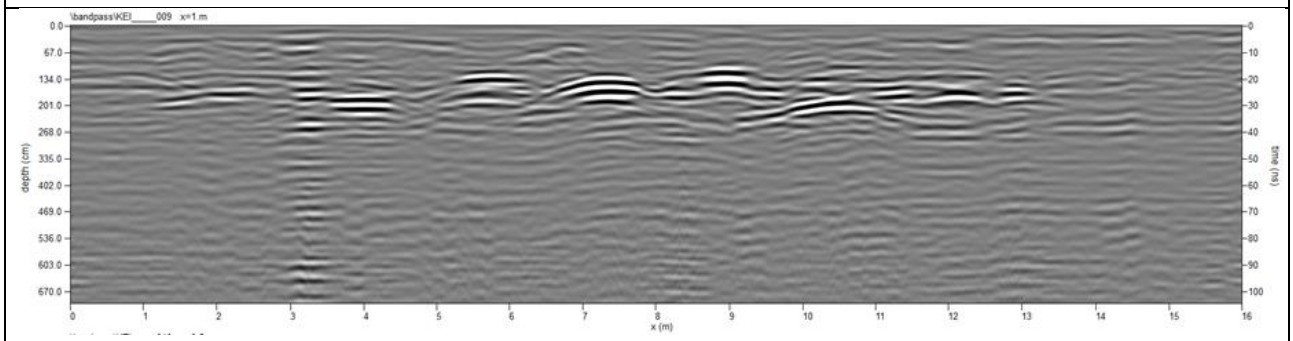
\bandpass\KEI____009 x=1.m
depth (cm)
time (ns)
x (m)

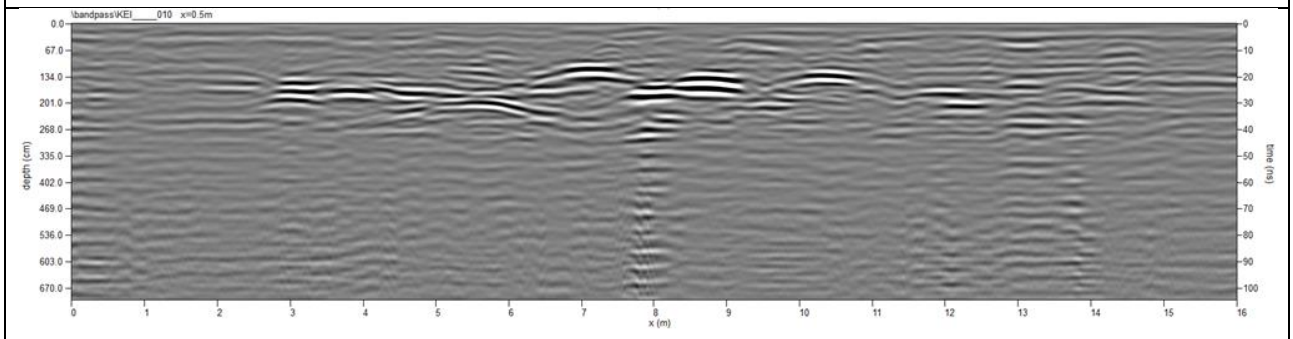
\bandpass\KEI____010 x=0.5m
depth (cm)
time (ns)
x (m)

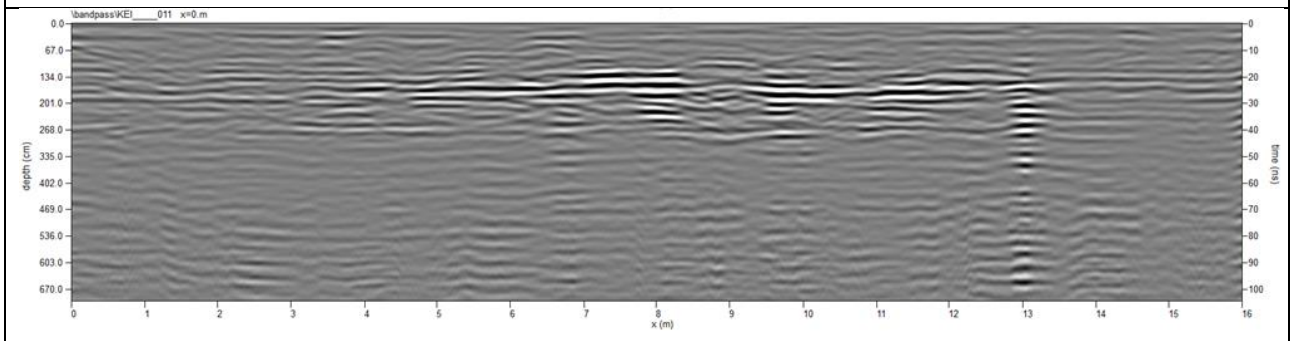
\bandpass\KEI____011 x=0.m
depth (cm)
time (ns)
x (m)

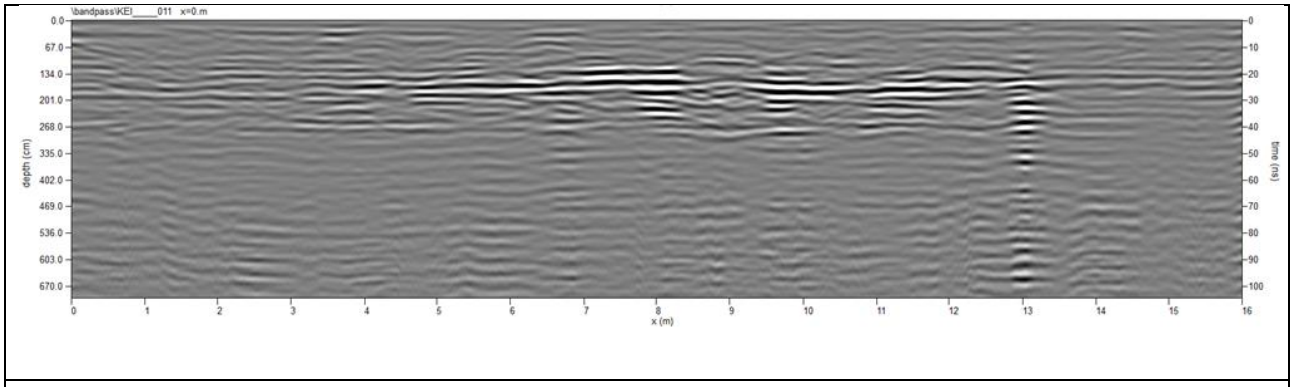

Keith Cemetery rows H and I. Data collected January 2022

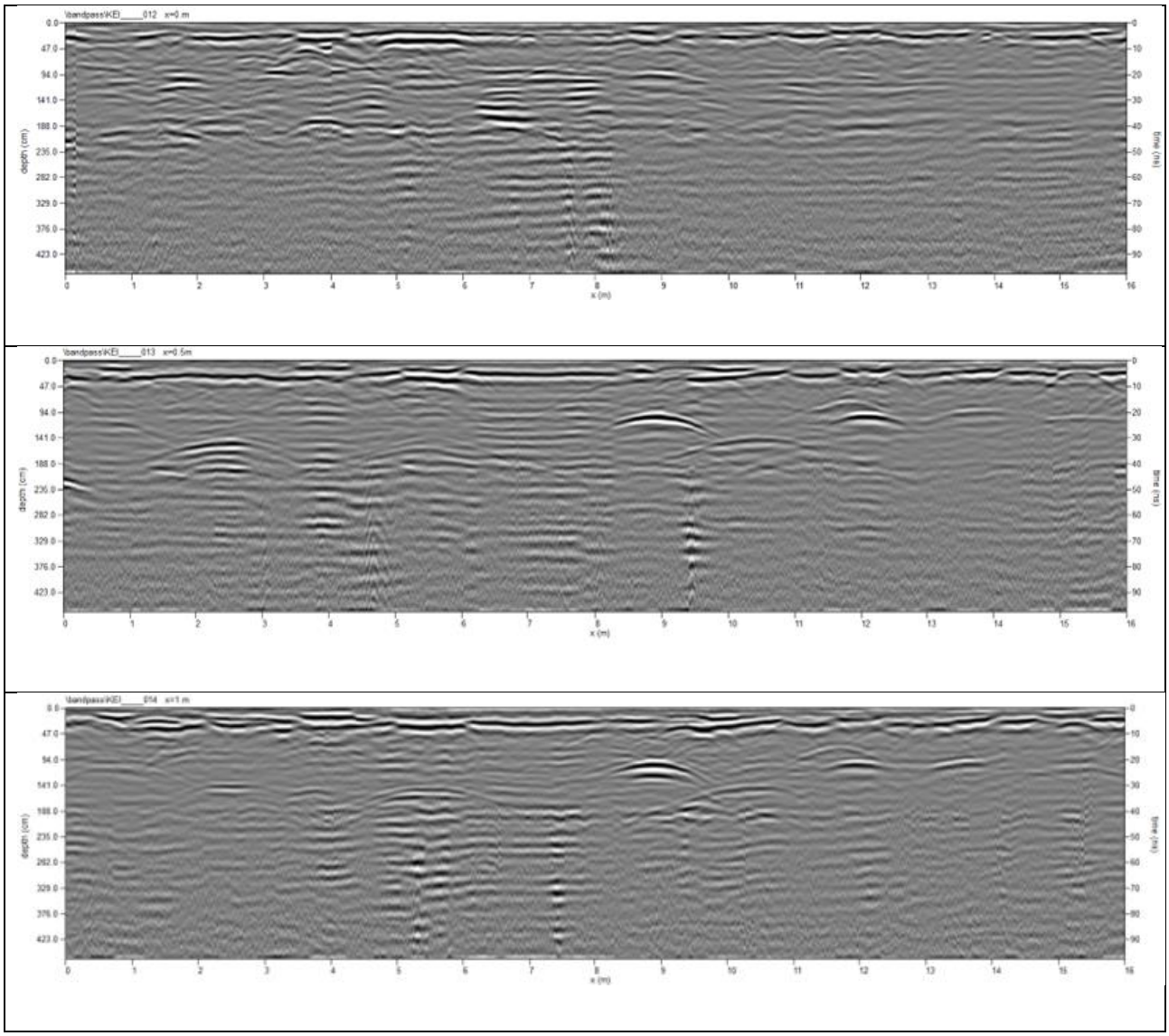

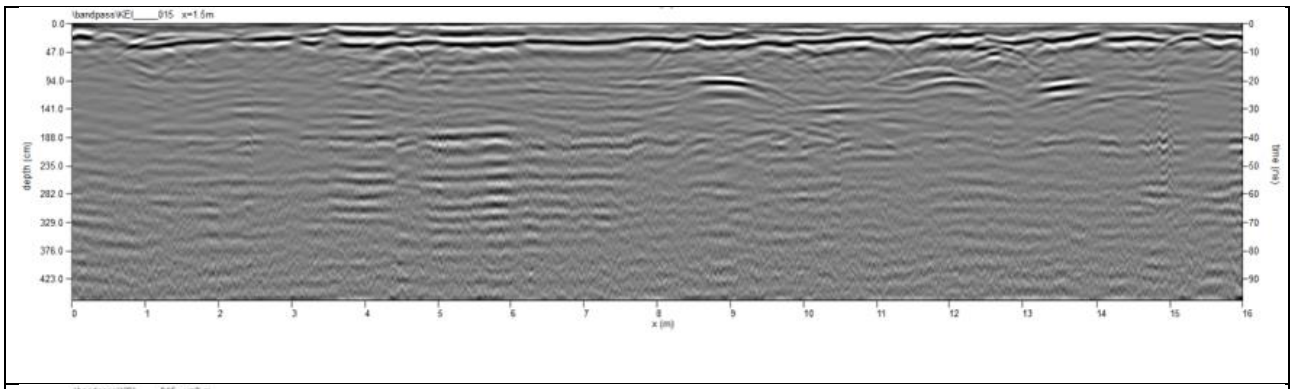
\bandpass\KEI____015 x=1.5m
depth (cm)
x (m)
time (ns)

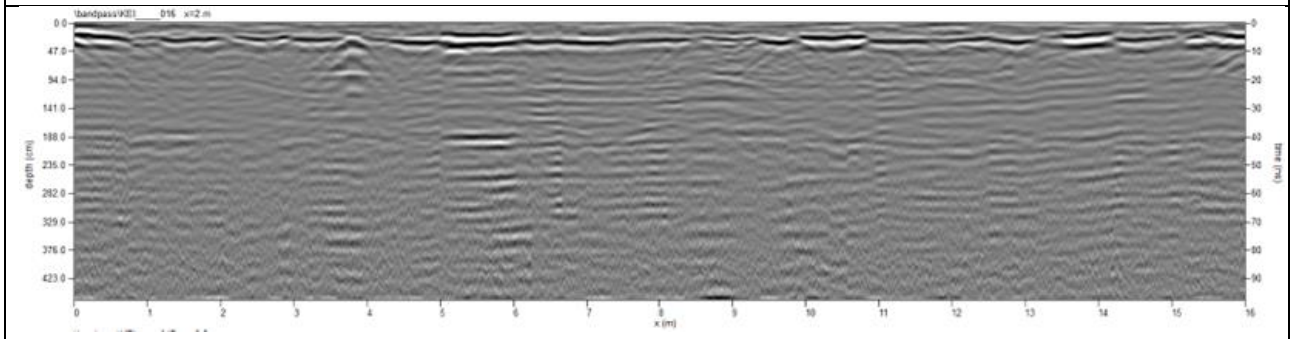
\bandpass\KEI____016 x=2 m
depth (cm)
x (m)
time (ns)

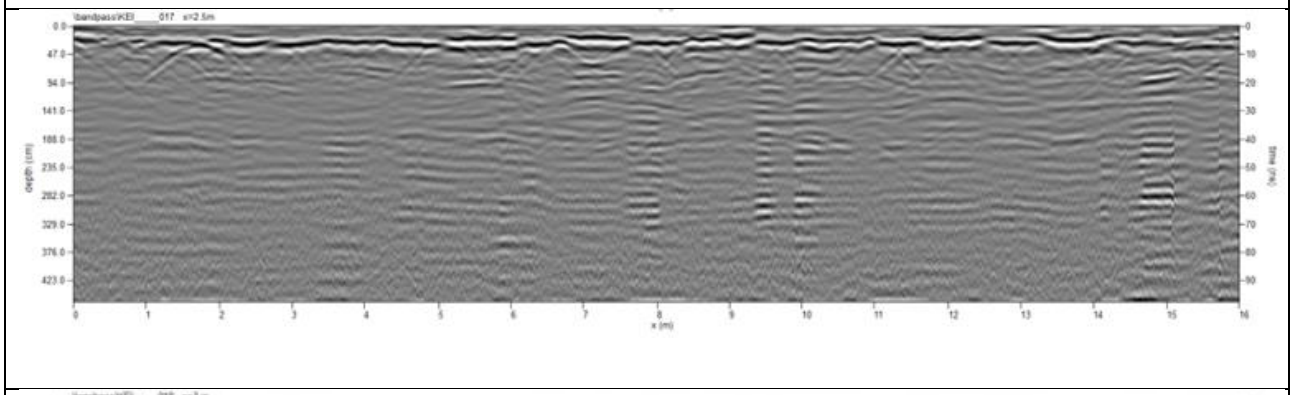
\bandpass\KEI____017 x=2.5m
depth (cm)
x (m)
time (ns)

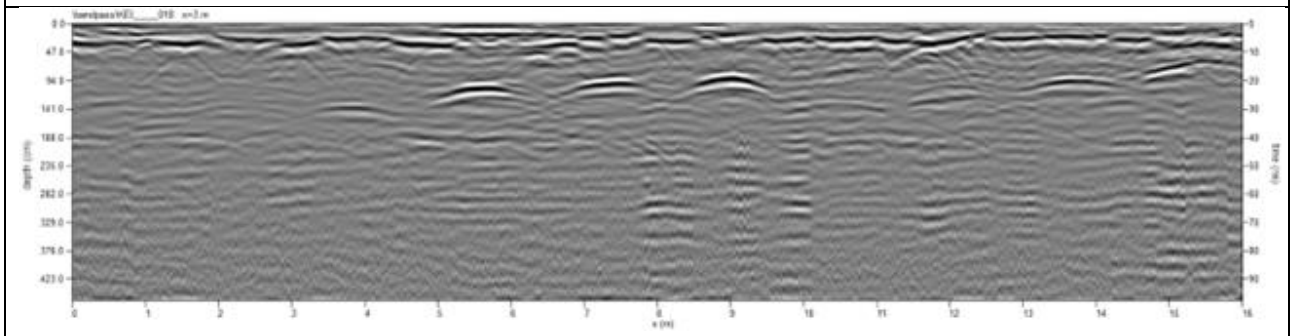
depth (cm)
x (m)
time (ns)

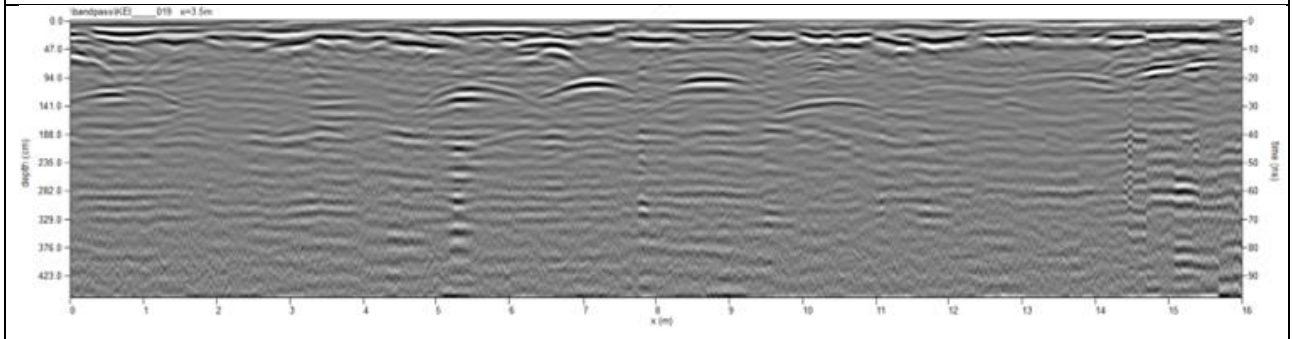
\bandpass\KEI____019 x=3.5m
depth (cm)
x (m)
time (ns)

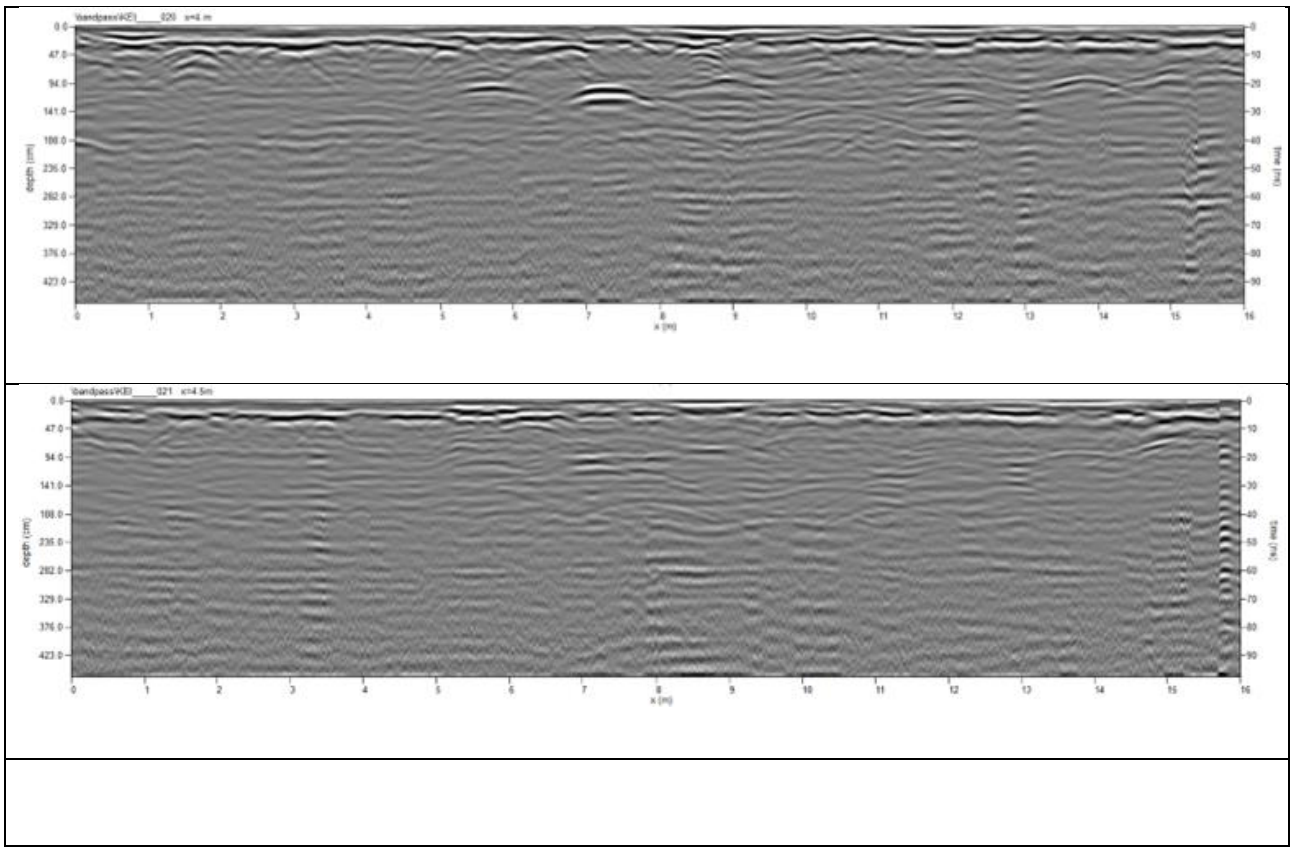

Keith Cemetery rows H and I. Data collected May 2022

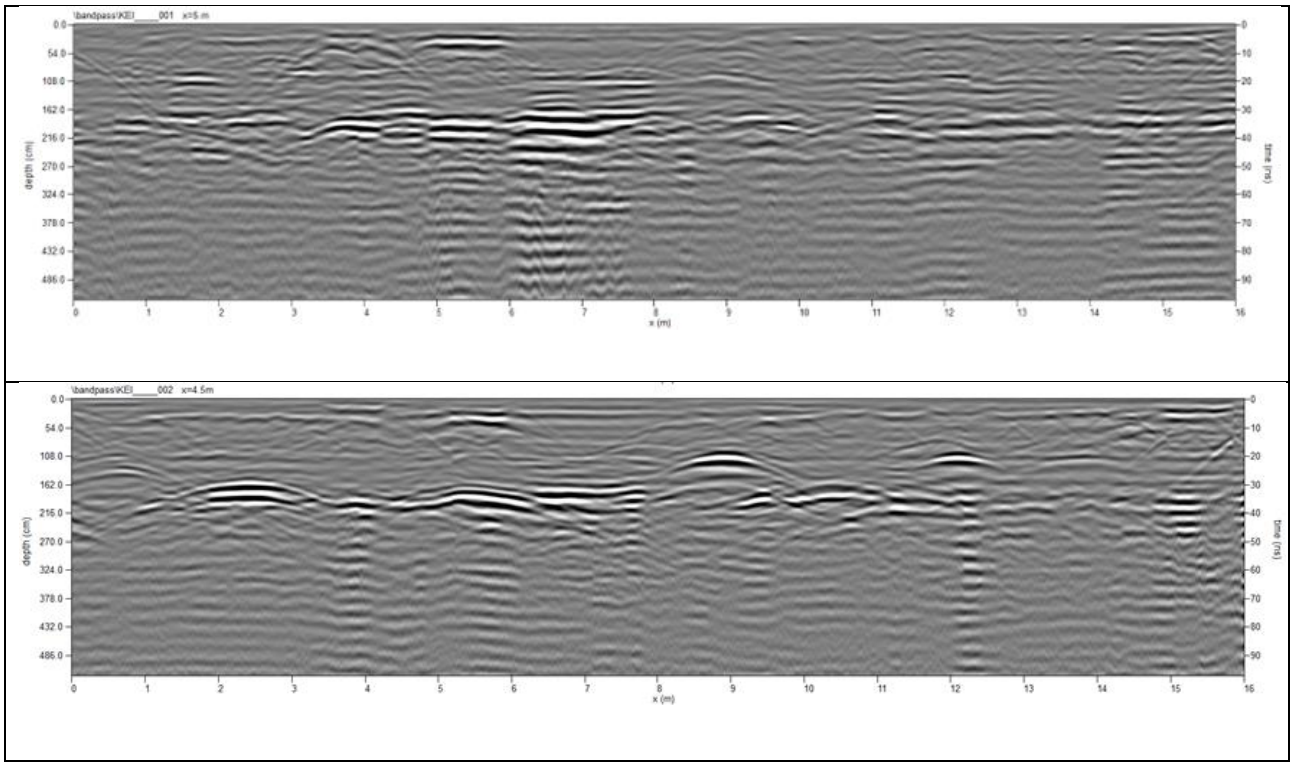

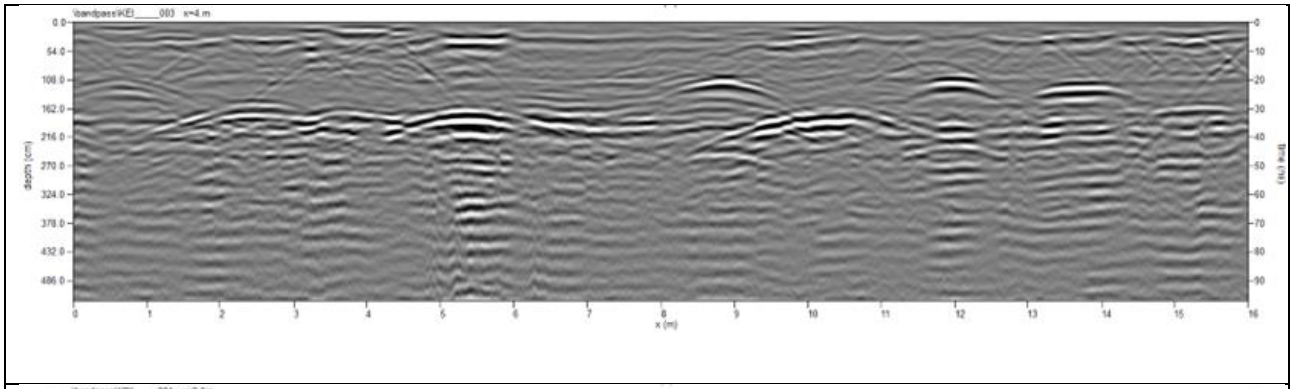
\bandpass\KEI____003 x=4 m
depth (cm)
x (m)
time (ns)

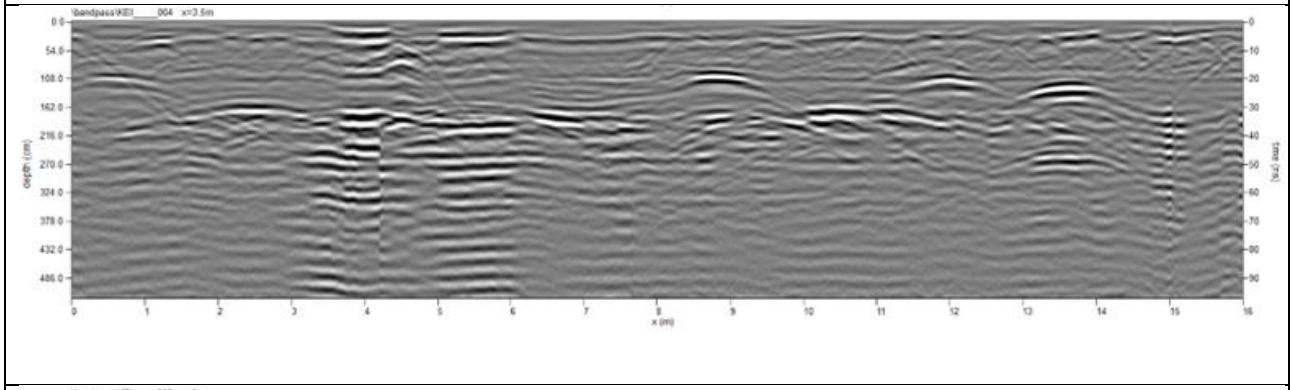
\bandpass\KEI____004 x=3.5m
depth (cm)
x (m)
time (ns)

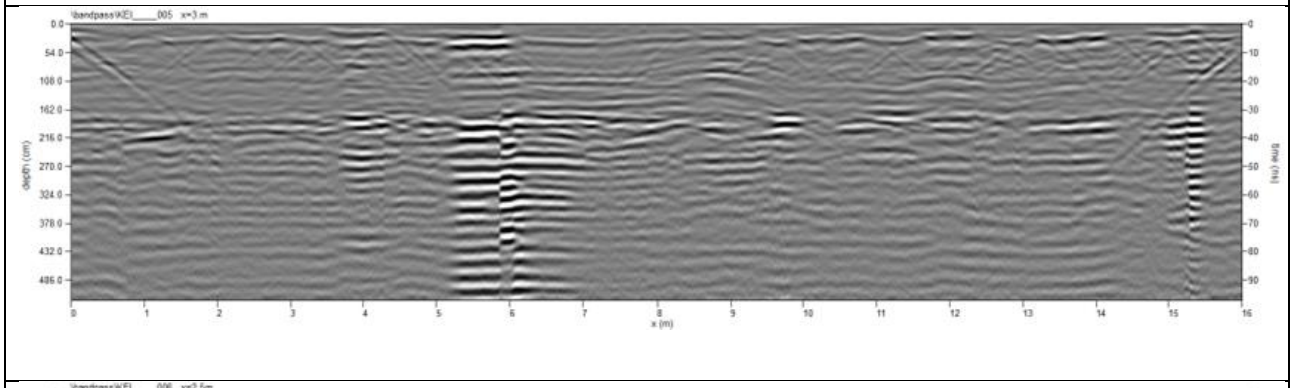
\bandpass\KEI____005 x=3 m
depth (cm)
x (m)
time (ns)

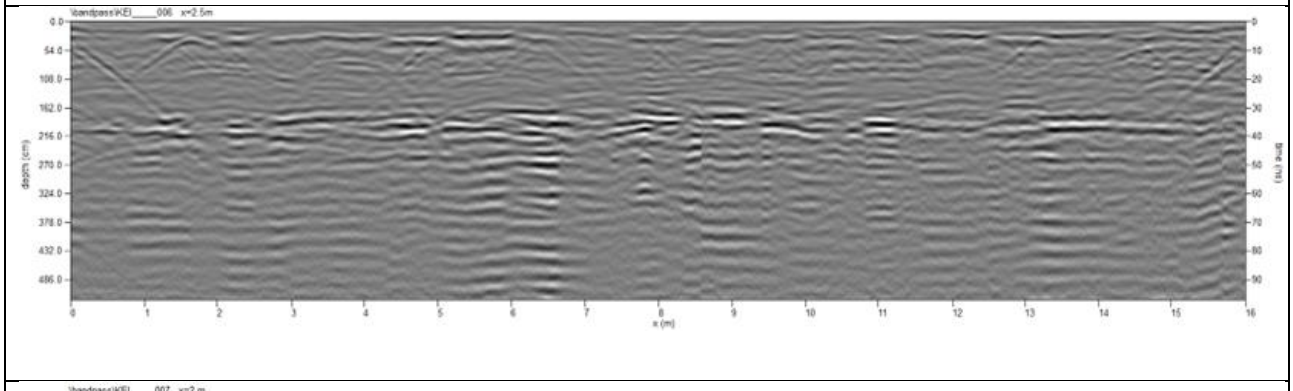
\bandpass\KEI____006 x=2.5m
depth (cm)
x (m)
time (ns)

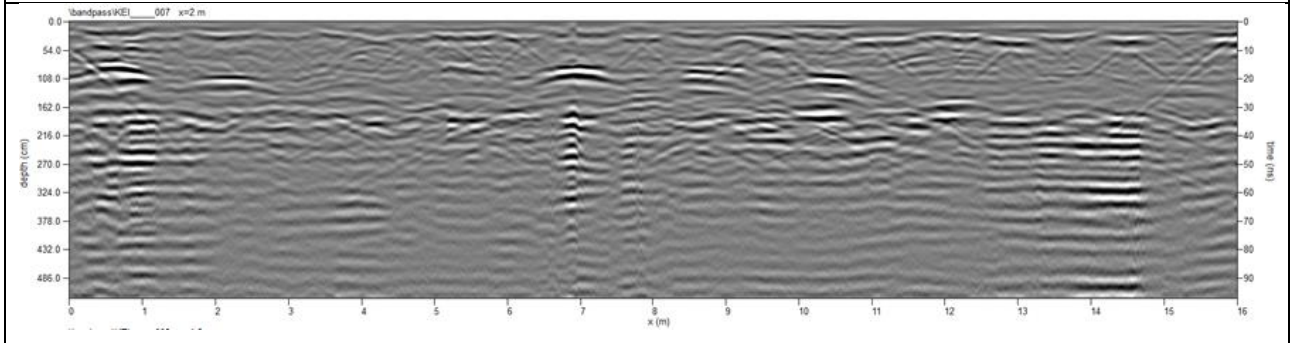
\bandpass\KEI____007 x=2 m
depth (cm)
x (m)
time (ns)

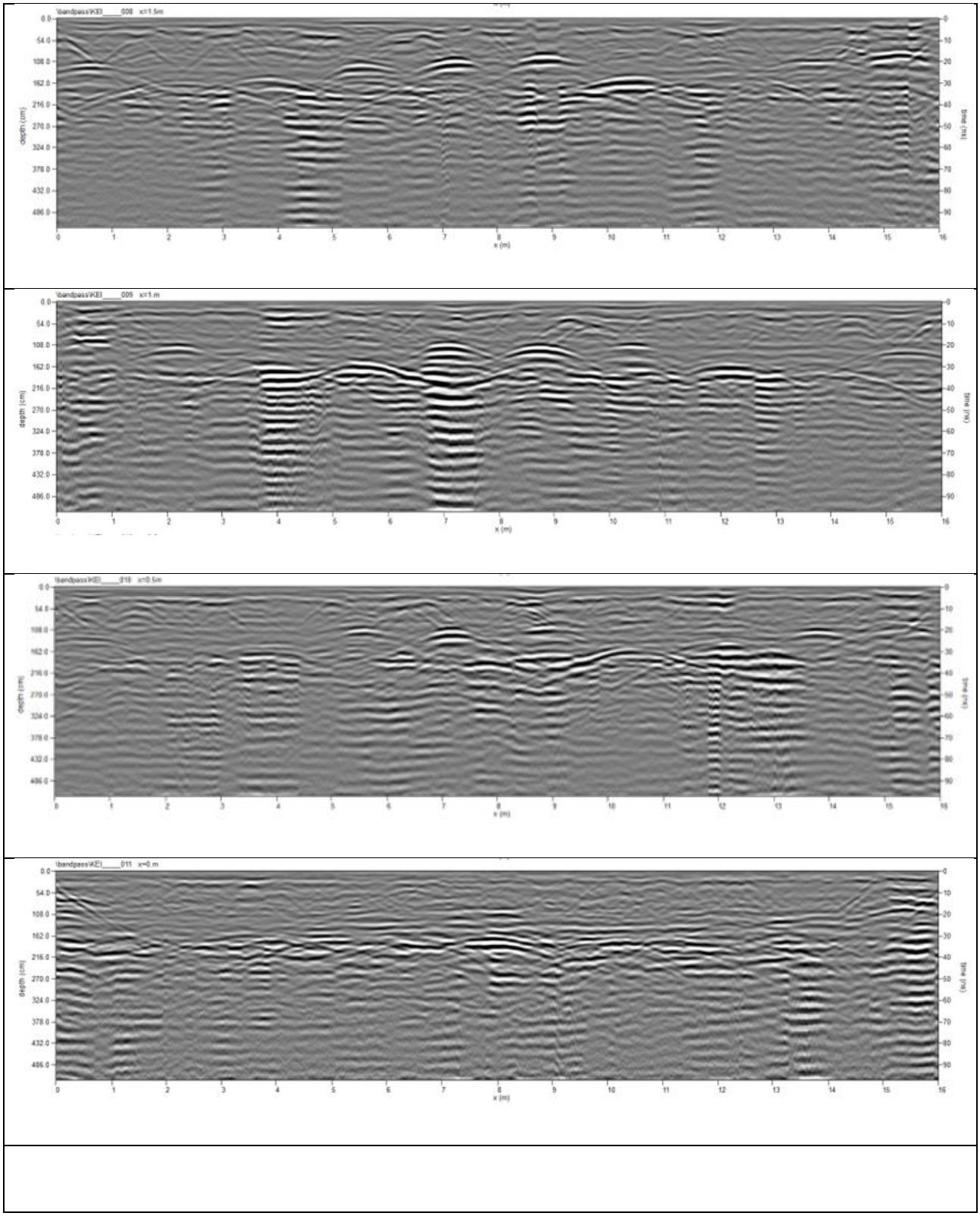

Keith Cemetery rows H and I. Data collected July 2022

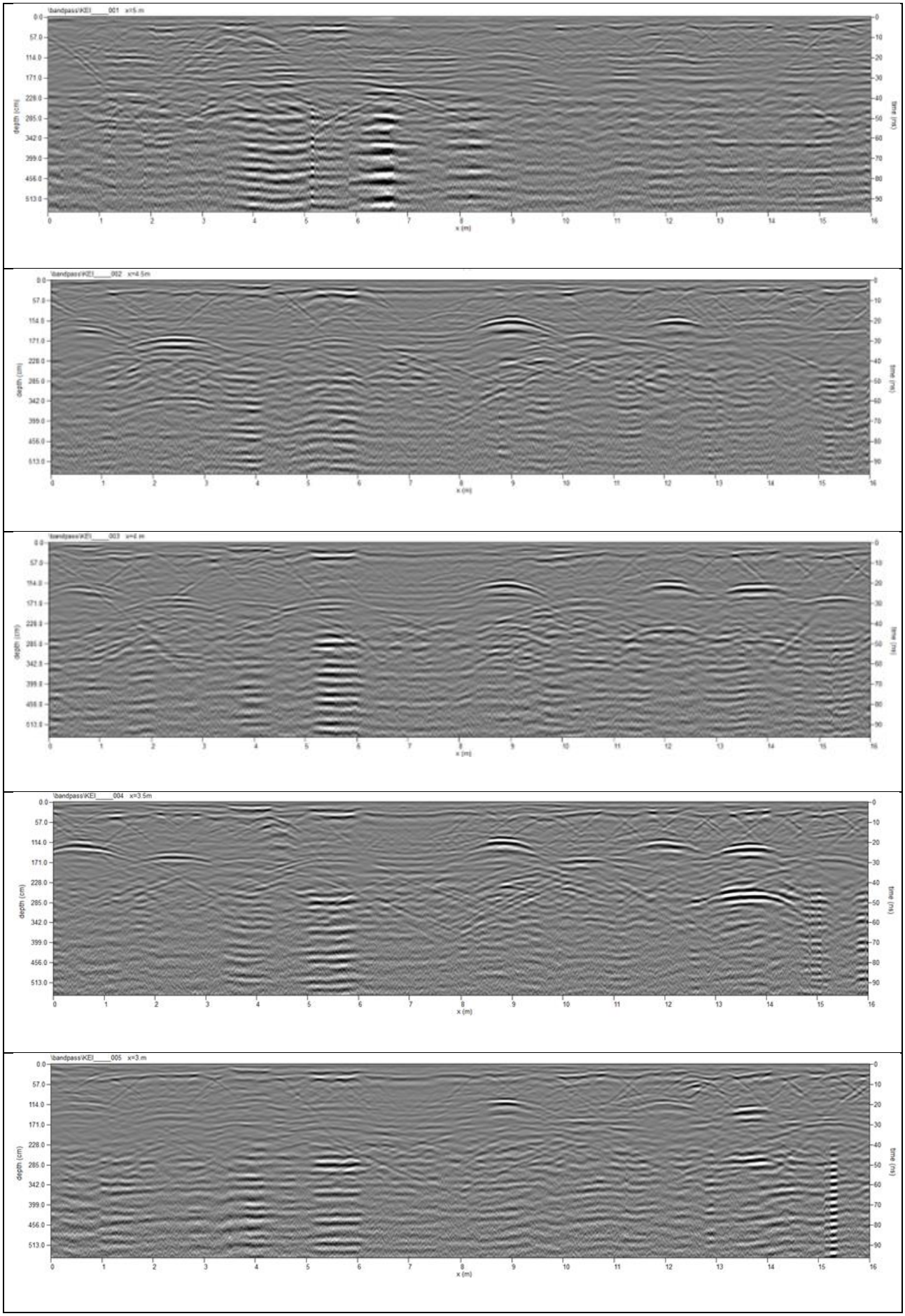
\bandpass\KEI_____001 x=5 m
\bandpass\KEI_____002 x=4.5m
\bandpass\KEI_____003 x=4 m
\bandpass\KEI_____004 x=3.5m
\bandpass\KEI_____005 x=3 m
depth (cm)
time (ns)
x (m)

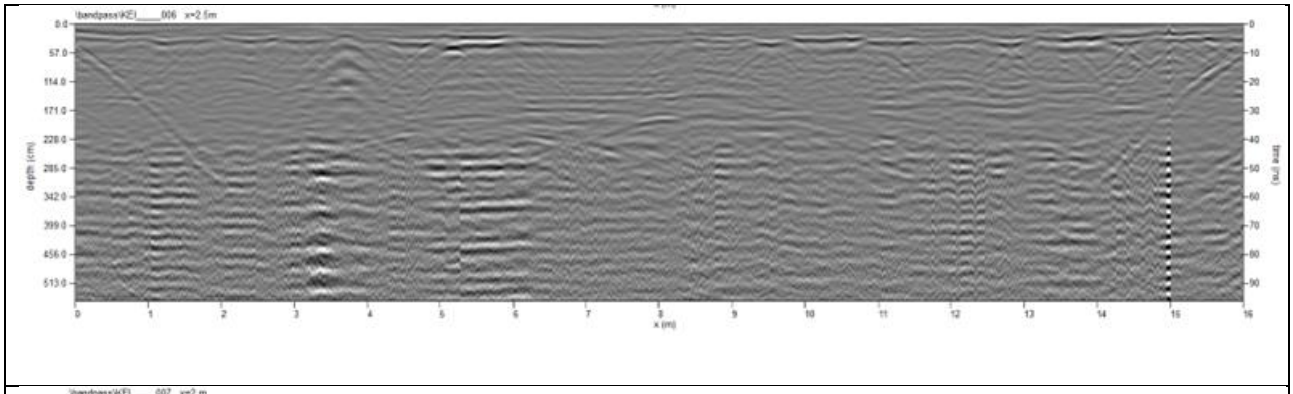
\bandpass\KEI____006 x=2.5m
depth (cm)
time (ns)
x (m)

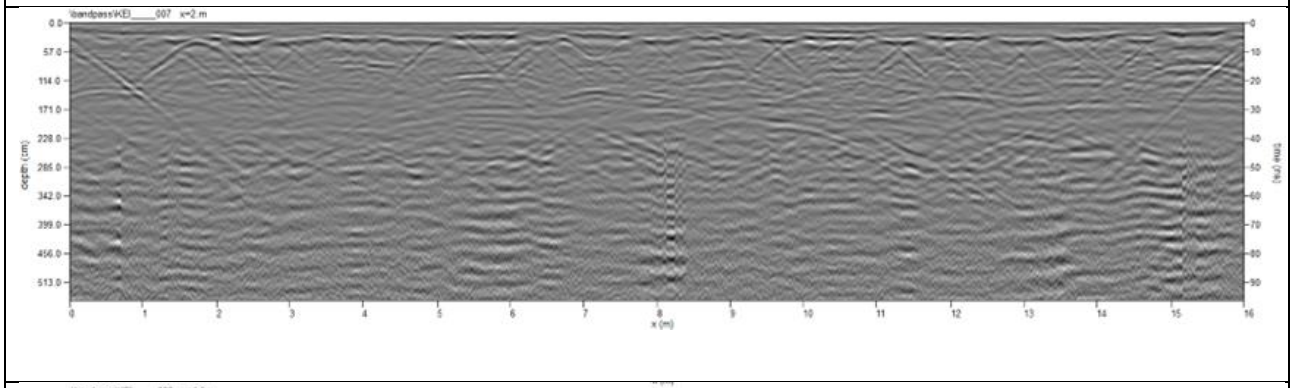
\bandpass\KEI____007 x=2.m
depth (cm)
time (ns)
x (m)

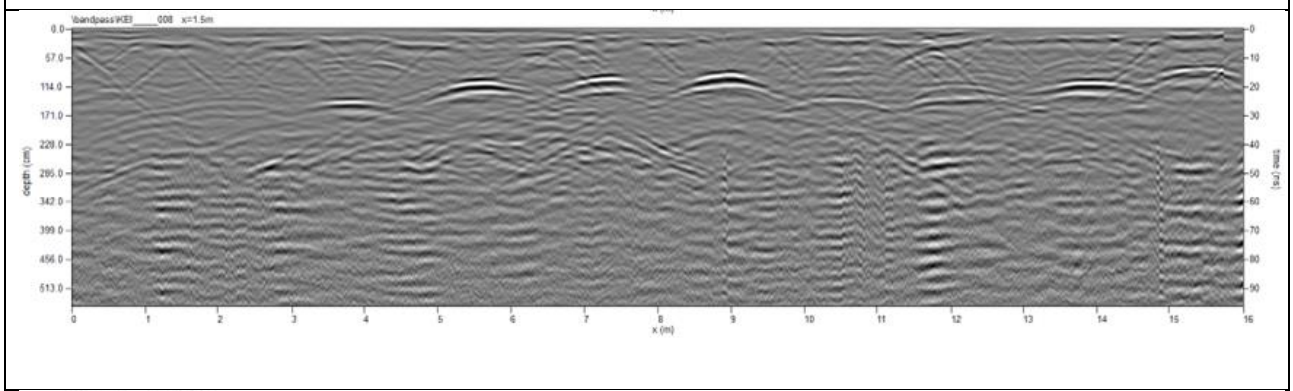
\bandpass\KEI____008 x=1.5m
depth (cm)
time (ns)
x (m)

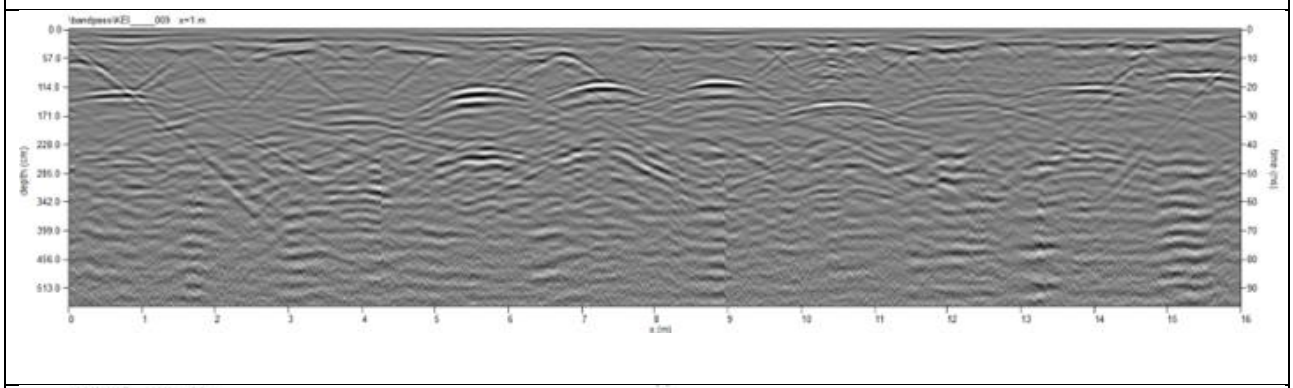
\bandpass\KEI____009 x=1.m
depth (cm)
time (ns)
x (m)

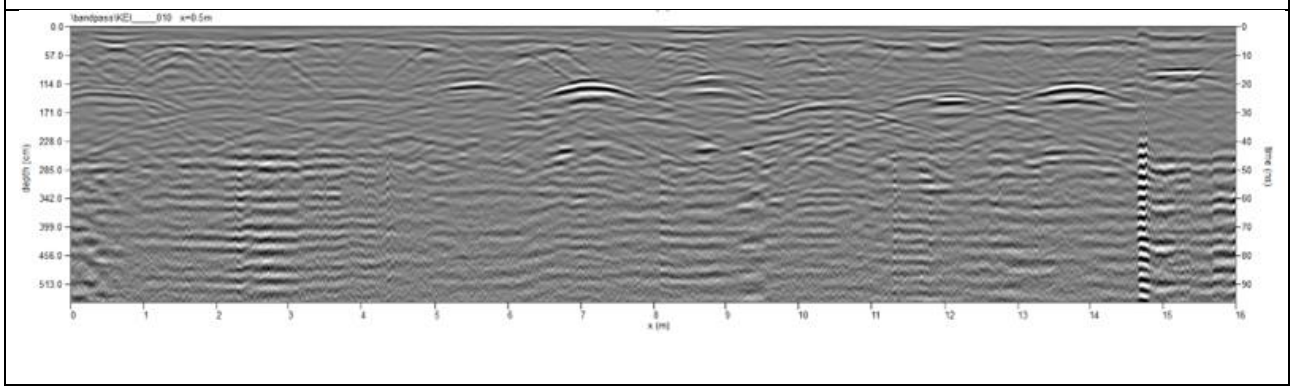
\bandpass\KEI____010 x=0.5m
depth (cm)
time (ns)
x (m)

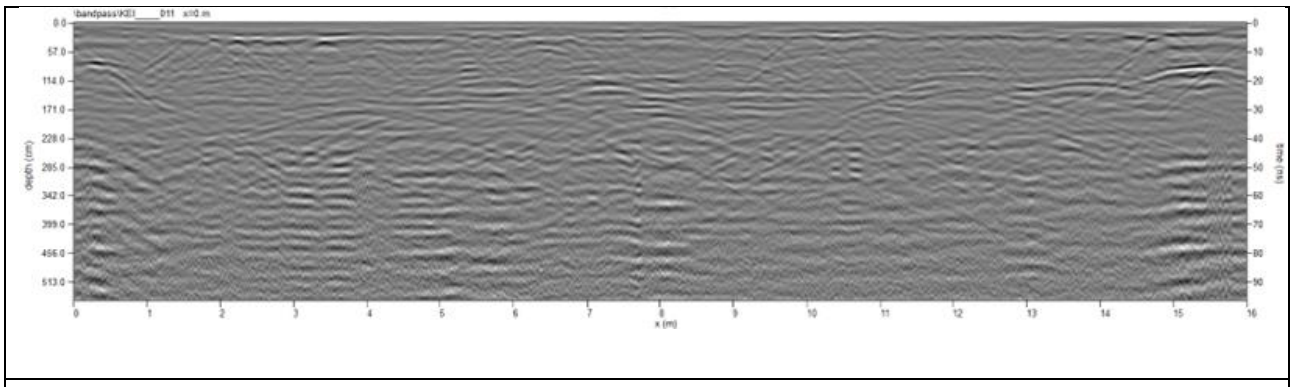

Keith Cemetery rows H and I. Data collected Sept 2022

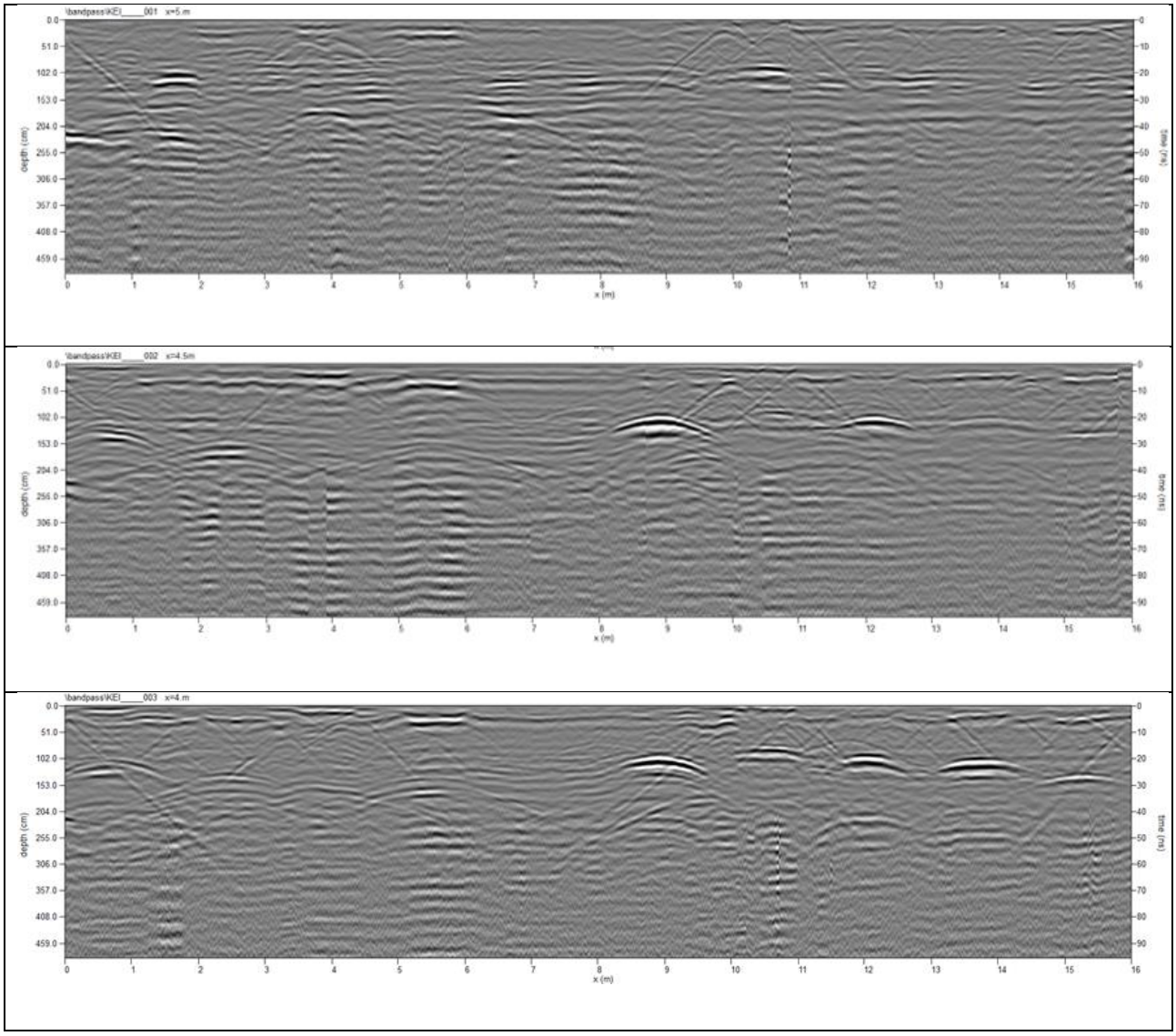

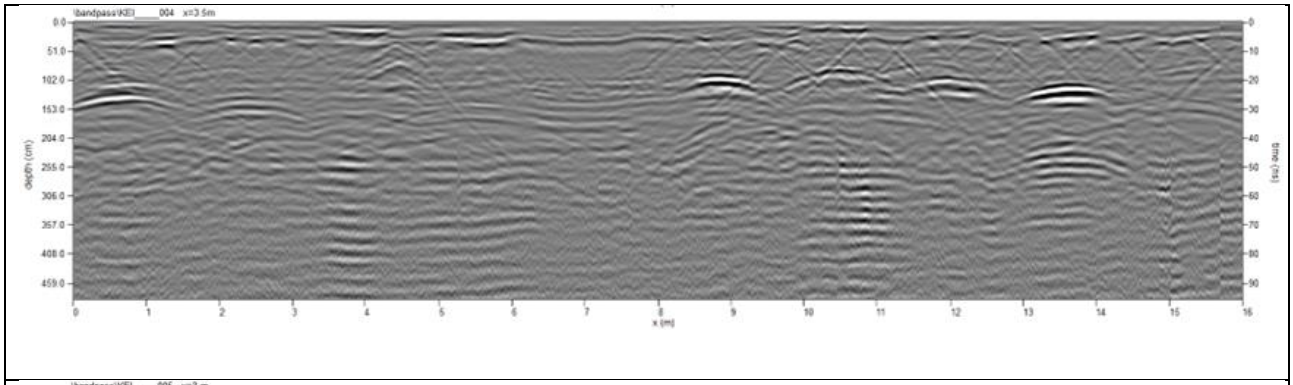
\bandpass\KEI____004 x=3.5m
depth (cm)
time (ns)
x (m)

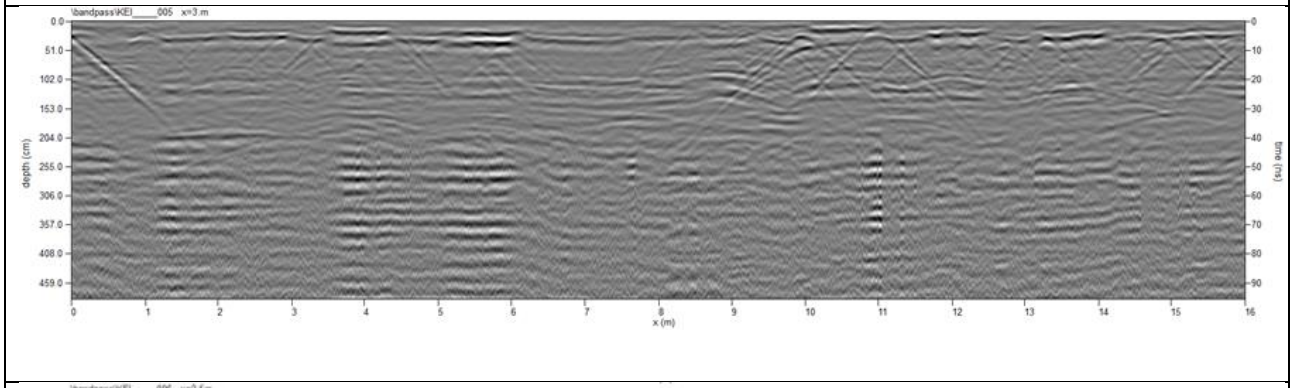
\bandpass\KEI____005 x=3 m
depth (cm)
time (ns)
x (m)

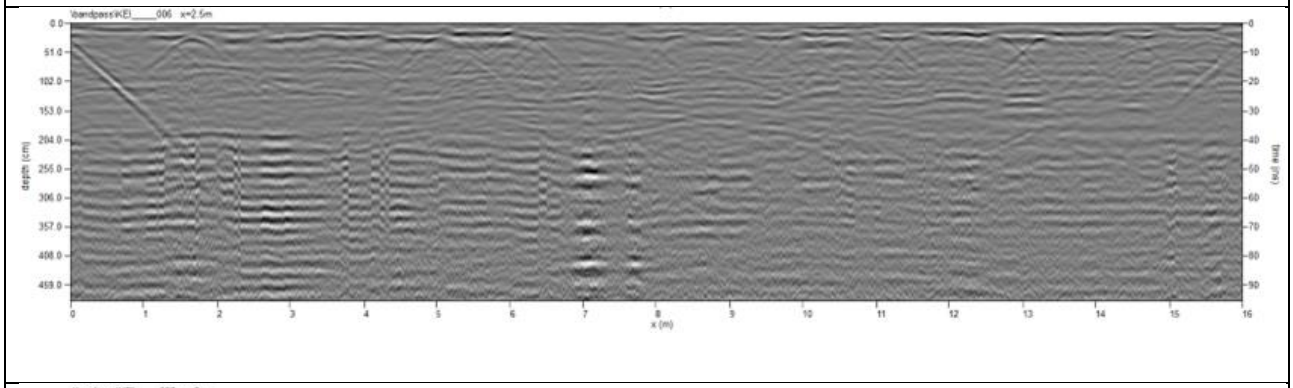
\bandpass\KEI____006 x=2.5m
depth (cm)
time (ns)
x (m)

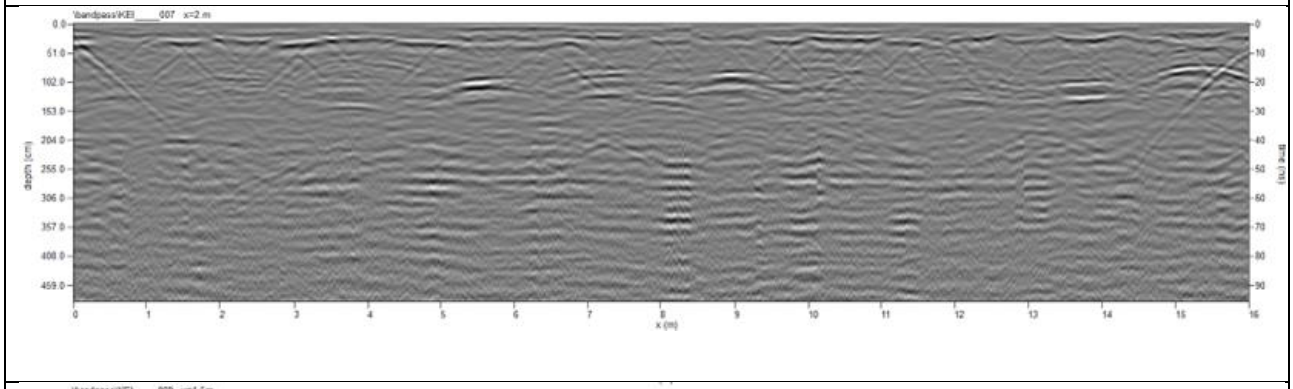
\bandpass\KEI____007 x=2 m
depth (cm)
time (ns)
x (m)

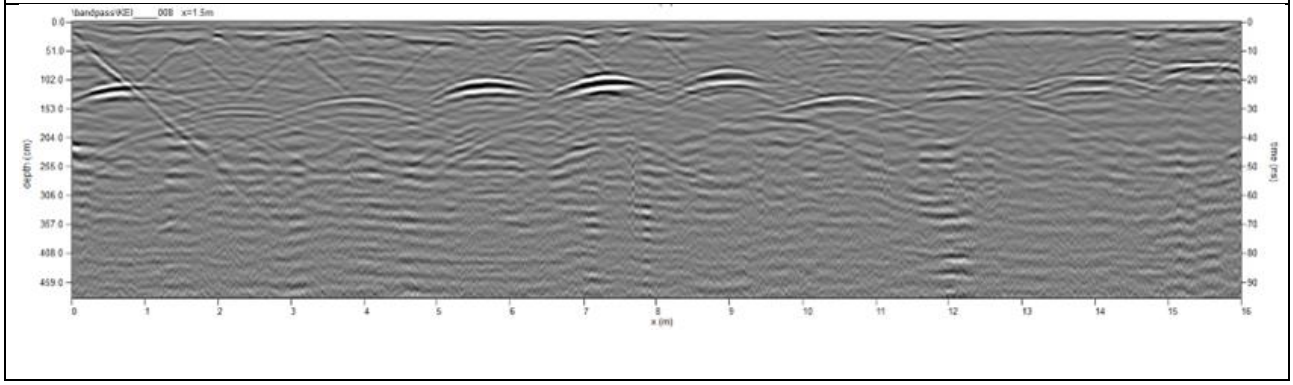
\bandpass\KEI____008 x=1.5m
depth (cm)
time (ns)
x (m)

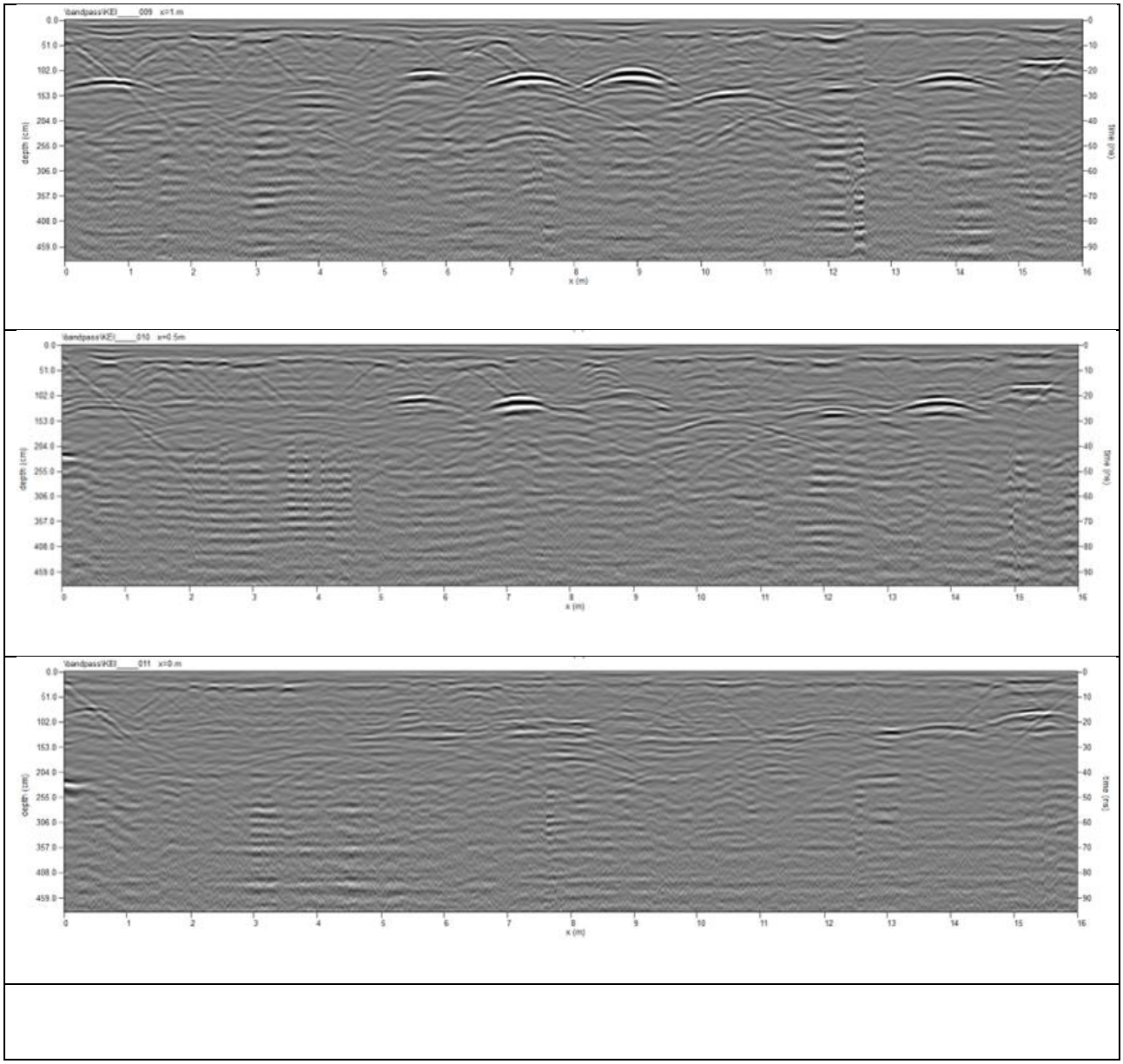

Keith Cemetery rows H and I. Data collected December 2022

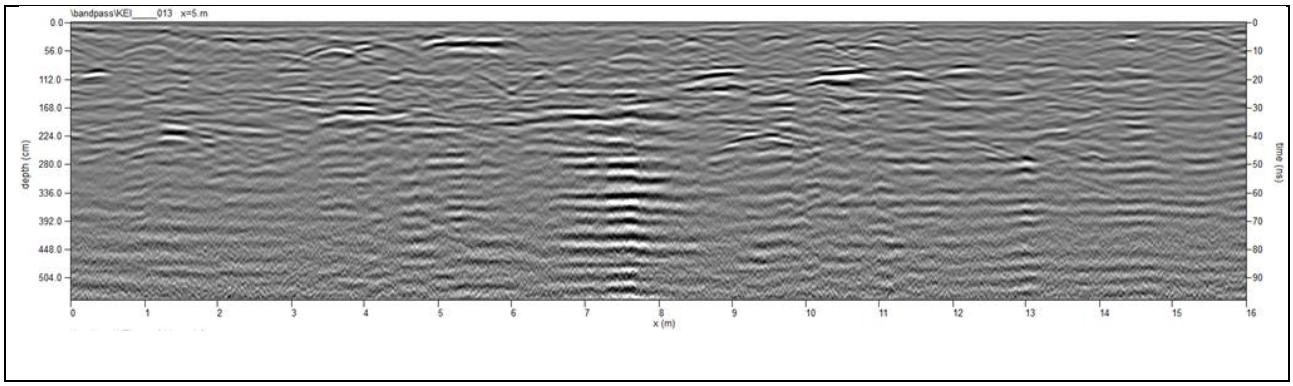

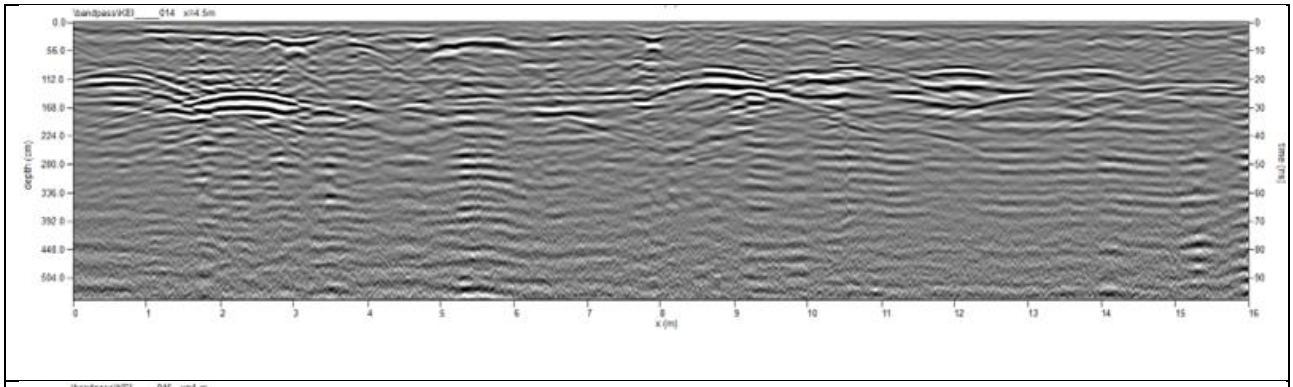
\bandpass\KEI____014 x=4.5m
depth (cm)
time (ns)
x (m)

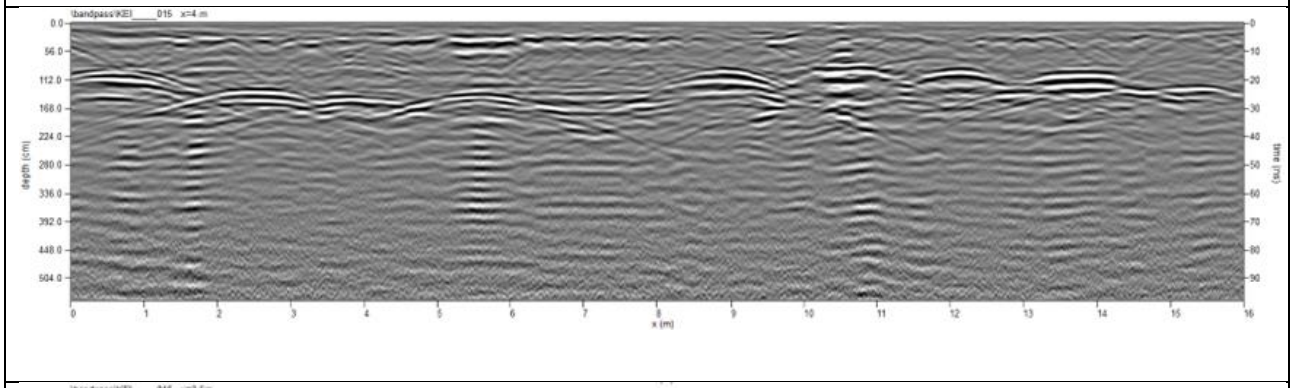
\bandpass\KEI____015 x=4 m
depth (cm)
time (ns)
x (m)

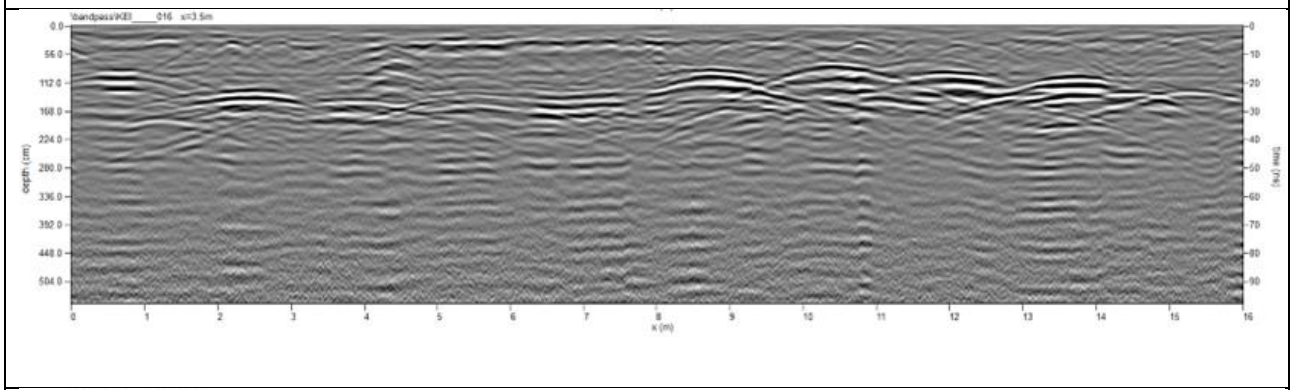
\bandpass\KEI____016 x=3.5m
depth (cm)
time (ns)
x (m)

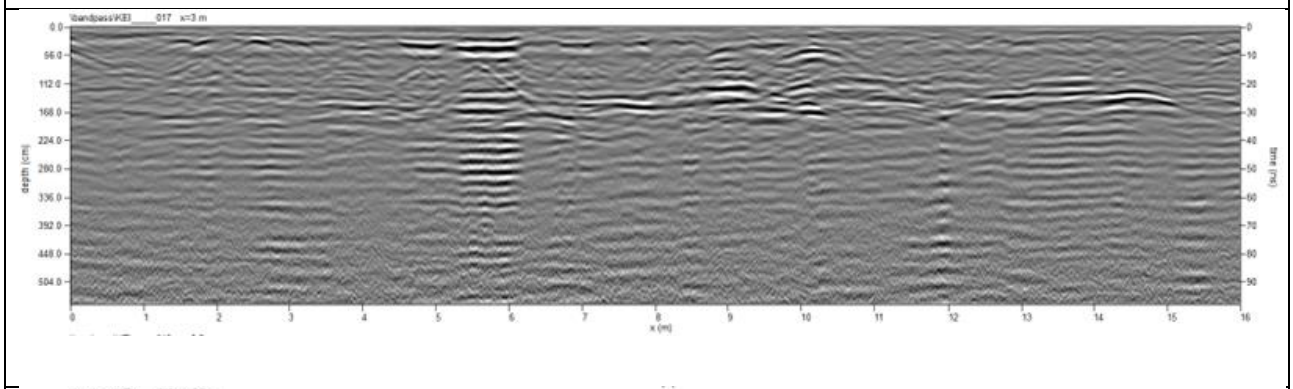
\bandpass\KEI____017 x=3 m
depth (cm)
time (ns)
x (m)

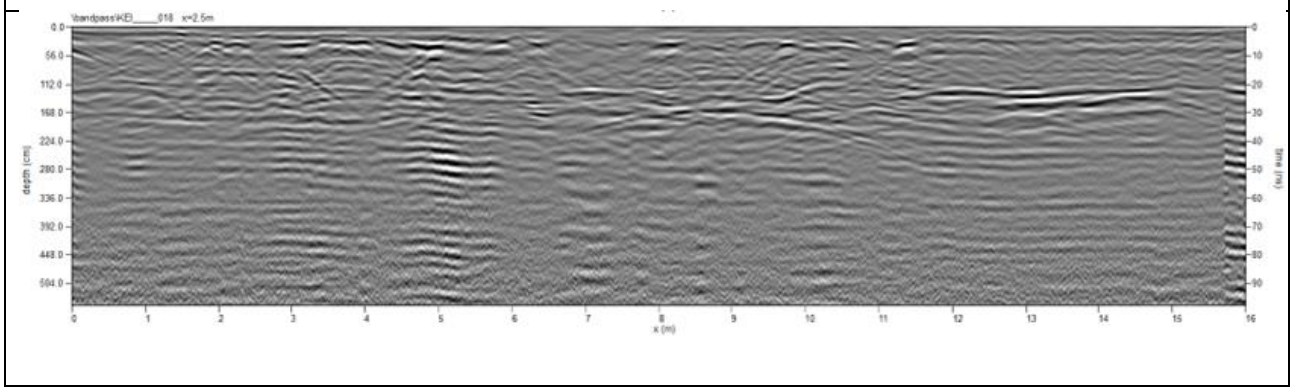
\bandpass\KEI____018 x=2.5m
depth (cm)
time (ns)
x (m)

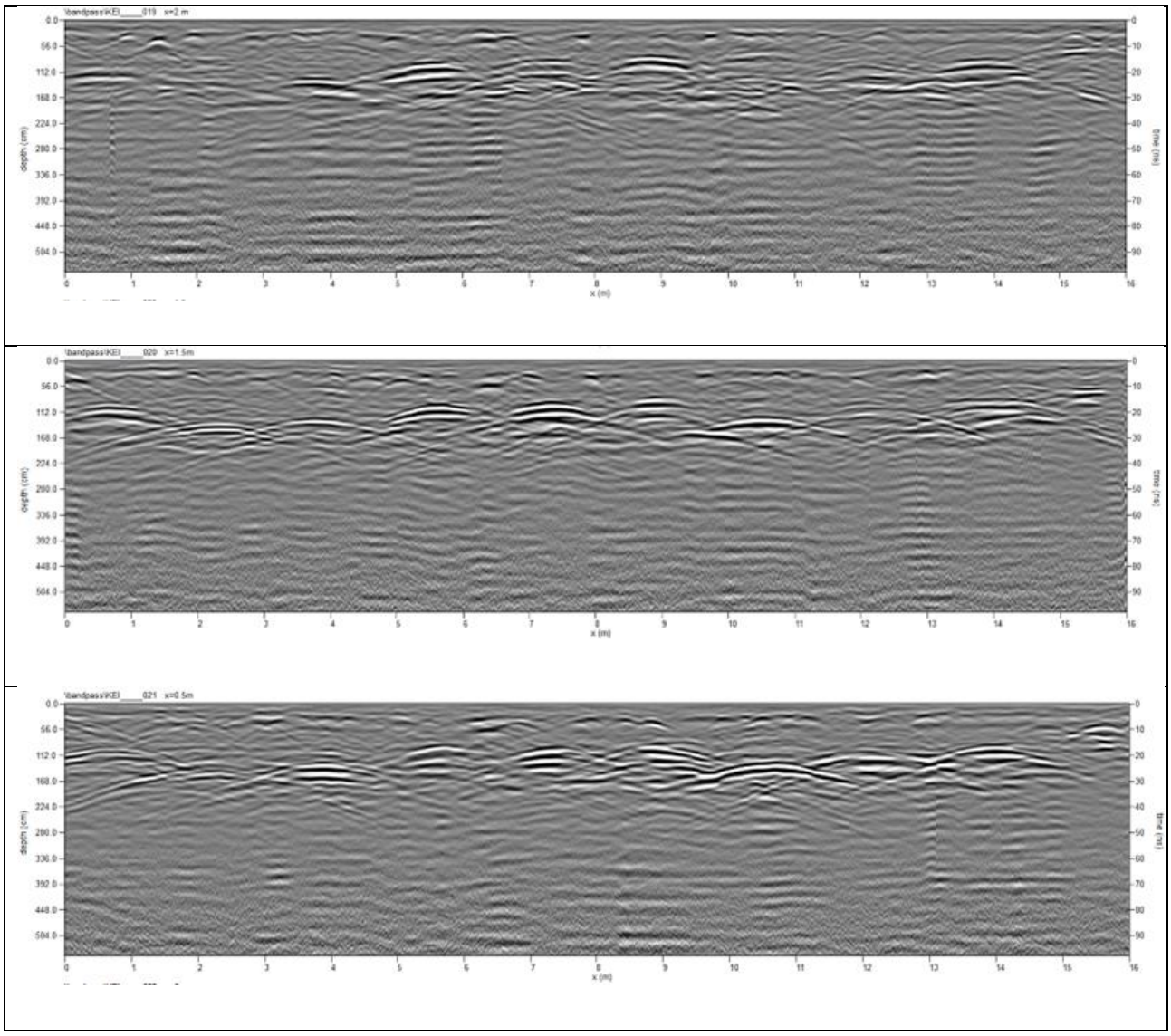

Keith Cemetery rows H and I. Data collected March 2023

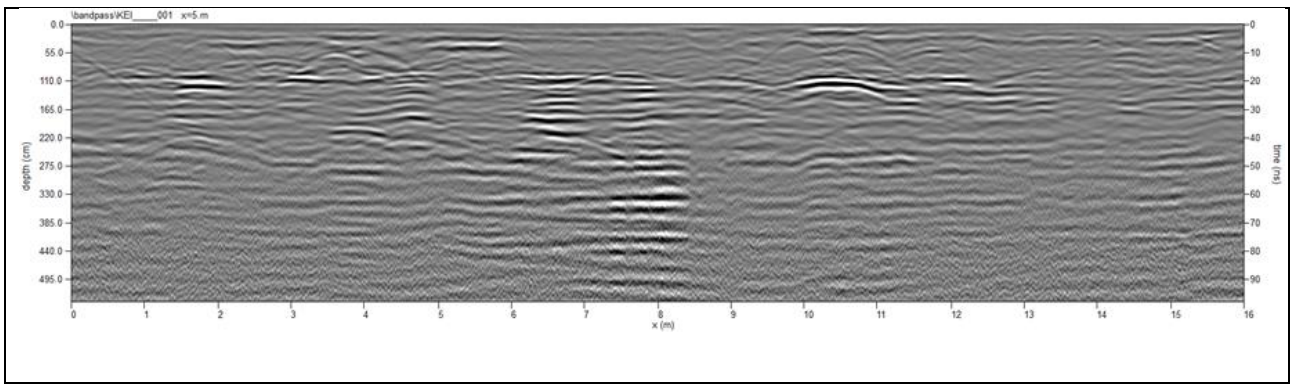

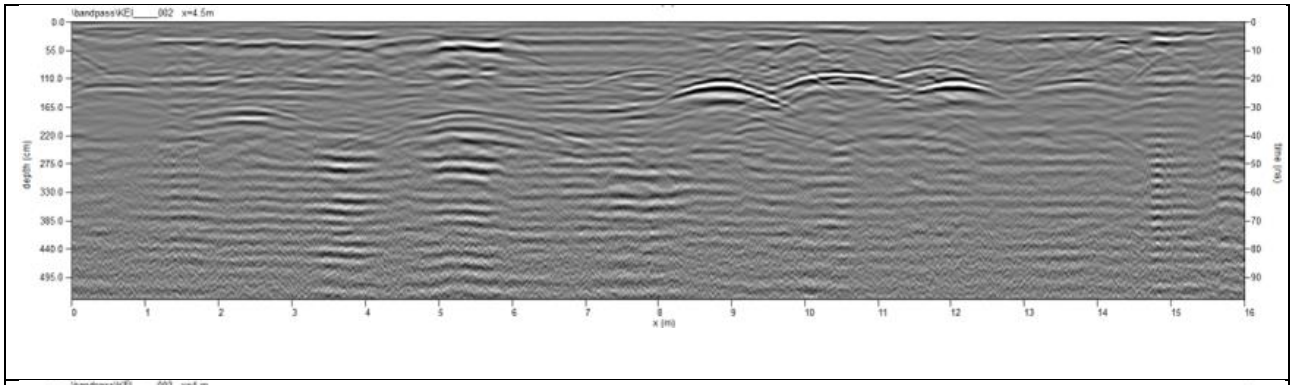
\bandpass\KEI____002 x=4.5m
depth (cm)
x (m)
time (ns)

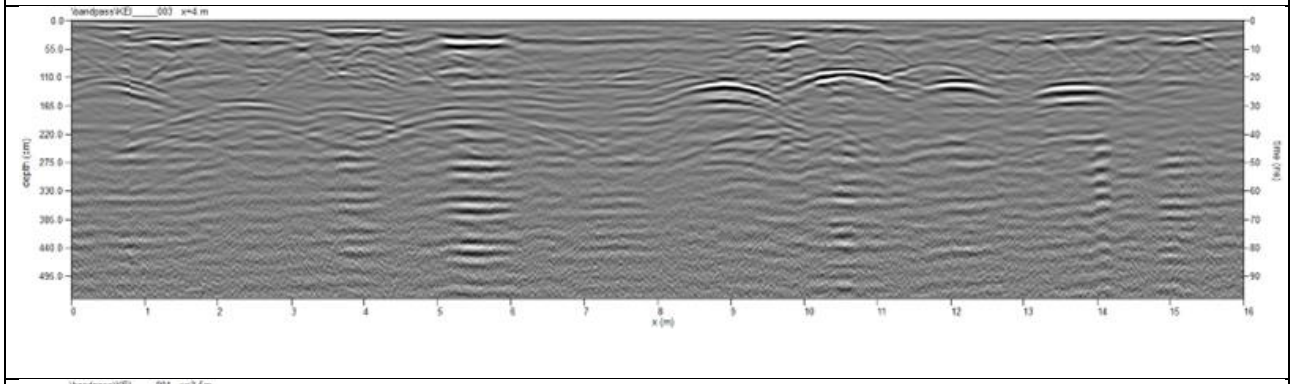
\bandpass\KEI____003 x=4 m
depth (cm)
x (m)
time (ns)

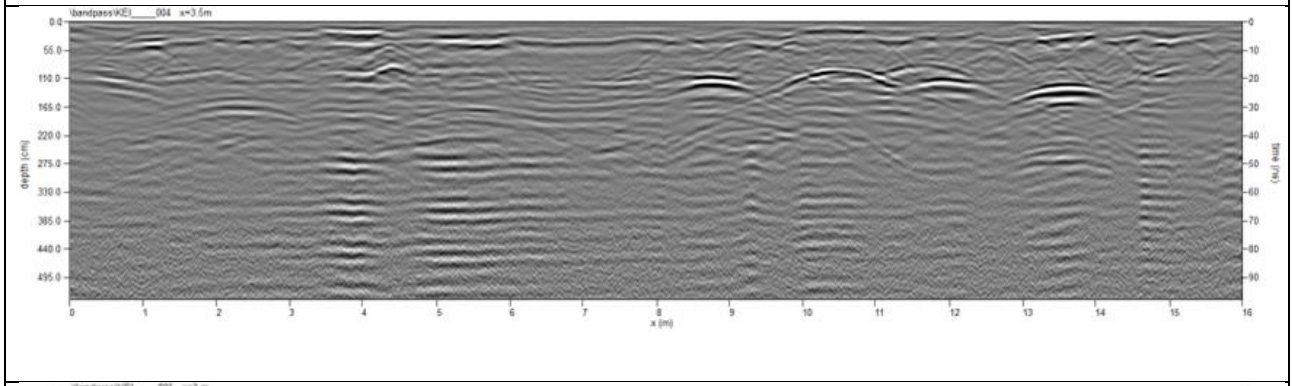
\bandpass\KEI____004 x=3.5m
depth (cm)
x (m)
time (ns)

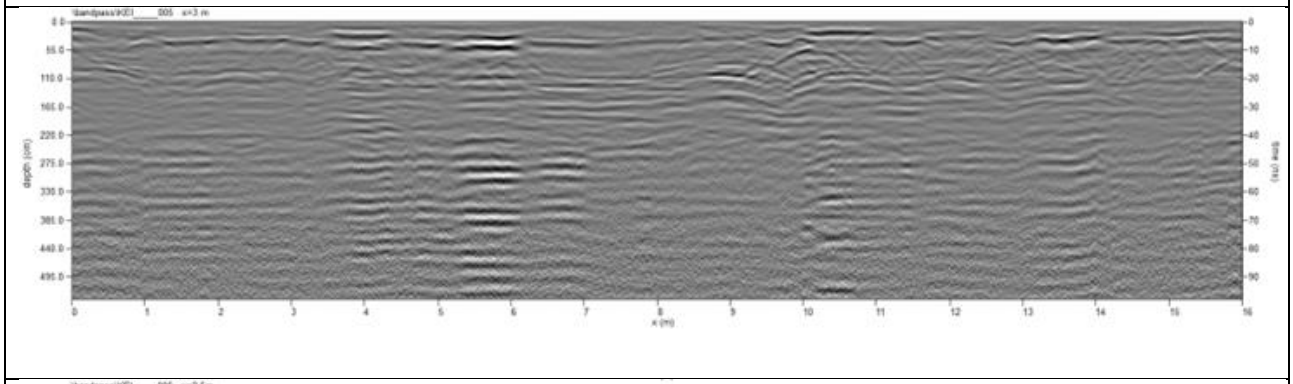
depth (cm)
x (m)
time (ns)

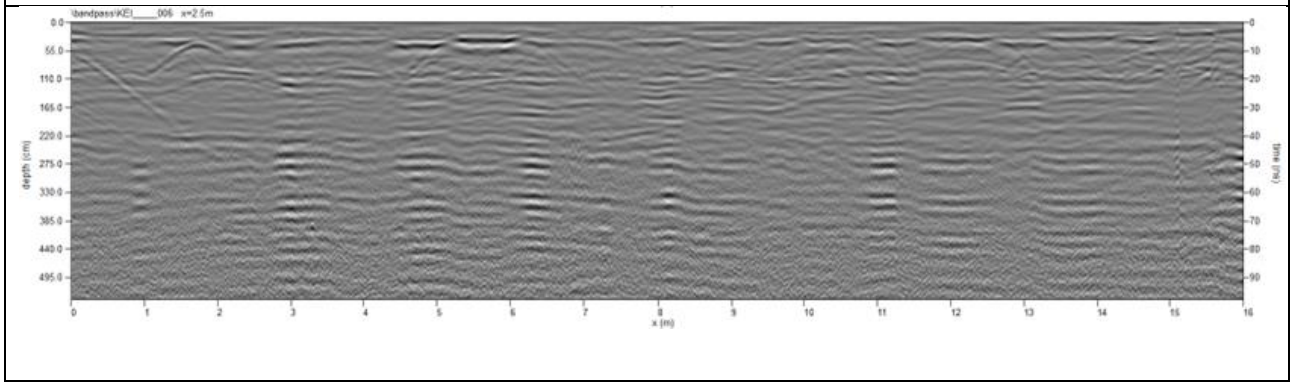
\bandpass\KEI____006 x=2.5m
depth (cm)
x (m)
time (ns)

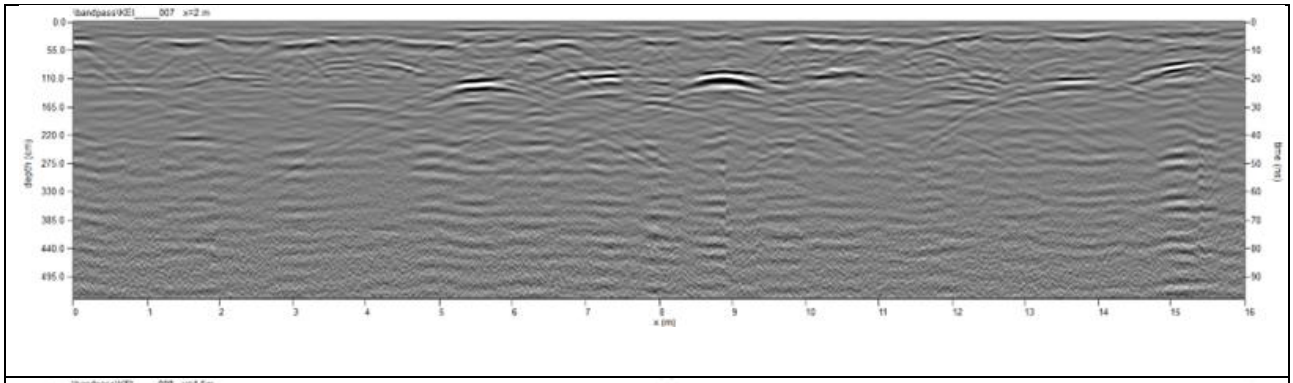
\bandpass\KEI_____007 x=2 m
depth (cm)
time (ns)
x (m)

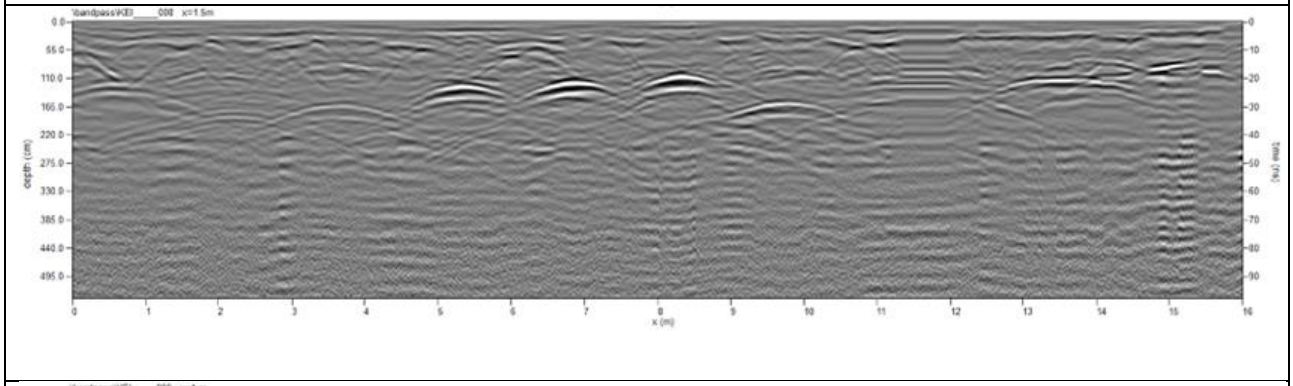
\bandpass\KEI_____008 x=1.5m
depth (cm)
time (ns)
x (m)

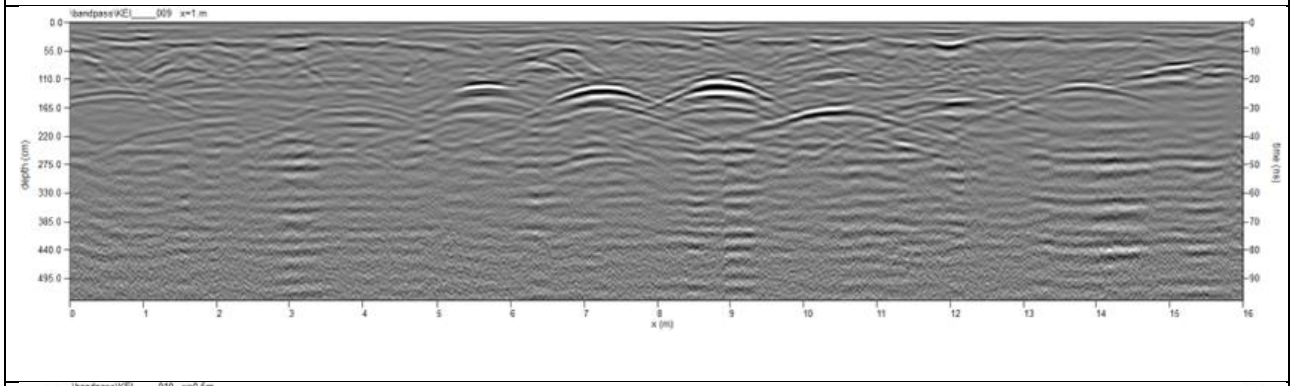
\bandpass\KEI_____009 x=1 m
depth (cm)
time (ns)
x (m)

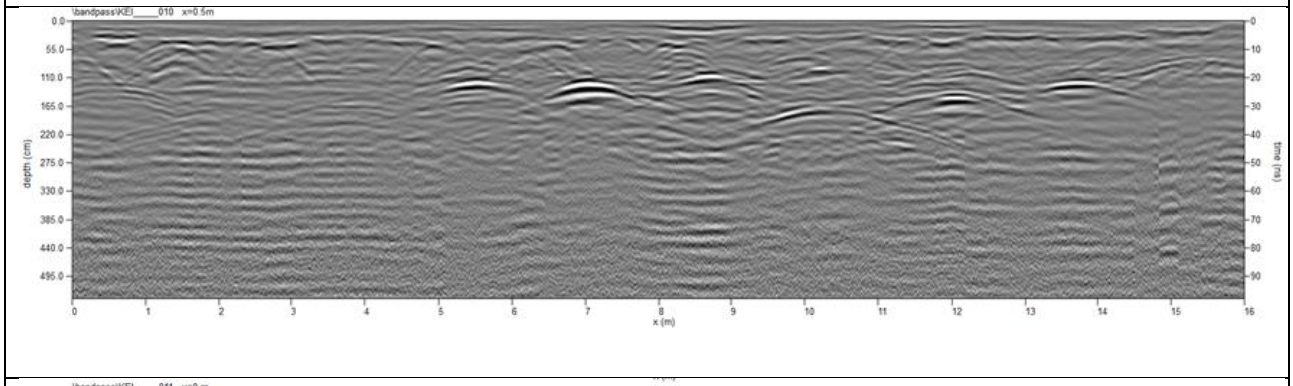
\bandpass\KEI_____010 x=0.5m
depth (cm)
time (ns)
x (m)

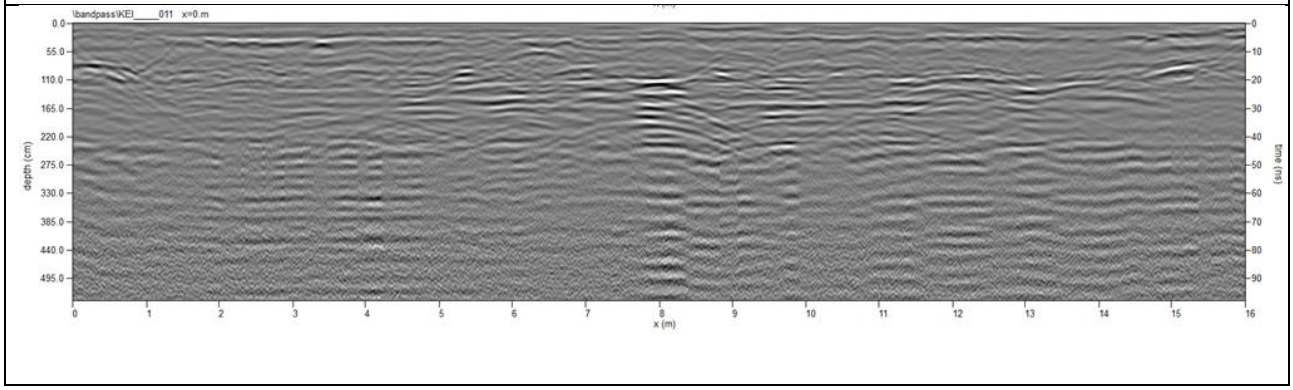
\bandpass\KEI_____011 x=0 m
depth (cm)
time (ns)
x (m)

7.1.2 Bordertown Cemetery Radargrams

Bordertown Cemetery Rows D and E. Data collected August 2020

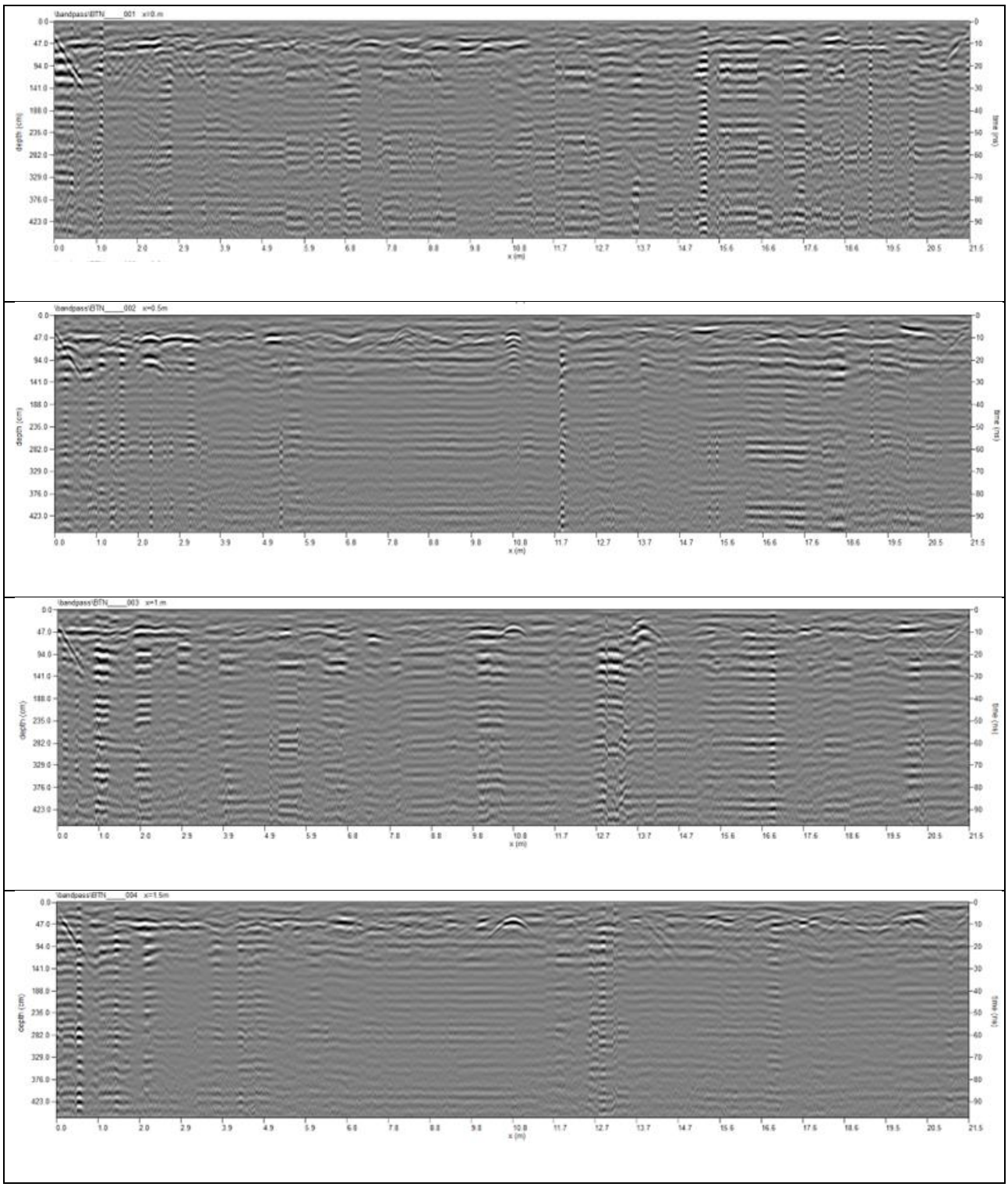

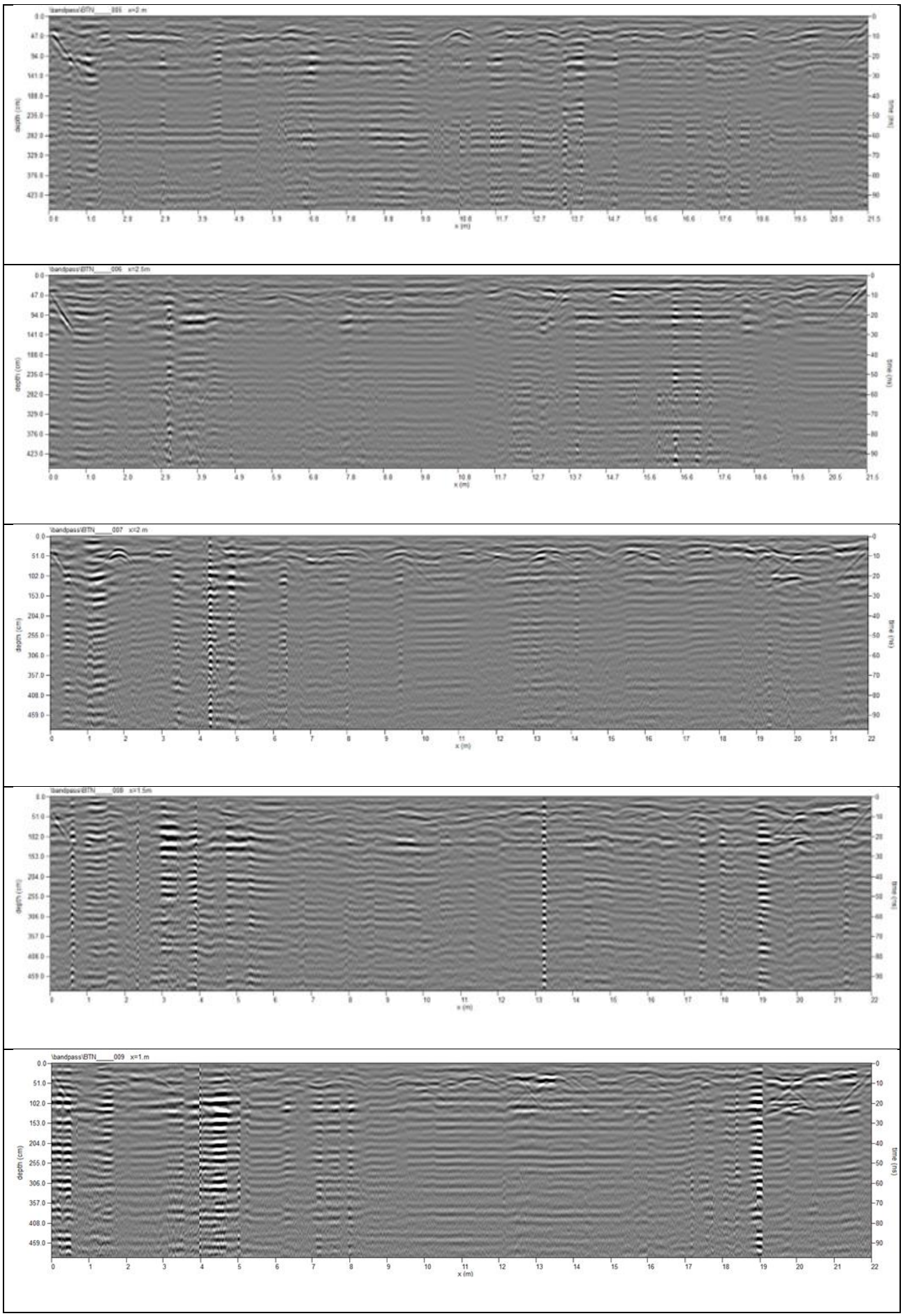
depth (cm)
time (ns)
x (m)

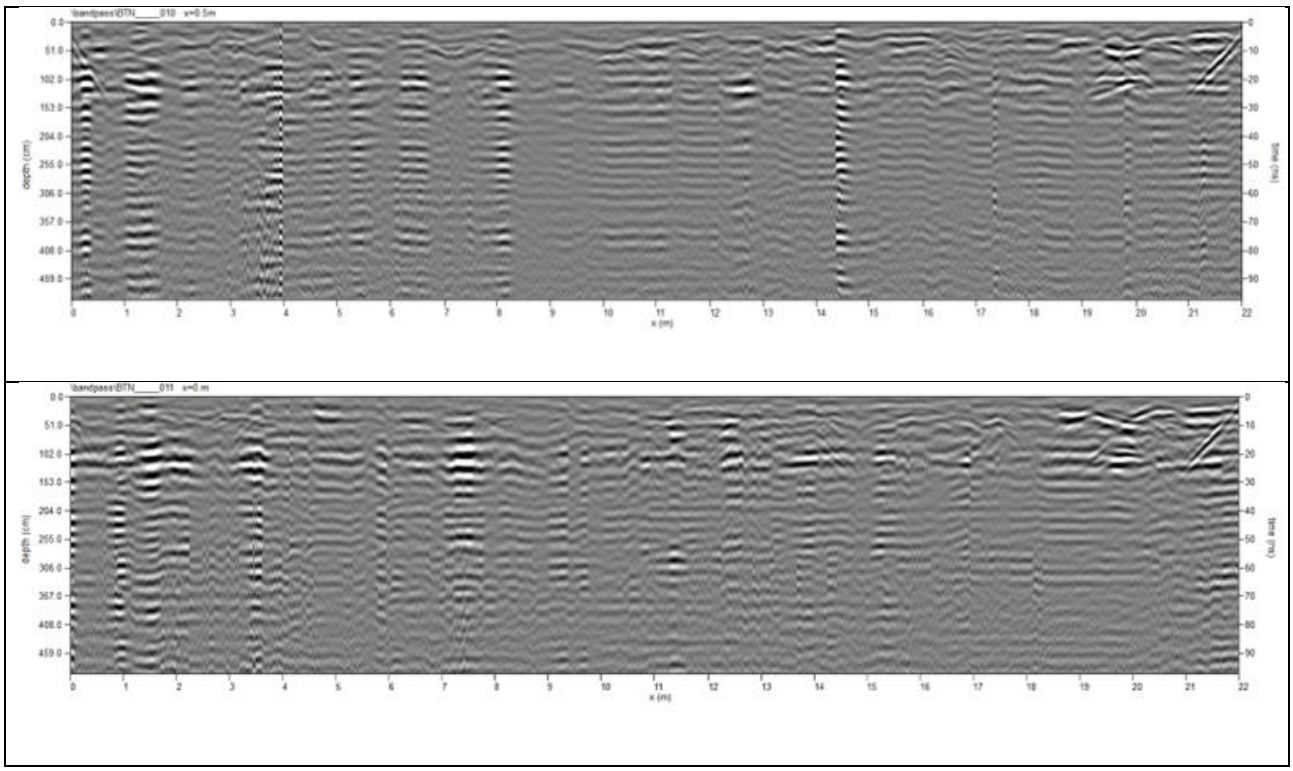

Bordertown Cemetery Rows D and E. Data collected October 2020

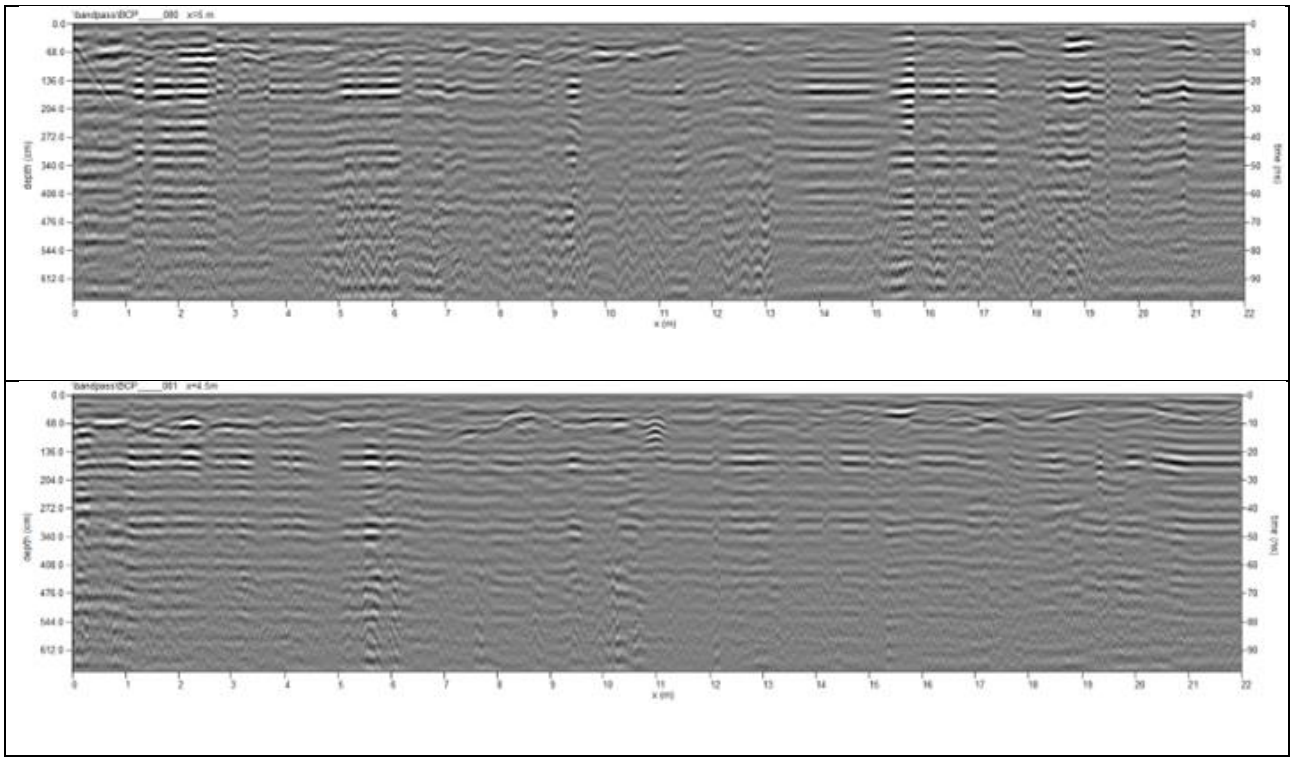

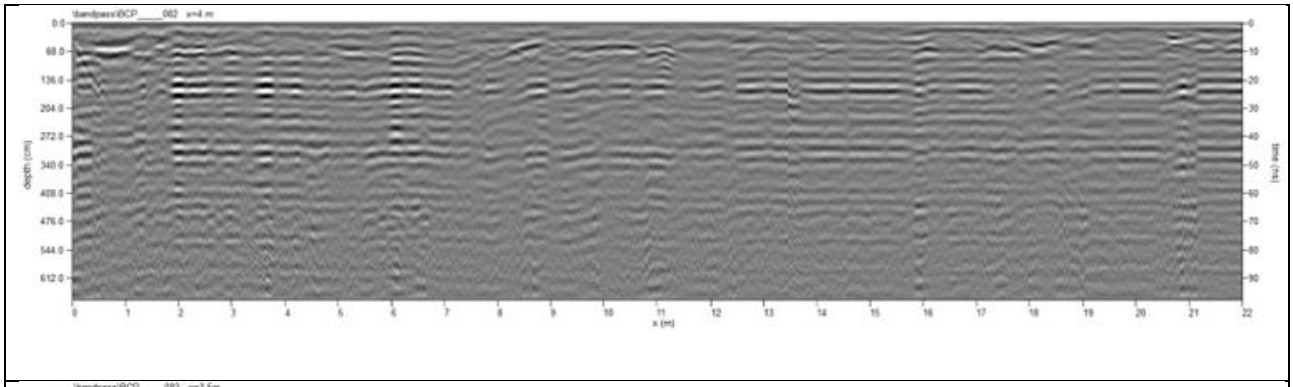

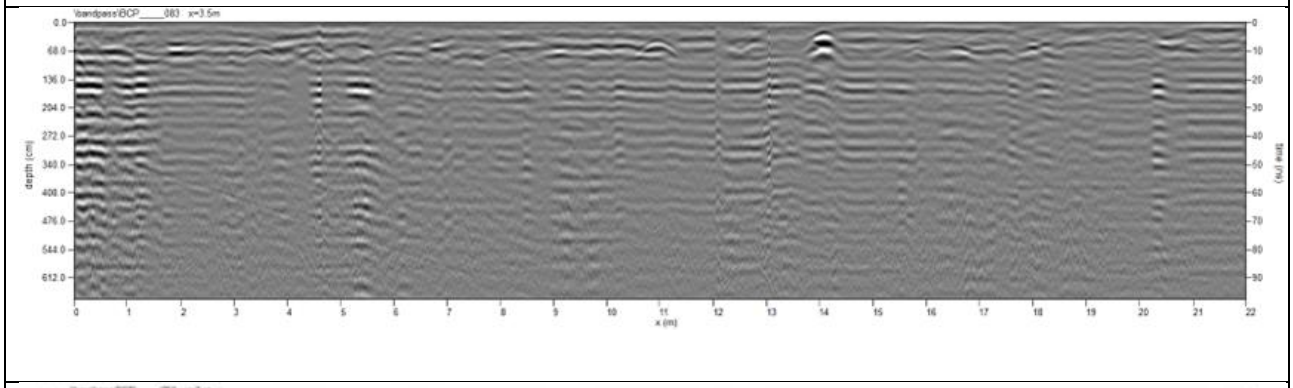

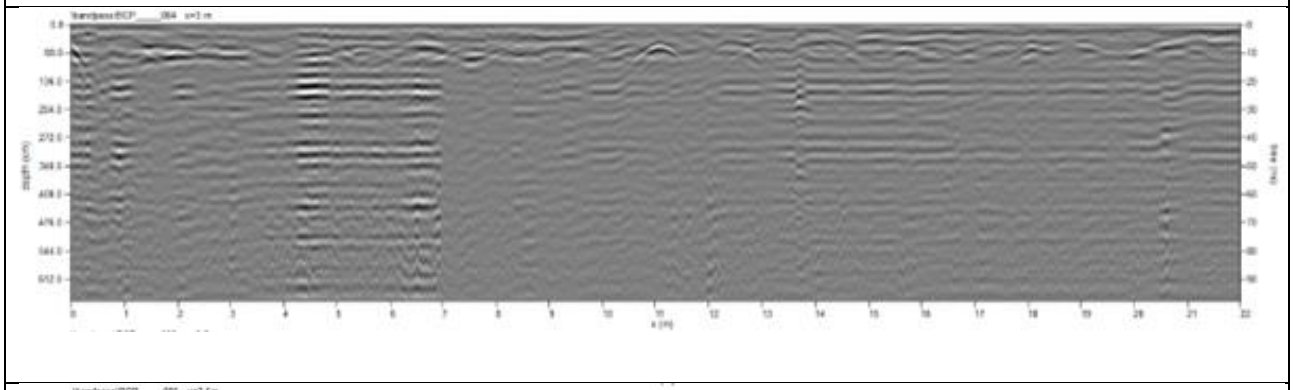

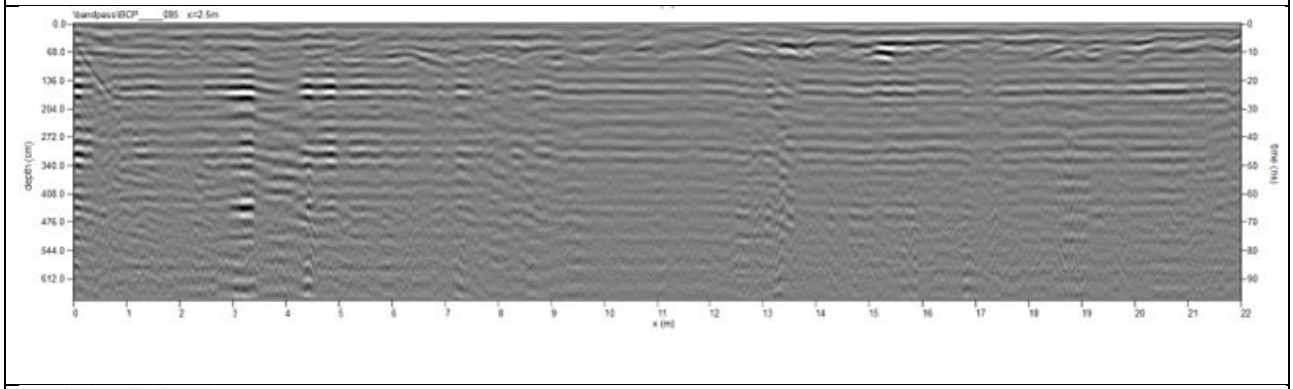

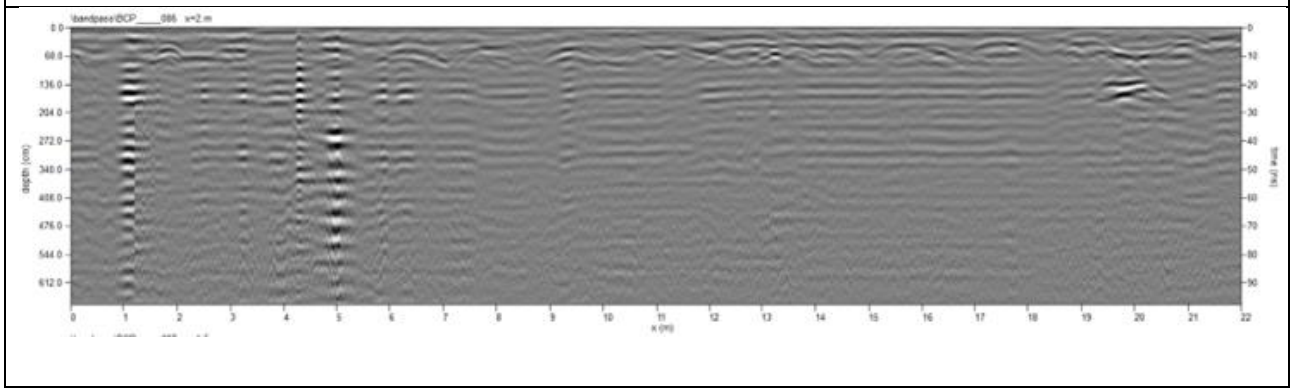

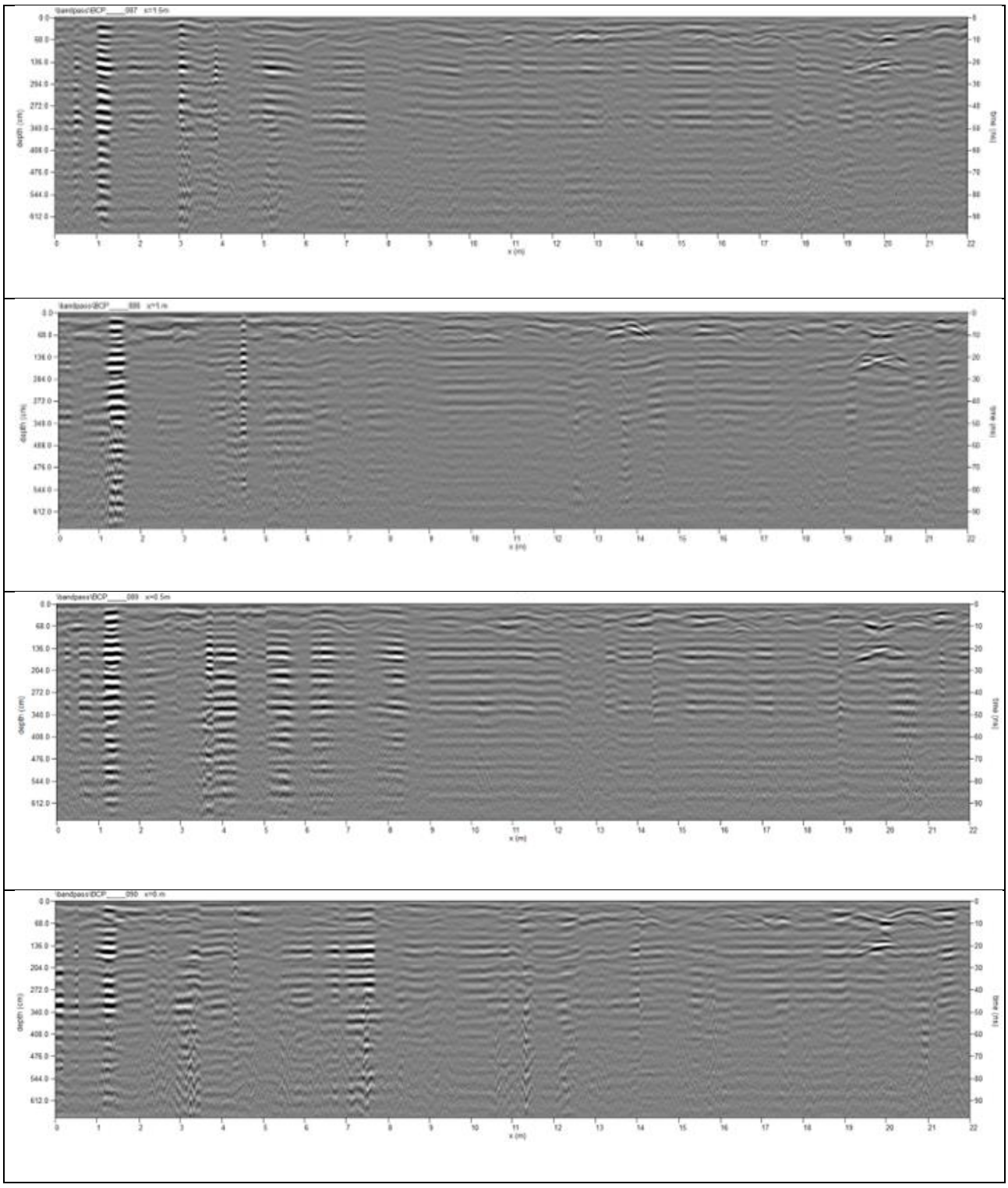

Bordertown Cemetery Rows D and E. Data collected January 2021

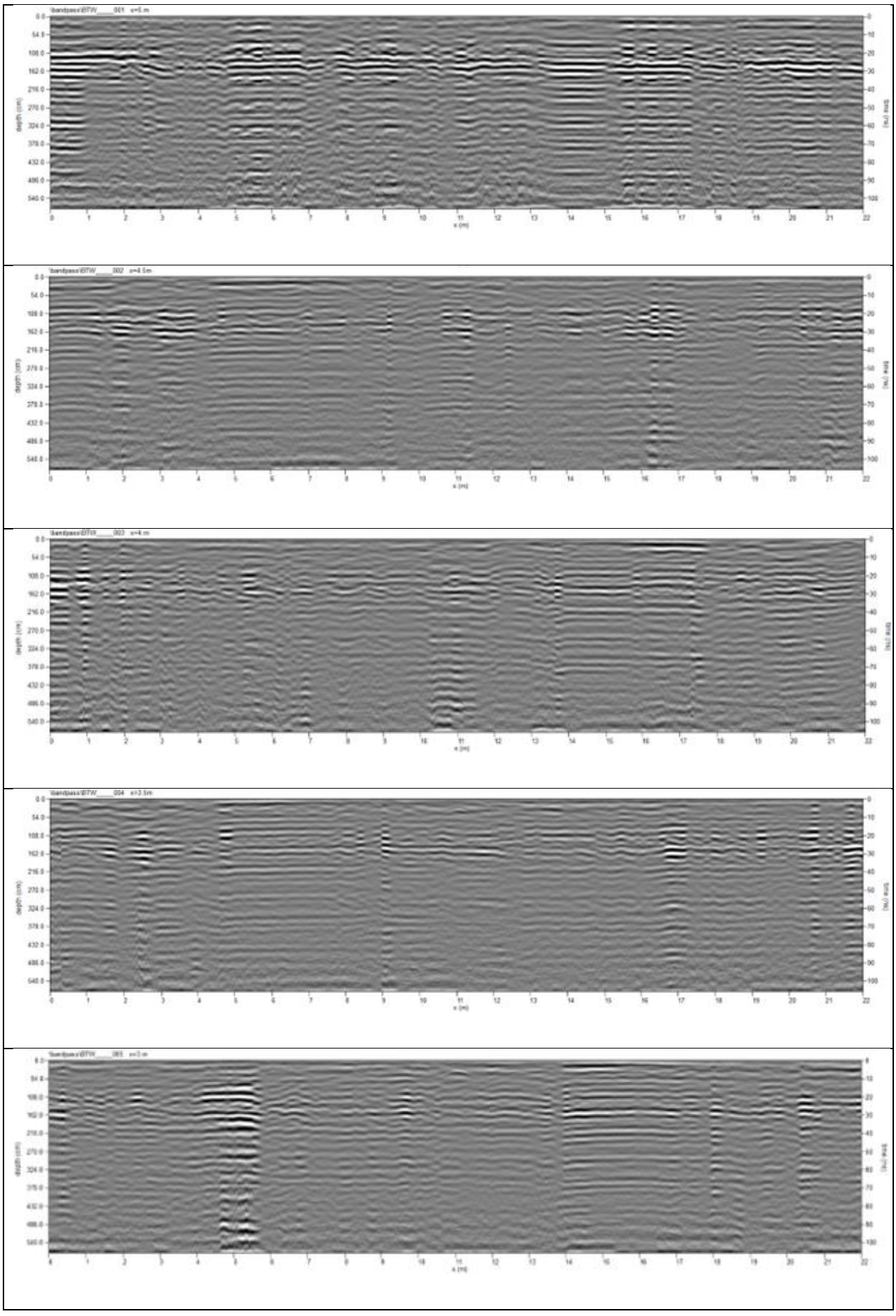

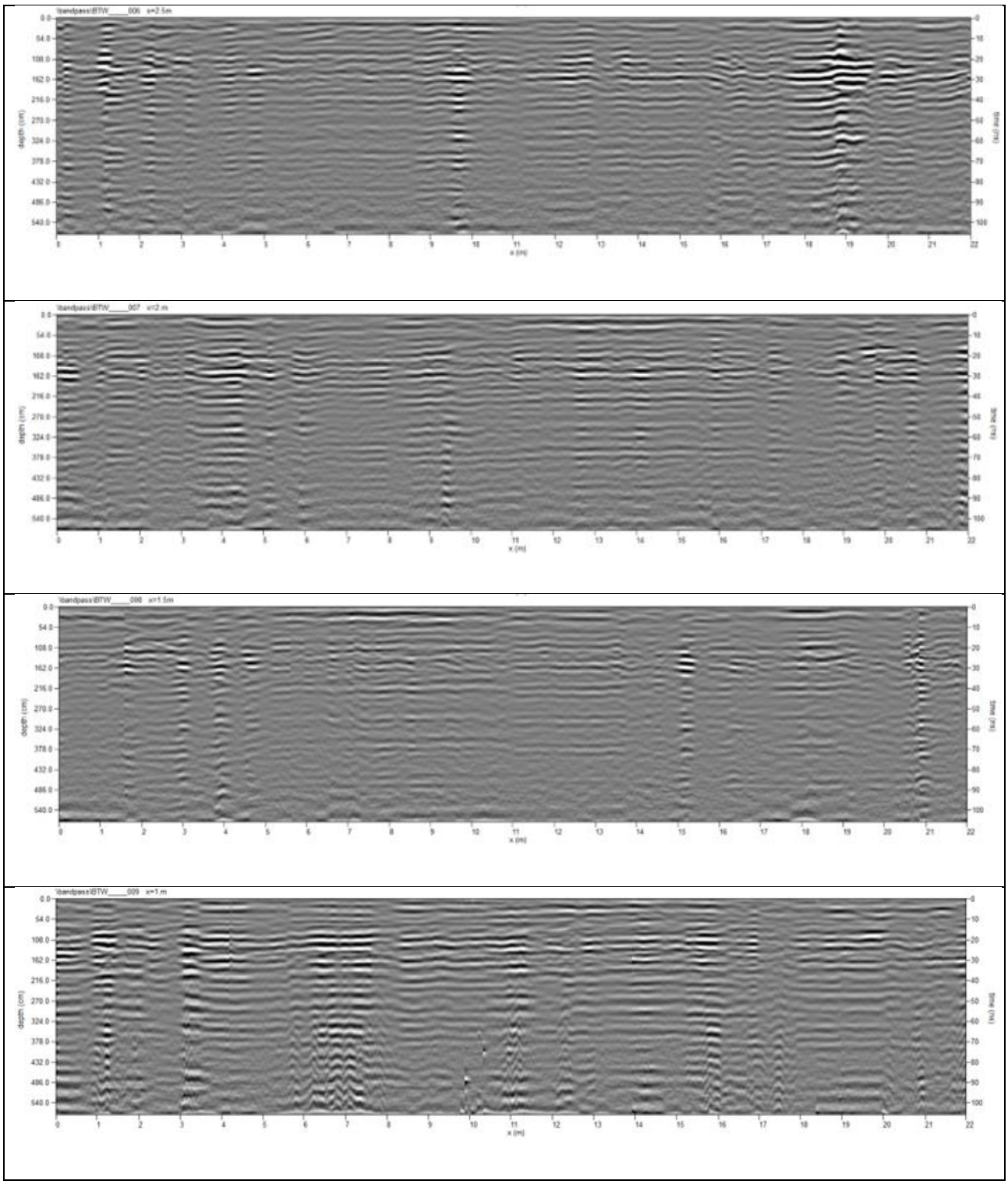

Bordertown Cemetery Rows D and E. Data collected January 2022

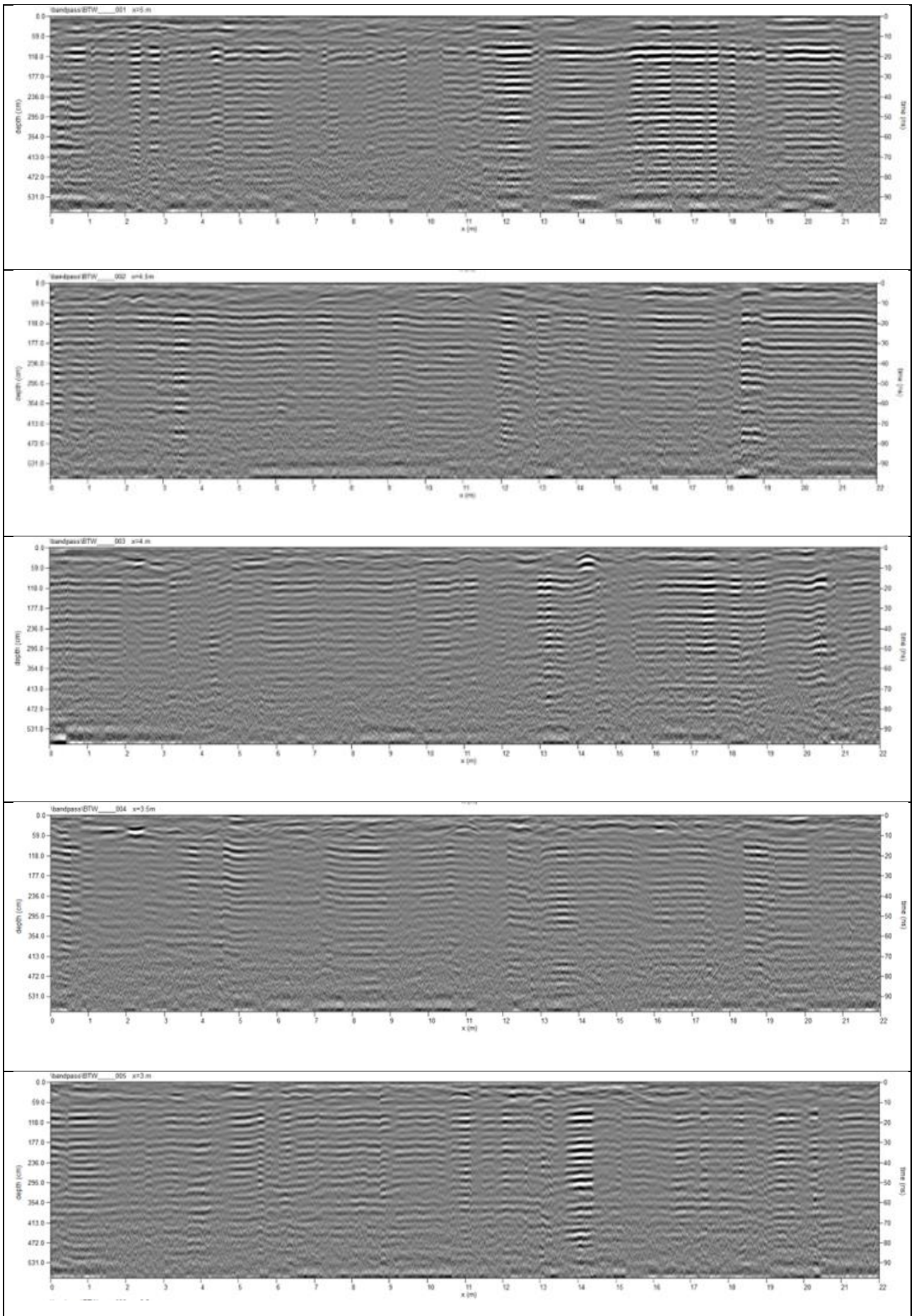
depth (cm)
x (m)

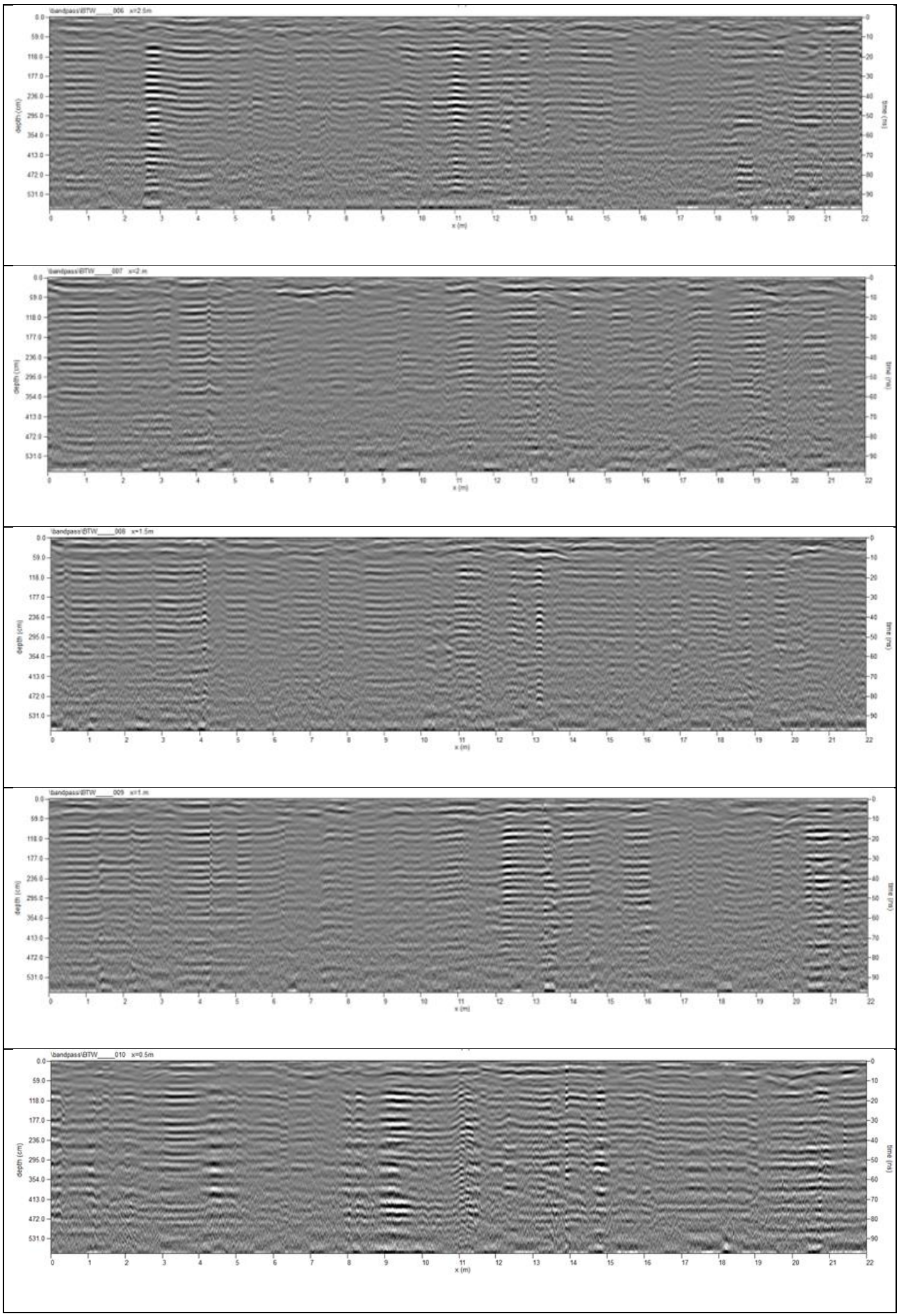
\bandpass\BTW____006 x=2.5m
\bandpass\BTW____007 x=2 m
\bandpass\BTW____008 x=1.5m
\bandpass\BTW____009 x=1 m
\bandpass\BTW____010 x=0.5m
depth (cm)
time (ns)
x (m)

Bordertown cemetery Rows D and E. Data collected May 2022

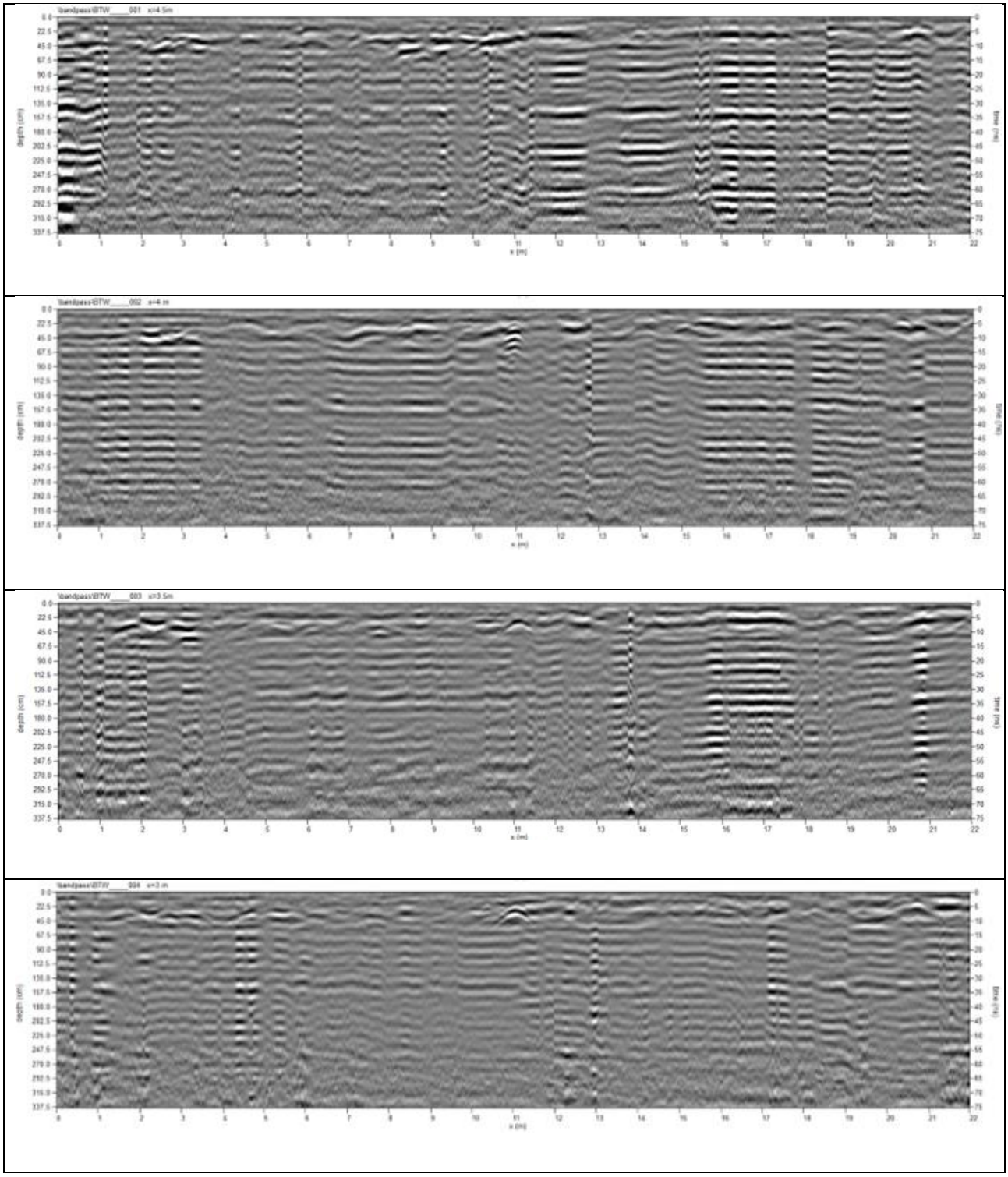

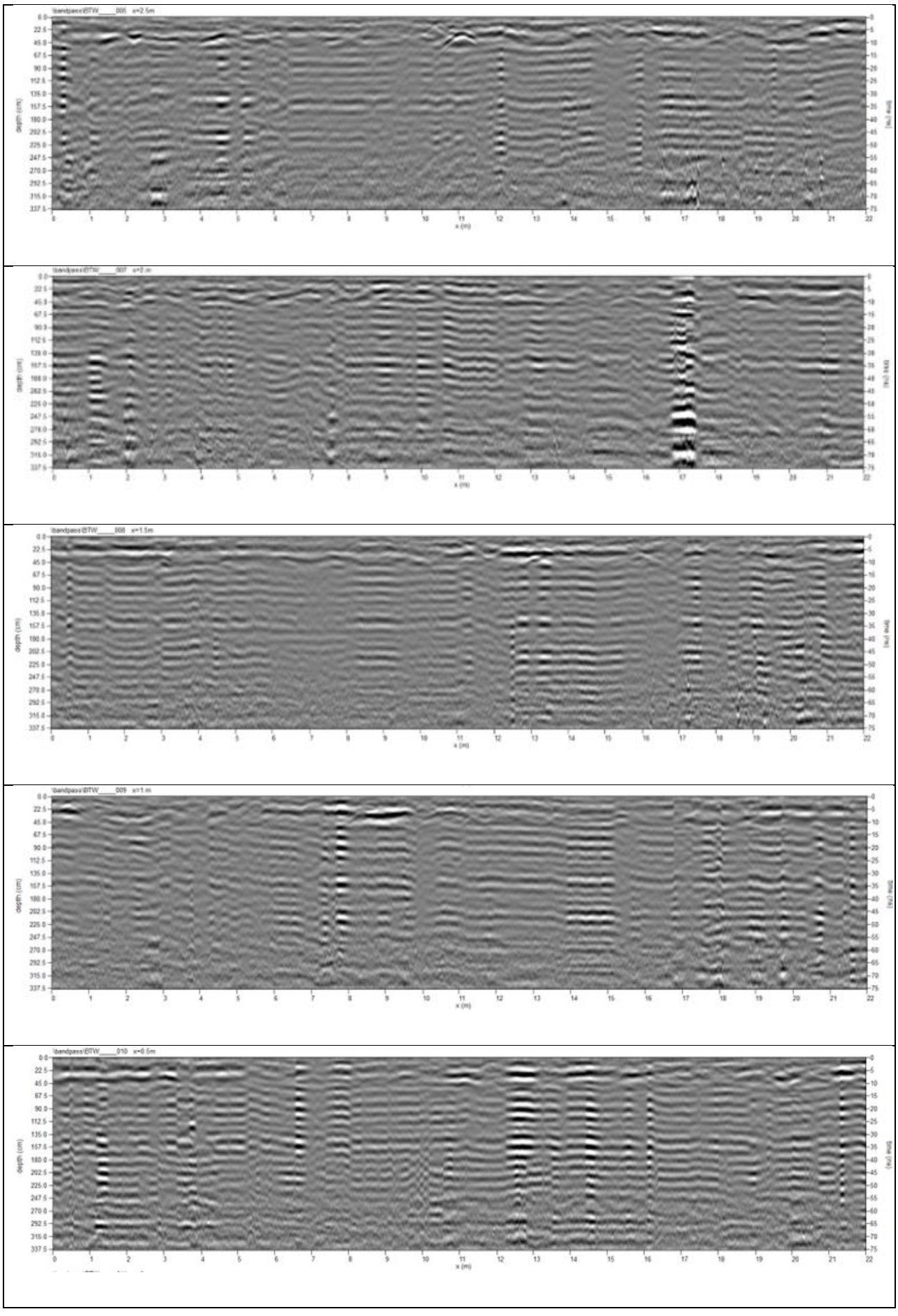

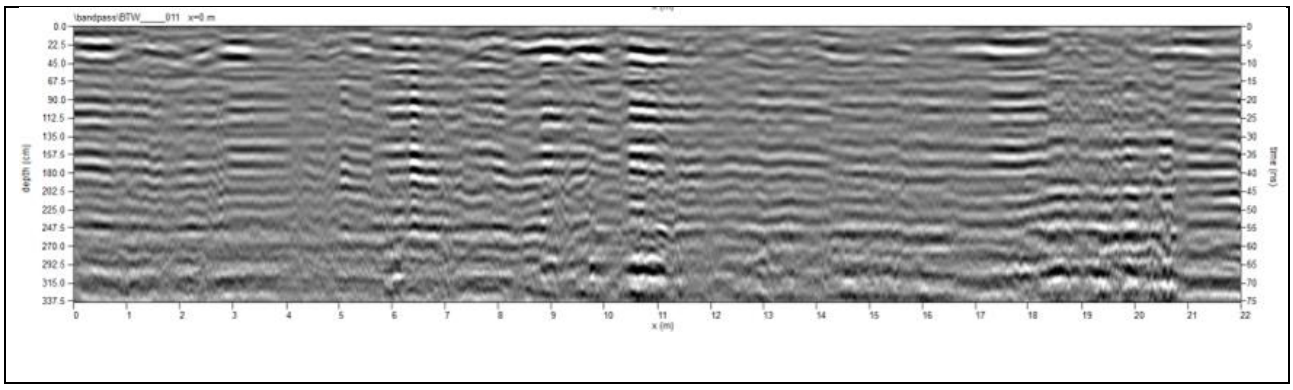

Bordertown Cemetery Rows D and E. Data collected July 2022

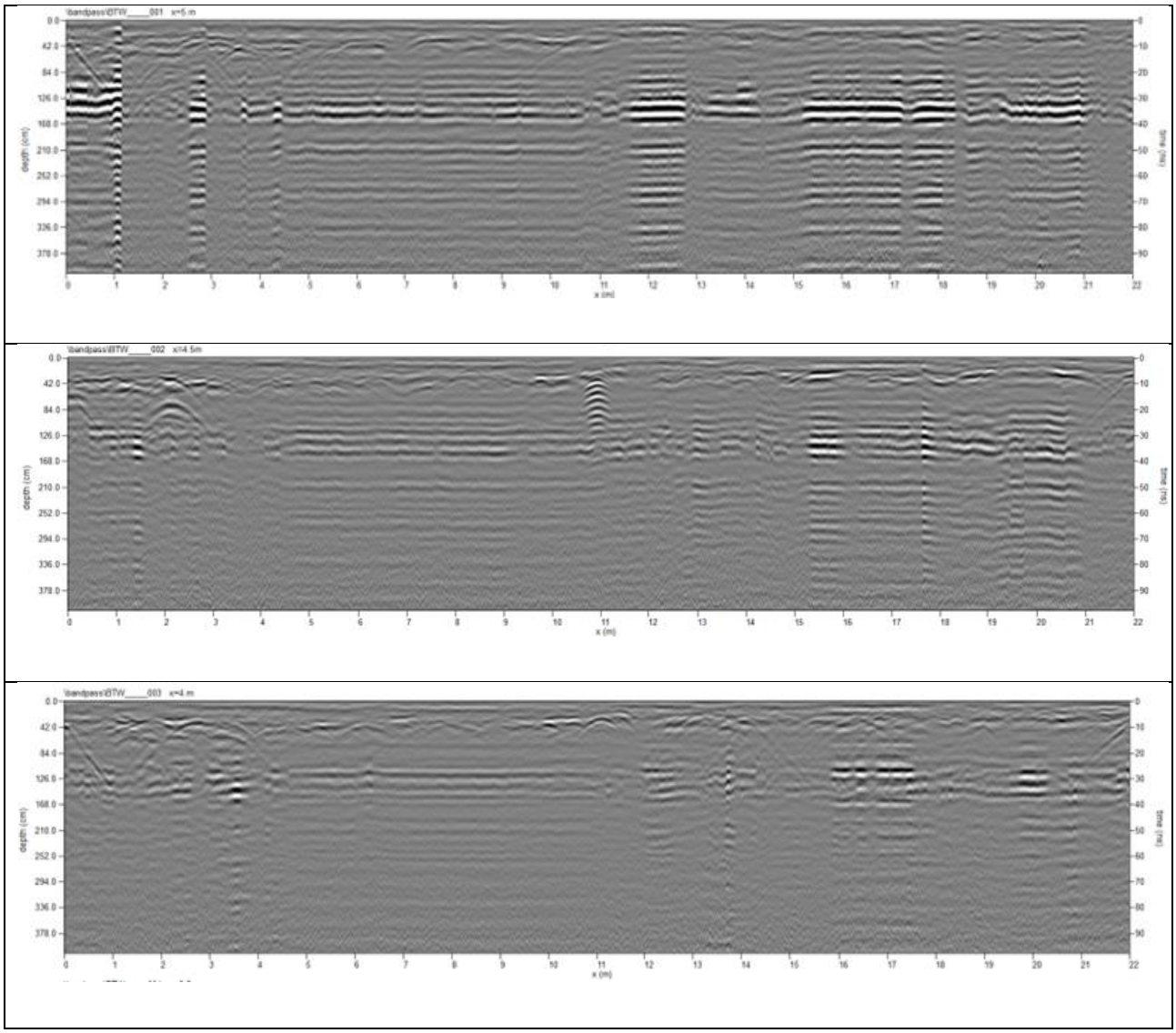

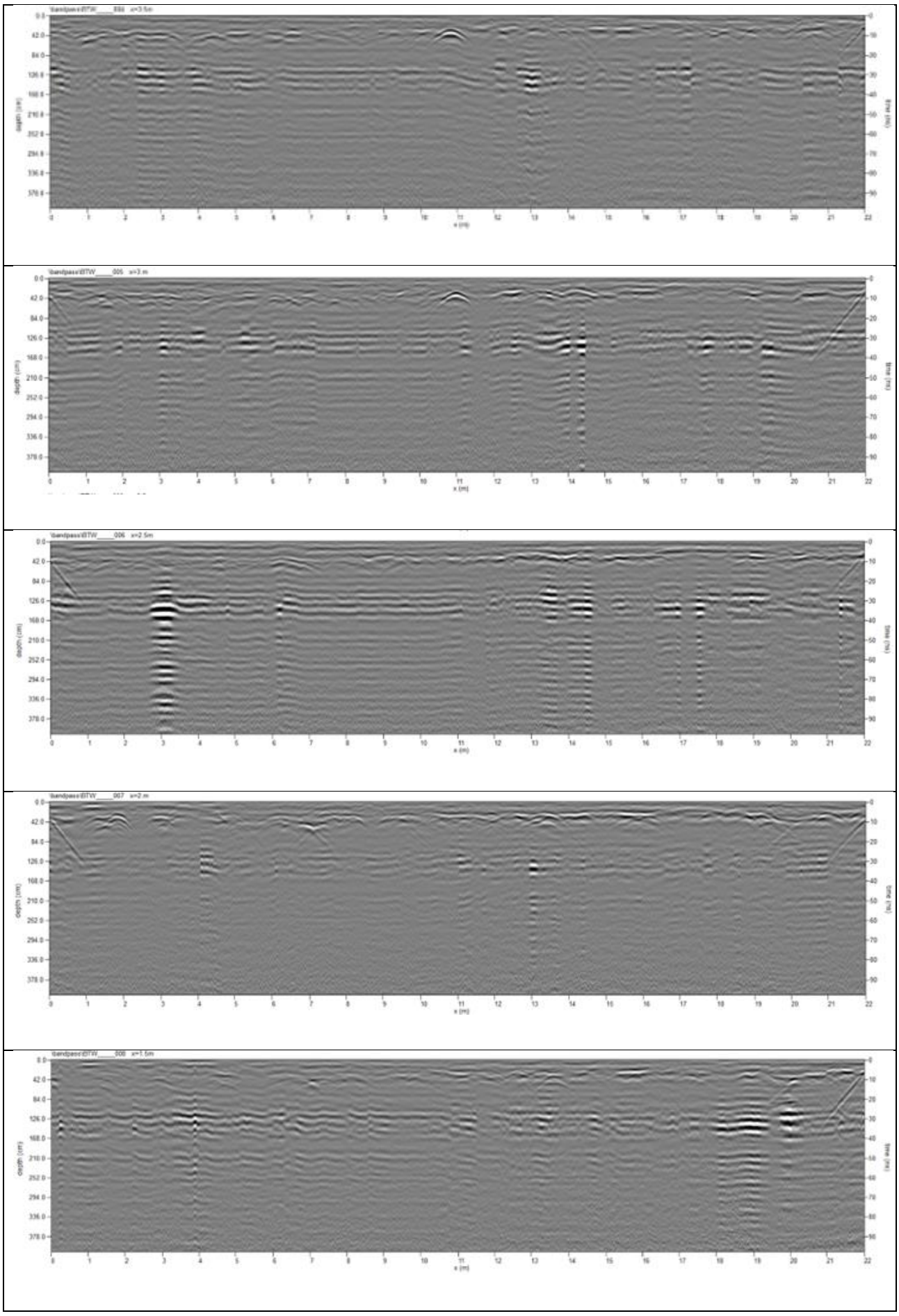

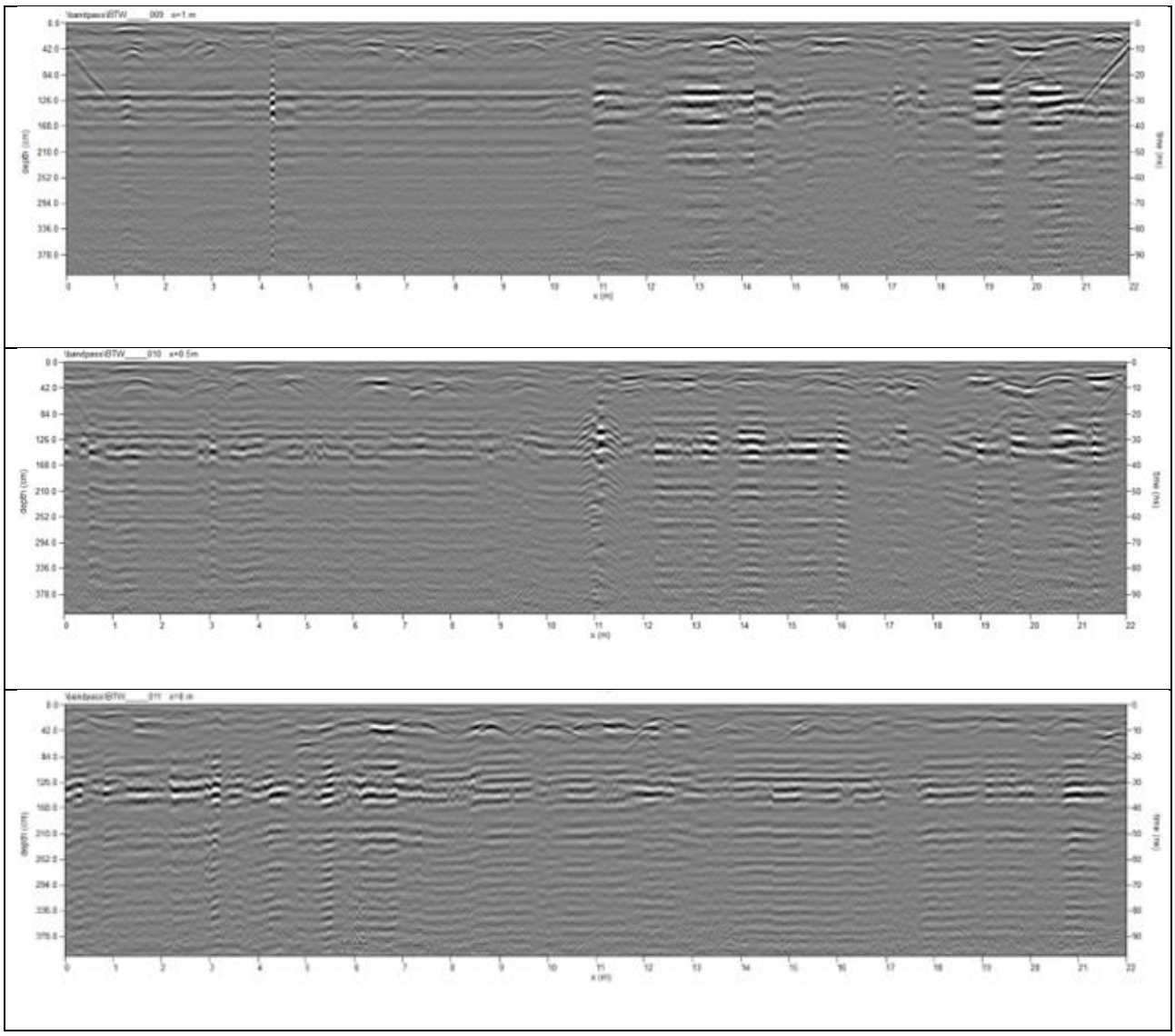

Bordertown Cemetery Rows D and E. Data collected September 2022

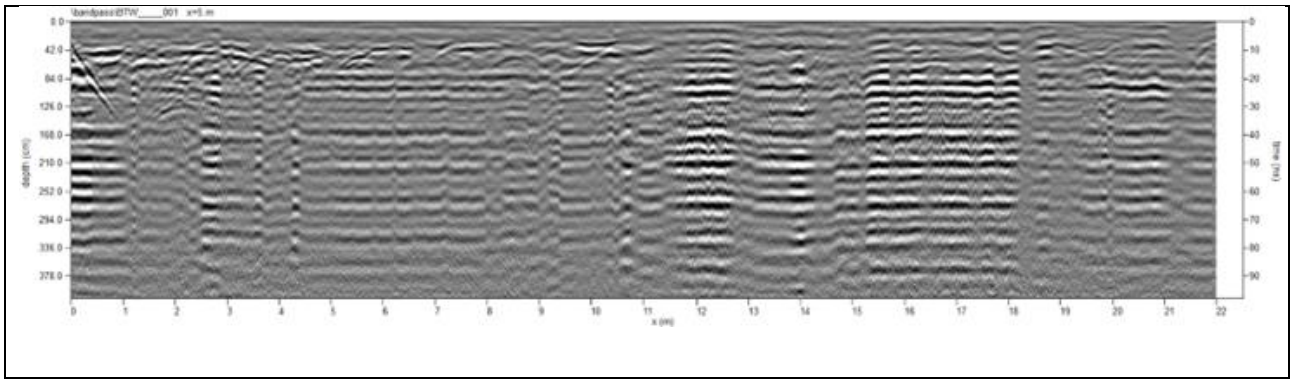

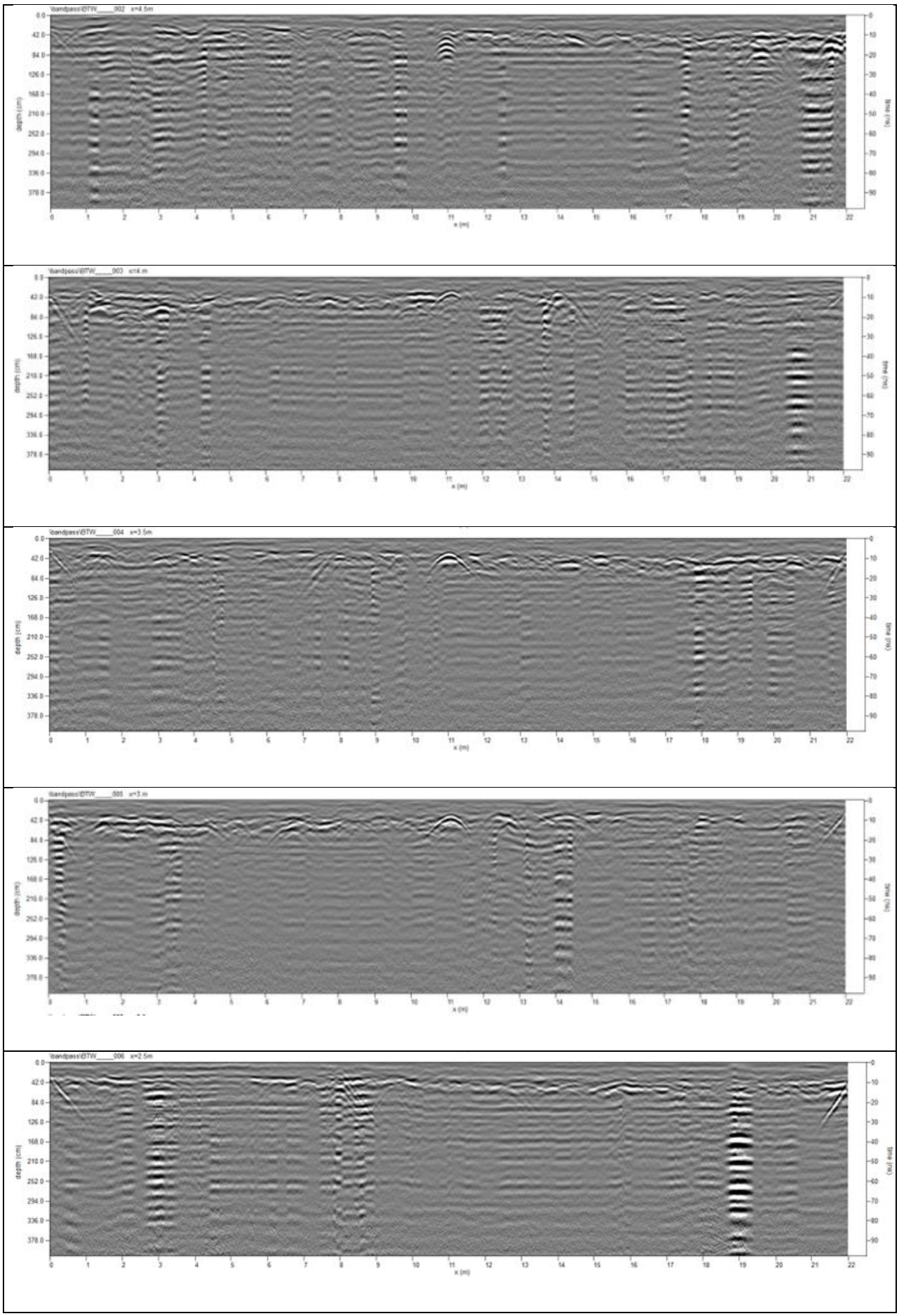
depth (cm)
x (m)
time (ns)

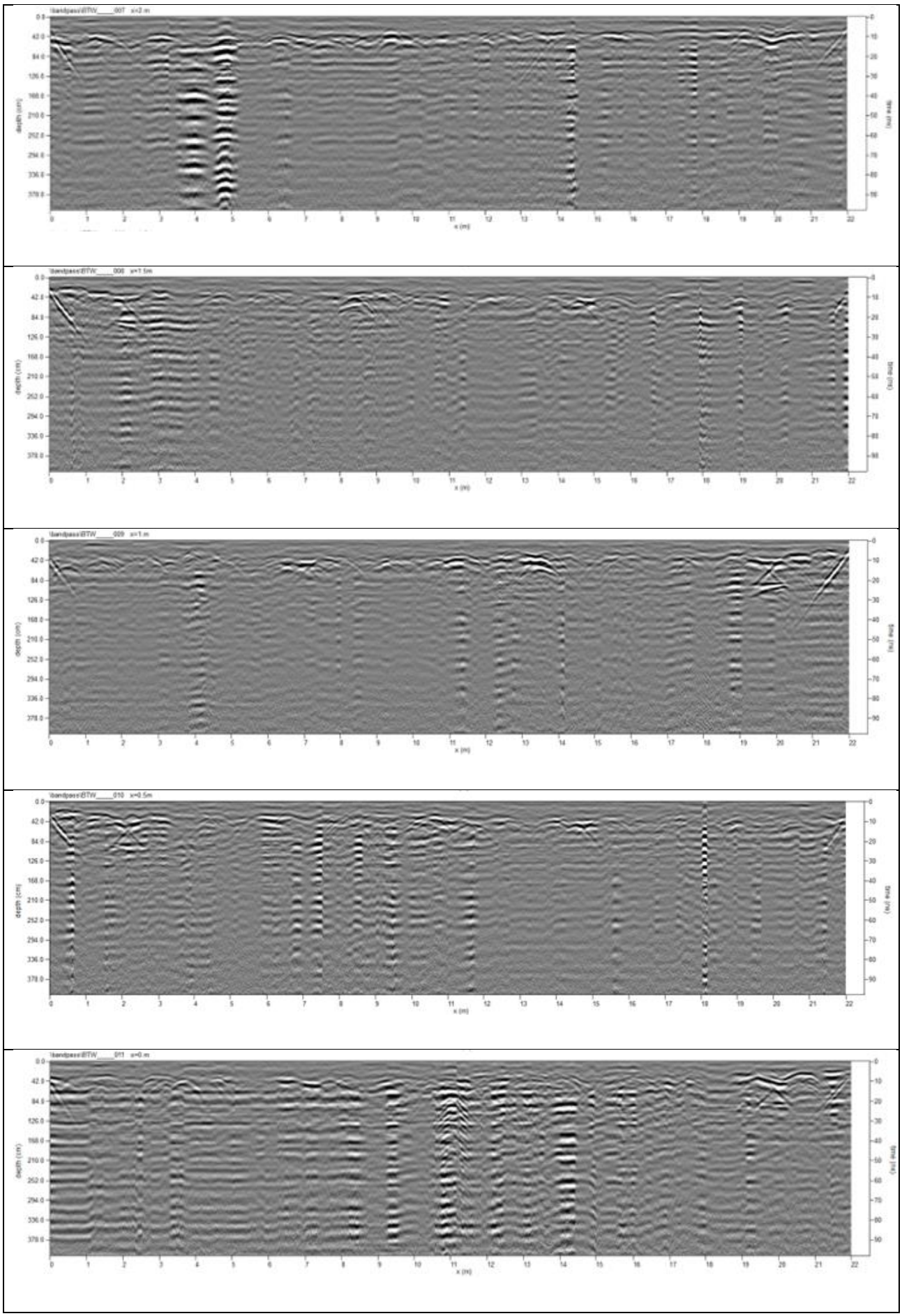

Bordertown Cemetery Rows D and E. Data collected December 2022

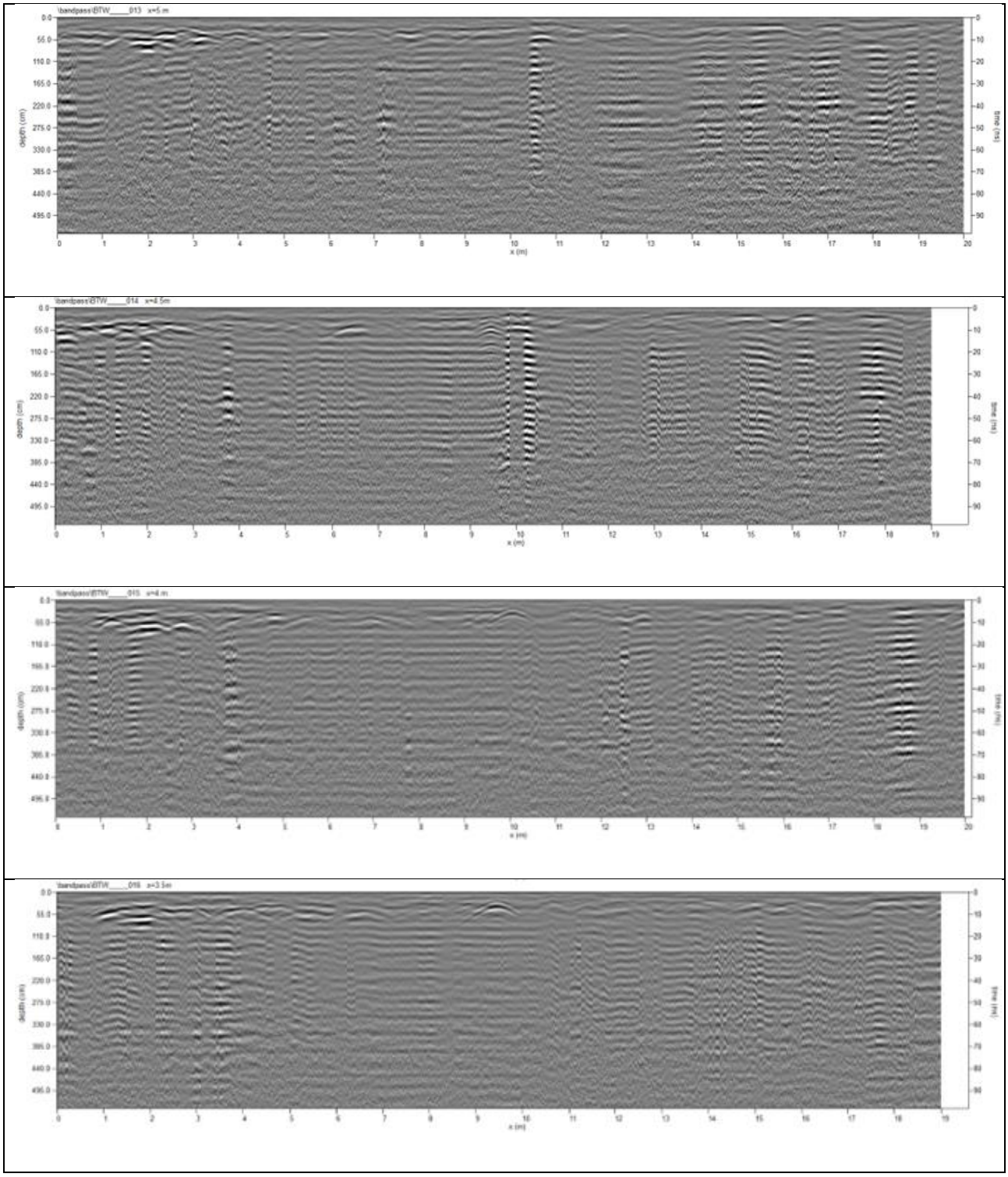

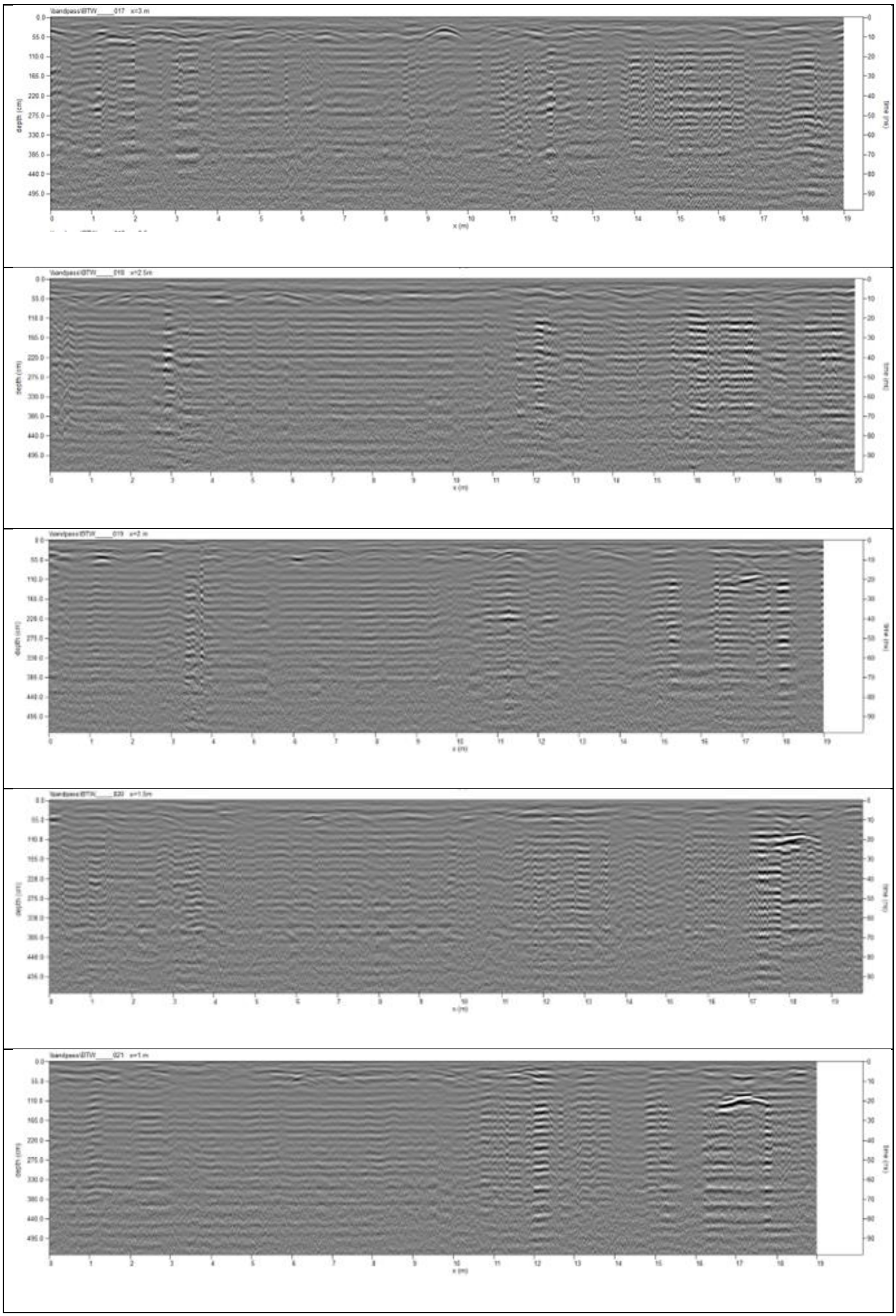

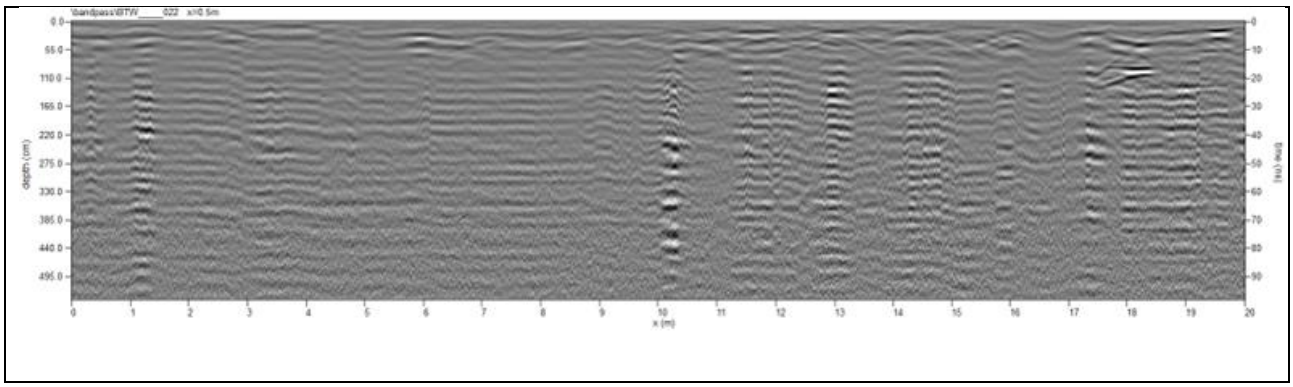

Bordertown Cemetery Rows D and E. Data collected March 2023.

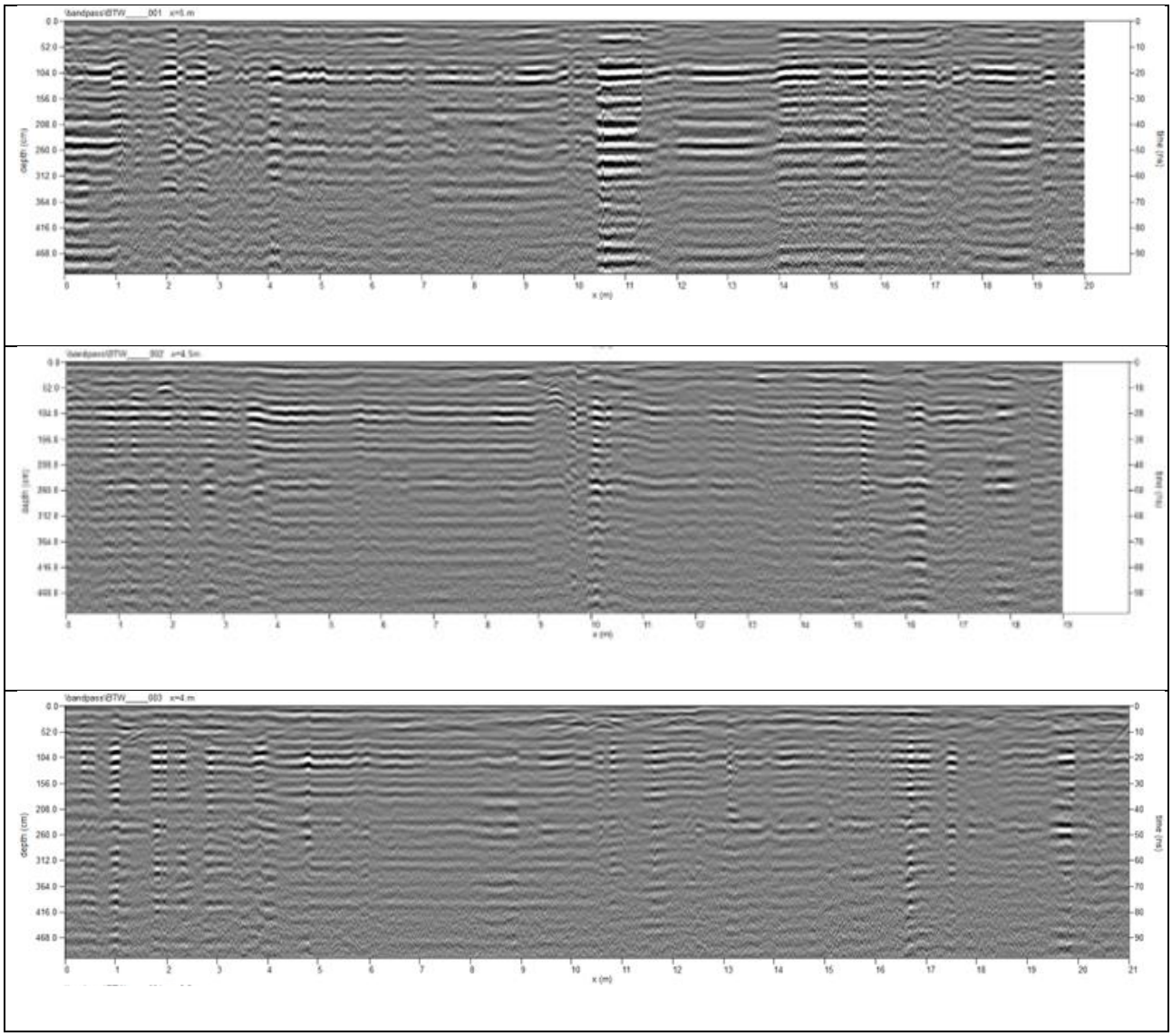

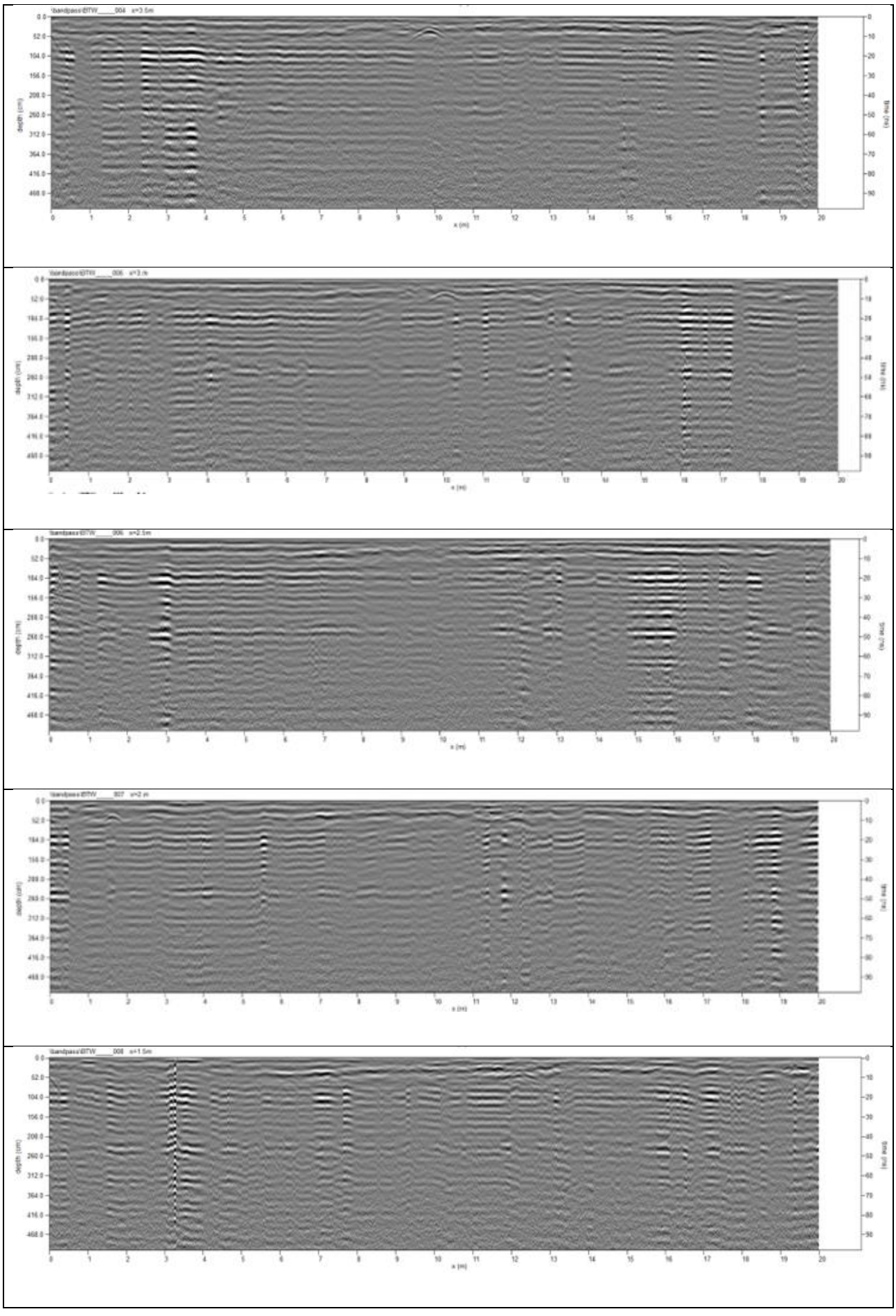

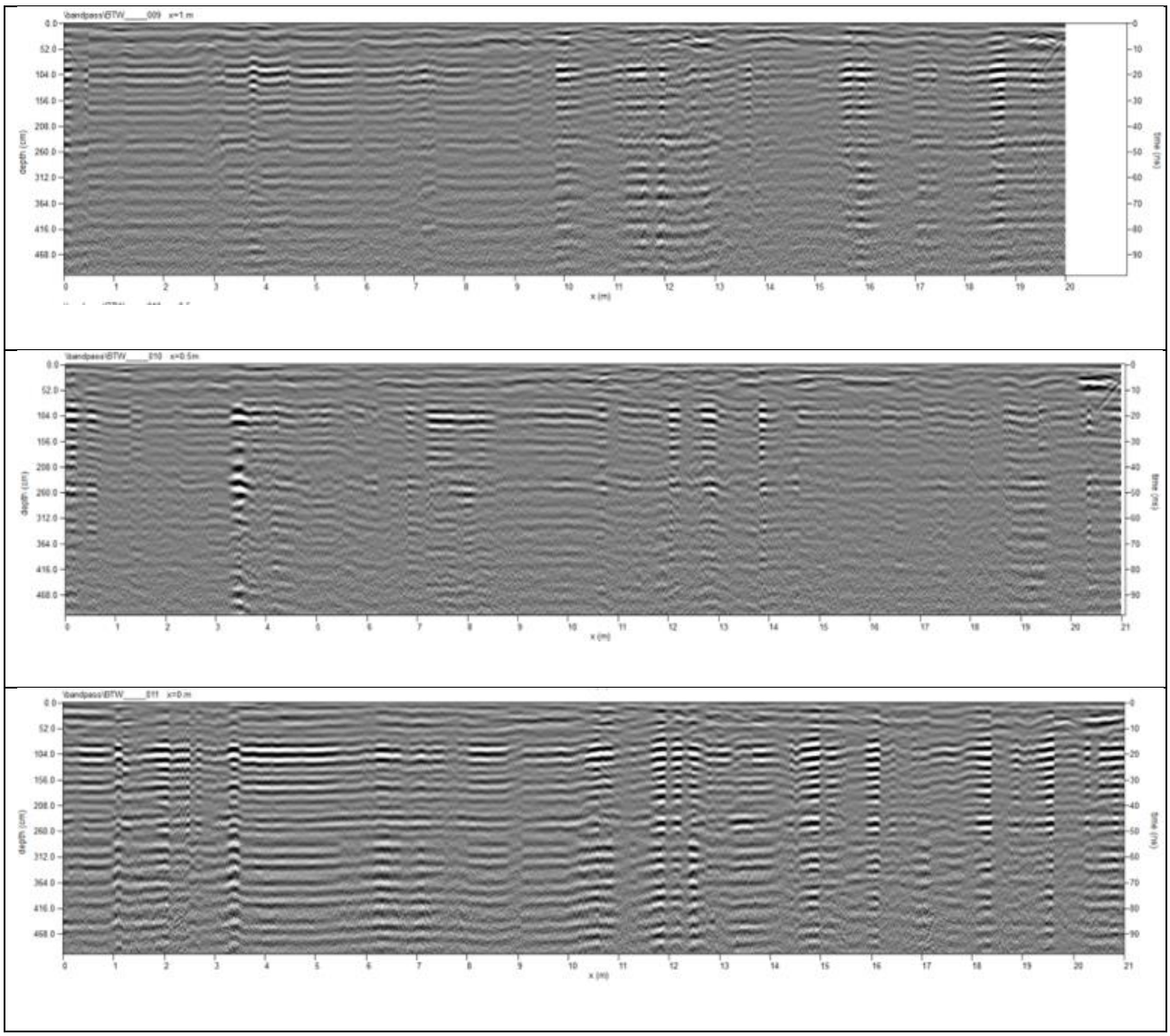

7.1.3 Port Lincoln RSL Cemetery Radargrams

RSL Cemetery Rows P and Q. Data collected September 2020

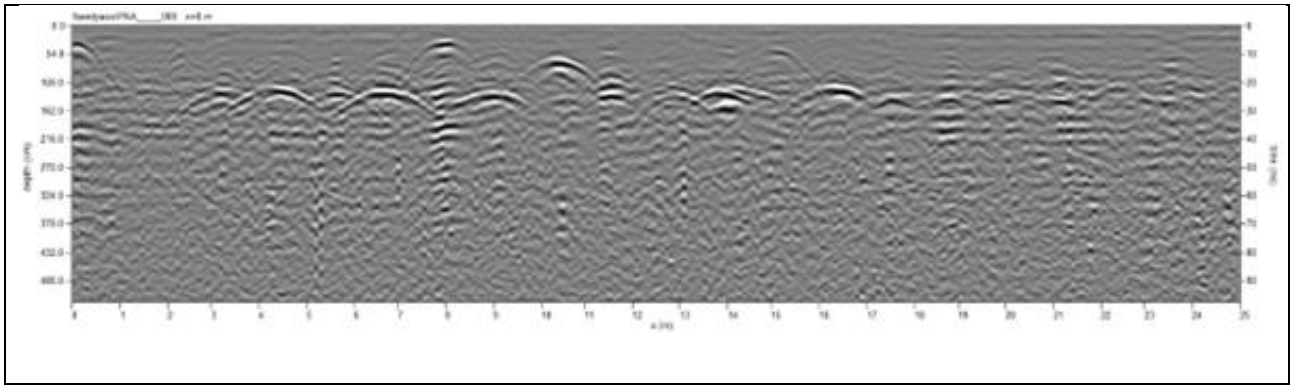

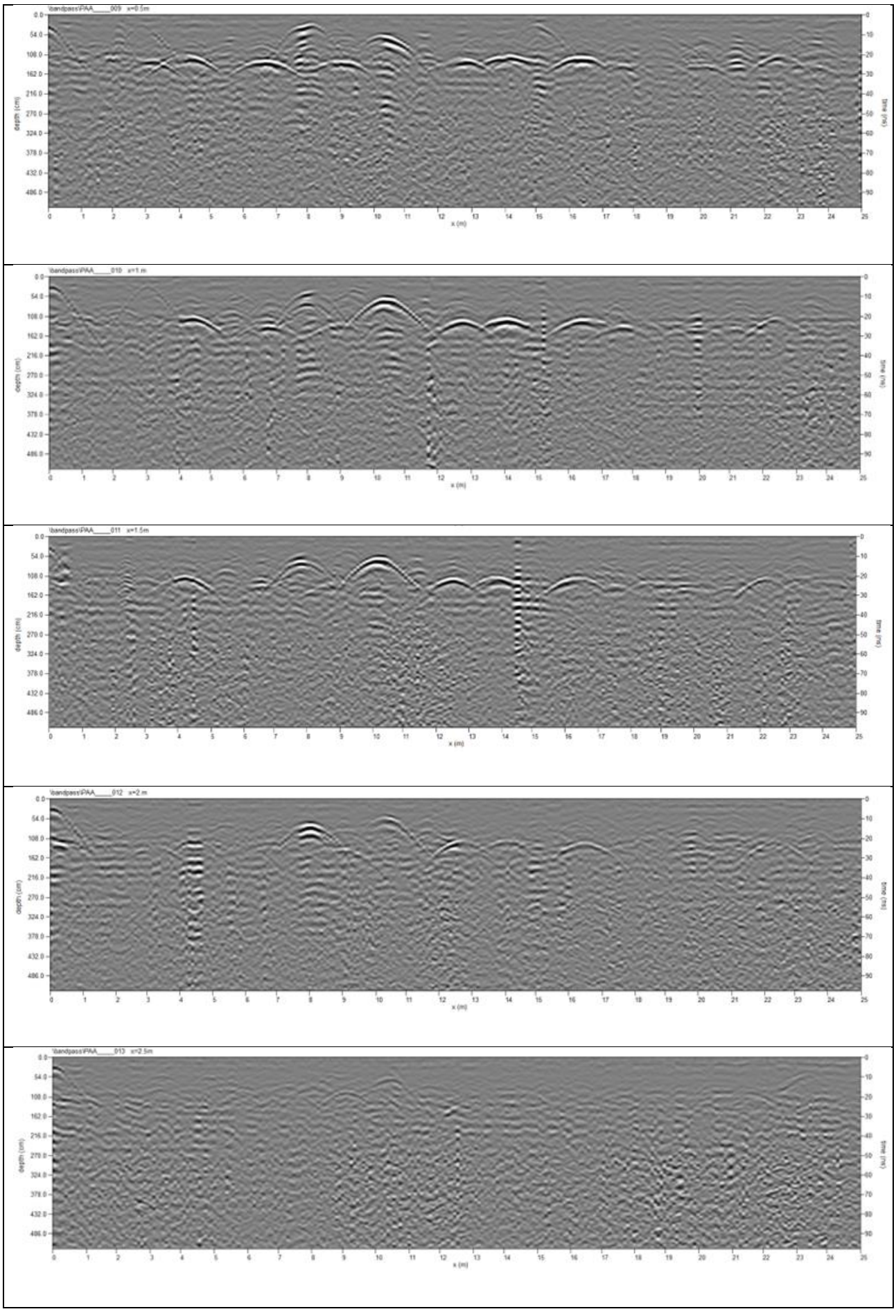
\bandpass\PAA_____009 x=0.5m
\bandpass\PAA_____010 x=1 m
\bandpass\PAA_____011 x=1.5m
\bandpass\PAA_____012 x=2 m
\bandpass\PAA_____013 x=2.5m
depth (cm)
time (ns)
x (m)

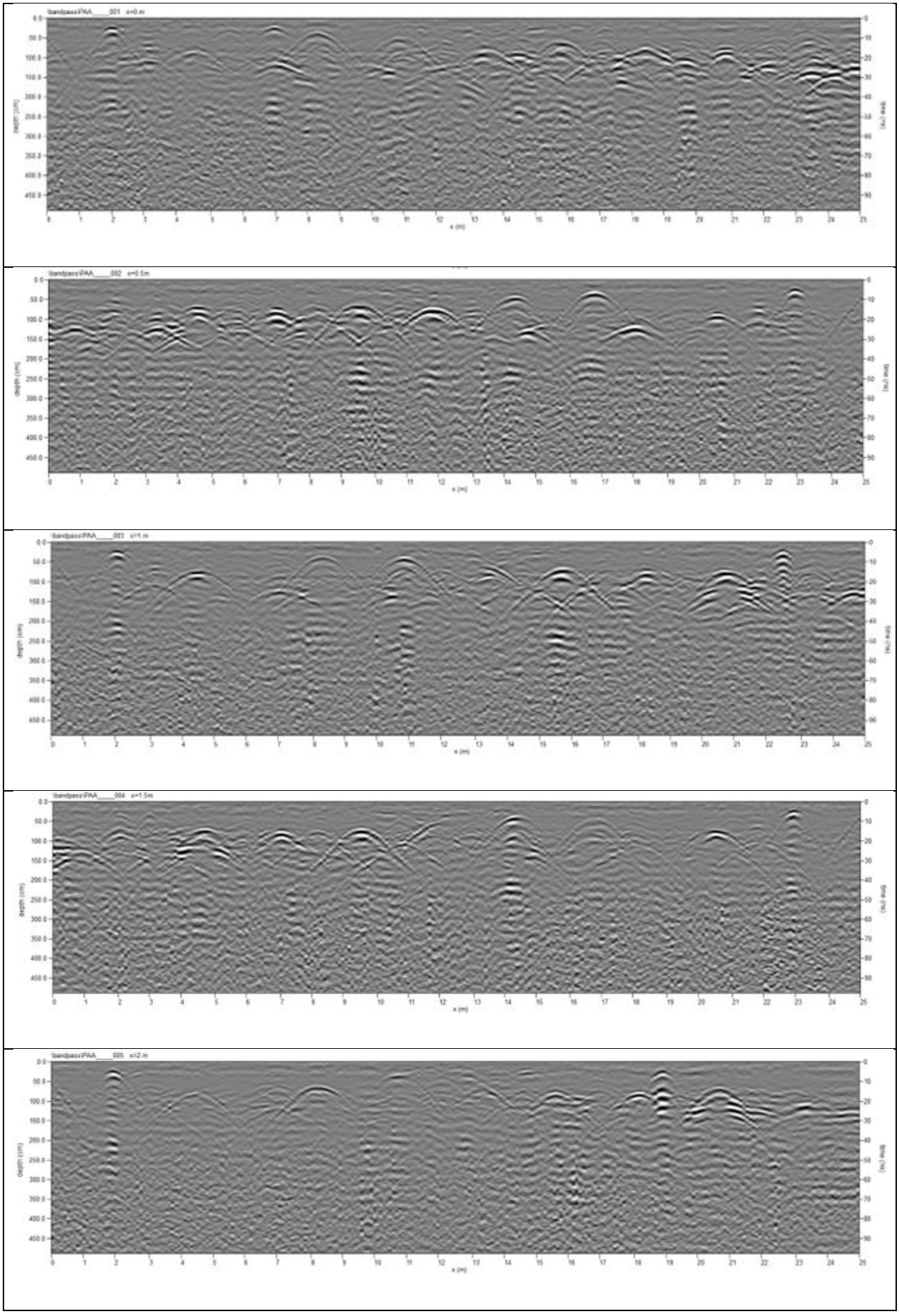

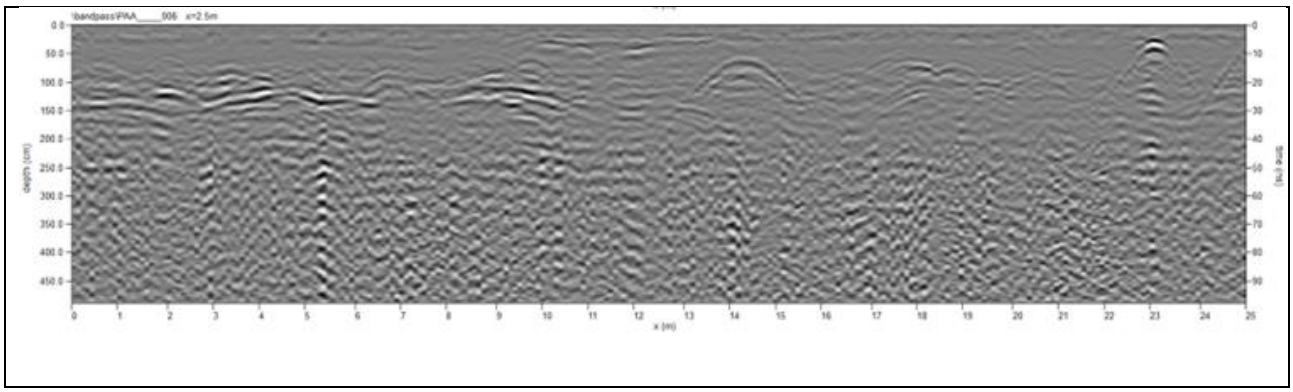

Port Lincoln RSL Cemetery Rows P and Q. Data collected December 2020

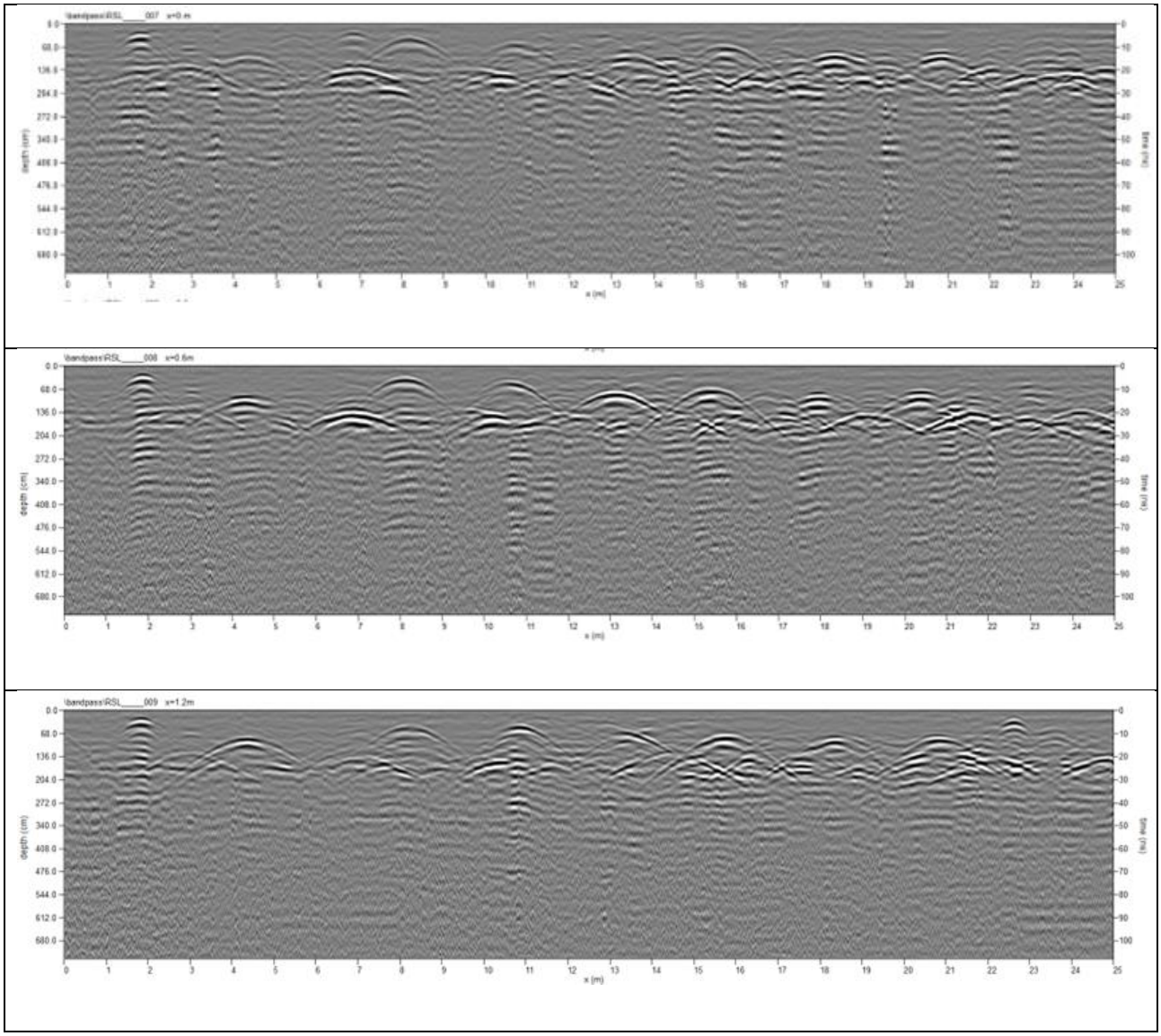

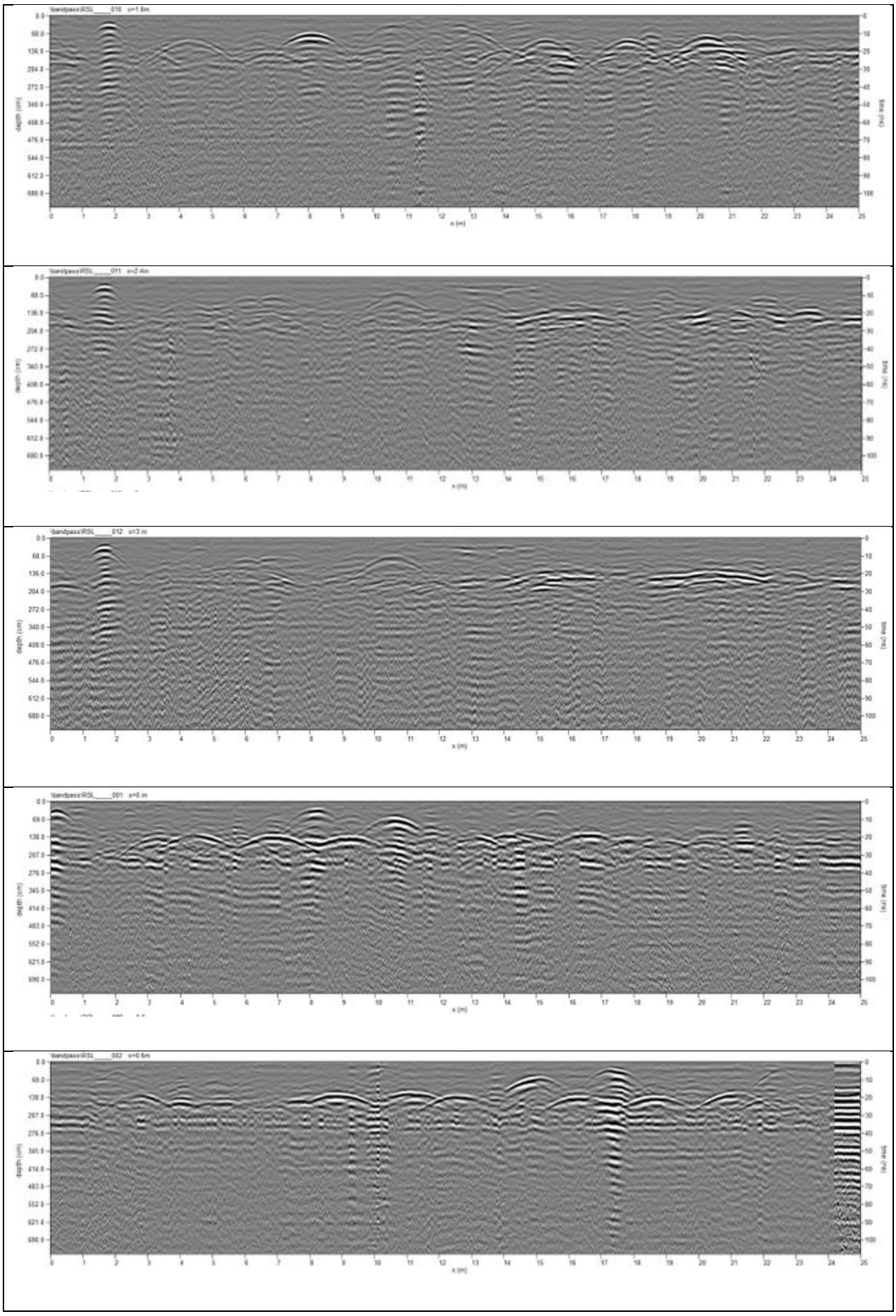
depth (cm)
time (ns)
x (m)

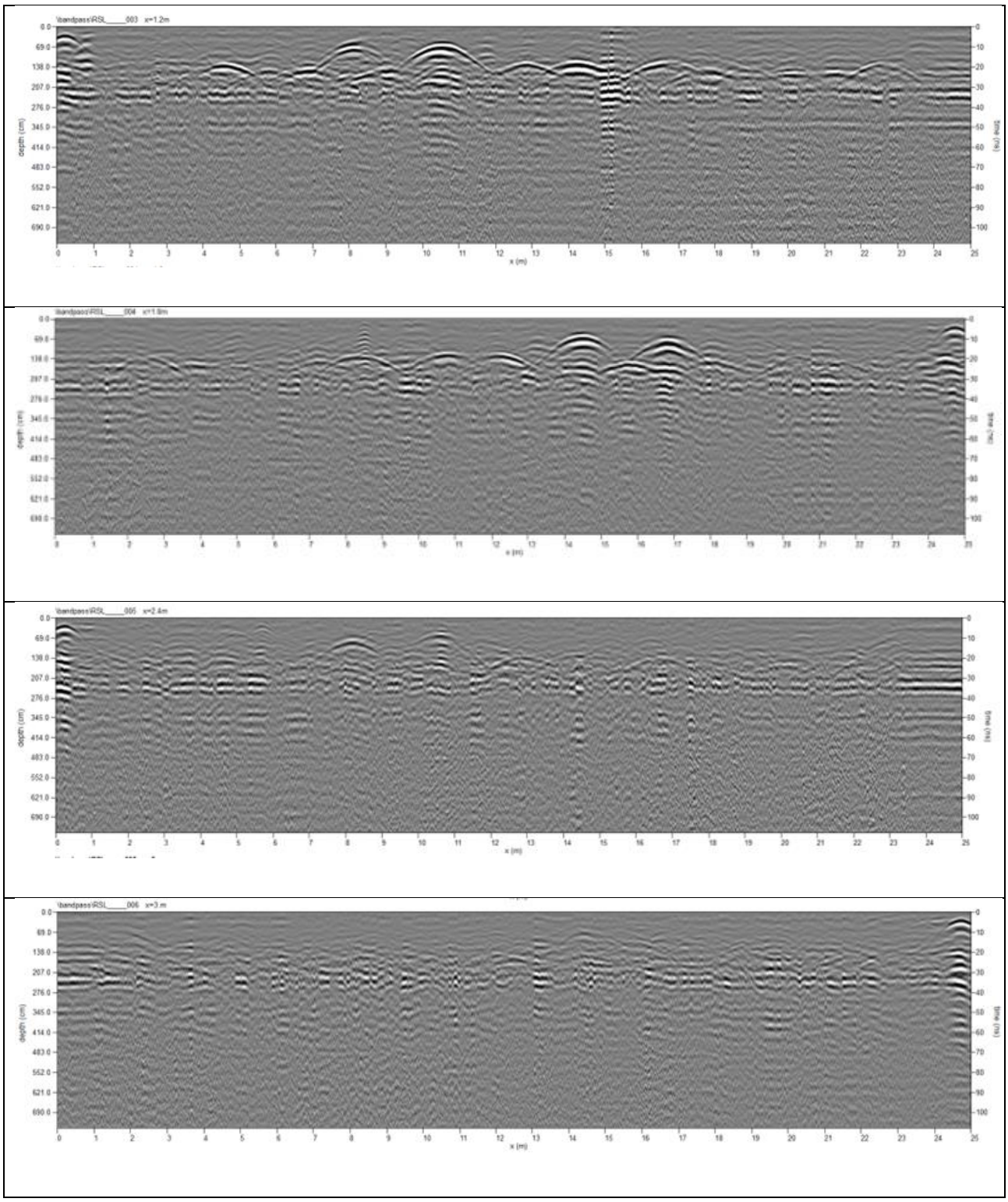

Port Lincoln RSL Cemetery Rows P and Q. Data collected March 2021

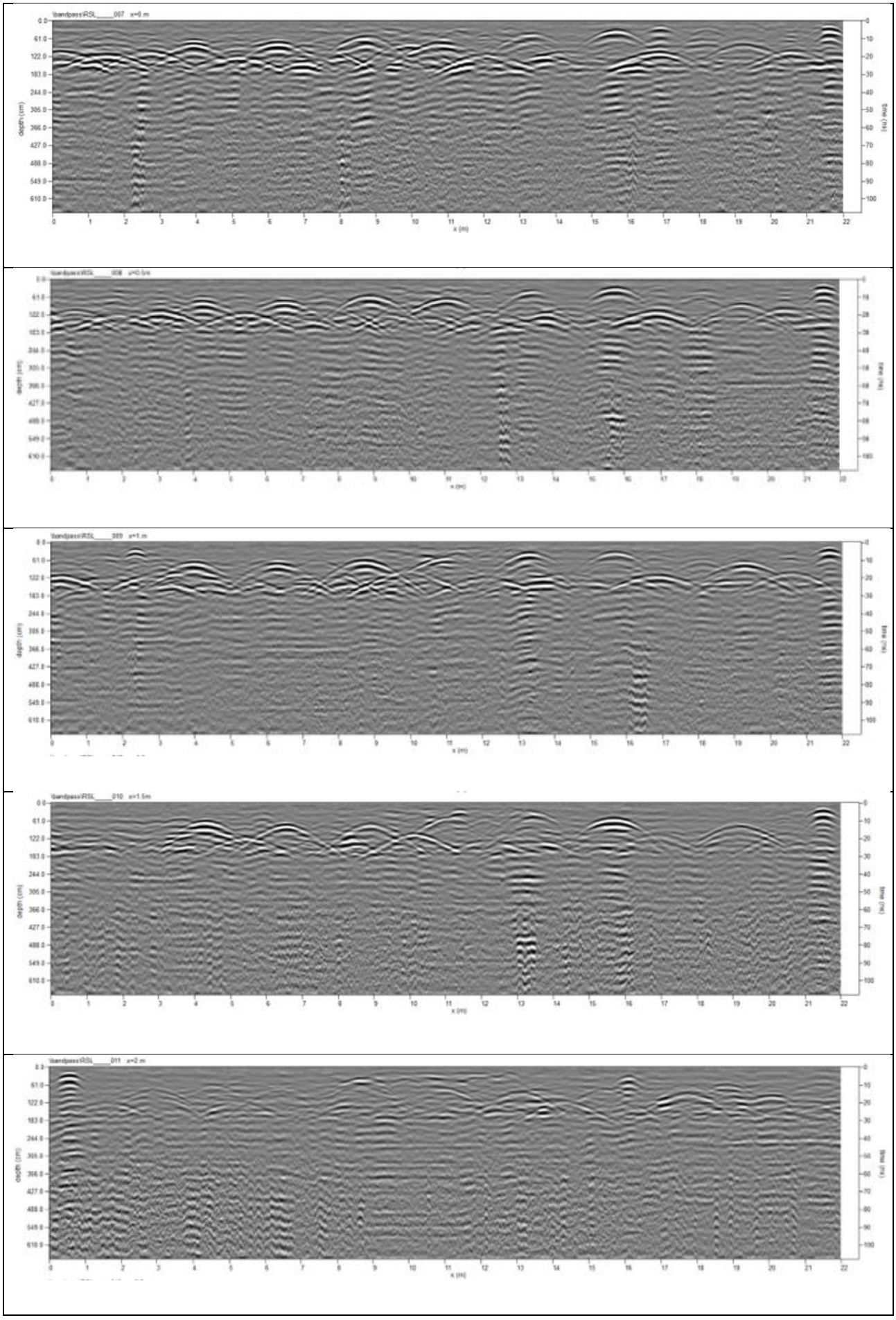

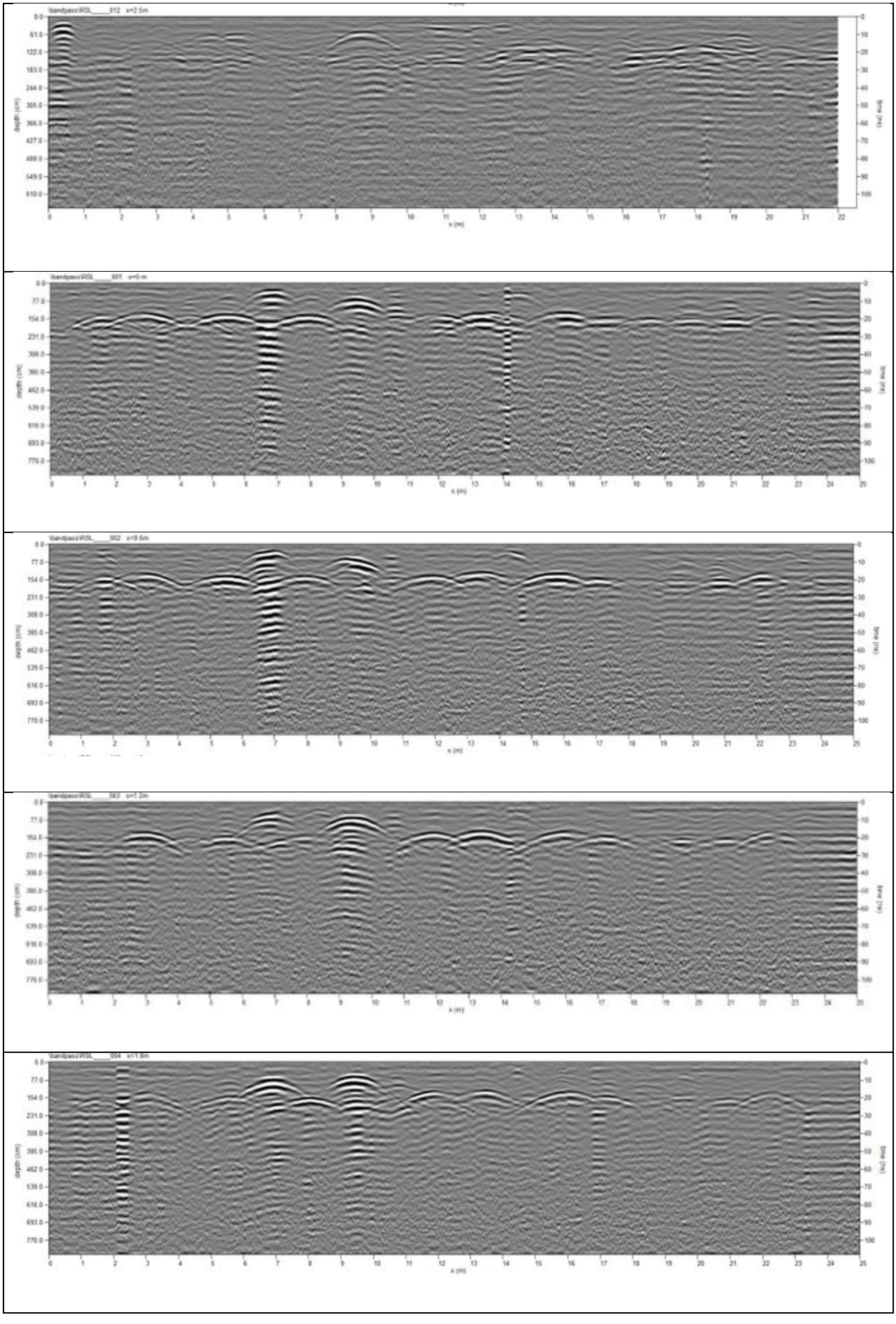

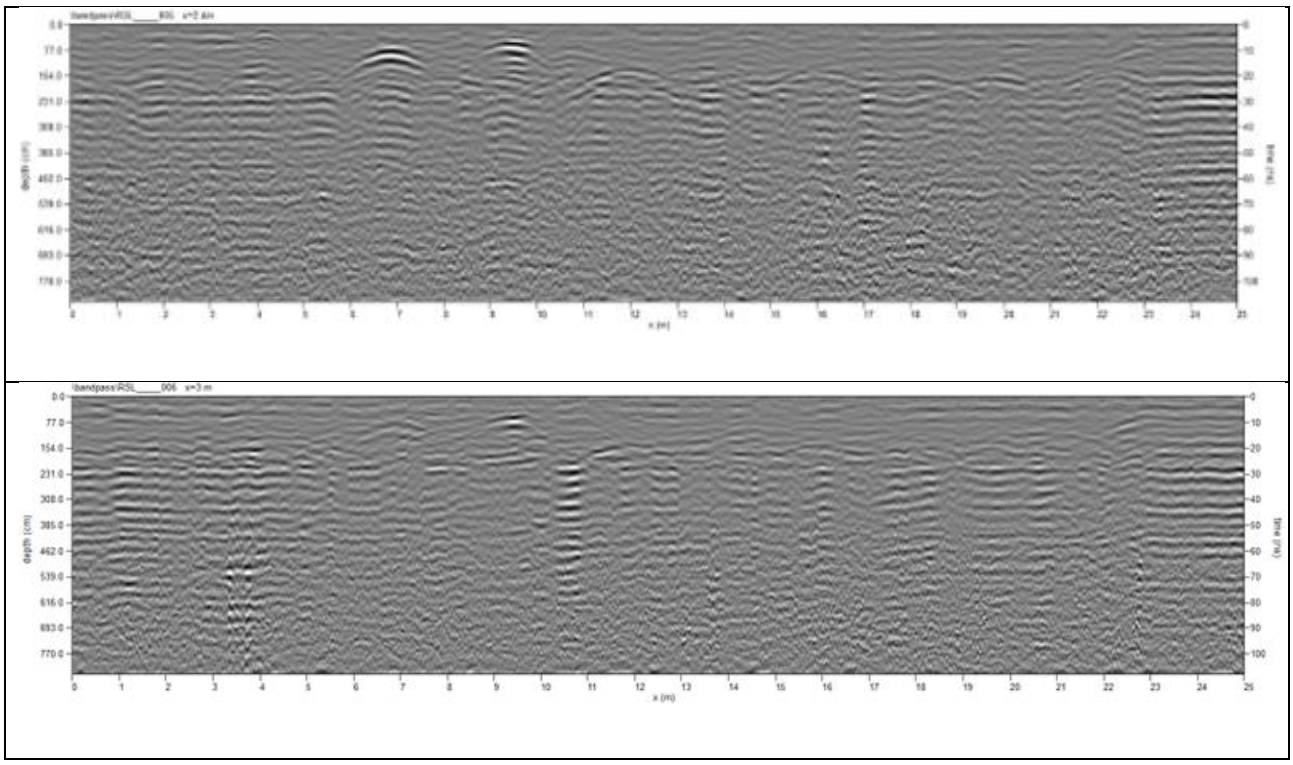

Port Lincoln RSL Cemetery Rows P and Q. Data collected June 2021

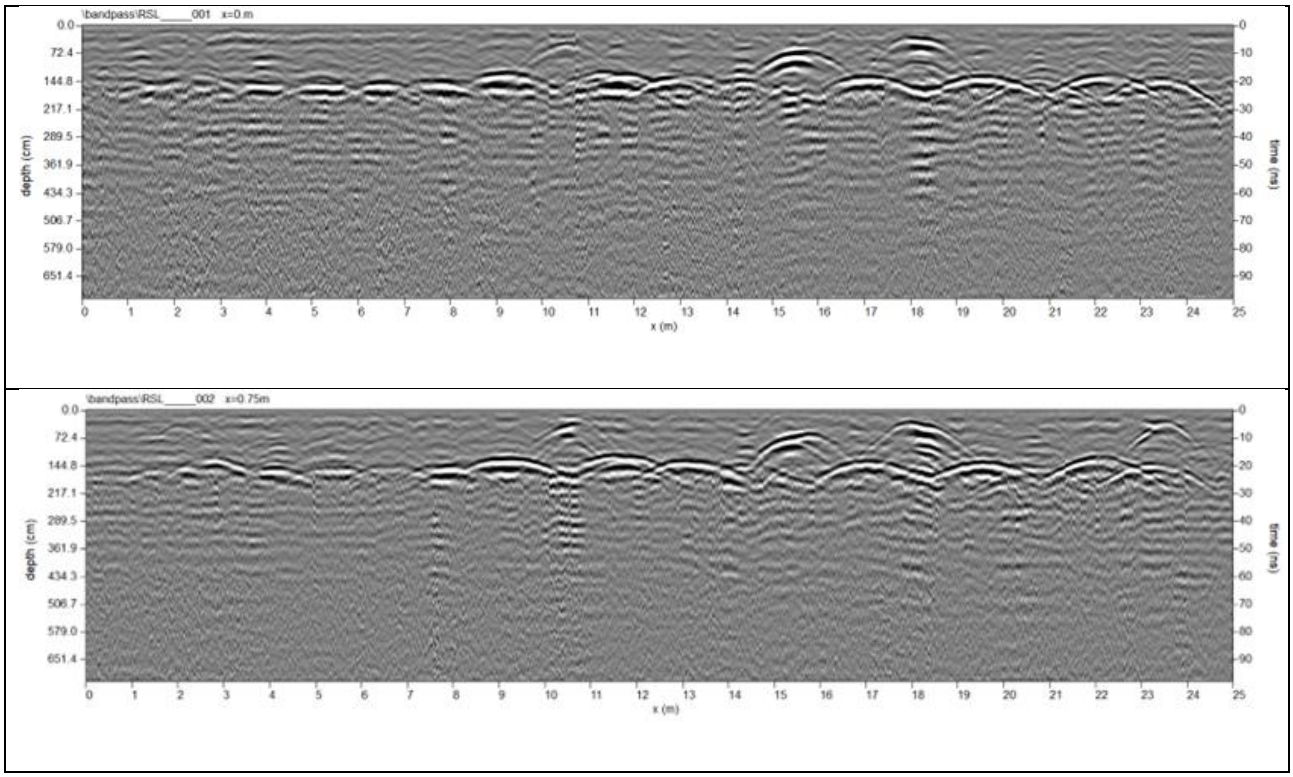

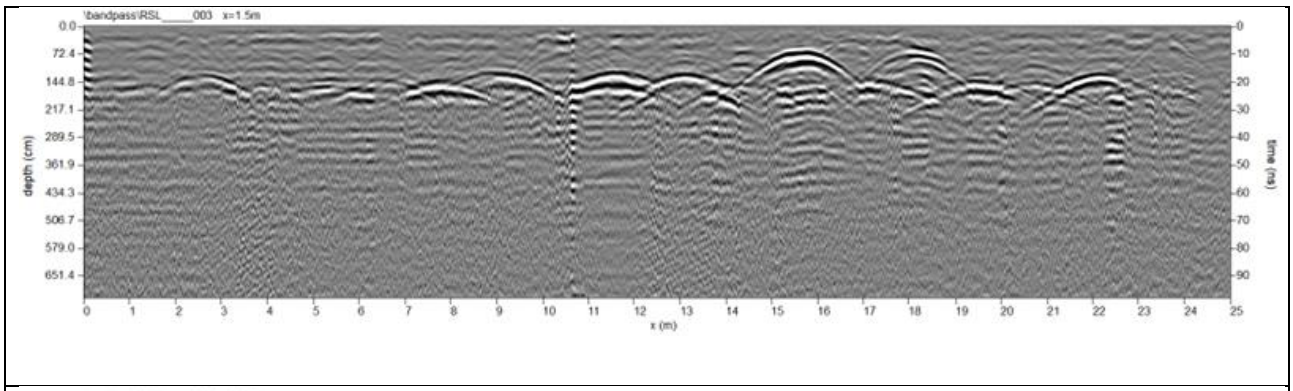
\bandpass\RSL_____003 x=1.5m
depth (cm)
time (ns)
x (m)

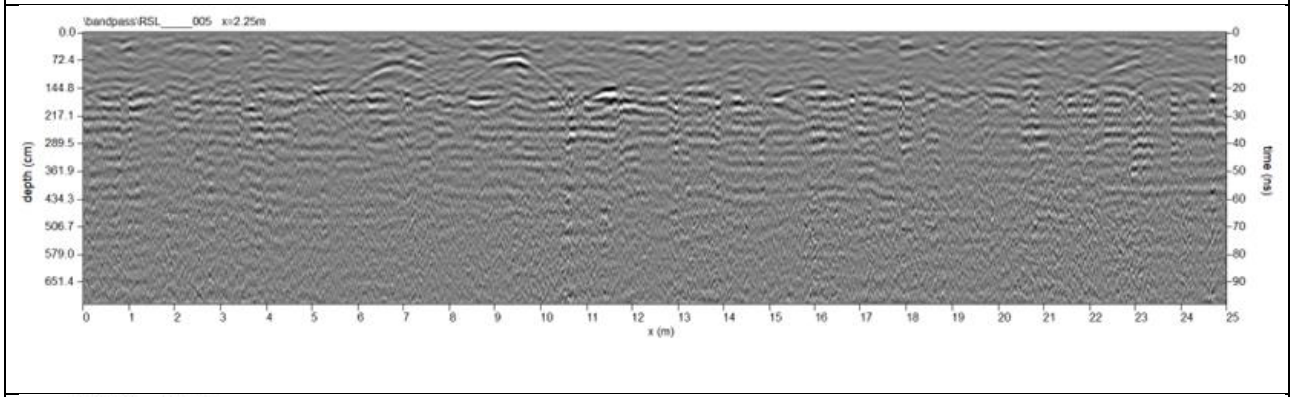
\bandpass\RSL_____005 x=2.25m
depth (cm)
time (ns)
x (m)

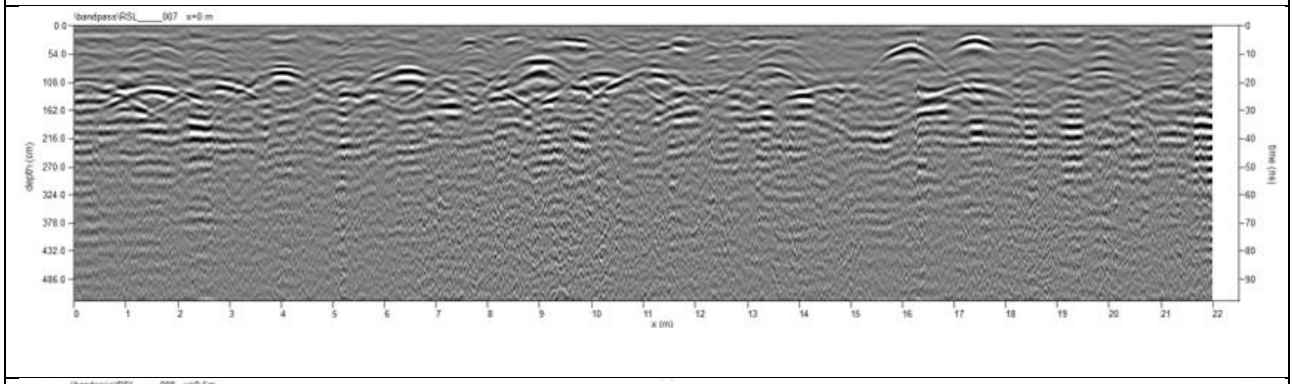
\bandpass\RSL_____007 x=0 m
depth (cm)
time (ns)
x (m)

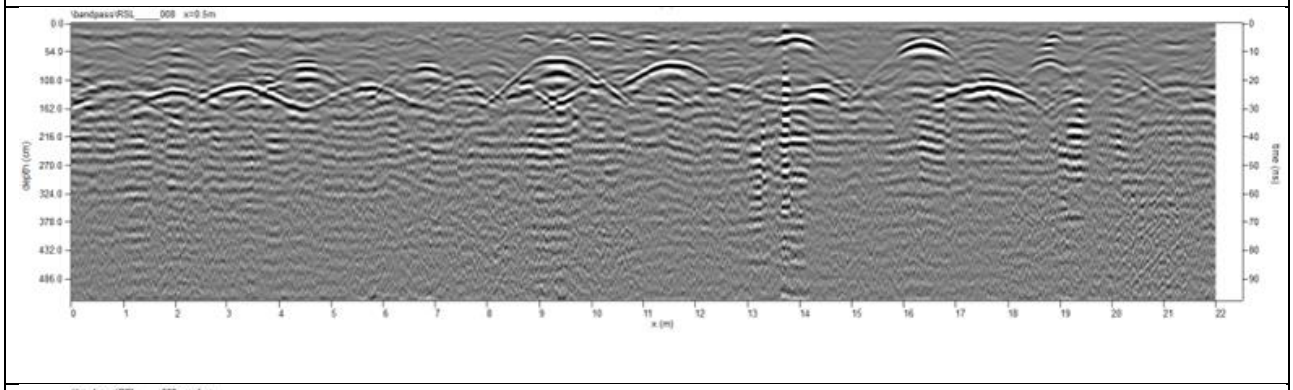
\bandpass\RSL_____008 x=0.5m
depth (cm)
time (ns)
x (m)

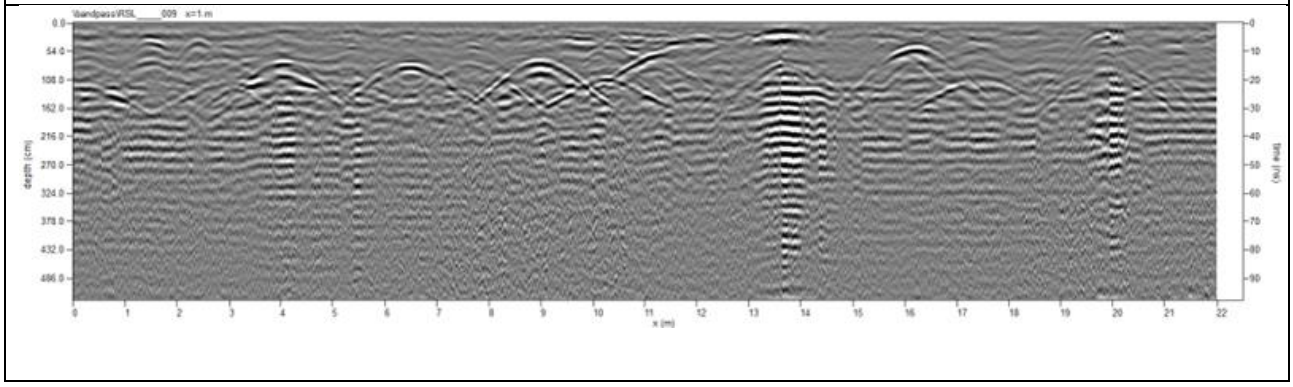
\bandpass\RSL_____009 x=1 m
depth (cm)
time (ns)
x (m)

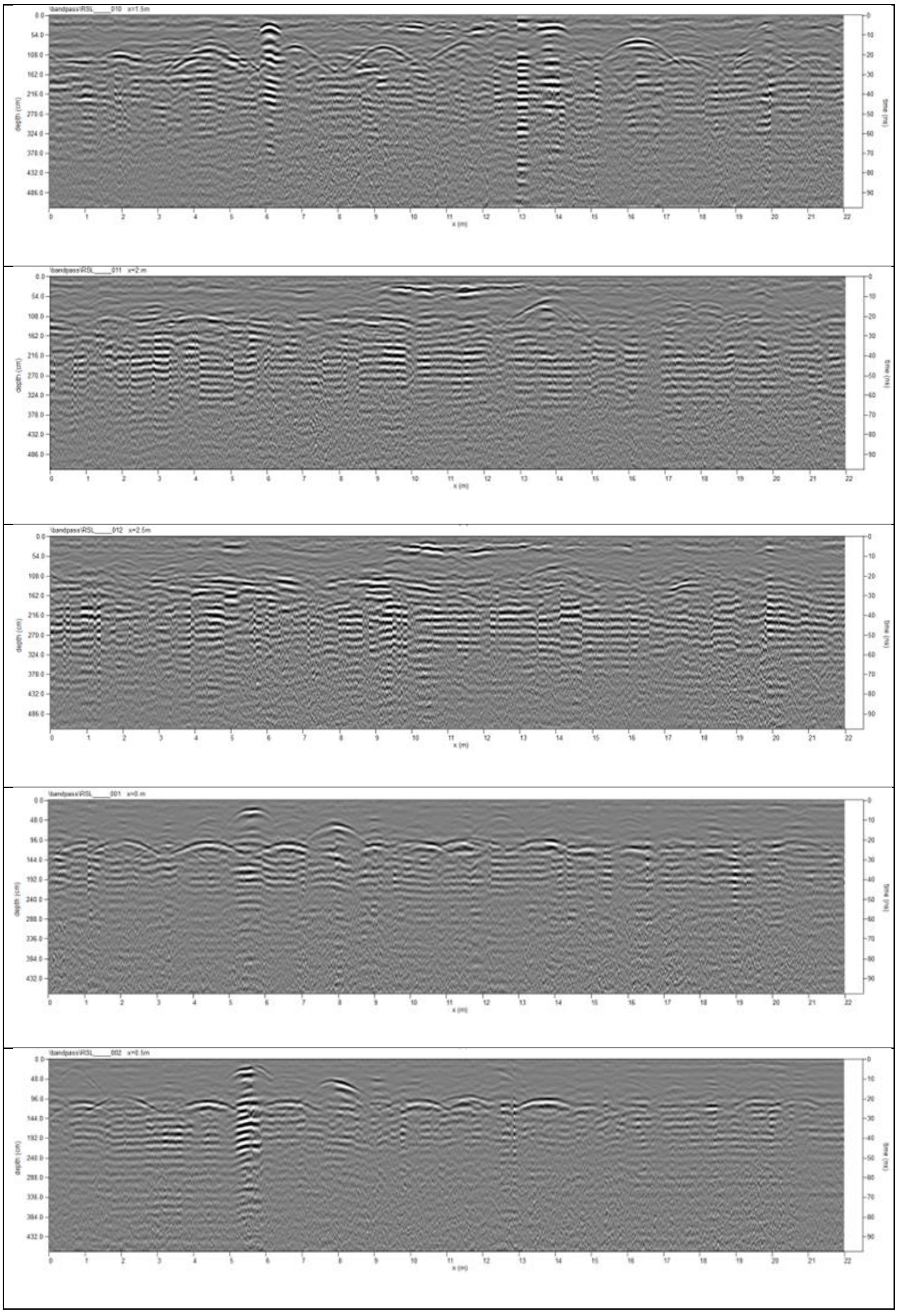
\bandpass\RSL____010 x=1.5m
\bandpass\RSL____011 x=2 m
\bandpass\RSL____012 x=2.5m
\bandpass\RSL____001 x=0 m
\bandpass\RSL____002 x=0.5m
depth (cm)
time (ns)
x (m)

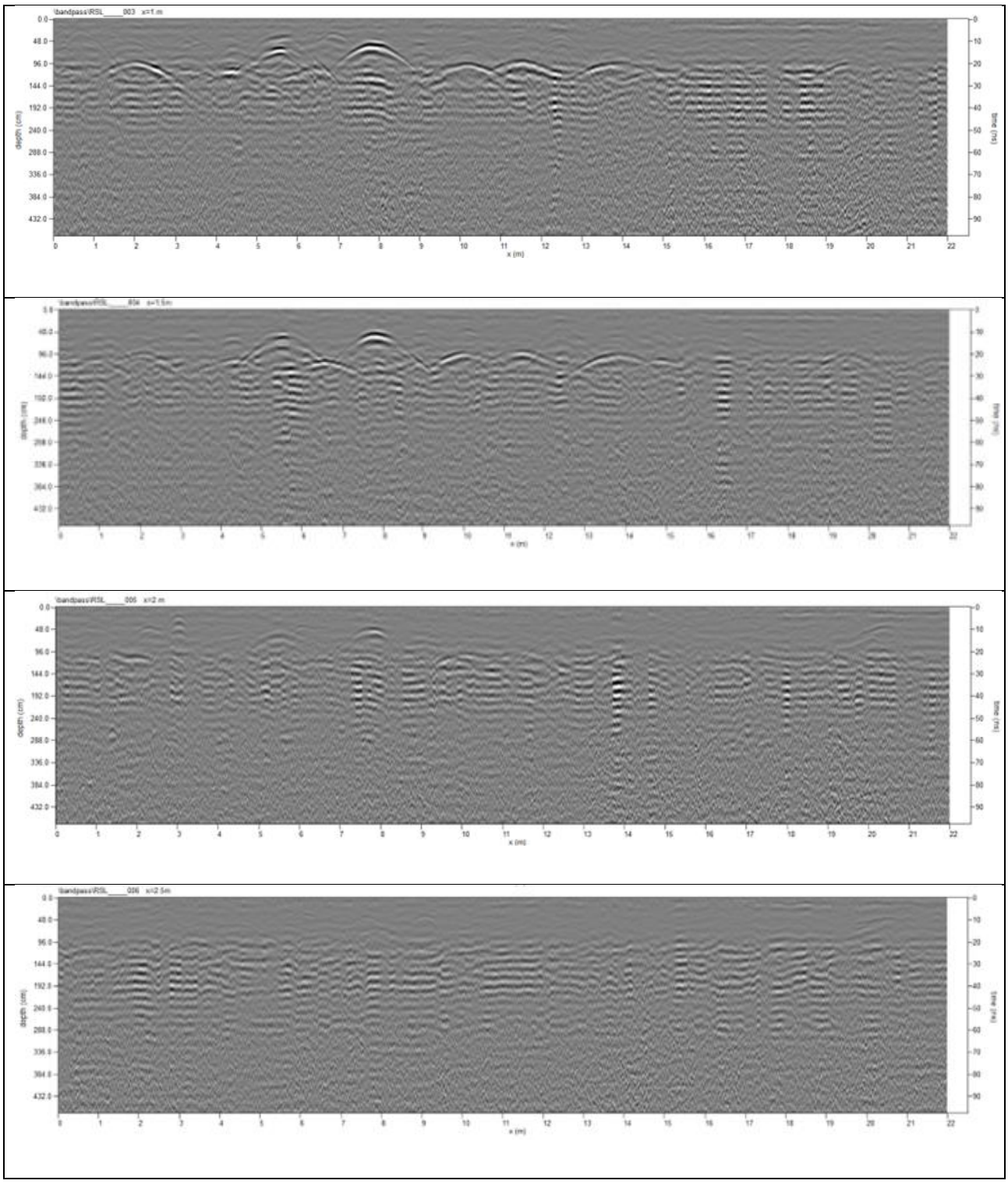

Port Lincoln RSL Cemetery Rows P and Q. Data collected September 2022

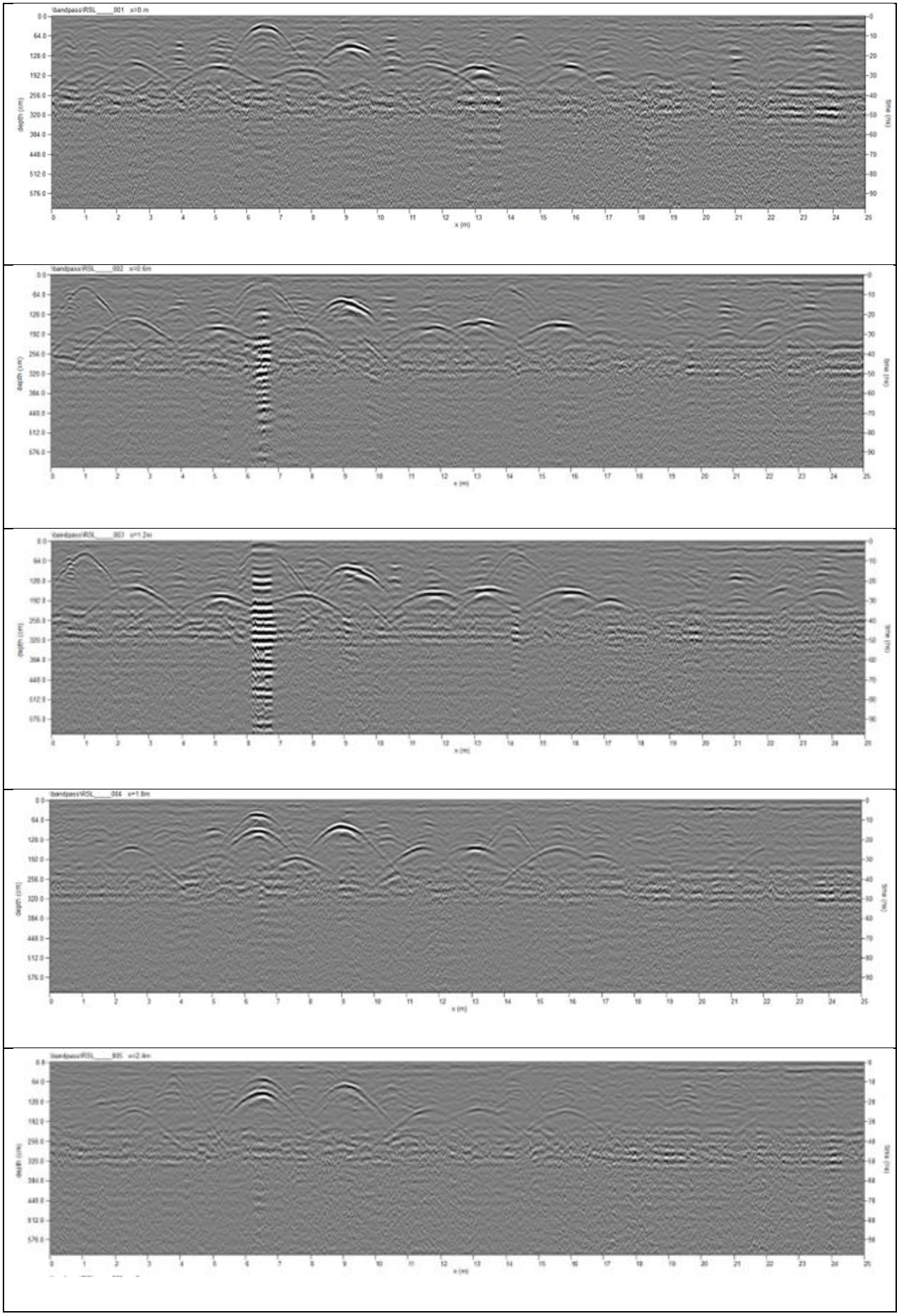

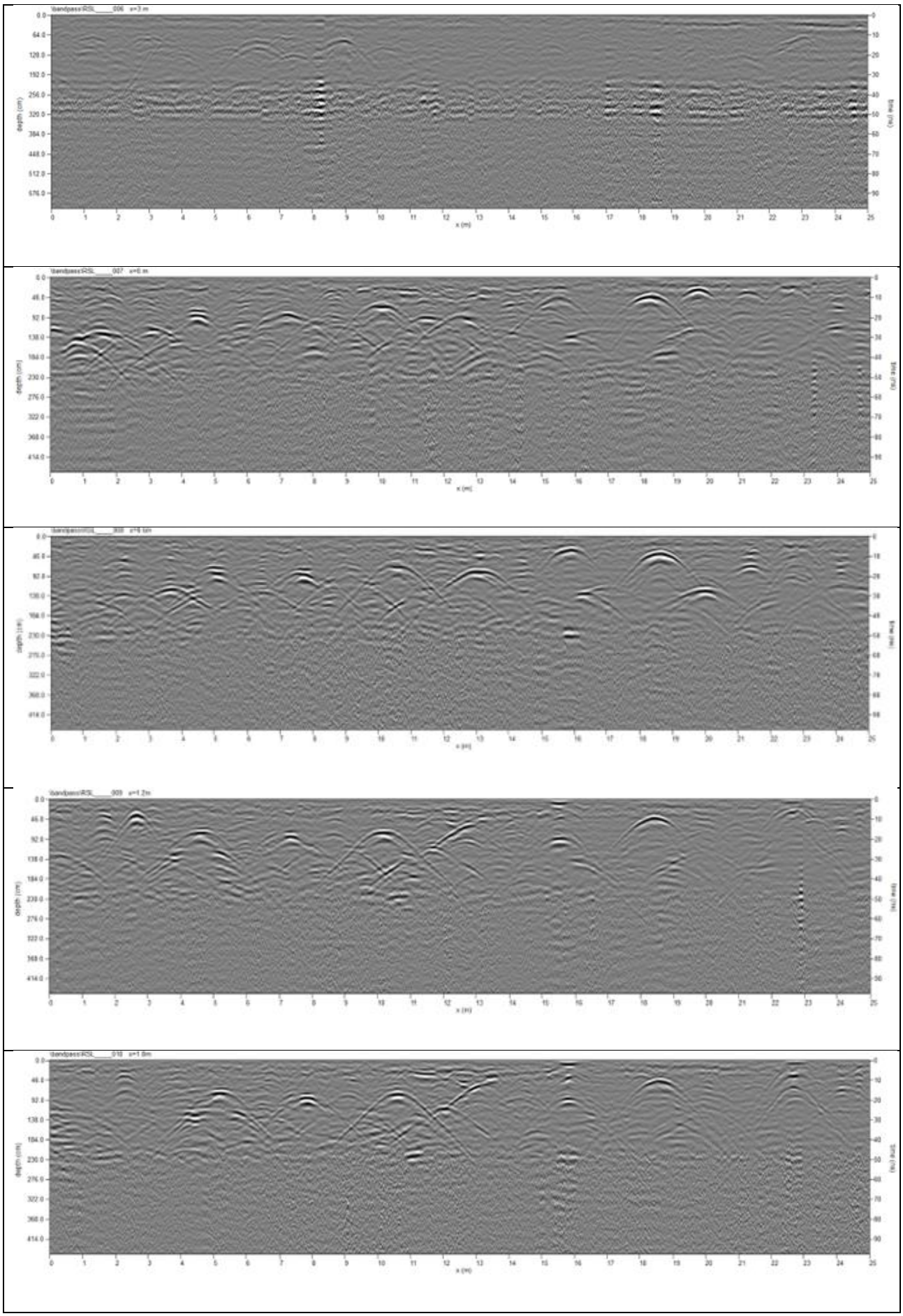

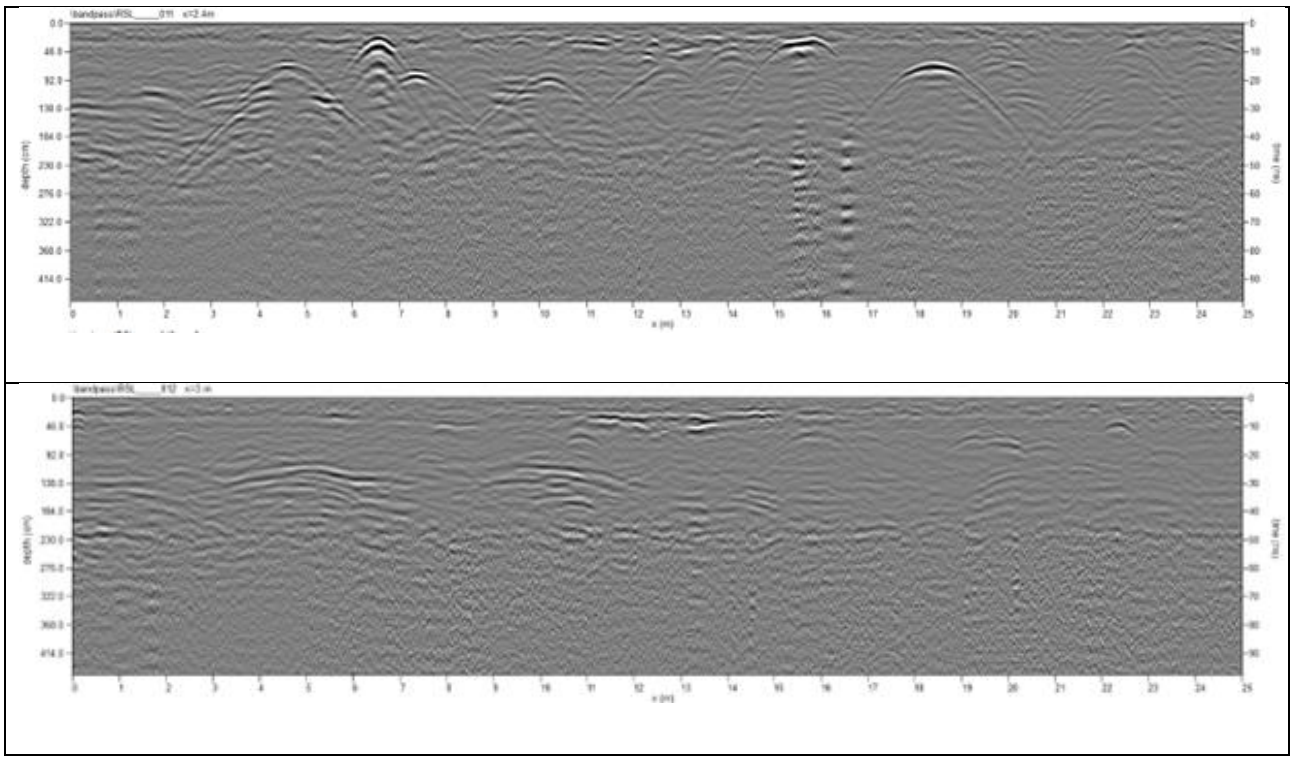

Port Lincoln RSL Cemetery Rows P and Q. Data collected December 2022.

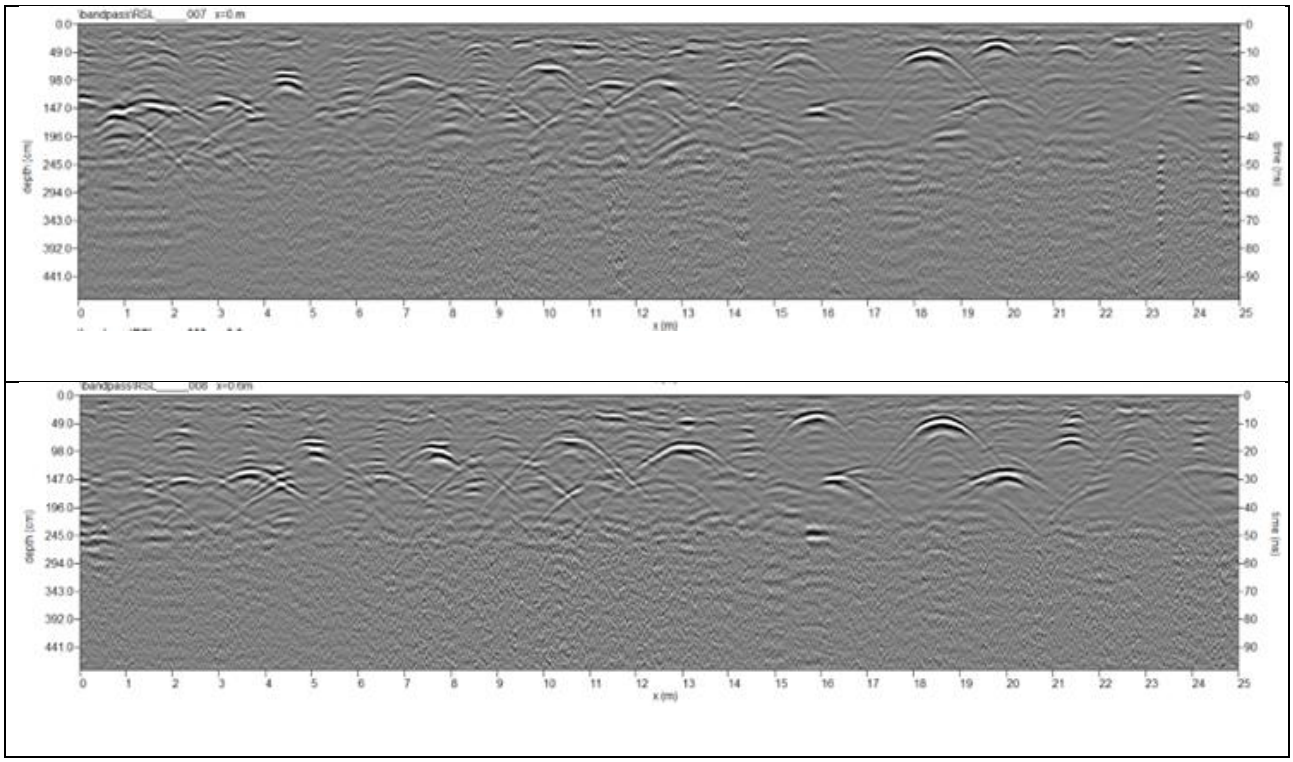

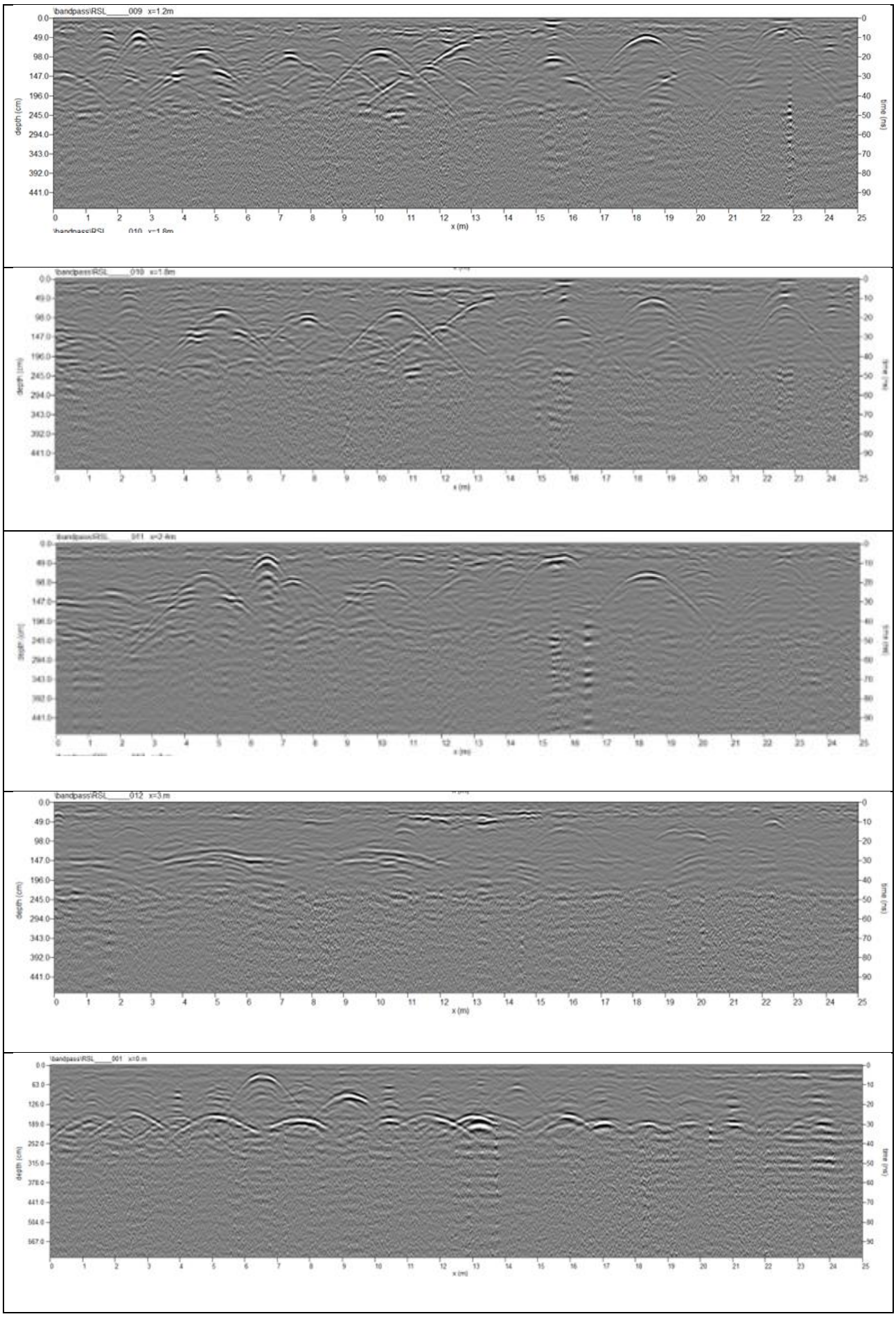
\bandpass\RSL_____009 x=1.2m
depth (cm)
time (ns)
x (m)
\bandpass\RSL_____010 x=1.8m
depth (cm)
time (ns)
x (m)
depth (cm)
time (ns)
x (m)
\bandpass\RSL_____012 x=3 m
depth (cm)
time (ns)
x (m)
\bandpass\RSL_____001 x=0 m
depth (cm)
time (ns)
x (m)

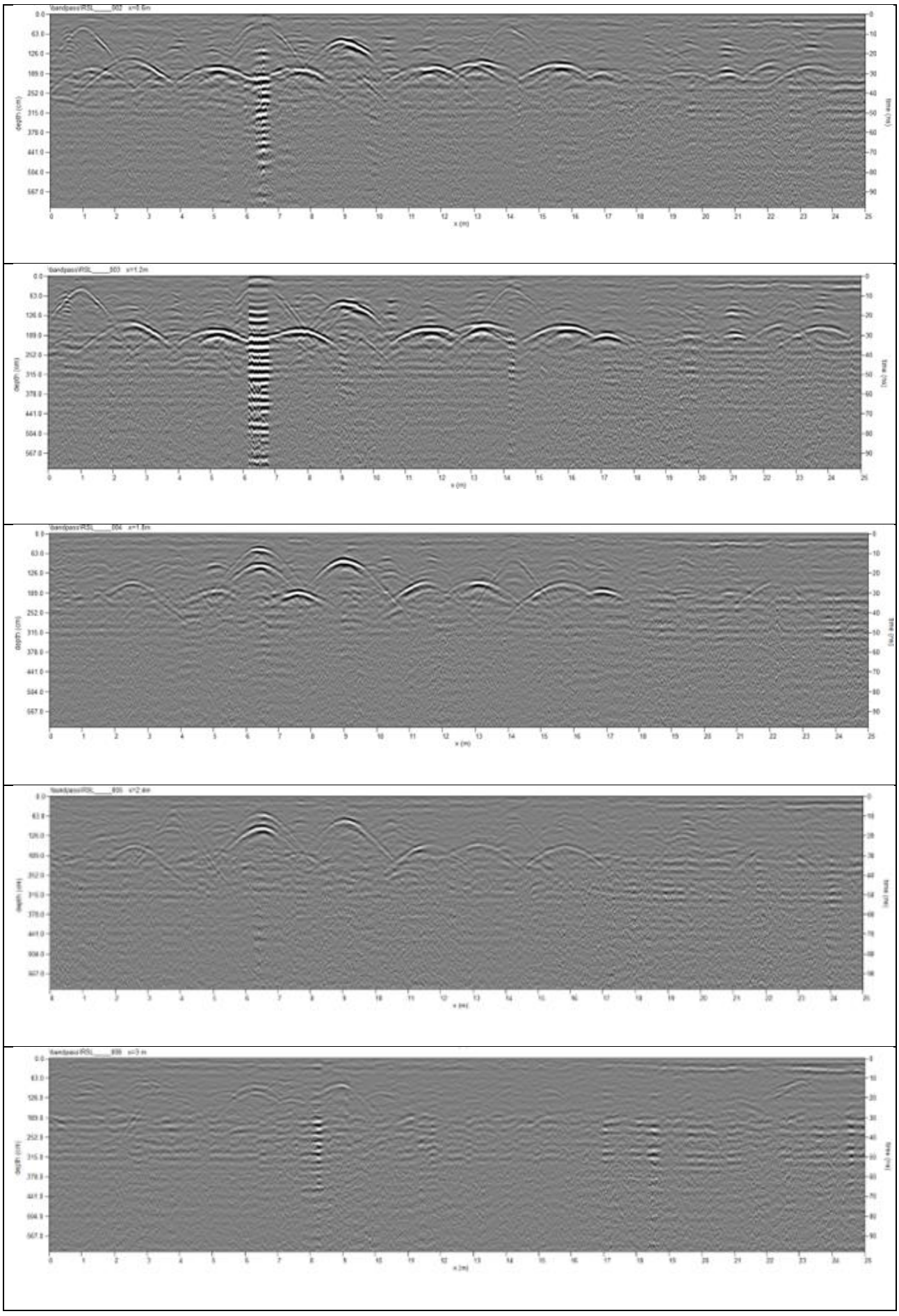

Port Lincoln RSL Cemetery Rows P and Q. Data collected March 2023

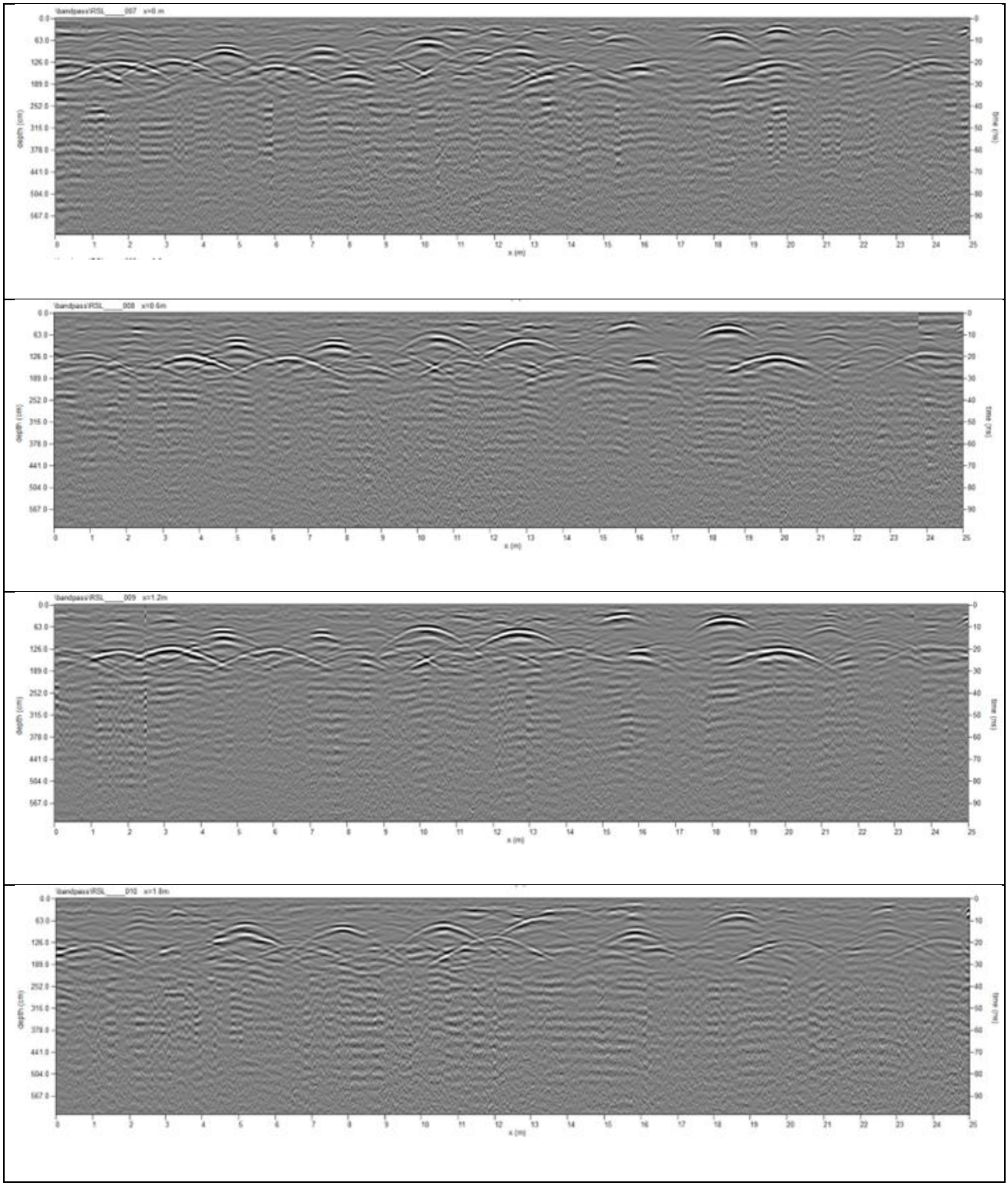

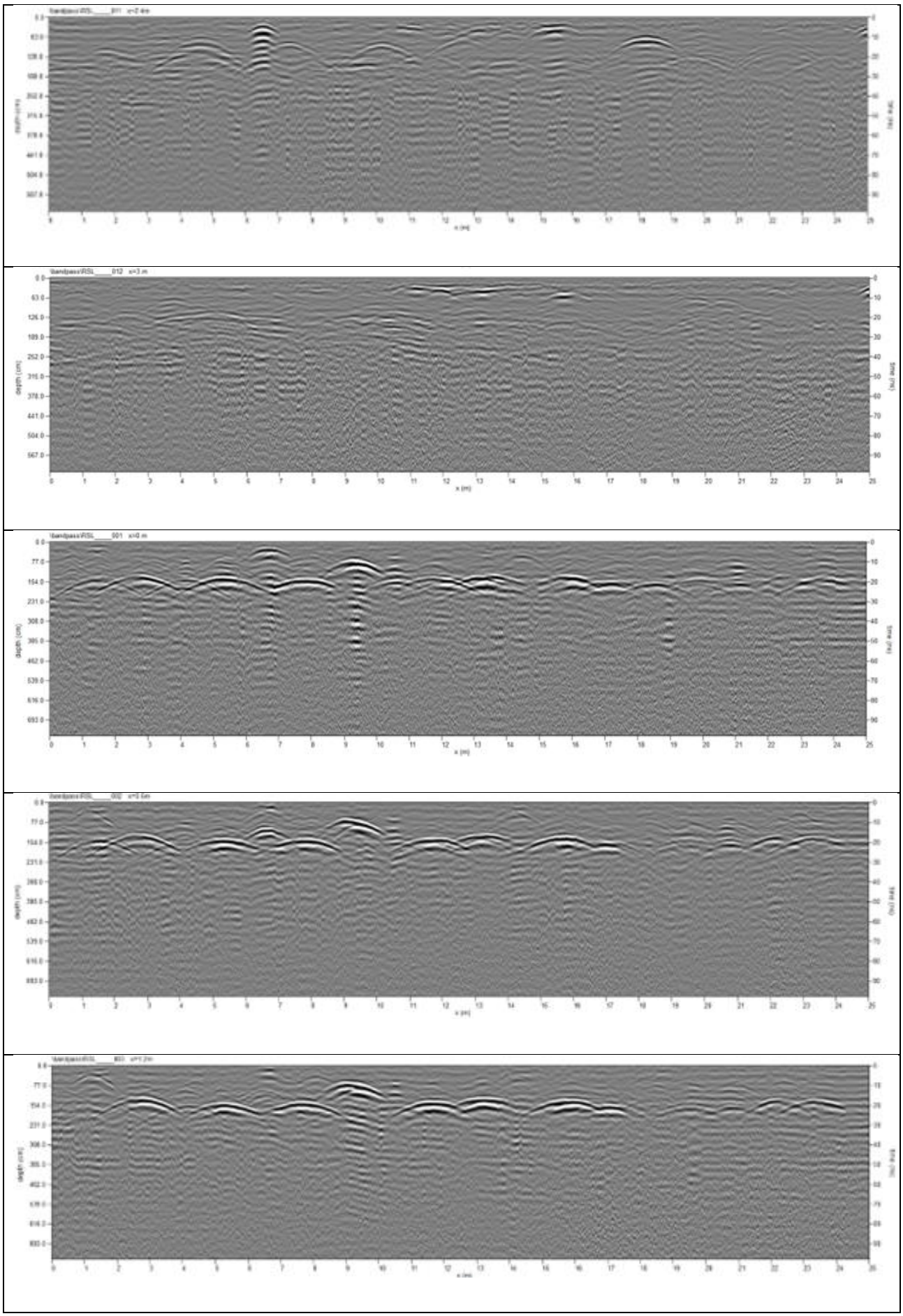

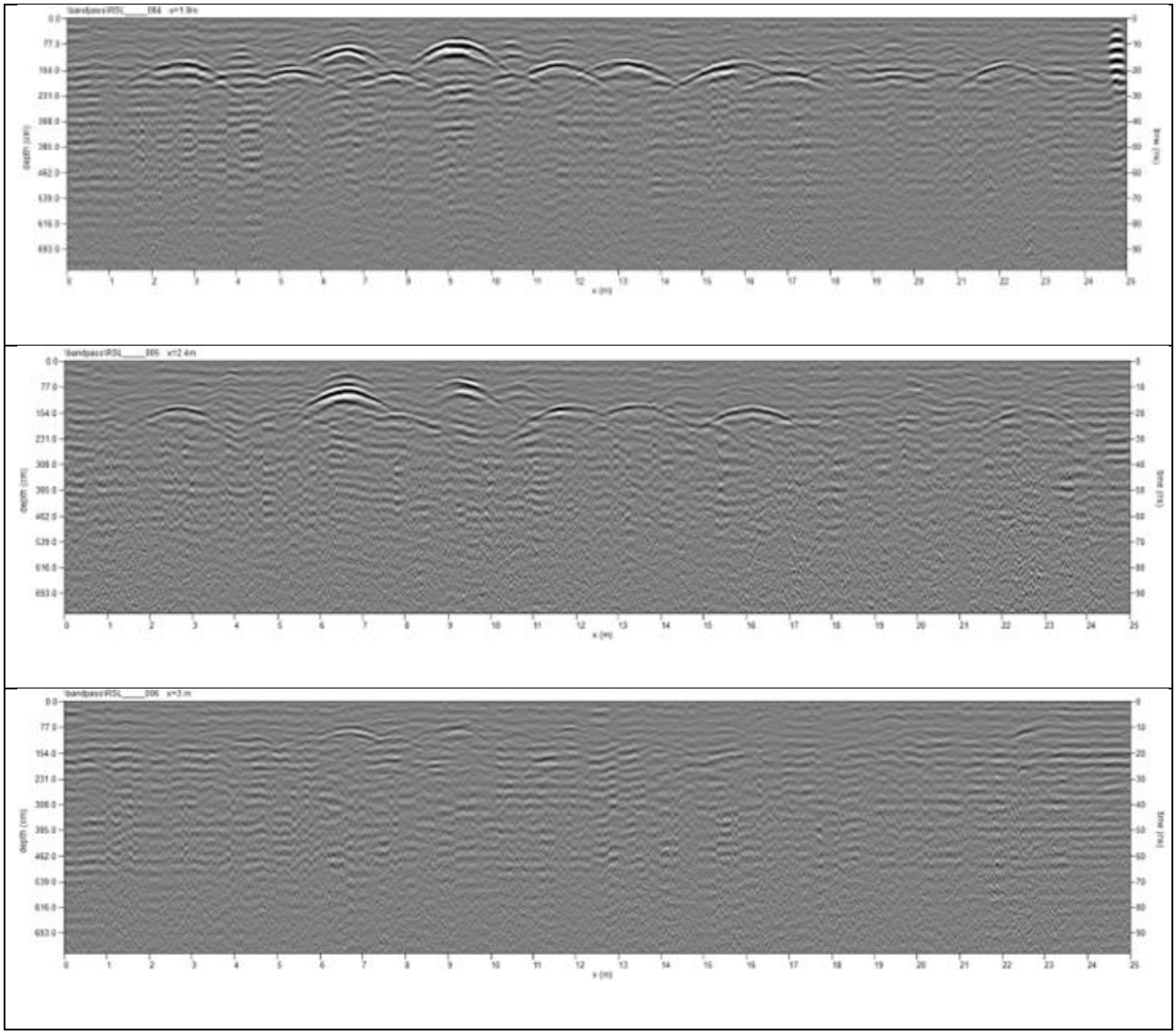

7.2 Appendix B Weather data, all sites

7.2.1 Port Lincoln

2020		Jan	Feb	Mar	Apr	May	Jun	Jul	Aug	Sep	Oct	Nov	Dec
	1st	0	5	0	0	3.6	9.2	0	0	0	1.2	0.2	3
	2nd	0	0	2.4	0	2.4	1		0	0.4	0	0	0
	3rd	0	0	0	0	0.6	0	0.6	0	0.8	0	0	0
	4th	1.2	0	0.8	12.4	0	0	0.6	0	0	6.2	0.4	0
	5th	3	0	0	0	0	0	0	0	0	30.2	0	0
	6th	0	0	0	0.4	0	0	0	0	0	3.4	0	0
	7th	0	0	0	2	0.6	1.4	0	0	0	0	0	0.6
	8th	0	0	0	0	3.4	0	0	2.6	0	37	0	0
	9th	0	0	0	0	18.6	0	0	9.4	0	0.2	0	0
	10th	0.2	0	0	0	0.2	0.2	1	0.8	0	0	0	0
	11th	1.6	0	0	0	0.2	0	5.6	3.8	0	0	1.6	0

	12th	0	0	0.4	0	0	0	5.8	3.8	2	0	0.6	0
	13th	0	0.4	0.8	0	0.6	5	0.8	0.2	12.8	0	0.2	8.8
	14th	0	0.2	0	0	0.2	11.8	0	2.8	0	0	0.2	1.6
	15th	0	0	0	0	0	0.6	0.2	2.2	0	0	0	0
	16th	0	0	0	0	0	0.8	0	0	0	0.4	0	0
	17th	0	0	0	0.4	0	0.6	0.2	0.2	19.4	0	0	0
	18th	0	0	0	0	0.2	0	0	8.2	1	0	0	0
	19th	0	0	0	0.8	0	0.4	1.6	21.8	2.2	0	0	0
	20th	0	0	0	0	7.2	9.8	0	5.6		0	0	0
	21st	0	0	0	0	6	7	0.2	4.4	1.4	0.4	0	0
	22nd	0	0	0	0	0	0.4	0	5.6	3.4	1	0.2	0
	23rd	5.6	0	0	5.2	2	0.6	0	1.8	1.8	5	0	0
	24th	0	0	0	3	0.6	0	0.2	0.4	3.8	0	0	0
	25th	0	0	0	0.2	0.4	0	3.4	0	10	0.8	0	0
	26th	0	0	0	16.8	0	0	0.4	0	0.6	0.6	0	0
	27th	0	0.2	0	0	0.2	0.2	0	0.2	0.2	0.4	0	0
	28th	0	0	0	0	0.2	0	0.2	0	0.6	0	0	0
	29th	0	0	2.6	6.6	0.2	0	0	0	0	0	7	0
	30th	0		0	24.8	0	0	0.2	0	12.8	3.6	0	0
	31st	0		0		8	0	0.2	0		0.6	0	0
	Monthly Total	11.6	5.8	7	72.6	55.4	49	21.2	73.8	73.2	91	10.4	14

2021		Jan	Feb	Mar	Apr	May	Jun	Jul	Aug	Sep	Oct	Nov	Dec
	1st	0	0	0.2	0	0	0	0.2	8.4	0	0.2	0	0
	2nd	0	0	0	0	0	0.4	13.8	0.4	0	0	0	0
	3rd	0.4	0	0	0	0	2.6	3.4	4.2	0.8	0	7.2	0
	4th	0.6	4.8	0	0	0	1.2	0.6	1	2.4	2	0	0
	5th	0	14	0	0	0	0.2	2.2	0.8	0.4	1.8	0	0
	6th	0	4	0	0	0	0.4	0	0.2	0	0	5	0
	7th	0.2	0.2	0	0	0	0	0	0	0	0	0	0
	8th	0	0	0	0	1.8	16.4	0	0	0.2	0	0	0
	9th	0	0	0	0	0.2	6.2	1.6	0	0	0	0	0
	10th	0	0	0	0	5.6	0.6	0.2	0	0	0	0	0
	11th	0	0	0	0	0	0.2	0	5.6	0	0	0	0
	12th	0	0	0	0	0.2	0	1.2	0.2	2.4	0	3.2	0
	13th	0	0	0.4	0	1	0	0.4	0.2	1.8	5	4.8	0
	14th	0	0	0	0.6	0.2	0	1.4	0.4	0	19.4	6.2	0
	15th	0	0	0	0.8	0.2	0	7.6	0	0	2.2	0.4	0
	16th	0	0	2.4	1.6	0	3.4	22	0	0	0	0	0
	17th	0	0	0.2	0	0	0	5.8	0	0	0	0	0
	18th	0	0	0	0.6	0.2	12.4	0	0.2	0.8	0	0	0
	19th	0	0	0	0	0	0	0.2	0	0	0	0	0
	20th	0	0	0	1	0	0	7	0.6	1.4	0	6.4	0
	21st	0	0	0	0.2	0	0	0	0.2	0.8	0.4	0.2	0
	22nd	0	0	0	2.4	0	0.2	11.6	0.2	0	0	0	0

	23rd	0	0	0	0.4	0	7	10	5.8	0	0	0.4	0
	24th	0	0	0	0	0	10	3.4	0.4	0	0	0.2	0
	25th	1.6	0	0.4	0	15	15.6	16.6	0.4	1.2	0	0	0
	26th	6.6	0	0.2	0	2.8	2	2	2	0	0	0.4	0
	27th	0	0.2	0	0	0	0.2	0	0	0	0.8	0	0
	28th	0	0	0	0.2	0	0.2	4.4	0.6	0	11.4	0	0
	29th	2	0	0	0	0	0	0.8	2.4	0	23	0	0
	30th	0	0	0	0	0	0	0	0.2	2.6	0	0	0
	31st	0		0.2	0	0		0.8	0		0		0
	Monthly Total	11.4	23.2	4	7.8	27.2	79.2	117	34.4	14.8	66.2	34.4	0

2022		Jan	Feb	Mar	Apr	May	Jun	Jul	Aug	Sep	Oct	Nov	Dec
	1st	0	0	0	0	0.2	0	0.2	1	0	0	13.8	0
	2nd	0	0	0	0	0.2	0	0	0.2	0.8	0	4.8	0
	3rd	0	0	0	0	0	0	2.6	18.6	0.2	0.2	1	0
	4th	0	0	0	0	1.8	2.2	0	0.2	0	24.4	0.4	0
	5th	0	0	0.2	0	1.8	9	0	16.8	0	15.2	0	0
	6th	0.4	0	0	1	4.8	5	0.2	1.2	0	0	0	0
	7th	0.8	0	0	0	0	3.6	2.2	1.2	1.4	2	0	0
	8th	0.2	0	0	0	0.2	1.2	0.2	0	9	1	0	0
	9th	0	0.6	0	0	0.2	0	0.4	0	17.2	0	0	3
	10th	0	0	0	0	0.2	0	0.2	4.8	0.6	0	0	0.2
	11th	0	0	0	0	0	0.8	0	0.4	0	0	0	0.8
	12th	0	0	0	0.6	0.2	0	2.8	0	0.2	15.2	14.2	1.4
	13th	0	0	0	0.2	0	0	0.8	3.2	0	0.2	42	0
	14th	0	0	0	2	1.2	0.6	0.4	3	1	9.4	3.2	0
	15th	0	0	0	13.4	0.4	8.4	0	1	1.2	0	0	0
	16th	0	27	0.2	0	2.4	3.6	0	7.2	12.4	0	0	0
	17th	0	8.6	18.2	0	0.4	0.2	5.6	0.2	3.4	0.2	0	0
	18th	0	0	0.2	0	0	0		11.4	1	1.4	0.8	0
	19th	0	0	0	6.6	0	0.8		3.4	0.2	0	4.2	0
	20th	0	0	0	0.6	0	2.6	0	2.8	0.6	0	6	0
	21st	0	0.6	0	0.8	0	0.4	0	1.2	1.8	0	0.8	1
	22nd	47.4	0	0	0	0	2.8	0	5.4	0	0	0	0
	23rd	0	0	0.2	0	0	1	0.4	5.6	0.2	0.2	0	0
	24th	2.2	0	0	0	0	0.6	2.2	0.4	0.2	2.2	0	0
	25th	3	0	0	0.4	6.4	0	10.8	0	2.2	1	0	0
	26th	0.2	0	0	0.2	2.4	2.4	1	0	7.2	0.4	0	0
	27th	47.2	0	0	0	0.4	0.4	0	0	0.8	0.2	0	0
	28th	0	0	0	0	1	0		0.2	0	0.2	0.4	0
	29th	0.2		0	0	1.6	0.2	0	0	0	0.2	0	0
	30th	0		0	1.4	24.6	0.6	4.4	0.4	0	1.6	0	0
	31st	0		0		3			0		8.6		0
	Monthly Total	102	36.8	19	27.2	53.4	46.4	34.4	89.8	61.6	83.8	91.6	6.4

2023		Jan	Feb	Mar	Apr	May	Jun	Jul	Aug	Sep	Oct	Nov	Dec
	1st	0		0	0.2	0.8	0	1.2					
	2nd	0	0.8	0	0.2	2.6	0	0.8					
	3rd	0	0.2	0	0	2	0						
	4th	0	0	0	0		0.2						
	5th	0	0	0	0	0.2	0						
	6th	0	0	0.2	0	5.2	0.2	7.2					
	7th	0	0	0	3.8	0.2	0.4	3.4					
	8th	0	0	1.2	0.6		21.8	5.4					
	9th	0	0	0	0	0.2	1.8	0.2					
	10th	0	0	0	0.2	0.2	0.4						
	11th	0	0	0	0		0.4	0.2					
	12th	0	0	0	3.4		0						
	13th	0	0	0	0.2		12.6						
	14th	0	0	0	0		1.8						
	15th	0	0	0	4		6.4	1.4					
	16th	0	0	0	3.2		1	0					
	17th	1	0	0	0	2.8	3.2	0.2					
	18th	12.6	0	0	1.4		2.6	0.4					
	19th	0	0	0	0	0.2	2.6	0.2					
	20th	0	0	0	0	0.2	0	2.6					
	21st	0	0	0.4	0.2	0.2	5	0.2					
	22nd	0	0	0	0		3.6	0.2					
	23rd	0	0	0	0		8.2	4.8					
	24th	0	0	0	0		19.6	0.4					
	25th	0	0	0.6	0	0.2	10.8	1.4					
	26th	0	0	4.8	0	2.4	0	0.2					
	27th	0	0	8	18.6	0.4	0.8						
	28th	0	0	2.6	0	3	0.2	0.2					
	29th	7.4		1.2	1	1.8	0.6	0.4					
	30th	0		0.8	0.2	0.8	0.2						
	31st	0		0				0.4					
	Monthly Total	21	1	19.8	37.2	23.4	104	31.4	0	0	0	0	0

7.2.2 Bordertown

2020		Jan	Feb	Mar	Apr	May	Jun	Jul	Aug	Sep	Oct	Nov	Dec
	1st	0			0	1.2	11.8	0	0	0	1.8	0	3.4
	2nd	0		2.63	9.6		0.6	0	0	0	0	0	0
	3rd	0	60.8	0	0		1	6	0	0		0	0
	4th		0.2	0		2.63	0	0	0	0		0	0
	5th		0	2		0	0	0	2.2	0		1.8	
	6th	1.43	0	0.6	13	0	0	3.63	0	0	11	0	

	7th	0	0	0	0	0	0	1	0	0	0	0	10.6
	8th	0	0	0	0	0.2	0	0	0	2.8	24.2	0	0.8
	9th	0	0	0	0		0	0	0	0	10.8	0	0
	10th	0	0	0	0		0	0	7.2	0	0	0	0
	11th		0	0		17.8	0	0	0	0	0	18.8	0
	12th		0	0		0	0	0	3.4	0	0	1.2	0
	13th	3.03	0	0		5		16	3.8	0	0	0.2	0
	14th	0	0	0	1.24	0		0	0.2	16.6	0		0.2
	15th	0	0	0	0	0	8.03	0	0	0	0		0
	16th	0	0	0	0.4	0	1	0	0	0	0	0.63	0
	17th	0	0	0	0	0	1.2	0	0.8	0.4		0	4.8
	18th		0	0	0	0	0	0	3	1.2		0	0.4
	19th		1.8	0	0	0	0	0	12	0	3.03	0	0
	20th	7.43	0	0	1	9.2		3.03	8.4	0	0	0	0
	21st	0	0	?	0	9.8		0	8.4	6.2	0		0.6
	22nd	0	0	?	5	0	5.63	0	0	1.8	0		0
	23rd	7	0	0.83	0.2		0.3	0.2	0	3	0.8	3.03	0
	24th	0	0	0	0.2		0.8	0	5	2.2		0	0
	25th	0	0	0		2.03	0.8	0	0	13.8		0	0
	26th	0	0.8	0		0	0.6	0	0	0	6.23	0	0
	27th	0	0	0	17.6	0	0	0	0	0	0	0	0
	28th	0	0		0	0.4	0	0	1	2.03	0		0
	29th	0			7	0	0	0	0	0	0.8		0
	30th	0		1.63	2.6		0	0	0	0.4	9.2	4.83	0
	31st	0						0	1.4	0			0
	Monthly Total	18.9	63.6	7.69	57.9	48.3	31.8	29.9	56.8	50.4	67.9	30.5	20.8

2021		Jan	Feb	Mar	Apr	May	Jun	Jul	Aug	Sep	Oct	Nov	Dec
	1st	0	0	0	0	0	0	0	0	0	0	0	0
	2nd	0	0	0	0	0	0	0.4	11.8	0	0	0	0
	3rd	0	0	0	0	0.2	1.8	0	4	2.6	0	0	0
	4th	0.2	0	0	0	0	1	0	4.6	0	0	0.2	0
	5th	0	2	0	0	0	0	13.4	2.6	0	22	0	0
	6th	0	0	0	0	0	0	0	1.4	3.8	0	0	0
	7th	0	0	0	0	0	4	0	0	0.2	0.8	0	0.2
	8th	0	8.4	0	0	0	6.2	0	0	0.1	0	4	0
	9th	0	0	0.4	0.8	0	0.8	0	3.6	0	0	0	0
	10th	0	0	0	0	4.2	0	0	0	0	0	0	0
	11th	0	0	0.4	0	2.6	0.4	0	0.4	0	0	0	0
	12th	0	1.4	0	0.6	0	0	0	4.4	0	0	1.4	0
	13th	0	0	0	0	0.2	0	1.2	1.6	8.6	0	0	0
	14th	0	0	0	2.6	1.2	0	0.8	0	0.2	13.4	0	0
	15th	0.6	0	10.2	0	0	0.4	8.8	0	0	7.6	8	0
	16th	0	0	0	0	0	6.8	4.2	5.4	0	0	0.4	0
	17th	0	0	0	0	3	20.4	0	1.8	0.8	0	0	0

	18th	0	0	0	0	0.4	5.4	0	0	0	1.4	0	0
	19th	0	0	0	0	0	0	18	0	0	0	0	0
	20th	0	0	0	2.5	0	0	9.2	0.1	9	0	0	2.4
	21st	0	0	0	2.8	0	0.8	1	0	2.8	0	0	0
	22nd	0	0	0	1.6	0	0	0	0	0	0	0	0
	23rd		0	0	0	0	5	4.8	2.8	0.8	0	0	0
	24th		0	1	0	0	0.4	0	1.8	0.4	0	6.6	0
	25th		0	1.4	0	5.6	10	0	0	0	0	6	0
	26th		0	0	0	9.6	0	23	0.6	0	0	0	0
	27th	13.7	0	0	1	1	0	0.2	0	0	0	0	0
	28th	0	0	0	0	0.4	3.2	1.2	0	0	1	0	0
	29th	0		0.2	0	0	0.4	6.6	0	4.4	16	0	0
	30th	0		0	0	0	0	0.6	0	11.8	0	0	0
	31st	0		0		0.2		0	0		0		0
	Monthly Total	14.5	11.8	13.6	11.9	28.6	67	93.4	46.9	45.5	62.2	26.6	2.6

2022		Jan	Feb	Mar	Apr	May	Jun	Jul	Aug	Sep	Oct	Nov	Dec
	1st	0	0	3.6	0	0	1	0.2	4	0	0	9.4	0
	2nd	0	0	0	0	2.4	0.1	0	1.2	2	0	2.6	0
	3rd	0	0	0	0	0	0	0	3.2	0	0	2.2	0
	4th	0	0	0	0	2.6	0	0	1.6	0	0	0	0
	5th	0	0	0	0	0.8	0	0.4	1.4	0.2	8	0	0
	6th	0	0	0	0.4	0.2	32.4	0	0	0	8.6	0	0
	7th	0.2	0	0	0	0	7	0.4	0	0	2.6	0	0
	8th	0	0	0	0	0	0.2	0	17.6	19.2	0	0	0
	9th	0	0	0	0	1.4	1	0	0	5.6	0	0	0
	10th	0	0	0	0	0	1	0	0	0	0.6	2.8	0
	11th	0	0	0	0	0	0	2	6	0	0	0	0
	12th	0	0	0	0	7.8	0	6.4	1.4	1.6	0	0	3.2
	13th	0	0	0	0	0	0	2.4	0	0	7	0	2
	14th	0	0	0	0	0	1.6	0.2	0	0	11	25.6	0.4
	15th	0	0	6.2	0	0	1.6	0	6	7.6	0	0.6	0
	16th	0	0	0	0	3	1.6	0	1.4	0.4	0	0	0
	17th	0	0	5.3	0	3.2	0	0	0.1	0	1.4	0	0
	18th	0	0	0	0	1.4	0	9	1	0	0	0	0
	19th	0	0	0	7	0.2	0	0.2	2.8	17.2	0	0	0
	20th	0	0	0	1.4	0	0.4	0	0	0	0	0	0
	21st	0	0	0	0	0	2	0	0	5.2	0	18.6	0.4
	22nd	0	0	0	0	0	1.6	0	8	0	0	5	6
	23rd	0	0	0	0	0	1.2	0	12	0	0	1.4	0
	24th	0	0	0	0	0	2	0	2.1	0	14.2	0.2	0
	25th	0	0	0	0	0	0	8.2	1	0	16	0	0
	26th	0	0	0	0	7.4	0	2.2	0	6.6	0	0	0

	27th	10.6	0	0	0	0.4	2.4	0.4	0	0.8	3	0	0
	28th	0	2	0	0	0	0.2	0.8	0	0	1.4	3.4	0
	29th	0		0	0	0	0	0.8	0	0	0	0.2	0
	30th	0		0	0	13	2.8	0	6.4	0	0		0
	31st	0		0		3.8		0	0.2		5.8		0
	Monthly Total	10.8	2	15.1	8.8	47.6	60.1	33.6	77.4	66.4	79.6	72	12

2023		Jan	Feb	Mar	Apr	May	Jun	Jul	Aug	Sep	Oct	Nov	Dec
	1st	0	0	0	0	3	2.6	0					
	2nd	0	0.2	0	0	3.8	0	0					
	3rd	0	8.2	0	0	7.2	0	1.6					
	4th	0	0	0	0	0.6	0	5.6					
	5th	0	0	0	0		0.4	0.6					
	6th	0	11	6.3	0		6.6	2					
	7th	0	0	0	0		18.2	3.6					
	8th	0	0	5.5	0	4.6	13	0					
	9th	0	0	0	0	0.4	9.8	0					
	10th	0	0	0.6	0	0.4	0	13.2					
	11th	0	0	0	16.2	0.2	0	0.1					
	12th	0	0	0	13		0	0					
	13th	0	0	0	2.6		4.4	0					
	14th	0	0	0	0.4		12.6	0					
	15th	0	0	0	0		0.8	0					
	16th	0	0	0	0	0.8	0	0					
	17th	0	0	0	11.8		0	0					
	18th	3	0	0	0		0	0.6					
	19th	0	0	0	0	0.8	18.4	0					
	20th	0	0	0	0.6		0.4	1.2					
	21st	0	0	4.2	0.4		0	1.6					
	22nd	0	0	0	0	2.6	2	0					
	23rd	0	0	0	0		23	0					
	24th	0.4	0	0	0.2		0	1.8					
	25th	0	0	0	0	2.6	0	0					
	26th	0	0	0	0	7	3.4	0					
	27th	0	7.4	6.7	4.6		0.2	0					
	28th	0		0	3		5.6	8.6					
	29th	0		0.6	0	10.6	1.2	0					
	30th	2.4		0	0	3.4	1	0					
	31st			0		1.2		1					
	Monthly Total	5.8	26.8	23.9	52.8	49.2	124	41.5	0	0	0	0	0

7.2.3 Keith

2020		Jan	Feb	Mar	Apr	May	Jun	Jul	Aug	Sep	Oct	Nov	Dec
	1st	0	50.6	0	0	5.2	10.6	0	0	0	0.8	0	3.4
	2nd	0	2.4	2.4	6.6	2.2	1.2	6.4	0	0	0	0	0
	3rd	0	0.6	0	0	1.6	1.1	3.2	0	0	0	0	0
	4th	0	0	0	5.6	0	0	2.2	1.2	0.4	0	0.4	0
	5th	1	0	0.4	3.2	0	0	1	0.4	2.6	13.8	0.2	0
	6th	0	0	0	1.4	0	0	0.2	0	0	0.4	0	4.9
	7th	0	0	0	0	0	0	0	0	0	0	0	6.4
	8th	0	0	0	0	0	0	0	3.4	0.8	20.4	0	3
	9th	0	0	0	0	18.4	0	0	1.2	0	4.2	0	0
	10th	0	0	0	0	2	0	0	0	0	0	0	0
	11th	1.8	0	0	0.6	2.2	0	18	0	0	0	2.6	0
	12th	0	0	0	0	0	0	7.4	3.4	0.4	0	1	0
	13th	0	0	0.4	0	3.2	0	0.2	5	10.8	0	0.4	0
	14th	0	0	0	0	0	8.4	0	0.3	0.6	0	0	0
	15th	0	0	0	0	0	1.2	0	0	0	0	0	0
	16th	0	0	0	0.4	0	3	0	0.7	0	0.8	0	0
	17th	0	0	0	0	0	1.2	0	0	0.4	3.2	0	0.2
	18th	0	0	0	0	0	0	0	1.4	0.8	0	0	0
	19th	0	0	0	1.2	0	0	0	7	0	0	0	0
	20th	0	0	0	0.2	0	1.2	1	4.2	1.4	0	0	0
	21st	0	0	0	0	12.4	1.6	0.2	10.4	8.4	0	0	1.2
	22nd	0	0	0	8.6	0.2	2.2	0	6.4	1.8	0	1.6	1.2
	23rd	10.4	0	0	0	4.2	2.6	0	4.6	3	0.6	1.4	0
	24th	0.5	0	0	0	0.4	1	0	0.2	4.8	1	0	0
	25th	0	0	0	0	0	0.6	0	0	11.6	0	0	0
	26th	0	0.6	0	19.6	0	0.4	0	0	3.8	0	0	0
	27th	0	0	0	0	0	3	0	0	0.4	0	0	0
	28th	0	0.8	0	0	0.4	0	0	0	0	1	0	0
	29th	0	0	0	8.8	0.2	0	0.2	0	0	0.4	3.8	0
	30th	0		2	3.6	0	0	0.8	0.6	1.4	7	0	0
	31st	0		0		1.4		0	1.2	0	0		0
	Monthly Total	13.7	55	5.2	59.8	54	39.3	40.8	51.6	53.4	53.6	11.4	20.3

2021		Jan	Feb	Mar	Apr	May	Jun	Jul	Aug	Sep	Oct	Nov	Dec
	1st	0	0	0	0	0	0	2	12.2	0	2.6	0	0
	2nd	0	0	0	0	0	0	1.6	0	0	0	0	0
	3rd	0	0	0	0	0	0.8	12.8	5.2	0.4	5.2	0.2	0
	4th	0	0	0	0	0	2	4.4	6	3.6	2.8	0.2	0
	5th	0	24.4	0	0	0	0	1.4	1.8	2.6	1.4	0	0
	6th	0	7.4	0	0	0	0	0	0.4	1.2	0	1.2	0
	7th	0	0	0	0	0	0	0	1.2	0	0	2.2	0
	8th	0	0	0.6	0	0	10.6	0	1.6	0	0	0	0

	9th	0	0	0	0.4	0.9	1.8	0	0	0	0	0	0
	10th	0	0	0	0	1.6	0	0	0	0	0	0	0
	11th	0	0	0	0.8	1	0	0	0.6	0	0.3	0	0
	12th	0	1	0	0	0	0.2	0	4.2	0.6	0	1	0
	13th	0	0	1	0	0	1.4	0.2	2.6	3.2	0	0	0
	14th	0	0	8.4	1	1.6	0	1.6	0.4	0	8.2	4.8	0
	15th	0.2	0	0	0	3.6	0	1.2	0	0	2.6	2	0.2
	16th	0	0	0.2	0	0.4	6.4	6.4	0.4	0	1.6	2.2	0
	17th	0	0	0	0	0.6	10.2	18.2	0.4	0	0	0	0
	18th	0	0	0	0	1	1.2	1.8	0	0	0	0	0
	19th	0	0	0	0	0	2.2	0	0	0.6	0	0	1.4
	20th	0	0	0	2.8	0	0	8.4	0	7.4	0	0.2	0.4
	21st	0	0	0	2.6	0	0	1	0	3.4	0	0	0
	22nd	0	0	0	4	0	0	0	0	1.2	0	0	0
	23rd	0	0	0	1	0	4.2	4	5.6	0	0	0	0
	24th	0	0	0.6	0	0	0	3.2	0.8	0	0	0.4	0
	25th	12.8	0	2.6	0.3	5.2	14.4	17.8	0.2	0.4	0	2	0
	26th	0	0	0	0	7.8	0.2	4.4	0	0	0	0	0
	27th	0	0	0.4	0	1.4	4.4	0	0	0	0	0	0
	28th	0	0	0	0	0.3	0	1	0	0	0.6	0	0
	29th	5.2		0	0	0	0	6.8	0.6	1.6	21	0	0
	30th	0		0	0	0	0	0.2	0	6.6	0	0	0
	31st	0		0		0		0	0		0		0
	Monthly Total	18.2	32.8	13.8	12.9	25.4	60	98.4	44.2	32.8	46.3	16.4	2

2022		Jan	Feb	Mar	Apr	May	Jun	Jul	Aug	Sep	Oct	Nov	Dec
	1st	0	0	20	0	0	2.6	0	5.4	0	0	11	0
	2nd	0	0	24.2	0	0	0	0	2.6	4	0	5	0
	3rd	0	0	0.2	0	0	0	0	5.2	0	0	1	0
	4th	0	0	0	0	1.6	0.6	0	0	0	0	0	0
	5th	0	0	0	0	2	23.6	0.2	7.6	0	10.2	0	0
	6th	0	0	0.4	1.2	0.8	9.4	0	5.2	0	5.4	0	0
	7th	0	0	0	0	2.2	10	0	9.2	0	1.6	0	0
	8th	0	0	0	0	1.8	0	0	0	10	0.6	0	0
	9th	0	0	0	0	0	0.4	4.9	0	7.6	0	0	0
	10th	0	0	0	0	0	0.8	0	0	2.6	0	1.4	0
	11th	0	0	0	0	0	0.2	0	5.4	0	0	0	0
	12th	0	0	0	0	4.4	0	5.6	2.8	0.8	0	0.4	4.2
	13th	3.6	0	0	0	0	0.3	3.6	9	0	9.4	25.4	1.6
	14th	0	0	0	0	0.6	0	0	1.6	0	5	1.4	0.4
	15th	0	0	0.2	0	0.2	0	0	1.4	5.8	0.4	1	0
	16th	0	0	0	0	4.4	2	0	0.2	0.8	0	0	0
	17th	0	0	4.4	0	1	0	7.6	0	16.6	0	0	0
	18th	0	0	0	5.2	1.4	0	2.6	0.6	6.1	0	0	0
	19th	0	0	0	0	0.2	0	0	3.4	0.8	0	6	0

	20th	0	0	0	0.2	0	0.6	0	4.2	0	0	3.1	0
	21st	0	0	0	0	0	2.4	0	0	8.2	1	8	3.2
	22nd	0	0	0	0	0	1.4	0	0	0.2	0.2	0.8	4.8
	23rd	0	0	0	0	0	0.2	1.4	15.6	0	0	1	0
	24th	0	0	0	0	0	0.6	0.6	0.8	0.3	28.8	0.2	0
	25th	0	0	0	0	6.6	0	6.2	1.2	0	9.4	0	0
	26th	0	0	0	0	0.6	3.6	3.4	0.4	4.6	1.4	0	0
	27th	12.4	0	0	0	0	2	0.2	0	3.2	2.1	0	0
	28th	0.6	0	0	0	0.4	0	2	0	0	1.2	2.2	3.2
	29th	0.5		0	0	3.2	0	1.8	0	0	1.2	0	0
	30th	0		0	4.8	17	1	0	8.2	0.1	0	0	0
	31st	0		0		6.2		0.8	0.2		1.8		0
	Monthly Total	17.1	0	49.4	11.4	54.6	61.7	40.9	90.2	71.7	79.7	67.9	17.4

2023		Jan	Feb	Mar	Apr	May	Jun	Jul	Aug	Sep	Oct	Nov	Dec
	1st	0	0	0	0.4	2.2	1.4	1.6					
	2nd	0	0	0	0	1.2	0	0.6					
	3rd	0	7	0	0	7.4	0	0					
	4th	0	2.6	0	0	0	0	5					
	5th	0	0	0	0	0	0	0					
	6th	0	0	7	0	7.8	0.6	1.8					
	7th	0	0	3.2	21.6	1.4	27.8	10.6					
	8th	0	0	4.6	3	0.6	3.6	3.4					
	9th	0	0	0.1	0.4	1	6.6	8					
	10th	0	0	0	0	0	0.6	3.4					
	11th	0	0	0	0	0	0	0					
	12th	0	0	0	8	0	0	0					
	13th	0	0	0	1.4	0	7	0					
	14th	0	0	0	0.8	0	15.2	0					
	15th	0	0	0	2.4	0	0.2	0					
	16th	0	0	0	9.2	0.3	0	1.4					
	17th	0	0	0	0	0	0	0					
	18th	1	0	0	0	0	6.8	0					
	19th	0	0	0	0.6	0.8	20	0					
	20th	0	0	0	0.4	1.4	0.4	0.6					
	21st	0	0	1	0	1.2	0	1.8					
	22nd	0	0	0	0	0	1.2	0.2					
	23rd	0	0	0	0	0	30.4	0.3					
	24th	4.2	0	0	0	0	3.6	0.6					
	25th	0	6.8	0	0	0.2	0	0.2					
	26th	0	0	0	0	9.6	1.4	0					
	27th	0	0	9	3.8	1.6	0	0					
	28th	0	0		3.2	21.3	1.6	7.4					
	29th	2.2		0.5	0.8	1	0.8	0.4					
	30th	0			0	0.2	0.6	0					

	31st	0		1.8		0.2		0.4					
	Monthly Total	7.4	16.4	27.2	56	59.4	130	47.7	0	0	0	0	0

7.3 Appendix C Ethics Documents

7.3.1 Bordertown

PARTICIPANT INFORMATION SHEET AND OPT-OUT FORM

Title: 'Assessing a geophysical multi-modal approach in the location of unmarked graves under various seasonal conditions'

Chief Investigator

Andrew Frost

College of Humanities, Arts and Social Sciences

Flinders University

Tel: 0414296372

Email: Andrew.frost@flinders.edu.au

My name is Andrew Frost, and I am a Flinders University PhD student. I am undertaking this research as part of my degree. For further information, you are more than welcome to contact me. My details are listed above.

Description of the study

This project will investigate the role played by soil moisture in typical geophysical surveys. These geophysical surveys will be using resistivity and conductivity methods to assess soil disturbances, typical of human burial. By using existing, known graves, the responses from subsurface disturbances can be more accurately assessed.

Geophysical methods are non-destructive and non-invasive. No buried objects can be identified, neither physical nor structural. The names of the deceased will not be disclosed.

This project is supported by Flinders University, College of Humanities, Arts and Social Sciences.

Purpose of the study

This project aims to determine how seasonal environmental conditions affects the effectiveness of typical geophysical methods in locating unmarked graves.

Benefits of the study

Locating unmarked graves is seen as being culturally beneficial by Indigenous groups, local historical groups, church parish groups, and local government authorities, and so any research into current methodology will aid both researchers and the industry at large. To date, the affects of soil moisture, studied over a long period of time has not been thoroughly investigated.

Given that this is an area where knowledge is lacking it can be seen that a greater understanding of what causes graves to be identifiable in data from resistivity and conductivity surveys may give more insight into the relative strengths and weaknesses of these techniques for locating graves.

This research in these fields will provide some certainty in the interpretation of geophysical results, with particular focus of these results in Australian conditions.

Participant involvement and potential risks

This study will be undertaken in the Bordertown Cemetery, Rows D & E.

If you have a relative buried in these rows, and you would like to opt-out of this study, please use the contact details above.

Withdrawal Rights

You may, without any penalty, decline to take part in this research study. If you decide to take part and later change your mind, you may, without any penalty, withdraw at any time without providing an explanation. To withdraw, please contact the Chief Investigator.

Confidentiality and Privacy

Only researchers listed on this form have access to the individual information provided by you. Privacy and confidentiality will be assured at all times. The research outcomes may be presented at conferences, written up for publication or used for other research purposes as described in this information form. However, the privacy and confidentiality of individuals will be protected at all times. You will not be named, and your individual information will not be identifiable in any research products without your explicit consent.

No data, including identifiable, non-identifiable and de-identified datasets, will be shared or used in future research projects without your explicit consent.

Data Storage

The information collected may be stored securely on a password protected computer and/or Flinders University server throughout the study. Any identifiable data will be de-identified for data storage purposes unless indicated otherwise. All data will be securely transferred to and stored at Flinders University for at least five years after publication of the results. Following the required data storage period, all data will be securely destroyed according to university protocols.

Ethics Committee Approval

The project has been approved by Flinders University's Human Research Ethics Committee (insert project number here).

Queries and Concerns

Queries or concerns regarding the research can be directed to the research team. If you have any complaints or reservations about the ethical conduct of this study, you may contact the Flinders University's Research Ethics & Compliance Office team via telephone 08 8201 3116 or email human.researchethics@flinders.edu.au.

Thank you for taking the time to read this information sheet which is yours to keep. If you accept our invitation to be involved, please sign the enclosed Consent Form.

7.3.2 Keith

PARTICIPANT INFORMATION SHEET AND OPT-OUT FORM

Title: 'Assessing a geophysical multi-modal approach in the location of unmarked graves under various seasonal conditions'

Chief Investigator

Andrew Frost

College of Humanities, Arts and Social Sciences

Flinders University

Tel: 0414296372

Email: Andrew.frost@flinders.edu.au

My name is Andrew Frost, and I am a Flinders University PhD student. I am undertaking this research as part of my degree. For further information, you are more than welcome to contact me. My details are listed above.

Description of the study

This project will investigate the role played by soil moisture in typical geophysical surveys. These geophysical surveys will be using resistivity and conductivity methods to assess soil disturbances, typical of human burial. By using existing, known graves, the responses from subsurface disturbances can be more accurately assessed.

Geophysical methods are non-destructive and non-invasive. No buried objects can be identified, neither physical nor structural. The names of the deceased will not be disclosed.

This project is supported by Flinders University, College of Humanities, Arts and Social Sciences.

Purpose of the study

This project aims to determine how seasonal environmental conditions affects the effectiveness of typical geophysical methods in locating unmarked graves.

Benefits of the study

Locating unmarked graves is seen as being culturally beneficial by Indigenous groups, local historical groups, church parish groups, and local government authorities, and so any research into current methodology will aid both researchers and the industry at large. To date, the affects of soil moisture, studied over a long period of time has not been thoroughly investigated.

Given that this is an area where knowledge is lacking it can be seen that a greater understanding of what causes graves to be identifiable in data from resistivity and conductivity surveys may give more insight into the relative strengths and weaknesses of these techniques for locating graves.

This research in these fields will provide some certainty in the interpretation of geophysical results, with particular focus of these results in Australian conditions.

Participant involvement and potential risks

This study will be undertaken in the Keith Cemetery, Rows H & I.

If you have a relative buried in these rows, and you would like to opt-out of this study, please use the contact details above.

Withdrawal Rights

You may, without any penalty, decline to take part in this research study. If you decide to take part and later change your mind, you may, without any penalty, withdraw at any time without providing an explanation. To withdraw, please contact the Chief Investigator.

Confidentiality and Privacy

Only researchers listed on this form have access to the individual information provided by you. Privacy and confidentiality will be assured at all times. The research outcomes may be presented at conferences, written up for publication or used for other research purposes as described in this information form. However, the privacy and confidentiality of individuals will be protected at all times. You will not be named, and your individual information will not be identifiable in any research products without your explicit consent.

No data, including identifiable, non-identifiable and de-identified datasets, will be shared or used in future research projects without your explicit consent.

Data Storage

The information collected may be stored securely on a password protected computer and/or Flinders University server throughout the study. Any identifiable data will be de-identified for data storage purposes unless indicated otherwise. All data will be securely transferred to and stored at Flinders University for at least five years after publication of the results. Following the required data storage period, all data will be securely destroyed according to university protocols.

Ethics Committee Approval

The project has been approved by Flinders University's Human Research Ethics Committee (insert project number here).

Queries and Concerns

Queries or concerns regarding the research can be directed to the research team. If you have any complaints or reservations about the ethical conduct of this study, you may contact the Flinders

University's Research Ethics & Compliance Office team via telephone 08 8201 3116 or email human.researchethics@flinders.edu.au.

Thank you for taking the time to read this information sheet which is yours to keep. If you accept our invitation to be involved, please sign the enclosed Consent Form.

7.3.3 Pt Lincoln RSL

PARTICIPANT INFORMATION SHEET AND OPT-OUT FORM

Title: 'Assessing a geophysical multi-modal approach in the location of unmarked graves under various seasonal conditions'

Chief Investigator

Andrew Frost

College of Humanities, Arts and Social Sciences

Flinders University

Tel: 0414296372

Email: Andrew.frost@flinders.edu.au

My name is Andrew Frost, and I am a Flinders University PhD student. I am undertaking this research as part of my degree. For further information, you are more than welcome to contact me. My details are listed above.

Description of the study

This project will investigate the role played by soil moisture in typical geophysical surveys. These geophysical surveys will be using resistivity and conductivity methods to assess soil disturbances, typical of human burial. By using existing, known graves, the responses from subsurface disturbances can be more accurately assessed.

Geophysical methods are non-destructive and non-invasive. No buried objects can be identified, neither physical nor structural. The names of the deceased will not be disclosed.

This project is supported by Flinders University, College of Humanities, Arts and Social Sciences.

Purpose of the study

This project aims to determine how seasonal environmental conditions affects the effectiveness of typical geophysical methods in locating unmarked graves.

Benefits of the study

Locating unmarked graves is seen as being culturally beneficial by Indigenous groups, local historical groups, church parish groups, and local government authorities, and so any research into current methodology will aid both researchers and the industry at large. To date, the affects of soil moisture, studied over a long period of time has not been thoroughly investigated.

Given that this is an area where knowledge is lacking it can be seen that a greater understanding of what causes graves to be identifiable in data from resistivity and conductivity surveys may give more insight into the relative strengths and weaknesses of these techniques for locating graves.

This research in these fields will provide some certainty in the interpretation of geophysical results, with particular focus of these results in Australian conditions.

Participant involvement and potential risks

This study will be undertaken in the Happy Valley RSL Cemetery, Rows P & Q.

If you have a relative buried in these rows, and you would like to opt-out of this study, please use the contact details above.

Withdrawal Rights

You may, without any penalty, decline to take part in this research study. If you decide to take part and later change your mind, you may, without any penalty, withdraw at any time without providing an explanation. To withdraw, please contact the Chief Investigator.

Confidentiality and Privacy

Only researchers listed on this form have access to the individual information provided by you. Privacy and confidentiality will be assured at all times. The research outcomes may be presented at conferences, written up for publication or used for other research purposes as described in this information form. However, the privacy and confidentiality of individuals will be protected at all times. You will not be named, and your individual information will not be identifiable in any research products without your explicit consent.

No data, including identifiable, non-identifiable and de-identified datasets, will be shared or used in future research projects without your explicit consent.

Data Storage

The information collected may be stored securely on a password protected computer and/or Flinders University server throughout the study. Any identifiable data will be de-identified for data storage purposes unless indicated otherwise. All data will be securely transferred to and stored at Flinders University for at least five years after publication of the results. Following the required data storage period, all data will be securely destroyed according to university protocols.

Ethics Committee Approval

The project has been approved by Flinders University's Human Research Ethics Committee (insert project number here).

Queries and Concerns

Queries or concerns regarding the research can be directed to the research team. If you have any complaints or reservations about the ethical conduct of this study, you may contact the Flinders University's Research Ethics & Compliance Office team via telephone 08 8201 3116 or email human.researchethics@flinders.edu.au.

Thank you for taking the time to read this information sheet which is yours to keep. If you accept our invitation to be involved, please sign the enclosed Consent Form.

7.4 Appendix D ECE Results

Southern Cross University
PO Box 157 Lismore NSW 2480
P: +61 2 6620 3678
E: eal@scu.edu.au
www.scu.edu.au/eal
ABN: 41 995 651 524

AGRICULTURAL SOIL ANALYSIS REPORT

8 samples supplied by Flinders University of South Australia on 31/01/2023. Lab Job No.N6832
Analysis requested by Andrew Frost. Your Job: Andrew Frost
ADDRESS NOT PROVIDED

			Sample 1	Sample 2	Sample 3	Sample 4
		Sample ID:	B3	B6	B1	B1.5
		Crop:	N/G	N/G	N/G	N/G
		Client:	N/G	N/G	N/G	N/G
	Parameter	Method reference	N6832/1	N6832/2	N6832/3	N6832/4
	Exchangeable Calcium (cmol+/kg)	Rayment & Lyons 2011 - 15D3 (Ammonium Acetate)	8.3	19	8.6	16
	Exchangeable Calcium (kg/ha)		3,711	8,333	3,870	7,058
	Exchangeable Calcium (mg/kg)		1,657	3,720	1,728	3,151
	Exchangeable Magnesium (cmol+/kg)		0.87	5.7	8.6	10
	Exchangeable Magnesium (kg/ha)		236	1,546	2,331	2,757
	Exchangeable Magnesium (mg/kg)		105	690	1,041	1,231
	Exchangeable Potassium (cmol+/kg)		0.60	0.51	0.93	1.00
	Exchangeable Potassium (kg/ha)		527	443	818	875
	Exchangeable Potassium (mg/kg)		235	198	365	390
	Exchangeable Sodium (cmol+/kg)		0.11	1.1	5.4	8.5
	Exchangeable Sodium (kg/ha)		56	573	2,797	4,379
	Exchangeable Sodium (mg/kg)		25	256	1,249	1,955
	Exchangeable Aluminium (cmol+/kg)	**Inhouse S37 (KCl)	0.04	0.02	0.02	0.02
	Exchangeable Aluminium (kg/ha)		8.0	4.6	3.5	3.0
	Exchangeable Aluminium (mg/kg)		3.6	2.1	1.6	1.4
	Exchangeable Hydrogen (cmol+/kg)	**Rayment & Lyons 2011 - 15G1 (Acidity Titration)	0.18	0.17	0.06	0.12
	Exchangeable Hydrogen (kg/ha)		4.0	3.8	1.4	2.6
	Exchangeable Hydrogen (mg/kg)		1.8	1.7	<1	1.2
	Effective Cation Exchange Capacity (ECEC) (cmol+/kg)	**Calculation: Sum of Ca,Mg,K,Na,Al,H (cmol+/kg)	10	26	24	35
	Calcium (%)	**Base Saturation Calculations - Cation cmol+/kg / ECEC x 100	82	71	36	44
	Magnesium (%)		8.6	22	36	29
	Potassium (%)		6.0	1.9	4.0	2.8
	Sodium - ESP (%)		1.1	4.3	23	24
	Aluminium (%)		0.4	0.1	0.1	0.0
	Hydrogen (%)		1.8	0.6	0.3	0.3
	Calcium/Magnesium Ratio	**Calculation: Calcium / Magnesium (cmol+/kg)	9.5	3.3	1.0	1.6

Southern Cross University
PO Box 157 Lismore NSW 2480
P: +61 2 6620 3678
E: eal@scu.edu.au
www.scu.edu.au/eal
ABN: 41 995 651 524

AGRICULTURAL SOIL ANALYSIS REPORT

8 samples supplied by Flinders University of South Australia on 31/01/2023. Lab Job No.N6832

Analysis requested by Andrew Frost. Your Job: Andrew Frost

ADDRESS NOT PROVIDED

			Sample 5	Sample 6	Sample 7	Sample 8
		Sample ID:	RSL3	RSL6	RSL1	RSL1.5
		Crop:	N/G	N/G	N/G	N/G
		Client:	N/G	N/G	N/G	N/G
	Parameter	Method reference	N6832/5	N6832/6	N6832/7	N6832/8
	Exchangeable Calcium (cmol+/kg)	Rayment & Lyons 2011 - 15D3 (Ammonium Acetate)	21	21	19	18
	Exchangeable Calcium (kg/ha)		9,416	9,275	8,537	8,303
	Exchangeable Calcium (mg/kg)		4,204	4,141	3,811	3,707
	Exchangeable Magnesium (cmol+/kg)		1.7	1.7	1.3	1.2
	Exchangeable Magnesium (kg/ha)		474	453	354	314
	Exchangeable Magnesium (mg/kg)		212	202	158	140
	Exchangeable Potassium (cmol+/kg)		1.2	0.55	0.13	<0.12
	Exchangeable Potassium (kg/ha)		1,036	484	115	<112
	Exchangeable Potassium (mg/kg)		462	216	51	<50
	Exchangeable Sodium (cmol+/kg)		0.27	0.24	0.45	0.66
	Exchangeable Sodium (kg/ha)		142	124	233	341
	Exchangeable Sodium (mg/kg)		63	56	104	152
	Exchangeable Aluminium (cmol+/kg)	**Inhouse S37 (KCl)	0.01	0.02	0.01	0.01
	Exchangeable Aluminium (kg/ha)		2.6	3.2	2.6	2.8
	Exchangeable Aluminium (mg/kg)		1.2	1.4	1.2	1.3
	Exchangeable Hydrogen (cmol+/kg)	**Rayment & Lyons 2011 - 15G1 (Acidity Titration)	0.07	0.28	0.07	0.24
	Exchangeable Hydrogen (kg/ha)		1.7	6.3	1.7	5.3
	Exchangeable Hydrogen (mg/kg)		<1	2.8	<1	2.4
	Effective Cation Exchange Capacity (ECEC) (cmol+/kg)	**Calculation: Sum of Ca,Mg,K,Na,Al,H (cmol+/kg)	24	23	21	21
	Calcium (%)	**Base Saturation Calculations - Cation cmol+/kg / ECEC x 100	86	88	91	90
	Magnesium (%)		7.2	7.1	6.2	5.6
	Potassium (%)		4.9	2.4	0.6	0.3
	Sodium - ESP (%)		1.1	1.0	2.2	3.2
	Aluminium (%)		0.1	0.1	0.1	0.1
	Hydrogen (%)		0.3	1.2	0.4	1.2
	Calcium/Magnesium Ratio	**Calculation: Calcium / Magnesium (cmol+/kg)	12	12	15	16

Notes:

1. All results presented as a 40°C oven dried weight. Soil sieved and lightly crushed to < 2 mm.
2. Methods from Rayment and Lyons, 2011. *Soil Chemical Methods - Australasia*. CSIRO Publishing: Collingwood.
3. Soluble Salts included in Exchangeable Cations - NO PRE-WASH (unless requested).
4. 'Morgan 1 Extract' adapted from 'Science in Agriculture', 'Non-Toxic Farming' and LaMotte Soil Handbook.
5. Guidelines for phosphorus have been reduced for Australian soils.
6. Indicative guidelines are based on 'Albrecht' and 'Reams' concepts.
7. Total Acid Extractable Nutrients indicate a store of nutrients.
8. National Environmental Protection (Assessment of Site Contamination) Measure 2013, Schedule B(1) - Guideline on Investigation Levels for Soil and Groundwater. Table 5-A Background Ranges.
9. Information relating to testing colour codes is available on sheet 2 - 'Understanding your agricultural soil results'
10. Conversions for 1 cmol+/kg = 230 mg/kg Sodium, 390 mg/kg Potassium, 122 mg/kg Magnesium, 200 mg/kg Calcium
11. Conversions to kg/ha = mg/kg x 2.24
12. The chloride calculation of Cl mg/L = EC x 640 is considered an estimate, and most likely an over-estimate
13. ** NATA accreditation does not cover the performance of this service.
14. Analysis conducted between sample arrival date and reporting date.
15. This report is not to be reproduced except in full. Results only relate to the item tested.
16. All services undertaken by EAL are covered by the EAL Laboratory Services Terms and Conditions (
17. This report was issued on 6/02/2023.

7.5 Appendix E. Magnetic Susceptibility Results

Keith Cemetery

Depth (cm)	Sample ID	Raw Meas. in SI	Mass Susc. Meas. (SI)	Sample Weight (g)	Correct. Factor	Correct. Offset
30	001(LF)	2.45E-05	1.31E-08	22.47	5.41E-04	-3.29E-07
30	001(HF)	2.71E-05	1.47E-08	22.47	5.41E-04	-1.78E-08
30	001 FD %	-11.9365	-11.9365	0	1	0
30	002(LF)	2.78E-05	1.63E-08	22.47	5.41E-04	2.42E-06
30	002(HF)	2.58E-05	1.35E-08	22.47	5.41E-04	-9.70E-07
30	002 FD %	17.6465	17.6465	0	1	0
60	004(LF)	1.59E-05	6.90E-09	23.3	5.18E-04	-2.48E-06
60	004(HF)	1.72E-05	8.40E-09	23.3	5.18E-04	-1.08E-06
60	004 FD %	-20.4565	-20.4565	0	1	0
60	005(LF)	1.25E-05	7.30E-09	23.80	5.05E-04	1.85E-06
60	005(HF)	1.46E-05	6.80E-09	23.80	5.05E-04	-1.05E-06
60	005 FD %	6.0687	6.0687	0	1	0
100	006(LF)	1.65E-05	8.50E-09	23.80	5.05E-04	2.47E-07
100	006(HF)	1.45E-05	6.60E-09	23.80	5.05E-04	-1.39E-06
100	006 FD %	21.8469	21.8469	0	1	0
100	007(LF)	6.61E-06	3.20E-09	22.95	5.28E-04	-6.07E-07
100	007(HF)	1.06E-05	5.00E-09	22.95	5.28E-04	-1.06E-06
100	007 FD %	-58.7301	-58.7301	0	1	0
150	008(LF)	9.89E-06	6.40E-09	22.95	5.28E-04	2.15E-06
150	008(HF)	1.06E-05	4.50E-09	22.95	5.28E-04	-2.04E-06
150	008 FD %	28.6907	28.6907	0	1	0

Bordertown Cemetery

Depth (cm)	Sample ID	Raw Meas. in SI	Mass Susc. Meas. (SI)	Sample Weight (g)	Correct. Factor	Correct. Offset
30	003(LF)	5.46E-04	3.06E-07	5.58	5.58E-04	1.76E-06
30	003(HF)	4.92E-04	2.74E-07	5.58	5.58E-04	-1.46E-06
30	003 FD %	10.495	10.495	0	1	0
30	004(LF)	5.52E-04	3.07E-07	5.58	5.58E-04	-8.27E-07
30	004(HF)	4.95E-04	2.75E-07	5.58	5.58E-04	-1.07E-06
30	004 FD %	10.364	10.364	0	1	0
60	005(LF)	5.62E-04	3.38E-07	5.98	5.98E-04	2.92E-06
60	005(HF)	5.46E-04	3.26E-07	5.98	5.98E-04	-1.09E-06
60	005 FD %	3.644	3.644	0	1	0
60	006(LF)	5.83E-04	3.49E-07	5.98	5.98E-04	6.11E-07
60	006(HF)	5.49E-04	3.27E-07	5.98	5.98E-04	-1.66E-06
60	006 FD %	6.1681	6.168	0	1	0
100	007(LF)	3.35E-04	2.03E-07	6.02	6.02E-04	2.97E-06
100	007(HF)	2.97E-04	1.79E-07	6.02	6.02E-04	1.03E-06
100	007 FD %	11.753	11.753	0	1	0
100	008(LF)	3.46E-04	2.07E-07	6.02	6.02E-04	-2.65E-06
100	008(HF)	2.92E-04	1.77E-07	6.02	6.02E-04	1.57E-06
100	008 FD %	14.375	14.375	0	1	0
150	009(LF)	2.02E-04	1.38E-07	6.72	6.72E-04	3.38E-06
150	009(HF)	1.88E-04	1.25E-07	6.72	6.72E-04	-1.11E-06
150	009 FD %	9.2436	9.244	0	1	0
150	010(LF)	2.08E-04	1.39E-07	6.72	6.72E-04	-3.15E-07
150	010(HF)	1.88E-04	1.24E-07	6.72	6.72E-04	-3.19E-06
150	010 FD %	10.959	10.959	0	1	0

Depth (cm)	Sample ID	Raw Meas. in SI	Mass Susc. Meas. (SI)	Sample Weight (g)	Correct. Factor	Correct. Offset
30	001(LF)	2.86E-03	2.34E-06	16.24	8.17E-04	7.00E-09
30	001(HF)	2.58E-03	2.10E-06	16.24	8.17E-04	-4.14E-06
30	001 FD %	10.12	10.12	0	1	0
30	002(LF)	2.86E-03	2.33E-06	16.24	8.17E-04	5.41E-07
30	002(HF)	2.57E-03	2.10E-06	16.24	8.17E-04	-2.08E-06
30	002 FD %	10.11	10.11	0	1	0
60	003(LF)	2.58E-03	1.58E-06	20.43	6.09E-04	4.59E-06
60	003(HF)	2.30E-03	1.40E-06	20.43	6.09E-04	5.22E-06
60	003 FD %	10.91	10.91	0	1	0
60	004(LF)	2.59E-03	1.57E-06	20.43	6.09E-04	-1.49E-06
60	004(HF)	2.30E-03	1.40E-06	20.43	6.09E-04	-1.02E-06
60	004 FD %	11.08	11.08	0	1	0
100	005(LF)	1.73E-03	1.02E-06	21.00	5.88E-04	3.17E-06
100	005(HF)	1.57E-03	9.21E-07	21.00	5.88E-04	9.98E-07
100	005 FD %	9.49	9.49	0	1	0
100	006(LF)	1.74E-03	1.02E-06	21.00	5.88E-04	1.21E-08
100	006(HF)	1.55E-03	9.13E-07	21.00	5.88E-04	-4.15E-08
100	006 FD %	10.90	10.90	0	1	0
150	007(LF)	2.13E-03	1.08E-06	23.81	5.05E-04	-3.04E-07
150	007(HF)	1.99E-03	1.00E-06	23.81	5.05E-04	9.40E-09
150	007 FD %	6.78	6.78	0	1	0
150	008(LF)	2.12E-03	1.07E-06	23.81	5.05E-04	1.19E-06
150	008(HF)	1.99E-03	1.00E-06	23.81	5.05E-04	-9.79E-07
150	008 FD %	6.54	6.54	0	1	0